UC San Diego

UC San Diego Electronic Theses and Dissertations

Title

A direct displacement-based design of low-rise seismic resistant steel moment frames

Permalink

https://escholarship.org/uc/item/3dq3j07d

Author

Harris, John L.

Publication Date

2006

Peer reviewed|Thesis/dissertation

eScholarship.org Powered by the California Digital Library
University of California

UNIVERSITY OF CALIFORNIA, SAN DIEGO

A Direct Displacement-Based Design of Low-Rise Seismic Resistant Steel Moment Frames

A dissertation submitted in partial satisfaction of the

requirements for the degree Doctor of Philosophy

in

Structural Engineering

by

John L. Harris III

Committee in Charge:

Professor Chia-Ming Uang, Chair
Professor Robert Englekirk
Professor Enrique Luco
Professor Jeff Rabin
Professor Jose Restrepo
Professor Peter Shearer

2006

Copyright

John L. Harris III, 2006

All rights reserved.

The dissertation of John L. Harris III is approved, and it is acceptable in quality and form for publication on microfilm:

_____

_____

_____

_____

_____

_____
Chair

University of California, San Diego

2006

To Heather

Unquestioned answers are more dangerous than unanswered questions

Anonymous
(engraved on a church in New York City)

TABLE OF CONTENTS

LIST OF ABBREVIATIONS

AISC	American Institute of Steel Construction
ARS	Acceleration Response Spectra
ASCE	American Society of Civil Engineers
ATC	Applied Technology Council
BOCAI	Building Officials Code Administrators International
BSSC	Building Seismic Safety Council
CUREe	California Universities for Research in Earthquake Engineering
DBD	Displacement-Based Design
DDBD	Direct Displacement-Based Design
DRS	Displacement Response Spectra
EBD	Energy-based Design
EERI	Earthquake Engineering Research Institute
ELFA	Equivalent Lateral Force Analysis
ELSA	Equivalent Linear Static Analysis
EPP	Elastic Perfectly-Plastic (or Elastoplastic)
EQ	Earthquake
EYA	Equivalent Yield Analysis
FBD	Force-Based Design
FEMA	Federal Emergency Management Agency
IBC	International Building Code
ICBO	International Conference of Building Officials
ICC	International Code Council
LRFD	Load and Resistance Factor Design
LFRS	Lateral Force Resisting System
MCE	Maximum Considered Earthquake
MDOF	Multi-degree-of-freedom
MSSM	Modified Secant Stiffness Method
NBC	National Building Code

NEHRP	National Earthquake Hazards Reduction Program
NFPA	National Fire Protection Agency
NSA	Nonlinear Static Analysis
PBSE	Performance-based Seismic Engineering
PEER	Pacific Earthquake Engineering Research
PGA	Peak Ground Acceleration
RBS	Reduced Beam Section
RCS	Reduced Column Section
SAC	SEAOC ATC CUREe Joint Venture
SAP	Seismic Analysis Provision
SBC	Standard Building Code
SBCCI	Southern Building Code Congress International
SCWB	Strong Column Weak Beam
SDOF	Single-degree-of-freedom
SDP	Seismic Design Provision
SEAOC	Structural Engineers Association of California
SMRF	Special Moment Resisting Frame
SP	Structural Performance Level
SSM	Secant Stiffness Method
UBC	Uniform Building Code
VRS	Velocity Response Spectra

LIST OF FIGURES

LIST OF TABLES

PREFACE

This document on Direct Displacement-Based Design (DDBD) of steel moment frames is the result of an eight year journey that began in 1998. It covers the entire procedure – starting with an empty frame model to final design. As such, in developing this document emphasis was placed on outlining the entire process and supporting theory to provide the engineer with the requisite information. Where applicable, analysis and design procedures are simplified enough in an attempt to maintain transparency and integration into a design office.

DDBD has been on the forefront of research concerning alternative seismic analysis philosophies since its inception in 1993 by Nigel Priestley. With the introduction of Performance-Based Seismic Engineering (PBSE), DDBD has found a niche where other seismic analysis philosophies find limitations. Still, more research is required for DDBD to be accepted as a viable alternative to the conventional seismic design philosophy.

Structural steel has begun to come back into fashion since its decline due to pricing, tariffs, and the 1994 Northridge earthquake. It is the hope that researchers will continue to find new and innovative design methods to maintain its appeal in seismic engineering.

Lastly, thank you for taking the time to read this document. I invite you to offer me suggestions for improvement, criticisms, or questions.

John L. Harris III

June 2006

Email: jlh3@bellsouth.net

ACKNOWLEDGEMENTS

I am sincerely grateful to the following while preparing this document.

- God, for giving me the ability to think, though at times incorrectly.
- Heather, for her love, patience, and devotion. For you, I am.
- My family, whom without their support I would be a starving musician.
- My external committee members, Jeff Rabin and Peter Shearer.
- My departmental committee members, Bob Englekirk, José Restrepo, and Enrique Luco, for forging new directions in seismic engineering.
- My committee chair, Chia-Ming Uang, for teaching me that to be a great teacher you have to be a great student; for his support, guidance, and eagle eye for details.

CURRICULUM VITAE

1994	BSCE, North Carolina State University Raleigh, NC
1994 – 1995	Structural Engineer, Butler Manufacturing Laurinburg, NC
1995 – 1996	Structural Engineer, MGC Triad Raleigh, NC
1996-1998	Structural Engineer, Armour, Cape & Pond Atlanta, GA
1998-2000	Structural Engineer, DeSimone Consulting Engineers New York, NY
2002	MS, North Carolina State University Raleigh, NC
2002 – 2006	Teaching Assistant and Research Assistant Dept. of Structural Engineering University of California, San Diego
2006	Ph.D., University of California, San Diego

ABSTRACT OF DISSERTATION

A Direct Displacement-Based Design of

Low-Rise Seismic Resistant Steel Moment Frames

by

John L. Harris III

Doctor of Philosophy of Structural Engineering

University of California, San Diego, 2006

Professor Chia-Ming Uang, Chair

In recent years the tenets of Performance-Based Seismic Engineering (PBSE) have been introduced for design of earthquake resistant structures. Thus, it is necessary that a design methodology be capable of producing a system that can achieve a performance target. Research has identified limitations in conventional force-based design practices in meeting the needs of PBSE. In response, a significant movement has been made towards displacement-based design in an attempt to bypass these limitations.

This research proposes a Direct Displacement-Based Design (DDBD) methodology for design of new seismic resistant steel moment frames.

Two crucial issues in earlier DDBD methods that need resolution are (1) assumption of frame yield displacements and (2) determination of system equivalent damping. To resolve the first, a procedure using beam mechanics is proposed to construct a yield displacement profile. The procedure illustrates that yield displacement is essentially a function of beam geometry, suggesting that displacement ductility demand can be controlled via design.

Secondly, the total energy dissipated by the frame from beam yielding is commonly estimated by evaluating the base shear - roof displacement hysteresis. From which an estimate of equivalent damping is computed by applying a damping function developed for a single yield mechanism. This is limiting in that ductility contributions from each mechanism or the effects of higher mode contributions are not considered. A more rational procedure is proposed where floor ductility contributions are accounted for and an equivalent modal damping computed. In so doing, a better estimate of equivalent damping for design can be made.

Additionally, in order to maintain the cohesion between analysis and design, a methodology to capture P-Δ effects as well as a capacity design methodology is proposed to aid in preserving the structural stability of the frame during strong ground motion and provide a reliable system that can exhibit controlled deformations while satisfying the PBSE objective.

Lastly, five low-rise steel moment frames are designed using the proposed DDBD and subjected to twenty earthquakes. The results indicate that the analytical displacements generally agree with those assumed in design, illustrating that frames thus designed have a much greater potential in meeting a performance target.

Chapter 1 Introduction

1.1 Introduction

The recent trend in design of seismic resistant steel moment frames is towards a Performance-Based Seismic Engineering (PBSE) philosophy. In PBSE a structural system is designed to achieve pre-defined levels of damage under pre-defined levels of earthquake intensity. Damage levels, also known as performance limit states, are defined by deformation quantities such as strain, curvature, rotation, or displacement. Similarly, earthquake levels are characteristically defined as a function of return period for a particular site. The combination of performance limit state and earthquake intensity constitutes a 'performance level', while a series of performance levels constitutes a 'performance objective'. In 1995 the Structural Engineers Association of California (SEAOC) developed a conceptual framework for PBSE known as 'Vision 2000'. Fig. 1-1 demonstrates the concept of performance levels and objectives defined by SEAOC. *Tentative Guidelines for Performance-Based Seismic Engineering* was subsequently drafted as an appendix in SEAOC (1999).

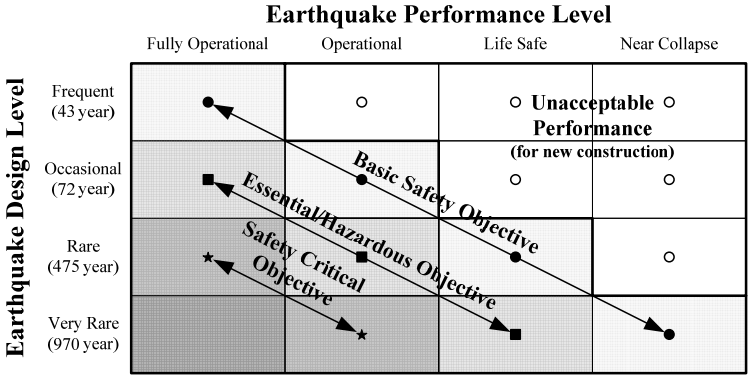

Figure 1-1. PBSE performance objectives (modified from SEAOC 1995)

Shortly afterwards, *FEMA 349: Action Plan for Performance Based Seismic Design* (EERI 2000) was produced by the Earthquake Engineering Research Institute (EERI) to increase PBSE awareness and streamline research efforts. In 2004 two chapters were published in *Earthquake Engineering: from engineering seismology to performance-based engineering* (CRC 2004) which outlines the movement towards PBSE: (1) Performance-Based Seismic Engineering: Development and Application of a Comprehensive Conceptual Approach to the Design of Buildings and (2) Performance-Based Earthquake Engineering. Currently, Applied Technology Council (ATC) as part of the ATC-58 project is working on *FEMA 445: Program Plan for Development of Next-Generation Performance-Based Seismic Design Guidelines* and *FEMA 446: Characterization of Seismic Performance for Buildings* which will build upon FEMA 349 and SEAOC (1995, 1999).

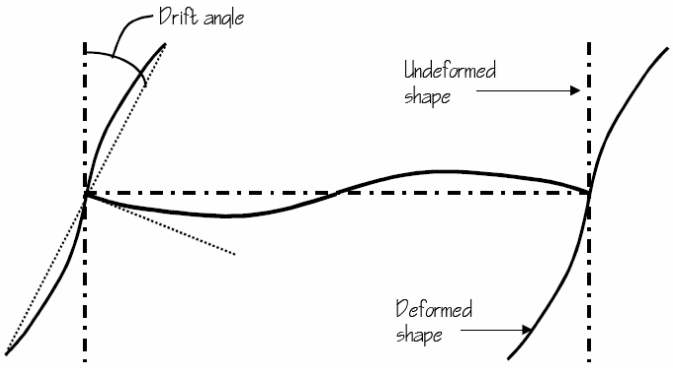

Figure 1-2. Drift angle illustration (SAC 2000)

In PBSE a performance objective typically specifies a target drift angle, θ_T, to define the desired damage level corresponding to each performance level. Fig. 1-2 graphically illustrates the drift angle concept. SEAOC (1999), Appendix I (Part B), in accordance with the Basic Safety Objective for Soil Type D, recommends the following

target values for a Zone 4 steel Special Moment Resisting Frame (SMRF) (Table 1-1 and Fig. 1-3). Here lies the fundamental difficulty of performance-based design. That is, quantitatively defining the degree of damage corresponding to each performance level target and the prediction of the earthquake magnitude leading to the attainment of the pre-defined damage level (Mazzolani et al. 2000).

Table 1-1. SEAOC recommended target values (Basic Safety Objective)

Performance Level (EQ) [1]	Qualitative Description	Qualitative Definition	θ_T (μ_θ) (*radians*)	PGA (*g*)	MCE PGA Reduction Factor
SP-1 (EQ I)	Operational	Yield mechanism; damage is negligible	0.005 (1.0)	0.16	0.24
SP-2 (EQ II)	Occupiable	Damage is minor to moderate; some repair is required	0.018 (3.6)	0.24	0.36
SP-3 (EQ III) (2/3 MCE)	Life Safe	Damage is moderate to major; extensive repairs are required	0.032 (6.2)	0.44	0.67
SP-4 (EQ IV) (MCE)	Near Collapse	Damage is major; repairs may be uneconomically feasible	0.040 (8.0)	0.67	1.00
SP-5	Collapse	Collapse is imminent			

1. see Fig. 1-3

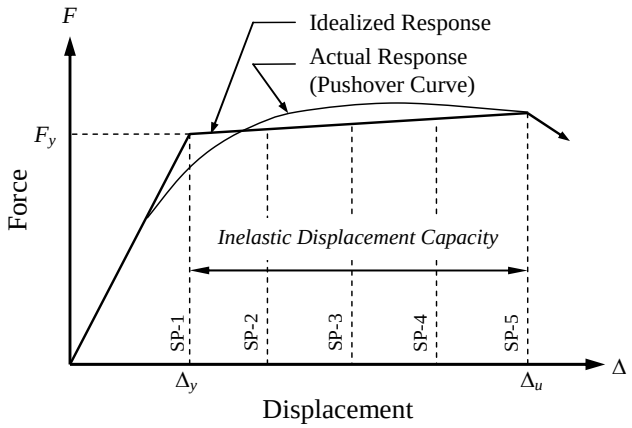

Figure 1-3. SEAOC performance levels

As a result of the introduction of PBSE it has become imperative that a seismic engineering methodology be capable of producing a system that can achieve a desired performance objective. In addition, for a design philosophy to be capable of satisfying PBSE, it must be able to evaluate seismic demands accurately, achieve a desirable

member hierarchy in the energy dissipation mechanisms, and predict the inelastic behavior under severe earthquakes (Lee and Goel 2001). In the past decade researchers have worked on adopting various methodologies to meet this need. These methods include: (1) Force-Based Design (FBD); (2) Displacement-Based Design (DBD); and (3) Energy-Based Design (EBD). EBD procedures have not been widely accepted in the work force; therefore, they will be disregarded in further discussions.

Prior to illustrating the concept of Direct Displacement-Based Design (DDBD) it is important to briefly introduce the FBD philosophy. Further, a discussion concerning the well established Equivalent Lateral Force Analysis (ELFA) is similarly required. This will provide a reference basis for discussing the inherent limitations observed in FBD as well as provide comparison points throughout this document.

1.1.1 Force-Based Design

The central focus of seismic code provisions is to reduce the probability of major damage to buildings when moderate earthquakes occur and to prevent the collapse of the main structure during severe earthquakes (Filiatrault 2003). Seismic codes are broken into two categories: (1) Seismic Analysis Provisions (SAP) and (2) Seismic Design Provisions (SDP). A few seismic codes currently in mainstream use in the U.S. are:

- ASCE 7: Minimum Design Loads for Buildings and Other Structures (ASCE 2005)
- International Building Code (IBC) (ICC 2003)
    - Uniform Building Code (UBC) (ICBO 1997)
    - National Building Code (NBC) (BOCAI 1999)

- Standard Building Code (SBC) (SBCCI 1999)
- NFPA 5000: Building Construction and Safety Code (NFPA 2003)
- FEMA 450: NEHRP Recommended Provisions for Seismic Regulations for New Buildings and Other Structures (BSSC 2003)
- Recommended Lateral Force Requirements and Commentary, 'Blue Book' (SEAOC 1999)
- FEMA 356: Prestandard and Commentary for the Seismic Rehabilitation of Buildings (ASCE 2000)

The latter three are source documents and are not considered jurisdictional seismic codes. The reader is referred to Berg (1983) and Kircher (2000) as well as the individual codes for respective histories. UBC, NBC, and SBC are listed though they have been merged into IBC. The intent and content of the 'Blue Book' published by SEAOC has been completely revised and future editions will not be considered a source document.

Table 1-2. Matrix of seismic analysis provisions (CRC 2004)

Category	Analysis Procedure	Force–Deformation Relationship	Displacements	Earthquake Load	Analysis Method
Equilibrium	Plastic Analysis Procedure	Rigid-plastic	Small	Equivalent lateral load	Equilibrium analysis
Linear	Linear Static Procedure	Linear	Small	Equivalent lateral load	Linear static analysis
	Linear Dynamic Procedure I	Linear	Small	Response spectrum	Response spectrum analysis
	Linear Dynamic Procedure II	Linear	Small	Ground motion history	Linear response history analysis
Nonlinear	Nonlinear Static Procedure	Nonlinear	Small or large	Equivalent lateral load	Nonlinear static analysis
	Nonlinear Dynamic Procedure	Nonlinear	Small or large	Ground motion history	Nonlinear response history analysis

These codes provide the design engineer with several SAPs (listed in Table 1-2) depending on the structural system, dynamic properties, Seismic Design Category, and system regularity. Although seismic codes provide SDPs typically they reference SDPs

published by external organizations. Table 1-3 lists a few of these organizations based on construction material.

Table 1-3. Matrix of seismic design provisions

Construction Material	Organization	Publication (Year) (as of this writing)
Structural Steel	American Institute of Steel Construction (AISC)	LRFD (2001) Seismic Provisions (2002) New Eds. in 2005
Concrete	American Concrete Institute (ACI)	ACI-318 (2005)
Timber	American Wood Council (AWC)	NDS (2001) New Ed. in 2005
Masonry	American Concrete Institute (ACI)	ACI-530 (2005)

The mostly widely researched and codified seismic engineering philosophy is FBD and is categorized as a design philosophy where the limit state is influenced by a satisfactory strength. That is, the structure is designed around an assigned equivalent lateral force computed via acceleration (see Earthquake Load in Table 1-2). This required elastic strength is a minimum requirement assumed to provide an acceptable degree of seismic safety and is expressed in codes as base shear. The check for damage control (inelastic displacements) under the design-level earthquake is a final check and the outcome of the design process.

1.1.1.1 Equivalent Lateral Force Analysis

Traditional seismic analysis of a steel moment frame typically employs ELFA for calculating the prescribed design base shear and associated equivalent lateral forces. In order to predict the lateral force effects from strong ground motion the engineer needs to

first estimate the fundamental period of the system, T_1. Seismic codes typically provide simplified equations for approximating an upper-bound 1st mode period. For example,

$$T_1 = C_u T_a \tag{1-1}$$

where

T_a = Approximate fundamental period $\left(= C_t h_n^{\,x}\right)$ (1-1a)

C_u = Upper limit coefficient (per code)

C_t = Period coefficient (per code)

h_n = Height of building frame above base (see Fig. 1-5)

x = Period coefficient (per code)

Eq. (1-1a) first appeared in ATC 3-06 (1978) and was derived using Rayleigh's method assuming: (1) equivalent static lateral forces are distributed linearly over the height of the building; (2) seismic base shear is proportional to $1/T_1^{2/3}$; and (3) heightwise distribution of stiffness is such that the interstory drift under linearly distributed forces is uniform over the height of the building (Goel and Chopra 1997).

Two response modification factors central to the ELFA procedure are: (1) Force Reduction Factor, *R*, and (2) Displacement Amplification Factor, C_d (shown in Fig. 1-4). According to NEHRP (BSSC 2003) for a steel SMRF: R = 8; C_d = 5.5; and Ω_o = 3. The force reduction factor specified in seismic codes used to determine the design strength attempts to encompass several factors: (1) amount of energy dissipation during inelastic response (damping and ductility), (2) the redundancy of the lateral force resisting system

(LFRS), and (3) the stiffness of LFRS (lower values are assigned to stiffer systems). A brief history of the force reduction factor can be found in ATC 19 (1996). The displacement amplification factor amplifies the elastic displacements determined from analysis to the expected inelastic displacements under the design-level earthquake.

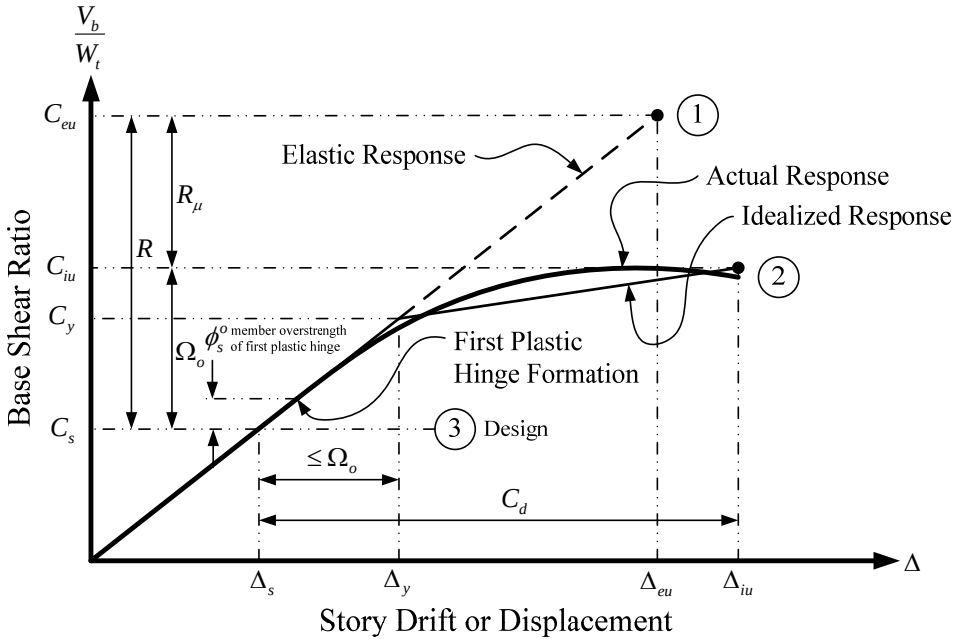

Figure 1-4. ELFA graphical representation (modified from Uang 1991a)

Once the approximate initial period is determined the design engineer enters into codified response spectra based on 5% viscous damping to calculate the ultimate elastic base shear (Level 1 force, $V_b = C_{eu} W_t$, in Fig. 1-4, where W_t = total seismic weight) and predicts the design base shear at first significant yield (Level 3 force, $V_b = C_s W_t$, in Fig. 1-4). This is accomplished by reducing the elastic base shear (Level 1 force) by the force reduction factor, *R*. The prescribed response spectrum is typically based on SDOF response. For illustration purposes, C_s can be computed for the descending branch of the Acceleration Response Spectrum (ARS) by

$$C_s = \frac{S_{D1}}{T_1\left(R/I\right)} \tag{1-2}$$

where

S_{D1} = Design spectral response acceleration at T = 1 *sec* (per code)

I = Occupancy importance factor (per code)

Any variation between the design base shear and actual base shear at first significant yield is due to member overstrengths, ϕ_s^o, of the first set of plastic hinges (see Fig. 1-4).

As evidenced by large R values stipulated in seismic codes, design provisions assume that a structure thus designed would reach an ultimate inelastic base shear (Level 2 force, $V_b = C_{iu}W_t$, in Fig. 1-4) two to four times the C_s design force level during a major earthquake (BSSC 2003). This is often the case when drift, not strength, controls member selections. This dissimilarity is identified as system overstrength, Ω_o (see Fig. 1-4).

The design base shear (Level 3 force) is distributed vertically to each floor (i.e., assumed concentrated masses) as equivalent lateral forces, F_i, as shown in Fig. 1-5. These forces are applied to the structural model in an elastic static analysis and the results used to proportion structural components in accordance with SDPs.

$$F_i = \rho_i V_b \frac{w_i h_{f,i}{}^k}{\sum_{i=1}^{n}\left(w_i h_{f,i}{}^k\right)} \tag{1-3}$$

where

w_i = Seismic weight at floor *i*

$h_{f,i}$ = Height of floor *i* above base

k = Period-dependent distribution coefficient (per code)

ρ_i = Redundancy factor for floor *i* (per code)

In Eq. (1-3), *k* is used to approximate variations in force distribution due to the changing fundamental mode shape and increasing response contributions from higher modes as the fundamental period increases. Taking *k* as unity implies that the fundamental mode shape is linearly proportional to the height above the base.

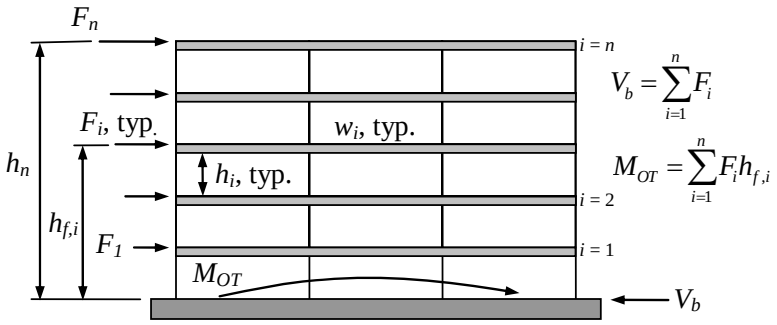

Figure 1-5. Lateral force distribution

Lastly, in addition to satisfying strength provisions the system should comply with inelastic displacement limits. Displacement limits are stipulated in seismic codes as story drift limits. The expected maximum displacement of each floor at the center of mass is determined by

$$\delta_x = \frac{C_d \delta_{xe}}{I} \tag{1-4}$$

where

δ_{xe} = Displacements determined from elastic analysis (see Fig. 1-6)

For drift analysis purposes the lateral forces applied in the elastic analysis to establish the displacements, δ_{xe}, can be calculated from Eq. (1-3) using the base shear computed using C_s determined with the *actual* 1st mode period in lieu of the strength value obtained from Eq. (1-1). This equates to two sets of design forces: (1) strength-level and (2) displacement-level. For simplicity design engineers sometimes disregard this difference and use strength-level lateral forces to check strength and displacement (conservative option). This practice is promoted in ASCE 7-05 (ASCE 2005), see Fig. 1-6. However, it is unclear what period should be used to compute *k* in Eq. (1-3).

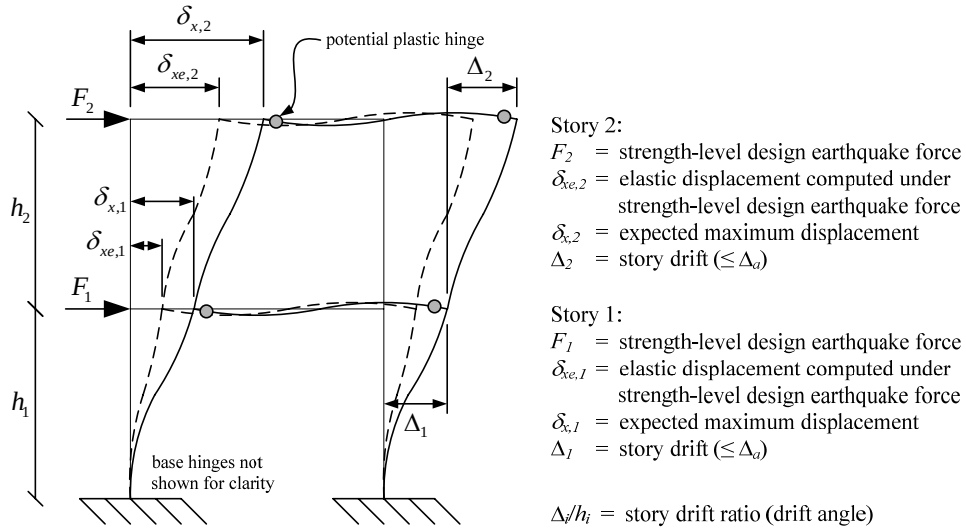

Figure 1-6. Displacement verification schematic (modified from ASCE 2005)

1.1.2 Statement of Problem

Conventional seismic engineering of steel moment frames generally follows a prescriptive FBD methodology where an ELFA is used to calculate component strengths at first significant yield. Current research, however, has identified inherent restrictions in FBD practices that limit system capabilities in meeting a performance target outlined in PBSE. Central to these limitations is the use of prescriptive response modification factors established independent of period and yield displacement. A corollary to this is that steel moment frames can be stiffer and stronger than is necessary to satisfy code drift limits (Harris 2004). Furthermore, the absence of a comprehensive capacity design philosophy that additionally incorporates the effects of higher mode response could lead to uncontrolled deformations and possibly undesirable column hinging (Harris 2004).

The following discussion summarizes a few limitations inherent in FBD in providing a system that can successfully achieve a performance target established by PBSE.

1.1.2.1 Total Weight Assumption

In accordance with ELFA the design base shear is determined with the total seismic weight, W_t, contributing to the 1st mode base shear. This is adopted to indirectly and approximately account for the contributions of higher modes (Chopra 1981). MDOF systems respond primarily elastically in the fundamental mode prior to development of inelastic actions (Medhekar and Kennedy 2000b). This contribution is appropriate for SDOF systems; however, the design base shear can be overestimated for MDOF systems

when the total mass is assumed to contribute solely to the 1st mode (Priestley 2003, Chopra 2005). This effect is illustrated in Fig. 1-7 (ρ is a beam-column stiffness ratio). Consequently for steel moment frames an increase in required strength is coupled with an increase in flexural stiffness leading to an inadvertent period shift from that assumed for design (disregarding additional strength and stiffness produced from member overstrength). This implies that an iterative analysis-design procedure is required.

Another limitation is that the "multi-mode" design base shear is distributed based on an assumed 1st mode shape that may not match the actual mode shape after the structure has been designed. In so doing, the base shear is distributed based on mass independently of the stiffness and strength of individual floors. It has been contended that higher modes are better accommodated in the capacity design phase rather than during the preliminary phase (Priestley 2003).

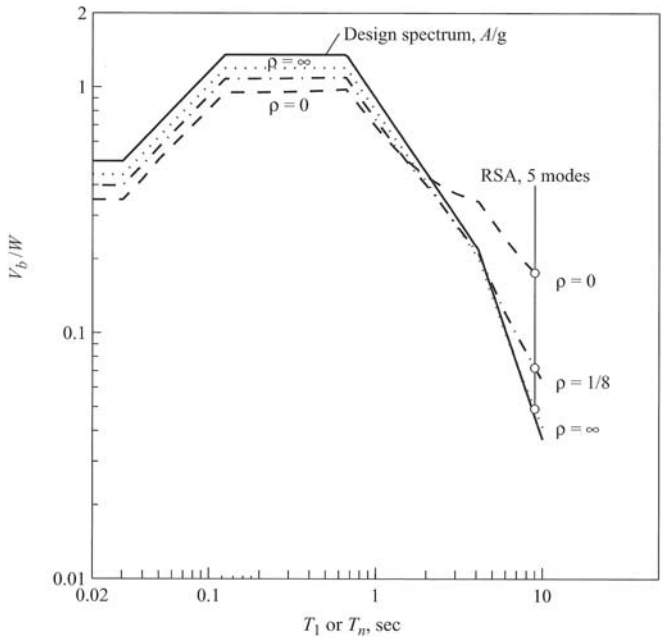

Figure 1-7. Base shear ratio vs. fundamental period (Chopra 2005)

1.1.2.2 Fundamental Period Assumption

To start the design process the engineer needs the fundamental period, or since the total mass is assumed to participate, the stiffness of the system. In lieu of a substantiated analysis seismic codes provide the engineer with simplified equations to approximate the fundamental mode. These equations were derived based on measured response of actual buildings during earthquakes. The formulas are calibrated to underestimate the fundamental period so that the computed base shear is conservative and to aid in arriving at an initial design (Newmark and Hall 1982). The reader is referred to ATC 3-06 (ATC 1978), Goel and Chopra (1997), and NEHRP 2003 (BSSC 2003) for detailed information.

There is no conceptual limitation with these equations since they are statistically derived from actual building response. The limitation is that the engineer is assuming a structural property before design of the structure. This implies that the analysis and design process should be iterative requiring convergence on the fundamental period. Seismic codes approach analysis and design independently and do not stipulate an iterative procedure.

Furthermore, the buildings used to derive these equations designed per earlier versions of the seismic code in California (prior to 1994). It is uncertain if these formulas can be applied to structures in other regions or structures designed by an alternative philosophy. Lastly, it was noted in the study that the intensity of shaking has little influence on the period of steel moment frames as long as there is no significant yielding

of the structure (Goel and Chopra 1997). This is contrary to FBD that assigns relatively high ductility values to steel moment frames.

1.1.2.3 Response Modification Factor Assumption

U.S. seismic codes require the design engineer to check inelastic displacement demands against code requirements, though service-level limit state verification has been removed (Uang and Bertero 1991). The maximum displacement demands are estimated by increasing elastic displacements determined by structural analysis, δ_{ex}, by a constant displacement amplification factor, C_d. However, the displacement amplification factor is determined independent of yield displacement and mechanism, and is typically specified less than the force reduction factor, R, and independent of overstrength, Ω_o. The limitations of such use are illustrated in Bertero (1986), Uang (1991a), Uang (1991b), and Uang and Maarouf (1993, 1994). Ultimately, due to the absence of yield displacements there is an incompatibility between the displacement amplification factor and ductility capacity. This is a consequence of having no methodology to determine the ratio of yield displacement to elastic displacement (see Fig. 1-4). Moreover, assuming a constant amplification factor implies that the mode shape does not change during inelastic response. Hence, displacement estimates are performed without evaluation of the strength and stiffness of individual floors, nor the effects of inelastic behavior.

The displacement-level lateral forces used to determine the elastic displacements, if selected, account for strength demands from higher mode effects thus possibly overestimating the analytical elastic displacements – even more pronounced if strength-

level lateral forces are used. Since two periods can be used to determine displacement-level and strength-level lateral forces, the design engineer is required to iterate between strength and stiffness by performing separate analyses.

Seismic codes limit maximum story drifts to 0.02*h* or 0.025*h* (where *h* is the height between floors) depending on the estimated 1st mode period (ASCE 7-05 stipulates that these values be reduced by ρ for a SMRF). These values are based on early research reporting that steel beams can accommodate post-yield rotations in the range of 0.01 to 0.015 *radians*, assuming an elastic rotation of 0.01 *radians* (AISC 2002). These rotation values have been subsequently revised based on later research; however, the codified allowable drift requirements have not been similarly revised. As such, the design engineer may find that substantial elastic stiffness requirements are placed on the frame when reducing the story drift limit by the displacement amplification factor. As a consequence, code drift limits tend to reduce design ductility levels to values significantly less than what can actually be accommodated (Priestley and Kowalsky 2000). This effect combined with the increase in stiffness due to member overstrengths created during design will produce higher than expected seismic forces and inconsistencies between actual and predicted damage levels. Ultimately, the system will most likely not experience the full ductility demand under the design-level earthquake, and it is questionable if the system could satisfy this capacity if pushed to this demand. The system will have difficulty attaining the performance objective. As a side note, it appears that the story drift limit could be assigned to account for the service-level limit state.

In parallel, the elastic force demands produced from the strength-level lateral forces are checked against yield capacities, albeit approximate since a conventional elastic analysis cannot account for geometric and material nonlinearities including inelastic redistribution, and the same ductility measure is assumed for all modes. Nonetheless, there are no codified requirements to insure that the ductility capacity does in fact match the initially assumed response modification factors. This implies that a ductility capacity can be assigned to a structural system regardless of its geometry and member strengths, and that the stiffness of a structure solely determines its displacement response (Priestley and Kowalsky 2000). Lastly, using constant response modification factors does not ensure the same level of safety against collapse for all structures (Bertero 1986, Uang 1991a,b).

Bertero (1986) tabulated the shortcomings of a constant *R* value.

(1) A single value assigned to *R* used for all buildings of a given frame type independent of height, geometry, and framing layout cannot be justified.

(2) The values assigned to *R* will likely not produce the desired performance under the design-level earthquake.

(3) *R* is intended to account for ductility; however, a constant ductility cannot be used to uniformly reduce the elastic spectral demands to the design spectral demands.

(4) Overstrength of buildings in different seismic regions will likely vary considerably. *R* should be dependent on seismic zone.

1.1.2.4 Elastic Analysis Assumption

$P-\Delta$ and $P-\delta$ effects (global and local geometric nonlinear effects respectively, or 2nd order effects) should be included in the structural analysis. Few elastic analysis software packages account for the local $P-\delta$ effect. Additionally, geometric imperfections are not typically modeled in analysis. Thus, an incompatibility exists between the static (or dynamic) analysis demands and component capacities determined from inelastic design interaction equations. That is, strength and stability of a system and its members are related, but the interaction is treated separately in LRFD steel design specifications.

In seismic engineering where members are required to respond and maintain structural integrity in the inelastic region an elastic analysis will produce conservative demands. This in effect will inherently contribute to member overstrength. Furthermore, displacements are used to determine damage levels and since geometric imperfections are accounted for in member design interaction equations and not the analysis, a discrepancy exists in the final displacement ductility prediction. These analysis limitations are neglected in this document, thus, this discussion is included to provide insight into future research needs.

1.1.3 Displacement-Based Design

As a result of these fundamental limitations inherent in FBD and ELFA, displacement-based design (DBD) methods are being investigated as alternative means to satisfy performance objectives. A recent paper by Sullivan et al. (2003) discussed several

DBD procedures capable of achieving PBSE. Sullivan et al. characterized the various design procedures by two key parameters: (1) the role that deformation plays in the design process, and (2) the type of analysis used in the design process. The resulting matrix of design procedures is shown in Table 1-4. The reader is referred to Sullivan et al. (2003) for details regarding any of the procedures listed. One of the more promising approaches is Direct Displacement-Based Design (DDBD) proposed by Priestley (1993) and revisited by Priestley (2003) – identified by the shaded region in Table 1-4.

Table 1-4. Matrix of design procedures (modified from Sullivan et al. 2003)

	Deformation-Calculation Based (*DCB*)	Iterative Deformation-Specification Based (*IDSB*)	Direct Deformation-Specification Based (*DDSB*)
Response Spectra: *Initial Stiffness Based*	Moehle (1992) FEMA 274 (ATC 1997) UBC[1] (ICBO 1997) Panagiotakos & Fardis[1,2] (1999) Albanesi et al. (2000) Fajfar (2000)	Browning[1] (2001)	SEAOC (1999) Aschheim & Black (2000) Chopra & Goel (2001)
Response Spectra: *Secant Stiffness Based*	Freeman (1978) ATC-40 (ATC 1996b) Paret et al. (1996) Chopra & Goel (1999)	Gulkan & Sozen (1974)	Kowalsky et al. (1995) SEAOC[1] (1999) Priestley & Kowalsky[1] (2000)
Direct Integration: *Time-History Analysis Based*	Kappos & Manafpour[2] (2000)	N/A	N/A

1. Method has been developed for particular structural types and is not intended for application to other structural types.
2. Method has been developed with specific limit states in mind that must be checked during design.

It is the expectation that a DDBD methodology will be more suited for PBSE than FBD by means of reverse engineering. While both philosophies begin the design process with a design ductility demand, DDBD differs in that the initial system stiffness and member strengths are the final design outcome. More importantly, the use of yield displacements is a fundamental part of this methodology. In so doing, the design ductility demand can be more strongly associated with frame ductility capacity than prescriptive

response modification factors. Furthermore, it is proposed that this philosophy results in a more reasonable design lateral force distribution since the proportionality between strength and stiffness is directly accounted in analysis and design by modeling an inelastic system. For these reasons, this philosophy could provide more efficient member sizes and produce a system more readily capable of accomplishing a performance target than its FBD counterpart (Harris 2004).

1.1.3.1 Direct Displacement-Based Design

DDBD is built upon the foundation outlined by the ‘substitute structure’ approach proposed for reinforced concrete frames by Shibata and Sozen (1976). In this method an inelastic frame is replaced by an equivalent elastic frame with its stiffness and damping properties related to but different from the elastic frame. Since the substitute structure is elastic, classical modal analysis procedures and elastic response spectra can be employed to calculate design forces. As stated by Shibata and Sozen (1976), this method is explicitly a design (and not an analysis) procedure with deliberate consideration of displacement in the design process.

In expanding the substitute structure approach to include analysis, DDBD aspires to design a structure to achieve a displacement rather than be bounded by a limit. In so doing, the premise is that a design base shear can be assigned based on a design displacement. This conceptually differs from FBD where a design base shear is assigned based on a design acceleration. The argument is that structural damage is more directly related to displacement than acceleration. The basic steps of the current DDBD approach

are described next. More detailed explanations follow in Chapter 2. The steps should be coupled with the graphical representation shown in Fig. 1-8.

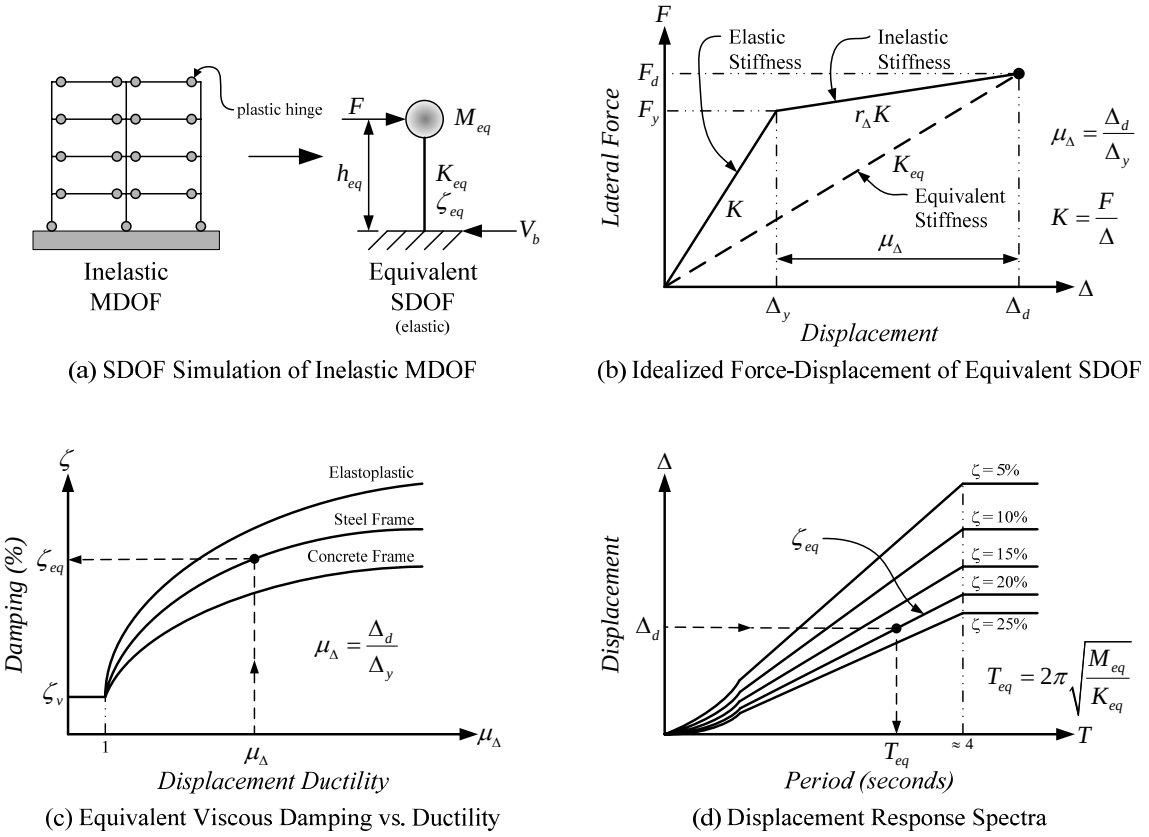

Figure 1-8. Graphical illustration of DDBD (modified from Priestley 2003)

Step 1: Selection of Seismic Demand

The seismic demand for DDBD is a Displacement Response Spectrum (DRS) generated for an elastic SDOF for several levels of damping (see Fig. 1-8(d)).

Step 2: Selection of Target Displacement

In accord with the intention of PBSE a performance target is chosen to represent the desired damage level when subjected to a given earthquake intensity. This target is

characterized as the design displacement, Δ_d, shown in Fig. 1-8(b). The target displacement for design of a structural system can be defined by strain-based damage criteria, curvatures, rotations, or directly by story drift ratio, θ_T.

Since a design spectrum (Step 1) is typically generated for a SDOF, a focal course of action in DDBD is to transform a MDOF structure into an equivalent SDOF with quantitative stiffness, mass (or weight, W_{eq}), height, h_{eq}, and damping, ζ_{eq}, illustrated in Fig. 1-8(a). This transformation is performed by applying a design displacement profile, $\{\delta_d\}$, which is a function of the target drift ratio (i.e., drift of the most critical structural component(s)). The displacement profile is chosen to correspond with the inelastic fundamental mode at the design-level of seismic excitation (Priestley 2003). The defining properties of the equivalent SDOF are as follows.

$$\Delta_d = \frac{\sum_{i=1}^{n}\left(w_i \delta_{d,i}{}^2\right)}{\sum_{i=1}^{n}\left(w_i \delta_{d,i}\right)} \tag{1-5}$$

$$W_{eq} = \frac{\sum_{i=1}^{n}\left(w_i \delta_{d,i}\right)}{\Delta_d} \tag{1-6}$$

$$h_{eq} = \frac{\sum_{i=1}^{n}\left(w_i \delta_{d,i} h_{f,i}\right)}{\sum_{i=1}^{n}\left(w_i \delta_{d,i}\right)} \tag{1-7}$$

The seismic weight from Eq. (1-6) is typically 60% - 90% of the total seismic weight, W_t, used in FBD. The remaining portion participates in the higher modes.

Step 3: Determination of Yield Displacement

The yield displacement, Δ_y, of the equivalent SDOF is commonly assumed and iterated based on design choices.

Step 4: Calculation of Equivalent Damping

With both target and yield displacement known (Steps 2 and 3) the displacement ductility demand, μ_Δ, of the equivalent SDOF can be estimated by

$$\mu_\Delta = \frac{\Delta_d}{\Delta_y} \tag{1-8}$$

Eq. (1-8) is an approximation of the system-level ductility demand of the MDOF system. Relations for equivalent damping, ζ_{eq}, can be defined as a function of displacement ductility for different materials and systems (see Fig. 1-8(c)), and are assumed to be a function only of the hysteretic loop shape.

Step 5: Calculation of Equivalent Period and Design Base Shear

The period of the equivalent SDOF, T_{eq}, at maximum response is obtained by entering the design-level DRS with the target displacement and reading across to the

appropriate response curve and down to the equivalent period as shown in Fig. 1-8(d). The response curve that is selected is a function of the level of equivalent damping.

With the period of the equivalent SDOF the equivalent stiffness, K_{eq}, is obtained by classical SDOF dynamics theory. The equivalent stiffness is defined as the secant stiffness to maximum response (see Fig. 1-8(b)).

$$K_{eq} = 4\pi^2 \frac{M_{eq}}{T_{eq}^{\ 2}} \tag{1-9}$$

The base shear (level 2 force in Fig. 1-4) at the design limit state is obtained by multiplying the equivalent stiffness by the target displacement.

$$F = V_b = K_{eq}\Delta_d \tag{1-10}$$

Step 6: Structural Analysis and Member Design

At the target, the design base shear from Eq. (1-10) is distributed as equivalent lateral forces and applied to the structural model in an elastic analysis (see Fig. 1-5).

$$F_i = V_b \frac{w_i \delta_{d,i}}{\sum_{i=1}^{n} \left(w_i \delta_{d,i} \right)} \tag{1-11}$$

Comparison of Eqs. (1-3) and (1-11) suggests that $\delta_d \propto h^k$, albeit that DDBD employs an inelastic fundamental mode shape. For compatibility with the substitute structure, component stiffness should be representative of that at the design displacement. In so

doing, member-level secant stiffness is used in analysis for those components undergoing inelastic deformations. The results from the elastic analysis are used to determine the required member strengths.

As intuition might suggest, DDBD is philosophically different than FBD. First, the fundamental period of the structure is not established until after the structure is designed. The period is consequently not restricted to the limitations inherent in Eq. (1-1a). Furthermore, comparing Eqs. (1-3) and (1-11), the lateral force distribution in DDBD is not constrained to a height proportional displacement assumption but rather is dependent on the desired inelastic displaced shape. The benefit of using an inelastic mode shape is that modifications to the elastic mode shape from changes in component stiffness due to inelastic action are taken in to account at the beginning of the design (Priestley 2003). Inelastic displacement verification is therefore not needed since maximum displacements are the focal point of design whereas displacement verification is a final check in FBD as well as being independent of design decisions. The maximum displacements in FBD are simply bounded by the limit and if satisfactory, regardless of magnitude, the design process typically ceases. This further illustrates that FBD should be an iterative analysis-design procedure. Lastly, displacement ductility is explicitly used in the DDBD process in lieu of “one-size-fits-all” response modification factors.

1.2 Research Objective and Dissertation Layout

A majority of research on DDBD methods has concentrated on concrete systems or general philosophical approaches. Only a few activities have considered DDBD as

applied to steel systems and there remains a void of information regarding its use with steel moment frames. The objective of this research is to develop through analytical study a comprehensive DDBD methodology for new seismic resistant low-rise steel moment frames. ‘Comprehensive’ means that this research outlines and demonstrates the entire process, thus, the coupling of analysis and design is preserved.

The global DDBD procedure presented within this document is based on the procedure developed by Priestley (1993, 2003) and subsequently introduced in *Recommended Lateral Force Requirements and Commentary* (SEAOC 1999) in Appendix I, *Tentative Guidelines for Performance-Based Seismic Engineering*. Several other parameters which will be discussed are yield displacement for steel moment frames, equivalent damping, and Equivalent Yield Analysis, including correlated capacity design provisions with allowances for protection against higher mode effects.

The dissertation layout is as follows. In Chapter 2 a literature review of DDBD is presented as well as a detailed illustration of the current methodology and core supporting theory. In addition, limitations, modifications, and research needs are addressed. Chapter 3 discusses the determination of the target and yield displacement profile and the design and yield displacement of the effective SDOF for steel moment frames. Chapter 4 presents a methodology for determining the quantitative measure of equivalent damping for design of MDOF steel moment frames. Chapter 5 discusses the inclusion of second-order effects into DDBD. Chapter 6 concludes the proposed procedure by introducing the use of Equivalent Yield Analysis and Capacity Design. Lastly, Chapter 7 demonstrates the complete proposed procedure in design examples of

three- and six-story steel moment frames. The designed frames are evaluated with a 2nd order inelastic time-history analysis to allow comparison of frame response when subject to strong ground motion and judge the applicability of the design parameters. Chapter 8 concludes the proposed procedure.

1.3 Simplifications, Assumptions, and Material Properties

The procedures described in this research encompass a Direct Displacement-Based Design of seismic resistant steel moment frames. Consequently, several simplifications and assumptions are used more for assistance in the basic understanding of steel response than for accuracy in the development of the proposed procedures. It is the hope of the author to continue this research forward continually revising the process for accuracy and simplicity in order to develop a systematic design procedure. The following items are used throughout this document, unless noted otherwise.

1.3.1 Simplifications

A bilinear approximation of the actual force-displacement member behavior including post-yield stiffness is used as the hysteretic function to model plastic hinges, shown for example in Fig. 1-9 (no post-yield stiffness). This topic is covered in Chapter 3. It is understood that structural steel exhibits the Baushinger Effect during reloading as shown for example in Fig. 1-10; hence, the Ramberg-Osgood or trilinear hysteresis could be a better approximation.

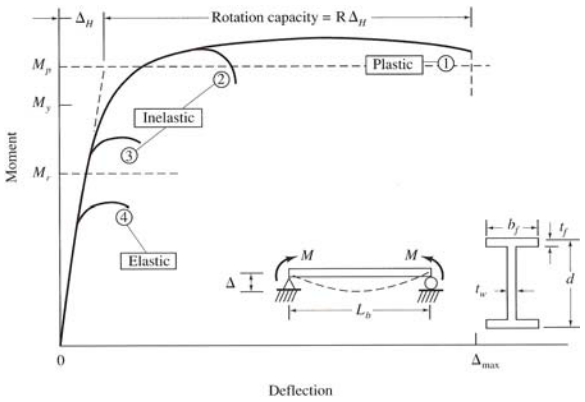

Figure 1-9. Member force-displacement graph of steel beam (Yura et al. 1978)

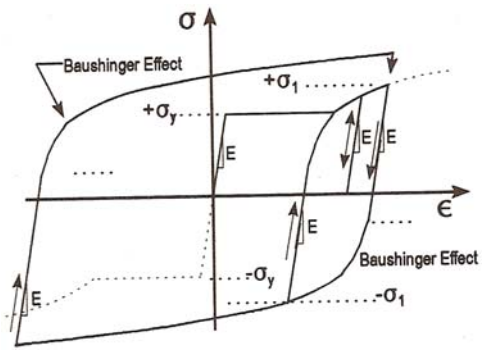

Figure 1-10. Cyclic behavior of steel with Baushinger Effect (Bruneau et al. 1998)

1.3.2 Assumptions

1. All elements are initially straight and prismatic, and plane cross-sections remain plane after deformation. The cross-section is symmetric about both principle axes and does not change during bending.
2. Flexural and lateral-torsional buckling are prevented. All members are assumed to be seismically compact (local buckling is allowed after formation of plastic hinge) and adequately braced to prevent out-of-plane deformations. Full plastic moment capacity is achieved (with reductions for the presence of axial but not shear or torsion forces).
3. Large rigid-body displacements are allowed, but member deformations and strains are considered small.
4. The element stiffness formulation is based on conventional beam-column stability functions, including axial and bending deformations, but not those associated with shear. Element bowing effects are neglected.
5. The formulation is limited by its ability to model plastic hinges only at the element ends. Plastic hinges can sustain inelastic rotations only. Strain

hardening is considered but stiffness and strength degradation is not considered.

6. All members are fabricated from isotropic homogeneous material. A linear stress-strain curve is assumed and is the same for compression and tension. Strains and stresses are constant across the width of the cross-section.
7. Composite action with concrete flooring is not considered.
8. All joints are assumed rigid and complete force transfer is assumed.
9. Vertical ground accelerations and soil-structure interaction are not considered.
10. Panel zone and shear deformations are not considered.
11. Structural torsional effects are not considered.

1.3.3 Material Properties

Unless otherwise noted, nominal steel material properties assumed in analysis and design are: yield stress ($F_y = 50\ ksi$), modulus of elasticity ($E = 29000\ ksi$), and shear modulus ($G = 0.4E = 11200\ ksi$).

Chapter 2 Review of Direct Displacement-Based Design

2.1 Introduction

In recent years the tenets of Performance-Based Seismic Engineering have been introduced for the design of earthquake resistant structures. Chapter 1 identified possible limitations in conventional force-based design in producing a system that can achieve a performance target and illustrated the need for an alternative seismic design philosophy. A significant movement during the past decade has been made towards a displacement-based design philosophy and Direct Displacement-Based Design (DDBD) has shown the most promising potential towards meeting this need.

The fundamental steps of DDBD were illustrated in Chapter 1. This chapter will concentrate on describing the steps in further detail while presenting the theory in support of this philosophy. Although the information provided in this chapter is generalized, requirements for adapting DDBD explicitly to steel moment frames and expanding upon the basic steps are provided in subsequent chapters.

2.2 Literature Review

Essential to the theory of DDBD is the understanding of its progression into the current methodology. Displacement-based design is not entirely a new subject of research for alternative seismic design philosophies. A review of past research reveals that this topic has progressed in the past decade into the current framework.

Gulkan and Sozen (1974) introduced a deformation-based design procedure for reinforced concrete frames that can be approximated as a SDOF. In this methodology the design base shear can be approximated by establishing a ‘damage stiffness’ coupled with a ductility level. Initial properties of the frame are known at the beginning and post-yield deformation based on ductility can be computed from an equivalent stiffness (elastic) and damping. The equivalent stiffness at a ductility level is taken as the secant stiffness (maximum lateral force divided by the maximum displacement). The peak displacement is calculated and checked against code limits. This study proposed the concept of “substitute damping.” Results from this study were also concluded by Shibata (1975).

Shibata and Sozen (1976a, 1976b, 1977) adapted the methodology proposed by Gulkan and Sozen (1974) to MDOF reinforced concrete frames. This research proposed that an inelastic frame can be converted to an equivalent elastic frame (‘substitute structure’) for estimating maximum displacements. The objective of this method is to establish the required strengths of the structural components such that a response displacement is not likely to be exceeded. As such, elastic member stiffness is known at the beginning and the substitute structure constructed based on a tolerable inelastic displacement. This study included a procedure for estimating a system-level substitute damping from SDOF damping.

Qi and Moehle (1991) and Moehle (1992) introduced a displacement-based design approach for reinforced concrete structures. This approach is based on comparison of curvature ductility capacity to demand. Since the capacity is known, the period and

member properties are known at the beginning. As a result, this procedure tends more to FBD where displacements are checked at the end of the process.

Priestley (1993) proposed the concept of Direct Displacement-Based Design where the initial period and member strengths are the final result of the procedure. It is proposed that the period of an inelastic system at a predetermined ductility level can be estimated by an elastic displacement response spectrum constructed for the appropriate level of damping. The stiffness of the inelastic system is taken as the secant stiffness to target response. The required elastic stiffness of the members is determined and members designed to achieve the desired ductility.

The DDBD procedure was initially developed for SDOF concrete bridge piers (Kowalsky et al. 1994, 1995) and was subsequently developed for multi-span concrete bridges (Calvi and Kingsley 1995, Priestley and Calvi 1997, Kowalsky 2002, Priestley and Calvi 2003). Calvi and Pavese (1995) illustrated the conceptual formulation of DDBD as applied to concrete building frames and was subsequently advanced and implemented for multi-story concrete building frames (Priestley et al. 1996, Priestley and Calvi 1997, Priestley 1998a, Priestley 1998b, Loeding et al. 1998, Priestley and Kowalsky 2000, Kowalsky 2001, Priestley 2003). As a side note, the reader is referred to Pettinga and Priestley (2005) for possible future revisions to DDBD of concrete frames.

Since the inception of DDBD many researchers have proposed other DDBD procedures or variations thereof. Many of these are listed in Table 1-4 and the reader is referred to these works. The following presents a selected few:

- Fardis et al. (1997) included design for gravity loads in DDBD and empirically derived expressions for the ductility capacity of concrete members.
- Heidebracht and Naumoski (1997) adopted DDBD for concrete moment resisting frames that are modeled as a shear beam.
- Fajfar (2000) proposed a generalized equivalent linear analysis procedure similar to that proposed by Qi and Moehle (1991) that incorporates an inelastic spectrum in lieu of an elastic spectrum constructed for the level of equivalent damping. Maximum displacement is the end result and checked against capacity.
- Xue (2001), Chopra and Goel (2001), and Xue and Chen (2003) proposed generalized DDBD procedures that incorporates an inelastic spectrum without the need for an equivalent structure and damping. Chopra and Goel (2001) contended that the formulation for equivalent damping overestimates the damping. As a side note, the formula used in that study was based on steady-state harmonic response at resonance. Also, based on research at that time, Borzi et al. (2001) proposed a methodology to construct an inelastic displacement spectrum.

Further information regarding general DDBD approaches (not related explicitly to steel structures) or variation thereof, discussions regarding the advantages of this philosophy, or other related topics can be found in Borzi and Elnashai (2000), Chandler and Mendis (2000), Smith and Tso (2002), Davisdon et al. (2002), Doherty et al. (2002),

Christopoulus et al. (2003), Pampanin (2003), Sullivan et al. (2003), Gutierrez and Alpizar (2004), Miranda and Lin (2004), Yavas and Saylan (2004), Thomsen and Wallace (2004), Park and Eom (2005), and Xue and Wu (2006).

The DDBD concept was initially applied to concrete bridges and buildings. Starting in 2000, researchers have been adapting DDBD, or variation thereof, to seismic resistant steel structures. The following is a brief review of research in this area.

Medhekar and Kennedy (2000a, 2000b) proposed a DDBD methodology for concentrically braced steel frames. It was noted in this study that little information is available on equivalent damping for steel structures responding inelastically and a methodology is needed. As a result, equivalent damping was not used in this study and 5% viscous damping in association with the equivalent stiffness was assumed. Lateral force resistance by the model frames for design purposes was provided by tension braces alone and, therefore, neglected the effects from buckling of the compression braces.

Aschheim and Black (2000) and Aschheim (2002) adapted a DDBD procedure that incorporates a yield point spectrum as a function of viscous damping and elastic system properties. As such, an acceptable yield displacement of the effective SDOF is a requisite in this method and an expression for approximating the yield displacement at the roof was proposed. This expression is derived independently of the desired or actual displacement profile at yield.

Harris (2002) proposed a DDBD methodology for steel moment frames following the basic steps. This study discussed the need of a yield displacement for the effective

SDOF computed based on a target yield displacement profile. This study also concentrated on the introduction of *Advanced Analysis* (Chen and Lui 1992, Chen and Toma 1994, Chen and Kim 1997) into the DDBD framework and general seismic design of steel frames. Harris (2004) subsequently expanded upon the original recommendations and provided response comparisons between a steel moment frame designed in accordance with DDBD and FBD. It was noted that a methodology to estimate a system-level equivalent damping is needed and that taking the displacements at the effective height to estimate ductility is more rational than using roof displacements.

Lin et al. (2002) illustrated a conceptual design example of DDBD applied to a steel moment frame. The yield displacement at the roof (independent of mode shape) was initially assumed and design iterated until convergence with elastic analysis results. Equivalent damping was computed for the effective SDOF using the Takeda model with the system-level ductility demand computed at the roof. Lin et al. (2003) subsequently expanded upon this example by introducing passive energy dissipation devices.

Kim and Seo (2004) presented a DDBD procedure for a concentrically braced steel frame with buckling-restrained braces. A methodology was proposed to predict the yield displacement at the roof assuming simultaneous yielding of all braces and neglecting contributions from column deformations and other sources. Steady-state harmonic system-level equivalent damping at resonance was assumed in this study.

Tsai et al. (2004) developed a DDBD procedure for a concentrically braced steel frame with buckling-restrained braces. The procedure was developed to match

experimental test results of a three-story frame. This methodology is similar to that proposed by Kim and Seo (2004) except the yield displacement computed from simultaneous brace yielding is amplified to account for other contributions. This procedure uses an inelastic spectrum in lieu of a damped elastic spectrum.

Lee et al. (2004) presented a PBSE design procedure derived based on the concept of energy balance, originally proposed by Uang and Bertero (1990), to determine the design base shear for a steel moment frame. Though this procedure is unrelated to DDBD, the procedure relies heavily on the selection of an acceptable yield displacement (assumed in this study). As such, there remains a need to develop a methodology to estimate the yield displacements for design purposes.

The progression of DDBD in research is evident in the literature review. In parallel with research publications, design engineers are beginning to understand the advantages of this philosophy and are implementing this philosophy in seismic design of structures. The California Department of Transportation (Caltrans 2001) has moved away from force-based design and has adopted a displacement-based design for concrete bridges. Still, there is a lack of information regarding a *complete* DDBD procedure explicitly adapted to steel structures. While the literature review presented a few research activities, full-scale experimental testing to verify the analytical results is needed.

2.3 Direct Displacement-Based Design

The global sequence of DDBD is graphically illustrated in Fig. 2-1. The process begins by characterizing the inelastic MDOF frame by an inelastic displacement profile

representative of the desired degree of damage. In Step A the inelastic MDOF is converted to an invented equivalent MDOF (substitute structure). In so doing, the transformation to the equivalent effective SDOF is readily accomplished in Step B. In Step C the design parameters are determined via the equivalent effective SDOF and applied to the equivalent MDOF in an elastic static analysis. In Step D the required elastic structural component properties are determined and design finalized.

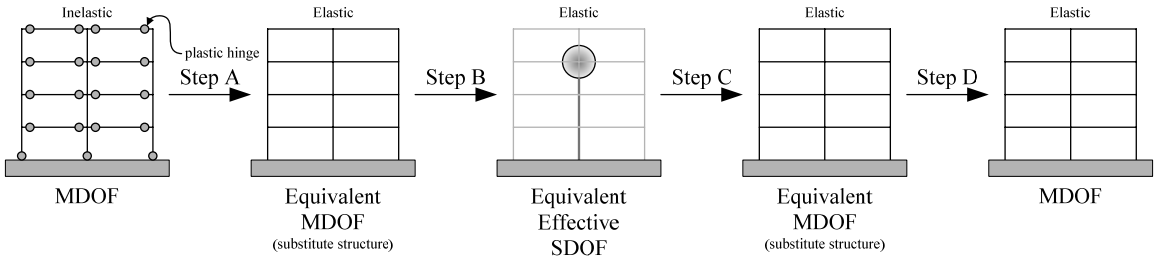

Figure 2-1. Global sequence used in DDBD

The six steps outlining the basic procedures involved in DDBD were introduced in Chapter 1. The first part of this section will discuss the theory in support of DDBD. The latter part (Section 2.3.2) will illustrate the basic steps in further detail while providing limitations and research needs.

2.3.1 General Theory

A crucial step in DDBD is the transformation of a MDOF structure into an effective SDOF structure as illustrated in Fig. 2-2. This transformation has been widely accepted among researchers as an acceptable means of approximating the global strength, stiffness, and ductility requirements of a MDOF system. The motivation in support of this

transformation is the application of a SDOF response spectrum specified in seismic codes to predict seismic demands on the actual system.

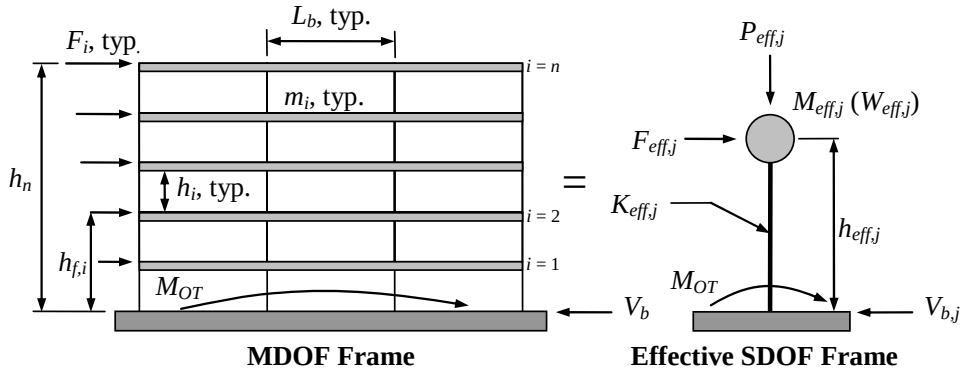

Figure 2-2. SDOF representation of MDOF

Prior to discussing the supporting theory, the use of the terminology 'effective' and 'equivalent' in describing system properties needs to be addressed. It appears from literature review that there is a tendency among researchers to substitute one term for the other. It is the opinion of the author that these terms are not interchangeable and should be clarified in order to preclude any confusion among colleagues and design engineers in the initial stages of learning the philosophy.

2.3.1.1 Modal, Effective, and Equivalent Effective SDOF Models

In accord with classical modal analysis, the coupled equations of motion of a MDOF system are decoupled into individual modes of vibration. Each mode of the MDOF is modeled by a *modal* SDOF, shown in Fig. 2-3(a), with properties: modal stiffness, K_j, and modal mass, M_j, where *j* is the mode index.

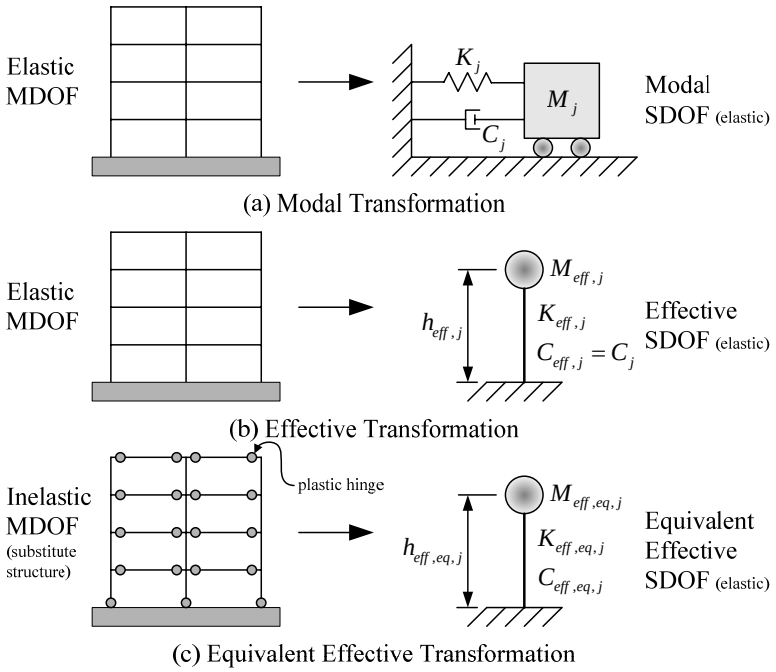

Figure 2-3. Graphical illustration of transformation classifications

In reference to Fig. 2-3(a), modal mass and stiffness for mode *j* are computed by classic modal analysis and are given as

$$M_j = \{\phi_j\}^T [M] \{\phi_j\} \tag{2-1}$$

$$K_j = \{\phi_j\}^T [K] \{\phi_j\} \tag{2-2}$$

where

$[K]$ = Stiffness matrix

$[M]$ = Mass matrix

$\{\phi_j\}$ = Mode shape for mode *j*

The mode shape in Eqs. (2-1) and (2-2) are the eigenvectors of the equation

$$\left[\left[K\right]-\omega_j^{\,2}\left[M\right]\right]\left\{\phi_j\right\}=\left\{0\right\} \tag{2-3}$$

where

ω_j = Natural circular frequency of mode j $\left(=2\pi\sqrt{\frac{K_j}{M_j}}\right)$ (2-3a)

Generally, all the mass is assumed to be concentrated at each floor and mass contributions to rotational dynamic degrees of freedom are considered negligible. As a result, the mass matrix is taken diagonal and the modal mass can be computed by

$$M_j=\sum_{i=1}^{n}\left(m_i\phi_{i,j}^{\,2}\right) \tag{2-4}$$

where

m_i = Lumped mass at floor i

$\phi_{i,j}$ = Modal coordinate of floor i for mode j

n = Number of floors

i = Node index

Node index i is synonymous with floor index corresponding to the horizontal dynamic degree of freedom.

If excited by an earthquake, each mode of the MDOF can be modeled by an *effective* SDOF, shown in Fig. 2-3(b), with properties: effective stiffness, $K_{eff,j}$, effective mass, $M_{eff,j}$, and effective height, $h_{eff,j}$. The previous two concepts represent elastic system response.

In the event that the system enters the inelastic region, the yielding system can be modeled by an *equivalent* elastic system. Accordingly, an inelastic MDOF can be modeled by an *equivalent* elastic *effective* SDOF, shown in Fig. 2-3(c), with properties: equivalent effective stiffness, $K_{eff,eq,j}$, equivalent effective mass, $M_{eff,eq,j}$, and equivalent effective height, $h_{eff,eq,j}$. The term 'elastic' is removed for brevity.

2.3.1.2 Transformation of MDOF to Effective SDOF

The following discussion details the transformation of an elastic MDOF system to an effective SDOF system. The transformation of the inelastic MDOF (equivalent MDOF) to the equivalent effective SDOF follows suit.

2.3.1.2.1 Effective Mass and Height of Effective SDOF

Similar to modal mass used in classical modal analysis, only a portion of the total mass of a MDOF frame is effective in producing the base shear, V_b, for a given mode *j* during earthquake excitation. This quantity of mass is known as 'effective mass'. In reference to Fig. 2-2, by assuming that the base shear is equal between the MDOF and effective SDOF ($\sum_{i=1}^{n} F_{i,j} = F_{eff,j}$), the effective mass, M_{eff}, for mode *j* is computed by

$$M_{eff,j} = \frac{\left(\sum_{i=1}^{n}\left(m_i\phi_{i,j}\right)\right)^2}{\sum_{i=1}^{n}\left(m_i\phi_{i,j}{}^2\right)} \tag{2-5}$$

When the effective mass is concentrated at a certain height above the base, the base overturning moments, M_{OT}, between the systems would similarly be matched (see Fig. 2-2). This height is known as the 'effective height' and represents the location of the resultant seismic force, F_{eff}. The effective height, h_{eff}, for mode *j* is computed by

$$h_{eff,j} = \frac{\sum_{i=1}^{n}\left(m_i \phi_{i,j} h_{f,i}\right)}{\sum_{i=1}^{n}\left(m_i \phi_{i,j}\right)} \tag{2-6}$$

where

$h_{f,i}$ = height of floor *i* above the base

Eqs. (2-1) through (2-6) are derived based on classical modal analysis and can be found in many textbooks pertaining to structural dynamics (Berg 1989, Clough and Penzien 1993, Chopra 1995).

This theory also requires that the period of both frames be equal for a given mode.

$$T_{eff,j} = 2\pi\sqrt{\frac{M_{eff,j}}{K_{eff,j}}} = T_j = 2\pi\sqrt{\frac{M_j}{K_j}} \tag{2-7}$$

It can readily be determined from Eq. (2-7) that effective mass and stiffness are related to their modal quantities by (see Appendix A)

$$M_{eff,j} = \Gamma_j^{\,2} M_j \tag{2-8}$$

$$K_{eff,j} = \Gamma_j^{\,2} K_j \tag{2-9}$$

where

Γ_j = modal participation factor for mode j

$$\left(= \frac{\sum_{i=1}^{n}\left(m_i\phi_{i,j}\right)}{M_j} = \frac{\sum_{i=1}^{n}\left(m_i\phi_{i,j}\right)}{\sum_{i=1}^{n}\left(m_i{\phi_{i,j}}^2\right)} \right) \tag{2-9a}$$

2.3.1.2.2 Effective SDOF Properties in DDBD

With regards to DDBD, no structural dynamic properties are initially known. Thus, a deflected shape (see Fig. 2-4) of the MDOF system for a given mode must be assumed ($\{\delta_j\} = A_j\{\phi_j\}$ where A_j is an arbitrary constant). The previous equations for effective mass and height for the fundamental mode become

$$M_{eff} = \frac{\left(\sum_{i=1}^{n}\left(m_i\delta_i\right)\right)^2}{\sum_{i=1}^{n}\left(m_i\delta_i^2\right)} \tag{2-10}$$

$$h_{eff} = \frac{\sum_{i=1}^{n}\left(m_i\delta_i h_{f,i}\right)}{\sum_{i=1}^{n}\left(m_i\delta_i\right)} \tag{2-11}$$

where

δ_i = Assumed displacement of floor i relative to the base

The mode index ($j = 1$) is removed from the previous equations for brevity. Unless otherwise noted, all subsequent equations are derived for the fundamental mode. The previous equations are also used for converting the equivalent MDOF frame into an

equivalent effective SDOF frame by employing an equivalent mode shape (i.e., inelastic mode shape). As such, the subscript *eq* is attached to the subscript *eff* (e.g., $M_{eff,eq,j}$).

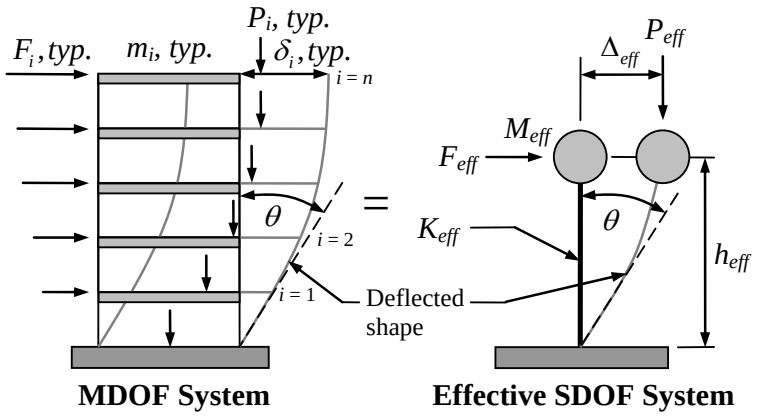

Figure 2-4. Deflected shape of MDOF and effective SDOF

2.3.1.2.3 MDOF Displacements and Effective SDOF Displacement

The transformation process additionally requires the design engineer to relate the displacement profile of the MDOF, $\{\delta_i\}$, to the displacement of the effective SDOF, Δ_{eff} (see Fig. 2-4). The effective displacement is computed such that the work done by the two systems are equal.

$$\underbrace{F_{eff}\Delta_{eff}}_{SDOF} = \underbrace{\sum_{i=1}^{n} F_i\delta_i}_{MDOF} \tag{2-12}$$

where

F_{eff} = Force on effective SDOF

F_i = Force on floor *i*

Eq. (2-12) infers that the displacement profile is proportional to the displacement of the effective SDOF which can be expressed as

$$\delta_i = c_i \Delta_{eff} \tag{2-13}$$

where

c_i = Non-dimensional displacement adjustment factor for floor *i*

Since the base shear, V_b, and overturning moment, M_{OT}, developed by the effective SDOF and MDOF (1st mode) are equivalent, this conversion process assumes that acceleration of each floor is proportional to displacement. Floor accelerations, a_i, are similarly related to the acceleration of the effective SDOF, a_{eff}, by

$$a_i = c_i a_{eff} \tag{2-14}$$

The reader is referred to Calvi and Kingsley (1995), Calvi and Pavese (1995) and Loeding et al. (1998a, 1998b) for further explanation of proportional accelerations. It follows that the force on the effective SDOF, F_{eff}, can be expressed as

$$F_{eff} = \sum_{i=1}^{n} F_i = \sum_{i=1}^{n} m_i a_i = a_{eff} \sum_{i=1}^{n} m_i c_i \tag{2-15}$$

Following Newton's second law and substituting Eq. (2-12) into Eq. (2-15), solving for the effective displacement leads to (see Appendix A)

$$\Delta_{eff} = \frac{\sum_{i=1}^{n} m_i \delta_i^2}{\sum_{i=1}^{n} m_i \delta_i} \tag{2-16}$$

Eq. (2-16) represents the lateral displacement of the effective mass at the effective height and is dependent on the assumed displacement profile of the MDOF system for the fundamental mode.

From Eq. (2-16), Eq. (2-10) for the effective mass is simplified to

$$M_{eff} = \frac{\sum_{i=1}^{n} m_i \delta_i}{\Delta_{eff}} \tag{2-17}$$

2.3.1.3 Nonlinear Static Analysis of SDOF System

Application of DDBD requires the MDOF frame be defined by an effective SDOF frame with effective system properties. This transformation provides the design engineer the benefit of using a prescriptive SDOF response spectrum specified in seismic codes to predict system response and, ultimately, the structural design forces when subjected to strong ground motion. For discussion purposes here, the effective SDOF shown in Fig. 2-5(a) will represent any inelastic SDOF system. The term ‘effective’ herein is used only to maintain coherence with the previous discussion concerning MDOF systems.

Fig. 2-5(a) shows an idealized bilinear force-displacement response of an effective SDOF system pushed past the yield displacement, Δ_y, to an inelastic

displacement, Δ_d. It has been proposed that an inelastic effective SDOF can be replaced by an equivalent elastic effective SDOF characterized by an equivalent stiffness and mass that will also respond to Δ_d as illustrated in Fig. 2-5(b). Because the equivalent effective SDOF system is elastic, input energy from horizontal ground motion is assumed to be dissipated by a fictitious viscous damper. The quantitative measure of this damping is identified as equivalent damping.

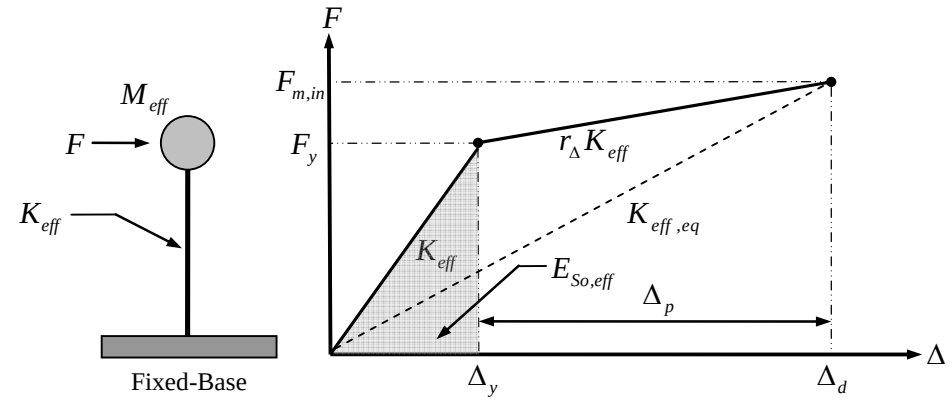

(a) Inelastic Effective SDOF

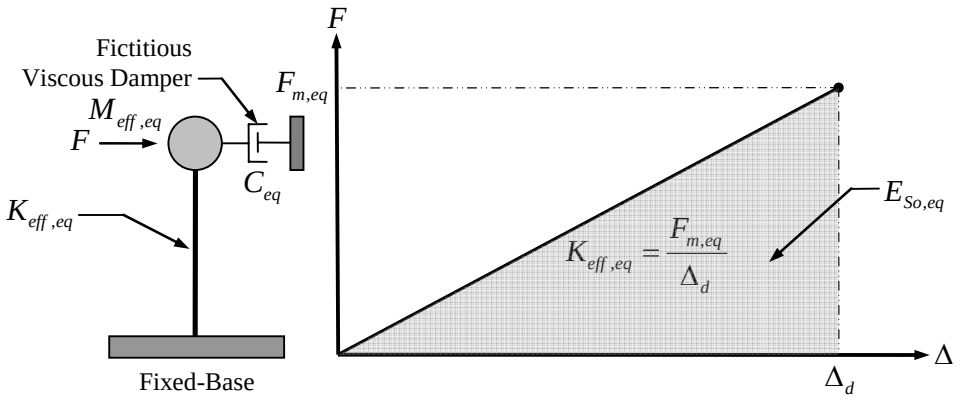

(b) Equivalent Effective SDOF

Figure 2-5. Force-displacement response of SDOF and equivalent SDOF

The primary benefit of this analysis technique is that it allows the design engineer to employ conventional elastic analysis techniques to determine the response and demand

magnitudes imposed on the system. This linearization approach has been termed Equivalent Linear Static Analysis (ELSA) and is the central concept of most nonlinear static analysis procedures currently being researched (e.g., DBD, Capacity Spectrum Method (ATC 1996, 2005), N2 Method (Fajfar 2000), to list a few).

This linearization technique additionally assumes that the pseudo-acceleration and pseudo-velocity of the equivalent and inelastic system are the same.

$$S_{a,in} = S_{a,eq} = \frac{4\pi^2}{T_{eq}^{\ 2}} \Delta_d \tag{2-18}$$

$$S_{v,in} = S_{v,eq} = \frac{2\pi}{T_{eq}} \Delta_d \tag{2-19}$$

where

$S_{a,eq}$ = Pseudo-acceleration of equivalent system

$S_{v,eq}$ = Pseudo-velocity of equivalent system

As such, the equivalent mass is typically taken equal to the effective mass, implying that the force developed in both systems at the peak displacement should be similarly matched (i.e., $F_{m,in} = F_{m,eq}$ in Fig. 2-5).

In accord with the Geometric Stiffness linearization approach (commonly referred to as the Secant Stiffness method) proposed by Rosenblueth and Herrera (1974), the equivalent stiffness is determined as the secant stiffness to maximum displacement. By geometry for the bilinear case shown in Fig. 2-6(a) the elastic and equivalent stiffness are related by (see Appendix A)

$$K_{eff} = K_{eff,eq} \frac{\mu_\Delta}{\left(1 + r_\Delta \left(\mu_\Delta - 1\right)\right)} \tag{2-20}$$

where

μ_Δ = Displacement ductility

r_Δ = Post-yield stiffness ratio

2.3.2 Direct Displacement-Based Design Methodology

In reference to Fig. 2-1, Step B is the central procedure of DDBD since seismic response and design parameters are approximated with the equivalent effective SDOF. The following discussion will concentrate on linking the basic DDBD steps with determination of the design parameters.

2.3.2.1 Step 1: Seismic Demand

The seismic demand used in DDBD is an elastic Displacement Response Spectrum (DRS) constructed for various levels of viscous damping, ζ, as shown in Fig. 2-6. The response spectrum is constructed for the response of an elastic SDOF system. Seismic codes contain provisions for constructing a 5% damped Acceleration Response Spectrum (ARS). The 5% damped DRS can be obtained from the 5% damped ARS by multiplying the spectral ordinates by

$$S_{d,5\%} = S_{a,5\%} g \frac{T^2}{4\pi^2} \tag{2-21}$$

where

$S_{d,5\%}$ = Spectral displacement at 5% damping

$S_{a,5\%}$ = Spectral acceleration at 5% damping

g = Acceleration of Gravity

T = Period

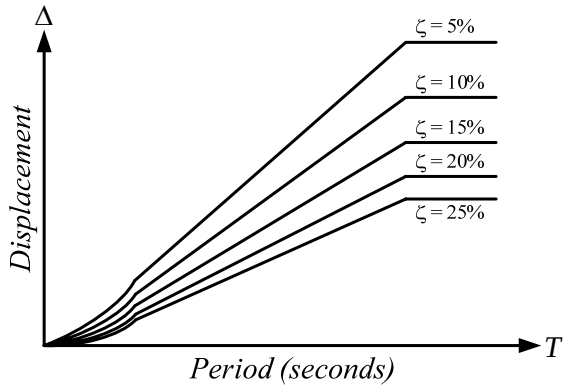

Figure 2-6. Displacement response spectra

Table 2-1. Spectral reduction factor

Equivalent Damping, ζ_{eq} (percentage of critical)	Adjustment Factor, B
≤ 2%	0.8
5%	1.0
10%	1.2
20%	1.5
30%	1.7
40%	1.9
≥ 50%	2

Response curves for higher damping values for far-field earthquakes can be constructed from NEHRP (BSSC 2003) by

$$S_{d\zeta\%} = \frac{S_{d5\%}}{B} \tag{2-22}$$

where

B = Adjustment factor (see Table 2-1)

ATC-55 (ATC 2005) states that the values listed in Table 2-1 can also be estimated by

$$B = \frac{4}{5.6 - \ln \zeta\%} \tag{2-23}$$

Alternatively, the relationship specified in Eurocode-EC8 (ECS 1998) derived by Bommer et al. (2000) can be used

$$S_{d,\zeta\%} = S_{d,5\%}\sqrt{\frac{10}{5+\zeta\%}} \tag{2-24}$$

where

$\zeta\%$ = Adjusted damping (in percent)

Near-fault earthquakes accompanied by large velocity pulses due to forward directivity effects may reduce the effectiveness of damping (Priestley 2003). As a result, Priestley (2003) proposed that displacement curves at higher damping values for near-fault earthquakes can be estimated by

$$S_{d,\zeta\%} = S_{d,5\%}\left(\frac{10}{5+\zeta\%}\right)^{\frac{1}{4}} \tag{2-25}$$

Bommer and Mendis. (2005) recommended the scaling factor proposed by Priestley (2003) and further stated that it is also necessary to ensure that the forward directivity pulse is depicted in the construction of the 5% damped DRS for these types of ground motion.

Reduction factors in Eqs. (2-23) through (2-25) are plotted along with the values presented in Table 2-1 in Fig. 2-7. There is not much deviation in the far-field spectral reduction factors. However, significant deviation occurs for near-fault motions. NEHRP does not currently suggest a different set of reduction factors for near-fault motions.

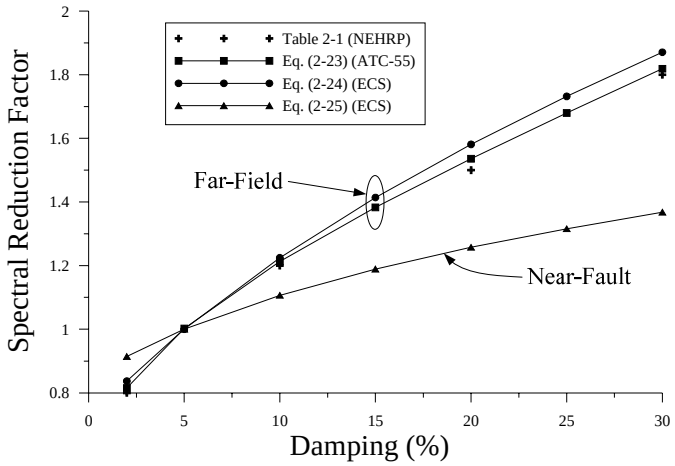

Figure 2-7. Spectral reduction curves

Bommer and Elnashai (1999) and Faccioli et al. (2004) pointed out that transformation of the ARS will generally not produce reliable displacements in the longer period range relevant for DDBD. As a result of this inaccuracy, Bommer et al. (2000) based on the work of Tolis and Faccioli (1999) proposed various DRS changes based on control periods, the most important being the point at which the spectral displacement becomes constant as period increases (see Fig. 2-6). According to NEHRP (BSSC 2003), this period ranges from 4 to 16 *seconds*, increasing exponentially with earthquake magnitude.

2.3.2.2 Step 2: Design Displacement Profile and Effective Displacement

A design displacement profile, $\{\delta_d\}$, is adopted for each performance level and represents the desired displaced shape of the frame. The profiles are constructed based on a target drift angle, θ_T, while considering the desired inelastic 1st mode shape. The damage level is set by selecting a drift angle which corresponds to the deformation of the most critical component(s).

Once the design displacement profile is chosen, the design engineer can compute the equivalent effective SDOF properties: $M_{eff,eq}$, or $W_{eff,eq}$, (Eq. (2-10)), $h_{eff,eq}$ (Eq. (2-11)), and design displacement, Δ_d (Eq. (2-16), where Δ_d is synonymous with Δ_{eff}).

The limitation here is in the definition of the design displacement profile. The author claims this to be the Achilles' heel of this procedure since estimated seismic response and design parameters are directly related to the assumed displacement profile which in return is a function of design choices. As such, does the displacement profile at the target include higher modes or is it simply based on the fundamental mode shape? Then, what is a reasonable approximation of the fundamental mode shape of a steel moment frame? Since stiffness and strength are the final outcome of this process, the assumed shape is used to control design selections in order to achieve this shape. This implies an iterative analysis and design procedure that requires convergence on the assumed shape. The design displacement profile to be used in analysis and design is discussed in Chapter 3.

The remaining portion of mass participates in the higher modes implying that these modes are not typically considered in design of potential plastic hinges (neglecting vertical accelerations). It has been contended that the higher modes are inadequately represented by elastic analysis and that higher modes are better accommodated in the capacity design phase rather than during the preliminary phase (Priestley 2003). Thus, what is a simplified method to provide protection against higher modes? This topic is covered in Chapter 6.

2.3.2.3 Step 3: Yield Displacement Profile and Effective Displacement

In parallel with Step 2, the design engineer must establish a yield displacement, Δ_y, of the equivalent effective SDOF. This is a crucial step in that selection will provide a definition of the target displacement ductility, μ_Δ, and locate the yield point (see Fig. 1-4). Currently, there are no recommendations for explicitly constructing the yield displacement profile of steel moment frames and researchers typically assume a yield drift ratio or utilize an inelastic design spectrum.

The importance of the yield and design displacement can now be recognized. Fundamentally, they determine the target displacement ductility for a given performance level which is the primary measure of damage. However, the current problem with this maximum displacement criterion is that it treats post-yield displacements and damage level independently. That is, there is no inclusion of the number of inelastic cycles the structure and comprising subassemblies experience prior to reaching maximum displacement.

Ductility is the quantitative measure of member deformation beyond the elastic limit without considerable loss in either strength or stiffness. Displacement ductility demand can be represented by either the kinematic or cyclic ductility relationship. The difference between the two is the latter takes in to account the possible changes of the origin of the inelastic excursion (Mazzolani and Piluso 1996).

Kinematic Ductility:

$$\mu_{\Delta} = \frac{\Delta_d}{\Delta_y} \tag{2-29}$$

Cyclic Ductility:

$$\mu_{\Delta} = \frac{\Delta_p}{\Delta_y} + 1 \tag{2-30}$$

where

Δ_p = Post-yield displacement (plastic)

The limitation here is in the assumption of the SDOF yield displacement, or even the yield displacement profile, $\{\delta_{dy}\}$, of the MDOF frame. What is the yield mechanism of the frame assumed in deriving the yield displacement(s)? Based on previous research results, it could be plausible to take the profile shape equal to the target profile shape. Then, what yield drift angle, θ_y, is used to construct the profile? Can a value of 0.5% as recommended by SEAOC (1999) and others (Priestley 1993, Moehle 1992) be adopted? Since the yield point is critical in this process, what is an acceptable serviceability limit?

The yield displacement profile to be used in analysis and design is the focal topic of Chapter 3.

Additionally, drift angle ductility will not equal displacement ductility for frames that displace in a non-linear fashion since drift angle ductility demands will vary vertically. This poses a limitation in quantitatively assigning a system-level displacement ductility demand. Many researchers take the displacement at the roof of the structure to characterize system-level ductility. It appears that a more rational approach is to take the displacements at the effective height (i.e., force resultant) to compute system-level ductility. Thus, how well does a displacement ductility determined from the effective SDOF displacements relate to the system-level ductility?

2.3.2.4 Step 4: Equivalent Damping

Equivalent damping, ζ_{eq}, in the equivalent elastic frame is used to model the energy dissipated by yielding in the inelastic frame. It has been proposed (see Chapter 4) that damping associated with the equivalent frame can be directly computed from a ductility-dependent equation for the effective SDOF. The results of these equations are graphically illustrated in Fig. 2-8.

In the author's opinion the displacement profile is the Achilles' heel of this process, it then follows that equivalent damping is the piercing arrow since ductility is related to the assumed displacement profiles. The ultimate question is how can the quantitative measure of damping be related between an effective SDOF dissipating energy with a single mechanism and a MDOF dissipating energy in multiple

mechanisms? Further, equating damping by the response of an effective SDOF neglects ductility contributions of each floor. A method for estimating the quantitative degree of damping in a MDOF frame for design purposes is proposed in Chapter 4.

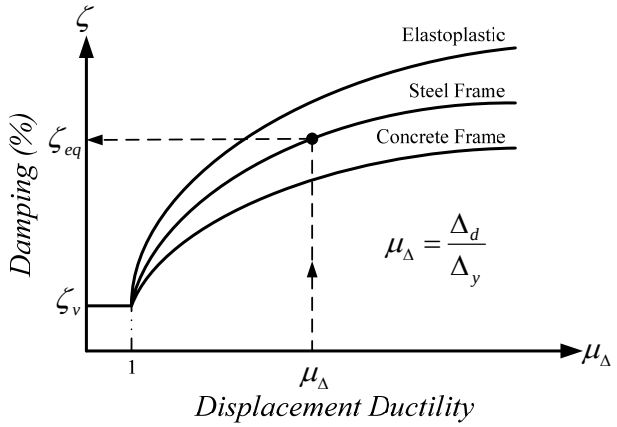

Figure 2-8. Equivalent damping

2.3.2.5 Step 5: Equivalent Effective Period and Design Base Shear

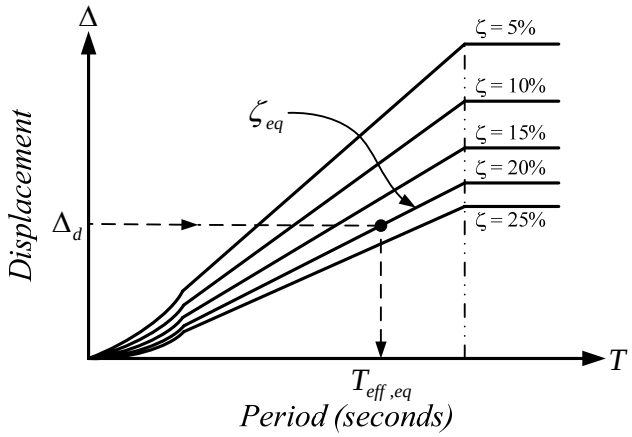

Figure 2-9. Design-level DRS

The equivalent period, $T_{eff,eq}$, can be obtained directly from the DRS constructed for the design-level earthquake (Step 1). The design engineer enters the DRS with the target displacement (Step 2) and reads off the equivalent period via the response curve for

the degree of equivalent damping (Step 4) as illustrated in Fig. 2-9. The displacement profile chosen is representative of the inelastic fundamental mode shape. As such, the equivalent period characterizes the equivalent 1st mode. Note that $T_{eff,eq} = T_{eq}$.

The equivalent effective stiffness (secant stiffness to target response) and design force can be determined from

$$K_{eff,eq} = 4\pi^2 \frac{M_{eff,eq}}{T_{eff,eq}^{\ 2}} \tag{2-34}$$

$$F_d = K_{eff,eq}\Delta_d = V_{bd} \tag{2-35}$$

2.3.2.6 Step 6: Structural Analysis and Component Design

The base shear computed at the target displacement is distributed heightwise and structural analysis conducted to determine component design strengths and stiffness.

$$F_i = V_{bd} \frac{w_i \delta_{d,i}}{\sum_{i=1}^{n} \left(w_i \delta_{d,i} \right)} \tag{2-36}$$

See Eq. (4-41) for the derivation of Eq. (2-36).

For compatibility with the substitute structure approach, component stiffness should be representative of that at the target displacement. In so doing, member-level secant stiffness is used for those components undergoing inelastic deformations. For moment frames where inelastic deformations (i.e., plastic hinges) are concentrated in the

beams, this is estimated by computing an equivalent moment of inertia, I_{eq},. Assuming elastoplastic response, this is found as

$$I_{b,eq} = \frac{I_b}{\mu_\delta} \tag{2-37}$$

where

I_b = Moment of Inertia of beam

μ_δ = Expected displacement ductility of beam $\left(= \frac{\delta_{d,i}}{\delta_{y,i}} \right)$ (2-37a)

The required equivalent member strengths are then determined by structural analysis and the required elastic member properties computed.

The limitation here is the approximation of the equivalent elastic stiffness of each yielding member. In so doing, the design engineer is iterating the stiffness of each section in the elastic analysis until convergence on the target displacement profile. Furthermore, design is based on the inelastic fundamental mode, thus force contributions from higher mode response could influence the actual stiffness of ductile sections at target.

In an attempt to simplify this process, it is recommended that an elastic analysis be performed on the yield displacement profile with lateral forces computed from the yield base shear, as proposed by SEAOC (1999) without the pre-reduction to account for overstrength. Sullivan et al. (2004) concluded that using response spectra with either initial stiffness or secant stiffness may be equally effective. The modified global sequence used in the proposed DDBD is graphically illustrated in Fig. 2-10.

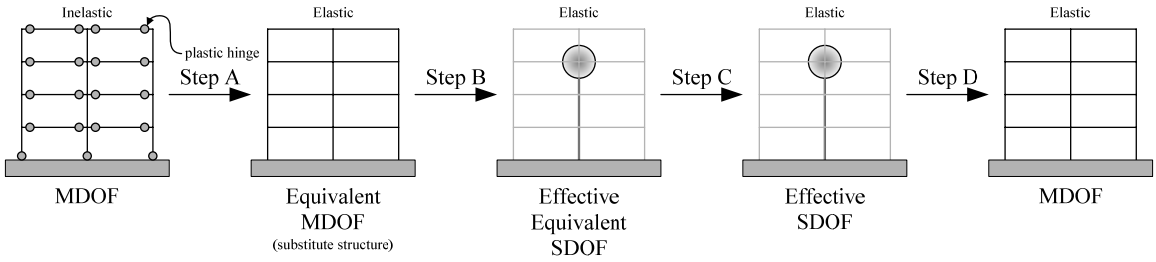

Figure 2-10. Modified global sequence used in proposed DDBD

In this DDBD scenario, the equivalent effective SDOF is converted to an effective SDOF (elastic) defined by the yield point properties in Step C. The effective stiffness is computed from Eq. (2-20) and the design force is

$$F_y = K_{eff}\Delta_y = V_{by} \tag{2-38}$$

The yield-level base shear is similarly distributed heightwise from

$$F_i = V_{by}\frac{w_i\delta_{dy,i}}{\sum_{i=1}^{n}\left(w_i\delta_{dy,i}\right)} \tag{2-39}$$

Structural analysis is performed and the required elastic member strengths and stiffness are directly determined at the yield point. This procedure is the subject of Chapter 6.

2.4 Conclusion

This chapter discussed the theory in support of Direct Displacement-Based Design. In addition, the fundamental steps of the current DDBD philosophy were discussed in further detail and accompanied by limitations of the procedures.

Chapter 3 Methodology for Estimating the Design Displacement Profiles

3.1 Introduction

In PBSE a performance objective is chosen based on an acceptable degree of damage and building use category. Once the design team has adopted the global design objective, individual performance levels coupled with earthquake intensities are outlined. Intrinsic in each performance level is a design target based on an allowable damage tolerance. This target is typically chosen in reference to story drift criterion. Although SEAOC (1999) specifies several performance levels within a performance objective, in reality only one performance level will govern structural design.

Moment frames resist imposed lateral displacements through flexural stiffness of the comprising members. Moment frames are classified by AISC into two types: (1) Type FR (fully rigid frames) and (2) Type PR (partially rigid frames). Type FR construction requires that members and connections be capable of transferring the full internally developed bending forces to adjacent members or supports. Experimental test data suggests that fully restrained seismically compact steel beams can successfully achieve an inelastic rotation of 0.3 *radians* and higher.

In DDBD of steel moment frames a target displacement profile, $\{\delta_d\}$, is adopted representing the desired inelastic displaced shape of the frame. The profile is constructed based on a target drift angle, θ_T, while considering the desired inelastic 1st mode shape.

Representing the deformed structure by an inelastic profile rather than the elastic mode shape is consistent with characterizing the structure by its secant stiffness to maximum response (Priestley 2003). Priestley additionally noted that the elastic and inelastic fundamental mode shapes are often very similar. Research has suggested that the elastic mode shape can be used to reasonably characterize the inelastic mode shape and has been adopted in NERHP 2003 (BSSC 2003). This assumption coincides with the use of a constant displacement amplification factor, C_d, used in FBD.

In addition, the yield displacement profile, $\{\delta_{dy}\}$, is of equal importance since it will provide an estimate of member and system-level ductility demands placed on the frame. However, there are currently no recommendations for explicitly constructing the yield profile. Researchers currently either assume a value (Lin et al. 2002, Lee et al. 2004, to list a few) or apply an inelastic design spectrum based on R-μ_Δ-T relationships (Xue and Chen 2003, Xue and Wu 2005, to list a few). Moreover, in the proposed DDBD procedure, the yield displacement profile is crucial in determining the design forces.

The first part of this chapter will discuss the construction of the target displacement profile for steel moment frames. The second part of the chapter will outline a procedure for constructing the yield displacement profile.

3.2 Target Displacement Profile

In the past decade several researchers have proposed target displacement profiles for use in DDBD. While the initial proposals were derived for reinforced concrete

moment frames and structural walls, research has shown that these profiles can be effectively applied to other construction material (e.g., steel moment and braced frames).

Priestley and Calvi (1997) proposed inelastic displacement profiles for reinforced concrete moment frames (listed in Table 3-1 and illustrated in Fig. 3-3(a)). Though these equations are approximations of the fundamental mode shape, they have been shown to be adequate for design purposes (Priestley 2003).

Table 3-1. Proposed design displacement profiles (fundamental mode)

Number of Stories (n)	$\delta_{d,i}$
$n \le 4$	$\theta_T h_{f,i}$
$4 < n < 20$	$\theta_T h_{f,i}\left(1-\frac{(n-4)h_{f,i}}{32h_{f,n}}\right)$
$n \ge 20$	$\theta_T h_{f,i}\left(1-\frac{h_{f,i}}{2h_{f,n}}\right)$

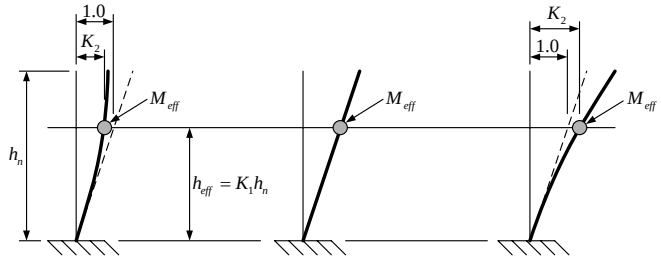

SHAPE 1 (Moment Frame Systems) SHAPE 2 (Dual Shear Wall - Moment Frame Systems) SHAPE 3 (Cantilevered Shear Wall)

# Stories	K_1 Effective Height Factor				K_2 Shape Factor					K_3 Effective Mass Factor=M_{eff}/M			
	Shape 1	Shape 2	Shape 3		Shape 1	Shape 2	Shape 3			Shape 1	Shape 2	Shape 3	
			H/L=2	H/L=5			μ=1	μ=2	μ=5			H/L=2	H/L=5
1	1.00	1.00	1.00	1.00	1.00	1.00	0.60	0.75	0.88	1.00	1.00	1.00	1.00
2	0.83	0.83	0.90	0.85	1.00	1.00	0.60	0.75	0.88	0.90	0.90	0.90	0.85
3	0.78	0.78	0.85	0.77	1.00	1.00	0.60	0.75	0.88	0.85	0.85	0.85	0.75
4	0.75	0.75	0.85	0.77	1.00	1.00	0.60	0.75	0.88	0.85	0.85	0.85	0.75
5	0.73	0.74	0.85	0.77	0.98	1.00	0.60	0.75	0.88	0.85	0.84	0.85	0.75
10	0.67	0.70	0.85	0.77	0.87	1.00	0.60	0.75	0.88	0.84	0.79	0.85	0.75
15	0.62	0.69	0.85	0.77	0.79	1.00	0.60	0.75	0.88	0.83	0.77	0.85	0.75
20	0.57	0.68	0.85	0.77	0.73	1.00	0.60	0.75	0.88	0.82	0.77	0.85	0.75
50	0.56	0.68	—	0.77	0.72	1.00	0.60	0.75	0.88	0.82	0.77	—	0.75

Where μ =displacement ductility

Figure 3-1. Proposed design displacement profiles (fundamental mode)

SEAOC (1999) proposed displacement profiles for various material-independent framing systems, shown in Fig. 3-1. Assigning profiles independent of construction material implies that the fundamental mode shape does not vary greatly between systems (e.g., concrete and steel moment frames). As seen in Fig. 3-1, SEAOC proposed the displacement of the effective SDOF in lieu of a MDOF displacement profile. These values are based on profiles proposed by Priestley and Calvi (1997).

Harris (2002, 2004) showed that the equations listed in Table 3-1 are reasonable approximations for steel moment frames limited to eight stories. Frames above these heights showed significant higher mode contributions to displacement response and deviation from the 1st mode shape assumption. This effect is also evident in research reports regarding computational analyses of the SAC steel moment frames (Gupta and Krawinkler 2000a) and other PBSE methodologies (Lee et al. 2004). It was additionally noted that the profiles assume the formation of base hinges in the first story columns and frames that did not form base hinges until well after beam hinges showed a strong tendency towards cantilever action (see Shape 3 in Fig. 3-1).

Table 3-2. Proposed design displacement profiles (fundamental mode)

Number of Stories (n)	Pinned-base $\delta_{d,i}$
$n \le 4$	$1.15\theta_T h_{f,i}\left(1-\frac{h_{f,i}}{3h_{f,n}}\right)$
$4 < n < 8$	$\left(1.15-0.025\left(n-4\right)\right)\theta_T h_{f,i}\left(1-\frac{h_{f,i}}{3h_{f,n}}\right)$ In regions of high seismicity, $n > 4$ not recommended

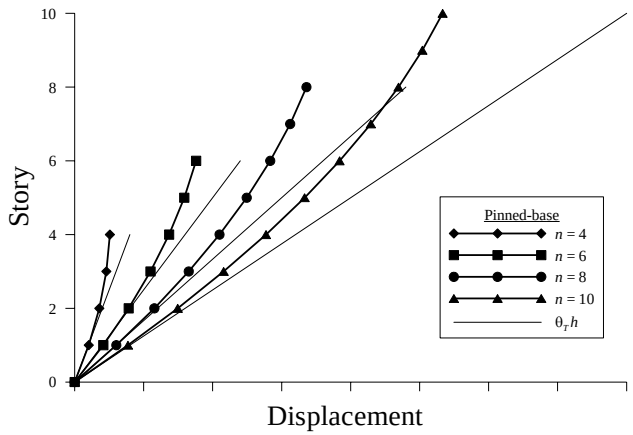

Figure 3-2. Proposed displacement profiles for pinned-base frames

Based on analytical research by the author, displacement profiles for pinned-base steel moment frames can be approximated from Table 3-2 (illustrated in Fig. 3-2). It is recommended that these frames be limited to eight stories in low-seismic regions and four stories in high-seismic regions due to the high elastic column stiffness required to meet the target drift ratio.

Karavasilis et al. (2006) proposed elastic and inelastic displacement profiles for steel moment frames for use in a PBSE methodology. This study concluded that the main structural characteristic that influences the displacement profile is the number of stories.

$$\delta_{d,i} = P_1 \theta_T h_i \left(1 - P_2 \frac{h_i}{h_n} \right) \tag{3-1}$$

where

P_1, P_2 = Profile coefficients (see Table 3-3)

Eq. (3-1) is plotted with those presented in Table 3-1 in Fig. 3-3(a).

Table 3-3. Displacement Profile Coefficients

Stories	Elastic Response		Inelastic Response	
(n)	P_1	P_2	P_1	P_2
1	1.00	0.00	1.00	0.00
3	1.00	0.18	1.00	0.10
6	0.85	0.20	0.90	0.20
9	0.70	0.21	0.75, 0.80, 0.85 [1]	0.30
12	0.62	0.22	0.70, 0.75, 0.80 [1]	0.35
15	0.55	0.24	0.65, 0.70, 0.75 [1]	0.40
18	0.52	0.25	0.60, 0.65, 0.70 [1]	0.40
20	0.50	0.25	0.55, 0.60, 0.65 [1]	0.40

1 Correspond with joint capacities: 1.1, 1.3, and 1.5 respectively

It was also found in that study that joint capacity ($\sum M_{p,c} / \sum M_{p,b}$) plays a role in the shape. The author believes this opinion to be inconsistent in that stiffness is proportional to strength. Thus, it is the extent of column deformations that influence the magnitude of displacements and not the shape (see Fig. 3-3(b)). Also, that study appears to be limited in some degree in that design and analysis of the analytical frames have been decoupled. That is, the predetermined frames were not designed to achieve a performance target under a given excitation but the input ground motions were scaled until a desired drift angle was achieved. It was also found that the number of bays does not significantly affect the inelastic displacement shape. Lastly, from an engineering standpoint, the design displacement profile should be independent of design choices (e.g., joint capacity) which are not usually known until after component design.

As can be seen in Fig. 3-3(b) the proposed shapes by Priestley and Calvi (1997) and Karavasilis et al. (2006) are practically equivalent for frame type buildings when normalized to an approximate 1st mode effective height ($\approx 0.67 h_{f,n}$). Therefore, the force distributions between the profiles differ only in magnitude with the profiles proposed by Karavasilis et al. resulting in higher design forces when $n > 4$. This implies that the

design displacements are smaller due to (1) higher mode response amplifying the story drift ratios thus reaching the target ratio and (2) member overstrength and column stiffness. Strength demands from higher modes are therefore directly accounted for in design forces. Since analysis and design appear to be decoupled in that study, it is uncertain what effects these profiles would have on an actual design scenario. At first glance, design would result in a stiffer and stronger frame than that using the profiles in Table 3-1 (neglecting overstrength and capacity design effects). The reduction in design displacements could be a feasible approach pending further design driven research.

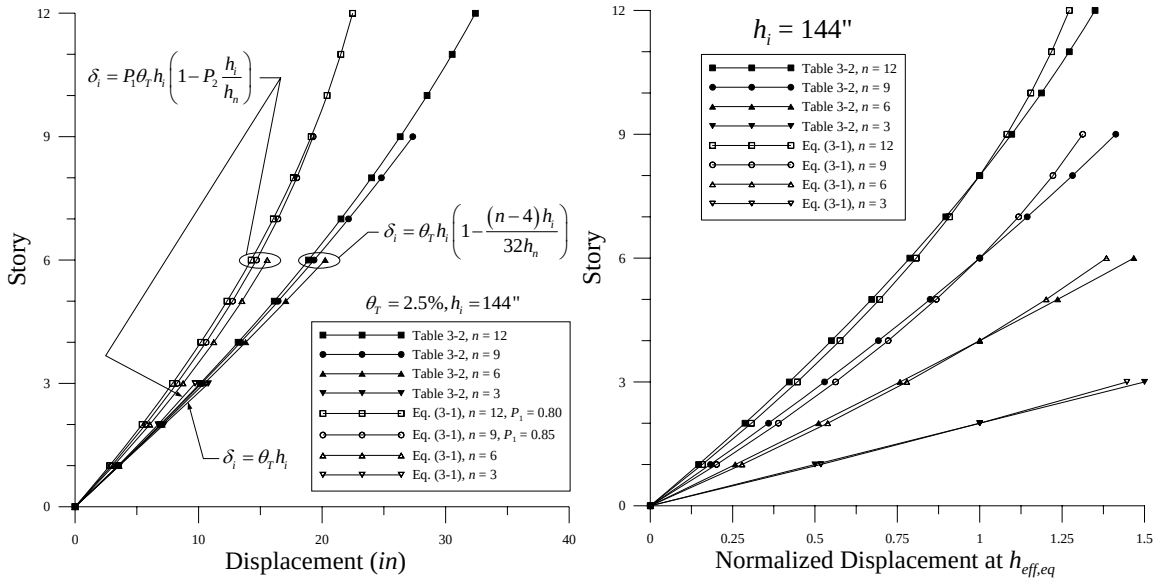

Figure 3-3. Proposed displacement profiles (*n* = 3, 6, 9, and 12)

Karavasilis et al. (2006) further concluded that the displacement profile is different in the elastic and inelastic range and that the proposed profiles are member independent. While this independence is reasonable for inelastic profiles, research suggests that elastic profiles are dependent on member geometry and design choices. It is the opinion of the author that these findings are likely a consequence of decoupling

design and analysis. There was no recommendation in this study as to the drift angle at the elastic (yield) profile. Also, there was no mention of requisite base hinge formations. Lastly, this study found that frames lower than six stories showed a small dispersion on maximum displacements.

Though several researchers have proposed target displacement profiles, the choice of the displaced shape used in design is somewhat arbitrary. The design engineer has freedom in selecting the desired response of a frame since the goal is to control behavior through design. However, lateral displacements at the onset of yielding are essentially a function of geometry and design choices. This correlation will recommend certain displaced shapes over others for different lateral force resisting systems. Assuming invariant displacement profiles to be valid, the displacement profile at yield should be examined to justify the chosen target displacement profile.

The objective of DDBD is to design a system for response in the fundamental mode and develops the potential plastic hinges assuming that the frame responds elastically essentially in the fundamental mode. Higher modes could have a significant effect on the response and design forces of a frame. Research has shown that displacements in low-rise frames are less sensitive to higher modes than are forces, presuming that the fundamental mode is the predominant mode of response. Also, higher modes can contribute more to frames dominated by cantilever action (Chopra 2005). It is recommended by the author that strength demands induced from higher modes be incorporated during capacity design in lieu of applying a reduction to the design displacements leading to increased design forces and reduction in expected ductility (i.e.,

damping). As such, the profiles listed in Table 3-1 are recommended for computing the design displacement (i.e., equivalent period) for analysis and design of steel moment frames limited to six stories.

Lastly, with the target displacement profile constructed based on a target drift limit, the corresponding target displacement of the equivalent effective SDOF can be computed as illustrated in Section 2.3.2.2.

3.3 Yield Displacement Profile

The next step is to construct the yield displacement profile, $\{\delta_{dy}\}$, and compute the corresponding yield displacement of the effective SDOF, Δ_y. With both target and yield displacement known, an estimate of the displacement ductility demand imposed on the structure and the amount of equivalent damping can be obtained.

Research (Priestley 1998, Aschheim 2002, Harris 2002) has proposed that the yield displacement profile of a frame can be estimated based on material properties, frame geometry, and predefined member geometry. Additional factors that influence the magnitude of displacements at yield for steel moment frames that need to be addressed are (1) extent of column deformations (including axial) and (2) panel zone and shear deformations. The following discussion outlines a procedure for identifying an approximate yield displacement profile.

Prior to discussing DDBD as applied to steel moment frames, it is important to illustrate the role that section curvature and member rotation play in predicting the

response of a frame and, ultimately, the quantitative measure of the frame ductility capacity.

3.3.1 Yield Strain

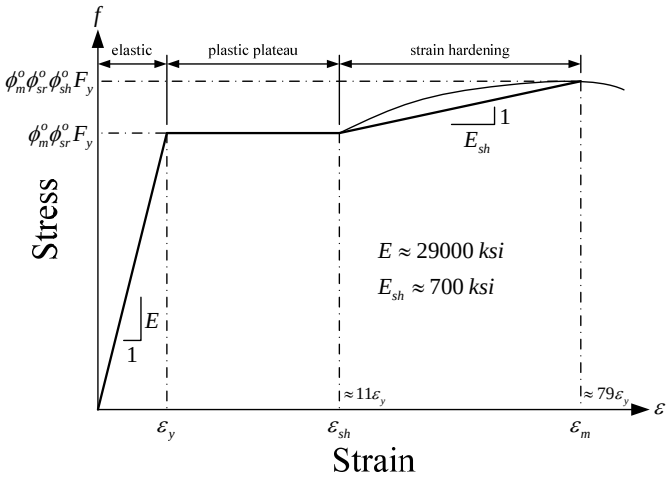

Figure 3-4. Idealized stress-strain relationship for commonly used structural steel

Two fundamental components to structural mechanics are stress, *f*, and strain, ε. Fig. 3-4 illustrates the idealized stress-strain relationship of commonly used structural steel. The idealized yield strain is

$$\varepsilon_y = \frac{F_{ya}}{E} = \frac{\phi_m^o \phi_{sr}^o F_y}{E} \tag{3-2}$$

where

F_{ya} = Actual yield stress

F_y = Nominal yield stress

E = Nominal modulus of elasticity

ϕ_m^o = Material overstrength $\left(= \frac{F_{ya}}{F_y} \right)$

ϕ_{sr}^o = Material overstrength from the effects of strain rate

Eq. (3-2) is applicable for compression and tension strains and assumes *E* is the same for each.

Randomness of the yield strength of a member in excess of the nominal value affects the formation of plastic hinges and, as a consequence, the response of the system. Additionally, the dependence of yield strength upon plate thickness should be considered for the prevention of local instability (Mazzolani and Pilusa 1996) and to account for the elongated range of stiffness reduction of a section prior to full plastification of thick flange plates. Values for material overstrength, ϕ_m^o (R_y per AISC), are proposed for various nominal yield strengths in Table 3-4 (values taken from AISC 2002).

Table 3-4. Material overstrengths

Steel	Shape	F_y (*ksi*)	ϕ_m^o
A36	W	36	1.5
A572	W	50	1.3
A992	W	50	1.1
A500	HHS	46	1.3
A53	Pipe	42	1.4

Furthermore, material strain hardening must be included in the determination of the maximum member capacity. The strain hardening overstrength factor, ϕ_{sh}^o, can be taken as 1.1 as proposed in AISC Seismic Provisions (AISC 2002). Lastly, material overstrength developed from the effects of strain rate, ϕ_{sr}^o, should also be considered.

3.3.2 Yield Curvature (Section Level)

For the discussion here, an idealized moment-curvature response (Fig. 3-5) is used for simplicity in predicting frame beam behavior. In this idealization, the member behaves elastically up to the plastic moment where all inelastic rotations occur within a zero-length plastic hinge (Beedle 1958; Chen and Sohal 1995, Bruneau et al. 1998).

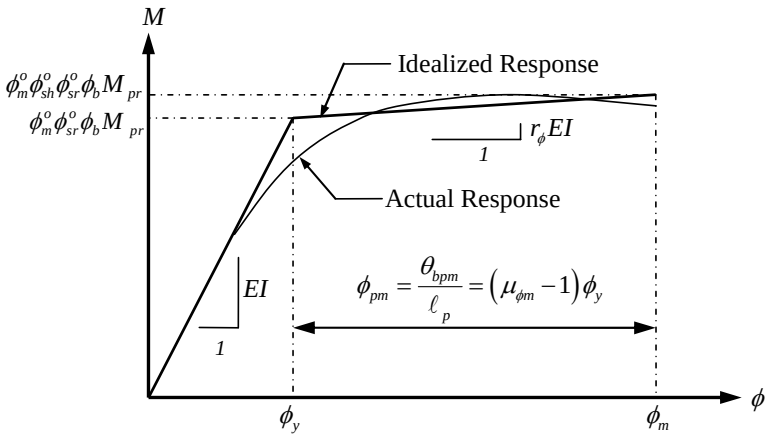

Figure 3-5. Moment-curvature response of W-section (strong axis)

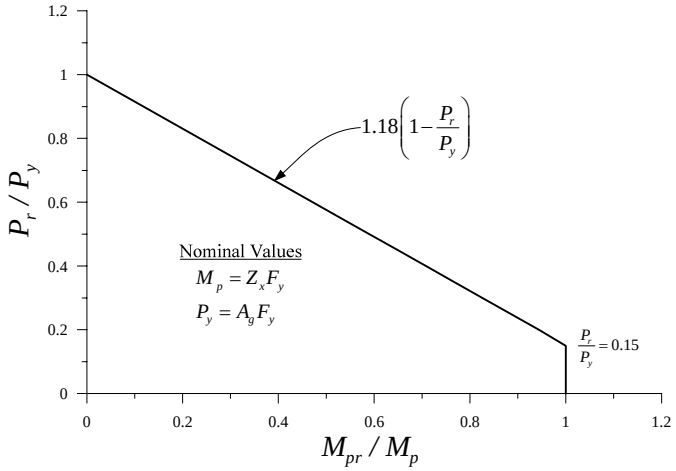

Figure 3-6. *P-M* interaction diagram of W-section (strong axis)

Fig. 3-6 illustrates an idealized *P-M* interaction diagram for a wide-flange section with bending about the major axis. The use of this interaction assumes that the beam is

compact and adequately braced out-of-plane in order to preclude instability, and includes an allowance for residual stresses (Salmon and Johnson 1996).

In accordance with Figs. 3-5 and 3-6, the idealized yield curvature of a frame beam subjected to a plastic moment, M_{pr}, reduced to account for the presence of an axial force, *P*, can be defined by (see Appendix A)

For $P \le 0.15P_y$

$$\phi_y = \frac{\phi_b M_{pr}}{EI} = \phi_b \phi_m^o \phi_{sr}^o \frac{2S_F}{d_b} \varepsilon_y \tag{3-3}$$

For $P > 0.15P_y$

$$\phi_y = \frac{\phi_b M_{pr}}{EI} = \phi_b \phi_m^o \phi_{sr}^o \frac{2.36S_F}{d_b} \left(1 - \frac{P}{P_y}\right) \varepsilon_y \tag{3-4}$$

where

M_{pr} = Reduced nominal plastic moment (see Fig. 3-6)

I = Moment of Inertia about major axis

S_F = Shape factor $\left(= \frac{Z_x}{S_x} \approx 1.15\right)$

Z_x = Plastic section modulus about major axis

S_x = Elastic section modulus about major axis

ϕ_b = Strength reduction factor for flexure (= 0.9 (AISC 2001))

d_b = Beam depth

P = Applied axial force

P_y = Nominal axial yield force $\left(= A_g F_y\right)$

A_g = Gross cross-sectional area

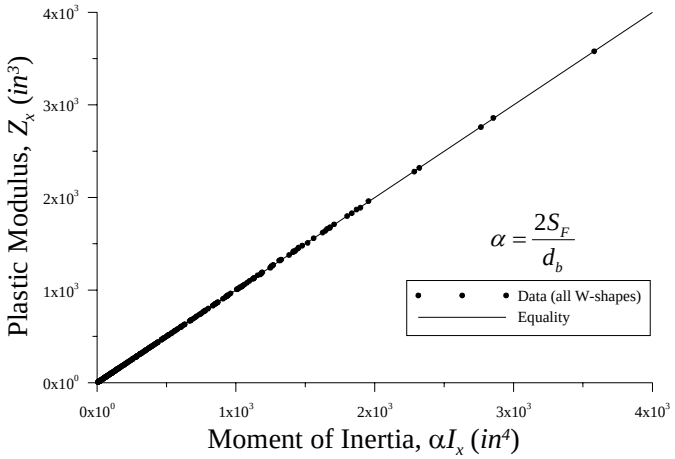

Figure 3-7. Relationship between Z_x and I_x (all W-shapes)

Evaluation of Eq. (3-3) demonstrates that the yield curvature is dependent only on section geometry, and is independent of flexural strength (Priestley and Kowalsky 2000). As a consequence, stiffness is proportional to strength (Priestley 1993). That is, flexural strength and stiffness are coupled, as can be seen in Fig. 3-7.

$$M_p \propto Z_x \text{ and } Z_x \propto I_x \tag{3-5}$$

Fig. 3-7 and Eq. (3-5) indicate that modifying the flexural strength of a section by changing Z_x proportionally alters the stiffness of the section. This proportionality contradicts the FBD assumption that an initial stiffness and, ultimately, an elastic system period can be determined independent of strength. That is, the action of allocating strength between members also changes the stiffness from the initial assumption, and, hence, implies an iterative analysis procedure (Priestley and Kowalsky 2000). Also, the

determination of a non-dimensional yield curvature indicates that the yield drift of a frame might possess the same independence (Priestley 1998). Due to the association between yield displacement and desired yield mechanism, the material overstrength factors should be used in computing the yield curvature.

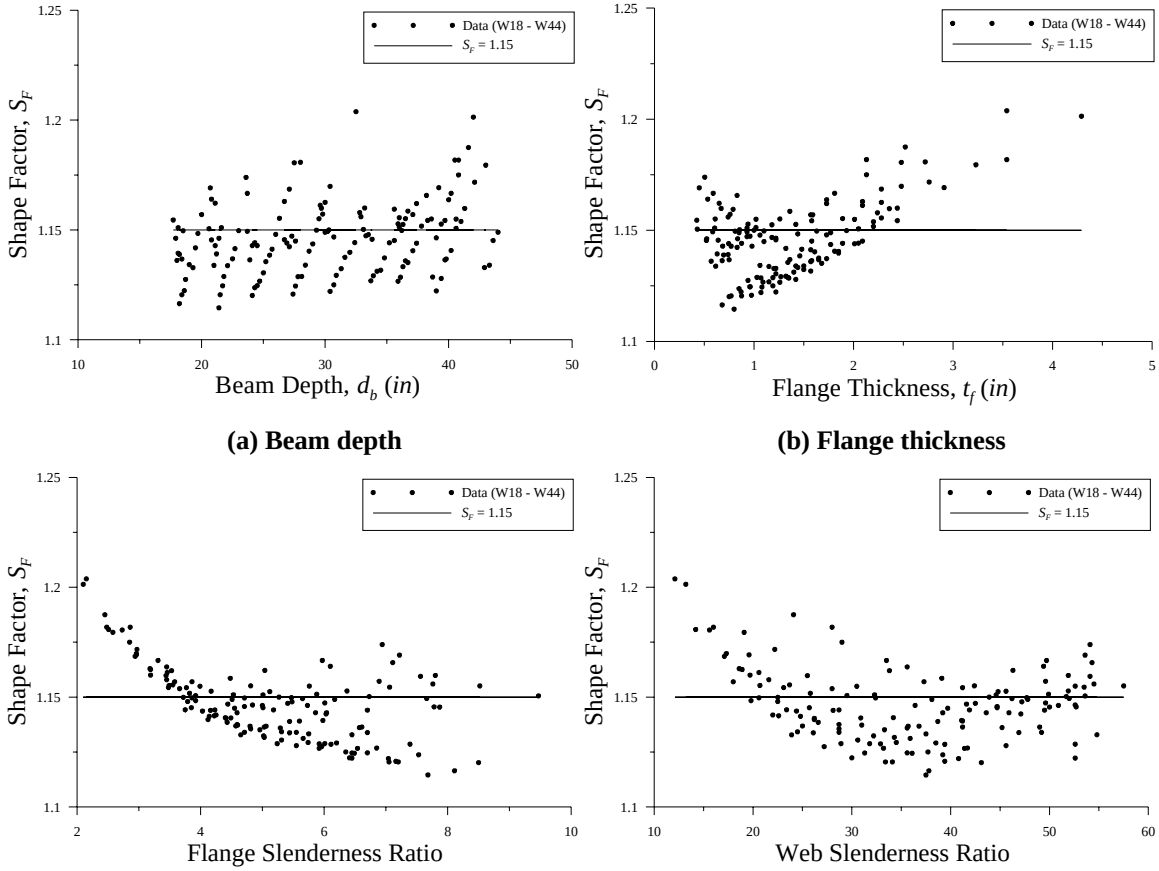

(a) Beam depth **(b) Flange thickness**

(c) Flange Slenderness Ratio **(d) Web Slenderness Ratio**

Figure 3-8. Relationship between S_F and section geometry (W18 – W44)

The shape factor, S_F, in Eqs. (3-3) and (3-4) can be assumed equal to 1.15 for design purposes for sections ranging from W18 to W44 as shown in Fig. 3-8. The maximum percent difference is 4.7% and -3.1%, which are typically seen with small and large flange and web width-thickness ratios respectively. As a side note, the sections with

the largest flange slenderness ratio are non-compact and not applicable (= 7.22 for 50 *ksi* steel (AISC 2002)).

A limitation of Fig. 3-6 is it is uncertain if the limit state at high axial force ratios is governed by buckling or formation of a plastic hinge. Normally the axial force ratio in frame beams is small due to large cross-sectional areas. Hence, Eq. (3-3) is typically all that is required for design. Unless otherwise noted, all further derivations are based on Eq. (3-3). It is recommended by the author that the force ratio in highly axially loaded columns where plastic hinges are desired be limited to 30%. Eq. (3-3) is also applicable to frame beams with Reduced Beam Sections (RBS) given that the ratio of plastic to elastic section modulus does not change.

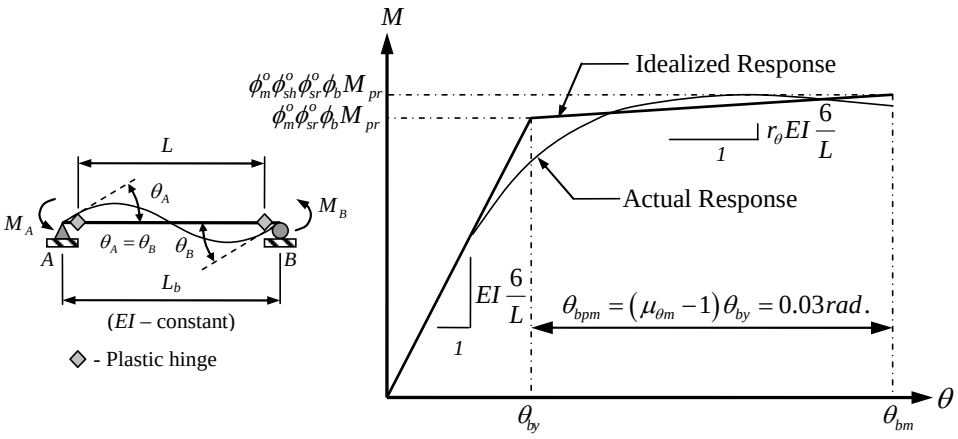

Figure 3-9. Moment-rotation response of W-section (strong axis)

Based on a minimum allowable plastic rotation, θ_{bpm}, of 0.03 *radians* associated with a moment strength of 1.1 (i.e., $\phi_{sh}^o = 1.1$) times the plastic moment capacity, the post-yield curvature stiffness ratio (see Fig. 3-5) is

$$r_{\phi} = \frac{\phi_y}{10\phi_{pm}} = 3.33\ell_p\phi_y \approx 7.67\phi_m^o\phi_{sr}^o\varepsilon_y \tag{3-6}$$

3.3.3 Yield Rotation (Member Level)

Fig. 3-9 illustrates the idealized moment-rotation relationship of a frame beam. Stability functions are utilized for determining frame beam yield rotation since second-order effects (P-Δ and P-δ) and the effect of an axial force on the bending stiffness of the element are accounted for (Chen and Lui 1992; Chen and Toma 1994; Chen and Kim 1997). It can be readily shown, based on the assumptions shown in Figs. 3-5, 3-6, and 3-9, that the idealized yield rotation of a frame beam subjected to equal end plastic moments and a compressive axial force can be determined by (see Appendix A)

For $P \le 0.15P_y$

$$\theta_{by} = \phi_y \frac{L}{6} \tag{3-7}$$

For $P > 0.15P_y$

$$\theta_{by} = \phi_y L\left(\frac{2\sin kL - kL(1+\cos kL)}{(kL)^2 \sin kL}\right) \approx \phi_y L\left(\frac{10}{60-(kL)^2}\right) \tag{3-8}$$

where

L = Beam length between adjacent plastic hinges $\left(= L_c - \ell_p\right)$

L_c = Clear length between adjacent column faces

ℓ_p = Plastic hinge length $\left(\approx d_b\right)$

$$k \quad = \text{Stability coefficient} \left(= \sqrt{\frac{P}{EI}} \approx \sqrt{\frac{P}{P_y} \frac{4S_F{}^2}{d_b{}^{1.96}} \varepsilon_y} \right) \tag{3-8a}$$

The stability coefficient (Eq. (3-8a)) is simplified based on Fig. 3-10 (see Appendix A).

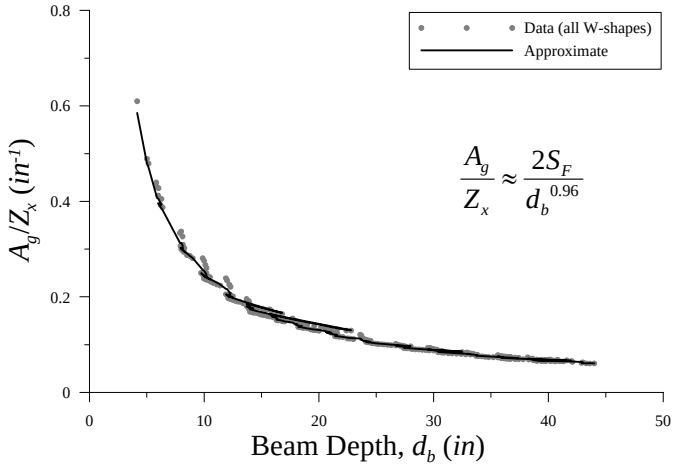

Figure 3-10. Stability coefficient relationship (all W-shapes)

The previous equations (1) neglect composite action, (2) assume that the member is sufficiently braced out-of-plane, and (3) assume that the maximum moment occurs at the ends of the member. Structures located in high seismic regions typically maintain a ratio of gravity moment to seismic moment demand for yield-level earthquakes on the order of 25%. Therefore, the effect of gravity load on a frame beam can be neglected (SAC 2000) and Eqs. (3-7) and (3-8) are all that is required. However, this effect should be incorporated in the determination of yield rotations for frame beams located in low seismic regions where the ratio of moments approaches unity. As a side note, the design engineer has the freedom to creatively configure floor framing layout such that gravity loads directly applied to beams are limited.

Taking M_{pr} as M_p for values of P less than $0.15P_y$ leads to a maximum error less than 5% (Beedle 1958; Bruneau et al. 1998). Additionally, until the axial force exceeds 30% of the axial plastic capacity, the reduction in moment capacity is typically less than 10% for wide-flange sections (Bruneau et al. 1998). Normally this criterion is not a concern for beams in moment frames since the axial load ratio is small due to large cross-sectional areas. Hence, Eq. (3-7) is typically all that is required for design.

The plastic moment capacity can be reduced further accounting for the presence of high shear forces. Conversely, the effect of shear force on the plastic moment capacity of frame members is insignificant due to high shear and moment occurring in localized zones where strain hardening of material will set in quickly permitting the moment capacity to exceed the nominal plastic value (Chen and Sohal 1995; Bruneau et al. 1998). Therefore, the plastic moment, before including the effect of an axial force, can be used in the design of framed members as long as the shear force does not exceed the plastic shear capacity, V_p (Chen and Sohal 1995).

Plotting Eq. (3-7) as a function of beam length (Fig. 3-11), it is clear that beam depths must be uniform for floors with equal bay lengths or vary in accordance with respective lengths in order to produce simultaneous beam hinging in a given floor. This also suggests that base columns should be the same depth, assuming constant height and an axial force ratio less than 30%. Ultimately, the yield displacement is essentially a function of beam geometry. This contradicts the assumption in FBD that constant response modification factors can be applied to comparable structures with internal geometric dissimilarities.

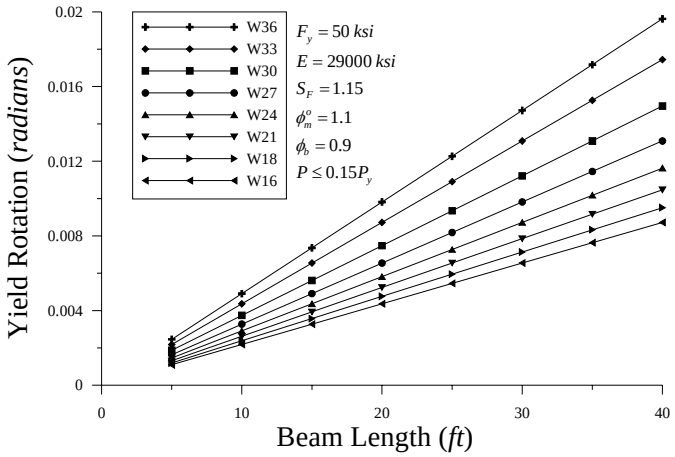

Figure 3-11. Yield rotation as a function of beam length

In accordance with the AISC Seismic Specifications (2002), a special moment frame with properly designed and detailed plastic hinges should be capable of reaching a post-yield rotation, θ_{bpm}, of 0.03 *radians*. The associated flexural strength of the beam at this plastic rotation is defined as $\phi_b \phi_m^o \phi_{sh}^o \phi_{sr}^o M_{pr}$. Therefore, the minimum allowable plastic curvature, ϕ_{pm}, is

$$\phi_{pm} = \frac{\theta_{bpm}}{\ell_p} \approx \frac{0.03}{d_b} \tag{3-9}$$

It also follows that the post-yield rotation stiffness ratio (see Fig. 3-9) is

$$r_\theta = 3.33\phi_y \frac{L}{6} = 3.33\theta_{by} \tag{3-10}$$

Typical wide-flange values of yield curvature and rotation for design purposes are presented in Table 3-5. It can be readily determined based on the parameters presented that $\mu_{\phi m} = 8.64$ and $r_\phi = 0.013$ for all depths. However, $\mu_{\theta m}$ and r_θ vary with member

length. Fig. 3-12 graphs the rotation ductility as a function of beam length. Assuming a relationship between displacement and rotation ductility, it is clear that ductility is not constant for a given framing system.

Table 3-5. Wide-flange member properties (F_y = 50 *ksi*)

d_b	ℓ_p	ϕ_y [1]	ϕ_{pm} [2]	ϕ_m	$\frac{\theta_{by}}{L}$ [3]	
		$\times 10^4$	$\times 10^4$	$\times 10^4$	$\times 10^6$	
14	14	2.80	21.43	24.23	46.74	
18	18	2.18	16.67	18.85	36.35	
21	21	1.87	14.29	16.16	31.16	$\phi_m^o = 1.1$
24	24	1.64	12.50	14.14	27.26	$\phi_{sh}^o = 1.1$
27	27	1.45	11.11	12.57	24.23	$\phi_{sr}^o = 1.0$
30	30	1.31	10.00	11.31	21.81	$\phi_b = 0.9$
33	33	1.19	9.09	10.28	19.83	$S_F = 1.15$
36	36	1.09	8.33	9.42	18.18	
40	40	0.98	7.50	8.48	16.36	
44	44	0.89	6.82	7.71	14.87	

1. Based on Eq. (3-3)
2. Based on plastic rotation of 0.03 *radians*
3. Based on Eq. (3-7)

For simplicity and in accordance with current analysis techniques, though a linearly elastic stress-strain relationship is assumed, stiffness degradation from the effects of residual stresses and gradual yielding associated with flexure, and geometric imperfections inherent in LRFD (AISC 2001) design interaction equations are neglected in Eqs. (3-3) and (3-7). However, in seismic engineering where the members are required to maintain structural integrity in the inelastic region, this idealization will produce conservative demands possibly overestimating the required stiffness and strength of a frame thereby inherently contributing to system overstrength. Furthermore, since displacements are used to estimate damage levels and geometric imperfections are accounted for in member design interaction equations and not the analysis, a discrepancy exists in the final displacement ductility prediction.

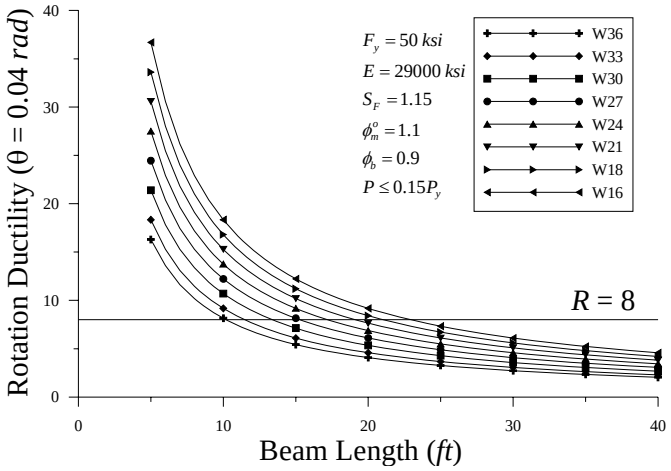

Figure 3-12. Rotation ductility as a function of beam length

These effects should be incorporated for more accurate analytical results. However, to the author's knowledge, an 'Advanced Analysis' (Chen and Lui 1992; SSRC 1993; Liew et al. 1993a, b; Chen and Toma 1994; Kim and Chen 1996a, b; Chen and Kim 1997; Chen 2000) is currently the only inelastic static analysis procedure that can effectively account for these effects, thus, eliminating the incompatibility between elastic analysis demand and inelastic member capacity. Though residual stresses can be large, they have no impact on the plastic moment capacity of a section (Beedle 1958; Bruneau et al. 1998).

3.3.4 Yield Displacements

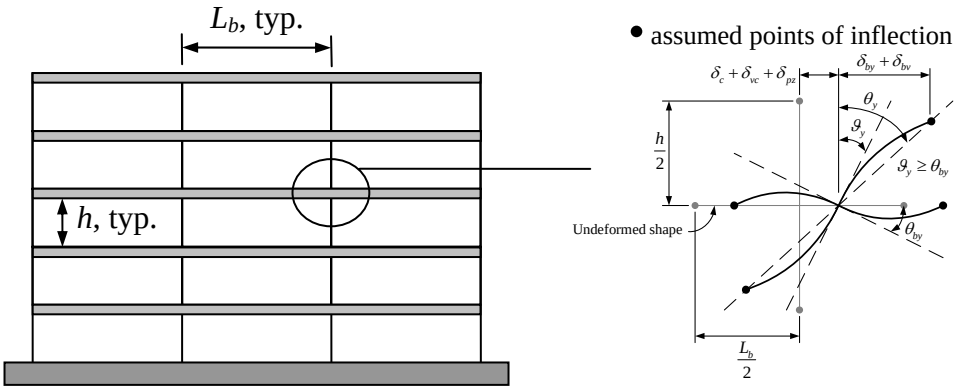

Figure 3-13. Sub-assembly response

Nodal displacement of moment frame assemblies, such as that shown in Fig. 3-13, consists of several components: (1) displacement due to beam rotations, (2) column deformations, and (3) panel zone and shear deformations. In accordance with the strong column-weak beam design philosophy, lateral yield displacement can be estimated by

$$\delta_y = \underbrace{\overbrace{\delta_{by}}^{beam} + \overbrace{\delta_c}^{column}}_{flexural\ deformations} + \underbrace{\overbrace{\delta_{pz}}^{panel\ zone} + \left(\overbrace{\delta_{vb}}^{beam} + \overbrace{\delta_{vc}}^{column} \right)}_{shear\ deformations} \tag{3-11}$$

where

δ_{by} = Lateral yield displacement of due to beam rotation

δ_c = Lateral displacement due to elastic column deformations

δ_{pz} = Lateral displacement due to panel zone deformations

δ_{vb} = Lateral displacement due to shear deformations of beams

δ_{vc} = Lateral displacement due to shear deformations of columns

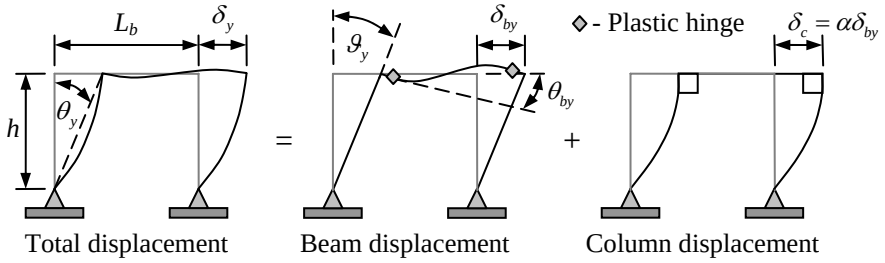

Figure 3-14. Lateral displacement schematic

To further illustrate this concept, Fig. 3-14 schematically shows the displacement contributions to a one-story single bay frame (neglecting the contributions of shear deformations). The yield displacement for a given floor *i* can be estimated by

$$\delta_{y,i} = \left(1 + \alpha_i + \beta_i\right)\delta_{by,i} \tag{3-12}$$

where

α_i = Lateral column displacement ratio $\left(= \dfrac{\delta_{c,i}}{\delta_{by,i}}\right)$

β_i = Lateral panel zone displacement ratio $\left(= \dfrac{\delta_{pz,i}}{\delta_{by,i}}\right)$

The displacement per bay *j* due to beam rotation at yield can be approximated by

$$\delta_{by,j} = \vartheta_{y,j} h_i = \theta_{by,j}\left[\frac{L_c - \ell_p}{L_b}\right]_j h_i \tag{3-13}$$

Beam depths are selected to provide comparable yield rotations for all beams in a given floor. Therefore, the total portion of the floor yield displacement due to beam rotations can be estimated by averaging Eq. (3-13) for all coupled bays.

$$\delta_{by,i} = \frac{\sum_{j=1}^{J} \delta_{by,j}}{J} \tag{3-14}$$

where J is the total number of bays in a frame floor and j is the bay index.

The column displacement ratio, α, in Eq. (3-12) is relatively arbitrary since the design engineer has freedom to decide the magnitude of elastic column deformations. A 10-40% increase ($\alpha = 0.1 - 0.4$), dependent on beam depths and degree of P-Δ effects (discussed in Chapter 5), provides a practical starting point in order to limit the likelihood of cantilever action or excessive column deformations possibly leading to undesirable column hinging. Shallow beam depths should correspond to lower column deformations due to a higher rotation at yield. Similarly, a lower α value should be selected when the gravity forces tributary to the frame generates significant P-Δ effects.

The additional lateral displacement due to panel zone deformations can be approximated by

$$\delta_{pz} = \frac{V_c h_c}{0.4 E A_{cw}} \tag{3-15}$$

where

h_c = Column height (measured between joint faces)

$\left(= h_i - \left(\frac{d_{b(i)} + d_{b(i-1)}}{2} \right) \right)$

A_{cw} = Cross-sectional area of column web $\left(= d_c t_w \right)$

Since neither the column shear force nor column size is initially known, panel zone deformations can be approximated in one of two ways. The first method requires the design engineer to assign an allowable stress to the column. The limiting strength value can be assigned to delineate between strong or weak panel zones and must be maintained through design. For example, a stress level of $V_c / A_{cw} = 0.5F_y$ can be selected. For this chosen value, Eq. (3-15) is simplified to

$$\delta_{pz} = 1.25\varepsilon_y h_c \tag{3-16}$$

The material overstrength factor, ϕ_m^o, need not be applied in this case as a preventive action against yielding.

The second method is to set $\beta = 0$ in Eq. (3-12), or some other estimated value as was done for column deformations, and iterate between analysis and design until convergence. The first approach is recommended for simplicity. Also, doubler plates are not included in Eq. (3-15).

In allocating a portion of lateral displacement to panel zone deformations the design engineer is challenged with modeling this effect in analysis. While researchers have proposed modeling methodologies (e.g., Krawinkler 1978, Gupta and Krawinkler 2002), they remain cumbersome and time-consuming for conventional analysis and design procedures. As a result, explicit displacement due to panel zone deformations is neglected in this research pending the development of a simplified analytical approach. For simplicity, the term in brackets in Eq. (3-13) maybe taken as unity to conservatively

account for the increase in lateral displacement due to panel zone deformations. In so doing, no rigid-end offsets should be used in the analytical model.

Yield displacement can similarly be converted to story yield drift angle.

$$\theta_{y,j} = \frac{\delta_{y,j}}{h_i} \tag{3-17}$$

The global floor and system yield drift angle can be estimated by

$$\theta_{y,i} = \frac{\sum_{j=1}^{J} \theta_{y,j}}{J} \tag{3-18}$$

$$\theta_{y,sys} = \frac{\sum_{i=1}^{n} \theta_{y,i}}{n} \tag{3-19}$$

In reference to Table 1-1 and Fig. -3, the selection of an accurate yield displacement at the SP-1 level is necessary for a reasonable measure of ductility. This currently cannot be accomplished by pre-defining the yield drift angle equal to 0.5% as suggested since yield rotation is essentially a function of beam geometry, as shown in Fig. 3-11. Therefore, yield properties corresponding to SP-1 in Fig. 1-3 should be determined based on $\theta_{y,sys}$. As a side note, the design engineer could select deeper beams if a lower system yield drift angle is required. With regard to FBD, if the maximum drift angle is taken as 2.5%, the required elastic drift angle is 0.46% (= 2.5%÷C_d) under displacement-level lateral forces. If strength-level lateral forces are used, as promoted in ASCE 7-05 (ASCE 2005), this would imply the first significant yield should occur at a

drift angle of 0.46%. The implication is that this would place high elastic stiffness requirements on the frame resulting in a stiffer and stronger frame that could have difficulty achieving the 2.5% drift angle.

The dependence of earthquake level and target demand is now evident since the effective period is determined from the respective DRS. However, proposing fixed PGA values unconnected to the strength and stiffness of a structure as listed in Table 1-1 considers them as independent. The design engineer may find that after designing for the controlling performance level, matching all other performance levels along the system force-displacement graph is unachievable (Fig. 1-3).

3.3.5 Displacement Profile

A displacement profile must be adopted for each performance level and represents the desired displaced shape of the frame. Research suggests that the elastic and inelastic mode shapes can be considered invariant (Fajfar et al. 1988, Qi and Moehle 1991, Fajfar 2000, Chorpra and Goel 2001). Thus, it is recommended that the yield displacement profile, $\{\delta_{dy}\}$, intending to represent the formation of the global yield mechanism is determined by substituting $\theta_{y,sys}$ for θ_T in Table 3-1. Note that adopting these profiles requires the development of base hinges in the first story columns.

Prior to any further discussion the definition of the global yield mechanism must be identified. In reference to Fig. 1-4 the formation of the global yield mechanism is defined by the idealized point Δ_y where a significant change in system stiffness occurs.

The global yield mechanism corresponds to a system displacement ductility of unity ($\mu_{\Delta}=1$). As indicated in Fig. 1-4 this point does not always correspond to the first yield point in MDOF frames. However, the design engineer can optimize and control hinge formations in the frame through design via the desired displacement profile.

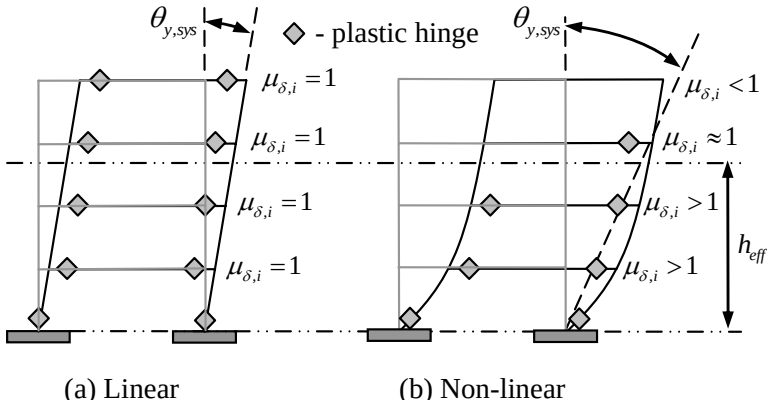

Figure 3-15. Global yield mechanism

In reference to Fig. 3-15, for linear displacement profiles, as proposed for frames up to four stories, the design objective is that all desired plastic hinges develop simultaneously. Conversely, for non-linear displacement profiles the design objective is chosen such that floors below the effective height at the global yield mechanism are inelastic by some degree. The nonlinear displacement profile assumes the formation of plastic hinges in the base of the first story columns in tandem with the development of beam hinges in the first floor. These definitions of the global yield mechanisms will be used throughout the remaining discussions.

The effective SDOF yield displacement, Δ_y, can be approximated by using the yield displacement profile, $\{\delta_{dy}\}$ with Eq. (2-26).

$$\Delta_y = \frac{\sum_{i=1}^{n} w_i \delta_{dy,i}^{\ 2}}{\sum_{i=1}^{n} w_i \delta_{dy,i}} \tag{3-20}$$

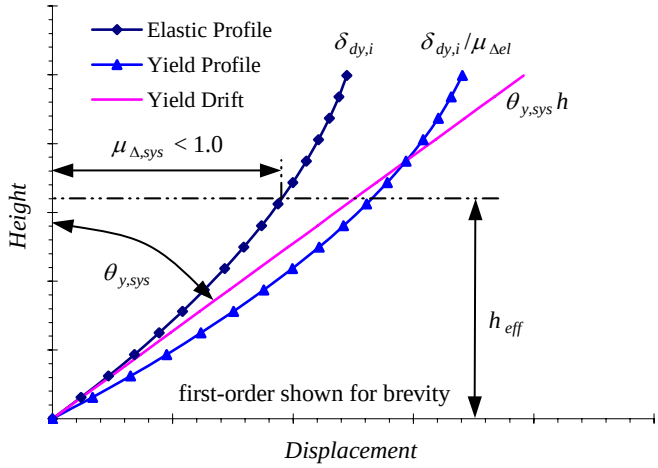

Figure 3-16. Non-linear yield displacement profile at yield point

When the chosen yield displacement profile is non-linear ($n > 4$) a modification to the profile in Table 3-1 is required. In reference to Fig. 3-16, the procedures described previously provide the yield displacement profile, $\{\delta_{dy}\}$, and 'Yield Drift', $\{\theta_{y,sys} h\}$, where $\theta_{y,sys}$ is the target drift angle at the lowest floor indicating that the first sequence of desired plastic hinges forms throughout the base and first floor beams. It can be seen in Fig. 3-16 that the yield displacement profile $\{\delta_{dy}\}$ does not correspond with the above definition of the global yield mechanism since the displacement profile is representative of the onset of the first significant yield. Accordingly, $\{\delta_{dy}\}$ is actually the 'Elastic Profile' depicted in Fig. 3-16.

It can be noticed in Fig. 3-16 when using the displacement profile $\{\delta_{dy}\}$ that the displacement ductility taken at the effective height is less than unity. The yield-level design forces, discussed subsequently in Chapter 6, are determined corresponding to the formation of the global yield mechanism. In this case, the effective SDOF yield displacement for frames up to eight stories can be estimated by

$$\Delta_{dy} = \theta_{y\,sys} h_{eff} \tag{3-21}$$

The 'Yield Profile', indicating the global yield mechanism, is determined by dividing the 'Elastic Profile' by the elastic displacement ductility, $\mu_{\Delta,el}$ (less than unity).

$$\mu_{\Delta,el} = \frac{\Delta_y}{\Delta_{dy}} \tag{3-22}$$

This topic forms the basis of Equivalent Yield Analysis discussed in Chapter 6. $\mu_{\Delta,el} = 1$ for linear displacement profiles.

3.3.6 Yield-level Earthquake and Serviceability Verification

It has been assumed up until this point that the target displacement controls design. That is, the main objective of the design engineer is to develop a system to match the target displacement, Δ_d. At this juncture, the design engineer needs to compare the yield-level PGA with that considered to be adequate in PBSE provisions. The yield-level earthquake can be approximated by reducing the design-level earthquake (e.g., ⅔×MCE).

$$PGA_y = \Re \times PGA_d \tag{3-23}$$

where

PGA_y = Peak Ground Acceleration of yield-level earthquake

PGA_d = Peak Ground Acceleration of design-level earthquake

$$\Re = \text{Reduction factor} \left(= \begin{cases} \dfrac{1}{\sqrt{2\mu_{\theta,sys} - 1}} & T_1 < 1.0 \\ \dfrac{1}{\mu_{\theta,sys}} & T_1 \geq 1.0 \end{cases} \right) \tag{3-23a}$$

$$\mu_{\theta,sys} = \text{Drift angle ductility} \left(= \frac{\theta_T}{\theta_{y,sys}} \right) \tag{3-23b}$$

If PGA_y is less than that prescribed in the PBSE code then the target performance level is adjusted to the yield point. It is apparent that this is directly related to the yield drift angle. The design engineer will most likely discover that moment frames typically possess a yield drift angle and, ultimately, a yield-level PGA greater than that specified by code. However, a steel braced frame has a considerably lower yield drift angle and, consequently, design could be governed by the yield-level PGA. This implies that there is high probability that the target objective at the design-level earthquake will not be matched and response will fall short of the target. If this is the case, the design engineer enters the yield-level DRS at, say, 2% damping and determines the 1st mode elastic period.

The goal of seismic design is to safe-guard against major failure and loss of life (Uang and Bertero 1991). As such, only one design-level earthquake is used in analysis.

In contrast, PBSE objectives stipulate several earthquake levels, albeit only one will govern design. One level that is of importance in PBSE is the ‘operational’ performance level. Discrepancies, however, exist in the definition of what constitutes operational. According to SEAOC (1999), it represents the yield point and is associated with a target drift ratio of 0.5%. As discussed previously, this cannot be adopted since the yield point is essentially defined by beam geometry and design selections. As such, structural damage of the building at this point is requisite.

Past seismic codes have defined ‘operational’ as the ability of a structure to resist minor earthquakes without structural damage, but possibly experience some non-structural damage (Uang and Bertero 1991). It was thus recommended that a two-level seismic design procedure be implemented where a service-level earthquake was defined and unconnected to the ductility requirements of the structure. However, serviceability checks have been removed from U.S. seismic codes.

Since yield displacement (associated with structural damage) is a critical design point in this philosophy, it is recommended that a two-level seismic analysis procedure be implemented: (1) displacement-level design and (2) service-level verification. It is proposed based on previous code requirements that the service-level drift angle be limited to 0.5% coupled with an earthquake intensity not to be less than 0.133×MCE. This value is associated with an R value equal to 5 (see Uang and Bertero 1991). The service-level PGA can be defined by

$$PGA_s = \frac{PGA_y}{200\theta_{y,sys}} \geq 0.133 PGA_{MCE} \tag{3-24}$$

where

PGA_s = Peak Ground Acceleration of service-level earthquake

PGA_y = Peak Ground Acceleration of yield-level earthquake

PGA_{MCE} = Peak Ground Acceleration of maximum considered earthquake

It follows from Eq. (3-24) that for frames with $T_1 \geq 1.0$

$$PGA_s = \frac{PGA_{MCE}}{300\theta_T} \geq 0.133 PGA_{MCE} \tag{3-25}$$

It can readily be computed that θ_T should be less than or equal to 2.5% in order to satisfy Eq. (3-25). This implies that service-level verification in earlier seismic codes was removed based on assignment of the drift limit, which coincides with the change from a ductility dependent limit to a fixed value. Consequently, although frames can successfully exceed 2.5% drift, it is recommended at this time to maintain the drift limit to satisfy the serviceability performance level. The primary difference then lies in the fact that displacement ductility is directly used in analysis and design resulting in a more efficient system.

3.4 Conclusion

This chapter outlined a methodology to construct the target and yield displacement profiles. These profiles are central to the determination of the displacement

ductility demands on each floor as well as the system. In Chapter 4, the importance of floor displacement ductility will be illustrated. It is recommended that system-level displacement ductility be measured with displacements taken at the effective height (i.e., effective SDOF displacements). This appears to be a more rational approach than using roof displacements since the effective height locates the resultant seismic force. Since the displacement profiles are assumed invariant, it follows that the effective and equivalent effective masses and heights are also the same. Lastly, the usefulness of the yield displacement profile goes beyond the proposed DDBD procedure. It can readily be applied in other seismic analysis and design philosophies (e.g., other DBD methods, FBD, Capacity Spectrum, Yield Point, etc.).

Chapter 4 Methodology for Estimating Equivalent Damping

4.1 Introduction

The ability of an elastic structure to dissipate input energy is identified as viscous damping, ζ_v, and is measured as the fraction of critical damping.

$$\zeta_{v,j} = c_j / c_{c,j} \tag{4-1}$$

where

c_j = Damping constant for mode j

$c_{c,j}$ = Critical damping coefficient for mode j $\left(= 2\sqrt{M_j K_j}\right)$ (4-1a)

The damping constant in Eq. (4-1) is selected such that the vibration energy it dissipates is equivalent to the energy dissipated by all damping mechanisms present in a structure for a given mode. Seismic codes assume systems inherently contain 5% viscous damping (includes some allowance for minor structural damage).

It is common engineering practice to design and detail structural components to exit the elastic region and respond inelastically when subjected to strong ground motion. The benefit of this type of design scenario is that the system will dissipate an increased amount of input energy through yielding of these mechanisms. This form of energy dissipation is referred to as 'hysteretic damping', ζ_h. The total degree of damping present in an inelastic system is typically formulated as the linear summation of viscous and hysteretic damping.

$$\zeta = \zeta_v + \zeta_h \tag{4-2}$$

Until recently there have been no explicit codified guidelines to quantifying the additional damping due to inelastic behavior at large deformations. In reference to FBD discussed in Chapter 1, the force reduction factor, *R*, is calibrated to implicitly approximate the increase in damping due to yielding for a wide range of system properties and geometries. As presented in Chapter 2, the *R* factor is strongly related to displacement ductility. The design engineer must then come to appreciate this generic value as it is uncertain if the *R* factor can readily be applied to an entire range of configurations in a specific class of structural systems since ductility can be essentially expressed as a function of beam length and depth. As such, it is questionable that two frames with different beam geometries will have the same level of damping if both attain the same inelastic displacement.

Seismic codes are beginning to adopt alternative seismic analysis procedures for the analysis of structures for seismic attack (see Table 1-2). Of these methods, Nonlinear Static Analysis (NSA) has received considerable attention lately with its adoption into NEHRP 2003 (BSSC 2003). The central philosophy supporting NSA is the Equivalent Linear Static Analysis (ELSA). The general theory for ELSA was discussed in Chapter 2. Due to ELSA employing an equivalent elastic system coupled with a level of equivalent damping to represent the response of an inelastic system, researchers are currently investigating various means to explicitly approximate hysteretic damping. Although a large amount of research has been conducted to determine component-level hysteretic functions (or SDOF), few relationships exist for quantifying the effects of local damping

on system-level damping. Additionally, this is extremely difficult to approximate for MDOF frames due to plastic hinge formation sequences being a function of earthquake characteristics, member overstrengths, and residual displacements.

Most displacement-based design philosophies currently being researched (see Table 1-4) use ELSA to determine seismic design parameters. They differ mainly in the selection of the equivalent properties. As such, the determination of the degree of equivalent damping for steel moment frames is the central focal point of this chapter. While the results presented are implicit to the proposed DDBD methodology, they can be applied in other alternative seismic analysis procedures that use ELSA.

Past research has identified that a bilinear with post-yield stiffness (‘bilinear hereafter) or elastic perfectly-plastic (EPP) hysteresis rule is best suited for representing the idealized cyclic response of a structural steel member when no axial force is present. These rules will be the main focus in the following discussion although a few other models are illustrated for comparison. Any other loop used to represent the response of a steel member may not be sufficient and could lead to significant error. The Ramberg-Osgood hysteresis rule that includes the Baushinger Effect (see Fig. 1-10) or a trilinear hysteresis is most likely best suited for structural steel and is a topic for further research in this area.

Lastly, many researchers use the term ‘equivalent viscous damping’ to quantify the level of damping in the equivalent elastic system. However, in reference to Eq. (4-2), some researchers are now questioning the use of ζ_v to represent the contribution of

viscous damping in the equivalent elastic frame. As a result, an equivalent ζ_v is being investigated – the reader is referred to Kwan and Billington (2003) and Priestley and Grant (2005). This would imply in the author's opinion that this contribution to damping should be referred to as 'equivalent viscous damping'. Within this document, this portion of damping is symbolized by $\zeta_{eq,v}$ to illustrate separation, although no proposals are recommended for computation (i.e., $\zeta_{eq,v} = \zeta_v$), and the term 'equivalent damping' is used to represent the total measure of damping'

4.2 Literature Review

4.2.1 Equivalent Damping in SDOF Systems

4.2.1.1 Steady-State Harmonic Excitation

Many researchers have proposed methodologies in order to estimate the quantitative measure of equivalent damping to be used in conjunction with the equivalent elastic SDOF when subjected to steady-state harmonic forces. These procedures vary based on the physical properties of the equivalent SDOF selected during derivation. The following discussion presents the background of a few of the more commonly known procedures: (1) Resonant Amplitude Matching, (2) Dynamic Equivalence (or Dynamic Stiffness), (3) Dynamic Mass, (4) Dynamic Critical Damping, and (5) Geometric Stiffness (or Secant Stiffness). Table 4-1 (located at the end of this section) presents a summary of the listed methodologies and the system properties used in the mathematical formulations.

Jacobsen (1930) first proposed the concept of equivalent linearization by replacing a nonlinearly damped elastic SDOF with an elastic SDOF with equivalent damping. In this process Jacobsen solved the damped equation of motion by applying a steady-state sinusoidal forcing function to an elastic SDOF that had the same natural period of the nonlinearly damped SDOF. The solution was integrated to determine the energy dissipated for one cycle of response. The measure of equivalent damping was determined by equating the energy dissipated by the elastic SDOF to that dissipated by the nonlinearly damped SDOF. Jacobsen additionally explained the uncertainty in selecting the one cycle criterion and that unless at or near resonance it does not offer a better solution than taking the equivalent time average of the damping force. It was also shown that this method could be employed with a broad category of damping functions, albeit restricted to essentially steady-state sinusoidal response.

Kryloff and Bogoliuboff (1943) subsequently proposed a linearization method where the nonlinear undamped equation of motion in the form

$$M\ddot{u} + Ku + F_{nl}(u, \dot{u}) = 0 \tag{4-3}$$

where

F_{nl} = Nonlinear restoring force

is replaced by an equivalent elastic damped equation in the form

$$M_{eq}\ddot{u} + C_{eq}\dot{u} + K_{eq}u = 0 \tag{4-4}$$

where

M_{eq} = Equivalent mass (taken equal to M)

K_{eq} = Equivalent stiffness

C_{eq} = Equivalent linear damping coefficient

Kryloff and Bogoliuboff stated that the equivalent damping coefficient and stiffness can be selected so that the solutions of Eqs. (4-3) and (4-4) are matched.

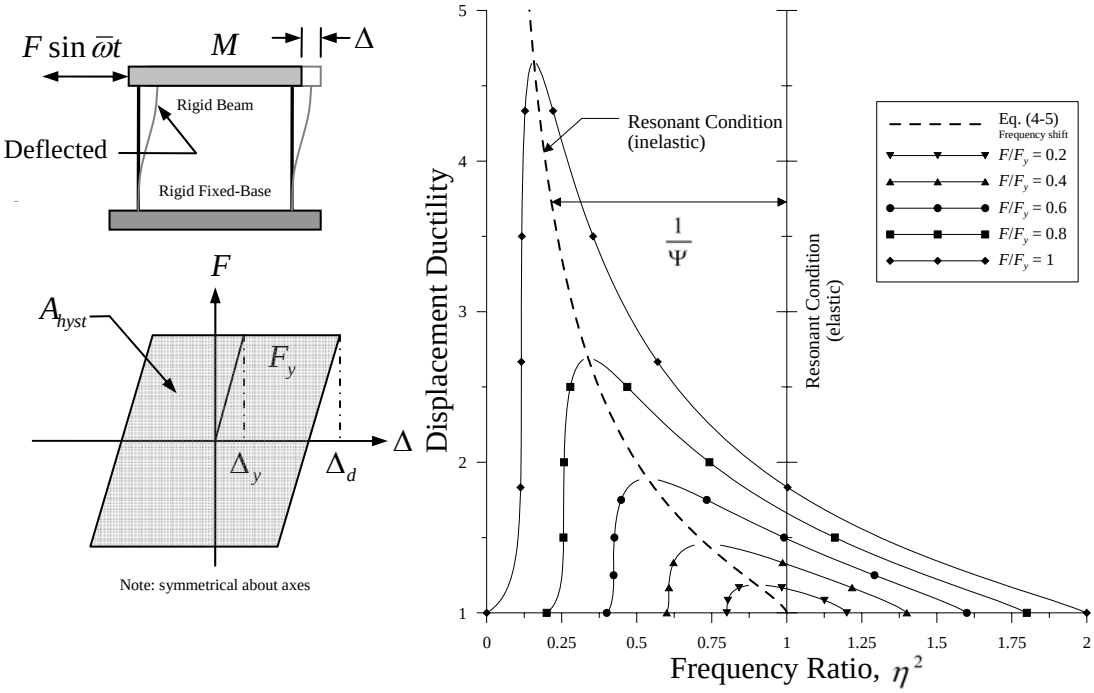

Figure 4-1. Steady-state response of elastoplastic SDOF to sinusoidal excitation

Caughey (1960a, 1960b, 1960c) based on the work of Kryloff and Bogoliuboff showed that the equivalent properties (stiffness and mass) could be derived such that the mean square difference between the solutions of Eqs. (4-3) and (4-4) is minimized. There was no identification of what value to use for the equivalent properties in this method. Fig. 4-1 illustrates the response of an elastoplastic SDOF subjected to varying intensity

steady-state harmonic forcing functions based on the theoretical solution proposed by Caughey (1960a). In Fig. 4-1, the equation tracing the peak displacement ductility (representing the inelastic resonant condition) is

$$\Psi = \eta^2 = \frac{1}{\pi}\left(\theta - \frac{\sin 2\theta}{2}\right) \tag{4-5}$$

where

η = Frequency ratio $\left(= \frac{\bar{\omega}}{\omega}\right)$ (4-5a)

$\bar{\omega}$ = Excitation frequency

ω = Undamped natural cyclic frequency $\left(= \sqrt{\frac{K}{M}}\right)$ (4-5b)

θ = Ductility coefficient $\left(= \cos^{-1}\left(1 - \frac{2}{\mu_\Delta}\right)\right)$ (4-5c)

It follows that Eq. (4-5) represents $\left(\frac{\bar{\omega}}{\omega_{in}}\right)^2 = 1$ where ω_{in} is the undamped natural cyclic frequency of the inelastic SDOF. The decrease in natural frequency ($\omega \to \omega_{in}$) dependent on response amplitude can be identified in Fig. 4-1.It can readily be determined that $\frac{\omega}{\omega_{in}} = \frac{1}{\sqrt{\Psi}}$ (frequency shift).

Jacobsen (1960) further discussed the adoption of equivalent damping into yielding systems. Jacobsen noted that complications arise when a frequency shift is present in that the damping ratio of the equivalent SDOF, $\zeta = c/c_c$, becomes a ratio of

quantities that vary with response amplitude. That is, ζ must vary to account for the variation in energy dissipation of the inelastic system.

Jennings (1968) pointed out that the success of Jacobsen's method (1930) is directly related to maintaining the natural frequency independent of response amplitude for all damping functions. Jennings further noted that in the case of an inelastic system the decrease in natural frequency caused by yielding presents problems that are not encountered in Jacobsen's original approach. It was proposed that the equivalent SDOF must have a variable resonant frequency and, thus, variable damping coefficient. Jennings concluded that the equivalent damping method gives an accurate description of steady-state response when subjected to sinusoidal excitation.

Since 1960, several researchers have proposed various methods based on those proposed by Jacobsen and Caughey (previously listed). The following discussion briefly explains these methods. The methods presented are based on the energy matching procedure outlined by Jacobsen. The theory of energy matching can be expressed mathematically as follows and is derived based on an undamped inelastic SDOF system ($\zeta_v = 0\%$) with an elastic perfectly-plastic hysteresis ($r_\Delta = 0$ in Fig. 4-2) while subjected to a steady-state sinusoidal forcing function, $F \sin \bar{\omega} t$.

4.2.1.1.1 Theory of Energy Matching

The energy dissipated by viscous damping, $E_{D,v}$, in one cycle of steady-state harmonic vibration of an elastic SDOF with mass, M, and stiffness, K, is

$$E_{D,v} = 2\zeta_v \omega M \int_0^{2\pi/\omega} \dot{u}(t)^2 \, dt \tag{4-6}$$

where

ζ_v = Viscous damping ratio

$\dot{u}(t)$ = Steady-state velocity response $\left(= \bar{\omega} \cos\left(\bar{\omega} t - \phi\right) \Delta\right)$ (4-6a)

ϕ = Undamped phase angle $\left(= \begin{cases} 0^\circ & \bar{\omega} < \omega \\ 90^\circ & \bar{\omega} = \omega \\ 180^\circ & \bar{\omega} > \omega \end{cases} \right)$

Solving Eq. (4-6) for one cycle of steady-state motion yields

$$E_{D,v} = 2\pi\zeta_v \frac{\bar{\omega}}{\omega} K\Delta^2 = 4\pi\zeta_v \eta E_{So} \tag{4-7}$$

where

Δ = Maximum displacement (response amplitude)

E_{So} = Elastic strain energy $\left(= \frac{1}{2} K\Delta^2 \right)$ (4-7a)

In reference to Fig. 4-2, for a viscously undamped equivalent SDOF with mass, M_{eq}, and stiffness, K_{eq} (secant stiffness), Eq. (4-7) becomes

$$E_{D,v} = 2\pi\zeta_{eq,h} \frac{\bar{\omega}}{\omega_{eq}} K_{eq} {\Delta_d}^2 = 4\pi\zeta_{eq,h} \eta_{eq} E_{So,eq} \tag{4-8}$$

where

ω_{eq} = Resonant frequency of the equivalent SDOF $\left(= \sqrt{\frac{K_{eq}}{M_{eq}}} \right)$ (4-8a)

$\zeta_{eq,h}$ = Equivalent hysteretic damping

η_{eq} = Equivalent frequency ratio $\left(= \frac{\bar{\omega}}{\omega_{eq}} \right)$ (4-8b)

$E_{So,eq}$ = Equivalent elastic strain energy $\left(= \frac{1}{2} K_{eq} \Delta_d{}^2 \right)$ (4-8c)

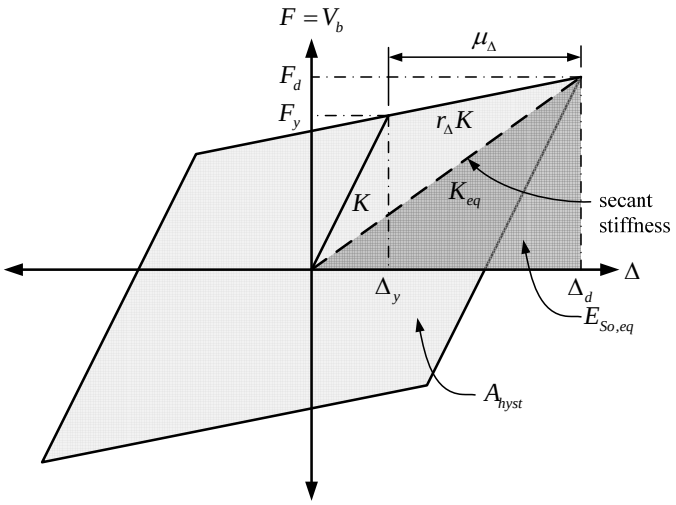

Figure 4-2. Bilinear hysteresis loop

The energy dissipated by yielding is equated as the area of the hysteresis loop for one cycle, A_{hyst}, shown in Fig. 4-2. The area of a bilinear loop can be computed by

$$A_{hyst} = \frac{4K\Delta_d\Delta_y}{\mu_\Delta}\left(\mu_\Delta - r_\Delta\left(\mu_\Delta - 1\right) - 1\right) \tag{4-9}$$

The energy dissipated by yielding in the inelastic SDOF must equal the energy dissipated by equivalent hysteretic damping, $\zeta_{eq,h}$ in the equivalent SDOF. Equating Eqs. (4-8) and (4-9) and solving for the damping term gives

$$\zeta_{eq,h} = \frac{A_{hyst}}{2\pi\eta_{eq}K_{eq}\Delta_d{}^2} \tag{4-10}$$

As shown by Eq. (4-10), equivalent hysteretic damping is dependent upon excitation frequency. It is commonly accepted practice among researchers to equate the energy dissipated assuming the structure is vibrating at resonance, $\eta_{eq} = 1$, where the response of an elastic system is most sensitive to damping. This implies that $\bar{\omega} = \omega_{eq}$ where ω_{eq} is matched to the resonant frequency of the inelastic SDOF, ω_{in}, at Δ_d. Obviously, this simplification would not be correct at any other forcing frequency; however, it has been argued that it is a reasonable estimate (Chopra 2001).

4.2.1.1.2 Method 1 – Resonant Amplitude Matching

Hudson (1965) proposed an analytical method where the stiffness and mass of the equivalent SDOF are taken equal to the elastic stiffness and mass of the inelastic SDOF. Hudson derived its applicability for a bilinear hysteresis. By equating the energy dissipated by the two systems at the resonant steady-state amplitude a closed form solution for the equivalent damping was derived. The end results are shown in Table 4-1 and plotted in Fig. 4-3. Hudson additionally stated that good agreement exists between

the analytical results and the exact numerical solution presented by Iwan (1961). Jennings (1968) subsequently applied this method to an elastoplastic SDOF.

Based on results presented by Caughey (1960), Jennings (1968) conducted an analytical investigation into several dynamic methods. Since the goal of the method proposed by Caughey was to minimize the difference between the response of the inelastic and elastic systems, there was no initial assumption of the quantitative measure of the equivalent SDOF properties.

4.2.1.1.3 Method 2 – Dynamic Equivalence (or Dynamic Stiffness)

Jennings (1968) characterized the equivalent SDOF by an equivalent stiffness such that the resonant frequencies of the two structures are identical. The mass of the two systems was arbitrarily chosen equal in the derivation of the resonant frequency shift. The equivalent viscous damping factor was derived by equating the energy dissipated for one cycle by the inelastic SDOF and the equivalent SDOF at resonance. The results are presented in Table 4-1 and plotted in Fig. 4-3.

As can be seen in Fig. 4-3(a), this method can produce very large damping quantities after a displacement ductility of 3. This occurs because the critical damping coefficient, c_c, decreases as a function of the response amplitude while simultaneously decreasing proportionally with the decrease in resonant frequency.

$$c_c = 2\Psi\sqrt{KM} \tag{4-11}$$

4.2.1.1.4 Method 3 – Dynamic Mass

Jennings (1968) proposed a solution taking the elastic stiffness of the two systems equal while varying the mass of the equivalent SDOF to model the frequency shift achieved by yielding. The mass was chosen such that the resonance frequencies of the two systems were matched. The results for elastoplastic response are presented in Table 4-1 and plotted in Fig. 4-3.

With this method the frequency shift remains the same as in the case of Dynamic Stiffness. The clearly defined decrease in equivalent damping in Fig. 4-2(a) is due to the critical damping coefficient, c_c, increasing with response amplitude, which is in contrast with Dynamic Stiffness.

$$c_c = \frac{2\sqrt{KM}}{\Psi} \tag{4-12}$$

4.2.1.1.5 Method 4 – Dynamic Critical Damping

Jennings (1968) proposed this method where the equivalent SDOF is defined such that the critical damping coefficient remains constant while maintaining the frequency shift due to yielding. The results for elastoplastic response are presented in Table 4-1 and plotted in Fig. 4-3.

The apparent difference between this method and the other dynamic methods is related to the choice of the equivalent system properties. An interesting conclusion is that all the dynamic methods maintain the same damping coefficient.

$$c = 4\pi\mu_{\Delta}\left(1-\mu_{\Delta}\right)\frac{\sqrt{KM}}{\Psi} \tag{4-13}$$

4.2.1.1.6 Method 5 – Geometric Stiffness (or Secant Stiffness)

Rosenblueth and Herrera (1964) proposed a ‘geometric stiffness’ method to determine the equivalent damping at resonance. In this model the stiffness of the equivalent SDOF was taken as the slope of the line connecting the extreme points of the hysteresis loop of the inelastic SDOF. For this reason the equivalent stiffness is commonly referred to as the ‘secant stiffness’. Since the secant stiffness is directly correlated to the force, the mass of the two systems was assumed equal. The results for elastoplastic and bilinear response are presented in Table 4-1 and plotted in Fig. 4-3.

Table 4-1. Equivalent hysteretic damping (SDOF - steady-state harmonic excitation)

	Method	Hysteresis	Excitation	Equivalent SDOF Properties: Stiffness K_{eq}	Mass M_{eq}	Period T_{eq}	Hysteretic Damping $\zeta_{eq,h}$	Reference	Initial Damping $\zeta_{eq,v}$
1a	Resonant Amplitude Matching	EPP [1]	Harmonic $\bar{\omega} = \omega_{eq}$	K	M	T	$\frac{2}{\pi}\frac{(\mu_\Delta - 1)}{\mu_\Delta^{\,2}}$	Hudson (1965) Jennings (1968)	0%
1b		Bi-linear	Harmonic $\bar{\omega} = \omega_{eq}$	K	M	T	$\frac{2}{\pi}\frac{(\mu_\Delta - 1)(1 - r_\Delta)}{\mu_\Delta^{\,2}}$	Hudson (1965)	0%
2	Dynamic Equivalence (i.e., Dynamic Stiffness)	EPP [1]	Harmonic $\bar{\omega} = \omega_{eq}$	$M\omega^2\Psi$ [2]	M	$\frac{T}{\sqrt{\Psi}}$ [2]	$\frac{2}{\pi}\frac{(\mu_\Delta - 1)}{\mu_\Delta^{\,2}}\frac{1}{\Psi}$ [2]	Jennings (1968) Based on Caughey (1960)	0%
3	Dynamic Mass	EPP [1]	Harmonic $\bar{\omega} = \omega_{eq}$	K	$\frac{K}{\omega^2\Psi}$ [2]	Same as 1	$\frac{2}{\pi}\frac{(\mu_\Delta - 1)}{\mu_\Delta^{\,2}}$	Jennings (1968) Based on Caughey (1960)	0%
4	Dynamic Critical Damping	EPP [1]	Harmonic $\bar{\omega} = \omega_{eq}$	K	M	Same as 1	$\frac{2}{\pi}\frac{(\mu_\Delta - 1)}{\mu_\Delta^{\,2}}\frac{1}{\sqrt{\Psi}}$ [2]	Jennings (1968) Based on Caughey (1960)	0%
5a	Geometric Stiffness (i.e., Secant Stiffness)	EPP [1]	Harmonic $\bar{\omega} = \omega_{eq}$	$\frac{K}{\mu_\Delta}$	M	$T\sqrt{\mu_\Delta}$	$\frac{2}{\pi}\left(1 - \frac{1}{\mu_\Delta}\right)$	Rosenblueth and Herrera (1964) Jennings (1968)	0%
5b		Bi-linear	Harmonic $\bar{\omega} = \omega_{eq}$	$K\frac{\left(1 + r_\Delta(\mu_\Delta - 1)\right)}{\mu_\Delta}$	M	$T\sqrt{\frac{\mu_\Delta}{\left(1 + r_\Delta(\mu_\Delta - 1)\right)}}$	$\frac{2}{\pi}\frac{(1 - r_\Delta)(\mu_\Delta - 1)}{\mu_\Delta\left(1 + r_\Delta(\mu_\Delta - 1)\right)}$	Adopted from Rosenblueth and Herrera (1964)	0%

1. Elastoplastic (Elastic Perfectly-Plastic (EPP))

2. $\Psi = \frac{1}{\pi}\left(\theta - \frac{\sin 2\theta}{2}\right)$ where $\theta = \cos^{-1}\left(1 - \frac{2}{\mu_\Delta}\right)$

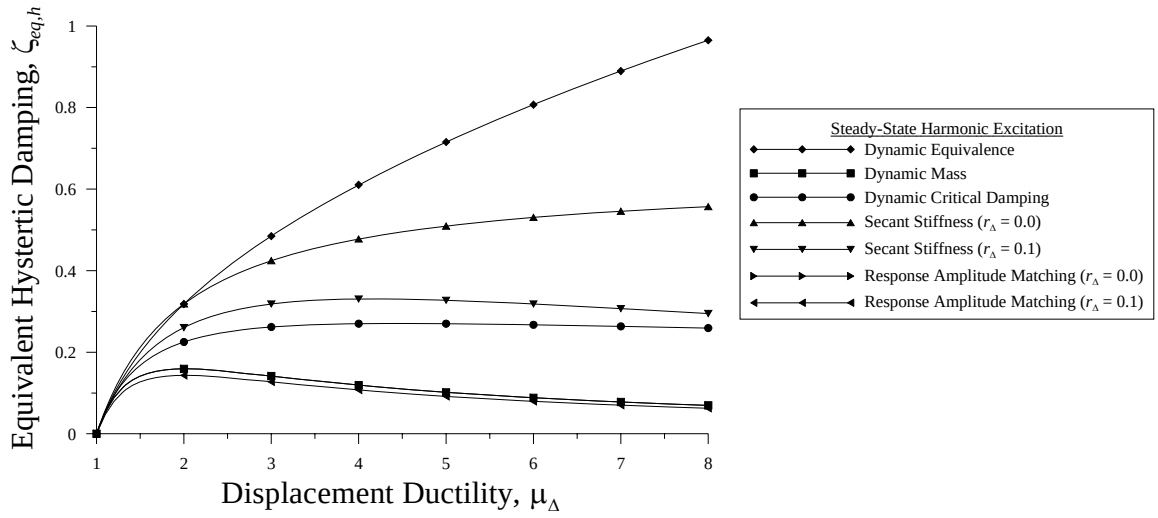

(a) Equivalent hysteretic damping (assumes resonant condition)

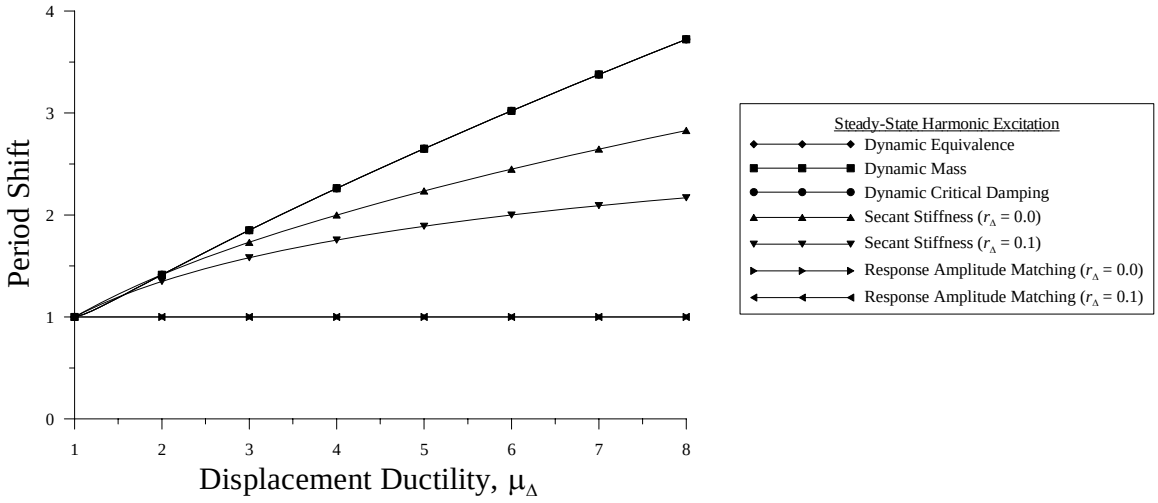

(b) Period shift

Figure 4-3. Equivalent hysteretic damping and period shift (steady-state excitation)

4.2.1.1.7 Summary

As evident in Table 4-1 and Fig. 4-3(a), different definitions of equivalent properties provide widely varying damping values at various response amplitudes. However, as differing as the damping equations are for EPP response, the product of the equivalent stiffness and damping, $K_{eq}\zeta_{eq}$, is constant among the methods (Hadjian 1982).

This can be deduced because the area of the hysteresis loop and maximum displacement is constant (see Eq. 4-10 with $\eta_{eq} = 1$). Fig. 4-3(b) presents the period shift as a function of displacement ductility. Though a wide range of period shift is evident, all methods result in the same initial period because the resonant amplitudes were matched in the derivations. The same conclusion can be drawn for bilinear response. Therefore, it is the selection of the equivalent system properties to be used in the linear analysis that needs to be investigated.

Jennings (1968) concluded that equivalent damping is dependent on whether the frequency shift and amplitude nonlinearities of the response are to be modeled, and what equivalent properties are prescribed to represent the inelastic SDOF. Jennings concluded that the Resonant Amplitude Matching method, due to its simplicity, clarity, and conservative results, is the preferred method. It was also noted that this methodology is the most readily adaptable for earthquake-like excitation.

Merritt (1978) performed an analytical comparison between the Geometric Stiffness and Resonant Amplitude Matching methods. This study concluded that the latter is unreliable and although the former underestimates the maximum response by up to 30% (assuming resonance) any additional work in the field of equivalent damping should focus on the Secant Stiffness method since it accounts for the frequency shift more adequately. It was recommended that a damping modification factor be applied to the damping curve due to a presumed overestimation of the actual amount of damping. It was proposed that this adjustment factor could be defined based on a least square fit to the inelastic response amplitude.

Hadjian (1982) revisited the previously illustrated methods and pointed out the deficiencies in selecting the equivalent stiffness equal to the elastic stiffness of the inelastic SDOF, while maintaining the same mass.

(1) There is no period elongation as the response amplitude increases, except where the equivalent mass is chosen respectively.
(2) The damping curves of Methods 1 and 3 are contrary to what is expected (i.e., damping increases relative to ductility).
(3) There is no design basis for reaching a maximum damping value at a ductility of 2 (Methods 1 and 3)

Hadjian further concluded that there does not appear to be a compelling reason for assuming the critical damping remains the same in Method 4 and that Method 1 results in excessively degrading stiffness and an over-damped situation at high ductility levels. This is contrary to what current research experiments and seismic codes demonstrate. Additionally, any combination of equivalent stiffness and mass can be selected to achieve the resonant frequency.

Hadjian noted that the use of constant mass between the two systems was an arbitrary decision in Jennings' derivation. Therefore, according to Hadjian, the Secant Stiffness method is the best choice for modeling equivalent damping since it provides an upper-bound softening of the inelastic SDOF. Additionally, Hadjian recommended that the period shift be modeled with a Modified Dynamic Equivalence method. This method would incorporate an equivalent mass determined from the secant stiffness.

$$M_{eq} = \frac{M}{\mu_{\Delta}\Psi} \text{ (EPP response)} \tag{4-14}$$

This modified process will give the damping curve provided by the Secant Stiffness method and the period shift provided by the Dynamic Equivalence method (theoretically exact solution solved by Caughey). Since the response acceleration is supposedly the same between the equivalent and inelastic SDOF, selecting an equivalent mass not equal to the actual mass of the inelastic SDOF disconnects its direct tie to design force (Kowalsky and Ayers 2002) and, as a result, this modified proposal would not be well suited for design.

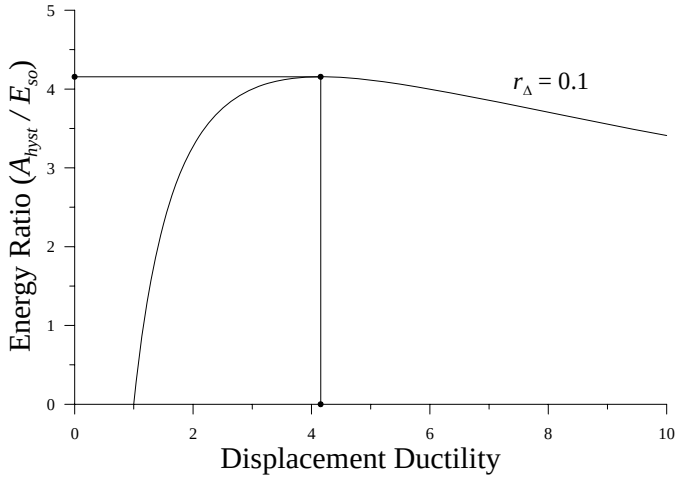

Figure 4-4. Energy ratio

Explanations (2) and (3) previously listed may also apply to the damping curve provided by the Secant Stiffness method with bilinear response, where damping achieves a maximum value at some ductility dependent on r_{Δ} (4.16 when $r_{\Delta} = 0.1$). This variation can be theoretically proven when noticing that the ratio of the area of the hysteresis loop to the equivalent strain energy reaches an apex at a ductility of 4.16 (see in Fig. 4-4).

Consequently, more damping is required in the equivalent system when the response amplitude is less than a ductility of 4.16. Likewise, less damping is required at higher ductility levels as the ratio begins a convergence to unity. However, one must question this logic from a design perspective – that damping decreases as ductility increases. This reasoning does not imply that the method is erroneous; simply that it proves the differences between the methods and definitions of the equivalent system properties.

Based on the previous discussion, the Secant Stiffness method is the best choice for modeling the equivalent elastic SDOF for:

(1) Connection to design force and application to various hysteretic loops
(2) Simplicity and ease of design integration and modeling the period shift
(3) Understanding response graphically and intuitively

The methods assumed an undamped SDOF in order to directly compute the degree of hysteretic damping at resonance. It has been proposed for a damped SDOF that the total amount of equivalent damping be computed as the linear summation of viscous and hysteretic damping.

$$\zeta_{eq} = \zeta_{eq,v} + \zeta_{eq,h} \tag{4-15}$$

where

$\zeta_{eq,v}$ = Equivalent viscous damping $\left(=\zeta_v\right)$

Taking only the area of the loop and adding the viscous damping component neglects any change in viscous damping inherent in the inelastic system.

Lastly, the previous methods neglect *P*-Δ effects and a rigid beam was assumed in the derivations, thus, yielding occurred in zero-length plastic hinges only in the columns (see Fig. 4-1). Consequently, plastic hinge lengths and elastic column displacements that would arise if hinges were forced to develop in the beam were not considered. This implies that the previous methodologies are restricted only to member-level hysteresis rules where *P*-Δ effects can be neglected. It was additionally assumed that the damping function used in the equivalent equation of motion does not significantly affect the equivalent natural frequency (i.e., equivalent damped natural frequency, $\omega_{D,eq}$).

4.2.1.2 Earthquake Excitation

The extension of equivalent damping for steady-state vibration can also be applied to systems subjected to earthquake-like excitation. However, the major weakness in this approach is that ground motion during an earthquake is not purely harmonic or even steady-state. The transient waves will probably not have enough time to damp out prior to completion of seismic attack. Furthermore, it is not likely that ground motions will strongly influence the development of a resonant condition.

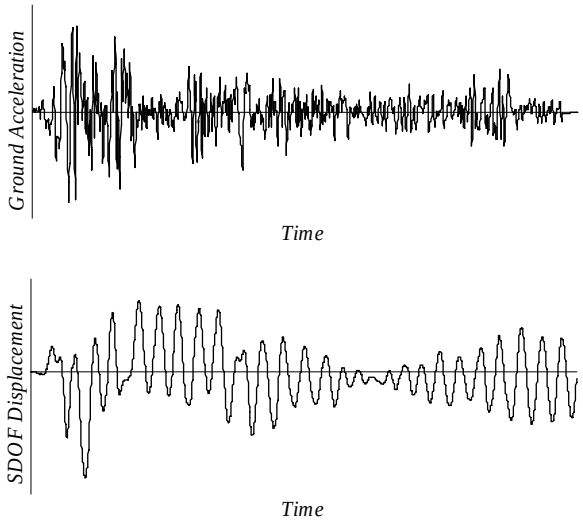

Figure 4-5. SDOF Response

Although ground motion accelerations are often of a complex nature containing a wide frequency range, displacement response of a structure can be a fairly smooth harmonic motion of variable amplitude (Hudson 1965), illustrated in Fig. 4-5. Thus, several researchers have proposed methods for determining equivalent damping based on the theory of harmonic steady-state excitation. The methods presented are summarized in Table 4-3 (located at the end of the discussion).

4.2.1.2.1 Method 1 – Hudson (1965)

Hudson (1965) showed that many of the cycles of earthquake response will occur at response amplitudes much less than the maximum. As a result, a reduction factor of one-third applied to the Resonant Amplitude Matching method was proposed to account for the decrease in energy dissipation. Hudson noted that equivalent damping for earthquake-like excitation does not vary much over a large range of yield ratios and, thus,

the total deformation of an elastoplastic SDOF is independent of the yield ratio. The results are presented in Table 4-3 and plotted in Fig. 4-6.

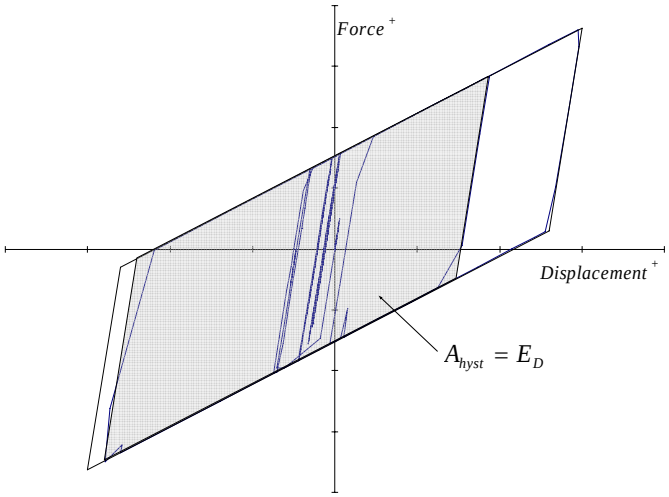

Figure 4-5. Bilinear hysteresis loop from earthquake excitation

Jennings (1968) concluded that the application of a dynamic or geometric method for quantifying equivalent damping for earthquake-like excitation would require that a response amplitude not equal to the maximum be determined since residual drifts can occur in the inelastic system. Consequently, additional errors could be introduced thereby limiting the use of any of the steady-state methods. The quantitative measure of damping determined by a steady-state method decreases as residual drifts increase since the system begins to vibrate about a new equilibrium point. This phenomenon is commonly referred to as the 'crawling effect', illustrated in Fig. 4-5. Jennings concluded that the Response Amplitude Matching method is the most adaptable method for earthquake-like excitation.

4.2.1.2.2 Method 2 – Gulkan and Sozen (1974)

Gulkan and Sozen (1974) performed experimental testing of one-story one-bay concrete frames subjected to a 13 *Hz* harmonic ground motion and the Taft (1952) time-history. In this model, plastic hinges formed in the columns. The equivalent stiffness of the frames was taken as the ratio of maximum absolute acceleration to maximum absolute displacement. It was acknowledged that this approach is equivalent to the taking the secant stiffness. Gulkan and Sozen matched the input energy to the energy dissipated by damping over the entire time-history.

$$E_I = M\int_0^t \ddot{u}_g(t)\dot{u}(t)dt \tag{4-16}$$

$$E_D = 2\zeta_{eq}\omega_{eq}M\int_0^t \dot{u}(t)^2 dt \tag{4-17}$$

Assuming that the relative velocities of the two systems are the same, equivalent damping can be determined by

$$\zeta_{eq} = \frac{T_{eq}}{4\pi}\frac{\int_0^t \ddot{u}_g(t)\dot{u}(t)dt}{\int_0^t \dot{u}(t)^2 dt} \tag{4-18}$$

where

T_{eq} = Equivalent period $\left(= 2\pi\sqrt{\frac{M}{K_{eq}}}\right)$ (4-18a)

Following the Takeda hysteresis model (Takeda et al. 1974), with no post-yield stiffness and assuming 2% viscous damping, an equivalent damping model, termed

‘substitute damping’, was developed for reinforced concrete flexural members. A relationship for the period shift was additionally developed, although comparable but not based on the steady-state Secant Stiffness method. The results are presented in Table 4-3 and plotted in Fig. 4-6.

It was noted in this study that the displacement arising from earthquake loading would be significantly smaller than the peak response obtained from the full hysteresis loop. Thus, the damping value will be overestimated and the maximum response underestimated if a steady-state solution was employed (Miranda and Ruiz-Garcia 2002). This damping model was adopted by Shibata (1975) and Shibata and Sozen (1976a, 1976b, 1977) for the ‘Substitute Structure’ approach for reinforced concrete frames. It has been additionally verified experimentally by Bonacci (1994), and incorporated into a DDBD methodology for reinforced concrete bridge piers and building frames by Calvi and Kingsley (1995) and Calvi and Pavese (1995) respectively. Shimazaki (2000) proposed this model for steel members by revising the factor 0.2 to 0.25 and concluded it provides a reasonable and conservative lower-bound damping curve. Teshigawara et al. (2000) adopted this approach and observed also that using 0.25 in lieu of 0.2 gives a reasonable lower-bound estimate to substitute damping.

4.2.1.2.3 Method 3 – Iwan and Gates (1979)

Iwan and Gates (1979) and Iwan (1980) proposed an empirical methodology for determining the equivalent damping and associated period shift for SDOF systems with mid-range periods. The goal of this statistical investigation was to minimize the spectral

error as a function of displacement ductility. There was no presumption of the initial stiffness or mass of the inelastic SDOF. This research included a class of six hysteresis models with 2% viscous damping subjected to twelve earthquakes representative of a variety of different types of excitation. The results are presented in Table 4-3 and plotted in Fig. 4-6.

The primary conclusions from Iwan's studies are that the optimal value of equivalent damping never exceeds 14% and that peak displacement is relatively insensitive to equivalent damping. Thus, it is insensitive to the definition of the equivalent period (Kowalsky and Ayers 2002). Xue (2001) concluded that for ductility ratios less than 4 for reinforced concrete, this model gives the most accurate results when compared to Kowalsky et al. (1994), ATC (1996), and Reinhorn (1997). It was additionally noted by Xue that ATC (1996) provides the smallest error for ductility ratios greater than 4. Lastly, Iwan and Gates (1979) took the output frequency as the natural frequency of the equivalent linear system (i.e., resonance) resulting in quantities independent of excitation; hence, it may be less efficient for earthquake problems (Levy et al. 2006).

4.2.1.2.4 Method 4 – Kowalsky et al. (1994)

Kowalsky et al. (1994) proposed an analytical damping model for reinforced concrete members based on the Takeda hysteresis model. In this approach, the stiffness was taken as the secant stiffness at maximum response and it was assumed that response had a 5% post-yield stiffness ratio, r_{Δ}, and 5% viscous damping. The mass was also held

constant throughout inelastic response. Kowalsky et al. concluded that this model compares well with that obtained by Gulkan and Sozen (1974) and provides a reasonable lower-bound damping curve when compared to experimental results. It was noted that taking this model as a lower-bound estimate of the achieved damping is on the conservative side and, therefore, better suited for design objectives. The results are presented in Table 4-3 and plotted in Fig. 4-6.

This damping curve has been widely adopted into various reinforced concrete DDBD approaches (Priestley et al. 1996, Priestley & Kowalsky 2000, Kowalsky 2001, Kowalsky 2002, Miranda and Ruiz-Garcia 2002, Priestley 2003, Priestley and Calvi 2003).

4.2.1.2.5 Method 5 – ATC-40 (1996)

ATC-40 (1996) proposed a damping curve to be applied to reinforced concrete members and period shift based on the steady-state bilinear Secant Stiffness method. In this approach, a hysteretic damping modification factor, κ, (presented in Table 4-2) was introduced to account for response variations due to earthquake excitations. The results are presented in Table 4-3 and plotted in Fig. 4-6.

Table 4-2. Damping modification factor

Type	β_o	κ
Type A	≤ 0.1625	1.0
	> 0.1625	$1.13-0.51(\pi/2)\beta_o$
Type B	≤ 0.25	0.67
	> 0.25	$0.845-0.446(\pi/2)\beta_o$
Type C	Any value	0.33

Akkar and Miranda (2003), in their critical evaluation of the proposed ATC-40 damping model, concluded that

(1) Maximum inelastic displacements for short period structures are overestimated by a factor of two.
(2) Type A model overestimates the damping and, thus, underestimates the maximum inelastic displacement on average of 30-40% for periods greater than 0.6 *sec*.
(3) Type B and C models overestimate the maximum inelastic displacement for periods greater than 0.6 *sec*.
(4) The overestimations increase as the force reduction factor, *R*, used in current force-based design increases.

4.2.1.2.6 Method 6 – Judi et al. (2002)

Judi et al. (2002) proposed a substitute damping model, similar to Gulkan and Sozen (1974), and recommended that ATC-40 employ a 'substitute damping' model in lieu of the model based on the steady-state bilinear Secant Stiffness method. The results are presented in Table 4-3 and plotted in Fig. 4-6. Blandon and Priestley (2005) pointed out that the use of a substitute damping model is not practical for design purposes since the curve would be different for each earthquake.

4.2.1.2.7 Method 7 – Iwan (2002)

Iwan (2002) presented a revised set of damping and period shift curves based on both random-like far-field and pulse-like near-fault ground motions. These new curves minimize both the mean value of the error and standard deviation. Iwan concluded that the new optimal linearization parameters provide a significant improvement over the

traditional methods based on either response amplitude or performance point error measures, and that the current Capacity Spectrum Method (using the secant stiffness) overestimates both the equivalent period and damping of inelastic systems. Iwan further stated that both methods may predict about the same average response for some range of cases, and that this does not imply they are equally effective outside this region. The results for an elastoplastic SDOF are presented in Table 4-3 and plotted in Fig. 4-6.

4.2.1.2.8 Method 8 – Kwan and Billington (2002)

Kwan and Billington (2002) statistically derived expressions for equivalent damping and period shift based on minimizing the root mean square of errors between the displacement response spectra of the inelastic SDOF and the equivalent SDOF. In this research twenty earthquake motions were used to derive equations applicable to a wide range of hysteretic models. It was recognized that the proposed models are somewhat insensitive to ground motion. Further, it was concluded that the Secant Stiffness method overestimates the period shift and equivalent damping, albeit based on steady-state excitation. Lastly, a modification factor to the viscous damping component was recommended to model the effects of changing stiffness. The results for an elastoplastic SDOF are presented in Table 4-3 and plotted in Fig. 4-6.

4.2.1.2.9 Method 9 – Priestley (2003)

Priestley (2003) proposed damping functions based on steady-state theory for various structural components. In addition, Priestley proposed a modification factor for near-fault earthquakes accompanied by velocity pulses that may reduce the effectiveness

of damping. This factor is applied directly to the Displacement Response spectra for use in his DDBD procedure. This modification factor was subsequently investigated by Bommer and Mendis (2005) who concluded that this modification is appropriate for motions affected by forward directivity. The results for an elastoplastic SDOF are presented in Table 4-3 and plotted in Fig. 4-6.

4.2.1.2.10 Method 10 – Harris (2004)

Harris (2004) proposed a damping modification factor, κ, (see ATC-40) of 0.5 to be applied to the steady-state bilinear Secant Stiffness method for steel beams in moment frames. This value was based on analytical results obtained from inelastic dynamic analysis of four, six, eight and sixteen story frames subjected to twelve time-histories. The results are presented in Table 4-3 and plotted in Fig. 4-6.

This study attempted to represent the inelastic MDOF system damping directly from an effective SDOF independently of the number of yield mechanisms. This implies that all beams yield simultaneously and have the same level of ductility. The simplicity of this approach is more advantageous for design than determining a system-level damping value. However, system-level modal damping is most likely the best approach since it will explicitly account for individual damping mechanisms.

4.2.1.2.11 Method 11 – Blandon and Priestley (2005)

Blandon and Priestley (2005) proposed damping curves for six hysteretic models for use in a DDBD methodology based on an iterative statistical investigation of the

response of a SDOF subjected to six synthetic time-histories. This work was based on employing the approach proposed by Jacobsen and concluded that equivalent damping should be a function of equivalent period. Also, this research reported that a significant inaccuracy exists with most proposed damping equations when predicting the response of very short period frames, $T \leq 0.5 \ sec$. The results are presented in Table 4-3 and plotted in Fig. 4-6 for a bilinear hysteresis.

4.2.1.2.12 Method 12 – Dwairi et al. (2005)

Dwairi and Kowalsky (2004) and Dwairi et al. (2005) conducted an analytical investigation of the applicability of the steady-state equivalent damping approach combined with a period shift represented by the secant stiffness to maximum response. It was concluded that the peak displacement is underestimated due to an overestimation of the equivalent damping and shifting of the hysteresis loop due to residual displacements. This study noted that the overestimation of the damping is proportional to the amount of energy dissipated and ductility level. Damping modification factors were statistically derived and employed to reduce the steady-state equivalent damping measure. The period shift remained constant for simplicity and application in design. The results for an elastoplastic SDOF are presented in Table 4-3 and plotted in Fig. 4-6.

Table 4-3. Equivalent hysteretic damping (SDOF - earthquake excitation)

	Method	Hysteresis	Excitation	1	Equivalent SDOF Properties: Stiffness K_{eq}	Mass M_{eq}	Period T_{eq}	Hysteretic Damping $\zeta_{eq,h}$	Notes	Initial Damping $\zeta_{eq,v}$
1	Resonant Amplitude Matching	Bilinear	Harmonic $\bar{\omega} = \omega_{eq}$	A	K	M	T	$\frac{2}{3\pi}\frac{(\mu_\Delta - 1)(1 - r_\Delta)}{\mu_\Delta^{\,2}}$	Hudson (1965)	0%
2	Gulkan and Sozen (1974)	Takeda (no post-yield stiffness)	Harmonic and 1 EQ Far	E/A	$\frac{abs(a_{max})}{abs(\Delta_{max})} \approx \frac{F_{max}}{\Delta_{max}}$	M	$T\sqrt{\mu_\Delta}$	$0.2\left(1 - \frac{1}{\sqrt{\mu_\Delta}}\right)$	Concrete $\bar{\omega}$ = 13 *Hz*, ω = 16 *Hz* ω_{in} = 10 *Hz*	2%
3	Iwan and Gates (1979), Iwan (1980)	Multiple	12 EQ Far and Near	A	NA	NA	$T\left(1 + 0.121(\mu_\Delta - 1)^{0.939}\right)$	$0.0587(\mu_\Delta - 1)^{0.371}$	T = 0.4-4 *sec*	2%
4	Kowalsky et al. (1994)	Takeda	EQ	E/A	Secant Stiffness $\frac{F_{max}}{\Delta_{max}}$	M	$T_{cr}\sqrt{\frac{\mu_\Delta}{\left(1 + r_\Delta(\mu_\Delta - 1)\right)}}$	$\frac{1}{\pi}\left(1 - \frac{1 - r_\Delta}{\sqrt{\mu_\Delta}} - r_\Delta\sqrt{\mu_\Delta}\right)$	Concrete cr = cracked	5%
5	ATC-40 (1996)	Bilinear	EQ	A	Secant Stiffness $\frac{F_{max}}{\Delta_{max}}$	M	$T\sqrt{\frac{\mu_\Delta}{\left(1 + r_\Delta(\mu_\Delta - 1)\right)}}$	$\kappa\frac{2}{\pi}\frac{(1 - r_\Delta)(\mu_\Delta - 1)}{\mu_\Delta\left(1 + r_\Delta(\mu_\Delta - 1)\right)} = \kappa\beta_o$	Concrete See Table 4-2 for κ	0%
6	Judi et al. (2002)	EPP	EQ	A	Secant Stiffness $\frac{F_{max}}{\Delta_{max}}$	M	$T\sqrt{\mu_\Delta}$	$0.01\left(10.5(\mu_\Delta - 1)^{0.8} + 1.4T - 0.6\right)$	Type A – See ATC-40 $0.4 \le T \le 3$	5%
7	Iwan (2002)	EPP	EQ Far and Near	A	NA	NA	$\mu_\Delta < 4.0$ $T\left(1 + 0.126(\mu_\Delta - 1)^2 - 0.0224(\mu_\Delta - 1)^3\right)$ $\mu_\Delta \ge 4.0$ $T\left(1 + 0.171 + 0.119(\mu_\Delta - 1)\right)$	$\mu_\Delta < 4.0$ $5.07(\mu_\Delta - 1)^2 - 1.08(\mu_\Delta - 1)^3$ $\mu_\Delta \ge 4.0$ $11.7 - 1.58(\mu_\Delta - 1)$	T = 0.1-2 *sec*	?%
8	Kwan and Billington (2003)	EPP	20 EQ	A	NA	NA	$0.8T\sqrt{\mu_\Delta}$	$\frac{0.72}{\pi}\left(1 - \frac{1}{\mu_\Delta}\right)$	T = 0.1-1.5 *sec*	5%
9	Priestley (2003)	EPP		A	Secant Stiffness $\frac{F_{max}}{\Delta_{max}}$	M	$T\sqrt{\mu_\Delta}$	$\frac{1.5}{\pi}\left(1 - \frac{1}{\mu_\Delta}\right)$		5%
10	Harris (2004)	Bilinear	12 EQ Far and Near	A	Secant Stiffness $\frac{F_{max}}{\Delta_{max}}$	M	$T\sqrt{\frac{\mu_\Delta}{\left(1 + r_\Delta(\mu_\Delta - 1)\right)}}$	$\kappa\frac{2}{\pi}\frac{(1 - r_\Delta)(\mu_\Delta - 1)}{\mu_\Delta\left(1 + r_\Delta(\mu_\Delta - 1)\right)}$	Steel $\kappa = 0.5$	2%
11	Brandon (2004), Brandon and Priestley (2005)	Bilinear	6 EQ Articial	A	Secant Stiffness $\frac{F_{max}}{\Delta_{max}}$	M	$T\sqrt{\frac{\mu_\Delta}{\left(1 + r_\Delta(\mu_\Delta - 1)\right)}}$	$\frac{1.23}{\pi}\left(1 - \frac{1}{\sqrt{\mu_\Delta}} - \frac{r_\Delta\mu_\Delta}{10}\right)\left(1 + \frac{1}{(T_{eq} + 0.85)^4}\right)$		0%
12	Kowalsky and Dwairi (2004), Dwairi et al. (2005)	EPP	100 EQ Far and Near	A	Secant Stiffness $\frac{F_{max}}{\Delta_{max}}$	M	$T\sqrt{\mu_\Delta}$	$\frac{C_{EP}}{\pi}\left(1 - \frac{1}{\mu_\Delta}\right)$	$T_{eq} < 1$ $C_{EP} = 0.85 + 0.6(1 - T_{eq})$ $T_{eq} \ge 1$ $C_{EP} = 0.85$	2%

1. A – Analytical, E – Experimental

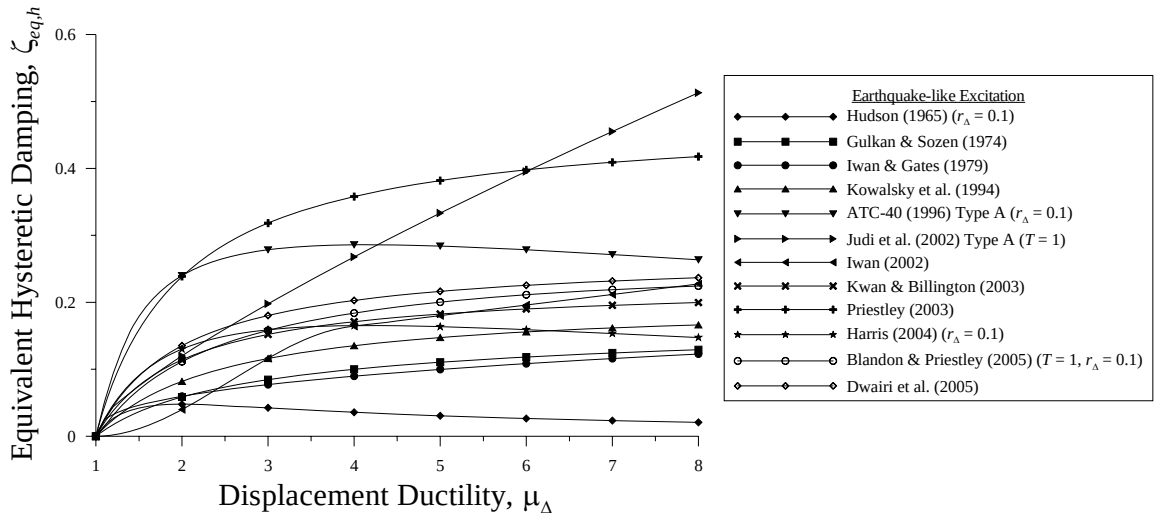

(a) Equivalent hysteretic damping

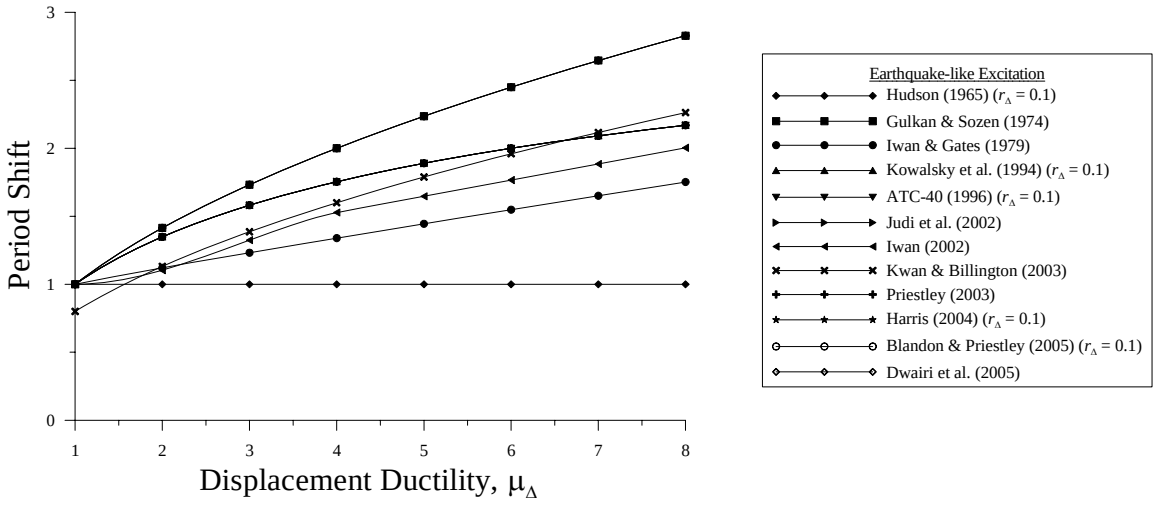

(b) Period shift

Figure 4-6. Equivalent hysteretic damping and period shift (earthquake excitation)

Although only selected response curves have been presented with supporting work, primarily EPP and bilinear, the reader is referred to the referenced works for damping curves for other hysteresis rules. Also, the reader is referred to other works not referenced for additional information (Otani 1981, Fardis and Panagiotakos 1996, Tzan and Pantleides 1998, Calvi 1999, Reddy and Pratap 2000, Riddell et al. 2002).

4.2.1.2.13 Summary

As evident in Fig. 4-6, the presented methods provide widely varying damping measures. This can be related to (1) the hysteresis function used in the derivation (i.e., Takeda, EPP, or bilinear) and (2) the method by which the curve was derived (i.e. secant stiffness, time integration, or statistical). Also, methods that use different period shifts will produce variations in damping curves.

The model proposed by Gulkan and Sozen is based on energy balance whereas Kowalsky et al. is based on Jacobsen's approach using the secant stiffness method and Iwan's method is derived based on statistical error reduction. The resemblance of Iwan's damping curve to that proposed by Gulkan and Sozen is coincidental since the curves were derived by different methods. Therefore, equivalent damping is directly related to the method by which it was derived and the curve should be applied accordingly and used with the respective period shift curves.

Hadjian (1982) proposed that the ratio of energy dissipated per cycle of the inelastic and equivalent SDOF at resonance depends on the product of the equivalent damping and stiffness. Therefore, Miranda and Ruiz-Garcia (2002) concluded that the difference between the normalized damping curves (normalized to T) of Kowalsky et al. (1994), Iwan (1980), and Gulkan and Sozen (1974) is relatively small for ductility levels less than 6. This investigation further concluded that the model presented by ATC-40 (1996) significantly underestimates the maximum inelastic displacements.

Many researchers reported that the concept of equivalent damping provides reasonable results justifying its use in seismic analysis. However, in specific cases when the ground motion is dominated by a single pulse-like excitation (near-fault motion), equivalent damping fails to recognize that the peak displacement is no longer a function of the energy dissipated (Kowalsky and Ayers 2002, Priestley 2003, Bommer and Mendis 2005) and an increase in error is probable. Reflecting on this logic, Priestley (2003) proposed a near-fault damping modification factor for constructing a SDOF displacement response spectrum for various levels of damping.

Furthermore, the concept of energy matching is more applicable to systems where several inelastic cycles that mobilize extensive energy dissipation precede the excursion to peak displacement (Kowalsky and Ayers 2002). The weakness of empirically derived curves based on variable period shifts is that they are not directly related to the design base shear, and, as a result, typically do not consider the hysteresis rule used in design (Dwairi et al. 2005). In the end, empirical equations are not well suited for design purposes.

Based on literature review it appears that an Alternative Secant Stiffness method (ASSM) is most suited for design purposes for earthquake-like excitation where design parameters are directly computed based on equivalent properties. The difference between the Secant Stiffness method (SSM) and ASSM is that equivalent damping is approximated by employing a damping modifier in the latter. All methods presented in Table 4-3 based on the SSM are categorized as an ASSM.

An ASSM is the best choice for DDBD since analysis and design are based on the secant stiffness which is a function of the inelastic displacement. As such, the period shift remains unaltered since it is related to what equivalent properties are used in the analysis and hysteresis loop. The weakness of this approach is that the period shift is based on a monotonic force-displacement response and neglects stiffness degradation due to multiple inelastic cycles. This will also affect the damping value due to proportionality with ductility, a topic for further research.

It can be reasoned that the damping model provided by Blandon and Priestley (2005) or Dwiari et al. (2005) is the most applicable for estimating equivalent damping of an SDOF whose equivalent response is modeled by the secant stiffness. Lastly, the total amount of damping can be estimated with Eq. (4-15).

4.2.2 Equivalent Damping for MDOF Systems

4.2.2.1 Steady-state Harmonic Excitation

To the author's knowledge, there is a limited amount, if any, literature concerning equivalent hysteretic damping in MDOF frames subjected to steady-state harmonic forcing.

4.2.2.2 Earthquake Excitation

The concepts discussed previously for SDOF systems for earthquake-like excitations can also be applied to MDOF systems. It has been proposed for a MDOF system with input energy being dissipated by multiple yielding members that equivalent

damping per yield mechanism can be defined by SDOF response and combined into a system-level damping. The benefit of this approach is that this global value can be used to represent equivalent damping in an effective SDOF.

4.2.2.2.1 Method 1 – Shibata and Sozen (1976)

Shibata and Sozen (1976, 1977) developed a procedure that associates the quantitative measure of each damping mechanism contribution to the system-level damping in proportion to its relative strain energy associated with a desired mode shape. In this 'substitute-structure' approach, system-level damping is referred to as a 'smeared' modal damping and is determined by

$$\zeta_{eq,sys} = \sum_{k=1}^{K} \left(\frac{E_{Seq,k}}{\sum_{k=1}^{K} E_{Seq,k}} \zeta_{eq,k} \right) \tag{4-19}$$

where

$E_{S\,j}$ = Equivalent elastic strain energy of member j

k = Member index

K = Total number of members dissipating input energy

$\zeta_{eq,k}$ in Eq. (4-19) is determined by Method 2 – Gulkan and Sozen (1974), see Table 4-3.

This procedure, or some modified version of, has been adopted into various DDBD methodologies (Kowalsky et al. 1994, Calvi and Kingsley 1995, Calvi and Palese 1995, Priestley and Calvi 1997, Priestley 1998, Loeding et al. 1998a, 1998b, Priestley

and Kowalsky 2000, Kowalsky 2002, Priestley 2003). As a side note, the design engineer must be aware of which ductility (displacement, rotation, curvature, etc.) is used when determining the member-level damping value.

4.2.2.2.2 Method 2 – Decanini et al. (2001)

Decanini et al. (2001) proposed a method to evaluate the hysteretic energy demand on each floor in reference to the story shear. In this study, the system-level hysteretic energy demand of a predetermined MDOF frame was calculated based on response of an effective SDOF (pushover curve) and then allocated to each floor by

$$E_{H,i} = \left(\frac{\alpha_i}{\sum_{i=1}^{n} \alpha_i} \right) E_{H,sys} \tag{4-20}$$

where

$E_{H,i}$ = Hysteretic energy demand of floor *i*

$E_{H,sys}$ = Total hysteretic energy demand

α_i = Story coefficient $= V_{yi}\delta_{yi}\left(\mu_{\delta i} - 1\right)$ (EPP response)

This suggests that system-level energy dissipation can be represented by first mode response. The limitation here is that variations in ductility demands imposed by higher modes are not accounted. It was shown that this difference is small in frames less than eight stories. Though this study evaluated hysteretic energy demands per floor, a procedure to estimate hysteretic damping per floor or system was not presented.

This method is more advantageous for integration into DDBD than the method proposed by Shibata and Sozen since it explicitly models contributions from floor ductility demands. It seems plausible to adopt this philosophy by evaluating the hysteresis loops of each floor. As a result, the frame could be discretized into an array of SDOF systems: one SDOF for each floor and one array for each mode of vibration. In so doing, an equivalent damping methodology developed for a SDOF could be applied to each floor.

In adopting this approach into DDBD, a system-level modal damping can be computed to represent the measure of damping in the effective SDOF. This approach would be best suited for new construction where the entire floor can be designed as an integrated assembly in order to achieve the desired displacement ductility. As such, plastic hinges in a floor would be designed to develop simultaneously so that a force-displacement response, such as that shown in Fig. 4-2, could be constructed. The following section outlines the proposed equivalent damping procedure for MDOF frames based on the previous suggestion.

4.3 Determination of Equivalent Damping for MDOF Frames

The literature review discussed several methodologies available for quantifying the degree of equivalent damping. A majority of the procedures were derived based on the response of an inelastic SDOF system. As is, they are not easily adaptable to MDOF systems. Though a couple procedures have been proposed for multi-story frames, there remains a need in adopting a procedure into a seismic design scenario.

Due to the large number of damping methodologies proposed for a SDOF, it is conceivable that a straightforward approach for a MDOF could be based on SDOF response. Many researchers investigating equivalent linearization methods have adopted this concept and use a system-level force-displacement response of an effective SDOF or base shear – roof displacement response to estimate equivalent damping. These approaches, while simple and advantageous, neglect the ductility contributions of each yield mechanism or, on a larger scale, floor ductility contributions.

The following discussion proposes a methodology to compute the level of equivalent damping to be used for design of steel moment frames in the proposed DDBD procedure. Since DDBD uses the secant stiffness to determine response amplitudes, the proposed methodology is based on an ASSM (see Section 4.2.1.2.13). The first part of this discussion deals with inelastic SDOF frames subjected to steady-state harmonic force excitation. Subsequently, the methodology is adapted to inelastic multi-story frames. The discussion concludes with the integration of the methodology into the proposed DDBD procedure.

An elastic frame subjected to an external force of sufficient magnitude to generate internal resisting forces in excess of the yield capacity of the comprising structural components will cause the frame to develop plastic hinges at these ‘over stressed’ locations as illustrated in Fig. 4-7(a). Frame response in this condition is governed by inelastic behavior and the frame is referred to as an ‘inelastic frame’.

Energy input into an inelastic frame is dissipated through yielding of structural components and viscous damping inherent in the frame. It has been proposed by researchers that hysteretic damping can be modeled as viscous damping. In so doing, the inelastic frame is replaced with an equivalent elastic frame as illustrated in Fig. 4-7(b). The total energy dissipated by the inelastic frame is modeled by equivalent damping, ζ_{eq}, in the equivalent elastic frame. Alternatively, a fictitious equivalent linear damper, c_{eq}, can be used to model damping as shown in Fig. 4-7(b). Two possible damper locations are illustrated: (1) based on story drifts (Method 1) and (2) based on relative displacement with the base (Method 2). These methods are discussed subsequently.

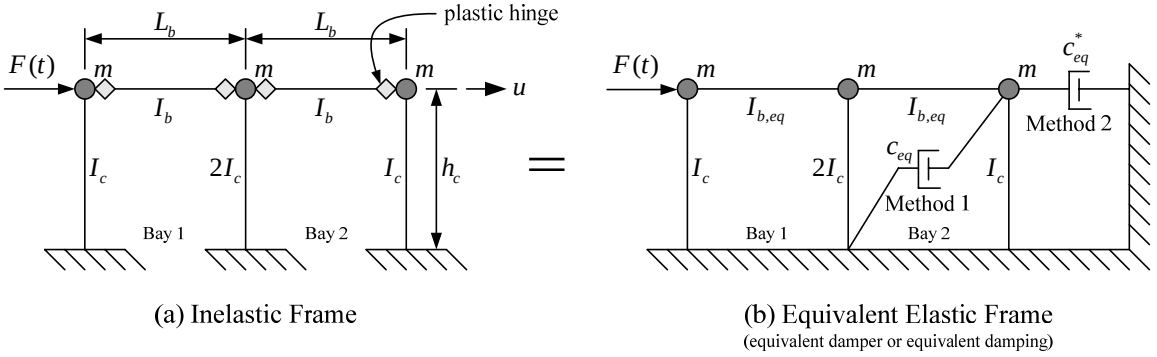

Figure 4-7. Frame schematic (one-story)

The goal of this linearization procedure is to provide an equivalent elastic frame whose maximum elastic responses will match the peak displacements and forces of the inelastic frame. Many linearization techniques for inelastic frames have been proposed since 1960. Of these methods, DDBD utilizes the Secant Stiffness method (SSM) to develop the equivalent elastic frame. The SSM is preferred over other methods for its graphical simplicity and ease of integration into a design scenario.

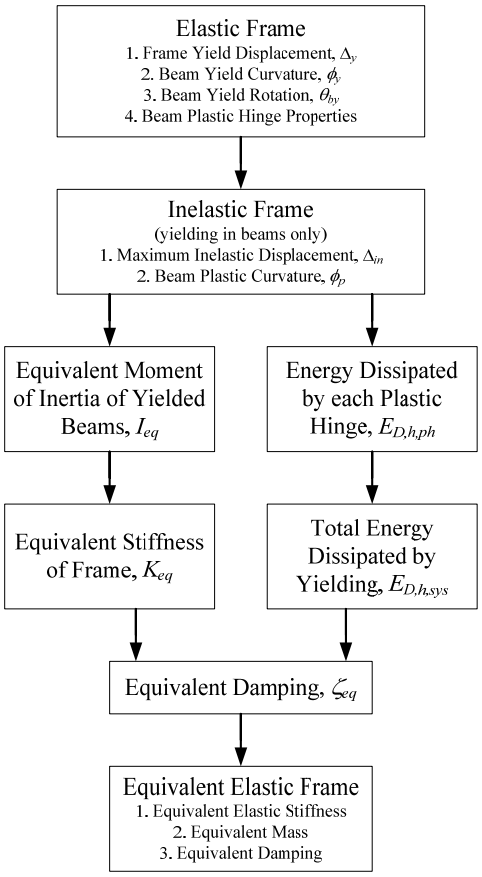

Figure 4-8. Flowchart of Secant Stiffness method (inelastic SDOF frame)

Prior to discussing the concept of equivalent damping as applied to an inelastic MDOF frame and integration into DDBD of a steel moment frame, it is important to illustrate its application to a SDOF inelastic frame. This will allow grounds for error to be identified and rectified.

4.3.1 Harmonic Forcing Excitation – SDOF Inelastic Frames

The flowchart in Fig. 4-8 outlines the SSM as applied to an inelastic moment frame that can be modeled as a SDOF.

4.3.1.1 Equivalent Elastic Frame

To construct the equivalent elastic frame, shown in Fig. 4-7(b), inelastic members (beams in this example) are replaced by equivalent elastic members. This conversion is achieved by taking the secant stiffness of the moment-rotation response of the inelastic member and computing an equivalent Moment of Inertia, I_{eq} (see Fig. 4-9).

$$I_{eq} = \frac{I}{\mu_\theta}\left(1 + r_\theta\left(\mu_\theta - 1\right)\right) \tag{4-21}$$

Eq. (4-21) assumes that both member ends maintain equal rotation ductility. The stiffness of the equivalent elastic frame, K_{eq}, can then be determined by structural analysis.

4.3.1.2 Hysteretic Energy Dissipation

In reference to Fig. 4-7(a), the hysteretic energy dissipated by a plastic hinge though yielding, $E_{D,h,ph}$, in one cycle of steady-state response is the area enclosed by its moment-rotation hysteresis loop, $A_{hyst,ph}$, shown in Fig. 4-9.

$$E_{D,h,ph} = A_{hyst,ph} = 4M_p\theta_{by}\left(\mu_\theta - r_\theta\left(\mu_\theta - 1\right) - 1\right) \tag{4-22}$$

where

μ_θ = rotation ductility of hinge $\left(= \dfrac{\left(\phi - \phi_y\right)\ell_p}{\theta_{by}} + 1 \approx \dfrac{\phi_p}{\phi_y}\dfrac{6d_b}{L} + 1 \right)$ (4-22a)

r_θ = post-yield stiffness ratio - Eq. (3-10)

Eq. (4-22a) assumes the plastic hinge length, ℓ_p, is equal to the depth of the beam, d_b.

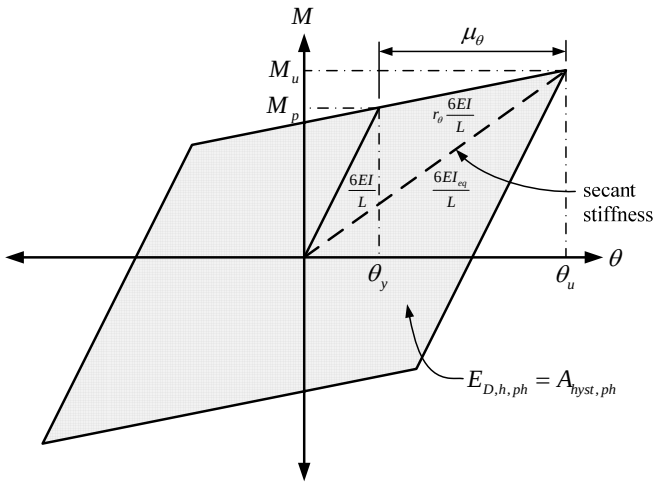

Figure 4-9. Moment-rotation hysteresis loop

The total amount of energy dissipated by hysteretic damping is the sum of the dissipated energies of all plastic hinges.

$$E_{D,h,sys} = \sum_{k=1}^{K} E_{D,h,ph,k} \tag{4-23}$$

where

k = Hinge index

K = Number of hinges

4.3.1.3 Equivalent Hysteretic Damping

Based on elastic harmonic theory, the energy dissipated by equivalent hysteretic damping (i.e., viscous) of the equivalent elastic frame in one cycle of steady-state response, shown in Fig. 4-10, is

$$E_{D,h,eq} = 2\pi\eta_{eq}\zeta_{eq,h}K_{eq}\Delta_{in}{}^{2} \tag{4-24}$$

The equivalent mass, M_{eq}, to define η_{eq} in Eq. (4-24) is taken equal to the mass, M.

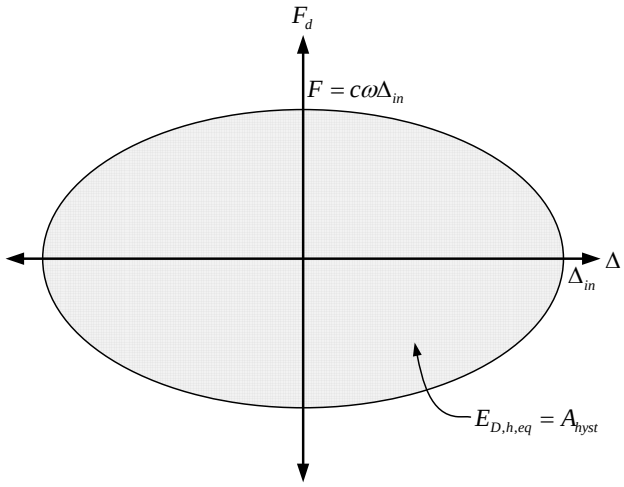

Figure 4-10. Equivalent hysteretic damping hysteresis (elastic)

The energy dissipated by the inelastic and equivalent elastic frame must be the same at the peak displacement. Equating the two values, $E_{D,h,sys} = E_{D,h,eq}$, the equivalent hysteretic damping ratio and constant are

$$\zeta_{eq,h} = \frac{E_{D,h,sys}}{2\pi\eta_{eq}K_{eq}\Delta_{in}{}^{2}} \tag{4-25}$$

$$C_{eq,h} = 2\zeta_{eq,h}\sqrt{K_{eq}M_{eq}} = 2\zeta_{eq,h}\omega_{eq}M_{eq} = \frac{E_{D,h,sys}}{\pi\bar{\omega}\Delta_{in}{}^{2}} \tag{4-26}$$

4.3.1.4 One-Story Example

Take for example the one-story frame shown in Fig. 4-7(a). System properties are:

Frame Properties:	Hinge Properties:	Dynamic Properties:
$E = 29000\ ksi$	$d_b = 24\ in$	$m = 0.647$
$I_c = 500\ in^4$	$M_p = 4792\ in\text{-}kip$	$m_i = 1.941$
$I_b = 1000\ in^4$	$\phi_y = 0.000165$	$K = 163.64\ k/in$
$h_c = 144\ in$	$\theta_y = 0.00793\ rad$	$T = 0.685\ sec$
$L_b = 288\ in$	$r_\phi = 0.013$	$\omega = 9.167\ rad/sec$
$F_y = 310\ kips$	$r_\theta = 0.026$	$\zeta_v =$ 0% (undamped)
$\Delta_y = 1.9\ in$		
$r_\Delta = 0.4$		

Beams are assumed axially rigid and no gravity load is applied to the system. The nodal masses are set only for horizontal inertia. Energy dissipation occurs only through hysteretic damping and yielding occurs only in the beam ends. Beam length, L, is taken equal to the bay length, L_b, for simplicity.

Table 4-4. Harmonic forcing functions

Index	F *kips*	F/F_y	Excitation Frequency, $\bar{\omega}$ *rad/sec*	Tabulated Results
Case 1	400	1.29	Case A - 0.5π	Table 4-2
Case 2	380	1.23	Case B - π	Table 4-3
Case 3	360	1.16	Case C - 1.5π	Table 4-4
Case 4	340	1.10	Case D - 1.75π	Table 4-5
Case 5	320	1.03	Case E - 2π	Table 4-6
Case 6	300	0.97	Case F - 2.5π	Table 4-7
Case 7	280	0.90	Case G- 3π	Table 4-8
Case 8	260	0.84	Case H – 4π	Table 4-9

The frame is subjected to the harmonic force cases listed in Table 4-4 in an inelastic dynamic analysis. Tables 4-5 to 4-12 present the results of the dynamic analysis and the results from Eq. (4-27) for the equivalent elastic frame with properties computed from Eqs. (4-21) to (4-26).

$$u(t) = \frac{F}{K_{eq}}\left(\frac{\left(1-\eta_{eq}{}^2\right)\sin\bar{\omega}t - 2\zeta_{eq}\eta_{eq}\cos\bar{\omega}t}{\left(1-\eta_{eq}{}^2\right)^2 + \left(2\zeta_{eq}\eta_{eq}\right)^2}\right) \tag{4-27}$$

ζ_{eq} in Eq. (4-27) is equal to $\zeta_{eq,h}$ in this example.

Table 4-5. Analysis results (CASE 1)

	Inelastic Frame			Equivalent Elastic Frame (SDOF)							% Difference	
$\overline{\omega}$ *rad/sec*	Δ_{in} *in*	μ_θ	$E_{D,h,sys}$ *in-kips*	$I_{b,eq}$ *in^4*	K_{eq} *k/in*	η_{eq}	ζ_{eq}	c_{eq}	Δ_{eq} *in*	$E_{D,h,eq}$ *in-kips*	Δ	E_D
0.5π	5.40	5.36	2581	208	100	0.22	65	17.97	4.03	1443	-25.2	-44.1
π	4.77	4.62	2144	237	104	0.43	34	9.56	4.44	1858	-6.9	-13.4
1.5π	10.56	11.83	6409	109	83	0.72	15	3.88	9.15	4815	-13.3	-24.9
1.75π	43.50	53.21	30912	45	69	0.92	4	0.95	33.89	18760	-22.1	-39.3
2π	35.14	42.50	24570	49	70	1.04	4	1.01	44.73	39809	27.3	62.0
2.5π	8.93	9.81	5215	126	86	1.18	10	2.65	10.06	6624	12.7	27.0
3π	5.05	4.93	2325	224	102	1.30	11	3.09	5.27	2533	4.4	8.9
4π	2.46	1.70	415	599	141	1.47	5	1.74	2.39	394	-2.6	-5.1

Table 4-6. Analysis results (CASE 2)

	Inelastic Frame			Equivalent Elastic Frame (SDOF)							% Difference	
$\overline{\omega}$ *rad/sec*	Δ_{in} *in*	μ_θ	$E_{D,h,sys}$ *in-kips*	$I_{b,eq}$ *in^4*	K_{eq} *k/in*	η_{eq}	ζ_{eq}	c_{eq}	Δ_{eq} *in*	$E_{D,h,eq}$ *in-kips*	Δ	E_D
0.5π	5.04	4.93	2325	224	102	0.216	66	18.52	3.75	1282	-25.7	-44.9
π	4.05	3.70	1599	289	111	0.415	34	9.88	3.91	1493	-3.4	-6.7
1.5π	9.27	10.19	5442	122	85	0.711	17	4.28	8.12	4182	-12.3	-23.1
1.75π	39.31	47.98	27812	47	70	0.917	4	1.04	30.52	16763	-22.4	-39.7
2π	32.95	39.84	22993	51	71	1.041	5	1.07	42.21	37734	28.1	64.1
2.5π	8.58	9.41	4978	130	87	1.175	11	2.74	9.64	6291	12.4	26.4
3π	4.88	4.71	2198	233	104	1.290	11	3.12	5.07	2378	4.0	8.2
4π	2.37	1.59	349	639	144	1.460	5	1.57	2.31	332	-2.5	-4.9

Table 4-7. Analysis results (CASE 3)

	Inelastic Frame			Equivalent Elastic Frame (SDOF)							% Difference	
$\overline{\omega}$ *rad/sec*	Δ_{in} *in*	μ_θ	$E_{D,h,sys}$ *in-kips*	$I_{b,eq}$ *in^4*	K_{eq} *k/in*	η_{eq}	ζ_{eq}	c_{eq}	Δ_{eq} *in*	$E_{D,h,eq}$ *in-kips*	Δ	E_D
0.5π	4.67	4.45	2042	245	105	0.213	66	18.96	3.45	1113	-26.2	-45.5
π	3.26	2.69	1003	388	123	0.395	31	9.56	3.34	1053	2.5	5.0
1.5π	7.94	8.55	4471	140	89	0.697	18	4.80	7.08	3557	-10.8	-20.4
1.75π	34.85	42.29	24444	49	70	0.913	5	1.17	27.03	14702	-22.4	-39.9
2π	30.82	37.26	21470	53	71	1.039	5	1.15	39.52	35303	28.2	64.4
2.5π	8.21	8.89	4674	136	88	1.167	11	2.81	9.29	5981	13.1	28.0
3π	4.71	4.52	2085	242	105	1.283	11	3.18	4.87	2228	3.4	6.9
4π	2.29	1.49	292	678	146	1.447	4	1.41	2.23	277	-2.7	-5.3

Table 4-8. Analysis results (CASE 4)

	Inelastic Frame			Equivalent Elastic Frame (SDOF)							% Difference	
$\overline{\omega}$	Δ_{in}	μ_θ	$E_{D,h,sys}$	$I_{b,eq}$	K_{eq}	η_{eq}	ζ_{eq}	c_{eq}	Δ_{eq}	$E_{D,h,eq}$	Δ	E_D
rad/sec	*in*		*in-kips*	in^4	*k/in*				*in*	*in-kips*		
0.5π	4.21	3.87	1700	278	110	0.209	67	19.47	3.13	941	-25.6	-44.7
π	2.47	1.72	424	594	141	0.369	21	7.02	2.75	525	11.3	23.9
1.5π	6.57	6.82	3446	169	94	0.678	20	5.40	6.01	2885	-8.5	-16.3
1.75π	29.94	36.05	20754	53	71	0.907	6	1.34	23.32	12595	-22.1	-39.3
2π	28.66	34.45	19804	55	72	1.035	5	1.22	36.87	32767	28.6	65.5
2.5π	7.85	8.43	4401	142	89	1.160	11	2.90	8.88	5639	13.2	28.1
3π	4.54	4.34	1979	251	106	1.275	11	3.24	4.65	2078	2.5	5.0
4π	2.20	1.40	237	722	149	1.434	4	1.24	2.14	224	-2.8	-5.4

Table 4-9. Analysis results (CASE 5)

	Inelastic Frame			Equivalent Elastic Frame (SDOF)							% Difference	
$\overline{\omega}$	Δ_{in}	μ_θ	$E_{D,h,sys}$	$I_{b,eq}$	K_{eq}	η_{eq}	ζ_{eq}	c_{eq}	Δ_{eq}	$E_{D,h,eq}$	Δ	E_D
rad/sec	*in*		*in-kips*	in^4	*k/in*				*in*	*in-kips*		
0.5π	2.91	2.26	746	457	129	0.192	56	17.83	2.51	552	-14.0	-26.0
π	2.02	1.15	88	873	157	0.349	6	2.20	2.31	116	14.4	30.9
1.5π	5.20	5.13	2443	216	101	0.653	22	6.11	4.94	2209	-4.9	-9.6
1.75π	24.59	29.35	16786	60	73	0.899	7	1.61	19.38	10423	-21.2	-37.9
2π	26.51	31.85	18264	57	72	1.031	6	1.32	33.83	29750	27.6	62.9
2.5π	7.51	8.01	4149	148	90	1.153	11	2.98	8.45	5260	12.6	26.8
3π	4.37	4.09	1827	265	108	1.264	11	3.23	4.49	1928	2.7	5.6
4π	2.12	1.30	175	778	152	1.418	3	0.99	2.06	165	-2.7	-5.4

Table 4-10. Analysis results (CASE 6)

	Inelastic Frame			Equivalent Elastic Frame (SDOF)							% Difference	
$\overline{\omega}$	Δ_{in}	μ_θ	$E_{D,h,sys}$	$I_{b,eq}$	K_{eq}	η_{eq}	ζ_{eq}	c_{eq}	Δ_{eq}	$E_{D,h,eq}$	Δ	E_D
rad/sec	*in*		*in-kips*	in^4	*k/in*				*in*	*in-kips*		
0.5π	1.89	1.00	0	1000	163	0.171	0	0.00	1.89	0	0	0
π	1.94	1.05	33	949	161	0.345	2	0.87	2.11	38	8.8	18.3
1.5π	3.92	3.51	1489	303	113	0.618	22	6.55	3.93	1496	0.2	0.5
1.75π	18.80	22.15	12522	70	75	0.885	9	2.05	15.14	8116	-19.5	-35.2
2π	24.39	29.10	16637	60	73	1.027	6	1.42	30.78	26505	26.2	59.3
2.5π	7.16	7.57	3892	155	91	1.146	12	3.08	8.01	4869	11.8	25.1
3π	4.20	3.89	1710	277	110	1.254	11	3.27	4.29	1777	1.9	3.9
4π	2.02	1.17	101	858	157	1.399	2	0.62	1.99	97	-1.8	-3.6

Table 4-11. Analysis results (CASE 7)

	Inelastic Frame			Equivalent Elastic Frame (SDOF)							% Difference	
$\overline{\omega}$	Δ_{in}	μ_θ	$E_{D,h,sys}$	$I_{b,eq}$	K_{eq}	η_{eq}	ζ_{eq}	c_{eq}	Δ_{eq}	$E_{D,h,eq}$	Δ	E_D
rad/sec	*in*		*in-kips*	in^4	*k/in*				*in*	*in-kips*		
0.5π	1.77	1.00	0	1000	163	0.171	0	0.00	1.77	0	0	0
π	1.92	1.02	12	981	162	0.344	1	0.33	1.96	12	1.9	3.9
1.5π	2.92	2.27	751	456	129	0.577	19	5.95	3.09	842	5.9	12.1
1.75π	12.68	14.47	7975	94	80	0.857	12	2.87	10.61	5582	-16.3	-30.0
2π	22.18	26.36	15016	63	73	1.021	6	1.55	27.34	22812	23.3	51.9
2.5π	6.81	7.15	3643	163	93	1.137	12	3.19	7.57	4506	11.2	23.7
3π	4.03	3.68	1589	291	111	1.244	11	3.30	4.08	1630	1.3	2.6
4π	1.93	1.04	24	962	162	1.378	0	0.16	1.93	24	-0.3	-0.6

Table 4-12. Analysis results (CASE 8)

	Inelastic Frame			Equivalent Elastic Frame (SDOF)							% Difference	
$\overline{\omega}$	Δ_{in}	μ_θ	$E_{D,h,sys}$	$I_{b,eq}$	K_{eq}	η_{eq}	ζ_{eq}	c_{eq}	Δ_{eq}	$E_{D,h,eq}$	Δ	E_D
rad/sec	*in*		*in-kips*	in^4	*k/in*				*in*	*in-kips*		
0.5π	1.64	1.00	0	1000	163	0.171	0	0.00	1.64	0	0	0
π	1.81	1.00	0	1000	163	0.343	0	0.00	1.81	0	0	0
1.5π	2.32	1.53	313	663	145	0.544	12	3.92	2.50	363	7.7	16.0
1.75π	6.79	7.11	3617	163	93	0.796	17	4.55	6.16	2979	-9.2	-17.6
2π	19.91	23.56	13355	68	74	1.015	7	1.71	23.71	18944	19.1	41.9
2.5π	6.44	6.67	3359	172	94	1.128	12	3.28	7.16	4156	11.2	23.7
3π	3.86	3.49	1475	305	113	1.234	11	3.34	3.88	1485	0.3	0.7
4π	1.81	1.00	0	1000	163	1.371	0	0.00	1.81	0	0	0

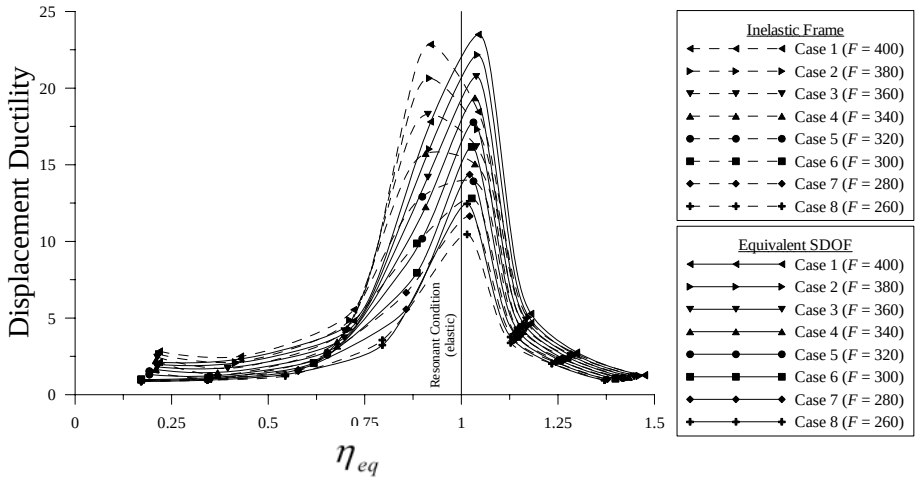

Figure 4-11. Displacement ductility comparison

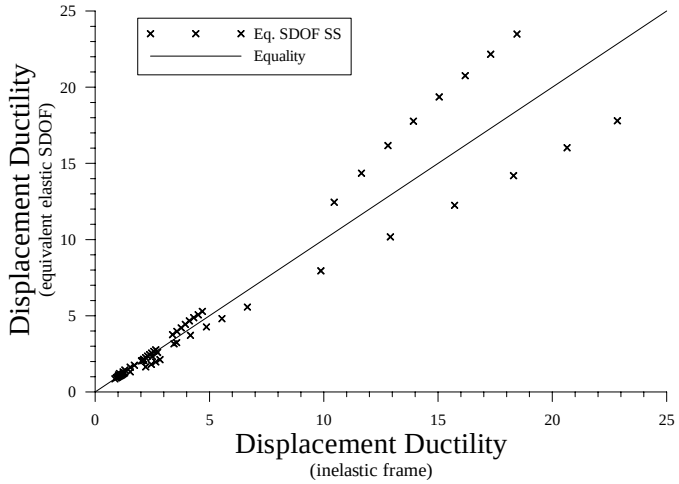

Figure 4-12. Displacement ductility comparison

Plotting displacement ductility responses, Figs. 4-11 and 4-12, large variations are evident at high displacement ductility levels, albeit outside the range of expected ductility of seismic resistant steel moment frames. Although ductility is a measure of inelastic response, it is used here to define the response of the equivalent elastic frame for comparison convenience. It is noticed that this procedure underestimates the displacement when $\eta_{eq} < 1.0$ and overestimates the displacement when $\eta_{eq} > 1.0$.

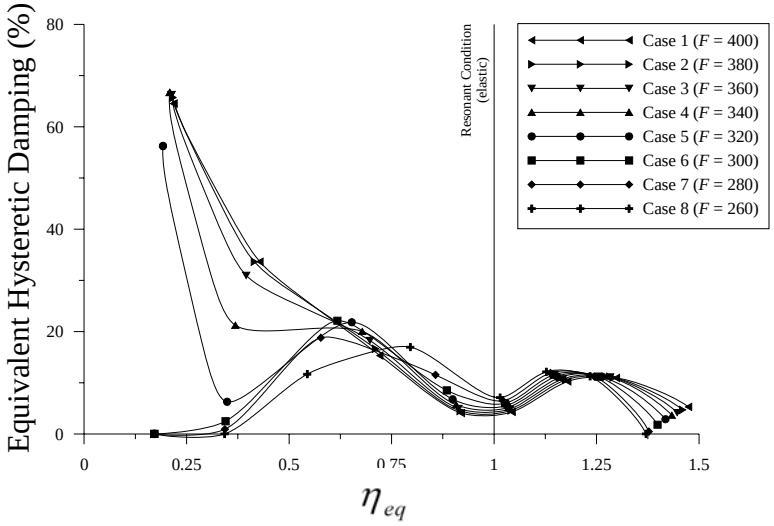

Figure 4-13. Equivalent hysteretic damping

Fig. 4-13 plots the equivalent hysteretic damping results as a function of equivalent frequency ratio for each force magnitude. Equivalent hysteretic damping is a function of force magnitude (i.e., input energy), equivalent frequency ratio, and ductility. It can be postulated that equivalent hysteretic damping reaches a minimum at the resonant condition. Furthermore, damping is not equal for the same ductility when $\eta_{eq} \leq 1$ and $\eta_{eq} \geq 1$. Consequently, assuming a resonant condition, $\eta_{eq} = 1$, for all cases can result in large variations between predicted and actual levels of damping. This topic is

discussed in more detail subsequently in Section 4.3.1.1.6. Fig. 4-14 expands Fig. 4-13 as a function of force ratio for spatial clarity.

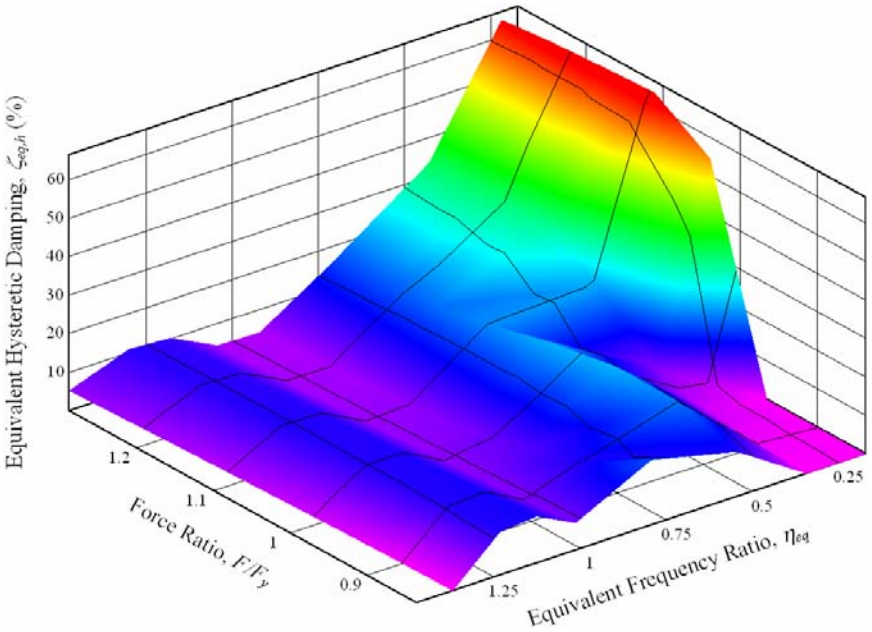

Figure 4-14. Equivalent hysteretic damping (spatial distribution)

It is evident from the results that the peak displacements of the two systems do not correspond with upwards of 26% difference. As a result, the energy dissipated by the two systems is not in accord with up to 45% variation. Further investigation is required to identify possible sources for such error.

4.3.1.5 Investigation of Sources of Error Using SSM

Fig. 4-15 illustrates the story shear-displacement response of the two systems for one cycle of steady-state response for Case 3-C (F = 360 *kips*, $\bar{\omega} = 1.5\pi$ *rad/sec*). Although considerable difference (10.8%) is noticed between maximum displacements achieved by the two systems, it is evident that the equivalent elastic stiffness is in

accurate agreement with the 'fictitious' secant stiffness of the inelastic frame. Equivalent stiffness can consequently be interpreted as a function only of the geometry of the hysteresis loop independent of rotation ductility of the beams and mass.

$$K_{eq} = K\left(\frac{1+r_{\Delta}\left(\mu_{\Delta}-1\right)}{\mu_{\Delta}}\right) \text{ (see Eq. (2-20))} \tag{4-28}$$

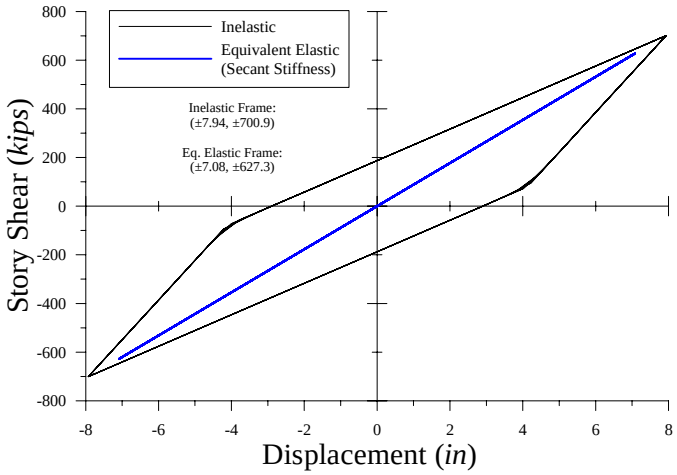

Figure 4-15. Steady-state story shear-displacement response (Case 3-C)

Assuming the mass remains constant, $M_{eq} = M$ during inelastic response the equivalent period shift and frequency shift are

$$\underbrace{\frac{T_{eq}}{T}}_{\substack{period\\shift}} = \sqrt{\frac{\mu_{\Delta}}{1+r_{\Delta}\left(\mu_{\Delta}-1\right)}} = \underbrace{\frac{\omega}{\omega_{eq}}}_{\substack{frequency\\shift}} \tag{4-29}$$

Fig. 4-16 plots the period shift results as a function of displacement ductility against Eq. (4-29). Excellent agreement exists between the results and the theoretical solution.

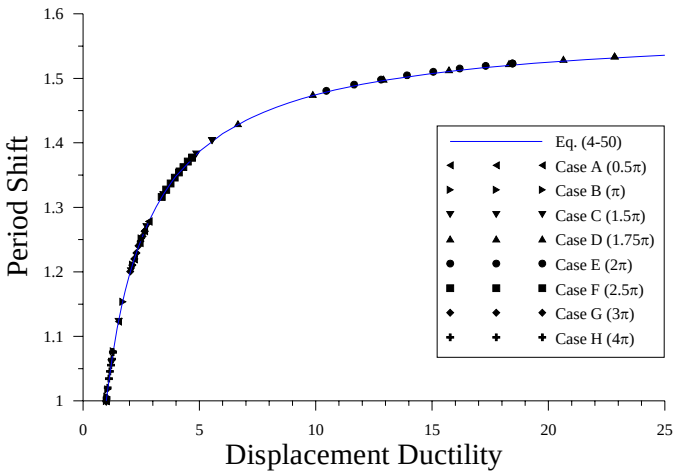

Figure 4-16. Period shift (SSM)

The area enclosed by the story shear-displacement hysteresis loop shown in Fig. 4-15 is 4522 *in-kip* (see Eq. (4-30).

$$A_{hyst} = 4V_y\Delta_y\left(\mu_\Delta - r_\Delta\left(\mu_\Delta - 1\right) - 1\right) = 4522 \ \textit{in-kips} = E_{D,h,sys} \tag{4-30}$$

This value is, for all intents and purpose, equal to the summed area of all moment-rotation hysteresis loops ($E_{D,h,sys} = 4471$ *in-kip*). The difference, though negligible, is due to additional lateral displacement due to column deformations which is not considered in the area of hysteresis loops of the plastic hinges. The energy dissipated by plastic work from the inelastic analysis is 4562 *in-kip*. Consequently, the quantitative amount of energy dissipated by hysteretic damping can be approximated using displacement ductility in lieu of rotation ductility. Eq. (4-25) can be rewritten as

$$\zeta_{eq,h} = \frac{E_{D,h,sys}}{2\pi\eta_{eq}K_{eq}{\Delta_{in}}^2} = \frac{2}{\pi}\frac{\left(1-r_\Delta\right)\left(\mu_\Delta - 1\right)}{\mu_\Delta\left(1+r_\Delta\left(\mu_\Delta - 1\right)\right)}\frac{1}{\eta_{eq}} \tag{4-31}$$

Fig. 4-17 plots the frequency-dependent equivalent hysteretic damping results as a function of displacement ductility against Eq. (4-31). Excellent agreement exists between the results and the theoretical solution. Also plotted in Fig. 4-17 is Eq. (4-31) assuming a resonant condition, $\eta_{eq} = 1$, is maintained. This assumption can lead to significant variation in predicted and actual damping levels. Still, relatively large variations in maximum displacements and energy dissipated are evident between the inelastic frame and equivalent elastic frame.

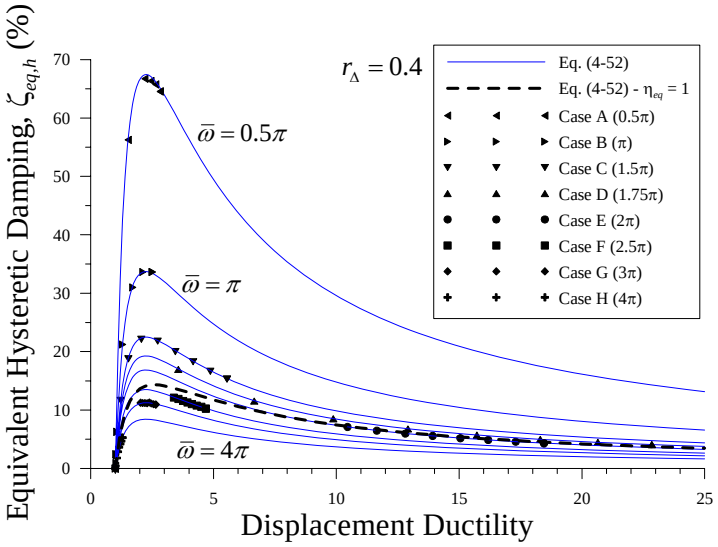

Figure 4-17. Equivalent hysteretic damping (SSM)

Two conclusions can be drawn as a result of the previous example. First, a resonant condition, $\eta_{eq} = 1$, leads to maximum ductility but does not coincide with the resonant damping condition. Two resonant damping conditions transpire dependent on η_{eq} and force ratio. Secondly, the objective of the SSM is to provide an equivalent elastic frame that achieves the same displacement and force as an inelastic frame. It is apparent from the previous example that applying this methodology (with constant mass assumed)

leads to theoretical agreement while resulting in discrepancies in maximum displacements and energy dissipation.

Based on the work by Kryloff and Bogoliuboff (1943), Caughey (1960) derived a theoretical steady-state frequency ratio, η, for an inelastic SDOF with a bilinear hysteresis loop using the method of slowly varying parameters.

$$\eta^2 = \underbrace{1+\gamma\left(\frac{\theta}{\pi}-\frac{\sin 2\theta}{2\pi}-1\right)}_{\text{resonant frequency shift }(\Psi)} \pm \gamma\sqrt{\left(\frac{F}{\gamma F_y \mu_\Delta}\right)^2 - \left(\frac{\sin^2\theta}{\pi}\right)^2} \tag{4-32}$$

where

Ψ = Resonant frequency shift (defined in above) (4-32a)

γ = $1-r_\Delta$ ($\gamma = 1$ - elastoplastic, $\gamma = 0$ - elastic) (4-32b)

θ = $\cos^{-1}\left(1-\frac{2}{\mu_\Delta}\right)$ (4-32c)

Fig. 4-18 plots the displacement ductility of the inelastic frame against the theoretical solution derived by Caughey (displacement ductility is limited to six for graphical clarity). Agreement is shown to exist between the results with the exception of very low excitation frequencies. This effect is due to the presence of transient waves in displacement response of the inelastic frame.

The resonant frequency shift (Caughey (Eq. (4-32a)) and Secant Stiffness (Eq. (4-29)) are additionally illustrated in Fig. 4-18. The period shifts of the two methods do not correspond. Since equivalent stiffness is a function of geometry of the hysteresis loop and

independent of mass, it can be reasoned that the assumption of constant mass is inconsistent thus leading to variation in peak displacement and force. In an attempt to minimize this error, a Modified Secant Stiffness method is proposed.

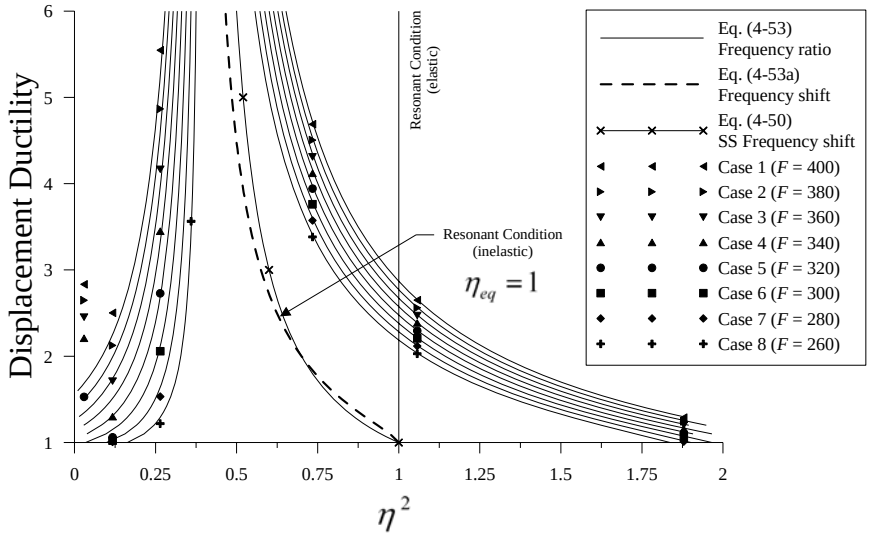

Figure 4-18. Displacement ductility response

4.3.1.6 Modified Secant Stiffness Method

It is proposed that in the Modified Secant Stiffness method (MSSM) the mass of the inelastic frame and equivalent mass of the equivalent elastic frame vary. Based on the solution derived by Caughey and using the secant stiffness (Eq. (4-28)), the equivalent mass ratio at the equivalent resonant frequency ratio, $\eta_{eq} = 1$ (see Fig. 4-18), is

$$\frac{M_{eq}}{M} = \frac{\left(1 + r_{\Delta}\left(\mu_{\Delta} - 1\right)\right)}{\mu_{\Delta}\Psi} \tag{4-33}$$

Fig. 4-19 plots the equivalent mass ratio as a function of displacement ductility and post-yield stiffness ratio, r_{Δ}. The equivalent mass ratios of the one-story example

frame are additionally plotted in the figure. Although it appears that the change in mass is negligible for the example frame ($r_\Delta = 0.4$), smaller post-yield stiffness ratios require greater mass ratios.

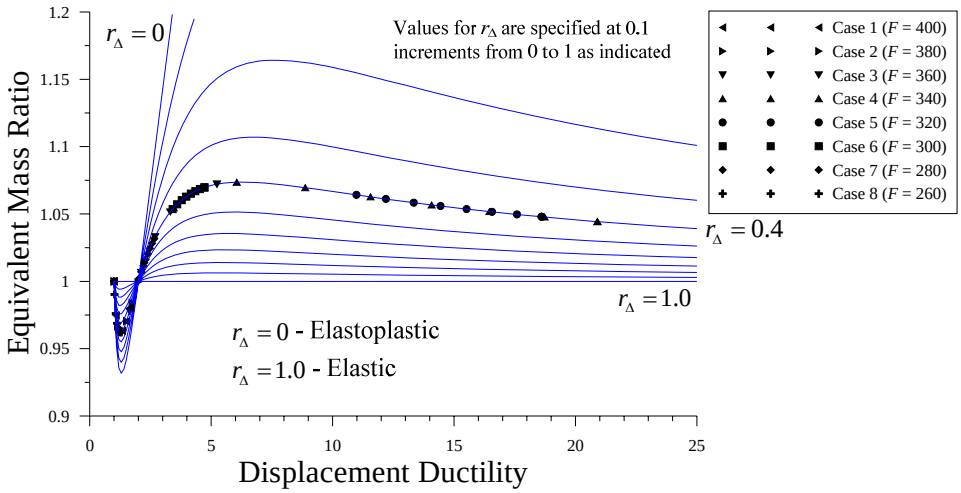

Figure 4-19. Equivalent mass ratio (MSSM)

Hadjian (1982) first proposed this modification (change in mass) and expressed it graphically for an elastoplastic system which illustrated that equivalent mass increases as displacement ductility increases. This conclusion was independent of excitation frequency, $\bar{\omega}$, (i.e., resonant condition was assumed) and was not numerically proven.

Similar to Eq. (4-32), the equivalent frequency ratio can be expressed as

$$\eta_{eq}^{\ 2} = 1 \pm \frac{\gamma \sqrt{\left(\frac{F}{\gamma F_y \mu_\Delta}\right)^2 - \left(\frac{\sin^2 \theta}{\pi}\right)^2}}{\Psi} \tag{4-34}$$

By superimposing Eqs. (4-32) and (4-34) it can be reasoned that the frequency shift remains constant independent of excitation frequencies, see Fig. 4-20 (displacement

ductility is limited to six for graphical clarity). This characteristic is evident when examining the method in which Eq. (4-34) was derived. It is therefore assumed that the equivalent mass ratio is not also a function of excitation frequency.

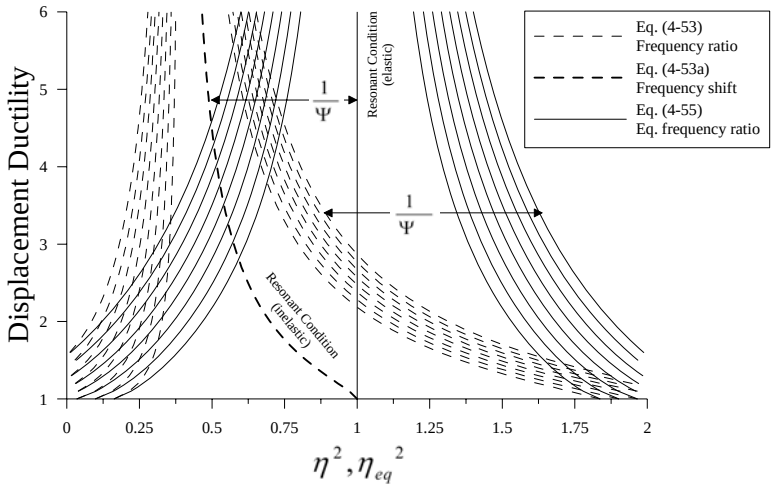

Figure 4-20. Variation in frequency ratios

The modified period and frequency shift is

$$\frac{T_{eq}}{T} = \sqrt{\frac{M_{eq}}{M}\frac{\mu_\Delta}{1+r_\Delta\left(\mu_\Delta - 1\right)}} = \frac{1}{\sqrt{\Psi}} = \frac{\omega}{\omega_{eq}} \tag{4-35}$$

The independency of period shift and excitation frequency does not however indicate that this holds true for equivalent hysteretic damping.

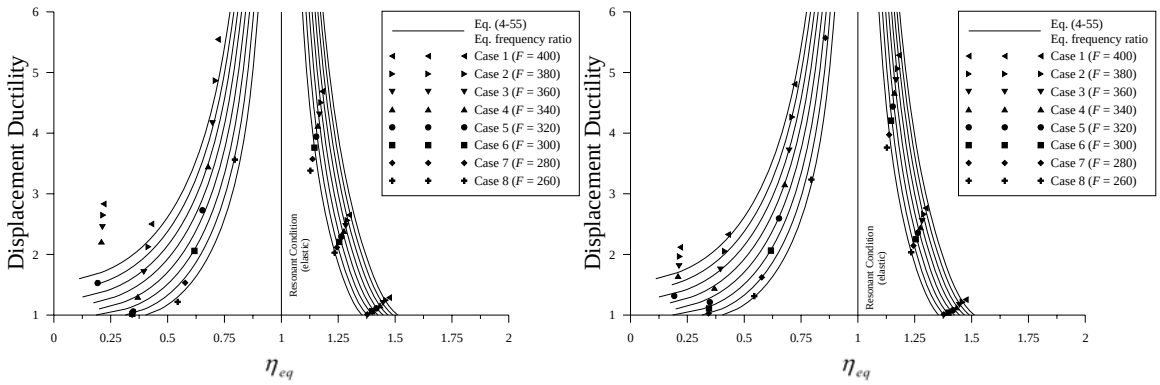

(a) Inelastic frame **(b) Equivalent elastic SDOF**

Figure 4-21. Equivalent frequency ratio

Fig. 4-21 plots Eq. (4-34) for all force ratios (Table 4-4) and the inelastic and equivalent elastic results (Fig. 4-21(a) and (b) respectively) as a function of equivalent frequency ratio (limited to six for clarity). Deviations in analytical results are evident.

Table 4-13. Theoretical displacement ductility

Index	F *kips*	Excitation Frequency, $\overline{\omega}$ *rad/sec*							
		0.5π	1π	1.5π	1.75π	2π	2.5π	3π	4π
Case 1	400	1.685	2.251	5.238	20.904	18.603	4.719	2.656	1.298
Case 2	380	1.508	1.989	4.602	18.725	17.590	4.533	2.567	1.255
Case 3	360	1.346	1.740	3.958	16.457	16.562	4.347	2.477	1.212
Case 4	340	1.203	1.511	3.315	14.077	15.515	4.161	2.389	1.168
Case 5	320	1.083	1.311	2.690	11.557	14.444	3.974	2.300	1.123
Case 6	300	Elastic	1.147	2.116	8.872	13.340	3.787	2.212	1.075
Case 7	280	Elastic	Elastic	1.638	6.056	12.193	3.600	2.125	1.022
Case 8	260	Elastic	Elastic	1.291	3.459	10.981	3.412	2.037	Elastic

Table 4-13 presents the theoretical displacement ductility at each excitation frequency from Eq. (4-34). The displacement ductility is then used to determine the properties of the equivalent elastic frame using the MSSM. Tables 4-14 to 4-21 present the analytical results from Eq. (4-27).

Table 4-14. Analysis results (CASE 1)

	Inelastic Frame			Equivalent Elastic Frame (SDOF)							% Difference	
$\overline{\omega}$	Δ_{in}	μ_θ	$E_{D,h,sys}$	M_{eq}	K_{eq}	η_{eq}	ζ_{eq}	c_{eq}	Δ_{eq}	$E_{D,h,eq}$	Δ	E_D
rad/sec	*in*		*in-kips*	*units*	*k/in*				*in*	*in-kips*		
0.5π	3.21		972	1.904	123	0.195	62	19.14	3.27	1009	1.9	3.8
π	4.29		1776	1.968	109	0.423	33	9.79	4.23	1733	-1.2	-2.4
1.5π	9.97		6015	2.081	84	0.742	15	4.09	9.45	5396	-5.3	-10.3
1.75π	39.80		28252	2.027	70	0.936	4	1.03	38.63	26616	-2.9	-5.8
2π	35.42		24986	2.034	71	1.067	4	1.01	34.29	23415	-3.2	-6.3
2.5π	8.98		5279	2.076	86	1.220	10	2.65	8.52	4744	-5.2	-10.1
3π	5.06		2351	2.003	102	1.320	11	3.10	4.92	2228	-2.7	-5.2
4π	2.47		423	1.868	141	1.448	5	1.75	2.56	455	3.7	7.6

Table 4-15. Analysis results (CASE 2)

	Inelastic Frame			Equivalent Elastic Frame (SDOF)							% Difference	
$\overline{\omega}$	Δ_{in}	μ_θ	$E_{D,h,sys}$	M_{eq}	K_{eq}	η_{eq}	ζ_{eq}	c_{eq}	Δ_{eq}	$E_{D,h,eq}$	Δ	E_D
rad/sec	*in*		*in-kips*	*units*	*k/in*				*in*	*in-kips*		
0.5π	2.87		721	1.883	130	0.189	57	17.72	2.96	764	3.0	6.0
π	3.79		1404	1.940	114	0.409	33	9.92	3.79	1406	0.1	0.1
1.5π	8.76		5113	2.075	87	0.730	17	4.50	8.32	4612	-5.0	-9.8
1.75π	35.65		25159	2.034	70	0.934	5	1.15	34.57	23660	-3.0	-6.0
2π	33.49		23548	2.037	71	1.066	4	1.06	32.41	22046	-3.2	-6.4
2.5π	8.63		5015	2.074	87	1.214	10	2.73	8.20	4526	-5.0	-9.7
3π	4.89		2224	1.996	103	1.310	11	3.14	4.77	2120	-2.4	-4.7
4π	2.39		362	1.868	143	1.435	5	1.61	2.48	390	3.8	7.7

Table 4-16. Analysis results (CASE 3)

	Inelastic Frame			Equivalent Elastic Frame (SDOF)							% Difference	
$\overline{\omega}$	Δ_{in}	μ_θ	$E_{D,h,sys}$	M_{eq}	K_{eq}	η_{eq}	ζ_{eq}	c_{eq}	Δ_{eq}	$E_{D,h,eq}$	Δ	E_D
rad/sec	*in*		*in-kips*	*units*	*k/in*				*in*	*in-kips*		
0.5π	2.56		491	1.870	138	0.183	47	15.15	2.66	528	3.7	7.5
π	3.31		1050	1.910	121	0.394	32	9.70	3.36	1081	1.5	2.9
1.5π	7.54		4199	2.063	90	0.714	18	4.99	7.19	3825	-4.6	-8.9
1.75π	31.33		21940	2.042	71	0.931	5	1.29	30.36	20594	-3.1	-6.1
2π	31.53		22089	2.041	71	1.064	5	1.13	30.52	20694	-3.2	-6.3
2.5π	8.28		4751	2.071	88	1.206	10	2.81	7.88	4304	-4.8	-9.4
3π	4.72		2096	1.989	105	1.298	11	3.18	4.62	2013	-2.0	-4.0
4π	2.31		301	1.869	146	1.422	4	1.43	2.39	323	3.6	7.3

Table 4-17. Analysis results (CASE 4)

	Inelastic Frame			Equivalent Elastic Frame (SDOF)							% Difference	
$\overline{\omega}$	Δ_{in}	μ_θ	$E_{D,h,sys}$	M_{eq}	K_{eq}	η_{eq}	ζ_{eq}	c_{eq}	Δ_{eq}	$E_{D,h,eq}$	Δ	E_D
rad/sec	*in*		*in-kips*	*units*	*k/in*				*in*	*in-kips*		
0.5π	2.29		288	1.870	147	0.177	34	11.13	2.38	310	3.8	7.7
π	2.88		725	1.884	130	0.378	28	8.88	2.96	768	2.9	5.8
1.5π	6.31		3286	2.041	95	0.692	20	5.57	6.07	3041	-3.8	-7.4
1.75π	26.80		18562	2.051	72	0.927	6	1.50	25.94	17389	-3.2	-6.3
2π	29.54		20603	2.045	72	1.062	5	1.20	28.65	19382	-3.0	-5.9
2.5π	7.92		4487	2.067	89	1.199	11	2.90	7.55	4077	-4.7	-9.1
3π	4.55		1972	1.981	106	1.287	11	3.22	4.47	1903	-1.7	-3.5
4π	2.22		238	1.873	149	1.409	4	1.22	2.30	254	3.3	6.6

Table 4-18. Analysis results (CASE 5)

	Inelastic Frame			Equivalent Elastic Frame (SDOF)							% Difference	
$\overline{\omega}$	Δ_{in}	μ_θ	$E_{D,h,sys}$	M_{eq}	K_{eq}	η_{eq}	ζ_{eq}	c_{eq}	Δ_{eq}	$E_{D,h,eq}$	Δ	E_D
rad/sec	*in*		*in-kips*	*units*	*k/in*				*in*	*in-kips*		
0.5π	2.06		118	1.892	156	0.173	16	5.61	2.12	124	2.6	5.3
π	2.50		441	1.868	140	0.363	22	7.18	2.59	475	3.8	7.7
1.5π	5.12		2399	2.005	102	0.662	22	6.18	4.99	2279	-2.5	-5.0
1.75π	22.00		14985	2.063	74	0.920	7	1.79	21.27	14006	-3.3	-6.5
2π	27.50		19083	2.050	72	1.060	5	1.28	26.69	17968	-3.0	-5.8
2.5π	7.57		4221	2.063	90	1.190	11	2.99	7.23	3857	-4.4	-8.6
3π	4.38		1845	1.973	108	1.275	11	3.25	4.32	1797	-1.3	-2.6
4π	2.14		175	1.881	152	1.396	3	0.97	2.19	184	2.6	5.2

Table 4-19. Analysis results (CASE 6)

	Inelastic Frame			Equivalent Elastic Frame (SDOF)							% Difference	
$\overline{\omega}$	Δ_{in}	μ_θ	$E_{D,h,sys}$	M_{eq}	K_{eq}	η_{eq}	ζ_{eq}	c_{eq}	Δ_{eq}	$E_{D,h,eq}$	Δ	E_D
rad/sec	*in*		*in-kips*	*units*	*k/in*				*in*	*in-kips*		
0.5π	2.18		209	1.876	151	0.351	13	4.43	2.26	223	3.4	7.0
π	4.03		1584	1.954	112	0.624	22	6.59	4.01	1567	-0.5	-1.1
1.5π	16.89		11174	2.076	76	0.907	9	2.27	16.31	10414	-3.5	-6.8
1.75π	25.40		17516	2.054	73	1.057	6	1.38	24.71	16583	-2.7	-5.3
2π	7.21		3956	2.058	91	1.181	11	3.08	6.93	3653	-3.9	-7.7
2.5π	4.21		1720	1.964	109	1.262	11	3.28	4.17	1688	-0.9	-1.9
3π	2.05		106	1.895	156	1.384	2	0.64	2.08	110	1.7	3.4
4π	2.18		209	1.876	151	0.351	13	4.43	2.26	223	3.4	7.0

Table 4-20. Analysis results (CASE 7)

	Inelastic Frame			Equivalent Elastic Frame (SDOF)							% Difference	
$\overline{\omega}$	Δ_{in}	μ_θ	$E_{D,h,sys}$	M_{eq}	K_{eq}	η_{eq}	ζ_{eq}	c_{eq}	Δ_{eq}	$E_{D,h,eq}$	Δ	E_D
rad/sec	*in*		*in-kips*	*units*	*k/in*				*in*	*in-kips*		
0.5π		Elastic										
π		Elastic										
1.5π	3.12		906	1.898	125	0.581	20	6.29	3.18	943	2.0	4.1
1.75π	11.53		7177	2.084	81	0.880	12	3.13	11.12	6669	-3.6	-7.1
2π	23.22		15887	2.060	73	1.053	6	1.49	22.64	15105	-2.5	-4.9
2.5π	6.85		3690	2.052	92	1.170	12	3.18	6.62	3438	-3.5	-6.8
3π	4.05		1597	1.955	111	1.249	11	3.29	4.02	1576	-0.7	-1.3
4π	1.95		31	1.922	161	1.373	1	0.21	1.96	32	0.6	1.2

Table 4-21. Analysis results (CASE 8)

	Inelastic Frame			Equivalent Elastic Frame (SDOF)							% Difference	
$\overline{\omega}$	Δ_{in}	μ_θ	$E_{D,h,sys}$	M_{eq}	K_{eq}	η_{eq}	ζ_{eq}	c_{eq}	Δ_{eq}	$E_{D,h,eq}$	Δ	E_D
rad/sec	*in*		*in-kips*	*units*	*k/in*				*in*	*in-kips*		
0.5π		Elastic										
π		Elastic										
1.5π	2.46		413	1.868	141	0.542	14	4.62	2.55	445	3.8	7.7
1.75π	6.59		3490	2.047	94	0.813	17	4.66	6.38	3278	-3.1	-6.1
2π	20.91		14167	2.066	74	1.049	7	1.64	20.49	13607	-2.0	-4.0
2.5π	6.50		3424	2.045	94	1.159	12	3.29	6.29	3210	-3.2	-6.2
3π	3.88		1472	1.945	113	1.235	11	3.30	3.87	1466	-0.2	-0.4
4π		Elastic										

Fig. 4-22 plots Eq. (4-34) for the force ratios and displacement ductility results for the equivalent elastic frame (split at a displacement ductility of six for graphical clarity).

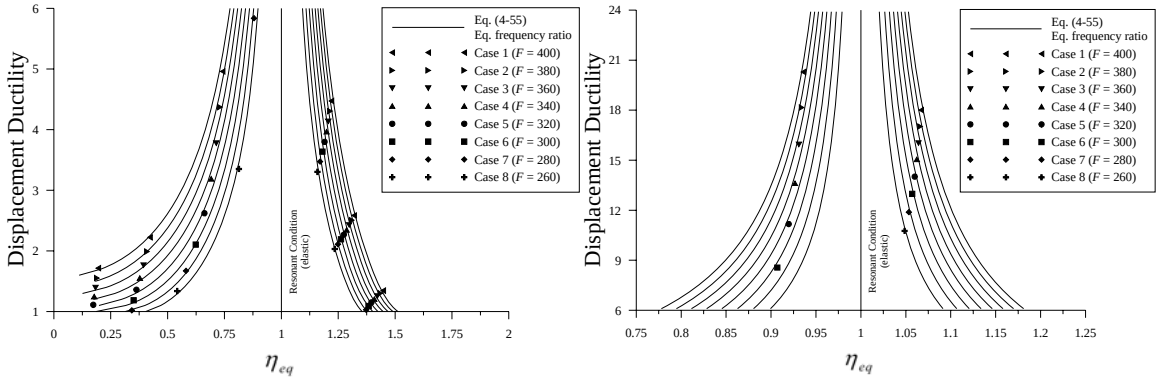

(a) Ductility 1 - 6 **(b) Ductility 6 – 24**

Figure 4-22. Displacement ductility response of equivalent elastic SDOF

Fig. 4-23 compares the displacement ductility between both methods (MSSM and SSM). The MSSM leads to better agreement in peak displacements between the two systems than the SSM.

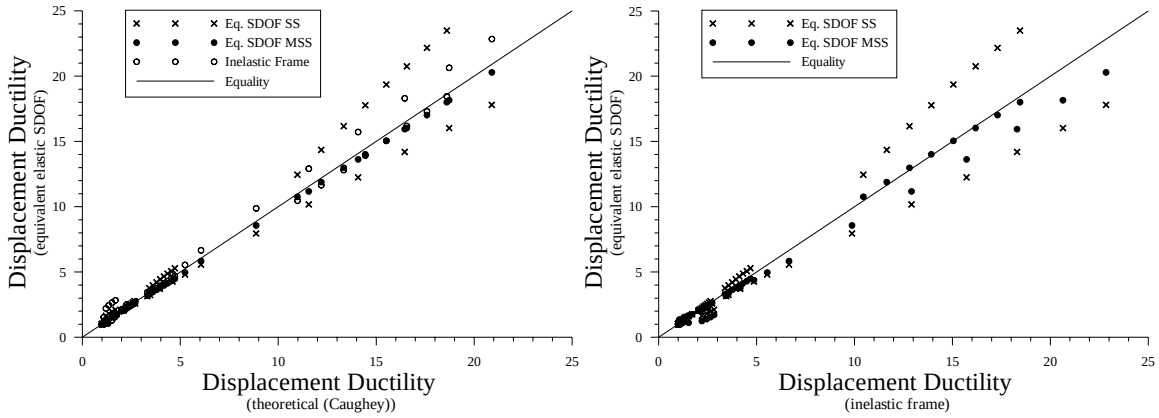

(a) Theoretical **(b) Inelastic**

Figure 4-23. Displacement ductility comparison

Fig. 4-24 plots the revised period shift results against the theoretical solution from Eq. (4-35). The period shift from the SSM, Eq. (4-29) is included for comparison. For

low displacement ductility (< 2) both methods give approximately the same period shift for $r_{\Delta} = 0.4$. Assuming Caughey's solution to be the correct impedence, the period shift is underestimated with the SSM at higher ductility demands due to the constant mass assumption. The large variation (5 data points) in Fig. 4-24(b) is due to the peak displacements of the inelastic frame being a function of transient waves at very low excitation frequencies.

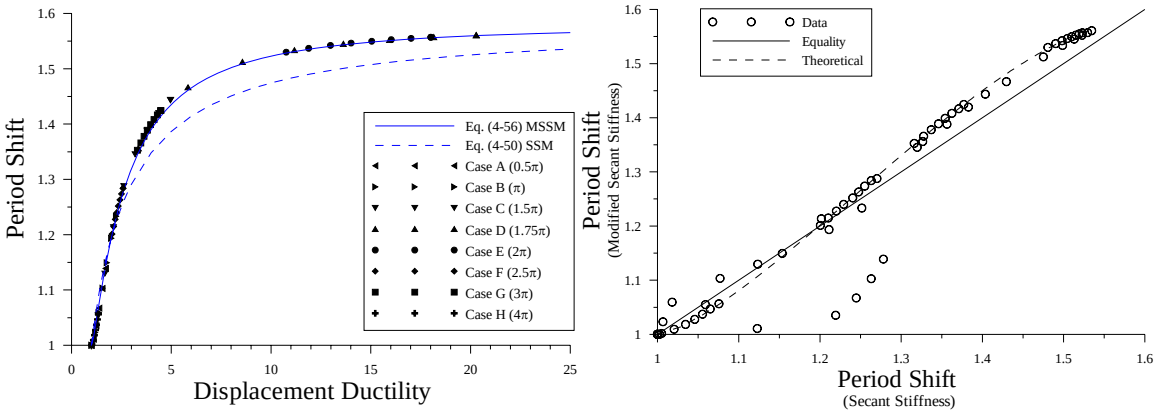

(a) Equivalent elastic SDOF **(b) Equivalent elastic SDOF**

Figure 4-24. Period shift (MSSM)

Fig. 4-25 plots the revised equivalent hysteretic damping results as a function of equivalent frequency ratio. The same general form results when compared to Fig. 4-13 though the magnitude of damping is shifted due to the change in equivalent frequency ratio. The most notable variation is seen for very low excitation frequencies for reasons previously discussed. Fig. 4-25 additionally plots the frequency-dependent damping curves, Eq. (4-31), for each excitation frequency. The data points correspond to the respective frequency curve illustrating that hysteretic damping is a function of input energy and ductility.

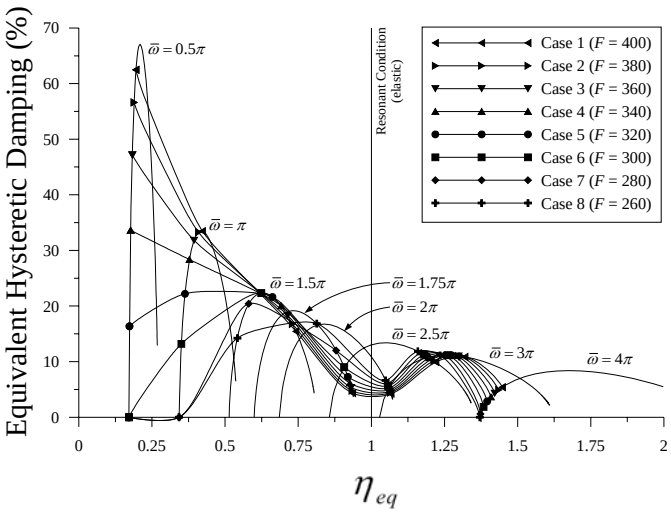

Figure 4-25. Equivalent hysteretic damping (MSSM)

Input energy for one cycle of steady-state response is

$$E_I = \pi F \Delta_{in} \sin\phi \tag{4-36}$$

where

$$\phi \;\; = Tan^{-1}\left(\frac{2\zeta_{eq,h}\eta_{eq}}{1-\eta_{eq}{}^2}\right) \tag{4-36a}$$

Energy balance would be represented at the intersection point, $E_I = E_D$. It follows that equivalent hysteretic damping can be expressed as

$$\zeta_{eq,h} = \frac{E_D\sqrt{\left(\eta_{eq}{}^2-1\right)^2}}{2\eta_{eq}\sqrt{\pi F\Delta_{in}{}^2 - E_D{}^2}} = \frac{F_y{}^2\sqrt{\left(\eta_{eq}{}^2-1\right)^2}}{2\eta_{eq}\sqrt{\left(\frac{F}{F_y}\frac{\pi}{4}\frac{\mu_\Delta}{\left(\mu_\Delta - r_\Delta\left(\mu_\Delta-1\right)-1\right)}\right)^2 - 1}} \tag{4-37}$$

Take for example $\bar{\omega} = 2.5\pi$ and superimpose Eq. (4-37) on to the frequency-dependent damping curve from Eq. (4-31) in Fig. 4-26. The assumption that damping

could be at a minimum at the equivalent resonant condition, as illustrated in Fig. 4-13 and 4-25, is evident from Fig. 4-26 where damping converges to zero at $\eta_{eq} = 1$.

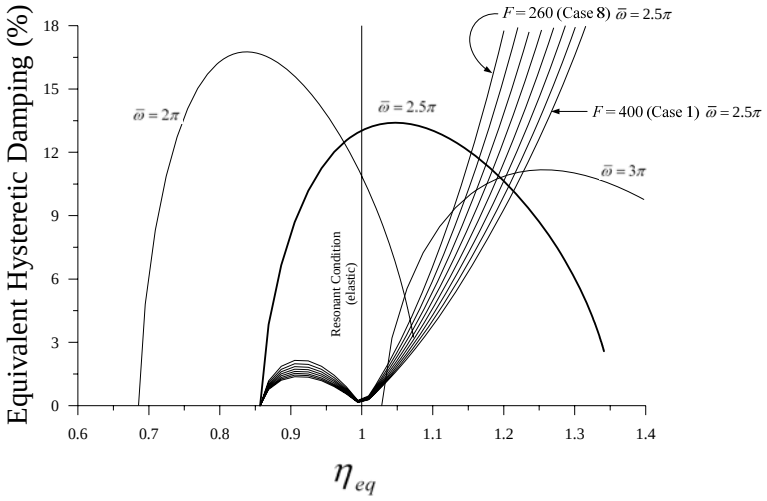

Figure 4-26. Input energy response for $\bar{\omega} = 2.5\pi$

However, this will not hold for all force ratios. This variation at resonance is due to the force magnitudes chosen resulting in an unbounded condition. The solutions of Eqs. (4-32) and (4-34) are unbounded when

$$\frac{F}{F_y} \geq \frac{4(1-r_\Delta)}{\pi} = 0.73 \text{ for } r_\Delta = 0.4 \tag{4-38}$$

It follows that

$$\mu_{\Delta,\max} = \frac{4(1-r_\Delta)}{4(1-r_\Delta) - \frac{F}{F_y}\pi} \text{ as } \eta_{eq} \text{ approaches unity} \tag{4-39}$$

A bounded solution results in a stable single-value damping ordinate. Fig. 4-27 plots the revised damping data points onto Fig. 4-25 for comparison. Other force ratios will cause the intersecting point to shift along the damping curve.

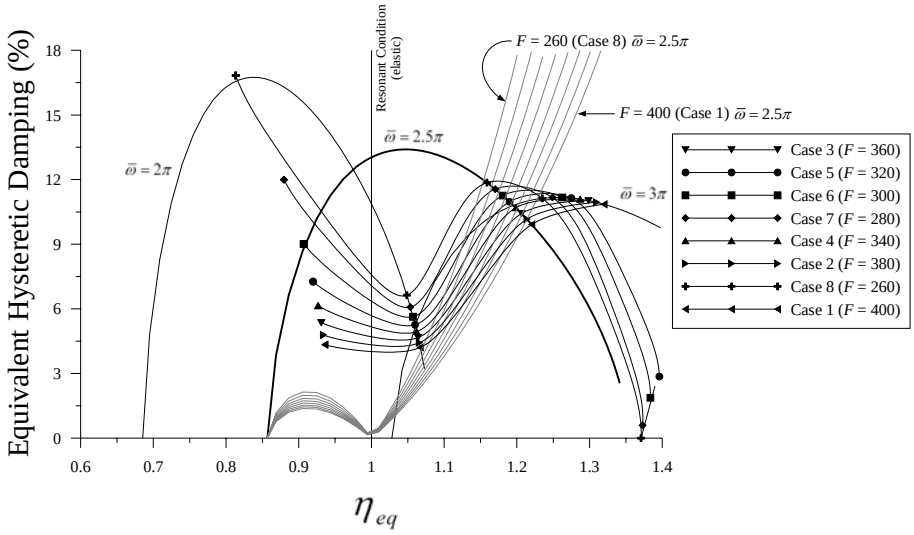

Figure 4-27. Energy balance comparison for $\bar{\omega} = 2.5\pi$

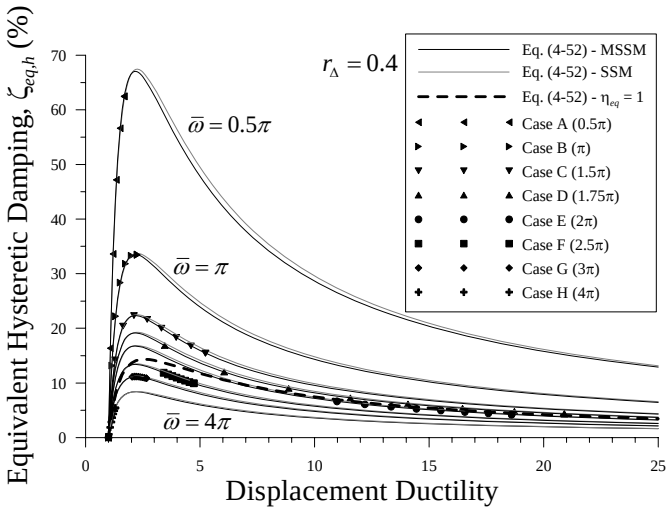

Figure 4-28. Equivalent hysteretic damping (MSSM)

Fig. 4-28 plots the revised equivalent hysteretic damping results as a function of displacement ductility. The damping curves for the MSSM and SSM (Eq. (4-31)) are

included for comparison. The damping curves shift slightly after the peak damping value is reached due to the change in peak inelastic displacement for $r_\Delta = 0.4$. The curves remain essentially unchanged for low ductility values.

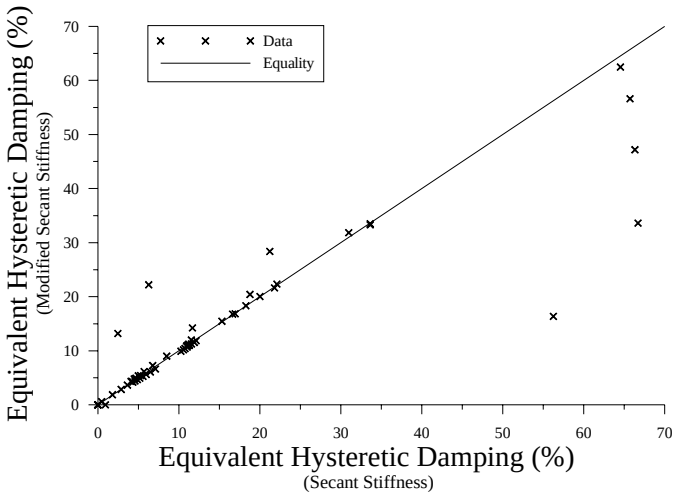

Figure 4-29. Equivalent hysteretic damping comparison

Fig. 4-29 compares the hysteretic damping values for the MSSM and SSM. For all intents and purpose, especially with regards to design, the MSSM method has no significant effect on the degree of equivalent damping with the exception of low excitation frequencies for $r_\Delta = 0.4$.

Figs. 4-30 plots hysteretic damping as a function of force magnitude and frequency ratio. Damping levels rapidly increase with high force ratios at low frequency ratios. The convergence to minimum damping at the resonant condition is illustrated. This minimization is due to an unbounded solution at the resonant condition. This effect vanishes when the solution is bounded. It is further evident that two resonant damping conditions exist. When $\eta_{eq} < 1$ the peak hysteretic damping is traced when $\eta_{eq,D} = 1$

where $\eta_{eq,D} = \bar{\omega}/\omega_{eq,D}$ and $\omega_{eq,D}$ is the equivalent damped natural cyclic frequency. When $\eta_{eq} > 1$ the maximum hysteretic damping is traced when $\eta = 1$. This line separates from $\eta_{eq} = 1$ when the apex of the damping curve is reached (Fig. 4-28) and remains essentially constant independent of force ratio. More plots are in Appendix C.

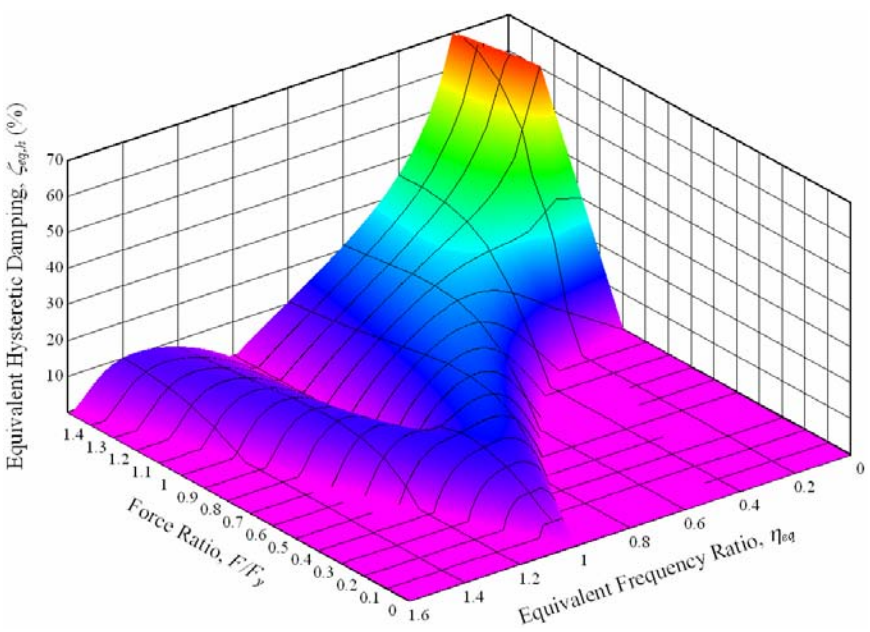

Figure 4-30. Spatial distribution of equivalent hysteretic damping for r_Δ = 0.4

Figs. 4-31 plots hysteretic damping as a function of force magnitude and displacement ductility for $\eta_{eq} \le 1$ (a) and $\eta_{eq} \ge 1$ (b). The sharp drop off at low force ratios is due to the system achieving a resonant condition (bounded solution) at the maximum displacement ductility. The validity of assuming a resonant condition for all cases can now be questioned. The data point corresponding to $\eta_{eq} = 1$ for each force ratio occurs once on the damping-ductility curve. Consequently, the damping curve at the resonant condition shown in Figs. 4-17 and 4-28 is then by definition the projection of these data points onto the vertical plane and thus not a valid comparison curve. Also, the

missing data to create the angled corner at high damping values in Figs. 4-78 and 4-79 is due to the solution reaching a mathematical stability limit.

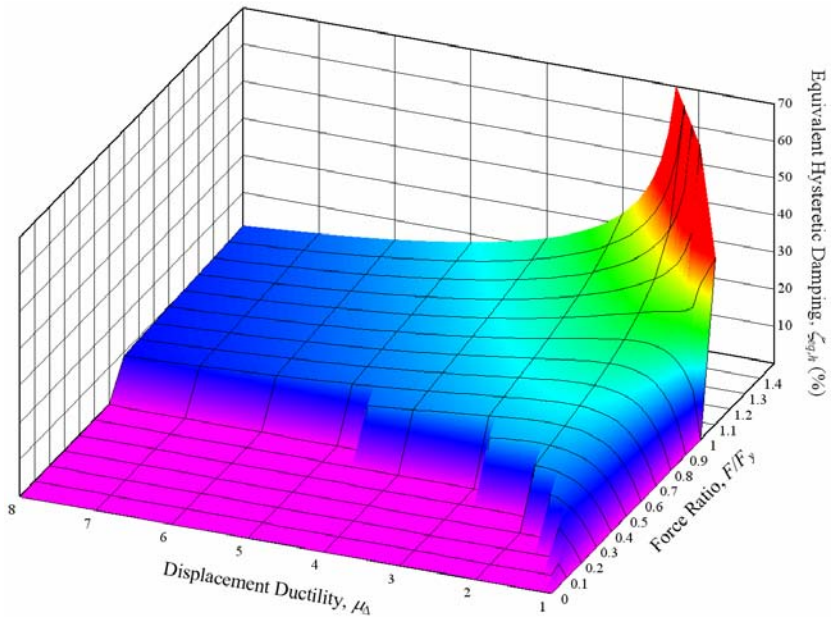

(a) $\eta_{eq} \leq 1.0$

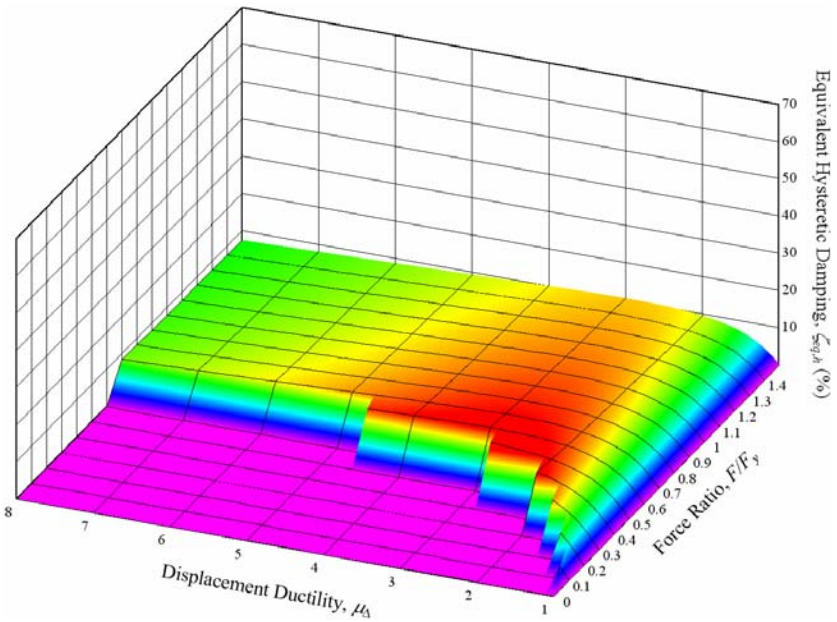

(b) $\eta_{eq} \geq 1.0$

Figure 4-31. Spatial distribution of equivalent hysteretic damping

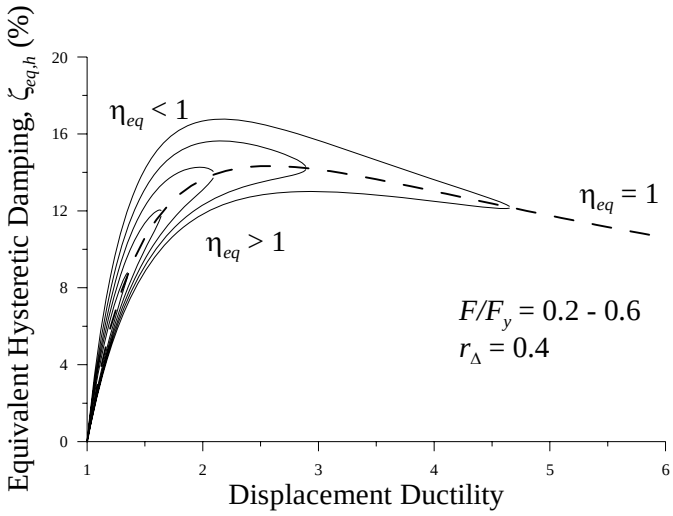

Figure 4-32. Damping – ductility curves (F/F_y = 0.2 - 0.6)

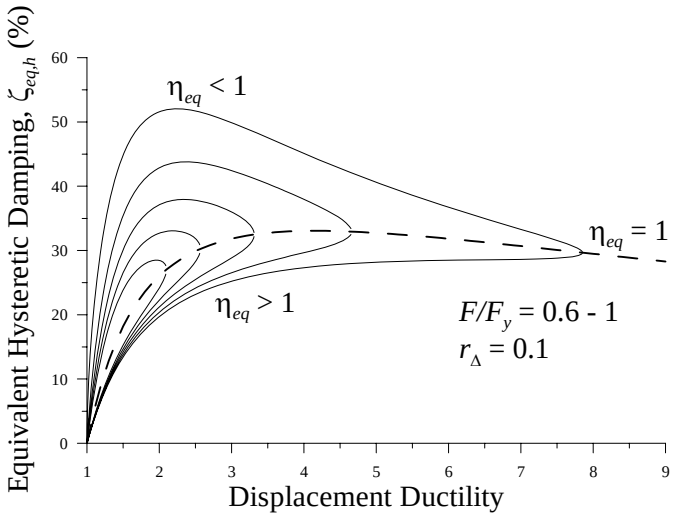

Figure 4-33. Damping – ductility curves (F/F_y = 0.6 – 1.0)

For low force ratios, as expected for seismic design, the maximum hysteretic damping is less than 20% when $\eta_{eq} \leq 1$ and 15% when $\eta_{eq} \geq 1$ for $r_\Delta = 0.4$. Plotting the damping-ductility curves for F/F_y = 0.2 to 0.6 (Fig. 4-32) it is evident that a resonant condition is a reasonable approximation in the absence of an excitation frequency. However, this does not hold true for smaller post-yield stiffness ratios. Fig. 4-33 plots the damping-ductility curves for F/F_y = 0.6 to 1.0 for $r_\Delta = 0.1$. If it is assumed that the

predominant excitation frequency produced from strong motion is greater than the equivalent natural frequency then assuming a resonant condition could be satisfactory in approximating the degree of damping for design. Ultimately, this implies that in order to apply this resonant theory to earthquake-like excitation a statistical evaluation must be conducted for a large number of recorded earthquakes for a particular location to derive a damping modification factor. Further, this damping factor would vary from region to region depending on frequency content.

4.3.1.7 Summary

The motivation of the MSSM is to obtain a better approximation of the equivalent system properties and, ultimately, the design force. Returning to Case 3-C previously illustrated for the SSM, Fig. 4-34 plots the story shear-displacement response of the equivalent elastic frame with properties determined from applying the MSSM. As evident, the MSSM leads to better response agreement.

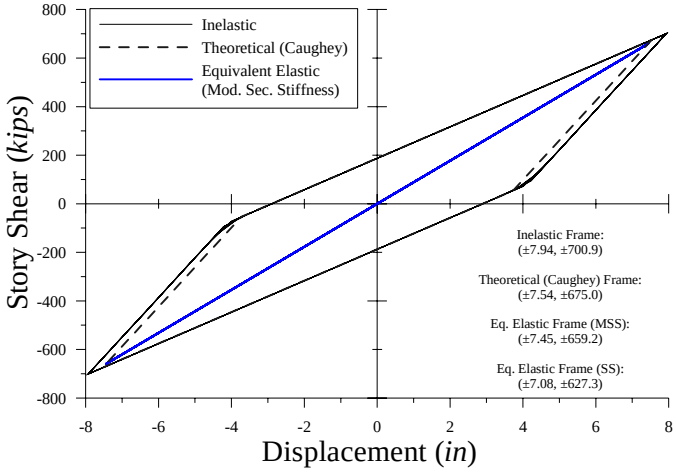

Figure 4-34. Steady-state story shear-displacement response (Case 3-C)

Other than errors developed through approximation of the secant stiffness, additional errors in maximum displacements between the theoretical solution and the MSSM are introduced simply due to the innate differences between the two methods: (1) method of slowly varying parameters for the benchmark results and (2) the exact solution of a damped elastic SDOF. Fig. 4-35 illustrates the flowchart summarizing the MSSM for a SDOF frame.

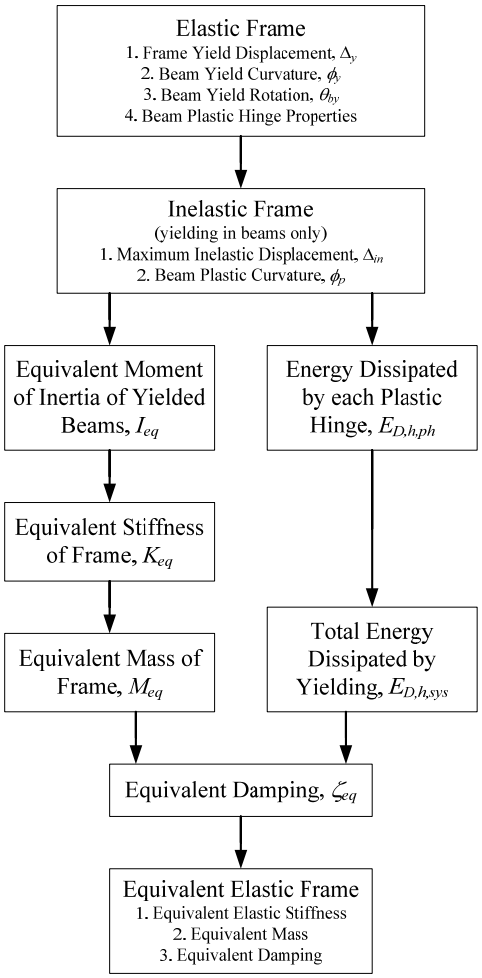

Figure 4-35. Flowchart of Modified Secant Stiffness method (inelastic SDOF frame)

4.3.2 Harmonic Forcing Excitation – MDOF Inelastic Frames

The Modified Secant Stiffness method (MSSM) proposed for a SDOF inelastic frame can also be applied to a MDOF inelastic frame. This application is based on examining the inelastic frame on a per floor basis. Fig. 4-36 illustrates the flowchart summarizing the MSSM for a MDOF moment frame.

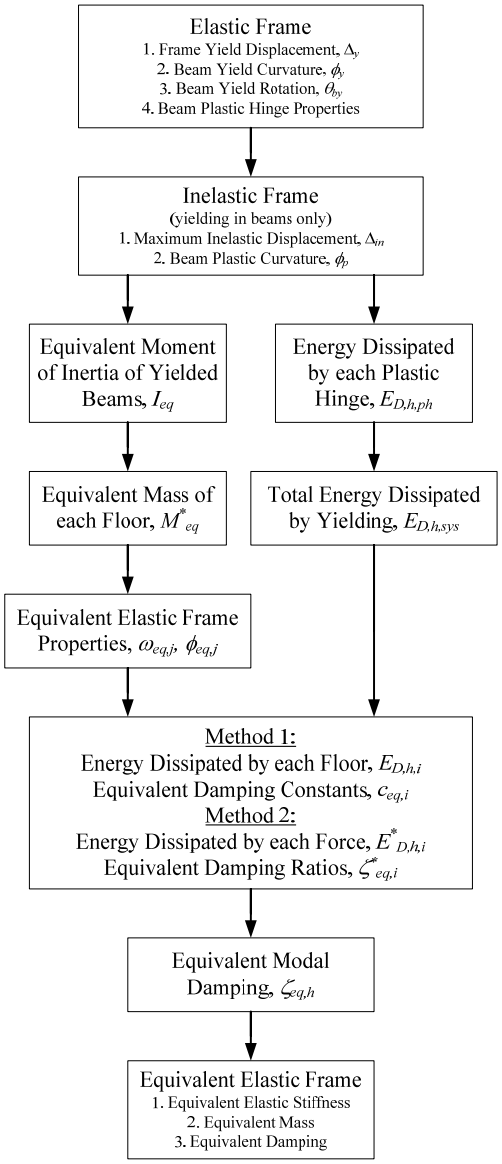

Figure 4-36. Flowchart of Modified Secant Stiffness method (inelastic MDOF frame)

4.3.2.1 MDOF Frame Lateral Force Distribution for Seismic Design

Structural dynamic theory provides the maximum restoring force of an elastic multi-story frame vibrating in the j^{th} mode at floor i as

$$F_{i,j} = \left(\omega_j{}^2 m_i\right) u_{i,j} \tag{4-40}$$

where

m_i = Horizontal inertia mass associated with lateral DOF i

i = DOF index (i.e., floor)

The base shear, V_b, due to mode j is thus the summation of Eq. (4-40) for all floors. It can readily be shown that the restoring force distribution for mode j can be expressed as

$$\left\{\phi_f\right\}_j F = \left\{\frac{m_i \phi_{i,j}}{\sum_{i=1}^{n}\left(m_i \phi_{i,j}\right)}\right\} F \tag{4-41}$$

Seismic codes typically use the fundamental mode shape (j = 1) in computing the horizontal design forces (see Chapter 1). Thus, Eq. (4-41) corresponds to Eq. (1-3) if the mode shape was assumed linear (k = 1) and Eq. (2-36) if $\phi_{i,j} = \delta_i$. When the mass is constant for all floors the force distribution and mode shape are invariant. Though the design force vector is based on a single mode, response of a frame can be influenced by multiple modes of vibration. It can be shown that a force distribution in accordance with Eq. (4-41) will not excite any other mode of vibration in an elastic frame due to modal orthogonality (Chopra 2005). The excited mode is thus referred to as the ‘active mode’.

4.3.2.2 Equivalent Elastic Frame

Similar to the one-story frame, the first step in this process is to determine the equivalent elastic member properties and the dynamic properties of the equivalent elastic frame. Determination of the equivalent Moment of Inertia of a beam follows that outlined for the one-story frame. It is similarly assumed here that plastic hinges develop only in the beam ends. The equivalent elastic natural frequency for mode *j*, $\omega_{eq,j}$, is determined by solving the eigenvalue problem

$$\left(\left[K_{eq}\right] - \omega_{eq,j}^{\ 2}\left[M_{eq}\right]\right)\left\{\phi_{eq,j}\right\} = 0 \tag{4-42}$$

where

$\left[K_{eq}\right]$ = Equivalent stiffness matrix

$\left[M_{eq}\right]$ = Equivalent mass matrix from Eq. (4-33)

$\left\{\phi_{eq,j}\right\}$ = Equivalent mode shape for mode *j* (eigenvectors of Eq. (4-42))

The mode shapes of the equivalent elastic frame, $\left\{\phi_{eq,j}\right\}$, could deviate from that of the benchmark frame, $\left\{\phi_j\right\}$. The extent of variation depends on how well the inelastic displacements maintain the elastic mode shape for the active mode. This constancy is contingent on component stiffness selections and the force distribution during inelastic response, as well as whether or not 1st floor column base hinges develop.

In addition to a possible change in mode shape during inelastic response a corresponding force redistribution would occur as the stiffness of the frame changes due

to yielding. Similarly, applying a mode-dependent equivalent force distribution results in orthogonal equivalent modes and, thus, only the active mode contributes to response of the equivalent frame. This is the basis of an ‘adaptive pushover’ analysis. Since the goal of this linearization procedure is to match peak displacements and forces, it follows that the base shear developed in both frames must concur. By setting the base shears equal, the equivalent force can be found from

$$F_{eq} = F \frac{\sum_{i=1}^{n} \phi_{f,i,j}}{\sum_{i=1}^{n} \phi_{f,eq,i,j}} \tag{4-43}$$

where

$$\left\{\phi_{f,eq}\right\}_j \quad = \text{Equivalent force distribution} \left(= \left\{ \frac{m_{eq,i}\phi_{eq,j}}{\sum_{i=1}^{n}\left(m_{eq,i}\phi_{eq,i,j}\right)} \right\} \right) \tag{4-43a}$$

It follows from Eq. (4-43) that force redistribution does not occur if the mode shapes do not vary between the elastic and inelastic frame.

After the equivalent frame has been constructed, the next step is to estimate the amount of equivalent hysteretic damping. Two methods are proposed: (1) stiffness-proportional damping (Section 4.3.1.2.3) and (2) mass-proportional damping (Section 4.3.1.2.4). The methods differ in how hysteretic damping is modeled. The latter method, although has no physical meaning, is computationally simpler and more easily integrated into a design provision.

4.3.2.3 Method 1 – Stiffness-Proportional Damping

In this method hysteretic damping is model by linear dampers placed between floors as shown in Fig. 4-37. This procedure is physically meaningful since yielding in the beams is a function of the relative displacements between floors (referred to as 'interstory displacements' or 'story drift').

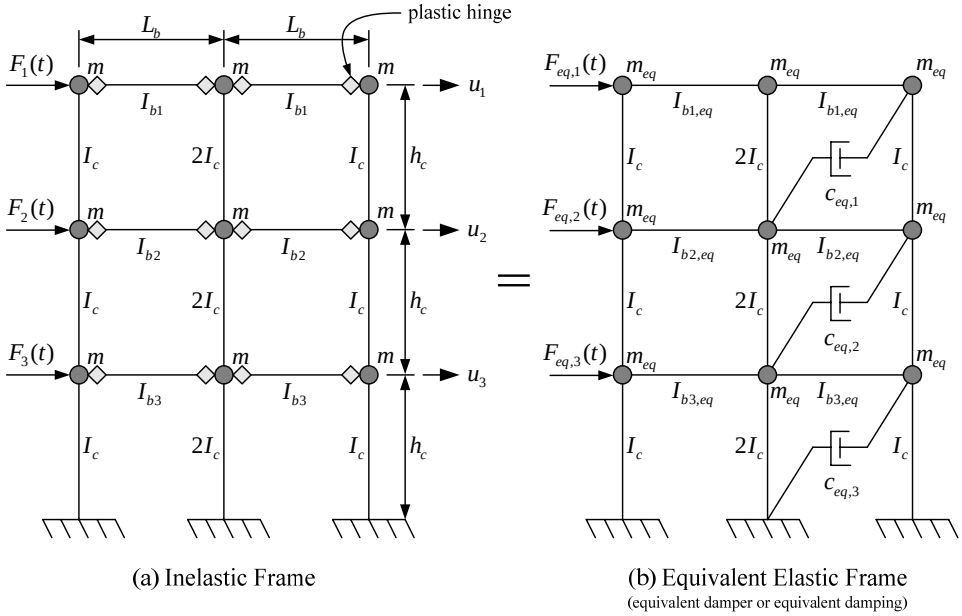

Figure 4-37. Method 1 schematic (stiffness-proportional damping)

4.3.2.3.1 Hysteretic Energy Dissipation

The objective of this step is to determine the energy dissipated by the system through yielding. Similar to the one-story frame the energy dissipated by a floor is found by summing the areas of the moment-rotation hysteresis loops of each plastic hinge.

$$E_{D,h,i} = \sum_{k=1}^{K} E_{D,h,ph,k} \tag{4-44}$$

Alternatively, the energy dissipated by a floor can be found by

$$E_{D,h,i} = A_{hyst,i} = 4V_{y,i}\bar{\delta}_{y,i}\left(\bar{\mu}_{\delta,i} - r_{\delta,i}\left(\bar{\mu}_{\delta,i} - 1\right) - 1\right) \tag{4-45}$$

where

$V_{y,i}$ = Yield-level story shear of floor i $\left(= \sum_{i=i}^{n} F_{y,i}\right)$

$\bar{\delta}_{y,i}$ = Interstory yield displacement of floor i $\left(= \delta_{y,i} - \delta_{y,i-1}\right)$

$\bar{\mu}_{\delta,i}$ = Interstory displacement ductility demand of floor i

The subscript δ is used to denote response of individual floors of a multi-story frame whereas Δ is used for a system-level model, as is the case for a SDOF frame or effective SDOF frame. The hysteretic energy dissipated by the system is the summation of Eqs. (4-44) or (4-45).

$$E_{D,h,sys} = \sum_{i=1}^{n} E_{D,h,i} \tag{4-46}$$

Energy dissipated by column base hinges in the 1st story should be included in Eq. (4-46).

4.3.2.3.2 Equivalent Hysteretic Damping

The hysteretic damping constant for each floor is computed by

$$c_{eq,h,i,j} = \frac{E_{D,h,i}}{\pi\eta_{eq,j}\omega_{eq,j}\bar{\delta}_{in,i}^{\ 2}} \tag{4-47}$$

where

$\bar{\delta}_{in,i}$ = Maximum interstory displacement of floor i $\left(=\delta_{in,i}-\delta_{in,i-1}\right)$

It follows that the equivalent hysteretic damping ratio is

$$\zeta_{eq,h,i,j}=\frac{c_{eq,h,i,j}}{2\omega_{eq,j}m_{eq,i}}=\frac{E_{D,h,i}}{2\pi\eta_{eq,j}\underbrace{\omega_{eq,j}{}^{2}m_{eq,i}}_{k^{*}_{eq,i,j}}\bar{\delta}_{in,i}{}^{2}}=\frac{1}{2\pi\eta_{eq,j}k^{*}_{eq,i,j}}\frac{E_{D,h,i}}{\bar{\delta}_{in,i}{}^{2}} \tag{4-48}$$

Since Eqs. (4-47) and (4-48) are mode-dependent, it follows that the energy dissipated and inelastic displacement must also be mode-dependent, which is valid due to the mode-dependent force distribution used in this process.

4.3.2.3.3 Equivalent Hysteretic Modal Damping

An equivalent hysteretic modal damping value could be estimated as an alternative to assigning damping values to each floor of the multi-story frame. This value is useful when converting the frame into an effective SDOF frame. Based on modal orthogonality, the equivalent elastic damping constant for the j^{th} mode is

$$C_{eq,h,j}=\left\{\phi_{eq,j}\right\}^{T}\left[C_{eq,h}\right]\left\{\phi_{eq,j}\right\} \tag{4-49}$$

The formulation of the equivalent damping matrix follows that of a shear beam stiffness matrix. For example, (DOFs are labeled from top down)

$$\left[C_{eq,h}\right]=\begin{bmatrix} c_{eq,1} & -c_{eq,1} & 0 & 0 & \cdots \\ & c_{eq,1}+c_{eq,2} & -c_{eq,2} & 0 & \cdots \\ & & c_{eq,2}+c_{eq,3} & -c_{eq,3} & \cdots \\ & sym. & & c_{eq,3}+c_{eq,4} & \cdots \\ & & & & \ddots \end{bmatrix} \tag{4-50}$$

It follows that the equivalent hysteretic modal damping ratio is

$$\zeta_{eq,h,j}=\frac{C_{eq,h,j}}{2\omega_{eq,j}M_{eq,j}}=\frac{\left\{\phi_{eq,j}\right\}^{T}\left[C_{eq,h}\right]\left\{\phi_{eq,j}\right\}}{2\omega_{eq,j}\sum_{i=1}^{n}m_{eq,i}{\phi_{eq,j}}^{2}} \tag{4-51}$$

4.3.2.4 Method 2 – Mass-Proportional Damping

In this method hysteretic damping is model by linear dampers placed at each floor and connected to a fictitious rigid wall as shown in Fig. 4-38. This method has no physical meaning since equivalent dampers cannot be placed as illustrated.

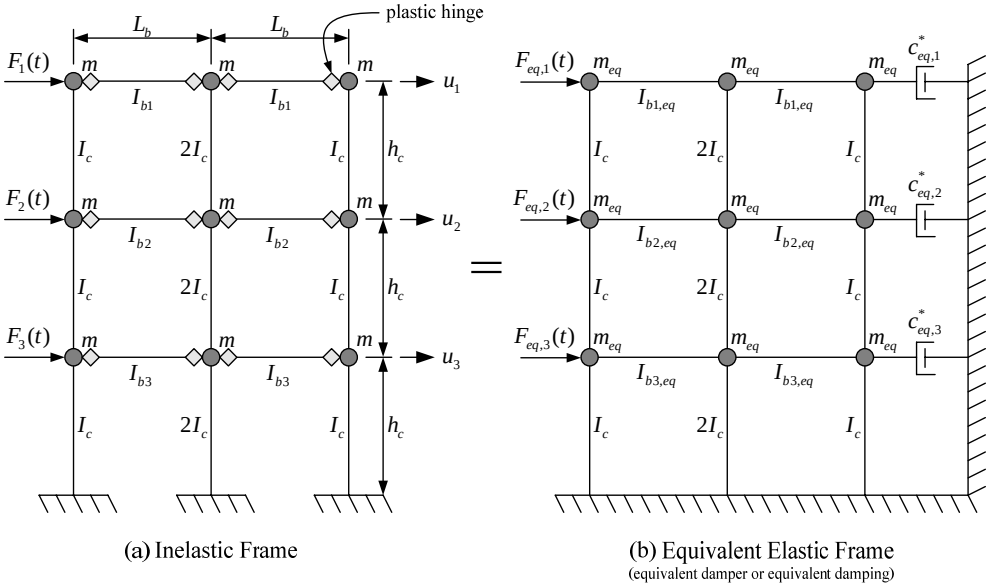

Figure 4-38. Method 2 schematic (mass-proportional damping)

4.3.2.4.1 Hysteretic Energy Dissipation

The total energy dissipated by the system through yielding of each floor is computed as shown in Method 1. It can be interpreted when evaluating Eqs. (4-44) and (4-45) that lower floors should contribute more to system energy dissipation than do upper floors. This is associated with the increase in strength demands on lower floors as the internal story shears increase. It can therefore be presumed that the energy dissipated by yielding per floor could be used to determine the value of equivalent hysteretic damping assigned to that floor in this method.

Bernal (1994) stated that damping forces are invariant to inertia forces. Therefore, the magnitude of energy dissipated should increase heightwise which is in contrast to the previous supposition. As a result, it is proposed that an energy-based normalization procedure be incorporated to estimate the portion of system energy dissipated by each floor. This concept is best understood by illustrating the effect of applied forces on frame response.

An idealized story shear - interstory displacement response of a three-story frame (see Fig. 4-38 for example) is shown for example in Fig. 4-39. The 1st floor contributes the most energy dissipation (area of V-δ loop). However, a moment-rotation loop of a plastic hinge in the 1st floor is a function of the story shear (summation of all applied forces above the 1st floor). Thus, the applied force at any subsequent floor contributes to energy dissipation on the 1st floor and only the respective shaded region is the energy dissipated due to the applied force at the 1st floor (F_3 in this example). This area becomes

the quantity of dissipated energy used to determine the equivalent hysteretic damping assigned to that DOF. Consequently, a portion of the total energy dissipated by the 1st floor is assigned to each subsequent floor. In the end, the magnitude of energy dissipated per floor increases heightwise.

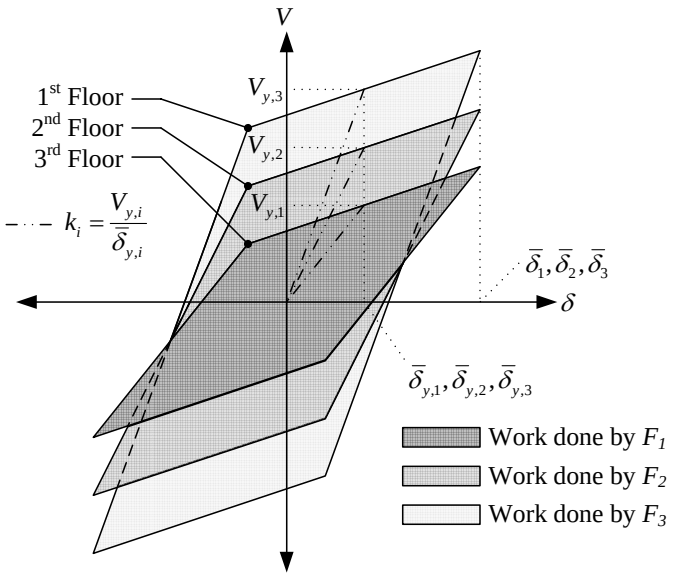

Figure 4-39. Idealized story shear – displacement response (three-story frame)

Assuming a 1st mode-based force distribution, $\{\phi_f\}_1$, and yield displacement profile shape, $\{\phi_1\}$, the total area of the system hysteresis loop of Fig. 4-39 is

$$E_{D,h,sys} = A_{hyst,sys} = A^*_{hyst,n} \sum_{i=1}^{n} \left(\phi_{f,i,1} \phi_{i,1} \left(\frac{r_{\delta,i} - 1}{r_{\delta,n} - 1} \right) \left(\frac{\mu_{\delta,i} - 1}{\mu_{\delta,n} - 1} \right) \right) \tag{4-52}$$

where

$A^*_{hyst,n}$ = Area of force-displacement of DOF n (Eq. (4-55))

n = Top DOF (3rd floor in this example (i = 1 in Fig. 4-39))

Eq. (4-52) is based on the approximation that all plastic hinges can be designed to form simultaneously vertically and horizontally. The normalization factor, τ, is defined as the measure of the hysteresis area of a given floor to the area of the hysteresis loop of the top floor ($i = n$).

$$\tau_i = \frac{\left(\phi_{f,i,1}\phi_{i,1}\left(\frac{r_{\delta,i}-1}{r_{\delta,n}-1}\right)\left(\frac{\mu_{\delta,i}-1}{\mu_{\delta,n}-1}\right)\right)}{\sum_{i=1}^{n}\left(\phi_{f,i,1}\phi_{i,1}\left(\frac{r_{\delta,i}-1}{r_{\delta,n}-1}\right)\left(\frac{\mu_{\delta,i}-1}{\mu_{\delta,n}-1}\right)\right)} \tag{4-53}$$

It follows that the portion of dissipated hysteretic energy assigned to each floor is

$$E^*_{D,h,i} = \tau_i E_{D,h,sys} \tag{4-54}$$

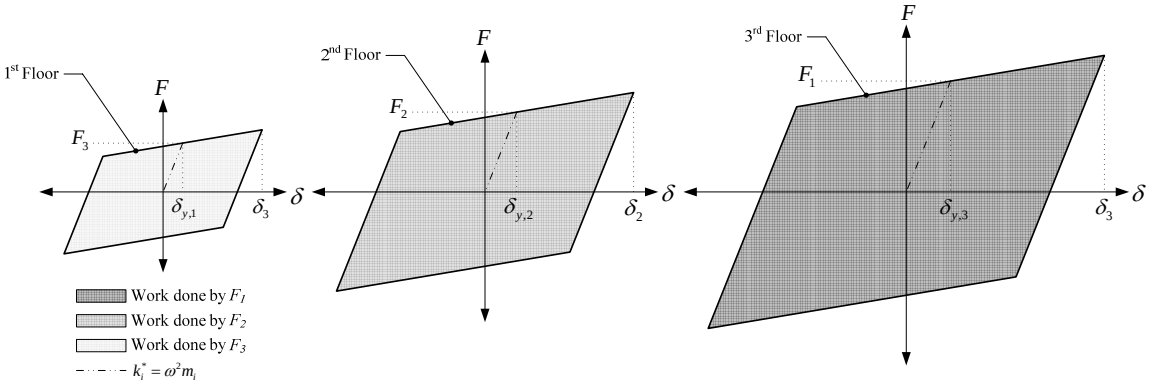

Figure 4-40. Idealized force – displacement response (three-story frame)

Alternatively, the area of the hysteresis loop for floor i due to the applied force, F_i (shaded region shown in Fig. 4-40) can be used.

$$E^*_{D,h,i} = A^*_{hyst,i} = 4F_{y,i}\delta_{y,i}\left(\mu_{\delta,i} - r_{\delta,i}\left(\mu_{\delta,i}-1\right)-1\right) \tag{4-55}$$

The shaded region in Fig. 4-39 if $\bar{\delta}_i$ is taken as δ_i is equal to the respective shaded regions in Fig. 4-40.

4.3.2.4.2 Equivalent Hysteretic Damping

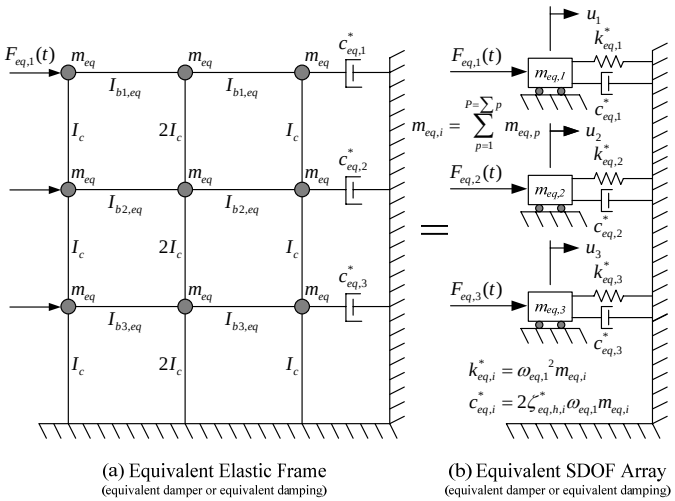

Figure 4-41. Method 2 schematic

As can be illustrated for an elastic MDOF frame subject to a mode-dependent force distribution, each floor of the equivalent elastic frame can be decoupled and treated as a SDOF – but related via natural frequency, $\omega_{eq,j}$ (see Fig. 4-41). This allows a mode-dependent hysteretic damping value to be assigned to each floor. The stiffness of each equivalent elastic SDOF system is

$$k^*_{eq,i,j} = \omega_{eq,j}{}^2 m_{eq,i} \tag{4-56}$$

From Eq. (4-8), the equivalent hysteretic damping ratio and constant per floor *i* are

$$\zeta^*_{eq,h,i,j} = \frac{1}{2\pi\eta_{eq,j}k^*_{eq,i,j}}\frac{E^*_{D,h,i}}{\delta_{in,i}{}^2} \tag{4-57}$$

$$c^*_{eq,h,i,j} = 2\zeta^*_{eq,h,i,j}\omega_{eq,j}m_{eq,i} = \frac{E^*_{D,h,i}}{\pi\eta_{eq,j}\omega_{eq,j}\delta_{in,i}{}^2} \tag{4-58}$$

4.3.2.4.3 Equivalent Hysteretic Modal Damping

Similar to Method 1 the equivalent elastic damping constant for the j^{th} mode is

$$C_{eq,h,j} = \{\phi_{eq,j}\}^T \underbrace{\left[C^*_{eq,h,j}\right]}_{diagonal}\{\phi_{eq,j}\} = \sum_{i=1}^{n}\left(c^*_{eq,h,i,j}\phi_{eq,i,j}{}^2\right) \tag{4-59}$$

It follows that the equivalent hysteretic modal damping ratio is

$$\zeta_{eq,h,j} = \frac{C_{eq,h,j}}{2\omega_{eq,j}M_{eq,j}} = \frac{\sum_{i=1}^{n}\left(\zeta^*_{eq,h,i}m_{eq,i}\phi_{eq,i,j}{}^2\right)}{\sum_{i=1}^{n}\left(m_{eq,i}\phi_{eq,i,j}{}^2\right)} \tag{4-60}$$

It can be seen when comparing Eqs. (4-51) and (4-60) that the latter is computationally simpler. However, Method 1 could be more applicable when the elastic and equivalent elastic mode shapes differ by more than 25%.

4.3.2.5 Three-Story Example

Take for example the three-story frame shown in Fig. 4-38. System properties and distributions are given are:

Frame Properties:
E = 29000 *ksi*
I_c = 1000 in^4
$I_{b2} = I_{b3}$ = 2000 in^4
I_{b1} = 1000 in^4
h_c = 144 *in*
L_b = 288 *in*

Dynamic Properties:
m = 0.647
m_l = 1.941
$k_{i,1}{}^*$ = 40 *k/in*
T_1 =1.384 *sec*
ω_1 = 4.54 *rad/sec*
ζ_v = 0% (undamped)

Hinge Properties:

DOF	d_b	M_p	ϕ_y	r_ϕ	θ_{by}	r_θ
i	*in*	*in-kip*	$\times 10^{-5}$	$\times 10^{-3}$	$\times 10^{-3}$	$\times 10^{-2}$
1	24	1955	6.74	5.39	3.24	1.08
2	24	4840	8.35	6.68	4.01	1.34
3	24	5620	9.69	7.75	4.65	1.55

Floor Properties:

DOF	V_y	Δ_y	r_Δ
i	*kips*	*in*	
1	100	2.50	0.10
2	170	1.76	0.13
3	201	0.77	0.18

$$\{\phi_1\} = \begin{Bmatrix} 1.000 \\ 0.704 \\ 0.307 \end{Bmatrix}$$

Beams are assumed axially rigid and no gravity load is applied to the system. The frame is subjected to a harmonic forcing function invariant to the 1st mode, $\{F(t)\} = \{\phi_f\}_1 F \sin \bar{\omega} t$, as shown in Fig. 4-39 and listed in Table 4-22. Yielding occurs only in the beam ends. The frame is designed such that all beam hinges form simultaneously under the given force distribution. The nodal masses are set only for horizontal inertia.

Table 4-22. Harmonic forcing functions

Index	F *kips*	Excitation Frequency, $\bar{\omega}$ *rad/sec*	Tabulated Results
Case 1	200		
Case 2	175	Case A - π	Table 4-23
Case 3	150		
Case 4	125	Case B - 2π	Table 4-24
Case 5	100		

An excitation frequency, $\bar{\omega}$, of π and 2π are chosen to insure that 1st mode steady-state response is achieved. Similar to the one-story example, it is found that response under low excitation frequencies contains transient response. Also, displacement response for some excitation frequencies outside the example range is coupled with higher modes during force redistribution. An adaptive force distribution would essentially remove this limitation. The 1st mode-based force distribution for this example is

$$\{\phi_f\}_1 F = \left\{ \frac{m_i \phi_{i,1}}{\sum_{i=1}^{n} (m_i \phi_{i,1})} \right\} F = \begin{Bmatrix} 1.000 \\ 0.7040 \\ 0.3071 \end{Bmatrix} F \qquad (4\text{-}61)$$

Fig. 4-42 illustrates the monotonic pushover response when subjected to the force distribution in Eq. (4-61).

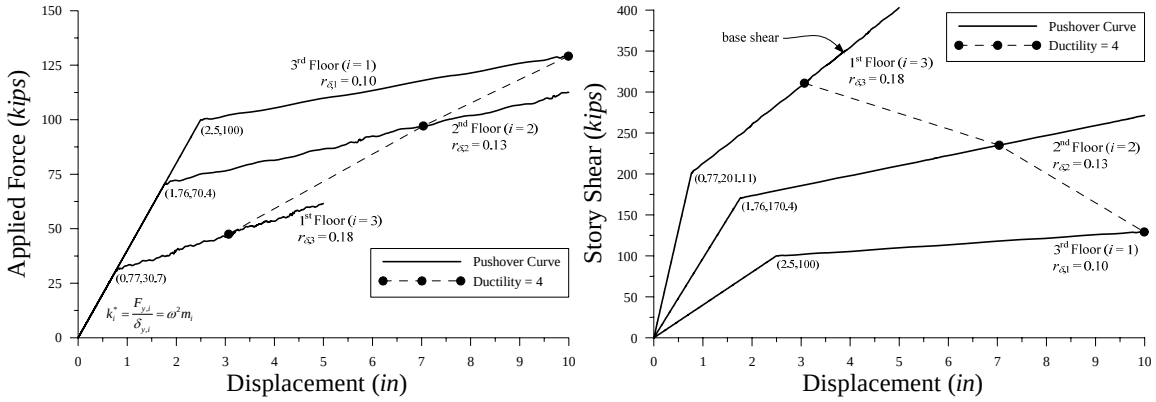

(a) force-displacement **(b) story shear-displacement**

Figure 4-42. Pushover curves

Tables 4-23 and 4-24 lists the results from dynamic analysis of the (1) inelastic frame, (2) undamped equivalent elastic frame with external linear dampers - Method 2, (3) equivalent elastic frame with modal damping – Method 2 (Method 1 values are shown for comparison), and (4) equivalent elastic SDOF per floor (see Fig. 4-41). The energy dissipated by the system was determined by Eq. (4-46) using rotation ductility of the plastic hinges (Eq. (4-22)).

Table.4-23. Analytical results (Case A)

		Inelastic Frame						Equivalent Elastic Frame with External Linear Dampers (Method 2)								Modal Damping			Eq. Elastic SDOF	
F	DOF (i)	δ_{in}	μ_θ	*Area*	$E_{D,h,sys}$	τ	$E_{D,h}^*$	$I_{b,eq}$	M_{eq}	$\omega_{eq,1}$	$T_{eq,1}$	$\phi_{eq,1}$	F_{eq}	$c_{eq,h}^*$	$\zeta_{eq,h}^*$	δ_{el}	$\zeta_{eq,h,1}$	$\zeta_{eq,h,1}$	δ_{el}	k_{eq}^*	δ_{el}
kips		*in*		*in-kips*	*in-kips*		*in-kips*	in^4	in^4	*rad/sec*	*seconds*		*kips*			*in*	Method 1	Method 2	*in*	*kip/in*	*in*
	3	3.13	6.86	2414		0.035	245	318	2.200			0.178		2.52	28.0	2.68			2.66	9.23	2.80
200	2	8.97	11.01	3064	6975	0.261	1823	206	2.336	2.048	3.068	0.555	232.05	2.30	24.0	8.41	20.6	21.0	8.33	9.80	8.53
	1	15.71	15.97	1498		0.704	4907	73	2.465			1.000		2.01	20.0	15.21			15.08	10.34	15.11
	3	2.80	6.07	2089		0.035	211	355	2.166			0.180		2.73	29.6	2.47			2.45	9.85	2.54
175	2	8.00	9.78	2688	6095	0.260	1586	228	2.300	2.132	2.947	0.557	202.60	2.51	25.6	7.68	22.1	22.5	7.60	10.45	7.75
	1	14.02	14.18	1319		0.705	4299	81	2.430			1.000		2.22	21.4	13.85			13.69	11.05	13.79
	3	2.46	5.26	1753		0.034	176	405	2.122			0.183		2.96	31.1	2.26			2.23	10.67	2.28
150	2	7.02	8.52	2301	5188	0.258	1340	258	2.251	2.242	2.802	0.559	173.19	2.76	27.3	6.96	23.8	24.1	6.87	11.32	6.96
	1	12.31	12.32	1134		0.708	3671	91	2.382			1.000		2.45	23.0	12.50			12.32	11.98	12.48
	3	2.11	4.43	1411		0.033	140	476	2.064			0.186		3.20	32.3	2.05			2.02	11.84	2.03
125	2	6.03	7.22	1903	4259	0.256	1092	300	2.187	2.395	2.624	0.563	143.77	3.04	29.1	6.23	25.7	25.9	6.12	12.54	6.15
	1	10.56	10.44	945		0.711	3027	106	2.316			1.000		2.75	24.8	11.10			10.91	13.28	11.14
	3	1.76	3.57	1060		0.031	104	582	1.993			0.191		3.41	32.9	1.80			1.77	13.53	1.76
100	2	5.01	5.91	1502	3310	0.252	835	361	2.101	2.605	2.412	0.567	114.40	3.37	30.8	5.37	27.8	27.9	5.27	14.26	5.22
	1	8.78	8.47	748		0.716	2371	128	2.226			1.000		3.12	26.9	9.48			9.29	15.10	9.57

Table.4-24. Analytical results (Case B)

		Inelastic Frame						Equivalent Elastic Frame with External Linear Dampers (Method 2)								Modal Damping			Eq. Elastic SDOF	
F	DOF (i)	δ_{in}	μ_θ	*Area*	$E_{D,h,sys}$	τ	$E_{D,h}^*$	$I_{b,eq}$	M_{eq}	$\omega_{eq,1}$	$T_{eq,1}$	$\phi_{eq,1}$	F_{eq}	$c_{eq,h}^*$	$\zeta_{eq,h}^*$	δ_{el}	$\zeta_{eq,h,1}$	$\zeta_{eq,h,1}$	δ_{el}	k_{eq}^*	δ_{el}
kips		*in*		*in-kips*	*in-kips*		*in-kips*	in^4	in^4	*rad/sec*	*seconds*		*kips*			*in*	Method 1	Method 2	*in*	*kip/in*	*in*
	3	1.05	1.75	308		0.034	31	1158	1.840			0.2384		1.42	10.3	1.05			1.05	25.59	1.08
200	2	2.66	2.32	405	915	0.261	239	877	1.848	3.729	1.685	0.6227	216.12	1.71	12.4	2.74	13.1	13.2	2.74	25.70	2.77
	1	4.15	3.03	203		0.705	645	338	1.870			1.0000		1.90	13.6	4.40			4.41	26.00	4.38
	3	1.03	1.65	267		0.041	30	1226	1.838			0.2512		1.43	10.0	1.01			1.01	27.83	1.02
175	2	2.49	2.03	316	728	0.280	204	998	1.836	3.891	1.615	0.6398	186.11	1.66	11.7	2.58	12.3	12.3	2.58	27.79	2.59
	1	3.71	2.45	146		0.679	494	414	1.840			1.0000		1.82	12.7	4.03			4.03	27.85	4.02
	3	0.98	1.53	218		0.045	23	1319	1.837			0.2678		1.23	8.2	0.98			0.98	30.50	0.98
150	2	2.33	1.72	220	525	0.293	154	1176	1.829	4.075	1.542	0.6615	156.36	1.43	9.6	2.41	9.9	10.0	2.41	30.37	2.42
	1	3.38	1.88	88		0.663	348	538	1.826			1.0000		1.54	10.3	3.64			3.65	30.32	3.64
	3	0.91	1.35	143		0.046	14	1492	1.843			0.2873		0.84	5.3	0.94			0.95	34.14	0.94
125	2	2.14	1.38	117	297	0.301	89	1456	1.832	4.304	1.460	0.6857	127.41	0.99	6.3	2.25	6.4	6.5	2.26	33.93	2.25
	1	3.06	1.37	37		0.652	194	734	1.827			1.0000		1.05	6.7	3.28			3.29	33.84	3.28
	3	0.82	1.13	53		0.051	6	1774	1.878			0.2969		0.45	2.7	0.86			0.86	37.46	0.82
100	2	1.87	1.14	42	118	0.251	30	1762	1.879	4.466	1.407	0.6924	101.10	0.43	2.6	2.00	3.1	3.1	2.01	37.48	1.90
	1	2.71	1.23	23		0.698	83	814	1.865			1.0000		0.57	3.4	2.89			2.91	37.18	2.76

Fig. 4-43 compares the displacements of the equivalent frames with the inelastic displacements. This procedure leads to agreement between the peak displacements.

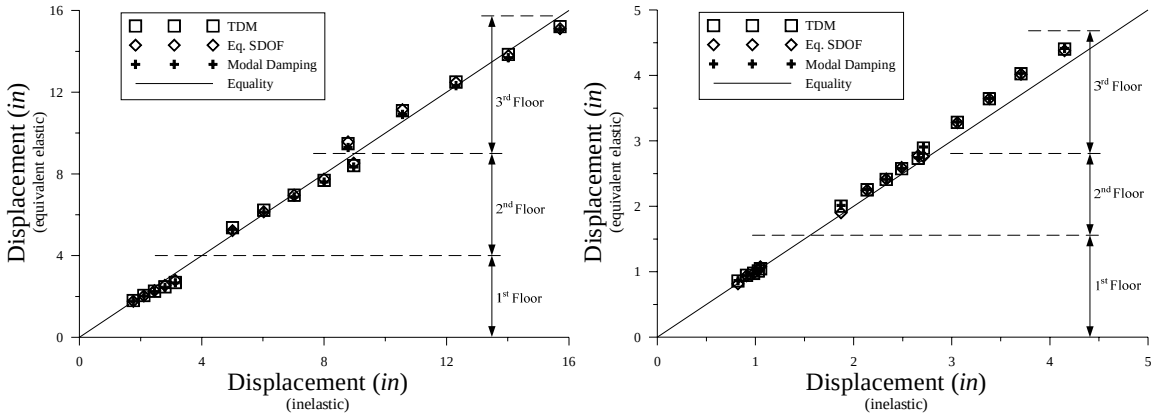

(a) Case A ($\overline{\omega} = \pi$) **(b) Case B ($\overline{\omega} = 2\pi$)**

Figure 4-43. Displacement comparison

Table 4-25 compares the equivalent hysteretic modal damping values obtained from the proposed methods. Damping values were calculated based on energy dissipated per floor using rotation ductility (Eqs. (4-44) and (4-66)) and displacement ductility (Eqs. (4-45) and (4-55)). Both methods yield equivalent results. Displacement ductility is recommended for convenience. Both methods give the same result if $\phi_j = \phi_{eq,j}$.

Table 4-25. Equivalent modal damping comparison

Case	Rotation Ductility			Displacement Ductility		
	Method 1	Method 2	% Diff.	Method 1	Method 2	% Diff.
1-A	20.6	21.0	2.01	20.2	20.4	1.45
2-A	22.1	22.5	1.76	21.5	21.8	1.49
3-A	23.8	24.1	1.43	22.9	23.3	1.54
4-A	25.7	25.9	1.06	24.5	24.9	1.63
5-A	27.8	27.9	0.48	26.2	26.7	1.77
1-B	13.1	13.2	0.44	12.1	12.2	0.61
2-B	12.3	12.3	0.44	10.9	10.9	0.12
3-B	9.9	10.0	1.23	9.1	9.2	1.32
4-B	6.4	6.5	1.34	6.6	6.8	2.67
5-B	3.1	3.1	0.53	2.8	2.9	3.64

Lastly, in the previous example, plastic hinges in the 1st floor column bases were purposely chosen not to develop. The formation of base hinges creates an additional complexity by requiring the use of an equivalent elastic column. The main difficulty with this is the determination of the axial force-dependent equivalent stiffness of the column with only one hinge developed. Another challenge is how to model this effect in an elastic analysis. For illustration only, the 1st floor column strengths were altered to allow the formation of column base hinges simultaneously with beam hinges to illustrate the change in fundamental mode shape during inelastic response (see Fig. 4-44).

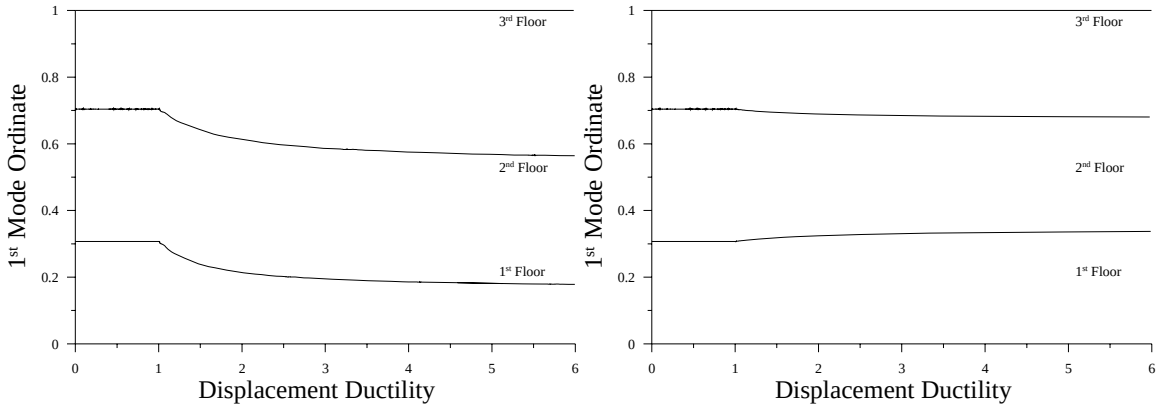

(a) without base hinges **(b) with base hinges**

Figure 4-44. Mode shape relationship (normalized to top floor)

The mode shape essentially remains unchanged as displacement ductility increases. As a corollary, if the design engineer assembles a system that develops a global yield mechanism with all hinges forming virtually simultaneously then the equivalent mode shape (inelastic) can be taken equal to the elastic mode shape. As a side note, decoupling strength and stiffness of the column as performed here requires the use of a Reduced Column Section (RCS) in the base. To the author's knowledge this concept has not been researched.

4.3.3 Earthquake Excitation – SDOF and MDOF Frames

The procedure presented for inelastic frames subject to steady-state harmonic excitation can be applied to frames excited by strong ground motion. Ground motions during an earthquake are not steady-state and are comprised of a collection of excitation frequencies with varying amplitudes. As a result, steady-state theory as previously outlined does not apply and, consequently, statistical investigations are required to determine a practical approximation of hysteretic damping.

The damping curve for earthquake excitation must be derived respective of the linearization methodology. For ease of integration into seismic analysis researchers have proposed modifications to steady-state theory. In so doing, the equivalent frequency ratio, η_{eq}, must be statistically approximated. Equivalent hysteretic damping can be approximated by modifying Eqs. (4-47) and (4-57).

$$c_{eq,h} = \kappa \frac{E_{D,h}}{2\pi\omega_{eq}\bar{\delta}_{in}^{\,2}} \text{ - Method 1} \tag{4-62a}$$

$$\zeta_{eq,h}^{*} = \kappa \frac{E_{D,h}^{*}}{2\pi k_{eq}^{*}\delta_{in}^{\,2}} \text{ - Method 2} \tag{4-62b}$$

where

$$\kappa \quad = \text{hysteretic damping modification factor} \left(= \frac{Z}{\eta_{eq}} \right) \tag{4-62c}$$

Z = Earthquake response adjustment for other factors

The best choice for approximating hysteretic damping for use in the proposed approach is the procedure derived by either Dwairi et al. (2005), Blandon and Priestley (2005), or Harris (2004) since these proposals are based on the use of the secant stiffness. Although these recommendations are based on studies of SDOF systems, it is assumed that they can be readily adopted in the proposed MSSM approach for a MDOF frame since each floor is treated individually.

Dwairi et al. (2005) determined κ to be 0.43 for elastoplastic response. Since this value was statistically derived, it is assumed that this value incorporates the change in frequency ratio during inelastic response and incorporates the fictitious change in mass. As a result, the derived factor should be modified to account for (1) post-yield stiffness (decrease) and (2) change in mass (decrease) to be applicable for Eq. (4-62). If the curve was decreased by approximately 90% it would closely correspond with that proposed by Blandon and Priestley (2005) for $r_{\Delta} = 0.1$. It is similarly assumed that the curve proposed by Blandon and Priestley (2005) incorporates the fictitious change in mass and, as a result, should decrease for use with the proposed methods. Furthermore, these curves are proposed for SDOF systems and it is uncertain if they can be applied to MDOF frames that can exhibit an increase in damping due to higher mode contributions.

Based on research by Harris (2004) and herein (Chapter 7), it is recommended that a value for κ be taken as 0.5 for steel moment frames less then three stories and 0.6 (= 1.2×0.5) for frames between three and six stories. The 1.2 factor is proposed to account for variations in damping due to possible contributions from higher modes. This factor could change depending on number of floors and expected floor displacement

ductility demands pending further research. Also, the change in mass is accounted in the damping formulation. Fig. 4-45 plots the three damping curves.

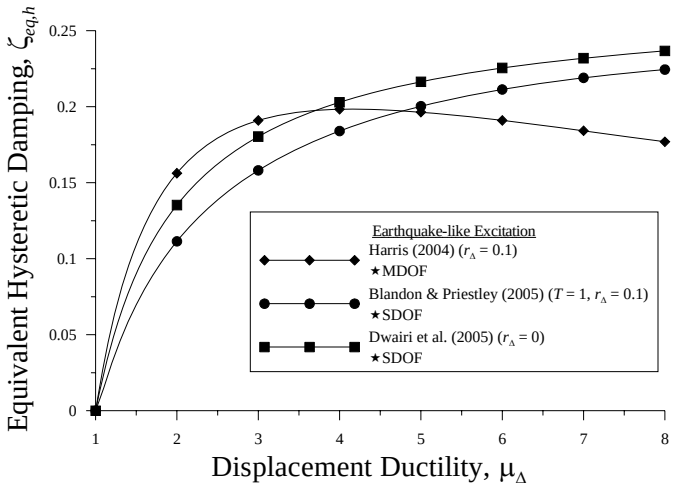

Figure 4-45. Equivalent hysteretic Damping

Lastly, the variation in yield-level design forces determined from the three damping curves result in even smaller variations in actual strength and stiffness properties of the structural components. This is primarily due to seismic design provisions and standard available hot-rolled steel sections providing a wide range of capacities that could satisfy the demand. For example, the design demand based on Blandon and Priestley may provide a W24×76 frame beam whereas a W24×68 and W24×62 are required by the demand determined from Dwairi et al. and the recommended value respectively. However, a W24×62 is not permitted by AISC seismic provisions (2005) due to local buckling requirements. Capacity design can also affect the required strength and stiffness of beams thereby resulting in a W24×76 or possibly heavier. In the end, the quantitative damping modification factor adopted is somewhat insensitive to design. The values derived by Dwairi et al. and Blandon and Priestley establish the

lower-bound limit whereas the upper-bound limit is determined from the recommended value for ductility demands less than 4.

4.3.4 Equivalent Damping For Use in DDBD

In reference to the basic DDBD steps, a target and yield displacement profile based on the fundamental mode shape is constructed in Steps 2 and 3 from which displacement ductility demands on each floor can be estimated. Based on the force distribution the amount of hysteretic energy dissipated by the system, $E_{D,h,sys}$, and portion thereof by each floor, $E^*_{D,h,i}$, (assuming Method 2) can be identified. It follows that the hysteretic damping ratio and constant for each floor are

$$\zeta^*_{eq,h,i} = \kappa \frac{E^*_{D,h,i} T_{eff,eq,\delta}{}^2}{8\pi^3 m_{eq,i} \delta_{d,i}{}^2} \text{ (Method 2)} \tag{4-63}$$

$$c^*_{eq,h,i} = \frac{4\pi}{T_{eq,\delta}} \zeta^*_{eq,h,i} m_{eq,i} \text{ (Method 2)} \tag{4-64}$$

The equivalent hysteretic modal damping constant and ratio are approximated by

$$C_{eq,h,\delta} = \frac{\sum_{i=1}^{n} \left(c^*_{eq,h,i} \delta_{d,i}{}^2 \right)}{\delta_{d,n}{}^2} \text{ (Method 2)} \tag{4-65}$$

$$\zeta_{eq,h,\delta} = \frac{\sum_{i=1}^{n} \left(\zeta^*_{eq,h,i} m_{eq,i} \delta_{d,i}{}^2 \right)}{\sum_{i=1}^{n} \left(m_{eq,i} \delta_{d,i}{}^2 \right)} \text{ (Method 2)} \tag{4-66}$$

The subscript δ is substituted for j in the previous equations to identify that modal and effective system properties are based on the target displacement profile, normalized such that the top DOF is unity (i.e., $\phi_\delta = \phi_j$).

Equivalent damping is assumed as the linear summation of the equivalent viscous and hysteretic damping.

$$\zeta_{eq} = \zeta_{eq,v} + \zeta_{eq,h} = \zeta_v + \zeta_{eq,h} \tag{4-67}$$

Equivalent viscous damping is customarily taken equal to viscous damping in the elastic frame. A viscous damping value between 2% and 5% is recommended, the first being more applicable to steel moment frames. In reference to Eq. (4-66), an iterative process is required since the equivalent period is not initially known. An equivalent damping value of 10% for $n < 3$ and 15% for $3 \le n \le 6$ is a reasonable starting value.

4.4 Conclusion

This chapter has proposed a methodology to compute a quantitative degree of damping for design of steel moment frames that bypasses the limitation of assuming a system-level force-displacement loop. The damping model plays a significant role in the seismic demand estimation and design when using an equivalent elastic frame to characterize the inelastic structural system (Xue 2002). Special attention should be drawn to the selection of a reasonably accurate damping curve. In addition, for design purposes the damping curve should slightly underestimate the actual damping. This provides a form of conservatism to safeguard the structure against possible failure modes. Vice

versa, if too high a damping value is accepted, design forces could be underestimated while actual displacements could exceed the target objective.

Finally, it is thought that using the 1st mode-based displacement profile to estimate the target damping level for low-rise short period steel moment frames where response is designed to be predominantly governed by the 1st mode provides a practical estimation of design forces while simultaneously maintaining a lower-bound damping value.

Chapter 5 *P*-Δ Effect

5.1 Introduction

In a *P*-Δ analysis force equilibrium is equated taking in to account the deformed structure. In reference to the SDOF shown in Fig. 5-1(a), when a lateral force, *F*, is applied to the mass, the mass displaces Δ_1 and force equilibrium confirms that the base shear developed is equal to the applied force. If the SDOF supports a vertical force, *P*, from gravity loads as illustrated in Fig. 5-1(b) and the same magnitude lateral force is applied, equilibrium about the deformed system (at Δ_1) demonstrates that the base shear developed is equal to the applied force plus an additional shear force due to an increase in base overturning moment, $P\Delta_1$. The response effect of this added overturning moment is modeled as an equivalent shear force on the system, $P\Delta_1/h_n$. This equivalent shear force causes the mass to undergo displacement Δ_2 beyond that produced by the lateral force. This supplementary action is identified as the 'second-order' or *P*-Δ effect. Analytical results are termed as being 'first-order' when the effects of vertical loads are not considered.

As intuition might suggest, a *P*-Δ analysis is iterative since the equivalent shear force is updated each analysis step. Thus, the graphical description illustrated in Fig. 5-1(b) is based on a single iteration *P*-Δ analysis. It is typical practice to terminate a second-order analysis when the change in displacement is less than 1% of the previous iteration.

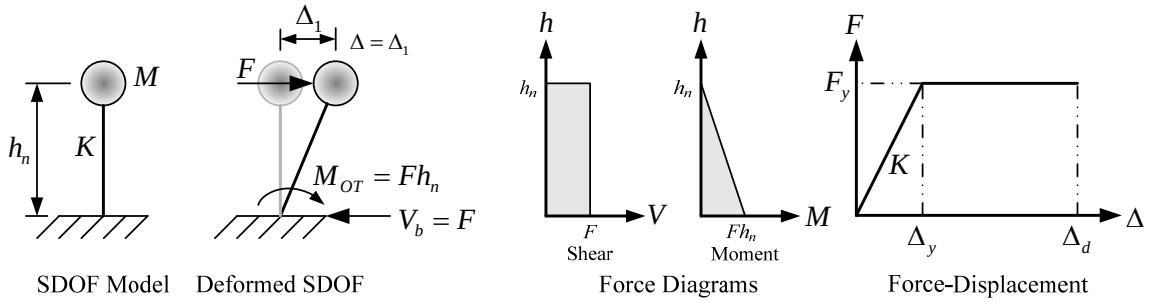

(a) First-order response of SDOF

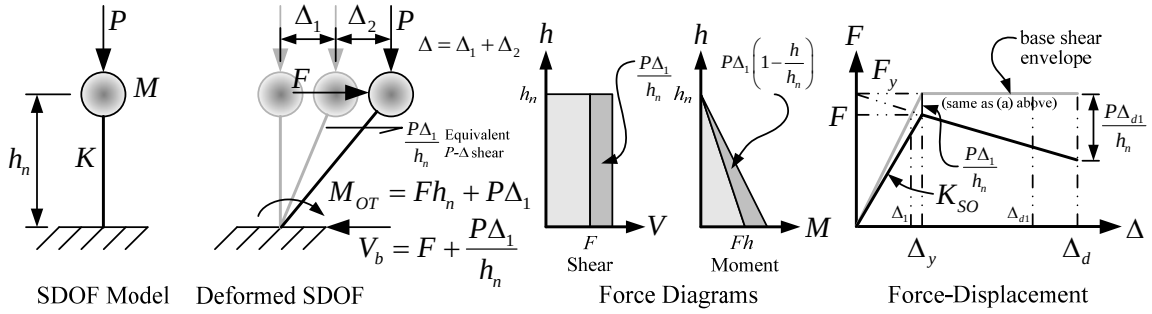

(b) Second-order (P-Δ) response of SDOF

Figure 5-1. SDOF response

Referring to the force-displacement graph shown in Fig. 5-1(b), including a vertical force has the affect of modifying the response of a system by causing a reduction in stiffness. The second-order elastic stiffness is computed by

$$K_{SO} = K - \frac{P}{h_n} = K\left(1-\theta\right) \tag{5-1}$$

where

θ = Stability coefficient $\left(= \dfrac{P}{Kh_n}\right)$ (5-1a)

K = First-order Stiffness

If the first-order natural cyclic frequency, ω_{FO}, is characteristically given by $\omega_{FO} = \sqrt{K/M}$ then the natural frequency and period including the second-order effect, ω_{SO} and T_{SO} respectively, are given by

$$\omega_{SO} = \sqrt{\frac{K(1-\theta)}{M}} = \omega_{FO}\sqrt{1-\theta} \tag{5-2}$$

$$T_{SO} = 2\pi\sqrt{\frac{M}{K(1-\theta)}} = \frac{T_{FO}}{\sqrt{1-\theta}} \tag{5-3}$$

Consequently, response results can vary significantly between the two systems (first and second-order) in a dynamic analysis.

As shown by Eq. (5-3), the period of the SDOF is lengthened by including the *P*-Δ effect. Thus, the motivation to incorporate the *P*-Δ effect in seismic design is fueled by the need to capture the change in fundamental period and, ultimately, the variation in lateral design forces. Fig. 5-1 indicates that the yield displacement does not significantly vary when the second-order effect is included (Priestley et al. 1993 , MacRae 1994, and Aschheim and Montes 2003). This conclusion is founded on the response of a SDOF system with known structural properties. This understanding can be viewed differently when structural properties are not yet identified and for MDOF frames as will be discussed subsequently.

According to NEHRP 2003 (BSSC 2003), taken from ATC-3 (1978), the ratio of second-order to first-order displacement assuming elastic response can be estimated by

$$\frac{\Delta}{\Delta_e} = \frac{1}{1-\theta} = \lambda_{\max} \tag{5-4}$$

where

$$\theta \quad = \text{Stability coefficient} \left(= \frac{P\Delta_{\max} I}{F h_n C_d} = \frac{P}{F}\left(\frac{\Delta_e}{h_n}\right)\right) < \left(\frac{0.5}{\beta C_d} \le 0.25\right) \tag{5-4a}$$

Δ_e = First-order elastic displacement (discussed in Chapter 1)

F = First-order lateral force (discussed in Chapter 1)

βC_d = Adjusted ductility demand (per code)

Setting $F/\Delta_e = K$ in Eq. 5-4(a) leads to P/Kh_n which is equal to Eq. (5-1a).

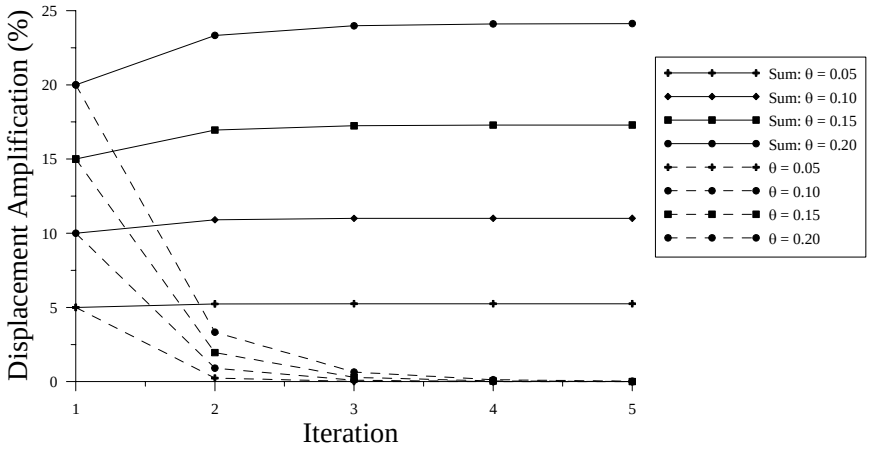

Figure 5-2. Percent displacement increase per iteration

The stability coefficient, θ, can be expressed as the first iteration percent increase in displacement due to the *P*-Δ effect (see Fig. 5-2), and Eq. (5-4) is the maximum displacement amplification after several iterations. From Fig. 5-2, higher stability coefficients require additional iterations to obtain a change between iterations to fall below a limiting value, say 1%. Past research has proposed that regular building

structures fall into the range of coefficients presented in Fig. 5-2. Thus, a single iteration *P*-Δ analysis is generally all that is required to adequately account for the increase in required strength for elastic frames.

In terms of dynamic response, Fig. 5-2 assumes that the acceleration of the mass and damping are independent of the 2nd order period (Eq. (5-3)). That is, any change in acceleration of mass or damping force as it undergoes additional displacement is neglected (i.e., *F* is determined from the first-order period). Take for example the SDOF presented in Fig. 5-1(a) with the following properties: M = 1.102 *k-sec*^{2}*/in*, K = 10.88 *k/in*, h_n = 200 *in*, and viscous damping = 5%. The period neglecting gravity force, T_{FO}, is 2 *seconds*. The response ordinates from the 5% damped response spectrum for TH-6 (see Appendix B) are: S_d = 15.55 *inches* (see Fig. 5-3) and S_a = 0.397*g*. Subjecting the SDOF to TH-6 in an elastic first-order dynamic analysis results in a displacement of 15.55 *inches* and an inertia force, *F*, acting on the system of 169.2 *kips*.

When considering the effect of the gravity force, *P*, a value for θ is chosen as 0.45 (P = 981.6 *kips*) and yields a second-order period, T_{SO}, equal to 2.7 *seconds*. The response ordinates from the 5% damped response spectrum for TH-6 are: S_d = 22.37 *inches* (see Fig. 5-3) and S_a = 0.314*g*. Subjecting the SDOF to TH-6 in an elastic second-order dynamic analysis results in a displacement of 22.37 *inches* and an inertia force, *F*, acting on the system of 133.5 *kips*. The base shear developed in the system is 243.3 *kips* (F+$P\Delta/h$ = 133.5+109.8). This illustrates that if the system were to be designed at yield

the design force would need to be 243.3 *kips*, which equates to a strength increase of 1.82 (243.3÷133.5) or 1.44 (243.3÷169.2).

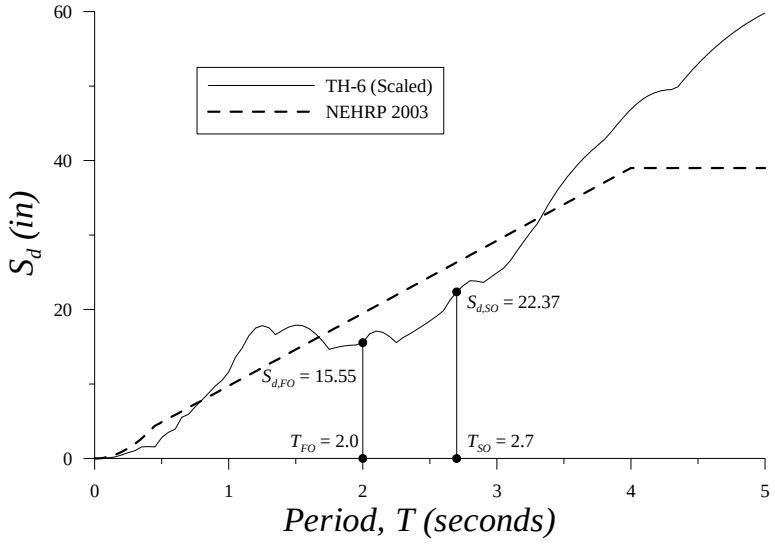

Figure 5-3. 5% damped DRS (TH-6)

From Eq. (5-4), the static displacement amplification is 1.82 leading to a displacement of 28.34 *inches* (15.55×1.82 – this value is also obtained after 10 iterations using first-order dynamic analysis results). However, the results obtained by the 2nd order dynamic analysis indicate a displacement amplification of 1.44 (22.37÷15.55). This discrepancy is due to displacement comparison at two different lateral force levels (F_{FO} = 169.2 *kips* and F_{SO} = 133.5 *kips*). Taking F_{FO} = 133.5 *kips* gives a first-order displacement of 12.27 *inches* resulting in a displacement amplification of 1.82. The amplification factors for 2%, 10%, 15% and 20% damping are 1.65, 1.55, 1.70, and 1.68 respectively and all require a strength and stiffness increase of 1.82. These values are dependent on ground motion characteristics and could widely vary between various earthquake records.

Entering the codified DRS (see Fig. 5-3) with the previous periods gives 19.5 and 26.3 *inches* respectively equating to a displacement amplification of 1.35. This value can also be obtained by Eq. (5-5) which was derived by Bernal (1987) for the region defined by the descending branch of the Acceleration Response Spectrum.

$$\frac{1}{\sqrt{1-\theta}} = \lambda_{\min} \tag{5-5}$$

The required strength increase in this scenario is still 1.82. Similarly, the amplification factor in Eq. (5-5) is based on two different lateral forces. Were the displacements compared at the same force level, say the second-order inertia force, the amplification factor would be Eq. (5-4). This concept is graphically illustrated in Fig. 5-4.

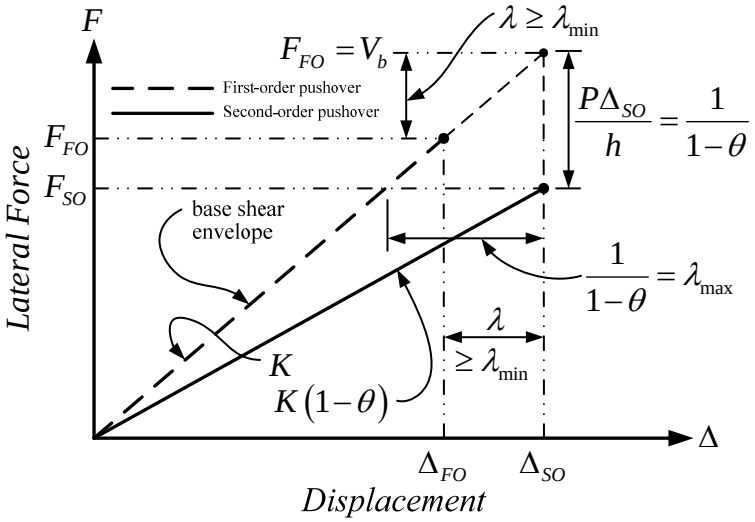

Figure 5-4. Elastic force-displacement response with *P*-Δ

As a result, presuming the dynamic analysis procedure is valid, design forces and displacements including the *P*-Δ effect would be overestimated if the reference lateral force and displacements were based on first-order system properties. Hence, if *P*-Δ

effects are judged to be necessary the second-order period should be used in analysis and design. Although scattered based on actual ground motion characteristics the displacement amplification factor for design purposes should be bounded by the upper limit set by Eq. (5-4) and the lower limit established with Eq. (5-5). Strength and stiffness amplification is determined with Eq. (5-4). Using Eq. (5-4) for both displacement and strength amplification implies that the first and second-order lateral forces are equivalent (see Fig. 5-4). Though the example stability coefficient is purposely selected high, the importance of including second-order effects into analysis (i.e., design fundamental period) is evident.

The theory in support of DDBD discussed in the previous chapters is based on first-order analysis principles. The following discussions propose revisions to include 2nd order effects. Including second-order effects is important in DDBD since the methodology is heavily dependent on displacements. The concepts proposed are based on non-conservative small displacement structural theory, the applied gravity force is assumed to remain vertical.

5.2 Literature Review

Second-order effects (P-Δ and P-δ) are required in computing buckling strengths of structural members and are inherent in member design specifications. It is thus required that structural analysis include second-order effects to maintain cohesion with member design equations. Local P-δ effects are outside the scope of this discussion.

Global *P*-Δ effects on static and dynamic frame response have been extensively researched in the past few decades. These research efforts range from simplified SDOF systems to complex tall building frames. However, there is still controversy in choosing an appropriate methodology for inclusion into an analysis and design philosophy and when this effect should be evaluated. Lastly, a common conclusion among researchers is that, generally speaking, their recommendation is an "acceptable means of limiting *P*-Δ effects." It is uncertain what is implied by the previous statement: (1) can *P*-Δ effects be neglected or (2) design would result in a satisfactory system. Research has illustrated the change in dynamic response when *P*-Δ is considered and that in some cases *P*-Δ has decreased the displacement response. Therefore, *P*-Δ effects could be explicitly modeled in analysis and design in order to utilize its beneficial advantages or protect members from the amplified forces when these effects are significant. As a side note, *P*-Δ effects do not change the yield rotation of the beams.

Rosenbleuth (1965) derived a simplified expression similar to the reserve-energy technique developed by Blume (1943) for adapting global *P*-Δ effects into analysis of a lateral force resisting structural frame. In this methodology, the total story shear (including effects from vertical loads) and relative displacement is used to compute the amplification of displacements and forces due to the sole action of these static forces.

$$x = \frac{x_v}{1 - \frac{\sum P}{V}\frac{x_v}{h}} \tag{5-6}$$

where

$x_{v,i}$ = Relative displacements between floors

Though this derivation concerned elastic frames, Rosenblueth recommended its application to inelastic frames and that the stiffness of an inelastic frame is taken as the tangent stiffness. This method, or variation thereof, has been widely adopted in seismic codes to determine amplification of elastic displacements (δ_{xe} in Chapter 1) and forces.

Andrews (1977) illustrated that a secondary consideration for including *P*-Δ effects for earthquake resisting frames is that the corresponding softening of the elastic system equates to a period elongation and thus a reduction in the base shear coefficient. However, the primary concern in this research was to limit *P*-Δ effects by providing a system with a stiffness restriction (provided via static displacement limits) and not development of an analysis and design procedure to explicitly account for *P*-Δ effects.

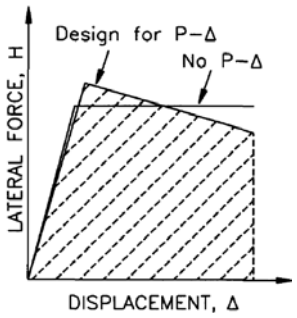

Figure 5-5. Static response of inelastic member (Paulay 1978)

Paulay (1978) illustrated that *P*-Δ effects can be neglected for concrete frames when the stability coefficient (using inelastic displacements) is less than 0.15. Paulay additionally detailed a design methodology where the strength of members could be increased in lieu of stiffness to protect against increased demands from *P*-Δ effects. In

this process the energy dissipated by the two systems are equivalent (see Fig. 5-5). Moss and Carr (1980) further concluded that *P*-Δ effects can be justifiably neglected in design of tall concrete frames when the maximum drift ratio is not significantly greater than 1%. They additionally concluded that providing an increase in strength rather than stiffness offers the most effective means of controlling displacement amplifications. Moehle (1992) recommended that the value proposed by Paulay be increased to 0.2.

Montgomery (1981) concluded in a more general sense that *P*-Δ effects should be considered in frame analysis when the ratio of maximum story drift to yield story drift exceeds 2. This study further concluded that the elastic stability coefficient approach, Eq. (5-4), adopted by seismic codes (at that time) provides reasonable results when the building is elastic or slightly inelastic. In contrast, it was noted that this method should not be used for systems responding in a strongly inelastic manner.

Tjondro et al. (1992) demonstrated that *P*-Δ effects can affect the dynamic response of MDOF steel frames when the maximum drift ratio is greater than 2% and can be ignored when amplification of drifts are less than 10%. Still, these research efforts concentrated on limiting the effects due to *P*-Δ and not explicitly account for such response in analysis and design.

Bernal (1987) contended that Eq. (5-4) underestimates the amplification factor for an elastoplastic SDOF and statistically derived the required dynamic strength increase.

$$\alpha = \overbrace{\frac{1}{\underbrace{1-\theta}_{Eq.(5-4)}}}^{elastic} \overbrace{\left(1+\beta\theta\right)}^{inelastic} \tag{5-7}$$

where

$$\beta \quad = P\text{-}\Delta \text{ coefficient } \left(=1.87\left(\mu_{\Delta}-1\right)\right) \tag{5-7a}$$

The challenge that Eq. (5-4) underestimates the amplification is not applicable since it is specialized for systems responding elastically and does not consider increases due to inelastic displacements (i.e., stiffness reduction). This implies that the stability coefficient should shift as the stiffness reduces. In accordance with the secant stiffness, Eq. (5-4) could be adapted for inelastic systems.

$$\alpha = \frac{1}{1-\mu_{\Delta}\theta} \text{ (EPP response)} \tag{5-8}$$

Eq. (5-8) has been adopted by the Mexican seismic code (MSC 1977). Fig. 5-6 plots Eqs. (5-4), (5-7), and (5-8) for an elastic SDOF (Fig. 5-6(a)) and an inelastic SDOF with $\mu_{\Delta} = 4$ (Fig. 5-6(b)). Eq. (5-8) illustrates good agreement with that derived by Bernal for stability coefficients less than 0.12.

As noted previously, the contention that Eq. (5-4) overestimates the amplification for elastic systems (Fig. 5-6(A)) is not compelling since first-order inertia forces were used for displacement comparison. As shown in Fig. 5-6(b), using the secant stiffness could be an adequate representation of the required strength and stiffness increase required to protect against demand increases from *P*-Δ effects and that the maximum

stability coefficient should be limited to 0.15. Lastly, Tremblay et al. (1998) statistically derived that $\beta = 1.53\left(\mu_{\Delta} - 1\right)$ in Eq. (5-7) for an elastoplastic SDOF systems (see Fig. 5-6(b)). The reduction from Eq. (5-7) is most likely due to the selected earthquake records.

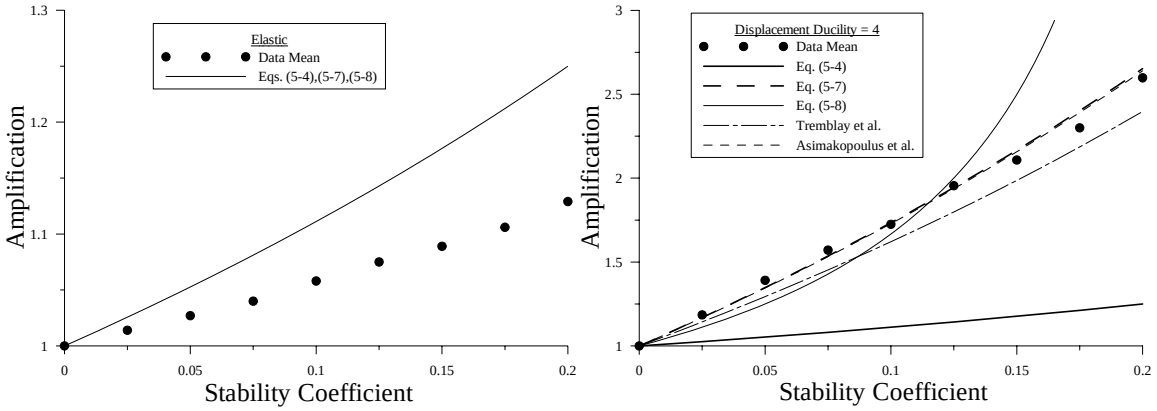

(a) Elastic **(b) Inelastic (elastoplastic)**

Figure 5-6. Amplification factor

Davidson et al. (1991) and Fenwick and Davidson (1994) statistically derived an equation to represent the required strength amplification for multi-story frames similar to Bernal (1987).

$$\alpha = \frac{1}{1-\theta}\left(1 + \beta\mu_{\Delta}\theta\right) \tag{5-9}$$

In this study, β was derived based upon an effective SDOF representation of the multi-story frame and compared to inelastic dynamic results of the multi-story frame. It was shown that the effective SDOF is adequate in defining an approximate amplification factor for a multi-story frame, although larger differences (conservative) were shown for shorter frames. Similar to Bernal (1987), displacement comparison was performed at the

first-order lateral force. Also, it is uncertain if the ratio of seismic weight and gravity load was varied in both these studies.

Bernal (1992, 1998) subsequently concluded that an effective SDOF is adequate for design purposes in predicting the dynamic instability (collapse intensity) of an MDOF system and instability is controlled by the shape of the MDOF yield mechanism. It was further noted that drift limitations provide control on initial stiffness but have no direct effect on the post-yield characteristic. Both Bernal (1987) and Mahin and Boroschek (1991) concluded that *P*-Δ effects can be ignored if the strength amplification to achieve a particular displacement ductility is less than 10%.

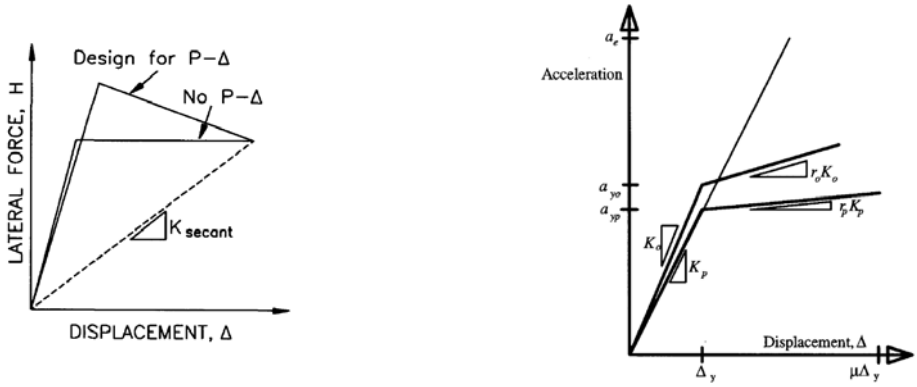

(a) MacRae et al. 1990 **(b) MacRae et al. 1993**

Figure 5-7. Static response of inelastic SDOF

MacRae et al. (1990), based on the effective SDOF principle, recommended a design procedure where the yield strength of the system with *P*-Δ could be increased such that the secant stiffness would match that of the SDOF without *P*-Δ (see Fig. 5-7(a)). This concept suggests that the inelastic displacement and applied force would similarly be matched. The increase in strength was modeled by amplifying the lateral inertia force by

the equivalent shear produced by the *P*-Δ effect. However, this process implies that the two systems are independent of each other in the sense that (1) the system with *P*-Δ illustrates an increase in effective damping while the two maintain the same period and (2) the base shears of the two systems are not concurrent. This procedure also implies that the yield displacement of the two systems varies and it is uncertain if the lateral inertia force was computed via the first or second-order period.

MacRae et al. (1993) and MacRae (1994) subsequently modified the approach by MacRae et al. (1990) for a SDOF system to check against *P*-Δ by including the second-order period when computing the lateral inertia force. The same yield displacement between both systems was maintained thus equating to an increase in stiffness as shown in Fig. 5-7(b). These studies also provided a design provision for systems that failed the *P*-Δ check. The key assumption in this proposal was that the strength of the system can be increased while not providing an increase in stiffness. It was concluded that the maximum stability coefficient for a concrete SDOF (Takeda model) for *P*-Δ to be ignored is 0.15 at $\mu_\Delta = 6$. Adopting this value for a bilinear SDOF with post-yield stiffness, it is proposed by the author that the first-order elastic stability coefficient be limited by

$$\theta \le 0.15\left(\frac{K_{secant}}{K}\right) = 0.15\left(\frac{\left(1+r_{\Delta^1}\left(\mu_\Delta - 1\right)\right)}{\mu_\Delta}\right) \le 0.1 \qquad (5\text{-}10)$$

Eq. (5-10) is dependent on displacement ductility and, therefore, provides a floating elastic stability limit. As a corollary, a high expected ductility results in a low elastic

stability coefficient limit. This implies that a set value, say 0.1 as outlined in NEHRP 2003 (BSSC 2003), can be non-conservative.

Gupta and Krawinkler (2000) performed inelastic dynamic analyses on the SAC steel moment frames and concluded that there is no simple procedure to permit a definite assessment of the collapse hazard due to *P*-Δ effects. It was recommended that the a system be designed such that it will not enter the negative post-yield slope region determined from a force-displacement pushover analysis. It was further noted that the stability coefficient method adopted by seismic codes is adequate in computing the amplification of force and displacement for frames responding essentially elastically.

Aschheim and Montes (2003) presented a simplified design procedure where a second-order yield point spectra can be developed. In this process, an effective SDOF is constructed from an actual SDOF such that dead load (i.e., seismic weight) is the only gravity load acting on the system. The effective height is adjusted to represent any additional gravity loads (i.e., live loads) that do not contribute to seismic weight. This concept is not suited for DDBD since it was formulated explicitly for the Yield Point Spectra method (Aschheim and Black 2000, Aschheim 2002). It was noted that this idealization is limited to a SDOF system and may not be appropriate for a MDOF frame if response is heavily influenced by *P*-Δ effects. Lastly, the design example presented results in a system with a negative post-yield slope (force-displacement) and was not verified by dynamic analysis.

Asimakopoulus et al. (2003) statistically derived a dynamic-based yield displacement amplification factor for an elastoplastic SDOF for inclusion in Direct Displacement-Based Design. In this concept, the yield displacement and, thus, strength were amplified to restrain response with *P*-Δ to a given ductility. This research proposed that β in Eq. (5-7) be taken as $2.396\left(\mu_{\Delta}-1.68\right)$, see Fig. 5-6(b). As shown in the figure, the amplification factors matches those proposed by Bernal (1987) for $\mu_{\Delta}=4$. Although no proposal was given in this study as to the manner in computing the yield displacement, it was contended that the amplification factor is derived to provide a SDOF with constant ductility. This study also proposed a global stability coefficient for an MDOF frame computed based on the number of bays and floors. This factor can be applied to amplify the effective SDOF yield displacement and strength in DDBD.

Conceptually, this method is not well suited for DDBD. First, a target displacement ductility is computed based on a fixed inelastic and yield displacement in DDBD. By amplifying the yield displacement the target ductility is modified and Eq. (5-7) implies an iterative procedure. It is assumed in this method that strength can be increased independent of stiffness (θ remains constant). Secondly, it is implied that the strengthened system will possess the same ductility (e.g., $\mu_{\Delta}=4$). If the initial ductility is based on a fixed target displacement, maintaining constant ductility equates to an increase in the inelastic displacement with *P*-Δ. This is graphically illustrated in Fig. 5-8.

As a result, it can be proposed that the stiffness can be increased while maintaining the yield displacement until the second-order displacement is matched with

the target. Thus, the period is shifted until response is satisfactory and the stability coefficient is modified. Conversely, DDBD could start with the desired second-order period and target displacement and result in the required first-order stiffness.

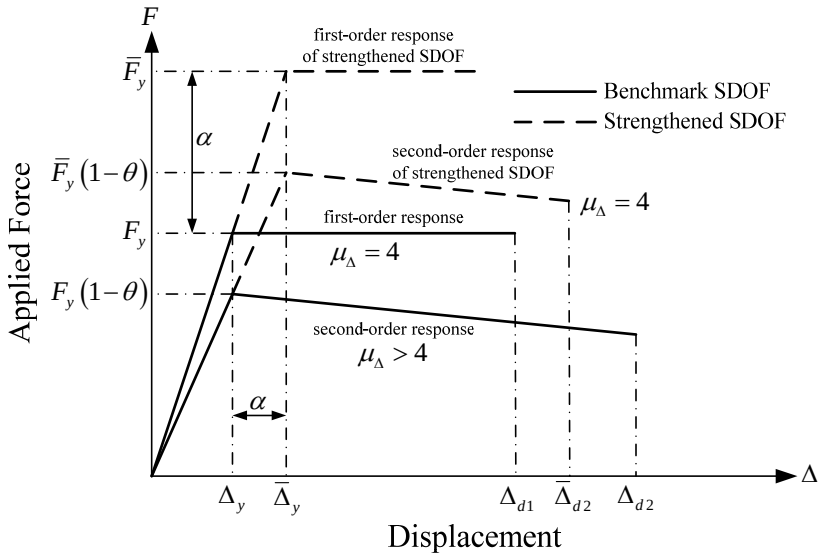

Figure 5-8. Response of amplified inelastic SDOF

Adam et al. (2004) proposed a methodology in which the stiffness of an effective SDOF can be amplified while maintaining the yield displacement. It was noted that *P*-Δ effects in MDOF frames depends on story strength and stiffness, distribution of gravity loads and the extent of inelastic behavior. Therefore, in this study the shape vector used in constructing the effective SDOF was determined from a 1st mode-based pushover analysis of the predefined generic MDOF frames including *P*-Δ (12 and 18 stories). It was concluded that the stability coefficient, θ, in general, increases as inelastic response increases. As a result, the increase in the elastic stiffness is computed via a relationship between the elastic and inelastic stability coefficients. The MDOF pushover curves illustrate that the frames examined have negative post-yield force-displacement

responses. It was further concluded that the proposed effective SDOF is appropriate to estimate *P*-Δ effects in non-deteriorating regular MDOF frames and that the *P*-Δ collapse capacities derived form the effective SDOF are, in most cases, conservative.

The progression of second-order analysis in earthquake engineering is evident based on the previous literature review. These methods were mostly concerned with SDOF oscillators and are dependent on a selected hysteresis function and chosen earthquake records. While limits for predetermined systems have been recommended whereas *P*-Δ effects can be neglected, there still remains a question of what method is appropriate for inclusion into a seismic analysis and design methodology, most notably a reverse engineering philosophy such as DDBD where displacement response is the key analysis and design parameter.

It can thus be proposed that the target inelastic displacement profile used in DDBD include *P*-Δ displacement amplifications, if required. In so doing, the design engineer aims to provide the system with the required story strength and stiffness to withstand second-order contributions based on the distribution of gravity forces. In the absence of dynamic-based approach explicitly tailored for DDBD, it is proposed that a two-level static stability coefficient approach be adopted. The two coefficients are computed for (1) the equivalent elastic system at the target displacement and (2) the elastic system at the yield displacement. In this scenario, the second-order equivalent period is directly computed and applied to compute the required first-order elastic stiffness and design forces. Stiffness amplification of the elastic system is applied via

capacity design (see Chapter 6). The subsequent discussions propose a methodology to explicitly include *P*-Δ into the proposed DDBD procedure.

5.3 Second-Order Yield Displacement Profile

Take for example the three-story frame shown in Fig. 5-9, based on the proposed DDBD procedures, consider design forces at yield are computed based on the required elastic stiffness, *K*, with no *P*-Δ. The design yield forces are then applied to the structural model in a 1st order elastic static analysis and member selections iterated until the required stiffness is achieved. For this discussion, all beams are assumed elastic perfectly-plastic and are designed to yield simultaneously under the design force distribution at Δ_y. The 1st order force-displacement response ($F_{y1} - \Delta_{y1}$) of the top floor to yield is shown in Fig. 5-9.

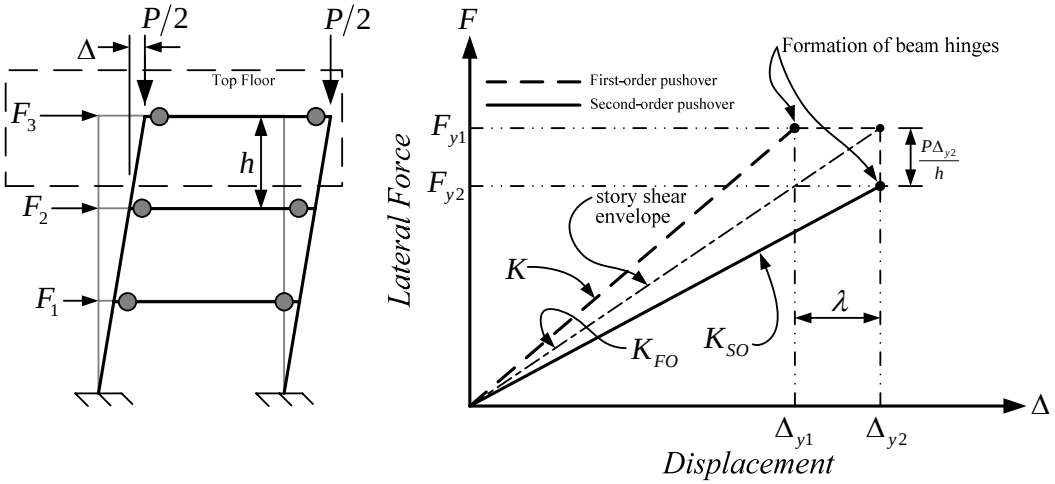

Figure 5-9. Amplification of yield displacement

If the same model (incrementally applied lateral forces) is analyzed with a second-order elastic analysis, the displacements computed at the point that all beams

reach yield will be larger than the first-order displacements determined previously due to an increase in column deformations associated with the addition of the equivalent lateral shears produced by the *P*-Δ effect. The 2nd order force-displacement response ($F_{y2} - \Delta_{y2}$) of the top floor to yield is shown in Fig. 5-9.

As shown in Fig. 5-9, the story shear at yield is amplified in the latter analysis due to the *P*-Δ effect and is concurrent to the first-order force. As a corollary, this displacement amplification should be modeled during analysis and design if *P*-Δ is going to be considered. The conclusion that yield displacement does not vary is valid only if the equivalent shears applied to account for the *P*-Δ effect are included in the design lateral forces. As a side note, this amplification is not visible in SDOF studies, such as that presented in Fig. 5-1.

This equates to two types of analysis and design: (1) without *P*-Δ (first-order) and (2) with *P*-Δ (second-order). The latter is further separated into two sub-classes: (1) first-order with *P*-Δ and (2) second-order with *P*-Δ. The two classes of second-order analysis differ only in that the equivalent lateral shears from *P*-Δ are included in the applied lateral forces.

With respect to the proposed DDBD procedure, if *P*-Δ effects are to be included in analysis an amplification factor applied to the *first-order* lateral yield displacement profile, $\{\delta_{dy,i}\}$, discussed in Chapter 3, is required to assimilate the increase in displacements. The *second-order* yield displacement profile, $\{\hat{\delta}_{dy}\}$, can be estimated by

$$\hat{\delta}_{dy,i} = \lambda_{y,i}\delta_{dy,i} \tag{5-11}$$

By assuming that each floor behaves independently of the others, the amplification factor, λ_y, is approximated by evaluating the total axial force to total horizontal force on a given floor *i*.

$$\lambda_{y,i} = \frac{1}{1 - \frac{\sum_{i=i}^{n} P_i}{\sum_{i=i}^{n} F_{el,i}} \left(\frac{\delta_{dy,i} - \delta_{dy,i-1}}{h_i} \right)} \tag{5-12}$$

where

$F_{el,i}$ = First-order with *P*-Δ lateral force on floor *i* (see Table 6-1)

h_i = Floor height below floor *i*

For simplicity, this factor can be approximated by

$$\lambda_y \approx \frac{F_{y^1}}{F_{y^2}} \tag{5-13}$$

where

F_{y^1} = First-order with *P*-Δ lateral force at yield (Eq. (5-29))

F_{y^2} = Second-order with *P*-Δ lateral force at yield (Eq. (5-26))

Since the total shear force on a given floor, $\sum F_{el}$, in Eq. (5-12) has not yet been determined, an iterative procedure is required and an amplification factor of 1.0 (i.e., no

P-Δ amplification) per floor can be initially assumed. Eq. (5-12) is similar to the *P*-Δ amplification factor (B_2) specified in LRFD specification (AISC 2001) and NEHRP seismic provisions (Eq. (5-4)). As illustrated previously, Eq. (5-12) requires displacement amplification at the same force magnitude; therefore, second-order forces determined from second-order structural properties are applied. The corresponding floor and system yield drift angle are

$$\hat{\theta}_{y,i} = \frac{\hat{\delta}_{y,i}}{h_i} \tag{5-14}$$

$$\hat{\theta}_{y,sys} = \frac{\sum_{i=1}^{n} \hat{\theta}_{y,i}}{n} \tag{5-15}$$

The yield displacement profile, $\left\{\hat{\delta}_{dy}\right\}$, intending to represent the global yield mechanism, is determined by substituting $\hat{\theta}_{y,sys}$ for θ_T in Table 3-1. With the second-order yield displacement profile identified, the transformation of the MDOF to the effective SDOF is performed and the quantities for M_{eff}, h_{eff}, and Δ_y determined. The target displacement profile is not influenced by *P*-Δ effects since second-order demands are incorporated in the analysis and component design in order to achieve the target.

5.4 Effective Gravity Force

Pertaining to the transformation of a MDOF to an effective SDOF discussed in Chapter 2, see Fig. 2-3, the additional overturning moment, ΔM_{OT}, developed under the $P-\Delta$ effect must also be equivalent for both systems.

$$\underbrace{\Delta M_{OT}}_{SDOF} = \underbrace{\Delta M_{OT}}_{MDOF} \tag{5-16}$$

Therefore, taken moments about the center point of the base provides

$$\underbrace{P_{eff}\Delta_{eff}}_{SDOF} = \underbrace{\sum_{i=1}^{n} P_i\delta_i}_{MDOF} \tag{5-17}$$

It follows that the equivalent effective gravity force is computed from

$$P_{eff,eq} = \frac{\sum_{i=1}^{n} P_i\delta_{d,i}}{\Delta_d} \tag{5-18}$$

Eq. (5-18) is an approximate expression developed to simplify the calculation of an effective stability coefficient, $\theta_{eff,eq}$, for calculating the change in 1st mode period (stiffness). Typically, this equation will result in a gravity force ratio similar to the mass ratio (total to effective). Fig. 5-10 compares, for example, the effective stability coefficient using Eq. (5-18) to the theoretical solution determined by dynamic analysis.

The similarity between Eq. (5-18) and Eq. (2-17) should be evident since the work done by the two systems must be in accord. The effective mass and effective gravity force might not always be the same. For example, the seismic weight might be composed of dead loads, *D*, and live loads, *L*, but there could be a component of live load that does not contribute to the lateral force via the seismic weight. In this case, Eq. (5-18) attempts to account for all gravity loads affecting the response stiffness of the system (i.e., second-order effective period) in order to employ a conventional response spectrum.

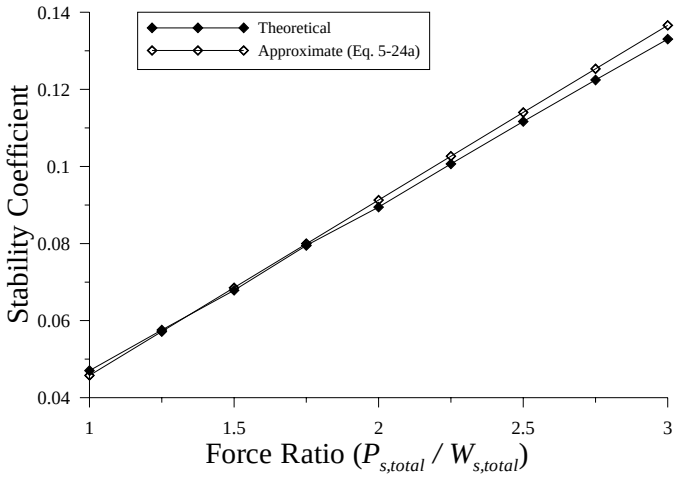

Figure 5-10. Stability coefficient comparison (1st mode)

Likewise, the effective gravity force at the yield point is

$$P_{eff} = \frac{\sum_{i=1}^{n} P_i \hat{\delta}_{dy,i}}{\Delta_y} \tag{5-19}$$

5.5 Equivalent Effective Period and Design Base Shear

If the target displacement, Δ_d, includes second-order effects then the equivalent effective period follows suit. Once the 2nd order period, T_{eff,eq^2}, is computed from the standard DRS (same manner as discussed in Chapter 2), the 2nd order equivalent effective stiffness (secant stiffness to target response) is readily computed by

$$K_{eff,eq^2} = 4\pi^2 \frac{M_{eff,eq}}{T_{eff,eq^2}^{\ 2}} \tag{5-20}$$

The corresponding second-order lateral force is calculated from

$$F_{d^2} = K_{eff,eq^2}\Delta_d \tag{5-21}$$

The respective base shear developed at target response is approximately given by

$$V_{bd} \approx F_{d^2} + \frac{P_{eff,eq}}{h_{eff,eq}}\Delta_d = F_{d^1} \tag{5-22}$$

In so doing, the first-order stiffness of the equivalent effective SDOF at maximum response, K_{eff,eq^1}, is then

$$K_{eff,eq^1} = K_{eff,eq^2} + \frac{P_{eff,eq}}{h_{eff,eq}} \tag{5-23}$$

The first-order target displacement, Δ_{d^1}, at F_{d^2} can be estimated by geometry.

$$\Delta_{d^1} = \left(\frac{K_{eff,eq^2}}{K_{eff,eq^2} + \frac{P_{eff,eq}}{h_{eff,eq}}} \right) \Delta_d = \frac{\Delta_d}{\left(1 - \theta_{eff,eq}\right)} \tag{5-24}$$

where

$$\theta_{eff,eq} \quad = \text{Effective stability coefficient} \left(= \frac{P_{eff,eq}}{K_{eff,eq^2} h_{eff,eq}} \right) \tag{5-24a}$$

Any variation in desired displacement profiles (yield and target) produces dissimilarity in the effective heights. Consequently, displacement comparison should be taken at the same height. Researchers commonly compute an approximate system ductility demand using displacements taken at the roof. Displacement comparison at the

effective height appears to be a more rational approach and can provide an improved measure. It is recommended that the equivalent effective height be used to determine the system ductility demand for design, albeit this process requires an additional modification factor as discussed next. This concept is graphically illustrated in Fig. 5-11.

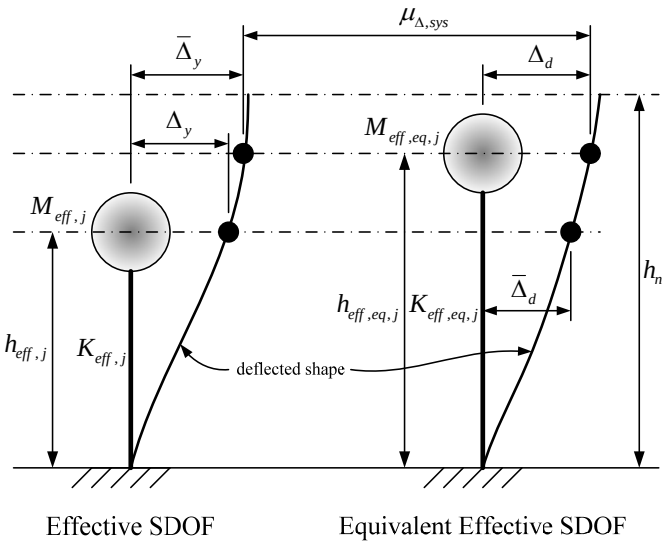

Figure 5-11. Displacement comparison of effective SDOF

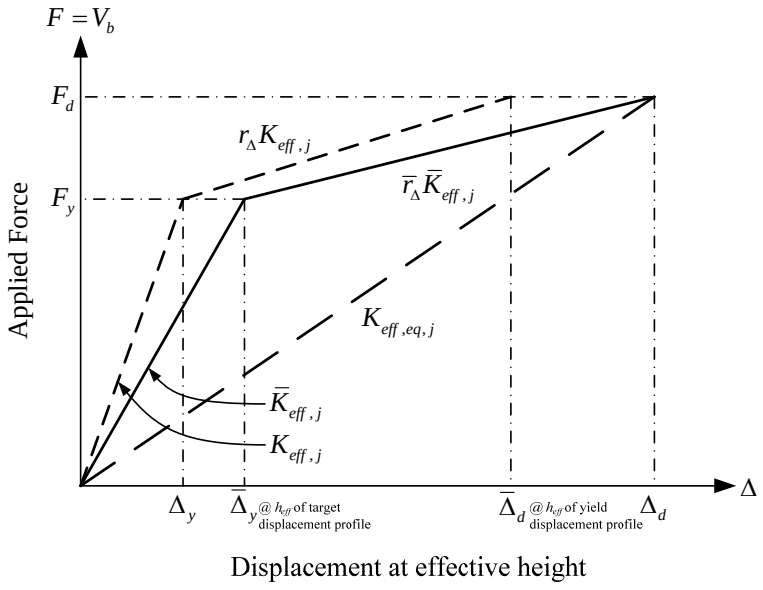

Figure 5-12. Force-displacement curve of effective SDOF

The effect of dissimilarity in effective heights on the force-displacement graph is shown in Fig. 5-12. The effective stiffness is modified due to the shift of yield displacement to the yield displacement at the equivalent effective height, $\bar{\Delta}_y$. Thus,

$$\bar{K}_{eff} = \frac{F_y}{\bar{\Delta}_y} \tag{5-XX}$$

The required effective stiffness is then

$$K_{eff} = \frac{F_y}{\Delta_y} = \bar{K}_{eff}\,\Upsilon \tag{5-XX}$$

where

Υ = Yield displacement ratio $\left(= \dfrac{\bar{\Delta}_y}{\Delta_y}\right)$ (5-XXa)

In the proposed DDBD procedure frame design is based on the required elastic stiffness of the system. The required 2nd order elastic stiffness from the secant stiffness to target response (see Appendix A) is computed from

$$K_{eff^2} = \eta\Upsilon\left(K_{eff,eq^2} + \left(1 - r_{\Delta^1}\right)\left(1 - \frac{1}{\mu_\Delta}\right)\frac{P_{eff,eq}}{h_{eff,eq}}\right)\left(\frac{\mu_\Delta}{1 + r_{\Delta^1}\left(\mu_\Delta - 1\right)}\right) \tag{5-25}$$

where

η = Stiffness amplification factor

Υ = Stiffness amplification factor due to change in h_{eff} (see above)

The corresponding lateral yield force and base shear are determined by

$$F_{y^2} = K_{eff^2}\Delta_y \tag{5-26}$$

$$V_{by^2} = F_{y^2} + \frac{P_{eff}}{h_{eff}}\Delta_y = F_{y^1} \tag{5-27}$$

Alternatively, the 1st order with *P*-Δ elastic stiffness (see Appendix A) is computed as

$$K_{eff^1} = \eta\Upsilon\left(K_{eff,eq^2} + \frac{P_{eff,eq}}{h_{eff,eq}}\right)\left(\frac{\mu_\Delta}{1 + r_{\Delta^1}(\mu_\Delta - 1)}\right) \tag{5-28}$$

The corresponding lateral yield force and base shear can be estimated by

$$F_{y^1} = V_{by^1} = K_{eff^1}\Delta_y \tag{5-29}$$

The stiffness amplification factor, η, is incorporated in Eqs. (5-25) and (5-28) to represent base shear amplification due to accidental torsion, the redundancy factor stipulated in current seismic codes, and other increases to building stiffness from other sources. It is the opinion of the author that these factors should be incorporated in the determination of the base shear strength rather than during member design as currently outlined in seismic codes thus contributing to member overstrength. As a side note, it is questionable if the lateral force resisting frame should be designed assuming it is the sole resisting system since other stiffness sources will assist in lateral force resistance. For simplicity, seismic codes do not consider external stiffness contributions, from interior gravity columns for example, to assist in force resistance.

P-Δ has the effect of reducing the response stiffness of the system. Consequently, the design engineer must provide the system with the first-order with *P*-Δ stiffness in order to achieve the desired second-order response. The design engineer must have *apriori* knowledge of the first-order post-yield frame response. That is, an understanding of r_{Δ^1} must be initially assumed based on experimental investigation. A value of 5-10% is recommended in SEAOC (1999). Research (Harris 2002, 2003, and 2004) suggests that the main factor influencing the value of r_{Δ^1} for steel moment frames is column stiffness.

5.6 Constructing Target Force - Displacement Curve

The idealized 1st mode target force - displacement graph can be constructed as shown in Fig. 5-13. The second-order post-yield stiffness ratio (see Appendix A) is computed by

$$r_{\Delta^2} = \frac{r_{\Delta^1}\left(1+\frac{h_{eff,eq}}{P_{eff,eq}}K_{eff,eq}\mu_\Delta\right)-1}{\left(\mu_\Delta + r_{\Delta^1}\left(1-\mu_\Delta\right)-1\right)+\frac{h_{eff,eq}}{P_{eff,eq}}K_{eff,eq}\mu_\Delta} \text{ need } \eta\Upsilon \qquad (5\text{-}30)$$

Eq. (5-30) can be used to determine the lower-bound limit of post-yield stiffness. The design engineer can then offset any negative post-yield stiffness through design via the required elastic stiffness. One mechanism for counteracting this occurrence is by increasing the stiffness of the columns in lieu of beams.

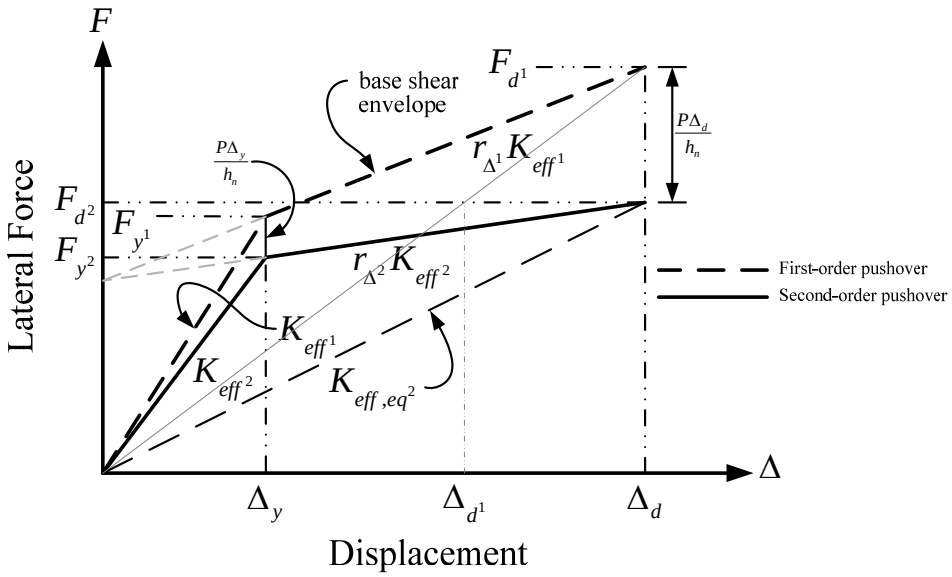

Figure 5-13. Target 1st mode force-displacement graph (pushover)

5.7 Determination of Equivalent Damping

Chapter 4 proposed a procedure to determine the quantitative degree of equivalent damping to be used in DDBD of steel moment frames. The pertinent system property in this procedure is the equivalent system period, $T_{eq,\delta}$. The previous discussion proposed a methodology to determine the 2nd order system stiffness whereas the equivalent period can be readily computed. As such, equivalent damping should be determined with respect to the 1st order system period.

The energy dissipated is computed as the area enclosed by the hysteresis loop. Fig. 5-14 illustrates the force-displacement response of a SDOF system with the *P*-Δ effect included (partial hysteresis loop). The total area of the loop can be computed by a first-order analysis (i.e., $F + P\Delta / h$). It follows that the hysteretic damping assigned to a floor can be approximated by

$$\zeta^*_{eq,h,i} = \underbrace{\kappa \frac{E^*_{D,h,i} {T_{eq,\delta^1}}^2}{8\pi^3 m_{eq,i} {\delta_{d,i}}^2}}_{Eq.(4\text{–}88)} = \kappa \frac{E^*_{D,h,i} {T_{eq,\delta^2}}^2}{8\pi^3 m_{eq,i} {\delta_{d,i}}^2 \left(1+\theta_{eff,eq}\right)} \tag{5-31}$$

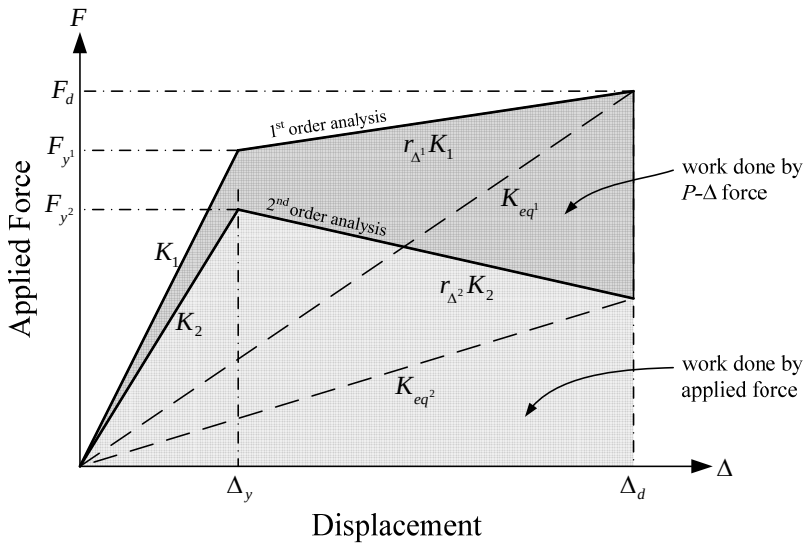

Figure 5-14. Force-displacement response

5.8 *P*-Δ Limits

NEHRP 2000 (BSSC 2000) and FEMA 356 (ASCE 2000) suggests that the *P*-Δ effect can be neglected when Eq. (5-4a) for each floor is less than 0.1, equating to a value for Eq. (5-12) of 1.1. NEHRP 2003 (BSSC 2003) limits Eq. (5-4a) to 0.1. Eq. (5-4a) is computed with drifts determined from strength-level lateral forces. The limit specified in NEHRP is based on engineering judgment and, additionally, elastic static displacements determined from a force distribution computed from the first-order fundamental period and that accounts for strength demands from higher mode contributions. The limit, however, is not based on displacements from the contributions from higher modes,

inelastic behavior, or the dynamic effects of gravity forces, and no limit is set based on the number of stories (such as that provided in EC8).

It is recommended for frames less than six stories, as limited within this document, that the *P*-Δ effect be modeled when the target story drift ratio is greater than 2% and independent of elastic displacements. This suggestion is applied in an effort to capture *P*-Δ effects originating from higher mode displacement response, albeit considered small in frames predominantly controlled by fundamental mode response.

If the target drift angle is greater than 2%, the design engineer is then challenged to determine whether or not *P*-Δ should be included. This process begins by assuming no *P*-Δ effects (i.e., $\lambda_{y,i} = 1$ for all floors) and results in a first-order effective stiffness. If the computed elastic stability coefficient of the effective SDOF and each floor satisfies Eq. (5-10) then design can proceed without including *P*-Δ, if so desired. This will provide a stability coefficient using the secant stiffness for the equivalent effective SDOF and each floor of the equivalent elastic MDOF less than 0.15.

If *P*-Δ is to be considered the stability coefficient using the first-order effective stiffness of the equivalent effective SDOF and each floor of the equivalent elastic MDOF should not exceed 0.33 (limed to 0.25 for essentially elastic frames). Stability coefficient limits for an elastic system are illustrated in Fig. 5-15. The design engineer could find that *P*-Δ effects will typically not significantly affect design until the gravity load present during an earthquake is approximately 1.5 times the reacting seismic weight. Any

additional demand increases above design are incorporated into Capacity Design discussed in Chapter 6.

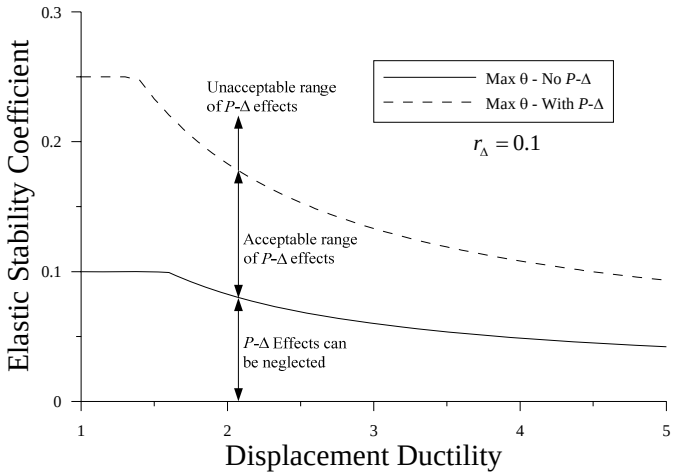

Figure 5-15. Elastic stability coefficient limits for expected ductility demand

5.9 Conclusion

This chapter outlined a methodology to explicitly include the *P*-Δ effect into the proposed DDBD procedure. The motivation for including second-order effects is to capture the change in fundamental period and to provide additional strength and stiffness capacity to ensure satisfactory and safe response. Still, the design engineer is charged with defining the prerequisite for such analysis.

Chapter 6 Development of an Elastic Analysis and Design Procedure

6.1 Introduction

DDBD is built upon the substitute structure philosophy developed by Shibata and Sozen (1976). While adopting this philosophy has many simplifying advantages, it does not, however, integrate easily into a design office methodology. The main drawback is that the equivalent elastic stiffness of each yielding member is iteratively approximated in the elastic analysis until convergence on the target displacement profile. Furthermore, design is based on the inelastic fundamental mode thus force contributions from higher modes could influence the actual stiffness of ductile sections at target.

As a means to developing a DDBD procedure more easily suitable for a design office it was proposed that design be based on a yield displacement profile and required elastic stiffness. The primary benefit of this proposal is that the design engineer can more readily analyze the system using elastic steel section properties during the iteration process to converge on the yield displacement profile. In parallel, force contributions from higher modes at the yield-level earthquake for low-rise short period frames are assumed to be small, pertaining to the design of members expected to develop plastic hinges. This philosophy thus advocates the development of all plastic hinges under the fundamental mode. Non-ductile members are subsequently protected from demands imposed by higher modes and other variables, discussed in Section 6.3. This seismic analysis procedure is termed ‘Equivalent Yield Analysis’ since the analysis of the system

is controlled by response demands determined from the equivalent stiffness at a target displacement.

6.2 Equivalent Yield Analysis

Equivalent Yield Analysis (EYA) is a concept adopted by the author for the elastic analysis of a multi-story frame. This concept separates conceptual hinge formations into groups assumed to develop simultaneously and, additionally, recognizes that an elastic analysis can only determine first level plastic hinge demands (i.e., first group of hinges chosen to develop in the frame).

The definition of the desired global yield mechanism was introduced in Chapter 3. For linear displacement profiles, the global yield mechanism indicates that all desired hinges form simultaneously and, likewise, are all assigned to the first level. An elastic analysis is therefore suitable for analyzing these systems. The goal is for the design engineer to select member strengths such that all desired hinges develop concurrently. In reference to Fig. 1-4, this design scenario attempts to optimize hinge formations such that $\Delta_s = \Delta_y$ and $C_s = C_y$.

Plastic hinges in frames responding in a nonlinear displacement profile typically form in a vertical traveling wave producing multi-level hinge formations, which cannot be effectively analyzed with an elastic analysis. In recognition of this incompatibility the calculated resultant yield force, F_y, is reduced to an *elastic* level, F_{el}, representative of

the first significant yield (formation of first level hinges - Δ_s in Fig. 1-4). The elastic design force can be computed by multiplying F_y by the elastic displacement ductility.

$$F_{el} = \mu_{\Delta,el} F_y \tag{6-1}$$

where

F_y = Resultant yield force from Eqs. (2-38), (5-26), or (5-29)

$\mu_{\Delta,el}$ = Elastic displacement ductility, Eq. (3-22)

Table 6-1 summarizes the design force F_{el} to be used in the proposed DDBD procedure for the various analytical cases.

Table 6-1. Resultant design force matrix

Analysis	Analysis Type	F_y	Displacement Profile	
			Linear	Nonlinear
Without *P*-Δ	1st Order	Eq. (2-38)	$F_{el} = F_y = V_{by}$	$F_{el} = \mu_{\Delta,el} F_y = V_{bel}$
With *P*-Δ	1st Order	Eq. (5-29)	$F_{el} = F_{y^1} = V_{by^1}$	$F_{el} = \mu_{\Delta,el} F_{y^1} = V_{bel^1}$
	2nd Order	Eq. (5-26)	$F_{el} = F_{y^2}$	$F_{el} = \mu_{\Delta,el} F_{y^2}$
			$V_{by^2} \approx F_{y^2} + \frac{P_{eff}}{h_{eff}} \Delta_y$	$V_{bel^2} \approx F_{el} + \frac{P_{eff}}{h_{eff}} \mu_{\Delta,el} \Delta_y$

The design force determined from Eq. (6-1) is vertically distributed heightwise (see Fig. 1-5) using the second-order yield displacement profile, $\left\{\hat{\delta}_{dy,i}\right\}$. $\left\{\hat{\delta}_{dy,i}\right\} = \left\{\delta_{dy,i}\right\}$ when *P*-Δ is not considered.

$$F_{x,i} = F_{el} \frac{w_i \hat{\delta}_{dy,i}}{\sum_{i=1}^{n} \left(w_i \hat{\delta}_{dy,i} \right)} \tag{6-2}$$

6.2.1 Structural Analysis

Once design forces are computed from Eq. (6-2), the design engineer analyzes the analytical model in an elastic analysis. A 2nd order analysis is required with Eq. (5-26) and typically requires a *P*-Δ column in the analytical model such as shown in Fig. 6-1. A 1st order analysis is used with Eqs. (2-38) or (5-29). In the latter case, the equivalent *P*-Δ shears are approximated in the design forces. The former is the recommended analysis.

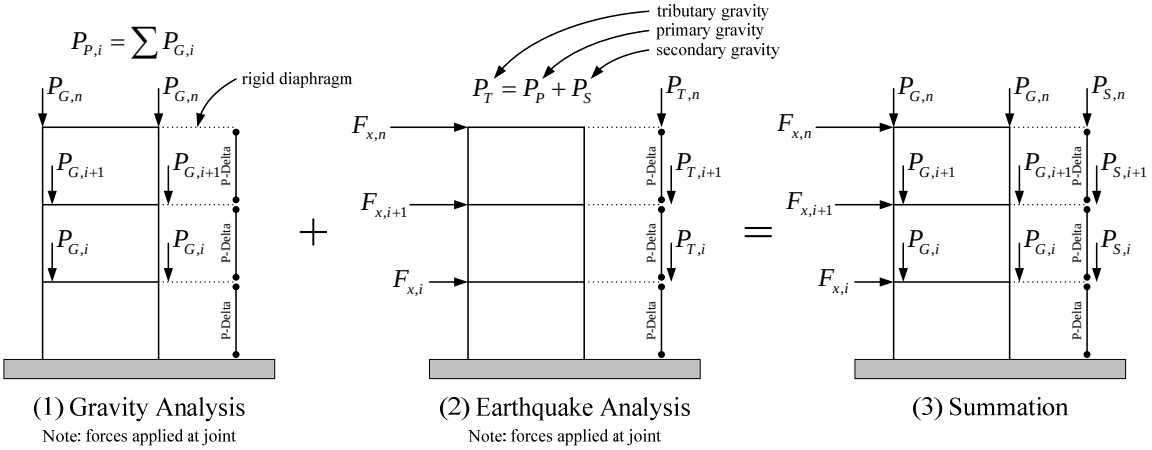

Figure 6-1. Structural analysis schematic

It is also recommended that structural analysis be broken into two stages: (1) gravity analysis (including vertical accelerations) and (2) earthquake analysis (graphically depicted in Fig. 6-1). The motivation in a combination analysis is that the design engineer can directly compute the contribution from seismic forces for use during capacity design. All gravity load tributary to the frame should be applied to the *P*-Δ column during the earthquake analysis since the effects from gravity loads are due to the displacement arising from the lateral forces. The tributary gravity force, P_T, on a given

floor is the summation of the primary gravity forces, P_P, (directly acting on frame) and secondary gravity forces, P_S, (indirectly acting on frame via lateral displacement).

6.2.2 Member Design Forces

First level force demands on the structural components are determined from structural analysis. Plastic design moments on beams are computed from

$$M_{EQ,b} = \eta_b M_{el,b} \tag{6-3}$$

where

$M_{el,b}$ = Moment demand on beam from elastic analysis

η_b = Moment amplification factor $\left(= \hat{\theta}_{y,i} \left(\frac{h_i}{\hat{\delta}_{dy,i} - \hat{\delta}_{dy,i-1}} \right) \right)$ (6-3a)

The moment amplification factor, η_b, in Eq. (6-3) modifies the moments to account for higher-level force demands. From Eq. (6-3a), $\eta_b = 1$ for linear displacement profiles (all moment demands are first level demands). On average, $\eta_b = 1$ for moment demands on beams in the first two floors for nonlinear displacement profiles (see Fig. 3-16).

Beams are designed for the plastic moment demands while maintaining the depths selected when determining the yield displacement profile. Any shape factor and beam depth differing from the nominal value used in estimating the yield rotation should be noted (e.g., W24×94, $S_F = 1.14$ and $d_b = 27.7$). Columns are designed using capacity design procedures, discussed subsequently, and the member selection process iterated

until convergence on the yield displacement profile. The design engineer could find that exact convergence on the yield profile is difficult when iterating stiffness and strength of columns during capacity design. Lastly, since yield displacement is related to yield curvature, the expected yield strength, $\phi_m^o \phi_{sr}^o F_y$, should be used when designing plastic hinges.

The fundamental difficulty in analyzing a system with forces generated at the yield point, or a reduced value, is that displacement profiles are assumed to be invariant at all performance levels (i.e., yield and target). Penalties arise in the selection of first story column sizes during capacity design possibly preventing the concurrent formation of plastic hinges at the column bases and first floor beams. This, including effects from other member overstrengths, will inherently affect the yield displacement profile and, ultimately, the design force distribution. As a result, the frame could experience lateral force redistribution as it travels from the elastic to inelastic state. This challenges the FBD assumption that a constant displacement amplification factor can be used for estimating maximum displacement demands and suggests that the chosen C_d value should reflect the desired yield mechanism.

6.3 Capacity Design

Capacity design of structures for earthquake resistance requires that distinct regions of desired critical members of the primary lateral force resisting system be chosen and designed for energy dissipation under severe imposed deformations (Paulay and Priestley 1992). These regions in moment frames are identified as plastic hinges as

discussed in Chapter 3 and illustrated as the design objective in Fig. 3-15. All other non-critical structural members must possess sufficient strength to resist the maximum demands originating from the selected regions. These non-critical members are designed to remain essentially elastic irrespective of the intensity of the ground motion or magnitudes of inelastic deformations (Paulay and Priestley 1992). This additionally includes member segments adjacent to critical regions, as well as the protection of critical regions from undesirable failure mechanisms (e.g., shear failure, elastic local buckling, and lateral-torsional buckling, etc.).

Prior to discussing capacity design as applied to steel moment frames, two key components fundamental to capacity design must be introduced.

1. The penalty for using steel in seismic resistant moment frames is that nominal member plastic moment capacities, $\phi_b M_p$, in all likelihood cannot be proportioned to exactly match that which is required by seismic analysis, M_{EQ}. Unless purposely allocated, $\phi_b M_p > M_{EQ}$ (M_{EQ} includes all load contributions). Furthermore, it is the actual strength of a member that is developed during seismic activity, not the nominal strength (Paulay and Priestley 1992). As a consequence, a system can develop significantly higher internal forces than those estimated from the initial analysis due to ‘member overstrengths’ (i.e., actual strength greater than that required). Member overstrength fundamentally leads to an energy dissipation capacity and available ductility different from that predicted (Mazzolani and Pilusa 1996).

2. Due to the complex nature of earthquake motion, excitation of higher modes can be expected during seismic attack. The objective of the proposed DDBD procedure is to design the potential plastic hinges for response in the fundamental mode. Thus, non-ductile members that are desired to remain nominally elastic must be protected from increased demands produced by higher modes. This component of capacity design is additionally employed to represent increased column demands from variation in system characteristics for MDOF systems while using SDOF response spectra, cantilever action, increase in P-Δ effects at large deformations, offset of inflection points away from mid-span, and changes in displacement profile as the frame enters the inelastic region of response. This portion of capacity design is referred to as 'Performance Overstrength' since the amplification factor intends to protect non-ductile members from the global performance of a system.

The proposed capacity design procedure for steel moment frames incorporates these two types of overstrength factors: (1) member (Section 6.3.1) and (2) performance (Section 6.3.2).

6.3.1 Overstrength of Ductile Members

Input energy during strong motion is dissipated in moment frames by plastic hinges. The strong column-weak beam (SCWB) design philosophy is encouraged for design of steel moment frames, and is a condition of the design displacement profile. In this philosophy, plastic hinges are designed to develop in the frame beams. Adjacent

columns are thus protected and designed to remain essentially elastic (with the exception of base hinges in the first story columns), see Fig. 3-15(a). The capacity design concept is graphically illustrated in Fig. 6-2.

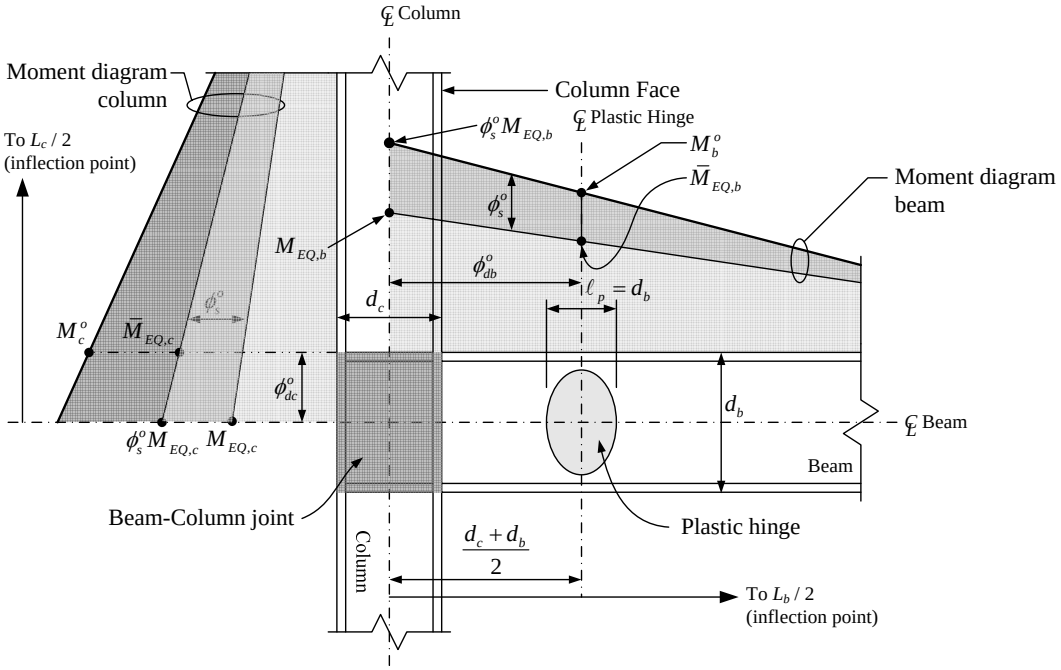

Note: only one beam and column shown for brevity

Figure 6-2. Capacity design schematic

The first step to insure that columns possess sufficient strength is to compute the maximum force demands that can be transferred to the column from adjacent beam hinges. Member overstrength of a critical region, ϕ_s^o, in a frame beam, referred to as 'flexural' overstrength, can be determined by

$$\phi_s^o = \frac{\phi_{sr}^o \phi_{sh}^o \phi_m^o M_{pr,b}}{\frac{\phi_{sf}^o}{\phi_d^o} \underbrace{\left(\phi_{db}^o M_{EQ,b}\right)}_{demand}} = \frac{M_b^o}{\bar{M}_{EQ,b}} \tag{6-4}$$

where

$M_{EQ,b}$ = Moment demand on beam from Eq. (6-3)

$\bar{M}_{EQ,b}$ = Moment demand on beam at plastic hinge $\left(=\phi_{db}^{o} M_{EQ,b}\right)$

$M_{pr,b}$ = Nominal plastic moment capacity of beam (see Chapter 3)

M_{b}^{o} = Ultimate plastic moment capacity of beam

ϕ_{m}^{o} = Material overstrength (see Chapter 3)

ϕ_{sr}^{o} = Material overstrength from the effects of strain rate

ϕ_{sh}^{o} = Material overstrength from the effects of strain hardening

ϕ_{sf}^{o} = Shape factor adjustment factor $\left(=\dfrac{S_{F,actual}}{S_{F,nominal}}\right)$ (6-4a)

ϕ_{d}^{o} = Beam depth adjustment factor $\left(=\dfrac{d_{b,actual}}{d_{b,nominal}}\right)$ (6-4b)

ϕ_{db}^{o} = Distance adjustment factor to plastic hinge

The strength reduction factor, ϕ_b, is not included in Eq. (6-4). This is recommended so that the ultimate moment capacity is not underestimated.

Since the strength ratio in Eq. (6-4) is taken at the critical region, a distance adjustment factor, ϕ_{db}^{o}, is incorporated to shift the analytical location of the required strength to the plastic hinge (e.g., from the column face or beam-column joint centerline). Assuming the center of the plastic hinge is located $d_b/2$ away from the column face and an inflection point at beam mid-span, the distance adjustment factors are

$M_{EQ,b}$ taken at column centerline:

$$\phi_{db}^{o} = 1 - \left(\frac{d_c + d_b}{L_b} \right) \tag{6-5}$$

$M_{EQ,b}$ taken at column face:

$$\phi_{db}^{o} = 1 - \left(\frac{d_b}{L_b - d_c} \right) \tag{6-6}$$

Depending on the nominal shape factor used for approximating the yield rotation, an additional variable, ϕ_{sf}^{o}, is incorporated to represent the actual to nominal ratio. A beam depth adjustment factor, ϕ_{d}^{o}, is also incorporated to represent the actual to nominal value.

The column design moment at the beam-column joint edge from flexural overstrength of the beam is (see Fig. 6-2)

$$\bar{M}_{EQ,c} = \phi_{dc}^{o} \phi_{s}^{o} M_{EQ,c} \tag{6-7}$$

where

$M_{EQ,c}$ = Moment demand on column $\left(= \eta_b M_{el,c} \right)$ (6-7a)

$M_{el,c}$ = Moment demand on column from elastic analysis

ϕ_{dc}^{o} = Distance modifier to beam-column joint edge $\left(= 1 - \frac{d_b}{L_c} \right)$ (6-7b)

The distance modifiers, ϕ_{db}^{o} and ϕ_{dc}^{o}, are derived assuming an inflection point at mid-span of the member (see Appendix A). This cannot always be valid since higher modes, gravity loads, and inelastic redistribution may shift the inflection point towards

the member end. Consequently, an additional factor is required to account for this variation and is incorporated in the performance overstrength factor discussed subsequently. Also, if design is to be conservatively based on centerline dimensions, the distance modifiers would be unity.

In the case of an interior column with beams framing into both sides, the flexural overstrength value is taken from the beam with the maximum value computed from Eq. (6-4) for simplicity. Alternatively, the beam overstrength values can either be averaged at the joint or a floor overstrength value can be computed. The flexural overstrength of a floor can be estimated by

$$\phi^{o}_{s,i} = \frac{\sum_{k=1}^{K} M^{o}_{b,k}}{\sum_{k=1}^{K} \bar{M}_{EQ,b,k}} = \frac{M^{o}_{b,i}}{\bar{M}_{EQ,b,i}} \tag{6-8}$$

where

k = Hinge index

K = Total number of hinges

Eq. (6-8) is applicable when all bay lengths in a story are nearly equal (not differing by more than 25%) . Otherwise, the design engineer should examine column design on a per joint basis. Lastly, it is recommended by the author that column depths be selected to satisfy $d_c \le d_b \le 2d_c$. Column depth is bounded in an attempt to limit higher mode contributions (highest limit) and cantilever action (lowest limit).

6.3.2 Performance Overstrength of Non-ductile Members

Performance overstrength represents the additional non-ductile member strength required to resist demands from higher modes and secondary behavioral uncertainties (listed previously). Higher modes can occur through two primary effects: (1) when earthquake induced higher mode effects govern system behavior, and (2) when a floor due to stiffness and strength irregularities attracts higher/lower demands than predicted thus altering the presumed lateral force distribution. Under the latter effect, the system could respond in an apparent higher mode due to reduced stiffness in localized portions of the structure from yielding.

While this factor does not play a role in the design of critical regions, it does factor into the design of non-ductile structural components. One approach to integrate this concept in design, as proposed by Paulay and Priestley (1992) and Mesa (2002) for concrete frames and structural walls, respectively, is to amplify the demand by a dynamic amplification factor. As such, in the proposed procedure protection is applied to non-ductile frame members through a dynamic amplification factor referred to as 'performance overstrength'.

The performance overstrength factor, ϕ_p^o, is divided into two categories: (1) higher modes (Section 6.3.2.1) and (2) secondary behavioral uncertainties (Section 6.3.2.2). This factor can be expressed as

$$\phi_p^o = \phi_{hm}^o \underbrace{\left(\phi_{P\Delta}^o \phi_{bu}^o\right)}_{secondary} \tag{6-9}$$

where

ϕ^o_{hm} = Protection factor against higher mode demands

$\phi^o_{P\Delta}$ = Protection factor against *P*-Δ effects at target displacement

ϕ^o_{bu} = Protection factor against secondary behavioral uncertainties

As a side note, in the early development of the proposed procedures (Harris 2002, 2003, 2004), the term plastic hinge sequencing factor, notated by ϕ^o_{ph}, was used to represent this effect. This term and notation is no longer applicable and is revised as presented.

6.3.2.1 Fundamental mode demand increase (higher modes)

The proposed approach promotes the design of ductile members by the fundamental mode and subsequently protects non-ductile members from increases in demands imposed by higher modes. The increase in 1st mode demands on non-ductile structural components at the yield point can be estimated by

$$\phi^o_{hm} = \frac{\sum_{i=1}^{n} m_i}{M_{eff,\delta}} = \frac{M_{total}}{M_{eff,\delta}} \tag{6-10}$$

where

$M_{eff,\delta}$ = 1st mode effective mass based on yield displacement profile

This approach differs from FBD practices where the total mass is used to determine the design base shear and lateral forces. As a result, demands on ductile structural components in FBD are determined from the “multi-mode” lateral forces possibly leading

to overly conservative beam strengths. Lastly, the amplification factor at the target performance level is determined by

$$\phi_{hm}^{o} = \frac{\sum_{i=1}^{n} m_{eq,i}}{M_{eff,eq,\delta}} = \frac{M_{eq,total}}{M_{eff,eq,\delta}} \tag{6-11}$$

The maximum value computed from Eqs. (6-10) and (6-11) is used in design.

6.3.2.2 Fundamental mode demand increase (behavioral uncertainties)

The first secondary behavioral factor in Eq. (6-9) represents the increase in demands originating from *P*-Δ effects at the target displacement.

$$\phi_{P\Delta}^{o} = \frac{\lambda_{T^2}}{\lambda_{y^2}} \leq 1.5 \tag{6-12}$$

where

λ_{y^2} = Second-order amplification factor at yield

$$= \left[1 - \frac{\sum_{i=i}^{n} P_i}{\sum_{i=i}^{n} F_{y^2,i}} \left(\frac{\hat{\delta}_{dy,i} - \hat{\delta}_{dy,i-1}}{h_i} \right) \right]^{-1}$$

λ_{T^2} = Second-order amplification factor at target

$$= \left[1 - \frac{\sum_{i=i}^{n} P_i}{\sum_{i=i}^{n} F_{d^2,i}} \left(\frac{\delta_{d,i} - \delta_{d,i-1}}{h_i} \right) \right]^{-1}$$

For simplicity, this factor can be approximated by

$$\phi^o_{P\Delta} \approx \frac{F_{d^1}}{F_{d^2}} \frac{F_{y^2}}{F_{y^1}} \leq 1.5 \tag{6-13}$$

Table 6-2 presents a possible range for the of secondary behavioral uncertainty factor, ϕ^o_{bu}, based on studies of regular steel moment frames. These values are to be used at the design-level earthquake (i.e., ⅔ MCE). This factor varies depending on the 1st mode elastic target period and is independent of ground motion characteristics and number of floors. The supposition of a constant value is in agreement with other research conducted on required column strengths in moment frames (Medina and Krawinkler 2005). The proposed values could change depending on the extent of cantilever action, unexpected strength increases, heightwise strength and stiffness distribution, and ground motion characteristics pending further research.

Table 6-2. Dynamic amplification factor values for behavioral uncertainties

Period (Elastic Target) (T_1)	ϕ^o_{bu}
0.5 – 1.0	1.10
1.0 – 1.5	1.15
1.5 - 2.0	1.20
2.0 – 3.0	1.25
3.0 – 5.0	1.30
> 5.0	1.40

Since columns in steel moment frames are designed to remain essentially elastic, a certain amount of reserve strength is provided by steel design equations. As a result, the behavioral uncertainty factor, ϕ^o_{bu}, can be taken as unity for frames with $T_1 \leq 2$ *seconds*. Further research is required to validate this presumption.

6.3.2.3 Performance overstrength factor

The design engineer applies this factor to force demands on non-ductile members and connections while adhering to the guidelines established in steel design specifications. The column design moment including all overstrengths is

$$M_c^o = \phi_p^o \bar{M}_{EQ,c} = \phi_p^o \left(\phi_{dc}^o \phi_s^o \eta_b M_{el,c} \right) \tag{6-14}$$

The column design moment is schematically illustrated in Fig. 6-2. Other force demands on the columns (i.e., shear and axial force) are computed in the same manner. Beam-to-column connection demands need only to be amplified by the flexural overstrength factor ϕ_s^o (no factor if ultimate plastic moment capacity is used in lieu of demands determined from elastic analysis). It is recommended that floor flexural overstrength factors be used in design rather than individual flexural overstrengths for frames with nearly equal bay lengths.

Demands at the base of the first story columns are not amplified by ϕ_p^o or ϕ_s^o in order to allow plastic hinges to develop. However, column base plates must be protected from failure due to the maximum forces developed in the first floor columns. Flexural overstrength of the base hinges could at times control over first floor beam flexural overstrengths and, as a result, should be applied to column demands above the first floor where cantilever action could dominate frame response and prevent the formation of a weak story in the first floor as the inflection point shifts towards the column end.

Lastly, in accordance with AISC seismic provisions, strong-column weak-beam (SCWB) at the joint centerline must be satisfied.

$$\frac{\sum M_{p,c}}{\sum M_{p,b}} = \frac{\phi_{db}^{o}}{\phi_{dc}^{o}} \frac{\sum M_{pr,c}}{\sum M_{b}^{o}} \geq 1.0 \tag{6-15}$$

where

$M_{pr,c}$ = Plastic moment capacity of column $\left(\geq M_{c}^{o}\right)$

Top floor columns at the roof need not satisfy Eq. (6-15) if elected. Recent research (Medina and Krawinkler 2005) illustrates that more stringent SCWB criteria above Eq. (6-15) appear to be needed and propose that ductile design should be incorporated in column ends. This was additionally noted by Harris (2004).

6.3.3 Force-Displacement Response Envelopes and System Overstrength

The application of a capacity design procedure to a moment frame results in two effects: (1) protection of non-ductile members from increased demands in order to maintain the strong-column weak-beam design philosophy and (2) producing an inadvertent period shift by strengthening non-ductile members. Under the latter effect, capacity design could have a significant effect on both the static and dynamic force-displacement envelopes since stiffness is proportional to strength. This alteration is important since any stiffening effects will shift the design yield and target displacements as well as possibly produce an increase in design forces.

After capacity design has been completed the design engineer can construct the static and dynamic response envelopes of the *actual* frame (force-displacement 'pushover' curves). The first step is to determine the *actual* 1st mode second-order effective stiffness, $K^{o}_{eff^2,1}$, of the frame (computed via structural analysis). Alternatively, the design engineer could calculate the 2nd order fundamental period and respective modal participation factor. The effective stiffness is then

$$K^{o}_{eff^2,1} = \Gamma_{1^2}{}^2 \sum_{i=1}^{n} \left(k^{*}_{i,1^2} \phi_{i,1^2}{}^2 \right) \tag{6-16}$$

The superscript attached to the mode index indicates second-order values. The stiffness ratio, Ω^{o}, is measured as the ratio of actual to target effective stiffness.

$$\Omega^{o} = \frac{K^{o}_{eff^2,1}}{K_{eff^2,\delta}} \tag{6-17}$$

During the next step, the design engineer approximates the force ratio, Λ^{o}, as the ratio of the 2nd order resultant yield force to the target resultant.

$$\Lambda^{o} = \frac{F^{o}_{y^2}}{F_{y^2}} \tag{6-18}$$

In accordance with an EYA, the design engineer can readily determine the flexural overstrength factor, ϕ^{o}_{s}, of the first plastic hinge(s) to develop. In some cases this single factor is adequate to define Λ^{o}. For example, a linear displacement profile could allow

most hinges to form simultaneously (if designed as such). Otherwise, an average of all member overstrength values, or at least 75%, can be acceptable. This factor is based largely on engineering judgment.

The yield displacement, Δ_y, can increase or decrease from the design value depending on the magnitude of column deformations. The revised yield displacement at the global yield mechanism, Δ_y^o, can be estimated by (see Appendix A)

$$\Delta_y^o = \left(\mu_{\Delta,el} \frac{\Lambda^o}{\Omega^o} \right) \Delta_y = \Theta^o \Delta_y \tag{6-19}$$

An important note is that beam contribution to yield displacement does not change since it is a function of geometry. This contradicts the assumption that a displacement ductility capacity can be estimated by taken the ratio of the force reduction factor, *R*, to the system overstrength factor, Ω_o, implying that stiffness is independent of strength.

The resultant force and displacement at the design target are adjusted by

$$F_{d^2}^o = \Lambda^o F_{d^2} \tag{6-20}$$

$$\Delta_d^o = \mu_{\Delta,sys} \Delta_y^o = \left(\mu_{\Delta,el} \frac{\Lambda^o}{\Omega^o} \right) \Delta_d \tag{6-21}$$

In the event that $\Delta_d^o > \Delta_d$, the design engineer should stiffen the columns to shift the displacements within the limit or select deeper beams. Revised 1st order force-displacement ordinates (base shear envelope) are computed from

$$F_{y^1}^o = F_{y^2}^o + \frac{P_{eff}}{h_{eff}} \Delta_y^o \approx V_{b,y}^o \tag{6-22}$$

$$F_{d^1}^o = F_{d^2}^o + \frac{P_{eff,eq}}{h_{eff,eq}} \Delta_d^o \approx V_{b,d}^o \tag{6-23}$$

The displacement profiles $\{\delta_d\}$ and $\{\delta_{dy}\}$ are adjusted to account for overstrength.

$$\{\delta_{dy}^o\} = \Theta\{\delta_{dy}\} \tag{6-24}$$

$$\{\delta_d^o\} = \Theta\{\delta_d\} \tag{6-25}$$

6.3.3.1 Monotonic Static 1st Mode Pushover Curve

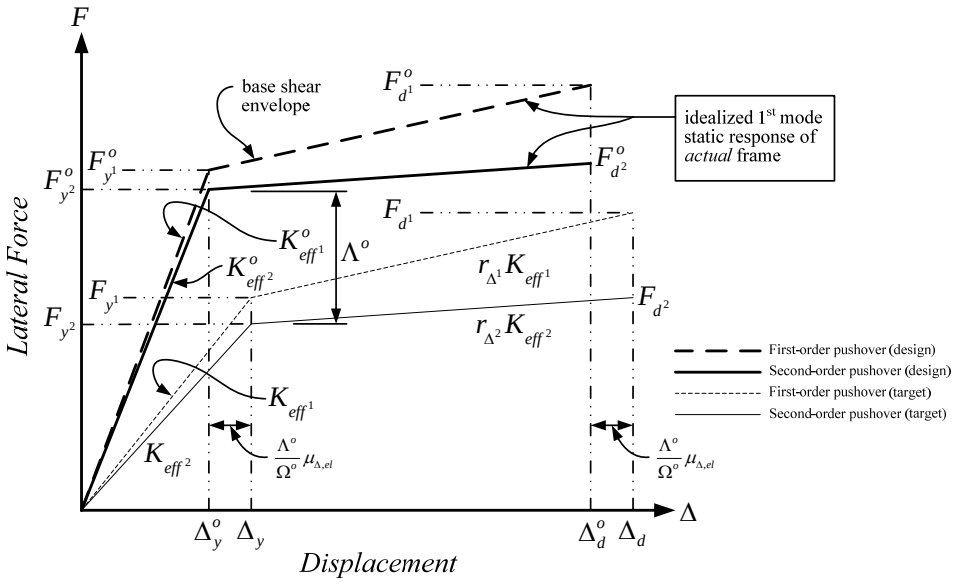

Figure 6-3. Static force - displacement graph (1st mode)

The revised ordinates computed from Eqs. (6-16) through (6-23) define the 1st mode static pushover curve of the *actual* effective SDOF, illustrated in Fig. 6-3. The idealized *actual* response is notated as 'design' to represent the capacity designed frame.

6.3.3.2 Dynamic Pushover Curve

Due to the likelihood of higher mode contributions to the response of the MDOF system during strong motion, an additional factor is applied to the *actual* 1st mode effective SDOF static pushover curve to predict the *actual* dynamic response. In constructing the dynamic pushover curve, the first-order static ordinates (base shear envelope) are amplified by ϕ_p^o, Eq. (6-9), to represent the change in static stiffness due to dynamic amplification, as shown in Fig. 6-4. The idealized *actual* dynamic response is notated as 'protected' to represent the capacity designed frame. The 'protected' curve signifies the minimum base shear that the frame has been designed to resist. An actual dynamic response curve from a time-history analysis in excess of this curve does not necessarily signify failure due to columns possessing reserve strength.

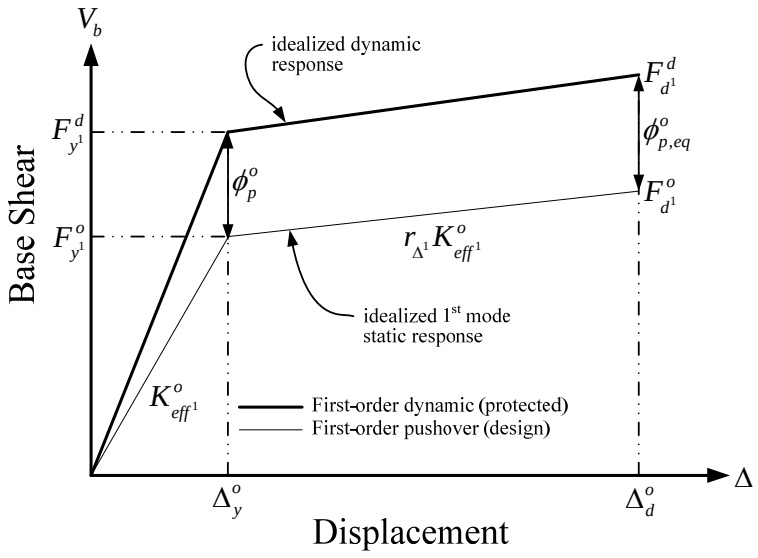

Figure 6-4. Dynamic base shear - displacement graph

Although not explicitly detailed into a design methodology, the reader is referred to Gupta and Krawinkler (2003) and Medina and Krawinkler (2005) for analytical results in support of providing this dynamic amplification for steel moment frames.

6.4 Conclusion

This chapter outlined a comprehensive analysis and capacity design methodology to be used with the proposed DDBD procedure. As evident, design and analysis are coupled and, as a result, the design engineer should be able to recognize changes to frame properties during capacity design. In truth, once the frame has been completely designed, the design engineer should return to the starting point of the proposed DDBD procedure and begin a new design iteration using the computed frame properties as the initial conditions of the 2nd iteration. The design engineer will most likely discover that the any variations between the end result of the 2nd iteration and the 1st iteration are negligible.

Optimizing hinge formations plays a vital role in controlling frame behavior during strong ground motion with positive and negative effects. At the least, the design engineer can now evaluate hinge sequencing by investigating the flexural overstrengths of the beams or floors. This suggests that an engineer should not select a beam based on its plastic moment capacity and moment of inertia independently. Furthermore, it is found the displacement ductility demand can be in part controlled via design.

Joint rotations and vertical stiffness distribution are additional design choices that need to be considered during the design of columns. The design engineer should select column depths that allow joints in a floor to have approximately equal rotations. This will

also provide beam design moment to be approximately the same, considering gravity loads do not cause large moment deviations in adjacent bays. Additionally, there should not be large stiffness variations from floor to floor, as is observed when large beam depths and/or column depths changes are incorporated. In the event that different beam depths are used between adjacent floors, column sizes should be selected to counteract the additional moment and shear demand placed on the lower floor while maintaining equivalent joint rotations.

Seismic codes specify a generalized overstrength value to be used in the design of non-ductile steel members. The author believes this procedure to be somewhat limiting since it applies a flexural overstrength factor prior to the design of any beams (similar to applying a force reduction factor prior to member selection). The use of a constant overstrength factor in the design of all non-ductile members could be conservative and contribute to the frame being stiffer and stronger than required. Conversely, it could be underestimated and result in column hinging. Therefore, it is recommended that overstrength factors not be used prior to ductile member design. The proposed procedure outlines a more rational approach, in the author's opinion, for determining the required overstrength factors, which is at the conclusion of the beam design process. This recommendation is also encouraged in the NEHRP 2003 (BSSC 2003).

The central goal of the proposed DDBD philosophy is to allow the engineer to design a system where the behavior is dictated from the start. This is in contrast to current seismic design where the frame behavior is the final product, and even then principally approximate. It is not justifiable to design a steel moment frame for seismic resistance by

selecting least weight beams and columns to satisfy demand and codified displacement control. Structural members are sometimes required to purposely have capacities in excess of the demand in order to control behavior. As a result, capacity-demand variations should be carefully examined and incorporated during capacity design.

Chapter 7 Seismic Analysis and Design of Steel Moment Frames Using DDBD

7.1 Introduction

Five steel moment frames are designed following the proposed DDBD methodology outlined in Chapters 2 through 6 – three three-story frames (Section 7.2) and two six-story frames (Section 7.3). Frame design begins with an empty model and follows through capacity design to the final product (see flowchart in Fig. 7-1). The final frames are evaluated with an inelastic dynamic analysis to investigate frame response when subjected to strong ground motion. Twenty time-history records – ten far-field and ten near-fault – are used in the analysis (Section 7.1.1). The dynamic analysis results are compared to the design parameters to determine applicability and identify any sources of error that could result in unsatisfactory performance by the proposed philosophy.

Two *idealized* frames are additionally constructed for comparison purposes – one three-story and one six-story (Section 7.4). Column stiffness and strength of the ductile structural components are modified until convergence on the target fundamental period (elastic) and yield displacement profile (development of the global yield mechanism). This will allow any sources of error due to flexural overstrengths and hinge formation sequences to be identified.

Lastly, two of the designed frames are subjected to filtered time-histories (modified to remove high frequencies) in an attempt to identify any variations in

analytical results due to the presence of higher modes – one three-story and one six-story (Section 7.5). A similar analysis is performed for the two idealized frames (Section 7.6).

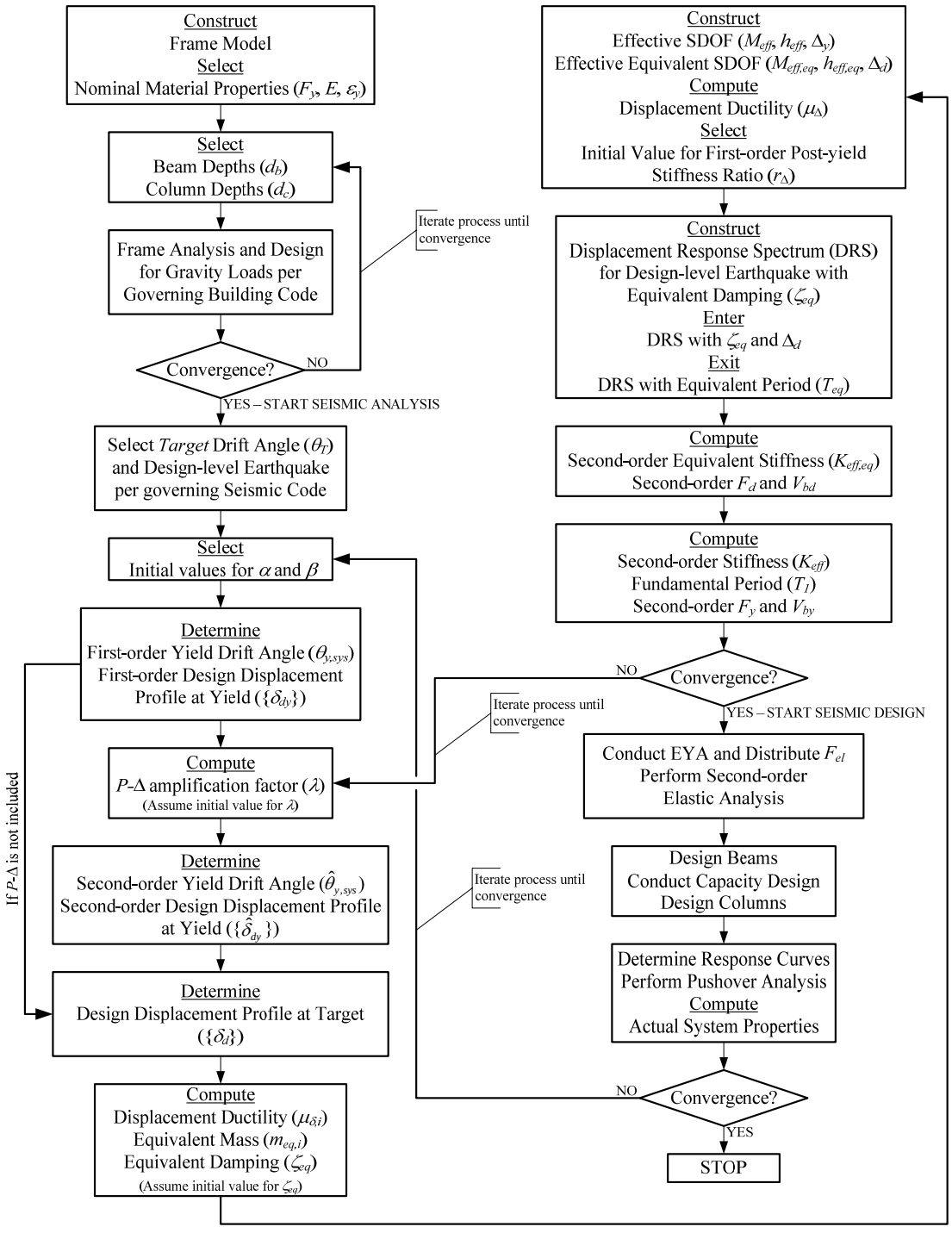

Figure 7-1. DDBD flowchart for steel moment frames

7.1.1 Earthquake Records and Design-level Response Spectrum

In accordance with NEHRP (2003), frame designs are based on a target drift angle, θ_T, of 0.025 *radians* at a design-level earthquake equal to ⅔ MCE. The MCE ARS is constructed with the parameters listed in Table App.B-1. The MCE response spectra are illustrated in Fig. App.B-1.

Twenty time-histories (listed in Table App.B-2) are selected to provide a wide range of ground accelerations, intensities, frequency content, and duration. Ten far-field earthquakes and ten near-fault earthquake records are selected from the Pacific Earthquake Engineering Research (PEER) Strong Motion Database (http://peer.berkeley.edu/smcat). The far-field time-histories are normalized to approximate the codified MCE. Near-fault records are not normalized.

Response spectra for the normalized earthquake records are shown in Appendix B. The 5% damped DRS and mean are plotted against the codified DRS in Figs. App.B-22 and App.B-23. As shown, differences in earthquake characteristics can result in variations between spectra. As a result, analytical deviations from the design displacement could be expected since frame designs are based on the codified spectrum. Though the time-histories comprise both far-field and near-fault records, only Eq. (2-23) is used to construct higher damping curves for the codified DRS. Consequently, analytical deviations could be expected for near-fault motions.

7.1.2 Structural Analysis

7.1.2.1 Inelastic Dynamic Analysis

RUAUMOKO (Carr 2004) is used for the dynamic and pushover analyses. Earthquakes are assumed uni-directional. A Lumped Mass Model is assumed so that masses are only associated to the translational degrees of freedom. As such, only *n* degrees of freedom (i.e., *n* modes) are used to determine frame response. The analysis is carried out using the Newmark-Beta method with $\beta = 0.25$. Second-order effects are included in the analysis by specifying a Simplified *P*-Δ Analysis. Rigid diaphragms are assumed for all floors.

Viscous damping, ζ_v, is modeled by Rayleigh damping using 2% for the first two modes for all frames. Consequently, viscous damping is computed based on the tangent stiffness of each member. The reader is referred to Carr (2004) for explanation of the use of tangent stiffness to model viscous damping. The first two modes were chosen in order to prevent any modes between those specified from falling below critical. For example, if modes one and three were selected as 2% of critical for the three-story frame, mode 2 has 1.4% damping. In all frames, viscous damping of the highest mode (three and six) is less than 3% and 10% respectively. Monotonic static pushover analysis is performed with viscous damping set to zero.

7.1.2.2 Elastic Static Analysis

STAAD (REI 2005) is used for the static analysis with rigid diaphragms assumed for each floor. Structural component design forces are computed from the analytical

results using the capacity design procedures presented in Chapter 6. Structural components are designed in accordance with AISC LRFD design provisions (AISC 2001) and AISC seismic provisions (AISC 2002).

7.1.3 Frame Design Parameters

For frame designs, the column amplification factor, α_i, is taken as 15% for each floor and panel zone and shear deformations are neglected. Beam lengths, L, are taken equal to the bay lengths, L_b, to conservatively approximate the contributions from panel zone and shear deformations. As such, rigid-end offsets at member ends are not incorporated in either analysis.

A992 steel is used for each member with material and strain hardening overstrength factor, ϕ_m^o and ϕ_{sh}^o respectively, set to 1.1. Material overstrength due to the effects of strain rate, ϕ_{sr}^o, is not considered. Plastic hinges are modeled by the beam-column interaction relationship with member-level bilinear hysteresis as shown in Figs. 3-5 and 3-6. Plastic hinge lengths, ℓ_p, are taken as d_b and d_c for beams and column hinges respectively. The first-order post-yield stiffness ratio of each floor, r_{δ^1}, and effective SDOF model, r_{Δ^1}, is assumed equal to 0.1. Non-ductile columns are modeled following the LRFD (AISC 2001) beam-column interaction with weak-axis flexural and lateral-torsional buckling prevented for both tension and compression. $P \le 0.2P_y$ is maintained during design of the 1st story columns to insure that plastic hinges at the base

develop prior to buckling. The axial and flexural strength reduction factors, ϕ_c and ϕ_b respectively, are taken as 0.9 per AISC LRFD specifications (2005).

The seismic floor weight and gravity load tributary to the frame (primary and secondary) are assumed equal. The horizontal inertia mass, *m*, is set equal to 1.294 *kips-s²/in*. Lastly, equivalent hysteretic damping for design purposes is determined using the damping modification factor, κ, equal to 0.6 (see Chapter 4).

7.2 Three-story Frame Design Example (FR-3F)

7.2.1 Frame Model and Design

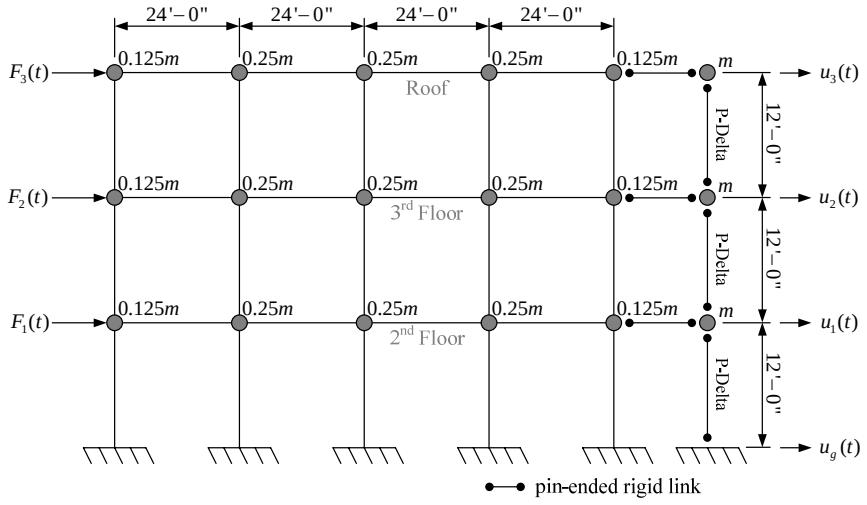

Figure 7-2. Frame schematic (three-story)

Three three-story frames are designed using the proposed DDBD methodology: (1) FR-3F-18 (W18 beams), (2) FR-3F-24 (W24 beams), and (3) FR-3F-30 (W30 beams). The frame model is shown in Fig. 7-2. W14 is chosen for the columns such that $2d_c \geq d_b$ is satisfied. Varying the beam depths between frames provides a basis for

response comparison, as well as effects of capacity design. The seismic floor weights are each set at 1000 *kips* – 50% respectively distributed as point loads to the frame columns and 50% to the *P*-Δ column.

Table 7-1. FR-3F model properties

Frame	DOF	h_i	$\delta_{d,i}$	$\theta_{by,i}$ [1]	$\lambda_{y,i}$	$\theta_{y,i}$ [2]	$\hat{\theta}_{y,i}$ [2]	$\theta_{y,sys}$	$\hat{\theta}_{y,sys}$	$\delta_{dy,i}$	$\hat{\delta}_{dy,i}$	$\mu_{\delta,i}$	$m_{eq,i}$ [3]	$\zeta_{eq,h,i}$ [3]
	(*i*)	(*in*)	(*in*)	(*rad*)		(*rad*)	(*rad*)	(*rad*)	(*rad*)	(*in*)	(*in*)			
FR-3F-18	1	144	3.60	0.01047	1.066	0.01204	0.01283	0.0120	0.0127	1.73	1.83	1.97	2580	0.154
	2	288	7.20	0.01047	1.052	0.01204	0.01266			3.47	3.65	1.97	2580	0.154
	3	432	10.80	0.01047	1.043	0.01204	0.01256			5.20	5.48	1.97	2580	0.154
FR-3F-24	1	144	3.60	0.00785	1.054	0.00903	0.00952	0.0090	0.0094	1.30	1.36	2.65	2769	0.184
	2	288	7.20	0.00785	1.043	0.00903	0.00942			2.60	2.72	2.65	2769	0.184
	3	432	10.80	0.00785	1.036	0.00903	0.00935			3.90	4.07	2.65	2769	0.184
FR-3F-30	1	144	3.60	0.00628	1.044	0.00722	0.00754	0.0072	0.0075	1.04	1.08	3.34	2929	0.195
	2	288	7.20	0.00628	1.035	0.00722	0.00748			2.08	2.16	3.34	2929	0.195
	3	432	10.80	0.00628	1.029	0.00722	0.00743			3.12	3.23	3.34	2929	0.195

1. based on $L = L_b$
2. based on $L_c - l_p = L_b$
3. based on $r_{\delta,i} = 0.1$

Table 7-2. FR-3F effective SDOF properties

Property	FR-3F-18 Target (*equivalent*)	FR-3F-18 Yield (*elastic*)	FR-3F-24 Target (*equivalent*)	FR-3F-24 Yield (*elastic*)	FR-3F-30 Target (*equivalent*)	FR-3F-30 Yield (*elastic*)
M_{eff}	6633	6655	7121	6655	7532	6655
h_{eff} (*in*)	336	336	336	336	336	336
P_{eff} (*kips*)	2571	2571	2571	2571	2571	2571
Γ_1	1.286	1.286	1.286	1.286	1.286	1.286
Υ	1.00	1.00	1.00	1.00	1.00	1.00
ζ_{eq}	17.4%	2.0%	20.4%	2.0%	21.5%	2.0%
Δ_d (*in*)	8.40	4.26	8.40	3.17	8.40	2.51
μ_Δ	1.97	1.00	2.65	1.00	3.34	1.00
T_{eff^2} (*sec*)	1.95	1.42	2.08	1.29	2.10	1.16
T_{eff^1} (*sec*)	1.85	1.38	1.96	1.26	1.99	1.14
K_{eff^2} (*kips/in*)	68.9	129.8	65.3	158.3	67.4	195.6
K_{eff^1} (*kips/in*)	76.5	137.5	72.9	166.0	75.1	203.2
F_{y^2} (*kips*)	578	553	548	502	566	492
F_{y^1} (*kips*)	643	586	613	526	631	511
r_{Δ^2}	0.047		0.057		0.065	

Table 7-3. FR-3F design forces

Frame	DOF (*i*)	$F_{x,i}$ (yield) (*kips*) *First-order*[1]	*Second-order*[2]
FR-3F-18	1	98	92
$F_{el^2} = 553$	2	195	184
$F_{el^1} = 586$	3	293	277
FR-3F-24	1	88	84
$F_{el^2} = 502$	2	175	167
$F_{el^1} = 526$	3	263	251
FR-3F-30	1	85	82
$F_{el^2} = 492$	2	170	164
$F_{el^1} = 511$	3	256	246

1. requires 1st order elastic analysis
2. requires 2nd order elastic analysis

Tables 7-1, 7-2, and 7-3 present the model properties, effective SDOF properties, and yield-level design forces respectively for each frame. Design values were determined after several iterations.

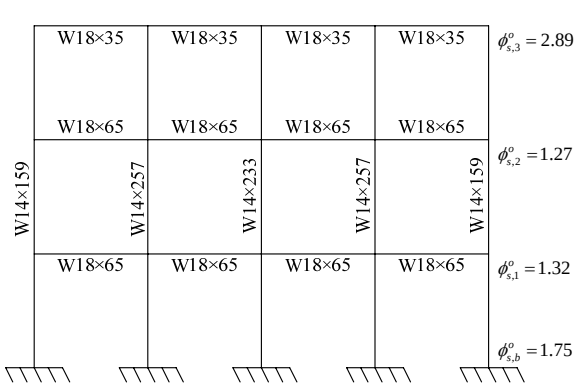

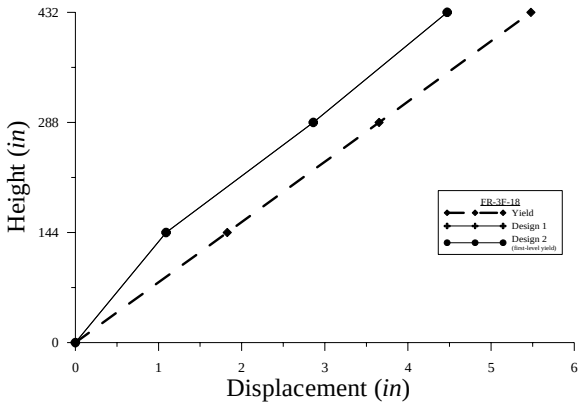

(i) Frame schematic **(ii) Displacement profile**

(a) FR-3F-18

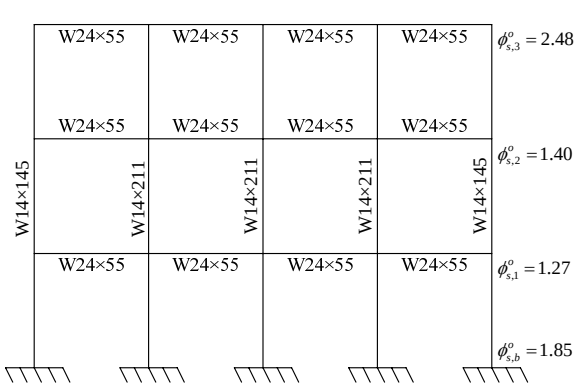

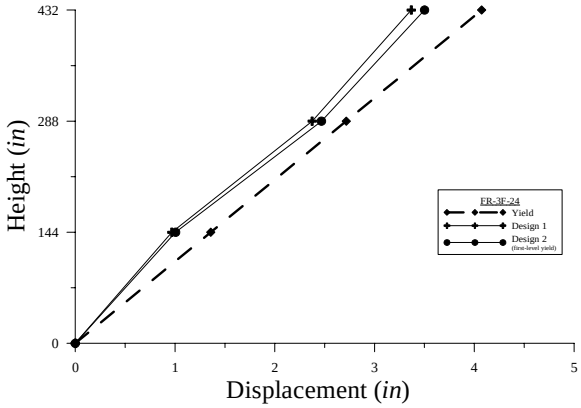

(i) Frame schematic **(ii) Displacement profile**

(b) FR-3F-24

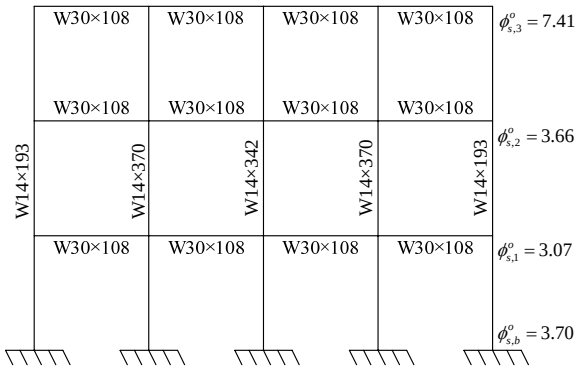

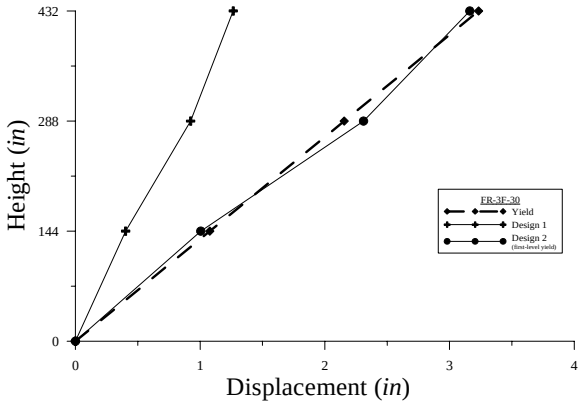

(i) Frame schematic **(ii) Displacement profile**

(c) FR-3F-30

Figure 7-3. Frame design

The frame models are analyzed in a 2nd order elastic analysis with the respective design forces. Member selections were iterated until the best fit to the yield displacement profile was achieved while maintaining the chosen member depths. Fig. 7-3 presents the final frame designs and displacement profiles. Three profiles are illustrated in each figure: (1) yield displacement profile ('Yield'), (2) displacement profile when subjected to the design forces ('Design 1'), and (3) displacement profile when the design forces are linearly amplified until the development of the first hinges ('Design 2'). Floor flexural overstrength values are indicated in the figure – the lowest value indicates location of first sequence of hinge formations and location of maximum drift ratio.

Table 7-4 lists the actual dynamic properties of the designed frames (ratio to elastic target values is included). As evident, member overstrengths and column stiffening from capacity design can significantly affect dynamic response. Most notably, a period shift occurs and, as a result, the design forces are amplified.

Table 7-4. Actual dynamic properties (FR-3F)

Property	FR-3F-18		FR-3F-24		FR-3F-30	
	Elastic	Ratio	Elastic	Ratio	Elastic	Ratio
M_{eff}	6218	0.93	6493	0.98	6644	1.00
h_{eff} (*in*)	347	1.03	340	1.01	336	1.00
P_{eff} (*kips*)	2403	0.93	2509	0.98	2567	1.00
Γ_1	1.283	1.00	1.261	0.98	1.252	0.97
T_{eff^2} (*sec*)	1.260	0.89	1.163	0.90	0.724	0.62
T_{eff^1} (*sec*)	1.231	0.89	1.139	0.90	0.781	0.69
K_{eff^2} (*kips/in*)	154.6	1.19	189.5	1.20	500.4	2.56
K_{eff^1} (*kips/in*)	162.0	1.18	197.6	1.19	430.0	2.12

Fig. 7-4 illustrates the 1st mode shapes (normalized to roof). In the figure, 'Target' is the normalized yield displacement profile and 'Design' is the normalized displacement

profile of the frame subjected to the design forces. Frame stiffening effects due to beam flexural overstrengths and capacity design of columns are evident in Figs. 7-3 and 7-4. It is determined that most beam hinges and 1st story column base hinges do not develop under the design forces and that beam hinges develop (except at the roof) prior to 1st story column base hinges – a condition of the chosen design displacement profile. Still, the linear force distribution is well represented.

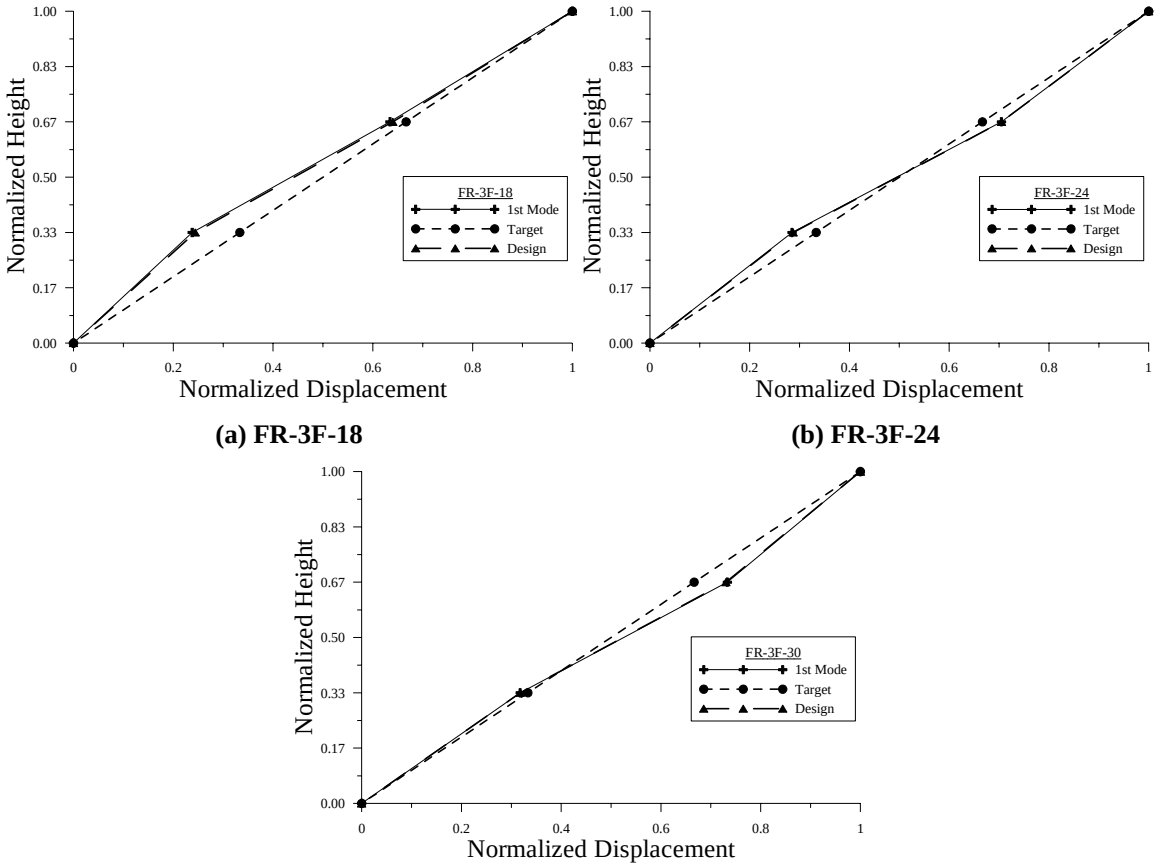

(a) FR-3F-18

(b) FR-3F-24

(c) FR-3F-30

Figure 7-4. Normalized 1st mode shape

7.2.2 Monotonic Static Pushover Analysis

A corollary to the noted stiffening effect is that a revision to the target yield displacement transpires. Table 7-5 presents the predicted static and dynamic response curve ordinates of the designed frames (see Chapter 6). The 'static' values include flexural overstrengths of the desired hinges and the 'dynamic' values incorporate the strengthening effect to protect against increased demands in the non-ductile members. Although ϕ_{bu}^{o} is used in design of columns, the listed values for ϕ_{p}^{o} do not include ϕ_{bu}^{o}.

Table 7-5. Static and dynamic predicted pushover ordinates (FR-3F)

Frame	Ω^{o}	Λ^{o}	Θ^{o}	Δ_{y}^{o} (*in*)	$F_{y^2}^{o}$ (*kips*)	$F_{y^1}^{o}$ (*kips*)	Δ_{d}^{o} (*in*)	$F_{d^2}^{o}$ (*kips*)	$F_{d^1}^{o}$ (*kips*)	ϕ_{p}^{o}	$F_{y^1}^{d}$ (*kips*)	$F_{d^1}^{d}$ (*kips*)
FR-3F-18	1.19	1.10	0.93	3.68	609	639	7.25	638	698	1.17	745	814
FR-3F-24	1.20	1.29	0.98	3.41	647	673	9.05	711	780	1.17	785	910
FR-3F-30	2.56	2.75	1.00	2.70	1352	1373	9.03	1621	1690	1.17	1602	1971

Fig. 7-5 plots the effective SDOF 'target' and expected 'static' and 'dynamic' pushover curves. The monotonic 'pushover' curve when subjected to the design force distribution is also shown. The assumed post-yield stiffness ratio, r_{Δ^1}, is accurate compared to the actual pushover curve.

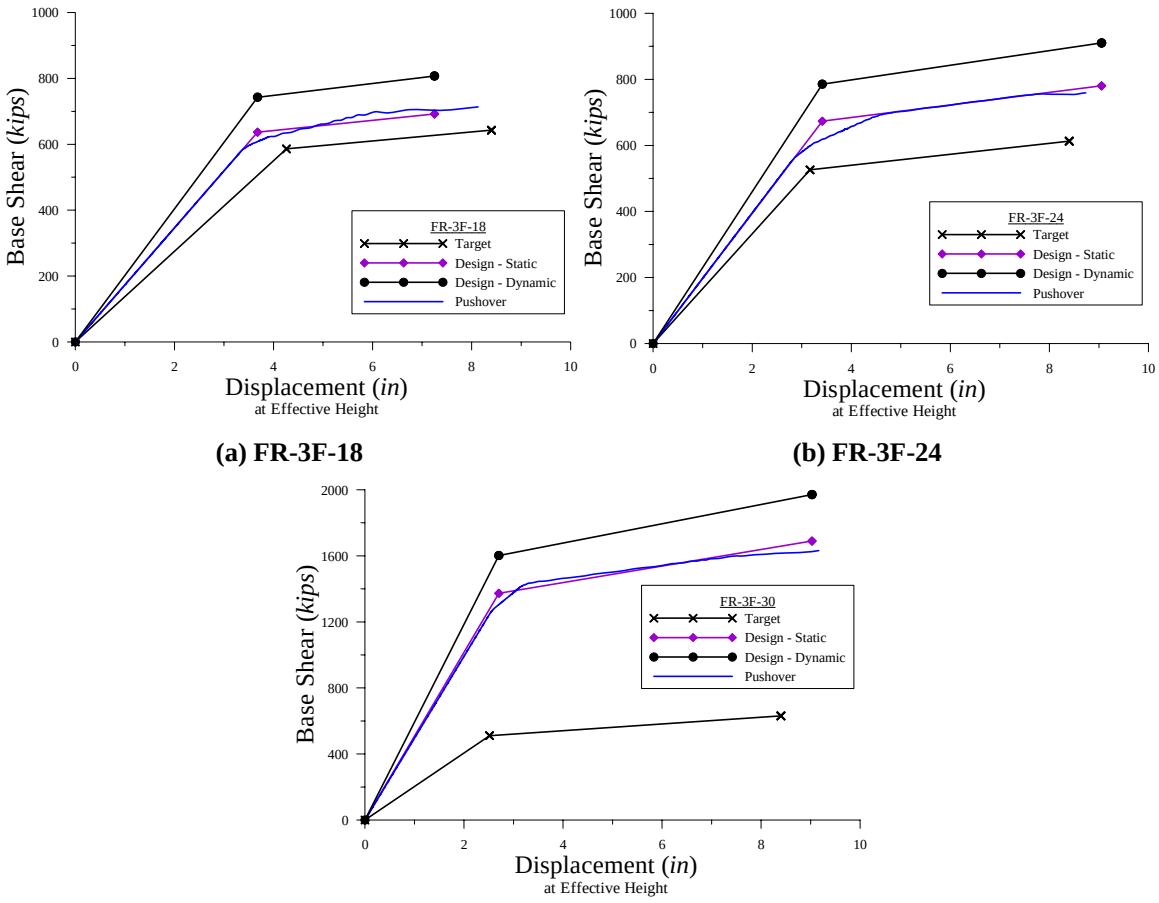

(a) FR-3F-18

(b) FR-3F-24

(c) FR-3F-30

Figure 7-5. Monotonic effective SDOF pushover curves

Fig. 7-6 presents the frame pushover curves under the design force distribution. The effects of overstrength and capacity design are evident. Deviation of the curves from the actual stiffness is due to differences between force distribution and 1st mode shape.

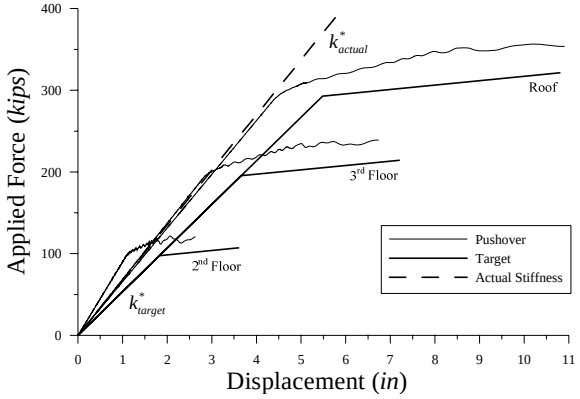

(i) Lateral force pushover

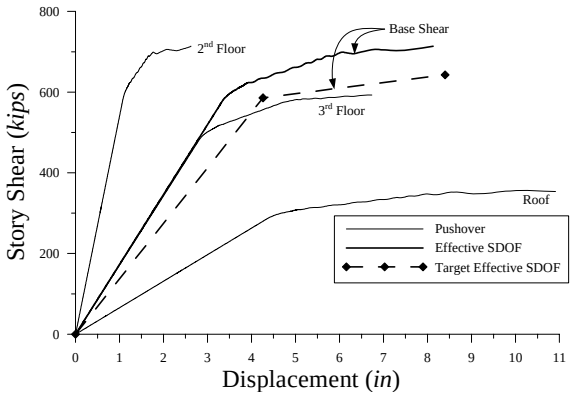

(ii) Story shear pushover

(a) FR-3F-18

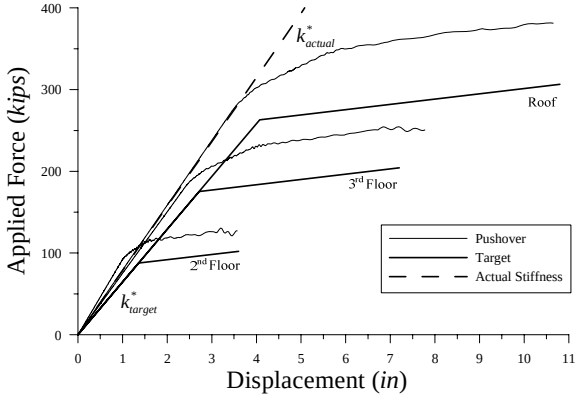

(i) Lateral force pushover

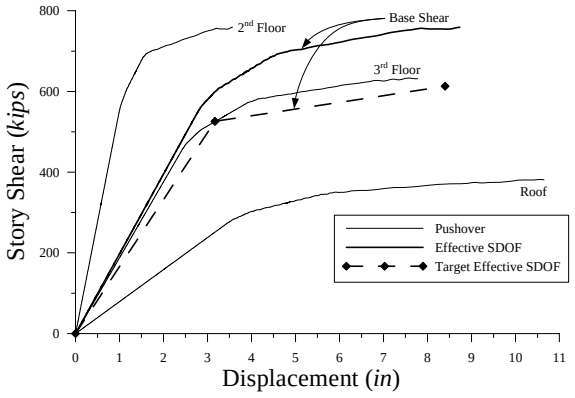

(ii) Story shear pushover

(b) FR-3F-24

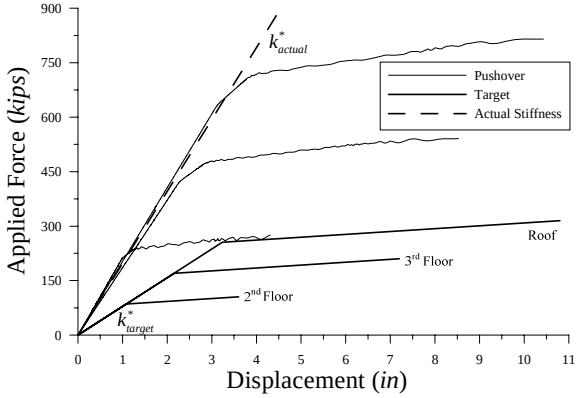

(i) Lateral force pushover

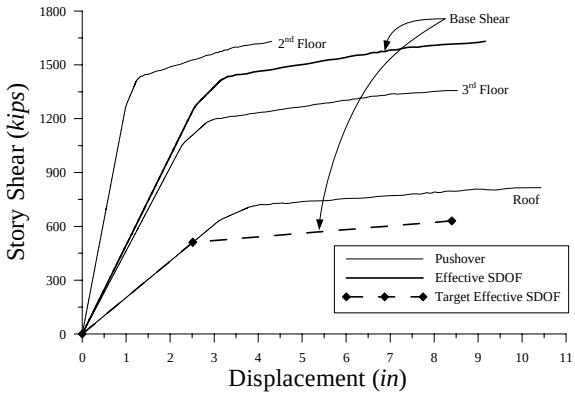

(ii) Story shear pushover

(c) FR-3F-30

Figure 7-6. Monotonic frame pushover curves

7.2.3 Dynamic Analysis

7.2.3.1 Displacement Envelopes and Dynamic Response Curves

The designed frames are evaluated with a 2nd order inelastic time-history analysis to evaluate frame response when subject to strong ground motion and to judge the applicability of the design parameters. Figs. 7-7, 7-8, and 7-9 present the displacement envelopes for the frames at the yield-level ($\Re$×MCE) and design-level (0.67×MCE) earthquake. The mean of the displacement envelopes is shown in the figures for comparison against the *revised* target profile (modified to account for overstrength – see Chapter 6). Dynamic pushover curves (base shear and base overturning moment) are additionally illustrated for each frame. Four levels of each earthquake (0.13, $\Re$, 0.45, and 0.67×MCE) are used to construct the pushover curves. The plots are classified as far-field and near-fault. Although the plots illustrate displacement envelopes, the difference between envelope and displacement profile at each nodal maximum is negligible.

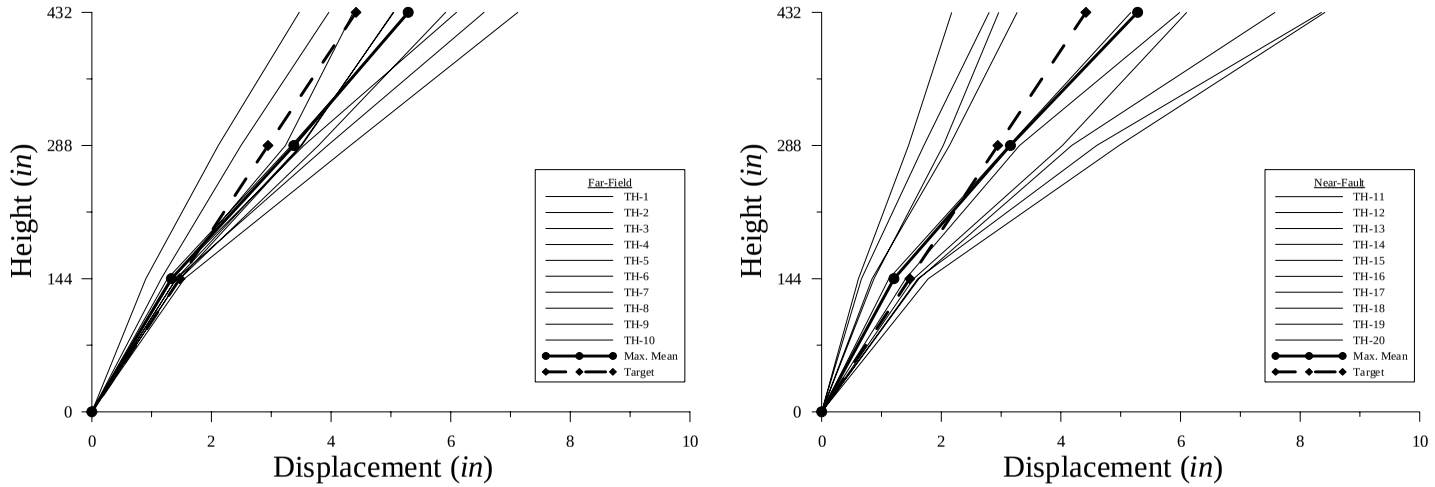

(a) Displacement profile (Yield - 0.27 × MCE)

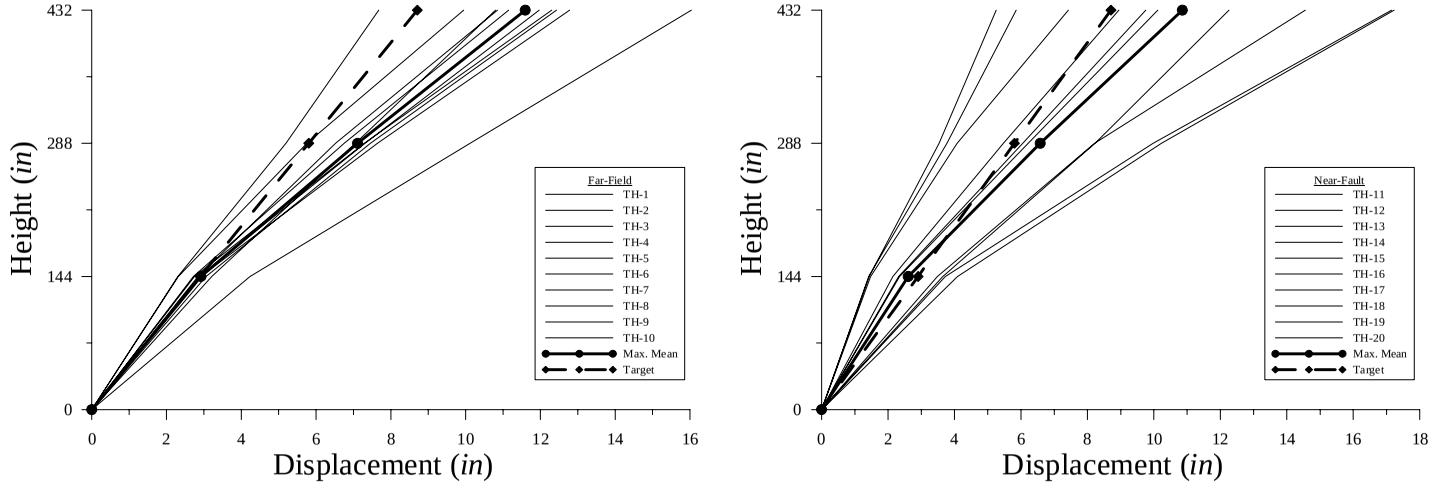

(b) Displacement profile (Target - 0.67 × MCE)

Figure 7-7. FR-3F-18 inelastic dynamic analysis results

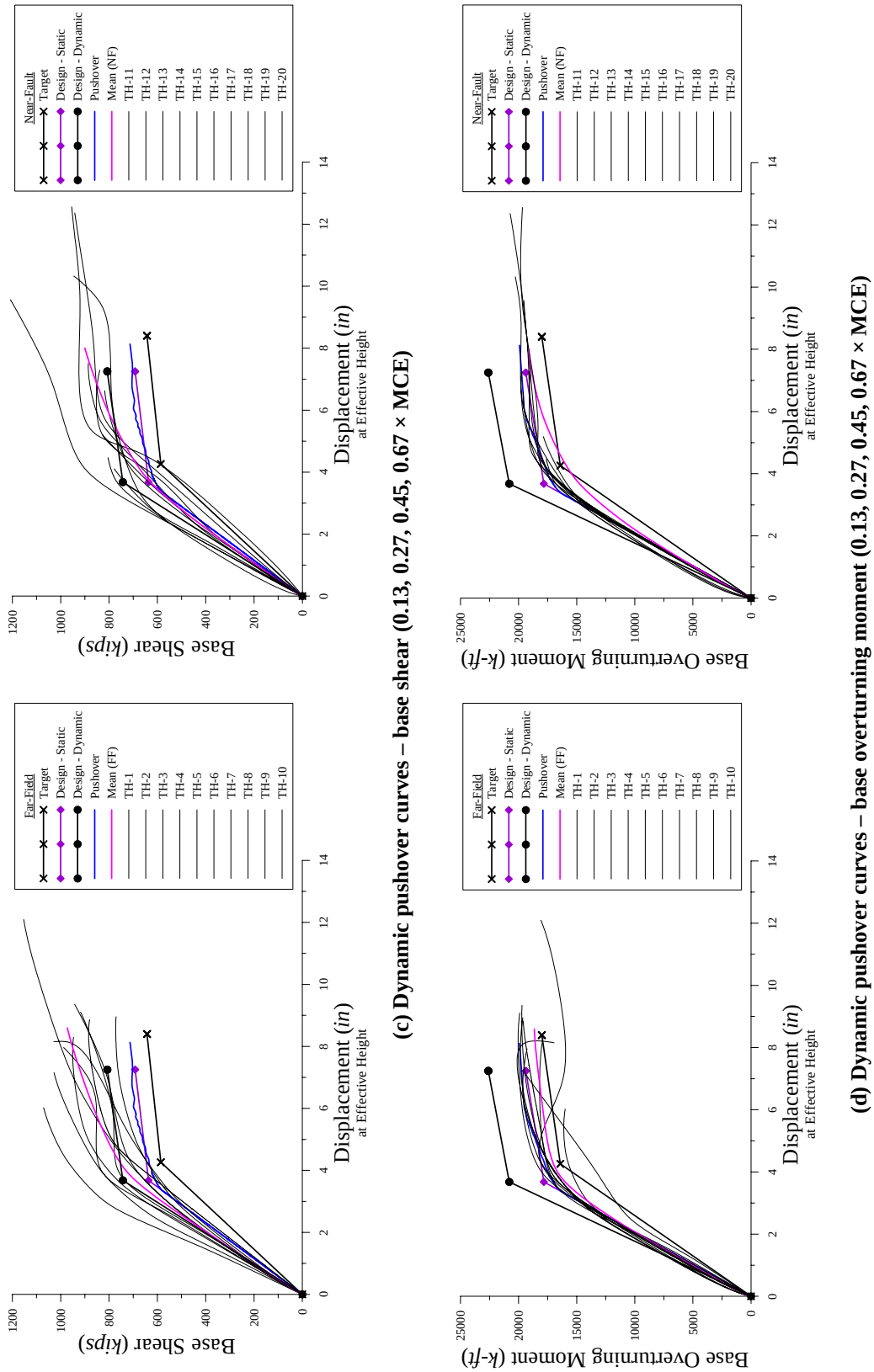

(c) Dynamic pushover curves – base shear (0.13, 0.27, 0.45, 0.67 × MCE)

(d) Dynamic pushover curves – base overturning moment (0.13, 0.27, 0.45, 0.67 × MCE)

Figure 7-7. FR-3F-18 inelastic dynamic analysis results (Cont'd)

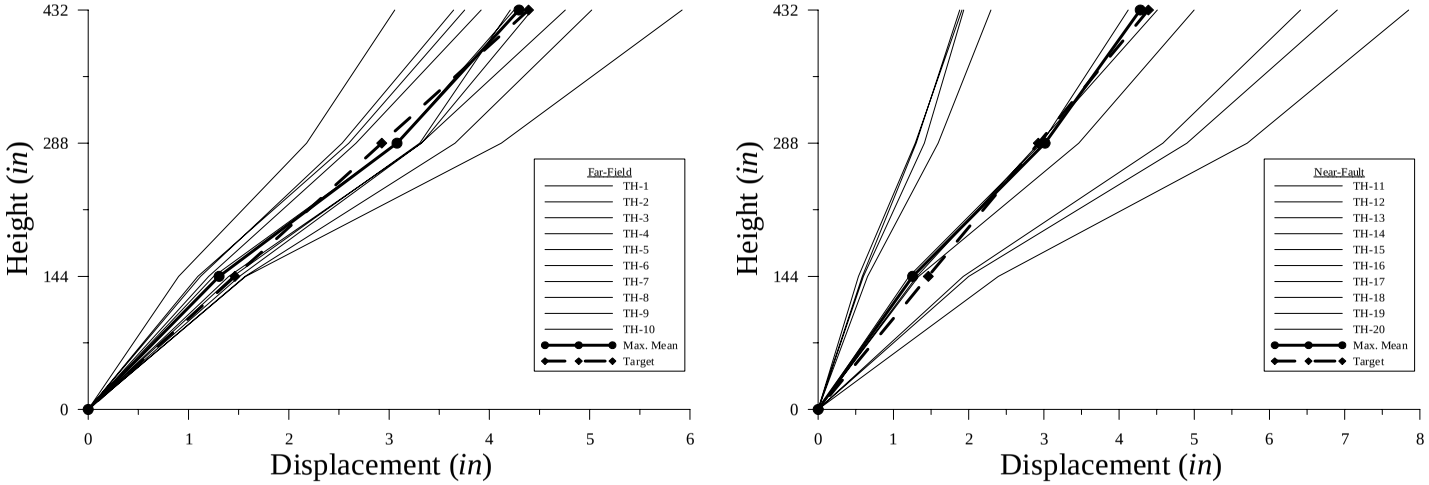

(a) Displacement profile (Yield - 0.25 × MCE)

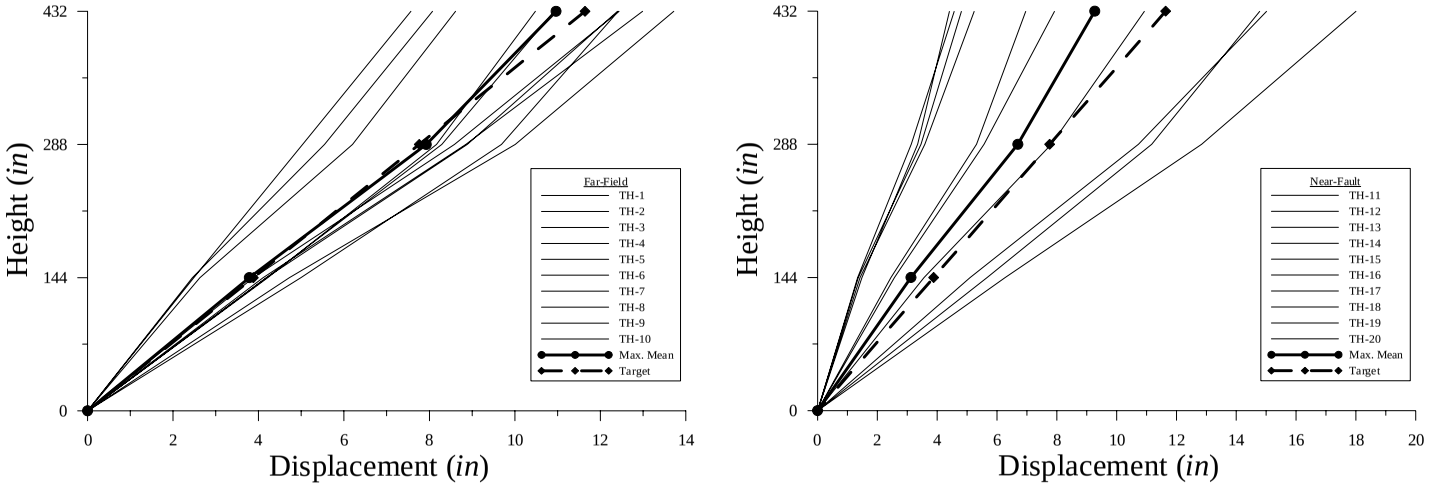

(b) Displacement profile (Target - 0.67 × MCE)

Figure 7-8. FR-3F-24 inelastic dynamic analysis results

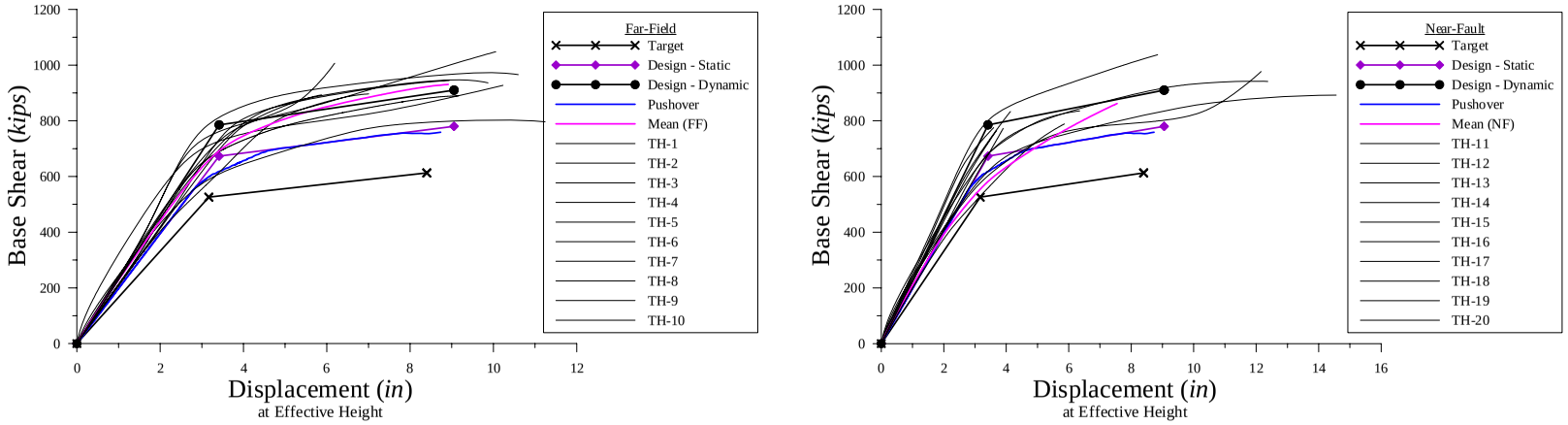

(c) Dynamic pushover curves – base shear (0.13, 0.25, 0.45, 0.67 × MCE)

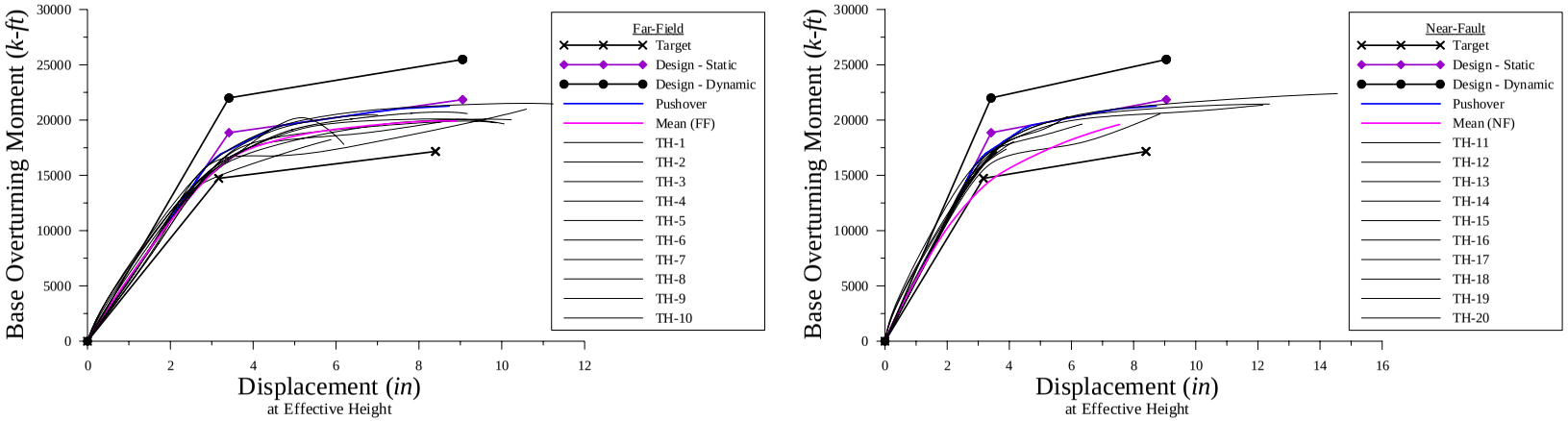

(d) Dynamic pushover curves – base overturning moment (0.13, 0.25, 0.45, 0.67 × MCE)

Figure 7-8. FR-3F-24 inelastic dynamic analysis results (Cont'd)

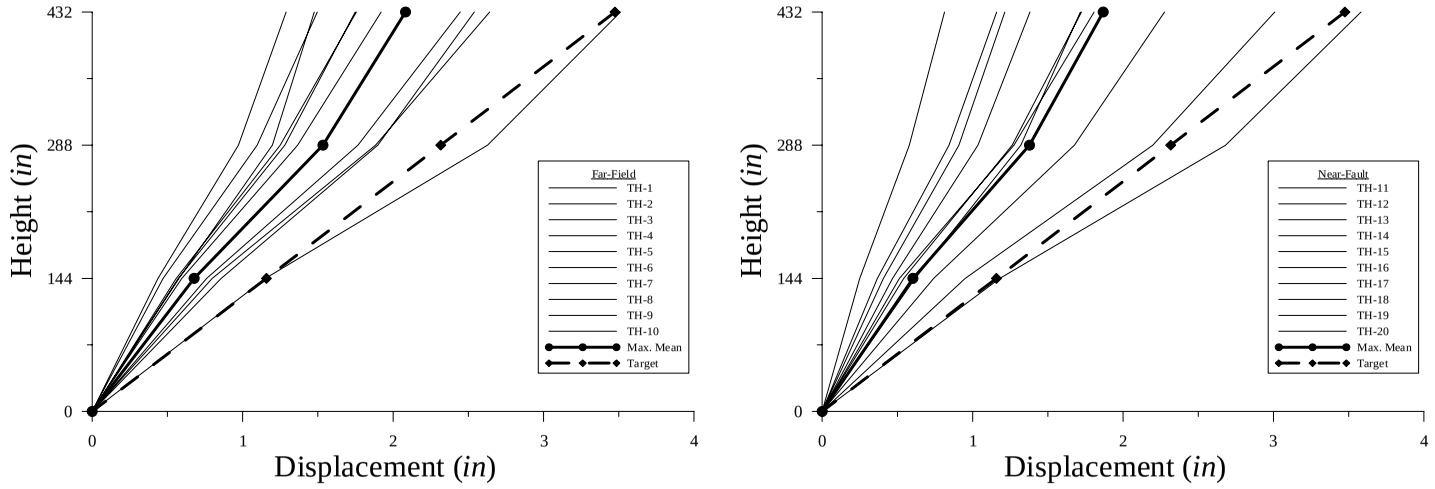

(a) Displacement profile (Yield - 0.20 × MCE)

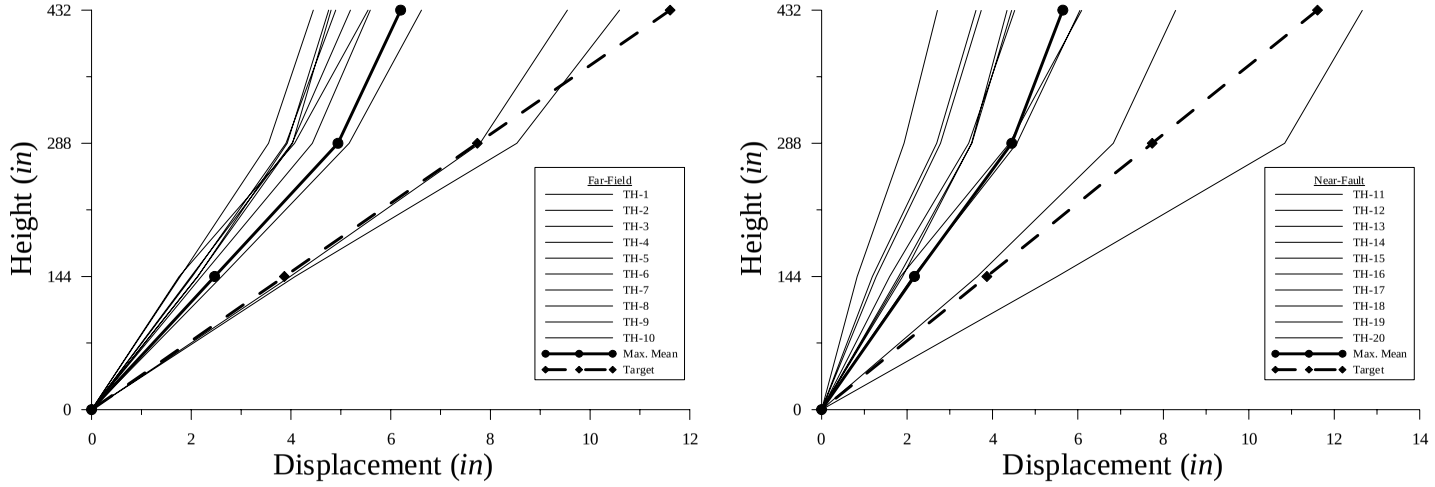

(b) Displacement profile (Target - 0.67 × MCE)

Figure 7-9. FR-3F-30 inelastic dynamic analysis results

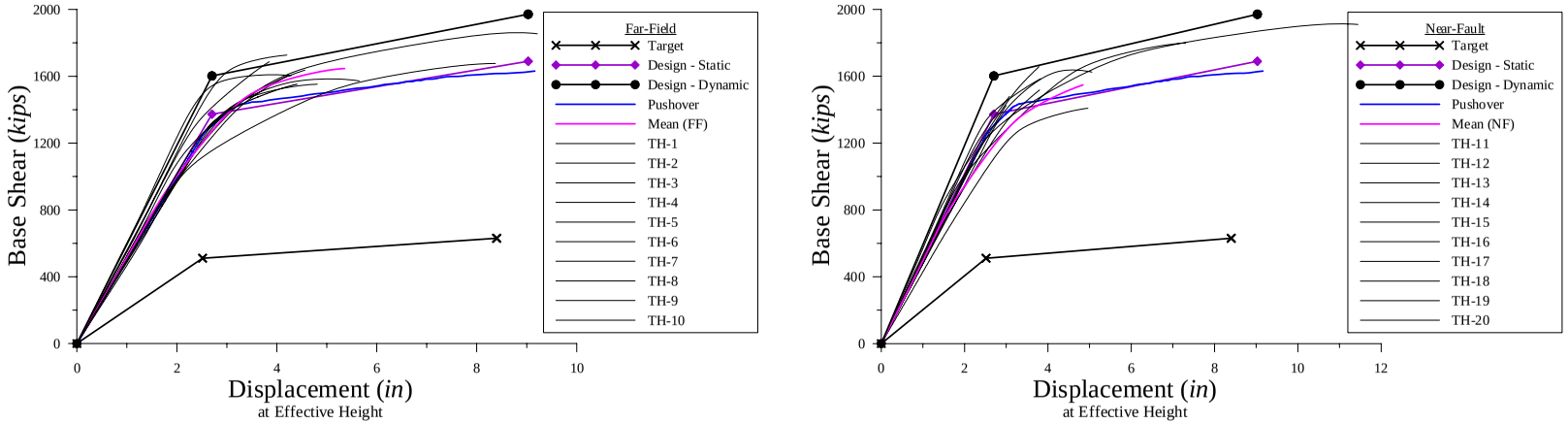

(c) Dynamic pushover curves – base shear (0.13, 0.20, 0.45, 0.67 × MCE)

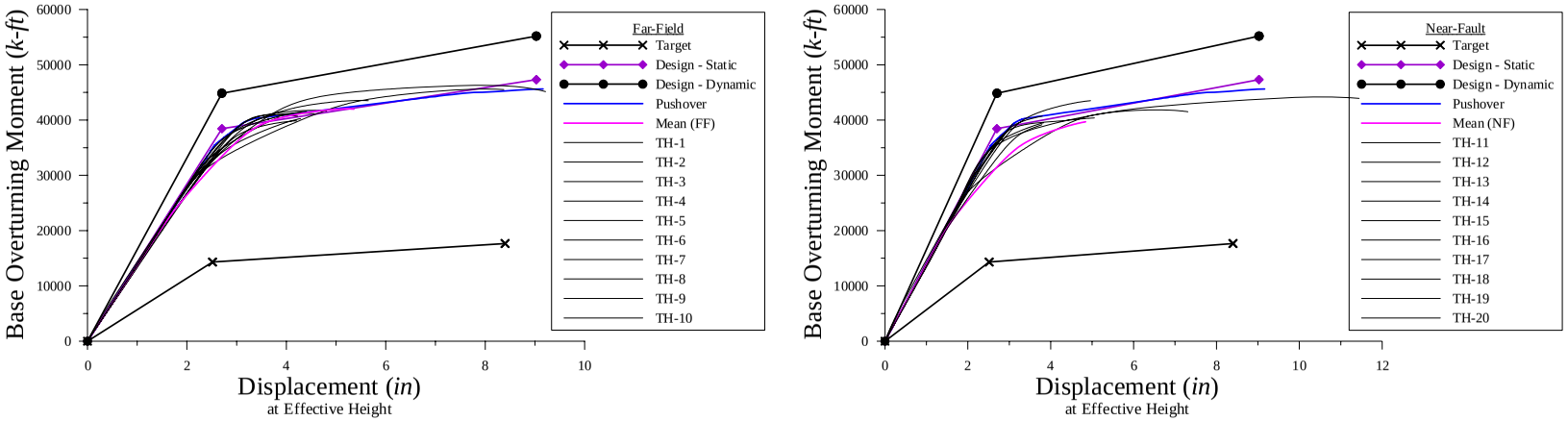

(d) Dynamic pushover curves – base overturning moment (0.13, 0.20, 0.45, 0.67 × MCE)

Figure 7-9. FR-3F-30 inelastic dynamic analysis results (Cont'd)

FR-3F-18

As seen in Fig. 7-7(a) and (b), good agreement exists between the mean envelopes and target profiles for the far-field earthquakes though the linear profile is not well represented. The frequency content and magnitudes are such that higher modes do contribute to frame behavior (see Fig. 7-7(c)). Although better agreement exists for the chosen near-fault records, ground motion characteristics associated with these type earthquakes result in wider scatter.

Contributions of higher modes are evident in Fig. 7-7(c) and (d) due to stiffness reduction of the beams, cantilever action, and earthquake characteristics (increase in base shear coupled with a decrease in base overturning moment). The frame thus relies heavily on column stiffness for resistance. Due to this effect, the columns were additionally strengthened during capacity design. Consequently, formation of base hinges is prevented and the frame is dominated by cantilever action.

FR-3F-24

As seen in Fig. 7-8(a) and (b), excellent agreement exists between the mean envelopes and target profiles for the far-field earthquakes. Similar to FR-3F-18, the frequency content and magnitudes are such that higher modes do contribute to frame behavior though a reduction is evident. This suggests that column depths play a role not only in post-yield stiffness but also on limiting higher mode contributions. Also, the increase in column strength for higher mode protection is lower than for FR-3F-18. Still, the frame has some cantilever action due to the absence or limited formation of base

hinges. Furthermore, near-fault motions do not allow the formation of 1st mode-based global yield mechanism for this frame (see curvature ductility, Table 7-7). Consequently, the system behaves similar to an essentially elastic frame for these records.

FR-3F-30

As seen in Fig. 7-9(a) and (b), large differences exist between the mean envelopes and target profiles. This effect is primarily due to the excessive level of strength and stiffness. As a result, the frame does not develop the desired global yield mechanism nor efficiently use the available ductility capacity (see curvature ductility, Table 7-8). Further, it can be seen that higher modes essentially do not contribute to frame response. It is thus recommended that frame designs be restricted to $\Lambda^o \leq 1.4$ and $\Omega^o \leq 1.4$, at which point the design engineer selects new beam depths for more effective use of strength and stiffness. The results also suggest that the displacement amplification factor, C_d, used in FBD is proportional to overstrength.

7.2.3.2 Curvature Ductility Envelopes

Fig. 7-10 illustrates the frame model with all possible hinge locations. Tables 7-6, 7-7, and 7-8 list the curvature ductility for each hinge developed in the frames at the presumed yield-level earthquake. In general, base hinges do not form at the presumed yield-level earthquake. This can affect the formation of the global yield mechanism (condition of design displacement profile) and, ultimately, the inelastic response of the frame. Also, the tables indicate that evaluating the floor flexural overstrengths provides a basis for evaluating hinge sequencing.

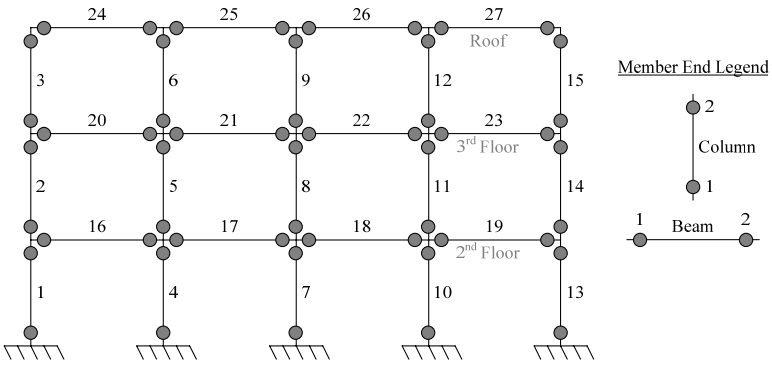

Figure 7-10. FR-3F plastic hinge model

Table 7-6. Curvature ductility envelopes (FR-3F-18) – 0.27×MCE

Floor	Member	End	TH-1	TH-2	TH-3	TH-4	TH-5	TH-6	TH-7	TH-8	TH-9	TH-10	TH-11	TH-12	TH-13	TH-14	TH-15	TH-16	TH-17	TH-18	TH-19	TH-20
Columns	1	1	---	---	---	---	---	---	---	---	---	---	1.08	---	---	1.02	---	---	---	---	---	---
	4	1	---	---	---	---	---	---	---	---	---	---	1.24	1.01	---	1.16	---	---	---	---	---	---
	7	1	---	---	---	---	---	---	---	---	---	---	1.24	1.02	---	1.17	---	---	---	---	---	1.00
	10	1	---	---	---	---	---	---	---	---	---	---	1.24	1.01	---	1.16	---	---	---	---	---	---
	13	1	---	---	---	---	---	---	---	---	---	---	1.08	---	---	1.02	---	---	---	---	---	---
2nd Floor	16	1	1.41	1.59	1.74	1.95	1.50	1.99	---	---	2.31	1.77	2.15	2.56	2.24	3.01	---	1.15	---	---	---	1.54
Beams		2	1.44	1.55	1.69	1.94	1.49	1.90	---	---	2.32	1.76	2.06	2.54	2.15	2.96	---	1.14	---	---	---	1.46
	17	1	1.40	1.51	1.72	2.00	1.44	1.90	---	---	2.40	1.79	2.04	2.45	2.18	2.89	---	1.13	---	---	---	1.49
		2	1.36	1.50	1.63	1.84	1.43	1.89	---	---	2.18	1.68	2.09	2.48	2.13	2.87	---	1.07	---	---	---	1.41
	18	1	1.36	1.50	1.63	1.84	1.43	1.89	---	---	2.18	1.74	2.09	2.48	2.11	2.87	---	1.07	---	---	---	1.40
		2	1.40	1.51	1.71	1.99	1.44	1.90	---	---	2.40	1.75	2.04	2.45	2.21	2.89	---	1.13	---	---	---	1.48
	19	1	1.44	1.55	1.68	1.93	1.50	1.95	---	---	2.33	1.77	2.06	2.54	2.17	2.96	---	1.12	---	---	---	1.47
		2	1.42	1.59	1.74	1.94	1.51	1.97	---	---	2.31	1.78	2.16	2.56	2.24	3.01	---	1.19	---	---	---	1.48
3rd Floor	20	1	1.76	2.41	1.41	2.46	1.05	2.72	---	1.08	3.15	1.63	3.68	4.55	2.22	4.21	---	1.84	---	---	---	2.72
Beams		2	1.79	2.45	1.38	2.33	1.02	2.71	---	1.02	3.07	1.56	3.70	4.49	2.17	4.21	---	1.83	---	---	---	2.71
	21	1	1.78	2.44	1.39	2.40	1.00	2.73	---	1.03	3.09	1.57	3.68	4.56	2.21	4.25	---	1.78	---	---	---	2.74
		2	1.75	2.44	1.34	2.38	---	2.65	---	1.00	3.04	1.52	3.70	4.47	2.12	4.13	---	1.78	---	---	---	2.61
	22	1	1.75	2.44	1.33	2.38	---	2.65	---	1.03	3.04	1.52	3.70	4.47	2.14	4.13	---	1.77	---	---	---	2.63
		2	1.80	2.45	1.38	2.39	---	2.73	---	---	3.11	1.58	3.68	4.56	2.20	4.25	---	1.78	---	---	---	2.64
	23	1	1.77	2.45	1.37	2.32	1.01	2.72	---	1.02	3.07	1.56	3.70	4.48	2.18	4.22	---	1.83	---	---	---	2.70
		2	1.81	2.48	1.41	2.46	1.03	2.72	---	1.05	3.18	1.68	3.73	4.54	2.24	4.22	---	1.78	---	---	---	2.71
Roof	24	1	1.44	2.53	1.15	2.54	1.88	2.53	1.06	1.25	2.81	1.79	4.05	5.22	1.92	4.49	---	1.85	---	---	---	3.43
Beams		2	1.43	2.50	1.14	2.53	1.87	2.47	1.02	1.15	2.86	1.78	3.88	5.03	1.88	4.47	---	1.66	---	---	---	3.42
	25	1	1.45	2.59	1.15	2.42	1.87	2.47	1.03	1.17	2.91	1.72	3.89	5.02	1.87	4.47	---	1.73	---	---	---	3.41
		2	1.40	2.42	1.10	2.42	1.86	2.46	---	1.14	2.71	1.72	3.89	5.09	1.86	4.46	---	1.69	---	---	---	3.40
	26	1	1.40	2.42	1.10	2.40	1.75	2.47	1.00	1.14	2.71	1.71	3.88	5.09	1.85	4.46	---	1.68	---	---	---	3.28
		2	1.45	2.60	1.11	2.61	1.92	2.48	1.03	1.17	2.92	1.82	3.98	5.01	1.92	4.47	---	1.73	---	---	---	3.47
	27	1	1.44	2.49	1.13	2.54	1.86	2.51	1.05	1.16	2.92	1.79	3.89	5.03	1.89	4.47	---	1.65	---	---	---	3.41
		2	1.49	2.62	1.14	2.54	1.87	2.52	1.06	1.24	2.78	1.80	4.06	5.21	1.93	4.55	---	1.84	---	---	---	3.42

Table 7-7. Curvature ductility envelopes (FR-3F-24) – 0.25×MCE

Floor	Member	End	TH-1	TH-2	TH-3	TH-4	TH-5	TH-6	TH-7	TH-8	TH-9	TH-10	TH-11	TH-12	TH-13	TH-14	TH-15	TH-16	TH-17	TH-18	TH-19	TH-20
Columns	1	1	---	---	---	---	---	---	---	---	---	---	1.52	2.18	---	1.52	---	---	---	---	---	---
	4	1	---	1.15	---	---	---	1.00	---	---	---	1.14	1.65	2.28	---	1.65	---	---	---	---	---	---
	7	1	---	1.15	---	---	---	1.00	---	---	---	1.14	1.65	2.28	---	1.65	---	---	---	---	---	---
	10	1	---	1.15	---	---	---	1.00	---	---	---	1.14	1.65	2.28	---	1.65	---	---	---	---	---	---
	13	1	---	---	---	---	---	---	---	---	---	---	1.52	2.18	---	1.52	---	---	---	---	---	---
2nd Floor	16	1	1.19	2.40	1.76	1.25	2.13	2.73	---	2.06	1.26	2.11	3.28	4.21	1.63	3.50	---	2.10	---	---	---	1.62
Beams		2	1.08	2.23	1.65	1.10	1.93	2.62	---	1.97	1.15	1.96	3.05	4.12	1.50	3.30	---	1.96	---	---	---	1.46
	17	1	1.08	2.23	1.64	1.10	1.98	2.59	---	1.94	1.13	1.96	3.07	4.07	1.50	3.31	---	1.96	---	---	---	1.47
		2	1.08	2.23	1.64	1.10	1.98	2.60	---	1.94	1.13	1.96	3.07	4.08	1.50	3.31	---	1.96	---	---	---	1.47
	18	1	1.08	2.23	1.64	1.10	1.98	2.60	---	1.94	1.13	1.96	3.07	4.08	1.50	3.31	---	1.96	---	---	---	1.47
		2	1.08	2.23	1.64	1.10	1.99	2.59	---	1.94	1.13	1.97	3.07	4.07	1.50	3.30	---	1.96	---	---	---	1.47
	19	1	1.09	2.23	1.63	1.09	1.99	2.63	---	1.96	1.14	1.97	3.05	4.12	1.53	3.37	---	1.93	---	---	---	1.46
		2	1.22	2.41	1.75	1.24	2.11	2.76	---	2.05	1.27	2.12	3.30	4.19	1.62	3.46	---	2.11	---	---	---	1.61
3rd Floor	20	1	---	2.06	1.26	1.37	1.57	2.51	---	1.42	1.22	1.75	2.78	3.61	1.13	3.00	---	1.91	---	---	---	1.93
Beams		2	---	2.05	1.15	1.29	1.56	2.50	---	1.41	1.12	1.74	2.73	3.52	1.04	2.93	---	1.89	---	---	---	1.83
	21	1	---	2.05	1.16	1.30	1.51	2.50	---	1.37	1.15	1.72	2.73	3.54	1.07	2.95	---	1.85	---	---	---	1.84
		2	---	2.05	1.16	1.30	1.52	2.50	---	1.37	1.15	1.72	2.76	3.54	1.06	2.95	---	1.85	---	---	---	1.84
	22	1	---	2.05	1.16	1.30	1.52	2.50	---	1.37	1.15	1.72	2.76	3.54	1.06	2.95	---	1.85	---	---	---	1.83
		2	---	2.05	1.16	1.30	1.51	2.50	---	1.37	1.15	1.72	2.73	3.54	1.06	2.95	---	1.85	---	---	---	1.84
	23	1	---	2.04	1.15	1.34	1.50	2.50	---	1.36	1.18	1.78	2.73	3.50	1.07	2.99	---	1.84	---	---	---	1.83
		2	---	2.15	1.26	1.37	1.59	2.58	---	1.43	1.21	1.75	2.73	3.59	1.15	2.99	---	1.91	---	---	---	1.85
Roof	24	1	---	---	---	---	---	---	---	---	---	---	---	1.06	---	---	---	---	---	---	---	---
Beams		2	---	---	---	---	---	---	---	---	---	---	---	1.03	---	---	---	---	---	---	---	---
	25	1	---	---	---	---	---	---	---	---	---	---	---	---	---	---	---	---	---	---	---	---
		2	---	---	---	---	---	---	---	---	---	---	---	---	---	---	---	---	---	---	---	---
	26	1	---	---	---	---	---	---	---	---	---	---	---	---	---	---	---	---	---	---	---	---
		2	---	---	---	---	---	---	---	---	---	---	---	---	---	---	---	---	---	---	---	---
	27	1	---	---	---	---	---	---	---	---	---	---	---	---	---	---	---	---	---	---	---	---
		2	---	---	---	---	---	---	---	---	---	---	---	---	---	---	---	---	---	---	---	---

Table 7-8. Curvature ductility envelopes (FR-3F-30) – 0.20×MCE

Floor	Member	End	TH-1	TH-2	TH-3	TH-4	TH-5	TH-6	TH-7	TH-8	TH-9	TH-10	TH-11	TH-12	TH-13	TH-14	TH-15	TH-16	TH-17	TH-18	TH-19	TH-20
Columns	1	1	---	---	---	---	---	---	---	---	---	---	---	---	---	---	---	---	---	---	---	---
	4	1	---	---	---	---	---	---	---	---	---	---	---	---	---	---	---	---	---	---	---	---
	7	1	---	---	---	---	---	---	---	---	---	---	---	---	---	---	---	---	---	---	---	---
	10	1	---	---	---	---	---	---	---	---	---	---	---	---	---	---	---	---	---	---	---	---
	13	1	---	---	---	---	---	---	---	---	---	---	---	---	---	---	---	---	---	---	---	---
2nd Floor	16	1	---	---	---	---	---	---	---	1.34	---	---	---	---	---	---	---	1.40	---	---	---	---
Beams		2	---	---	---	---	---	---	---	1.47	---	---	---	---	---	---	---	1.52	---	---	---	---
	17	1	---	---	---	---	---	---	---	1.47	---	---	---	---	---	---	---	1.59	---	---	---	---
		2	---	---	---	---	---	---	---	1.39	---	---	---	---	---	---	---	1.42	---	---	---	---
	18	1	---	---	---	---	---	---	---	1.39	---	---	---	---	---	---	---	1.42	---	---	---	---
		2	---	---	---	---	---	---	---	1.47	---	---	---	---	---	---	---	1.59	---	---	---	---
	19	1	---	---	---	---	---	---	---	1.47	---	---	---	---	---	---	---	1.52	---	---	---	---
		2	---	---	---	---	---	---	---	1.34	---	---	---	---	---	---	---	1.40	---	---	---	---
3rd Floor	20	1	---	---	---	---	---	---	---	---	---	---	---	---	---	---	---	---	---	---	---	---
Beams		2	---	---	---	---	---	---	---	---	---	---	---	---	---	---	---	---	---	---	---	---
	21	1	---	---	---	---	---	---	---	---	---	---	---	---	---	---	---	---	---	---	---	---
		2	---	---	---	---	---	---	---	---	---	---	---	---	---	---	---	---	---	---	---	---
	22	1	---	---	---	---	---	---	---	---	---	---	---	---	---	---	---	---	---	---	---	---
		2	---	---	---	---	---	---	---	---	---	---	---	---	---	---	---	---	---	---	---	---
	23	1	---	---	---	---	---	---	---	---	---	---	---	---	---	---	---	---	---	---	---	---
		2	---	---	---	---	---	---	---	---	---	---	---	---	---	---	---	---	---	---	---	---
Roof	24	1	---	---	---	---	---	---	---	---	---	---	---	---	---	---	---	---	---	---	---	---
Beams		2	---	---	---	---	---	---	---	---	---	---	---	---	---	---	---	---	---	---	---	---
	25	1	---	---	---	---	---	---	---	---	---	---	---	---	---	---	---	---	---	---	---	---
		2	---	---	---	---	---	---	---	---	---	---	---	---	---	---	---	---	---	---	---	---
	26	1	---	---	---	---	---	---	---	---	---	---	---	---	---	---	---	---	---	---	---	---
		2	---	---	---	---	---	---	---	---	---	---	---	---	---	---	---	---	---	---	---	---
	27	1	---	---	---	---	---	---	---	---	---	---	---	---	---	---	---	---	---	---	---	---
		2	---	---	---	---	---	---	---	---	---	---	---	---	---	---	---	---	---	---	---	---

As discussed in Chapter 3, the yield-level earthquake is dependent upon rotation ductility (see Eq. (3-23)). It is recommended that the yield-level earthquake be approximated by incorporating overstrength.

$$\Re \quad = \text{Reduction factor} \left(= \begin{cases} \dfrac{\Omega^o}{\sqrt{2\mu_{\theta,sys} - 1}} & T_1 < 1.0 \\ \dfrac{\Omega^o}{\mu_{\theta,sys}} & T_1 \geq 1.0 \end{cases} \right) \tag{7-1}$$

It follows that the revised yield-level earthquakes are 0.32, 0.29, and 0.49 × MCE for FR-3F-18, FR-3F-24, and FR-3F-30 respectively. Still, the lack of formation of the base hinges should be corrected in order to completely validate the chosen displacement profile and yield-level earthquake intensity.

Tables 7-9, 7-10, and 7-11 list the curvature ductility for each hinge developed in each frame at the design-level earthquake. From Chapter 3, the minimum allowable curvature ductility based on the chosen response parameters is approximately 8.6.

Member ductility values in excess of the allowable do not directly identify failure but do indicate unsatisfactory member performance.

Table 7-9. Curvature ductility envelopes (FR-3F-18) – 0.67×MCE

Floor	Member	End	TH-1	TH-2	TH-3	TH-4	TH-5	TH-6	TH-7	TH-8	TH-9	TH-10	TH-11	TH-12	TH-13	TH-14	TH-15	TH-16	TH-17	TH-18	TH-19	TH-20
Columns	1	1	2.86	2.89	3.22	5.12	3.58	2.51	2.07	2.19	2.82	3.10	4.57	3.96	1.93	4.22	---	1.90	---	---	1.70	4.16
	3	1	---	---	---	1.09	---	---	---	---	---	---	---	---	---	---	---	---	---	---	---	---
	4	1	2.91	2.95	3.25	5.16	3.61	2.57	2.16	2.27	2.91	3.16	4.47	3.94	2.01	4.23	---	2.00	---	---	1.80	4.20
	5	1	---	---	---	1.35	---	---	---	---	---	---	---	1.03	---	1.13	---	---	---	---	---	1.01
	6	1	---	---	---	1.62	---	---	---	1.05	---	---	---	---	---	---	---	---	---	---	---	---
	7	1	2.92	2.97	3.31	5.18	3.68	2.57	2.17	2.28	2.96	3.17	4.47	3.94	2.04	4.30	---	2.03	---	---	1.81	4.21
	8	1	---	---	---	1.50	---	---	---	---	---	---	---	1.16	---	1.30	---	---	---	---	---	1.10
	9	1	---	---	---	1.74	---	---	---	1.18	---	---	---	---	---	---	---	---	---	---	---	---
	10	1	2.91	2.95	3.25	5.16	3.61	2.57	2.17	2.27	2.91	3.16	4.47	3.94	2.01	4.23	---	2.00	---	---	1.80	4.20
	11	1	---	---	---	1.35	---	---	---	---	---	---	---	1.03	---	1.13	---	---	---	---	---	1.01
	12	1	---	---	---	1.62	---	---	---	1.05	---	---	---	---	---	---	---	---	---	---	---	---
	13	1	2.86	2.89	3.22	5.12	3.58	2.51	2.07	2.19	2.82	3.10	4.57	3.96	1.93	4.22	---	1.90	---	---	1.70	4.16
	15	1	---	---	---	1.09	---	---	---	---	---	---	---	---	---	---	---	---	---	---	---	---
2nd Floor	16	1	4.97	5.34	5.02	7.54	4.91	4.96	3.80	3.24	4.54	4.20	7.50	7.14	4.17	5.63	1.92	3.99	1.76	2.05	3.46	6.03
Beams		2	4.91	5.25	4.94	7.40	5.00	4.85	3.55	3.42	4.41	4.14	7.39	7.12	4.14	5.60	1.92	3.88	1.70	1.96	3.37	5.96
	17	1	4.90	5.30	5.00	7.30	4.86	4.97	3.58	3.17	4.61	4.05	7.41	7.12	4.15	5.48	1.88	3.85	1.72	1.96	3.36	5.83
		2	4.88	5.17	4.90	7.22	4.90	4.75	3.53	3.29	4.45	4.04	7.37	7.12	3.95	5.39	1.84	3.86	1.65	1.95	3.35	5.89
	18	1	4.88	5.17	4.91	7.22	4.86	4.74	3.53	3.29	4.45	4.04	7.38	7.12	4.02	5.40	1.81	3.86	1.65	1.95	3.35	5.88
		2	4.90	5.30	5.00	7.31	4.88	5.00	3.58	3.17	4.61	4.05	7.42	7.12	4.11	5.49	1.89	3.83	1.72	1.96	3.36	5.82
	19	1	4.91	5.24	4.95	7.40	5.00	4.87	3.55	3.45	4.41	4.14	7.39	7.07	4.15	5.60	1.92	3.88	1.71	1.96	3.37	5.95
		2	4.97	5.40	5.02	7.54	4.91	4.96	3.80	3.24	4.53	4.20	7.51	7.17	4.18	5.63	1.92	3.99	1.77	2.06	3.44	6.03
3rd Floor	20	1	6.29	7.08	6.50	8.95	4.89	6.67	5.75	4.58	5.73	5.51	10.00	10.10	5.17	8.75	1.99	4.85	1.72	3.55	4.35	6.20
Beams		2	6.30	6.84	6.67	8.69	4.87	6.81	5.50	4.56	5.78	5.53	9.93	10.13	4.99	8.74	2.14	4.73	1.64	3.54	4.35	6.29
	21	1	6.22	6.91	6.52	8.76	4.92	6.73	5.55	4.43	5.72	5.50	10.03	10.02	5.07	8.72	2.11	4.72	1.64	3.58	4.28	6.21
		2	6.22	6.85	6.65	8.39	4.69	6.63	5.59	4.47	5.77	5.51	9.83	10.12	4.93	8.74	2.05	4.78	1.64	3.46	4.28	6.19
	22	1	6.22	6.86	6.65	8.40	4.69	6.63	5.59	4.47	5.78	5.51	9.83	10.11	4.93	8.74	2.05	4.78	1.64	3.47	4.27	6.18
		2	6.22	6.92	6.53	8.76	4.92	6.74	5.58	4.43	5.72	5.50	10.04	10.01	5.07	8.72	2.10	4.72	1.65	3.59	4.28	6.21
	23	1	6.29	6.84	6.68	8.75	4.86	6.81	5.54	4.57	5.79	5.54	9.93	10.12	5.00	8.75	2.13	4.73	1.69	3.55	4.27	6.23
		2	6.29	7.09	6.51	8.93	4.89	6.73	5.71	4.59	5.74	5.52	10.01	10.10	5.18	8.76	1.98	4.84	1.70	3.56	4.38	6.23
Roof	24	1	6.25	7.00	6.86	10.81	6.38	6.50	6.23	7.01	6.16	5.80	10.50	10.29	5.15	9.37	2.09	4.64	1.61	4.01	4.12	7.53
Beams		2	6.04	7.11	7.06	10.68	6.36	6.54	6.00	6.96	5.69	5.80	10.48	10.40	5.14	9.36	2.08	4.62	1.60	4.00	4.11	7.53
	25	1	6.06	6.99	7.02	10.83	6.50	6.64	6.01	7.00	5.91	5.88	10.54	10.39	5.14	9.33	2.09	4.49	1.59	4.04	4.15	7.37
		2	6.06	7.01	6.94	10.88	6.08	6.35	6.03	7.01	5.49	5.76	10.38	10.35	5.12	9.42	1.99	4.61	1.58	3.90	4.02	7.38
	26	1	6.05	7.01	6.95	10.88	6.07	6.35	6.03	7.01	5.49	5.76	10.38	10.35	5.12	9.41	2.00	4.61	1.59	3.91	4.03	7.38
		2	6.06	7.00	7.03	10.83	6.49	6.66	6.02	7.01	5.92	5.88	10.54	10.39	5.13	9.41	2.01	4.50	1.60	4.05	4.04	7.36
	27	1	6.05	7.12	7.05	10.68	6.35	6.55	6.05	6.97	5.70	5.87	10.49	10.39	5.13	9.37	2.07	4.62	1.59	4.00	4.10	7.52
		2	6.16	7.00	6.96	10.82	6.37	6.52	6.22	7.02	6.16	5.77	10.51	10.28	5.14	9.38	2.08	4.65	1.70	4.02	4.12	7.52

Table 7-10. Curvature ductility envelopes (FR-3F-24) – 0.67×MCE

Floor	Member	End	TH-1	TH-2	TH-3	TH-4	TH-5	TH-6	TH-7	TH-8	TH-9	TH-10	TH-11	TH-12	TH-13	TH-14	TH-15	TH-16	TH-17	TH-18	TH-19	TH-20
Base	1	1	5.46	5.26	2.71	5.27	5.10	6.01	2.63	2.45	6.82	5.60	7.93	8.80	2.79	6.84	---	2.45	---	---	---	4.29
	4	1	5.43	5.32	2.80	5.37	5.13	6.01	2.74	2.53	6.80	5.55	7.81	8.66	2.84	6.71	---	2.56	1.08	---	1.04	4.35
	5	1	---	---	---	1.38	---	---	---	---	---	---	1.26	1.21	---	---	---	---	---	---	---	---
	7	1	5.43	5.31	2.80	5.38	5.13	6.01	2.74	2.44	6.82	5.55	7.81	8.66	2.84	6.71	---	2.55	1.08	---	1.04	4.35
	8	1	---	---	---	1.39	---	---	---	---	---	---	1.27	1.23	---	---	---	---	---	---	---	---
	10	1	5.43	5.32	2.80	5.37	5.13	6.01	2.74	2.53	6.80	5.55	7.81	8.66	2.84	6.71	---	2.56	1.08	---	1.04	4.35
	11	1	---	---	---	1.38	---	---	---	---	---	---	1.27	1.21	---	---	---	---	---	---	---	---
	13	1	5.46	5.26	2.71	5.27	5.10	6.01	2.63	2.45	6.82	5.61	7.93	8.80	2.79	6.84	---	2.45	---	---	---	4.29
2nd Floor	16	1	6.51	6.74	4.42	7.04	6.74	8.15	3.63	4.09	7.81	6.50	9.29	10.37	4.08	8.67	2.10	3.96	2.13	1.81	2.21	6.23
		2	6.40	6.75	4.71	6.48	6.32	7.77	3.47	3.95	7.53	6.31	8.66	10.21	3.98	8.45	1.98	3.72	2.00	1.71	2.09	5.95
	17	1	6.34	6.65	4.46	6.53	6.31	7.84	3.47	3.95	7.59	6.34	8.78	10.11	3.91	8.49	2.01	3.75	1.98	1.69	2.06	5.99
		2	6.34	6.65	4.47	6.53	6.47	7.84	3.47	3.97	7.46	6.33	8.80	10.11	3.91	8.48	2.00	3.75	1.98	1.69	2.06	5.99
	18	1	6.34	6.65	4.46	6.53	6.47	7.84	3.47	3.97	7.46	6.33	8.80	10.11	3.91	8.48	2.00	3.75	1.98	1.69	2.06	5.99
		2	6.34	6.65	4.47	6.53	6.31	7.84	3.47	3.94	7.59	6.34	8.78	10.11	3.91	8.49	2.01	3.75	1.98	1.69	2.06	5.99
	19	1	6.33	6.76	4.66	6.49	6.34	7.79	3.46	3.95	7.48	6.35	8.67	10.20	3.90	8.50	1.97	3.75	1.97	1.71	2.09	5.95
		2	6.54	6.75	4.45	7.05	6.64	8.15	3.69	4.07	7.90	6.49	9.29	10.36	4.12	8.65	2.14	3.90	2.14	1.83	2.18	6.22
3rd Floor	20	1	4.95	6.95	3.76	7.09	6.21	6.36	3.65	4.63	5.37	4.36	7.10	9.27	3.93	7.37	1.74	3.32	1.23	1.80	2.10	5.27
		2	4.80	6.69	4.16	7.17	5.88	6.52	3.70	4.59	4.93	4.18	6.77	8.99	3.96	7.23	1.70	3.37	1.14	1.71	2.08	5.39
	21	1	4.83	6.71	4.03	7.16	6.08	6.41	3.70	4.57	5.18	4.26	6.80	9.03	3.95	7.26	1.70	3.36	1.13	1.73	2.07	5.33
		2	4.83	6.83	4.02	7.15	5.96	6.41	3.70	4.58	5.18	4.26	6.98	9.07	3.95	7.27	1.70	3.36	1.14	1.73	2.07	5.34
	22	1	4.83	6.83	4.02	7.15	5.96	6.41	3.70	4.58	5.18	4.26	6.98	9.07	3.95	7.27	1.70	3.35	1.14	1.73	2.07	5.34
		2	4.82	6.71	4.03	7.16	6.08	6.41	3.70	4.57	5.18	4.26	6.79	9.03	3.95	7.27	1.71	3.36	1.14	1.73	2.07	5.33
	23	1	4.79	6.70	4.17	7.23	5.87	6.54	3.75	4.62	4.94	4.33	6.88	8.98	3.94	7.25	1.70	3.32	1.11	1.72	2.07	5.37
		2	4.94	6.96	3.77	7.08	6.19	6.38	3.64	4.66	5.38	4.30	7.05	9.25	3.92	7.38	1.80	3.33	1.21	1.84	2.08	5.25
Roof	24	1	2.56	4.97	1.62	6.75	4.97	3.44	2.44	3.01	2.36	1.98	4.74	6.93	2.45	4.87	---	1.70	---	---	---	4.38
		2	2.28	4.66	1.16	6.40	4.68	3.19	2.22	2.73	2.10	1.76	4.34	6.69	2.11	4.52	---	1.38	---	---	---	4.12
	25	1	2.28	4.68	1.25	6.42	4.68	3.19	2.22	2.75	2.15	1.76	4.51	6.69	2.12	4.55	---	1.39	---	---	---	4.05
		2	2.28	4.69	1.26	6.43	4.68	3.20	2.22	2.75	2.15	1.76	4.50	6.69	2.12	4.55	---	1.39	---	---	---	4.07
	26	1	2.28	4.68	1.26	6.43	4.68	3.19	2.22	2.75	2.06	1.76	4.50	6.69	2.12	4.55	---	1.39	---	---	---	4.07
		2	2.28	4.68	1.25	6.43	4.67	3.20	2.21	2.75	2.17	1.76	4.51	6.68	2.12	4.55	---	1.38	---	---	---	4.05
	27	1	2.23	4.68	1.17	6.41	4.61	3.20	2.20	2.75	2.18	1.81	4.44	6.67	2.11	4.52	---	1.42	---	---	---	4.10
		2	2.57	5.00	1.67	6.77	4.99	3.47	2.55	3.05	2.33	1.96	4.71	6.91	2.37	4.94	---	1.59	---	---	---	4.34

Table 7-11. Curvature ductility envelopes (FR-3F-30) – 0.67×MCE

Floor	Member	End	TH-1	TH-2	TH-3	TH-4	TH-5	TH-6	TH-7	TH-8	TH-9	TH-10	TH-11	TH-12	TH-13	TH-14	TH-15	TH-16	TH-17	TH-18	TH-19	TH-20
Columns	1	1	2.22	5.51	2.35	2.05	5.83	2.51	1.80	3.27	2.63	2.48	2.21	5.18	1.96	8.13	1.47	2.57	---	---	---	1.74
	2	2	---	1.56	---	---	2.40	---	---	---	---	---	---	1.65	---	4.74	---	---	---	---	---	---
	4	1	2.31	5.43	2.44	2.17	5.60	2.57	1.88	3.29	2.84	2.57	2.31	5.07	2.03	7.93	1.59	2.64	---	---	1.11	1.82
	5	2	---	1.65	---	---	2.45	---	---	---	---	---	---	1.69	---	4.64	---	---	---	---	---	---
	7	1	2.33	5.47	2.44	2.17	5.64	2.61	1.92	3.31	2.74	2.59	2.37	5.11	2.08	7.98	1.60	2.64	---	---	1.13	1.86
	8	2	---	1.82	---	---	2.64	---	---	---	---	---	---	1.91	---	4.86	---	---	---	---	---	---
	10	1	2.31	5.43	2.44	2.17	5.60	2.57	1.88	3.29	2.84	2.57	2.31	5.07	2.03	7.93	1.59	2.64	---	---	1.11	1.82
	11	2	---	1.65	---	---	2.45	---	---	---	---	---	---	1.69	---	4.64	---	---	---	---	---	---
	13	1	2.25	5.55	2.35	2.05	5.67	2.53	1.80	3.33	2.66	2.48	2.21	5.11	1.96	8.16	1.47	2.57	---	---	---	1.73
	14	2	---	1.56	---	---	2.33	---	---	---	---	---	---	1.64	---	4.74	---	---	---	---	---	---
2nd Floor	16	1	2.70	6.19	2.60	2.37	6.74	3.14	2.69	3.72	2.46	2.74	2.32	5.27	2.26	8.75	2.23	3.01	---	1.46	1.60	3.04
Beams		2	2.77	6.13	2.65	2.25	6.78	3.16	2.81	3.80	2.94	2.81	2.19	5.37	2.26	8.73	2.26	3.25	---	1.52	1.65	3.14
	17	1	2.75	6.10	2.70	2.40	6.72	3.17	2.71	3.86	2.59	2.82	2.27	5.37	2.35	8.75	2.41	3.09	---	1.54	1.66	3.09
		2	2.72	6.16	2.61	2.30	6.76	3.13	2.80	3.69	2.72	2.74	2.24	5.22	2.22	8.69	2.14	3.21	---	1.51	1.62	3.10
	18	1	2.72	6.16	2.61	2.30	6.78	3.16	2.81	3.67	2.72	2.74	2.22	5.22	2.21	8.69	2.14	3.21	---	1.50	1.66	3.10
		2	2.76	6.10	2.70	2.39	6.69	3.15	2.71	3.89	2.59	2.82	2.33	5.37	2.35	8.75	2.41	3.09	---	1.56	1.64	3.09
	19	1	2.77	6.13	2.65	2.25	6.75	3.16	2.81	3.80	2.95	2.81	2.18	5.37	2.26	8.73	2.26	3.25	---	1.53	1.65	3.14
		2	2.69	6.19	2.60	2.37	6.79	3.14	2.69	3.71	2.45	2.74	2.33	5.29	2.26	8.75	2.23	3.01	---	1.45	1.61	3.03
3rd Floor	20	1	1.61	3.61	1.38	1.27	3.90	1.56	2.14	2.54	1.94	1.38	1.00	2.57	1.26	3.35	1.31	2.21	---	---	1.01	2.61
Beams		2	1.72	3.54	1.42	1.36	3.89	1.65	2.17	2.75	1.93	1.48	1.05	2.60	1.29	3.47	1.40	2.24	---	---	1.01	2.78
	21	1	1.72	3.63	1.47	1.36	3.98	1.66	2.26	2.66	1.98	1.48	1.00	2.60	1.34	3.45	1.40	2.27	---	---	---	2.75
		2	1.71	3.54	1.45	1.35	3.85	1.65	2.17	2.72	2.04	1.47	1.05	2.53	1.33	3.37	1.41	2.30	---	---	---	2.75
	22	1	1.71	3.57	1.45	1.35	3.84	1.65	2.17	2.72	2.04	1.48	---	2.53	1.33	3.37	1.38	2.30	---	---	---	2.75
		2	1.72	3.61	1.47	1.36	3.98	1.66	2.26	2.66	1.97	1.49	---	2.60	1.34	3.45	1.42	2.27	---	---	---	2.75
	23	1	1.73	3.54	1.42	1.36	3.89	1.66	2.17	2.75	1.92	1.49	---	2.60	1.29	3.47	1.39	2.23	---	---	---	2.78
		2	1.61	3.61	1.38	1.27	3.90	1.56	2.14	2.55	1.94	1.38	---	2.57	1.26	3.35	1.30	2.23	---	---	---	2.61
Roof	24	1	---	---	---	---	---	---	---	---	---	---	---	---	---	---	---	---	---	---	---	---
Beams		2	---	---	---	---	---	---	---	---	---	---	---	---	---	---	---	---	---	---	---	---
	25	1	---	---	---	---	---	---	---	---	---	---	---	---	---	---	---	---	---	---	---	---
		2	---	---	---	---	---	---	---	---	---	---	---	---	---	---	---	---	---	---	---	---
	26	1	---	---	---	---	---	---	---	---	---	---	---	---	---	---	---	---	---	---	---	---
		2	---	---	---	---	---	---	---	---	---	---	---	---	---	---	---	---	---	---	---	---
	27	1	---	---	---	---	---	---	---	---	---	---	---	---	---	---	---	---	---	---	---	---
		2	---	---	---	---	---	---	---	---	---	---	---	---	---	---	---	---	---	---	---	---

Nearly all hinges for the three frames are below the allowable. It can be reasoned that FR-3F-18 and FR-3F-24 utilize more of the ductility capacity than FR-3F-30. This is associated with the optimum selection of beam depth that in return do not generate excessive flexural overstrength and stiffness. However, ground motion characteristics of the near-fault records do not provide the frames the ability to efficiently utilize the innate ductility capacity. In general, this is associated with lack of formation of a 1st mode-based yield mechanism. Also, near-fault motions affect the effectiveness of damping. Therefore, it is recommended that either a revised damping modification factor, κ, be derived or new DRS reduction factors (see Eq. 2-25) be computed for near-fault earthquakes.

7.2.3.3 Story Shear Envelopes

Fig. 7-11 plots the story shear envelopes at the design-level earthquake. The figures are separated into far-field and near-fault. Each figure illustrates the mean for

comparison against the capacity designed values (‘Protected’) and the numerical ratio of mean to ‘Design’ and mean to ‘Protected’ is provided.

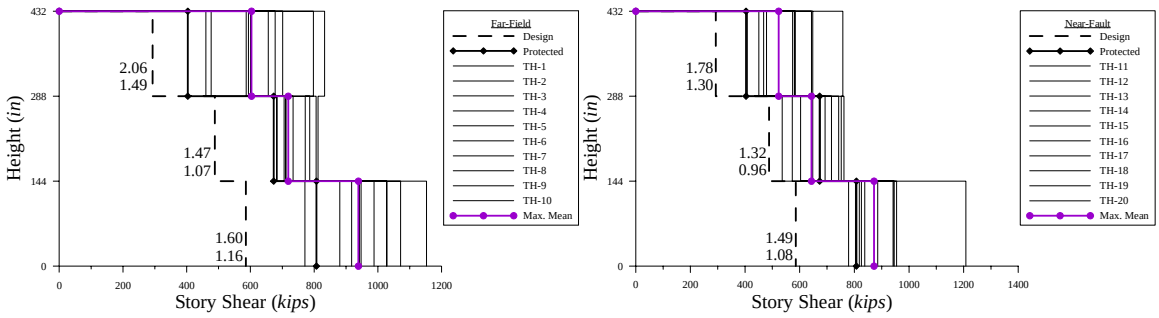

(a) FR-3F-18

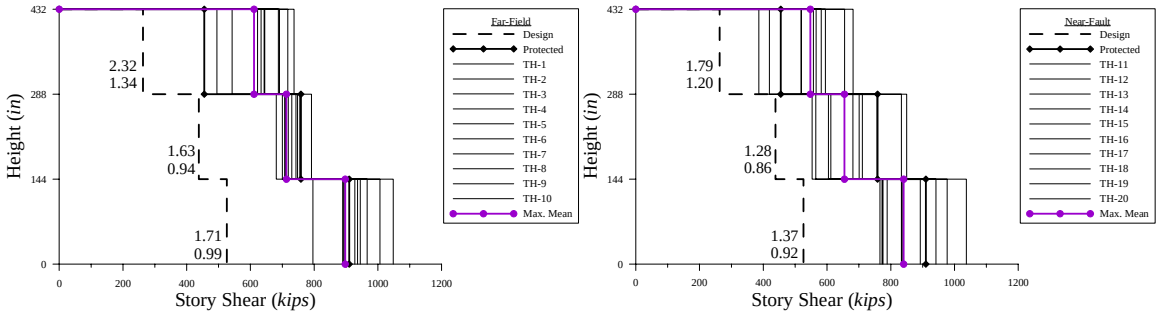

(b) FR-3F-24

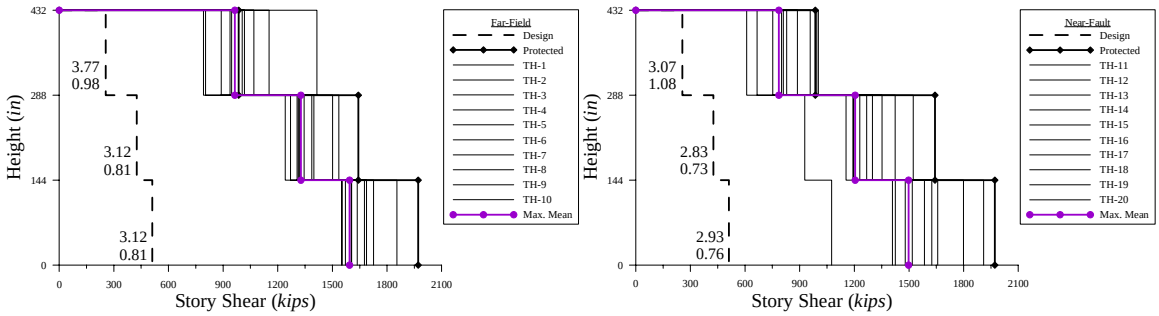

(c) FR-3F-30

Figure 7-11. Story shear envelopes

As evident in the figure, member overstrengths and higher modes play a significant role in the amplification of story shears beyond the ‘Design’ values. Good agreement exists between the mean and ‘protected’ values. One could postulate increasing the design lateral forces in the upper floors to reduce the ratio; however, this

effect is primarily due to high flexural overstrengths in the top floor and acceptable construction practices (using the same column for multiple floors). It is also evident that overstrength is dependent on design choices and assuming a generalized value as specified in seismic codes can lead to further stiffening of the frame.

In comparison with Tables 7-9 to 7-11, it is evident that the proposed capacity design procedure adequately protects non-ductile members from the increase in story shears due to flexural overstrength and contributions of higher modes. While a few columns develop plastic hinges, they do not destabilize the frame enough to develop a soft story. However, some earthquakes do illustrate unsatisfactory performance (see TH-4, 11, 12, and 14). It is plausible that the performance overstrength values listed in Table 6-5 could be increased for near-fault earthquakes.

7.2.3.4 Story Drift Envelopes

Though the displacement envelopes and displacement profiles at each nodal maximum are nearly identical for these frames, satisfactory response is evaluated by investigating the time-dependent story drift ratio envelopes. Fig. 7-12 illustrates the story drift envelopes at the design-level earthquake. The figures are categorized as far-field and near-fault. The mean of the story drift ratios is shown in each figure for comparison against the ‘Design’ value and the ratio of mean to ‘Design’ is provided.

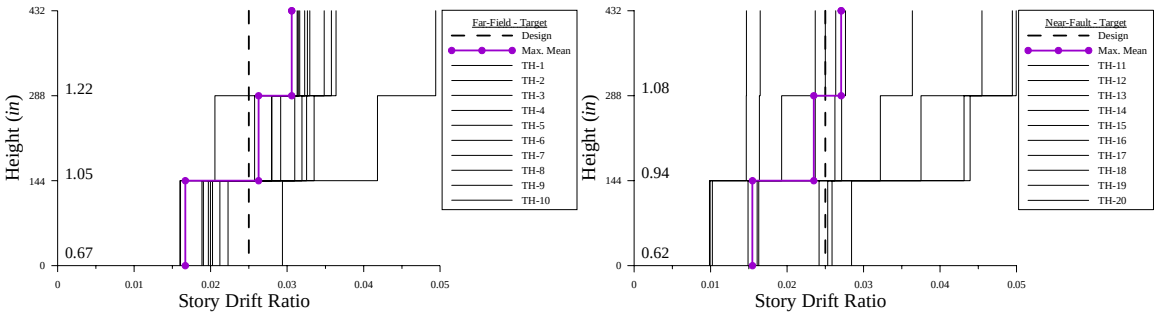

(a) FR-3F-18

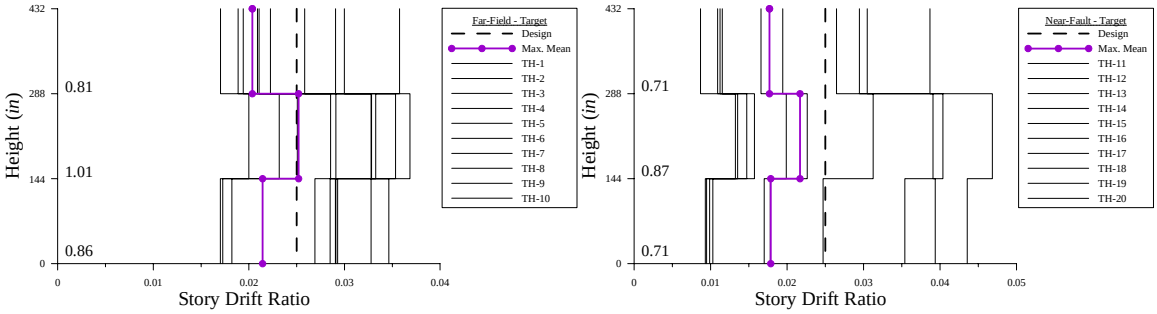

(b) FR-3F-24

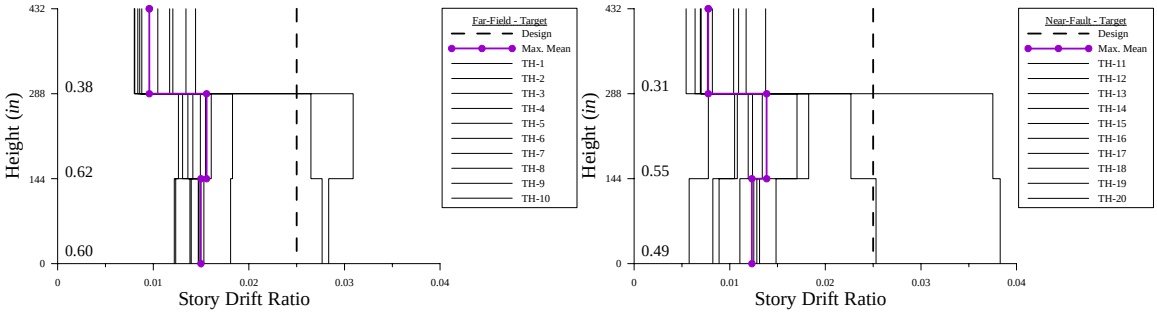

(c) FR-3F-30

Figure 7-12. Drift ratio envelopes (Target - 0.67×MCE)

As seen in Fig. 7-12(a), cantilever action dominates the response of FR-3F-18. This effect is primarily due to base hinges not forming concurrently with beam hinges. Base hinges do not form because column strengths were increased for protection against higher modes, which have a significant effect on this frame due to a sharp decrease in system stiffness upon formation of the global yield mechanism. This frame performs unsatisfactory in accomplishing the performance objective, albeit a corollary of design selections.

In contrast, FR-3F-24 responds in a mixed fashion with a combined frame–wall behavior. From Fig. 7-12(b), it is clear that the maximum drift ratio occurs in the 2nd floor which was indicated in Fig. 7-3(b). Although column base hinges do not form concurrently with the beam hinges in this frame, column stiffness and strength are reduced from FR-3F-18 due to an apparent reduction in higher mode contributions. As a result, base hinges form at a lower demand and the frame utilizes more of the available ductility capacity responding in a more linear fashion. This frame performs satisfactorily in meeting the performance objective. Therefore, it is recommended that the selection of nominal column depths be bounded by $0.55d_b \le d_c \le 0.75d_b$.

As indicated previously, FR-3F-30 is stiffer and stronger than that required to meet the performance objective. This is directly associated with the excessive flexural overstrengths created using deep beams. As a corollary, high elastic stiffness requirements are placed on the columns, leading to a reduction in higher mode contributions. This frame does not perform satisfactorily (in the opposite sense) in meeting the performance objective.

Lastly, Fig. 7-13 presents the story drift ratios at the yield-level earthquake. With the exception of FR-3F-30, frame response indicates that the proposed procedure provides an acceptable value for the drift angle at yield. FR-3F-18 indicates strong cantilever response at the assumed global yield mechanism resulting in formation of the first sequence of hinges to occur in the upper floor beams. Both FR-3F-24 and FR-3F-30 indicate a more linear response with the maximum drift ratio occurring at the location demonstrated by the floor flexural overstrength values.

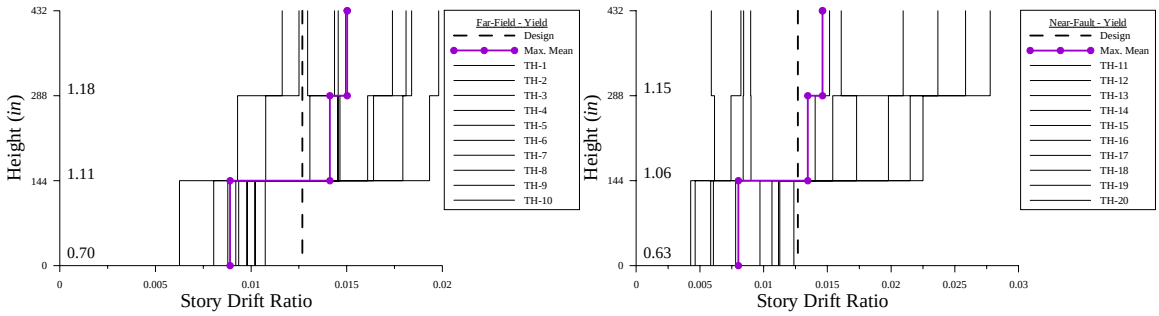

(a) FR-3F-18

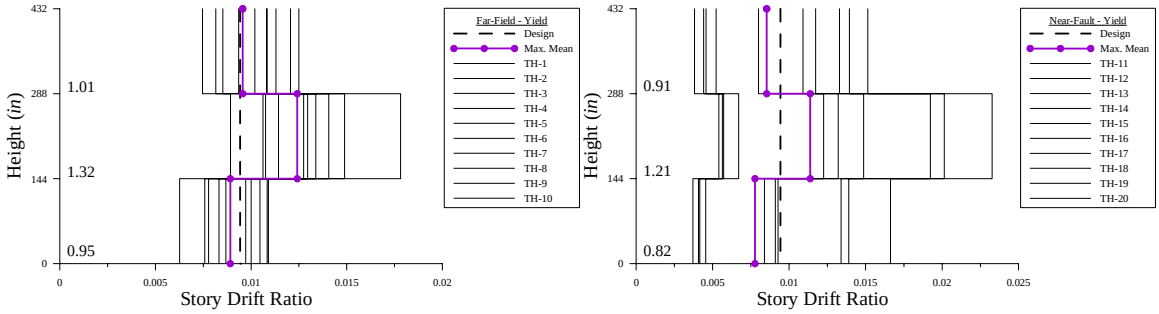

(b) FR-3F-24

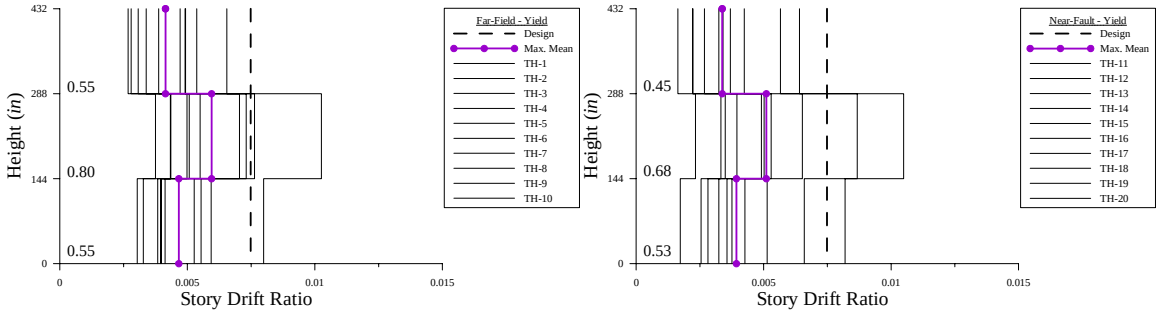

(c) FR-3F-30

Figure 7-13. Drift ratio envelopes (Target - ℜ ×MCE)

7.2.3.5 Effective Height

The dynamic pushover curves (base shear and base overturning moment) indicate higher mode contributions in FR-3F-18 and FR-3F-24. As a means to evaluate the extent of higher mode contributions, the actual effective height of the frame is compared to the design value. The actual effective height is computed as the time-dependent ratio of base overturning moment to base shear at each response maximum. Fig. 7-14 plots the

effective heights for the four levels of earthquake intensity at: (1) each maximum nodal displacement (three floors) and (2) each maximum story shear (three floors) – 60 points for each intensity.

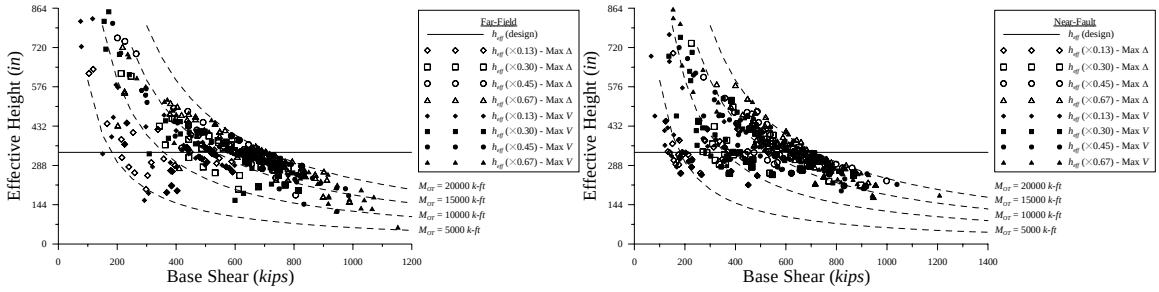

(a) FR-3F-18

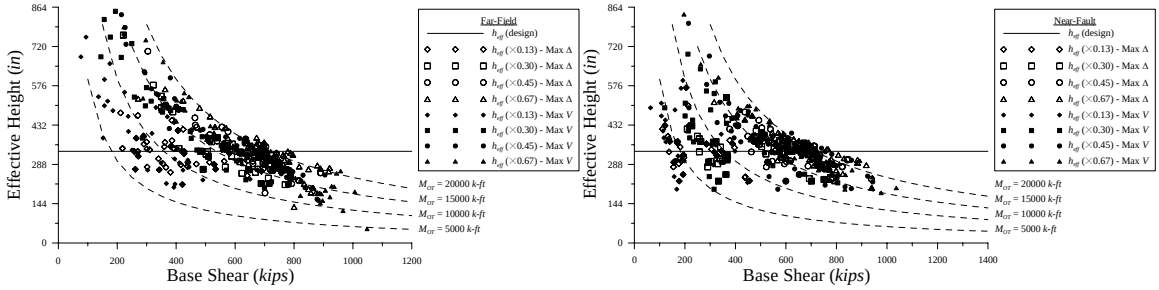

(b) FR-3F-24

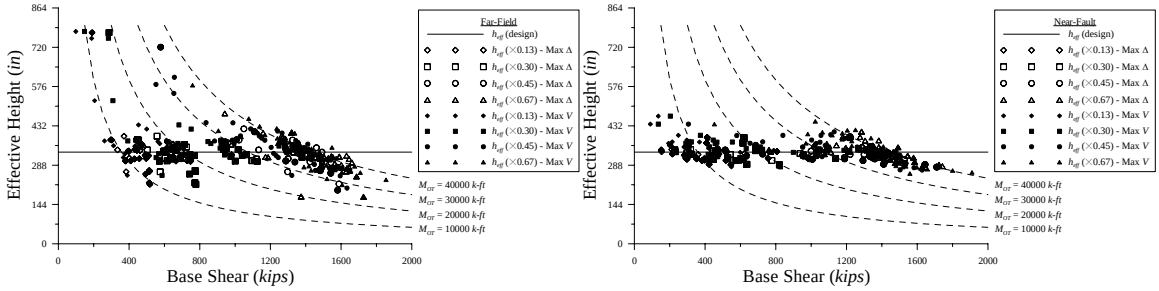

(c) FR-3F-30

Figure 7-14. Effective Height (0.13, ℜ , 0.45, 0.67 × MCE)

As seen in Fig. 7-14, a broad spectrum of effective heights is evident. First, effective height increases when the base shear drops below any story shear. In contrast, effective height decreases when any story shear acts in opposing direction of the base shear. This effect is graphically illustrated in Fig. 7-15. Also, the actual 1st mode-based

effective height can deviate from the design value due to variation between mode shape and target displacement profile (see Fig. 7-4). This variation is typically within +5% for cantilever and –5% for parabolic.

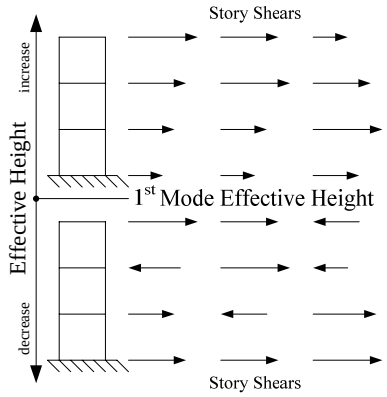

Figure 7-15. Effective height variation

In general, it can be seen in Fig. 7-14 that higher mode contributions have more effect on forces than displacements. FR-3F-18 indicates a larger contribution of higher modes to maximum nodal displacements than does FR-3F-24. This further suggests that beam-column depth ratios should be limited as recommended in order to produce a frame where higher modes have less impact on lateral displacements. The standard deviations of these frames are approximately 28% (FR-3F-18) and 23% (FR-3F-24) of the design effective height for displacements and 43% and 45% for story shears respectively. As a result, the damping modification factor, κ, is increased to 0.6 in an attempt to capture the increase in damping due to higher modes. Lastly, FR-3F-30 does not indicate a similar trend and maintains the effective height (19% and 29% standard deviation respectively). Ultimately, this comparison indicates that the linear profile shape is reasonable and that

higher mode protection to non-ductile members should be included during capacity design.

7.2.3.6 Serviceability

As discussed in Chapter 3, a two-level limit state DDBD procedure is proposed: (1) displacement limit states and (2) serviceability limit state. The minimum service-level earthquake is computed as 0.133×MCE and is associated with an allowable drift angle of 0.005 *radians*. Figs. 7-16, 7-17, and 7-18 present the displacement and drift angle envelopes at the service-level earthquake.

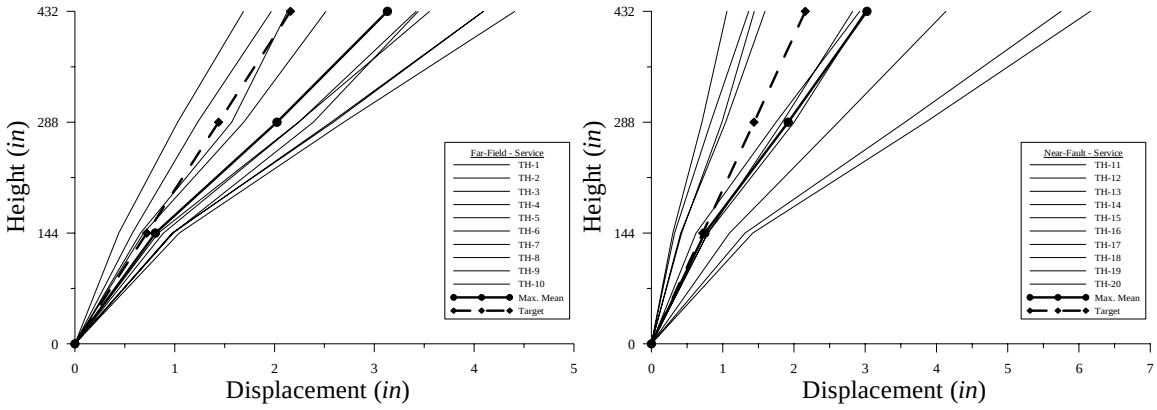

(a) Displacement envelopes

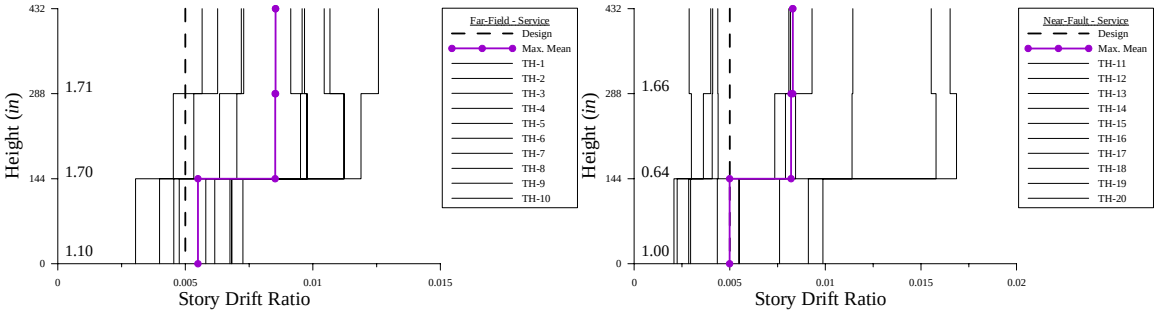

(b) Story drift ratio

Figure 7-16. Serviceability (FR-3F-18)

FR-3F-18 is strongly influenced by cantilever action due to stiffness distributions based on design selections. Assuming the service-level earthquake intensity to be acceptable, this frame does not perform satisfactorily in meeting the adopted 0.5% drift limit.

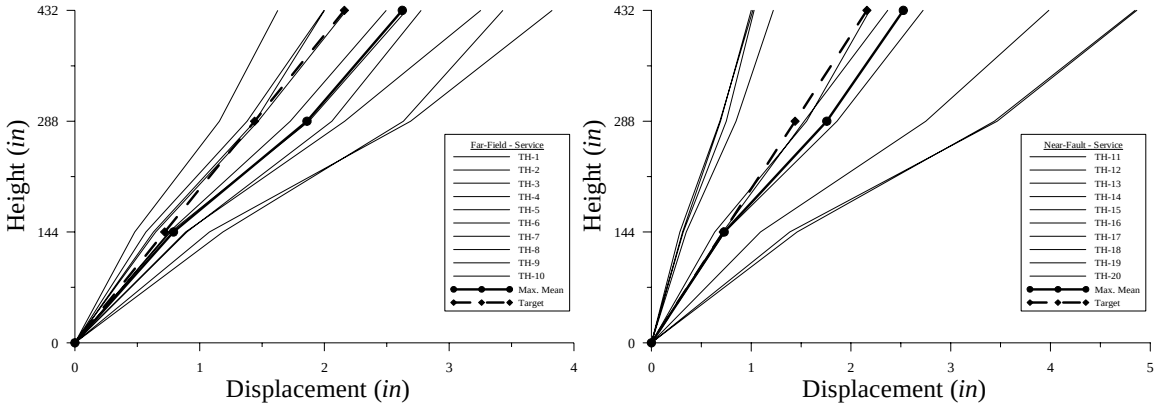

(a) Displacement envelopes

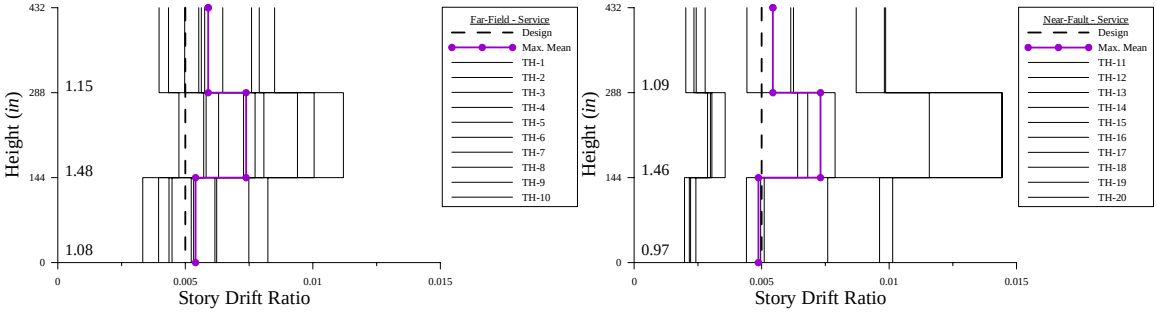

(b) Story drift ratio

Figure 7-17. Serviceability (FR-3F-24)

FR-3F-24 shows similar response as FR-3F-18 with a more linear response. One could postulate increasing the stiffness of the upper floors to reduce the drift ratios; however, this would most likely influence a stronger trend towards cantilever action since higher mode contributions to displacements are relatively low. This implies that construction practices (e.g., single column size for three floors) play a role in stiffness distribution. Thus, it is suggested that the performance overstrength factor be calibrated

also to provide a reliable stiffness to assist in decreasing the drift ratio at the service-level limit state. Additionally, it is plausible that the 0.5% drift limit could be relaxed, say 0.75%, since second-order effects are explicitly accounted. This relaxation would then indicate satisfactory performance for both FR-3F-18 and FR-3F-24 since the frames do not develop plastic hinges until approximately a 1% drift.

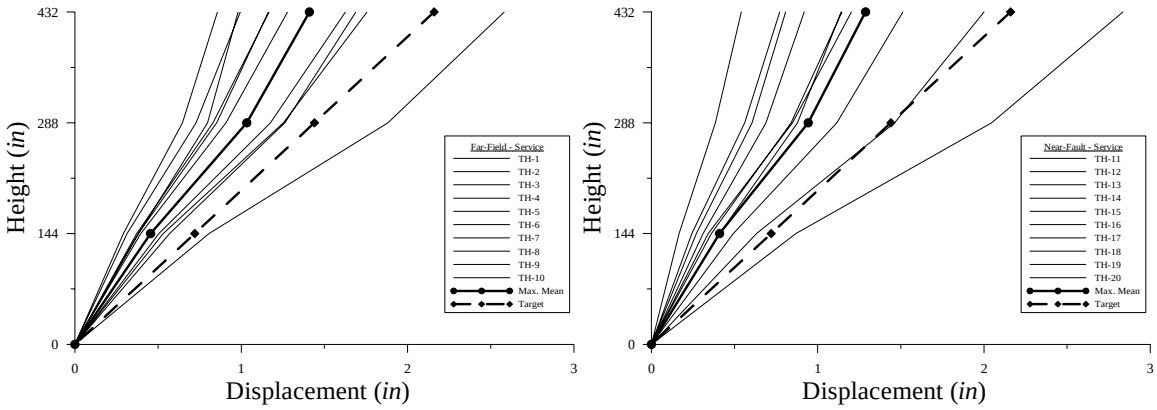

(a) Displacement envelopes

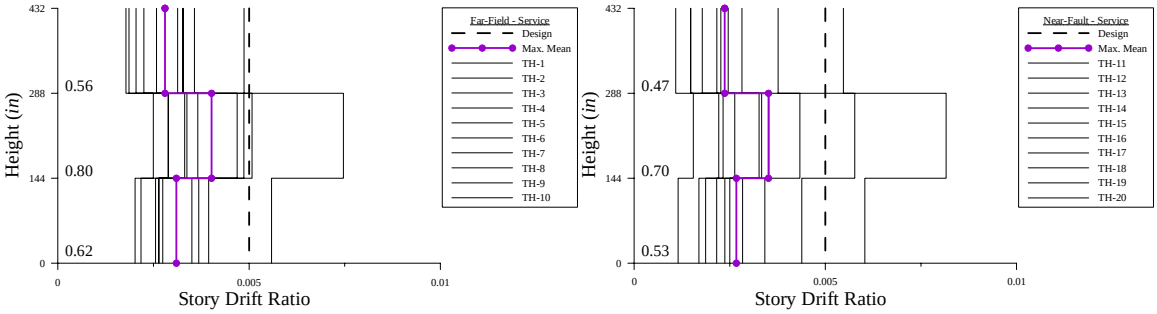

(b) Story drift ratio

Figure 7-18. Serviceability (FR-3F-30)

FR-3F-30 satisfies the drift limit due to an excessive level of strength and stiffness. As a result, this frame is not efficiently designed to achieve a performance target.

7.2.3.7 Effective SDOF Displacement Comparison

Fig. 7-19 plots the ratios of actual displacement at the effective height to (1) design displacement of the effective SDOF and (2) displacement from DRS at the equivalent period and damping. Upwards of 50% deviation is seen for actual-design displacement ratios. Larger deviations are seen with the DRS ordinate. The latter variation is primarily due to the period shift created by overstrength and capacity design and higher mode contributions, as well as their affects on ductility and damping. This variation corresponds to what is typically expected in earthquake engineering research.

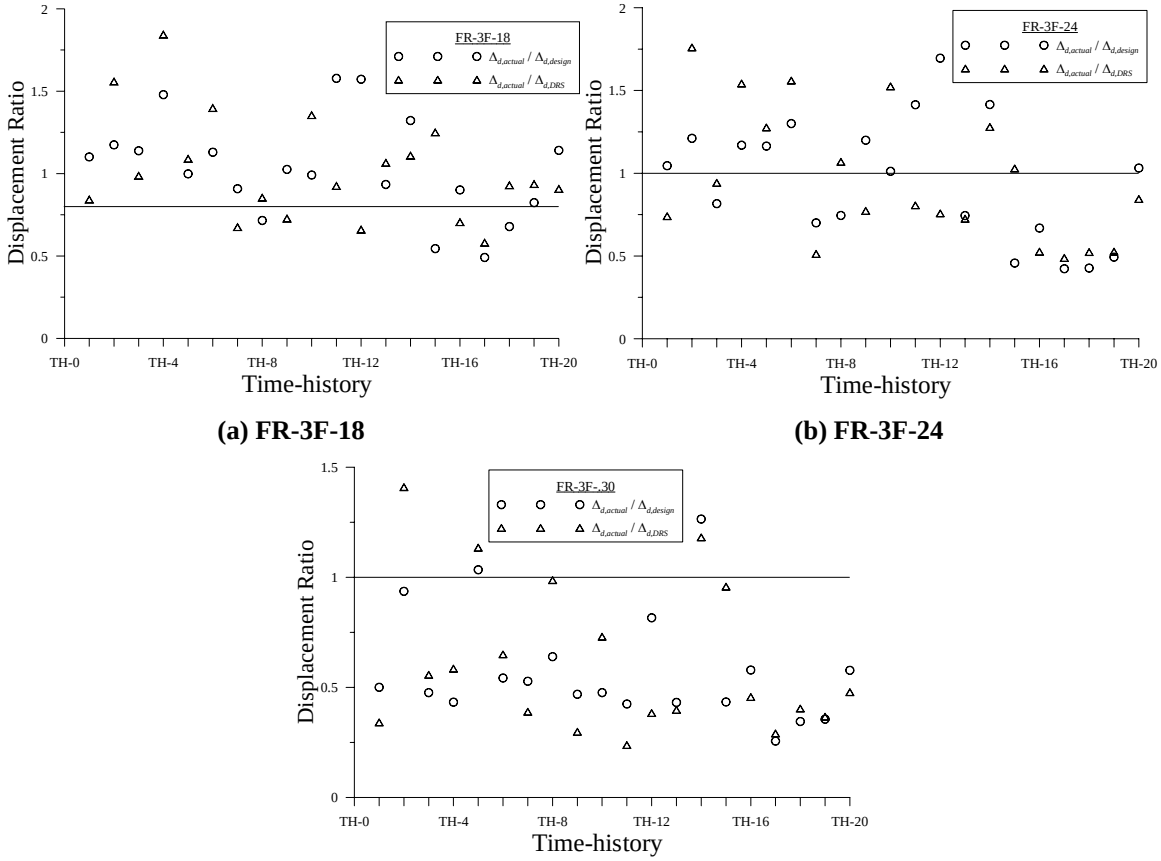

(a) FR-3F-18 **(b) FR-3F-24**

(c) FR-3F-30

Figure 7-19. Displacement ratio

7.2.3.8 Force-Based Design Parameters

Examination of the design parameters established by FBD indicates that stiffness and strength are treated independently and a frame thus designed could be stiffer and stronger than required to meet the performance objective. For comparison purposes, the strength-level fundamental period for FR-3F is

$$T_1 = C_u T_a = 1.4(0.028(36^{0.8})) = 0.69\ sec \begin{cases} \text{FR-3F-18 } T_1 = 1.38\ sec \rightarrow \overbrace{0.50}^{ratio} \\ \text{FR-3F-24 } T_1 = 1.26\ sec \rightarrow 0.55 \\ \text{FR-3F-30 } T_1 = 1.14\ sec \rightarrow 0.60 \end{cases}$$

The corresponding strength-level design base shear at first significant yield is

$$V_{by'} = \frac{S_{D1}}{T_1\left(R/I\right)} W_t = \frac{0.66}{0.69(8)} W_t = 0.12 W_t = 360\ kips \begin{cases} \text{FR-3F-18 } V_{by} = 586\ kips \rightarrow \overbrace{0.61}^{ratio} \\ \text{FR-3F-24 } V_{by} = 526\ kips \rightarrow 0.68 \\ \text{FR-3F-30 } V_{by} = 511\ kips \rightarrow 0.70 \end{cases}$$

This yields a design lateral force distribution (k = 1.095) and magnitude of

$$\{\phi_f\} = \begin{Bmatrix} 0.51 \\ 0.33 \\ 0.16 \end{Bmatrix} = \begin{Bmatrix} 1.00 \\ 0.64 \\ 0.30 \end{Bmatrix} \overbrace{\begin{Bmatrix} 1.00 \\ 0.63 \\ 0.24 \end{Bmatrix}}^{\text{FR-3F-18}} \overbrace{\begin{Bmatrix} 1.00 \\ 0.71 \\ 0.29 \end{Bmatrix}}^{\text{FR-3F-24}} \overbrace{\begin{Bmatrix} 1.00 \\ 0.73 \\ 0.32 \end{Bmatrix}}^{\text{FR-3F-30}} \text{ and } \{F_x\} = \begin{Bmatrix} 185 \\ 118 \\ 55 \end{Bmatrix} kips$$

As evident, the base shear and corresponding design forces are smaller than those used in the previous DDBD example, albeit independent of frame and member geometry. However, the force distribution agrees well with the fundamental mode shapes.

In this scenario, the design engineer would design the frame to resist the strength-level lateral forces and subsequently compute displacement-level lateral forces from the *actual* period, if desired. It follows that the displacement profile due to the displacement-level lateral forces and expected inelastic displacements should be limited to

$$\{\delta_{ex}\} = \begin{Bmatrix} 1.83 \\ 1.17 \\ 0.55 \end{Bmatrix} in. \ (\theta_{ex} = 0.46\%) \text{ and } \{\delta_{in}\} = \begin{Bmatrix} 10.04 \\ 6.44 \\ 3.02 \end{Bmatrix} in. \ (\theta_{in} = 2.5\%)$$

Iteration would terminate when the frame satisfies both the lateral forces and elastic displacement limits under the respective lateral forces.

The limitation here is that there is no direct ratio between $\{\delta_{ex}\}$ and $\{\delta_{y'}\}$ developed under the strength-level lateral forces and between $V_{by'}$ and $V_{by'}$ after the frame is designed to satisfy $\{\delta_{ex}\}$. This indicates that strength and stiffness are treated separately in FBD and requires multiple analysis-design iterations.

For comparison purposes, assume strength-level and displacement-level lateral forces are concurrent and all beams are designed to yield at $V_{by'}$. The beam depth would need to be 52 *inches* for a beam to yield at a drift ratio of 0.4% (assuming column deformations contribute 15%).

$$d_b \approx \frac{2S_F\varepsilon_y}{0.004}\frac{L}{6} \approx 52 \, in.$$

The deepest stock W-section available is W44. Accordingly, the drift ratio at yield is 0.55%. This implies that the columns would need to be stiffened considerably in order to

satisfy the 0.46% limit. As shown previously by FR-3F-30, stiff frames with excessive flexural overstrengths have difficulty meeting the 2.5% drift ratio target.

Conversely, a frame could be constructed with more efficient beam depths after several iterations evaluating the noted ratios. Assuming the base shear ratio of strength to displacement, R_{SD}, is 2 (beams yield at $V_{by'}$), the beam depth would need to be 26 *inches*.

$$d_b \approx \frac{2S_F\varepsilon_y}{0.004R_{SD}}\frac{L}{6} \approx 26$$

Thus, a frame designed with W27 beams would provide a drift ratio at $V_{by'}$ of 0.89%. This value is much closer to the values determined by the proposed procedure. However, the design engineer would need to perform several independent analyzes to determine that $R_{SD} = 2$. If R is taken equal to μ_Δ and $\mu_\theta \approx \mu_\Delta$, the expected maximum drift ratio is 7.12% whereas 0.46%×C_d yields 2.5%. This discrepancy is related to strength and stiffness being treated independently and, as a result, seismic codes provide varying prescriptive constraints for design. This example does not include the effects of flexural overstrength on frame strength and stiffness which would typically change the previous values. In the end, the proposed procedure is more rational since the proportionality between strength and stiffness is explicitly used in analysis and design. As a side note, inputting FR-3F-18 frame properties and assuming 85% of the design spectra allocated to the 1st mode results in a base shear nearly that computed in the previous DDBD example.

$$V_{by'} = \frac{0.85S_{D1}}{T_1\left(R/I\right)}W_{eff} = \frac{0.85(0.66)}{1.23(1.97)}2572 = 595\ kips$$

7.3 Six-story Frame Design Example (FR-6F)

7.3.1 Frame Model and Design

Two six-story frames are designed using the proposed DDBD methodology: (1) FR-6F-27 (W27 beams) and (2) FR-6F-33 (W33 beams). The frame model is shown in Fig. 7-20. Beam depths are varied in adjacent bays in accordance with Fig. 3-11 as well as steadily decreased heightwise every two floors. W14 and W24 are chosen for the columns for FR-6F-27 and FR-6F-33 respectively such that $2d_c \geq d_b$ is satisfied. Column splices occur on the 4th floor. The seismic floor weights are each set at 1500 *kips* – 25% respectively distributed as point loads to the frame columns and 75% to the *P*-Δ column.

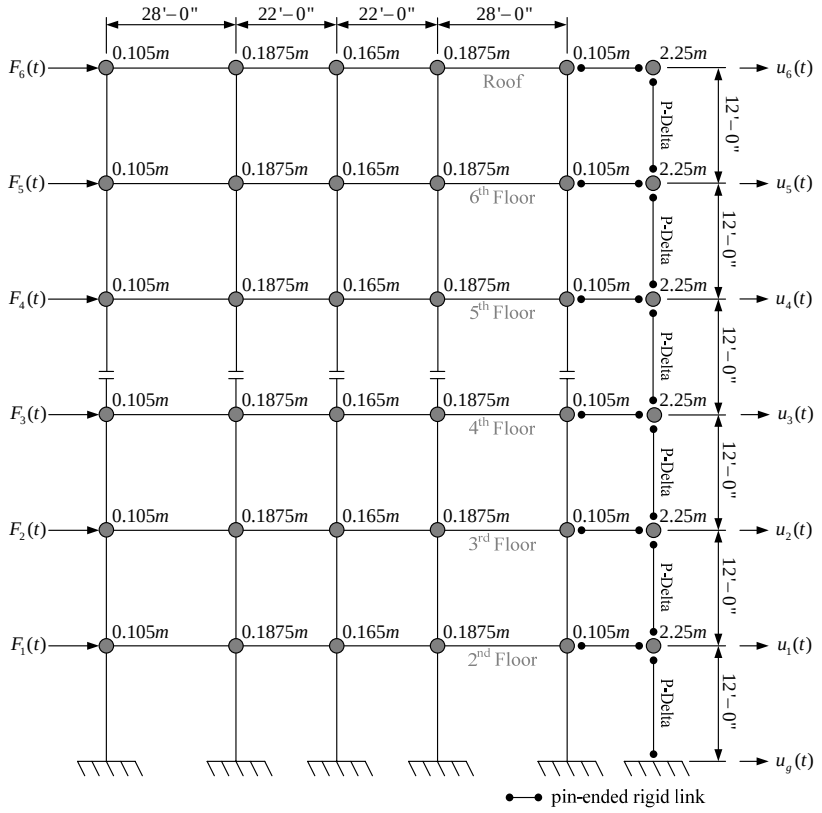

Figure 7-20. Frame schematic (six-story)

Tables 7-12, 7-13, and 7-14 present the model properties, effective SDOF properties, and yield-level design forces respectively for each frame.

Table 7-12. FR-6F model properties

Frame	DOF	h_i	$\delta_{d,i}$	d_b (Bay 1,4)	d_b (Bay 2,3)	$\theta_{by,i}$ [1]	$\theta_{by,i}$ [1]	$\lambda_{y,i}$	$\theta_{y,i}$ [2]	$\hat{\theta}_{y,i}$ [2]	$\theta_{y,sys}$	$\hat{\theta}_{y,sys}$	$\delta_{dy,i}$	$\hat{\delta}_{dy,i}$	$\mu_{\Delta,el}$	$\tilde{\delta}_{dy,i}$	$\mu_{\delta,i}$	$m_{eq,i}$ [3]	$\zeta_{eq,h,i}$ [3]
	(*i*)	(*in*)	(*in*)	(*in*)	(*in*)	(*rad*)	(*rad*)		(*rad*)	(*rad*)	(*rad*)	(*rad*)	(*in*)	(*in*)		(*in*)			
FR-6F-27	1	144	3.56	27	21	0.0081	0.0082	1.089	0.0094	0.0103	0.0101	0.0107	1.43	1.52	0.95	1.61	2.31	4016	15.7%
	2	288	7.05	27	21	0.0081	0.0082	1.076	0.0094	0.0101			2.84	3.02		3.18	2.26	3996	15.2%
	3	432	10.46	24	21	0.0092	0.0082	1.065	0.0100	0.0107			4.21	4.48		4.72	2.21	3975	14.7%
	4	576	13.80	24	21	0.0092	0.0082	1.057	0.0100	0.0106			5.56	5.91		6.22	2.17	3954	14.2%
	5	720	17.06	24	18	0.0092	0.0096	1.051	0.0108	0.0113			6.87	7.30		7.69	2.12	3933	13.7%
	6	864	20.25	24	18	0.0092	0.0096	1.046	0.0108	0.0113			8.15	8.67		9.13	2.07	3912	13.2%
FR-6F-33	1	144	3.56	33	27	0.0067	0.0064	1.076	0.0075	0.0081	0.0084	0.0089	1.20	1.26	0.95	1.33	2.79	4206	17.3%
	2	288	7.05	33	27	0.0067	0.0064	1.065	0.0075	0.0080			2.38	2.50		2.64	2.73	4184	16.8%
	3	432	10.46	27	24	0.0073	0.0072	1.056	0.0084	0.0088			3.53	3.71		3.91	2.67	4161	16.3%
	4	576	13.80	27	24	0.0073	0.0072	1.049	0.0084	0.0088			4.65	4.90		5.16	2.61	4138	15.8%
	5	720	17.06	27	21	0.0081	0.0082	1.044	0.0094	0.0098			5.75	6.06		6.38	2.55	4115	15.3%
	6	864	20.25	27	21	0.0081	0.0082	1.039	0.0094	0.0098			6.82	7.19		7.57	2.49	4092	14.8%

1. based on $L = L_b$
2. based on $L_c - l_p = L_b$
3. based on $r_{\delta,i} = 0.1$

Table 7-13. FR-6F effective SDOF frame properties

Property	FR-6F-27 Target (*equivalent*)	FR-6F-27 Yield (*elastic*)	FR-6F-33 Target (*equivalent*)	FR-6F-33 Yield (*elastic*)
M_{eff}	19393	19022	20298	19022
h_{eff} (*in*)	619	621	619	621
P_{eff} (*kips*)	7370	7350	7371	7350
Γ_1	1.378	1.375	1.378	1.375
Υ	---	≈1.00	---	≈1.00
ζ_{eq}	15.8%	+2.0%	17.4%	+2.0%
Δ_d (*in*)	14.69	6.64 (6.31)	14.69	5.51 (5.23)
μ_Δ	2.22	1.00	2.68	1.00
T_{eff^2} (*sec*)	3.27	2.21	3.33	2.04
T_{eff^1} (*sec*)	3.03	2.13	3.09	1.97
K_{eff^2} (*kips/in*)	71.6	153.3	72.3	181.0
K_{eff^1} (*kips/in*)	83.5	165.2	84.2	192.9
F_{y^2} (*kips*)	1052	1018	1062	997
F_{y^1} (*kips*)	1227	1097	1237	1062
r_{Δ^2}	0.031	---	0.041	---

Table 7-14. FR-6F design forces

Frame	DOF	$F_{x,i}$ (*elastic*) (*kips*)	
	(*i*)	*First-order*[1]	*Second-order*[2]
FR-6F-27	1	54	48
	2	107	94
$F_{el^2} = 967$	3	159	140
$F_{el^1} = 1042$	4	210	185
	5	259	229
	6	308	271
FR-6F-33	1	52	47
	2	104	92
$F_{el^2} = 947$	3	154	137
$F_{el^1} = 1009$	4	203	181
	5	251	224
	6	298	266

1. requires 1st order elastic analysis
2. requires 2nd order elastic analysis

For the remaining discussions and sections, the reader is referred to Section 7.2 for information concerning graphs and tables purposely removed to limit redundancy. Fig. 7-21 presents the final frame designs and displacement profiles.

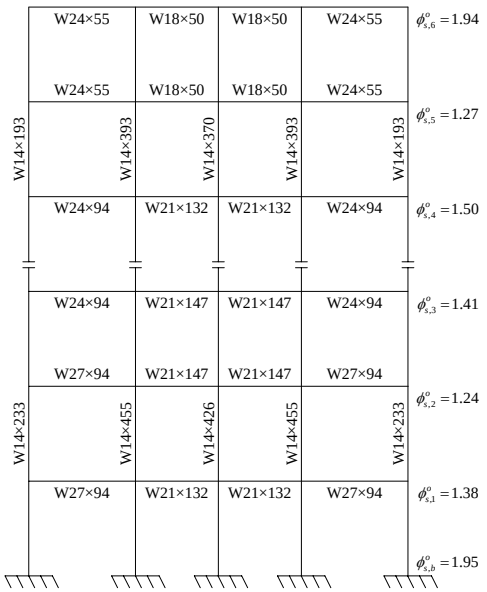

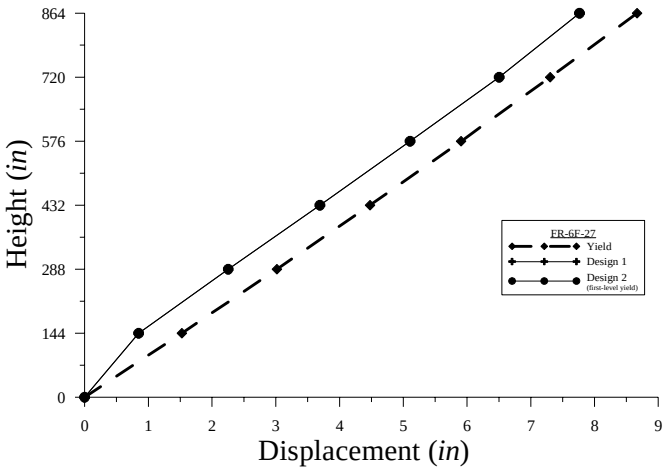

(i) Frame schematic **(ii) Displacement profile**

(a) FR-6F-27

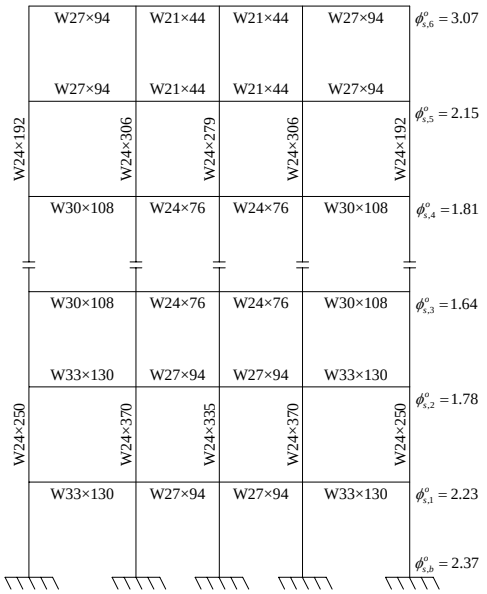

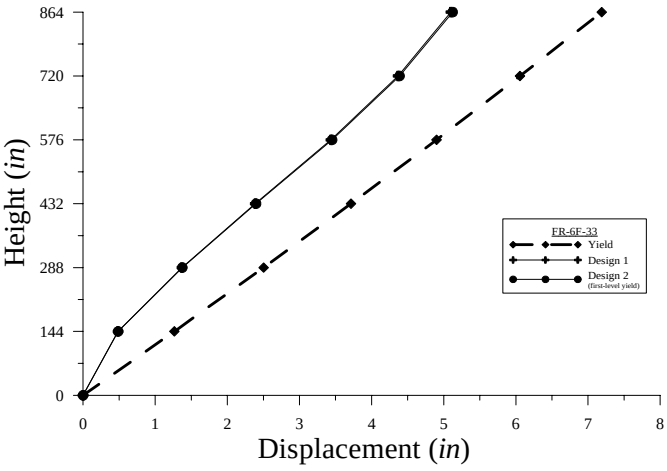

(i) Frame schematic **(ii) Displacement profile**

(b) FR-6F-33

Figure 7-21. Frame design

Table 7-15 lists the actual dynamic properties of the designed frames (ratio to elastic target values is included).

Table 7-15. Actual dynamic properties (FR-6F)

Property	FR-6F-27		FR-6F-33	
	Elastic	Ratio	Elastic	Ratio
M_{eff}	17830	0.94	17500	0.92
h_{eff} (*in*)	640	1.03	645	1.04
P_{eff} (*kips*)	6759	0.92	6688	0.91
Γ_1	1.376	1.00	1.354	0.98
T_{eff^2} (*sec*)	2.044	0.92	1.677	0.82
T_{eff^1} (*sec*)	1.980	0.93	1.641	0.83
K_{eff^2} (*kips/in*)	168.5	1.10	245.7	1.36
K_{eff^1} (*kips/in*)	179.5	1.09	256.6	1.33

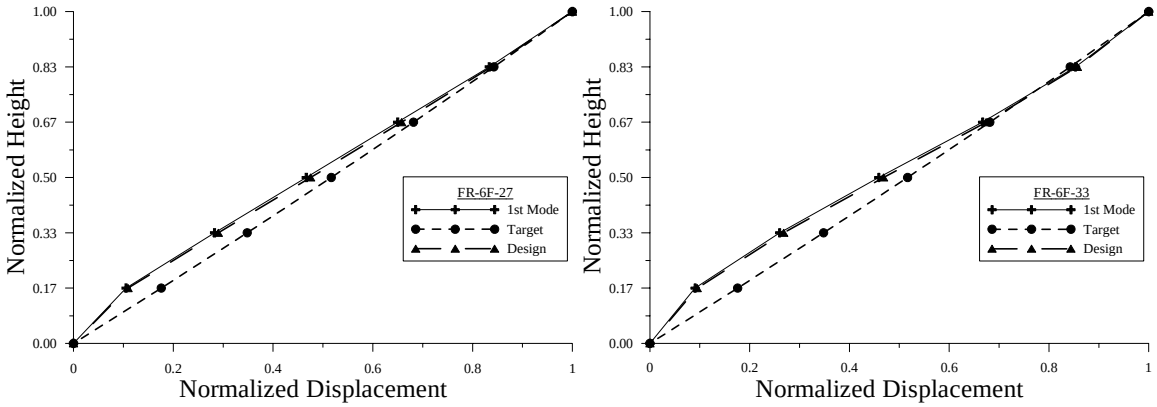

(a) FR-6F-27 **(b) FR-6F-33**

Figure 7-22. Normalized 1st mode shape

Fig. 7-22 illustrates the 1st mode shapes (normalized to roof). Frame stiffening effects due to beam flexural overstrengths and capacity design of columns are evident in Figs. 7-21 and 7-22. As a result, the lateral force distribution is slightly misrepresented thus allocating larger magnitudes to the upper floors. It is plausible that the design displacement profile at first-significant yield (i.e., first-level hinges) is not parabolic as assumed and could be modified as indicated. It is determined that most beam hinges and 1st story column base hinges do not develop under the design forces and that beam hinges develop (including the roof) prior to 1st story column base hinges.

7.3.2 Monotonic Static Pushover Analysis

Table 7-16 presents the predicted static and dynamic response curve ordinates of the designed frames and Fig. 7-23 plots the effective SDOF 'target' and expected 'static' and 'dynamic' pushover curves. The monotonic pushover curve is also shown.

Table 7-16. Static and dynamic predicted pushover ordinates (FR-6F)

Frame	Ω^o	Λ^o	Θ^o	Δ_y^o (*in*)	$F_{y^2}^o$ (*kips*)	$F_{y^1}^o$ (*kips*)	Δ_d^o (*in*)	$F_{d^2}^o$ (*kips*)	$F_{d^1}^o$ (*kips*)	ϕ_p^o	$F_{y^1}^d$ (*kips*)	$F_{d^1}^d$ (*kips*)
FR-6F-27	1.09	1.00	0.94	5.74	1018	1086	12.73	1052	1204	1.23	1330	1477
FR-6F-33	1.36	1.25	0.92	4.82	1246	1303	12.89	1348	1502	1.23	1596	1842

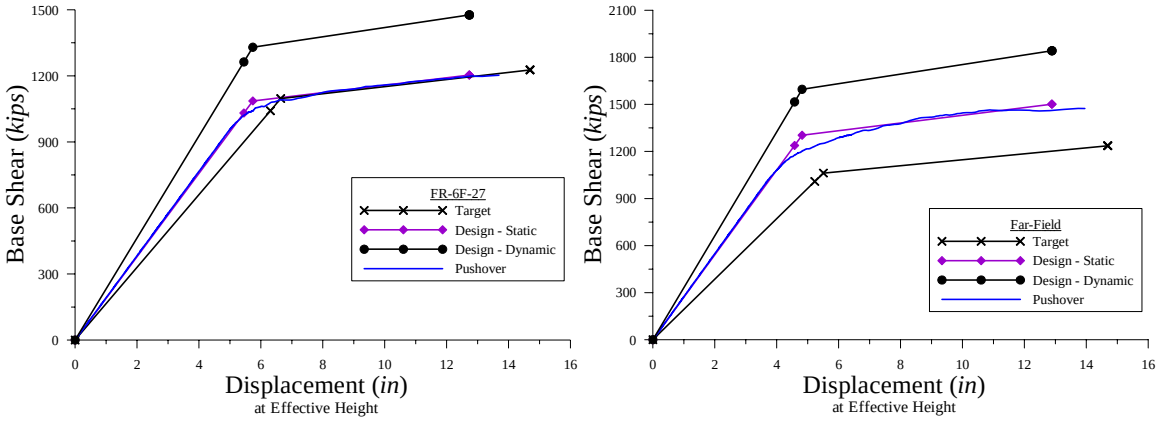

(a) FR-6F-27 **(b) FR-6F-33**

Figure 7-23. Target and predicted pushover curves

Fig. 7-24 presents the pushover curves under the design force distribution.

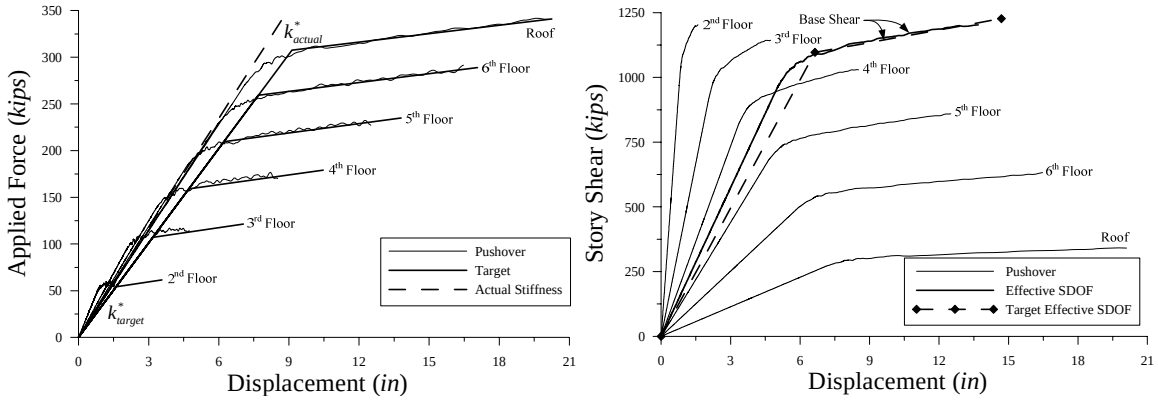

(i) Lateral force pushover **(ii) Story shear pushover**

(a) FR-6F-27

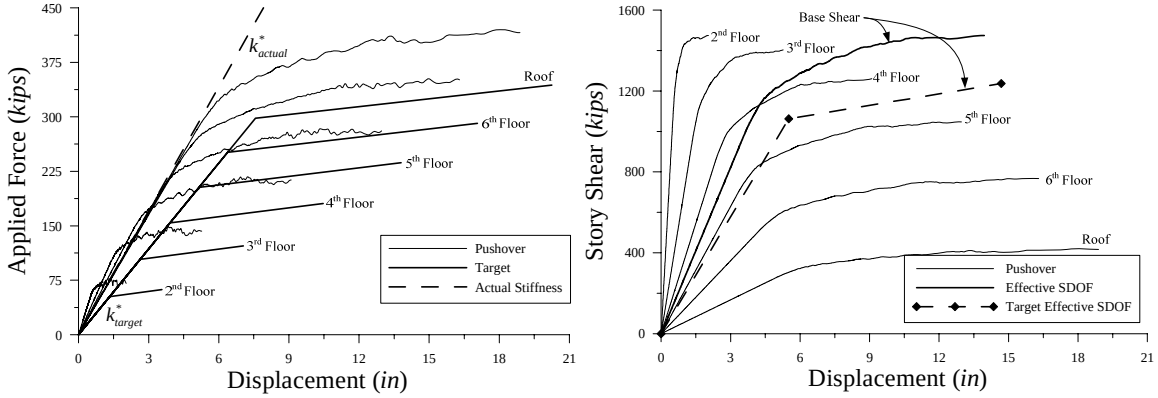

(i) Lateral force pushover **(ii) Story shear pushover**

(b) FR-6F-33

Figure 7-24. 1st mode pushover curves

7.3.3 Dynamic Analysis

7.3.3.1 Displacement Envelopes and Dynamic Response Curves

Figs. 7-25 and 7-26 present the displacement envelopes for the frames at the yield-level ($\Re \times$MCE) and design-level (0.67 × MCE) earthquake. Fig. 7-27 illustrates that the difference between displacement envelope and profile at each nodal maximum is small in these frames.

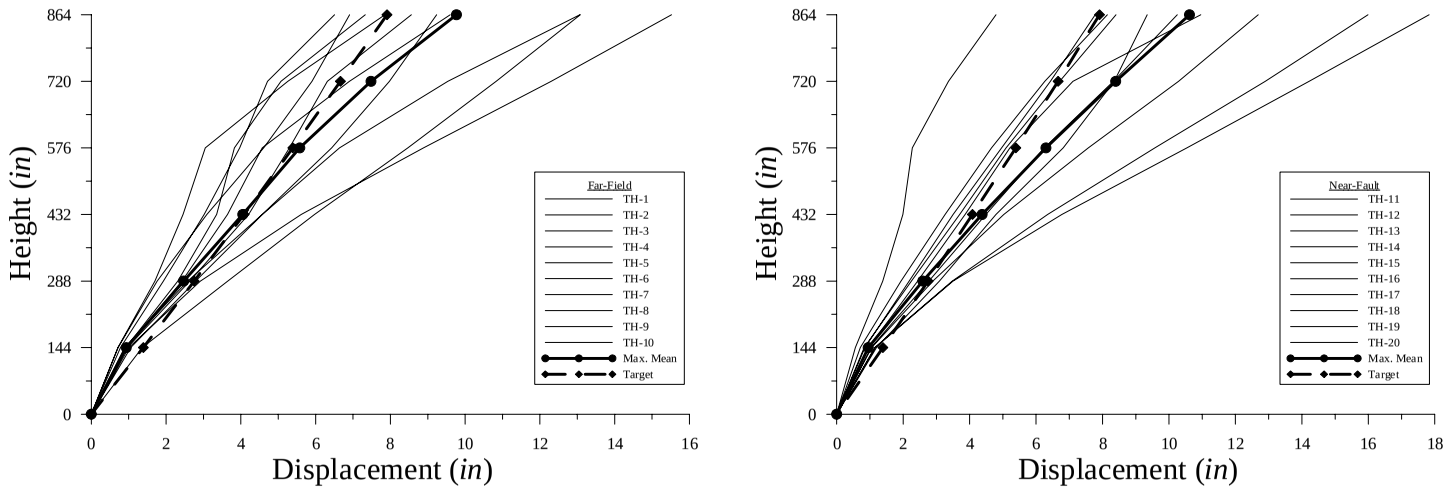

(a) Displacement profile (Yield - 0.30 × MCE)

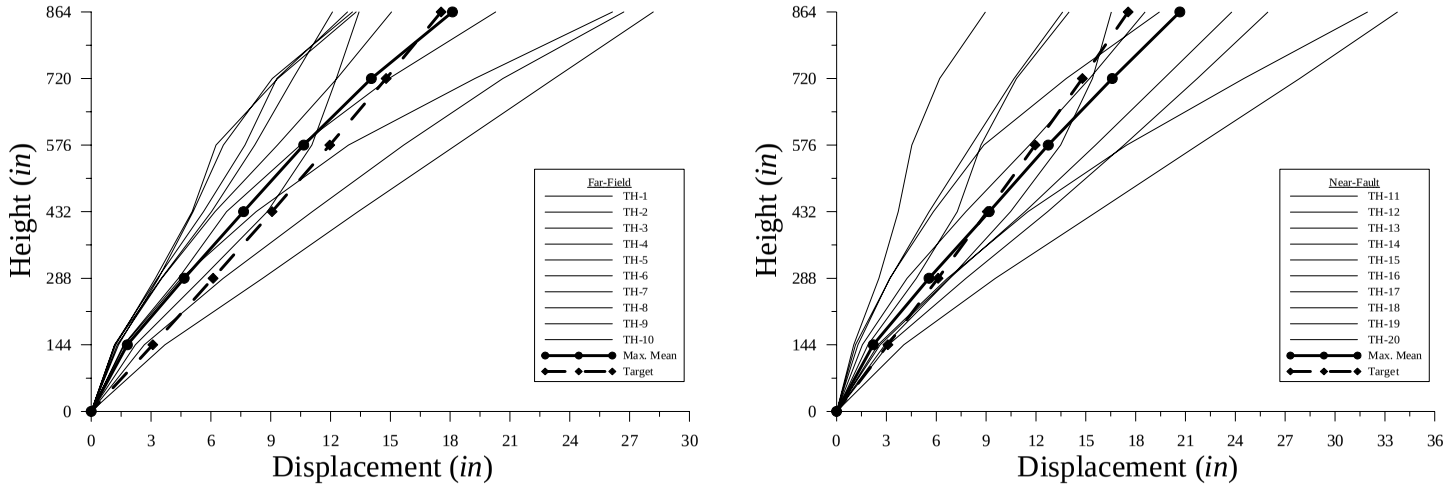

(b) Displacement profile (Target - 0.67 × MCE)

Figure 7-25. FR-6F-27 inelastic dynamic analysis results

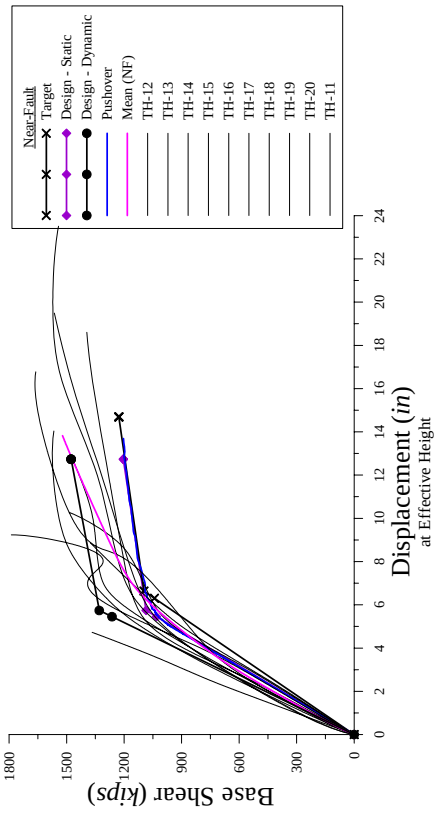

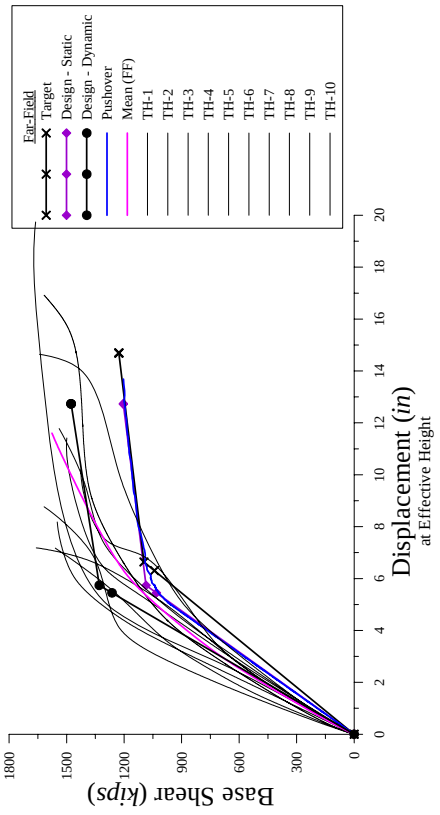

(c) Dynamic pushover curves – base shear (0.13, 0.30, 0.45, 0.67 × MCE)

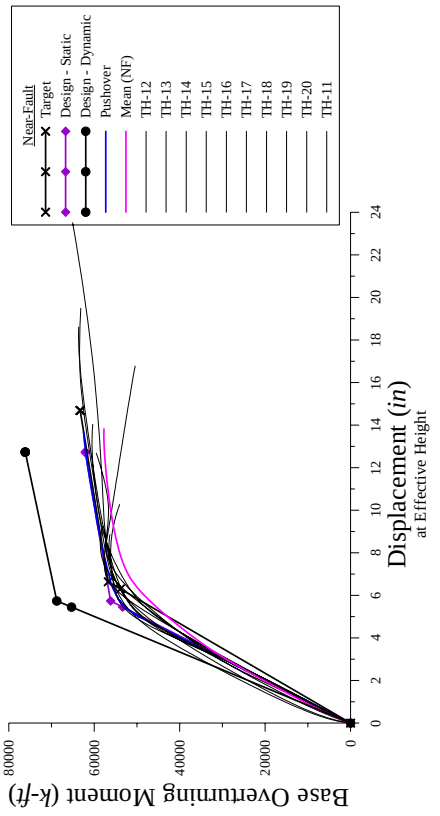

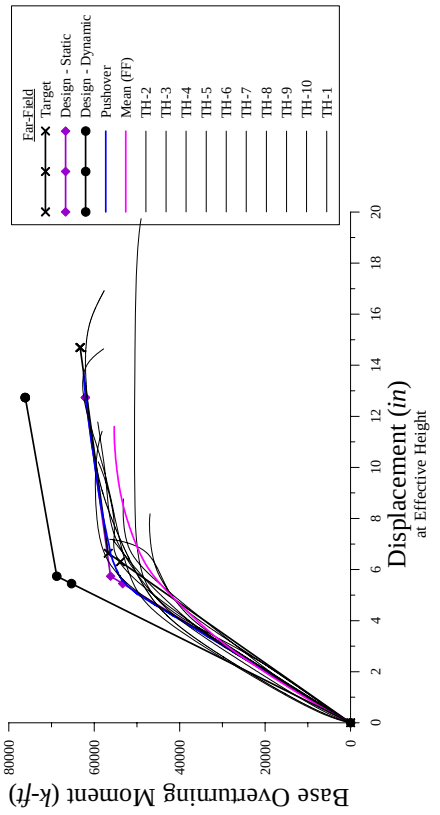

(d) Dynamic pushover curves – base overturning moment (0.13, 0.30, 0.45, 0.67 × MCE)

Figure 7-25. FR-6F-27 inelastic dynamic analysis results (Cont'd)

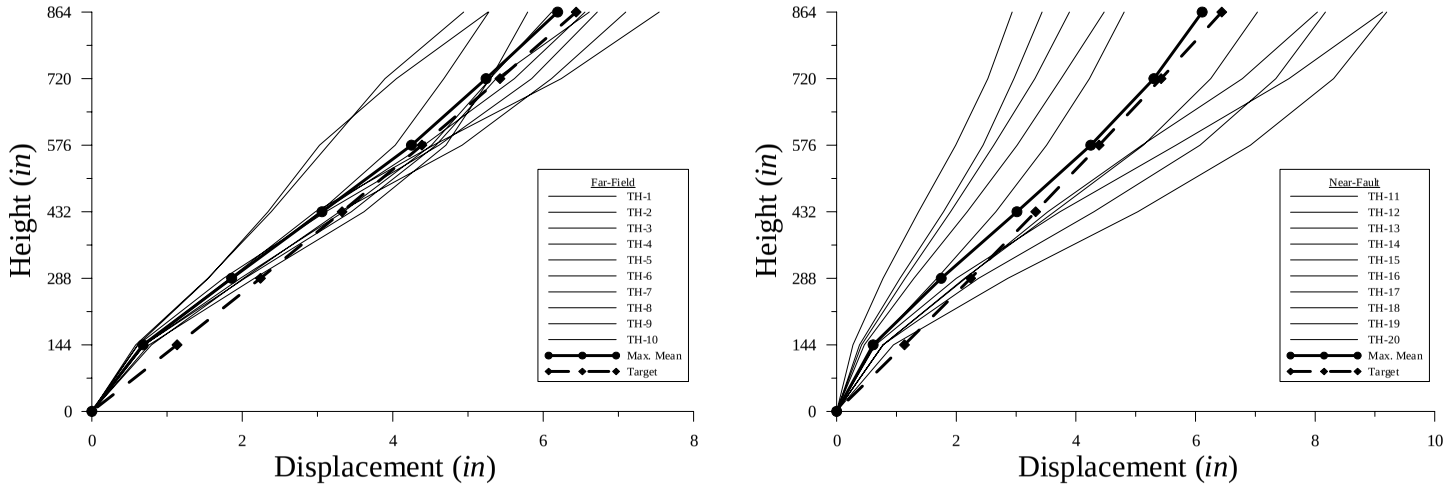

(a) Displacement profile (Yield - 0.25 × MCE)

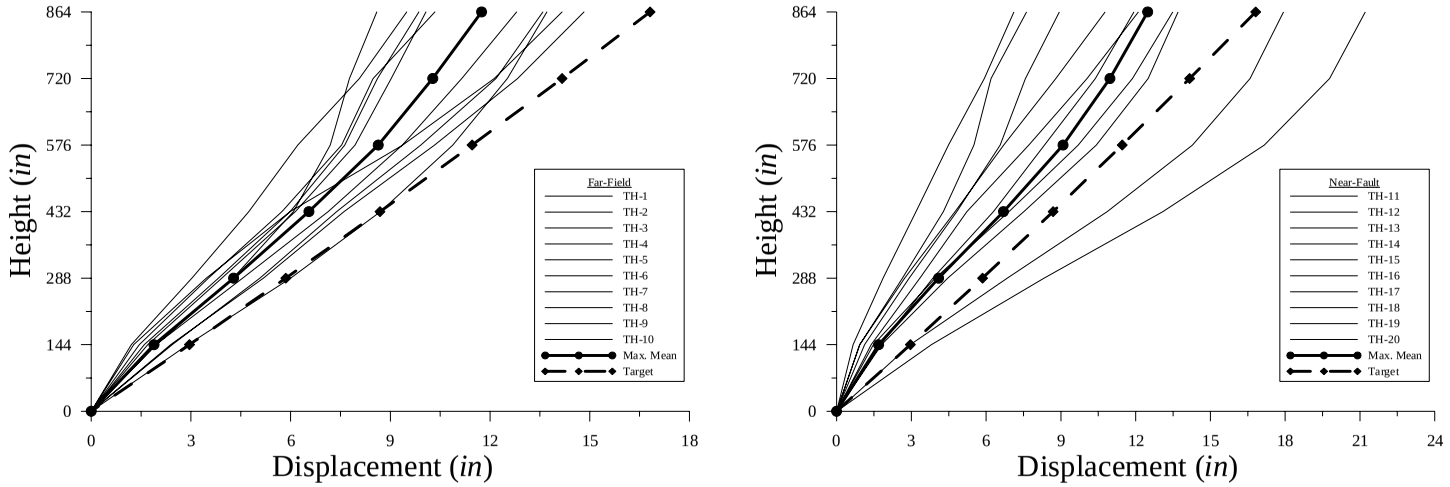

(b) Displacement profile (Target - 0.67 × MCE)

Figure 7-26. FR-6F-33 inelastic dynamic analysis results

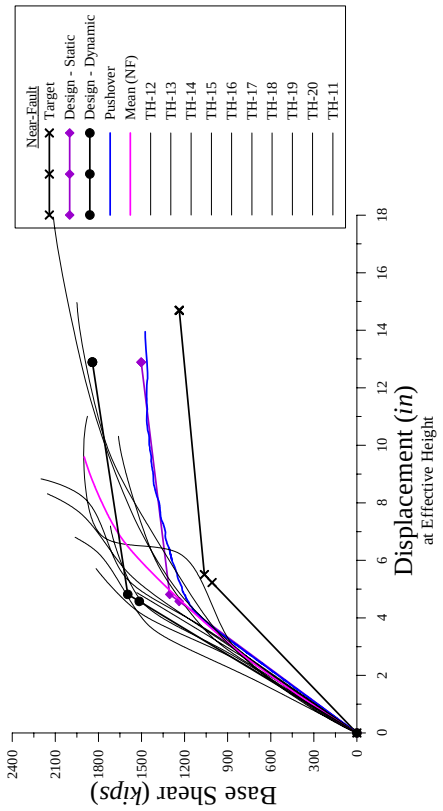

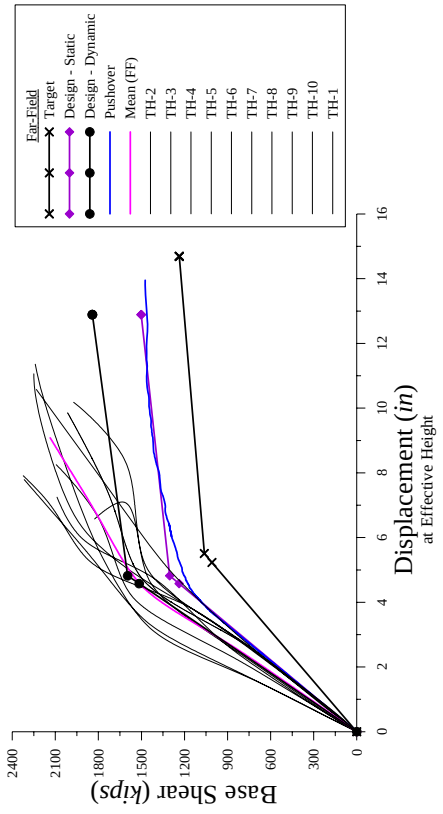

(c) Dynamic pushover curves – base shear (0.13, 0.25, 0.45, 0.67 × MCE)

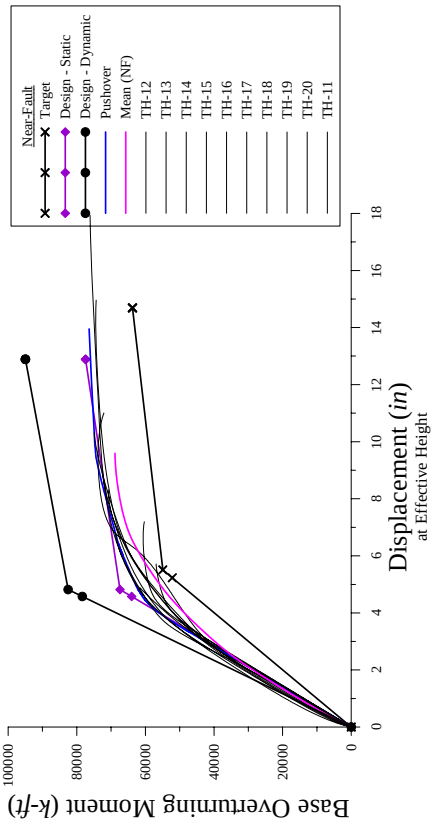

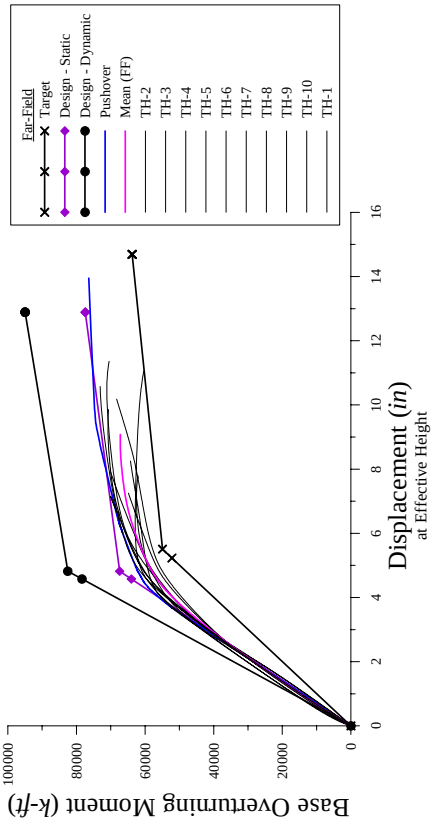

(d) Dynamic pushover curves – base overturning moment (0.13, 0.25, 0.45, 0.67 × MCE)

Figure 7-26. FR-6F-33 inelastic dynamic analysis results (Cont'd)

FR-6F-27

As seen in Fig. 7-25(a) and (b), good agreement exists between the mean envelopes and target profiles though cantilever action is clearly evident, implying the maximum drift ratio is first reached in the upper floors. The frequency content and magnitudes are such that higher modes contribute to frame behavior; more significantly than for the three-story frames (see Fig. 7-25(c)). As a corollary, the frame relies heavily on column stiffness for resistance and response is dominated by cantilever action similar to the three-story-frames. It is evident that the lack of base hinge formation can have a significant effect on the actual and design displacement profiles.

FR-6F-33

As seen in Fig. 7-26(a) and (b), reasonable agreement exists between the mean envelopes and target profiles, a better match is achieved at the yield-level. The frequency content and magnitudes are such that higher modes do significantly contribute to frame behavior (see Fig. 7-26(c)). Similar to FR-3F-30, the high strength and stiffness of the frame limits its ability to achieve the design target. The frame also displays some cantilever action due to the absence of base hinges at the yield-level and subsequently experiences some inelastic redistribution of forces at the design-level. This further emphasizes the requisite base hinge formations in the chosen design displacement profile.

As seen in the previous figures, higher mode contributions begin to dominantly affect these frames, even in the elastic region. Still, a trend is seen where the predicted dynamic pushover curve agrees with the analytical data. It is thus recommended that the

proposed DDBD methodology be restricted to steel moment frames up to six stories with fundamental periods less than 2.0 *seconds*.

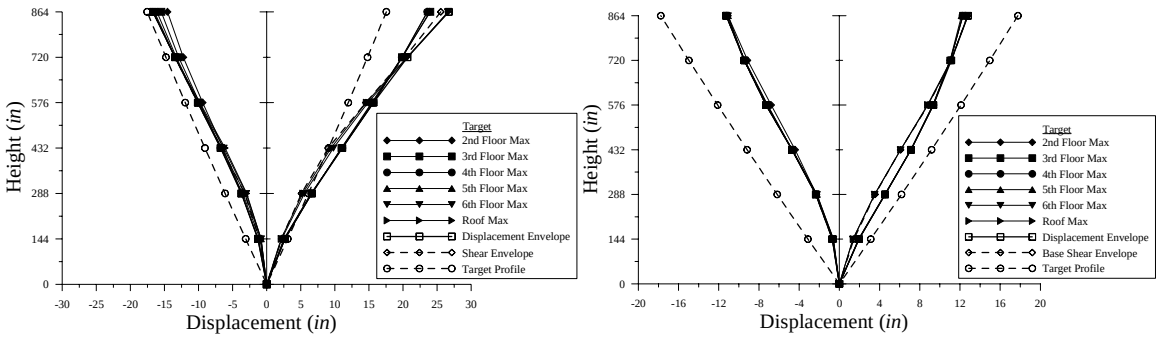

(a) FR-6F-27 **(b) FR-6F-33**

Figure 7-27. Displacement profiles (TH-1)

7.3.3.2 Curvature Ductility Envelopes

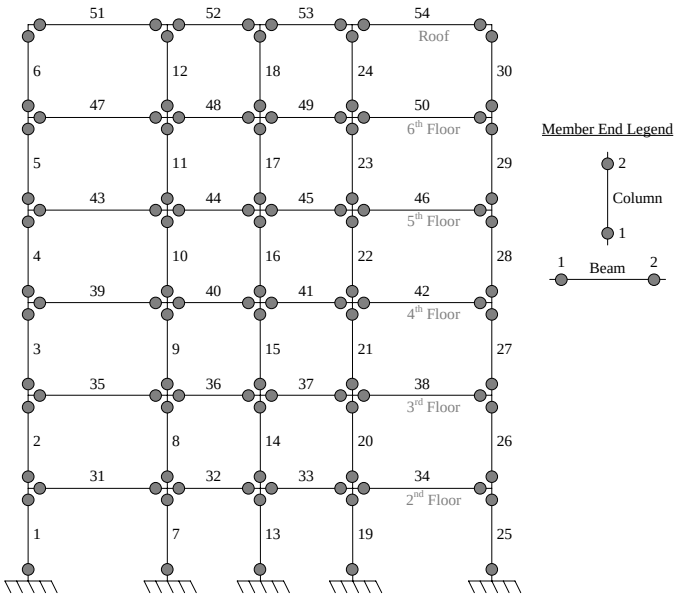

Figure 7-28. FR-6F plastic hinge model

Fig. 7-28 illustrates the frame model with all possible hinge locations. Tables 7-17 and 7-18 list the curvature ductility for each hinge developed at the presumed yield-level

earthquake. It is clear that base hinges do not form at the presumed yield-level though a majority of beam hinges have formed.

Tables 7-19 and 7-20 list the curvature ductility for each hinge developed at the design-level earthquake. Most hinges are below the allowable for the design-level earthquake. FR-6F-27 is dominated by cantilever action and experiences unsatisfactory performance for a few earthquake records (see TH-1, 5, 7, 9, 11, and 12). This suggests that the upper floors should be stiffened to assist in reducing cantilever action, albeit a response affect of delayed base hinge formations. FR-6F-27 also utilizes more of the ductility capacity than FR-6F-33.

Table 7-17. Curvature ductility envelopes (FR-6F-27) – 0.30×MCE

Floor	Member	End	TH-1	TH-2	TH-3	TH-4	TH-5	TH-6	TH-7	TH-8	TH-9	TH-10	TH-11	TH-12	TH-13	TH-14	TH-15	TH-16	TH-17	TH-18	TH-19	TH-20
Columns	**1**	1	---	---	---	---	---	---	---	---	---	---	---	---	---	---	---	---	---	---	---	---
	7	1	---	---	---	---	---	---	---	---	---	---	---	---	---	---	---	---	---	---	---	---
	13	1	1.07	---	---	---	---	---	---	---	---	---	---	---	---	---	---	---	---	---	---	---
	19	1	1.11	---	---	---	---	---	---	---	---	---	---	---	---	---	---	---	---	---	---	---
	25	1	1.06	---	---	---	---	---	---	---	---	---	---	---	---	---	---	---	---	---	---	---
2nd Floor	31	1	2.14	---	---	---	---	1.07	1.20	---	1.25	---	1.75	1.68	1.21	---	---	1.29	---	---	---	1.62
Beams		2	2.15	---	---	---	---	1.09	1.24	---	1.27	---	1.79	1.68	1.26	---	---	1.33	---	---	---	1.64
	32	1	2.45	---	1.22	---	1.23	1.36	1.53	1.16	1.57	---	2.06	2.01	1.54	1.28	---	1.61	---	---	---	1.93
		2	2.37	---	1.12	---	1.14	1.29	1.42	1.06	1.45	---	1.98	1.89	1.45	1.14	---	1.52	---	---	---	1.85
	33	1	2.37	---	1.11	---	1.14	1.29	1.42	1.05	1.45	---	1.98	1.89	1.45	1.14	---	1.52	---	---	---	1.85
		2	2.42	---	1.23	---	1.23	1.37	1.53	1.16	1.57	---	2.05	2.01	1.53	1.28	---	1.61	---	---	---	1.93
	34	1	2.13	---	---	---	---	1.12	1.24	---	1.27	---	1.79	1.68	1.25	---	---	1.34	---	---	---	1.64
		2	2.13	---	---	---	---	1.06	1.20	---	1.24	---	1.74	1.69	1.22	---	---	1.29	---	---	---	1.63
3rd Floor	35	1	2.79	---	1.78	---	1.00	1.44	1.80	---	2.65	---	3.11	3.56	1.56	1.26	---	2.14	---	---	1.01	1.86
Beams		2	2.83	---	1.82	---	1.05	1.44	1.80	---	2.65	---	3.11	3.59	1.59	1.26	---	2.18	---	---	1.05	1.91
	36	1	3.10	---	2.08	1.03	1.30	1.74	2.09	---	2.96	---	3.40	3.91	1.87	1.54	---	2.46	1.17	---	1.32	2.17
		2	3.05	---	2.02	---	1.22	1.64	2.00	---	2.86	---	3.36	3.78	1.78	1.46	---	2.37	1.08	---	1.23	2.10
	37	1	3.05	---	2.02	---	1.22	1.66	2.02	---	2.85	---	3.36	3.82	1.78	1.49	---	2.37	1.07	---	1.23	2.09
		2	3.10	---	2.08	1.03	1.29	1.73	2.09	---	2.96	---	3.40	3.89	1.86	1.53	---	2.47	1.17	---	1.32	2.20
	38	1	2.83	---	1.81	---	1.03	1.44	1.79	---	2.67	---	3.10	3.59	1.56	1.26	---	2.16	---	---	1.04	1.90
		2	2.79	---	1.78	---	1.00	1.45	1.82	---	2.63	---	3.11	3.56	1.57	1.26	---	2.17	---	---	1.01	1.88
4th Floor	39	1	2.92	---	1.82	1.14	1.20	---	2.08	---	3.73	---	3.90	4.68	1.85	1.36	---	2.90	---	---	---	2.18
Beams		2	2.82	---	1.76	1.06	1.13	---	2.01	---	3.65	---	3.77	4.62	1.76	1.29	---	2.88	---	---	---	2.09
	40	1	3.37	---	2.27	1.58	1.64	1.18	2.48	---	4.17	1.17	4.37	5.19	2.24	1.80	---	3.40	1.37	1.16	1.35	2.59
		2	3.12	---	2.07	1.37	1.43	---	2.31	---	3.98	---	4.08	4.92	2.10	1.59	---	3.17	1.18	---	1.16	2.41
	41	1	3.12	---	2.06	1.36	1.46	---	2.33	---	3.97	---	4.09	4.93	2.09	1.62	---	3.18	1.16	---	1.15	2.41
		2	3.36	---	2.27	1.57	1.63	1.19	2.47	---	4.17	1.17	4.33	5.20	2.23	1.78	---	3.40	1.38	1.15	1.35	2.60
	42	1	2.78	---	1.73	1.06	1.15	---	1.97	---	3.64	---	3.77	4.62	1.75	1.29	---	2.88	---	---	---	2.13
		2	2.93	---	1.83	1.14	1.20	---	2.14	---	3.73	---	3.90	4.68	1.84	1.37	---	2.91	---	---	---	2.16
5th Floor	43	1	2.95	1.84	1.14	---	2.01	1.55	3.31	1.48	4.11	---	4.06	5.40	1.97	2.92	---	3.35	---	---	1.22	1.35
Beams		2	2.93	1.84	1.11	---	1.99	1.54	3.29	1.47	4.10	---	4.05	5.39	1.97	2.95	---	3.29	---	---	1.21	1.35
	44	1	3.47	2.32	1.61	1.29	2.48	2.05	3.84	1.99	4.64	---	4.58	6.00	2.49	3.49	---	3.85	1.31	1.40	1.70	1.86
		2	3.27	2.15	1.41	1.04	2.30	1.85	3.67	1.76	4.46	---	4.38	5.75	2.28	3.23	---	3.65	1.11	1.22	1.53	1.65
	45	1	3.27	2.10	1.39	1.05	2.33	1.84	3.67	1.77	4.46	---	4.36	5.75	2.28	3.23	---	3.65	1.09	1.20	1.50	1.66
		2	3.46	2.35	1.61	1.26	2.46	2.05	3.85	2.00	4.62	---	4.59	6.00	2.46	3.48	---	3.87	1.31	1.41	1.74	1.86
	46	1	2.89	1.78	1.10	---	1.99	1.54	3.30	1.48	4.09	---	4.04	5.39	1.96	2.92	---	3.29	---	---	1.21	1.35
		2	2.96	1.86	1.13	---	2.04	1.54	3.31	1.49	4.10	---	4.05	5.41	1.97	2.93	---	3.36	---	---	1.25	1.36
6th Floor	47	1	3.16	3.08	1.51	1.60	3.21	2.83	4.73	3.98	4.33	1.94	4.86	6.98	2.01	5.00	---	4.56	1.04	1.87	1.75	1.77
Beams		2	3.19	3.07	1.52	1.62	3.19	2.81	4.82	3.74	4.50	1.93	4.84	7.07	2.05	4.93	---	4.91	1.13	1.92	1.74	1.82
	48	1	3.53	3.39	1.80	1.91	3.53	3.16	5.21	4.22	4.81	2.25	5.29	7.52	2.34	5.41	1.25	5.16	1.36	2.17	2.06	2.08
		2	3.56	3.43	1.83	1.93	3.54	3.18	5.19	4.42	4.88	2.26	5.24	7.54	2.34	5.38	1.27	5.15	1.39	2.24	2.07	2.16
	49	1	3.57	3.42	1.86	1.93	3.54	3.18	5.24	4.42	4.88	2.26	5.24	7.52	2.34	5.40	1.28	5.14	1.39	2.25	2.06	2.09
		2	3.51	3.39	1.80	1.90	3.53	3.16	5.20	4.22	4.81	2.25	5.28	7.56	2.33	5.37	1.22	5.18	1.35	2.16	2.08	2.08
	50	1	3.16	3.06	1.54	1.61	3.20	2.80	4.81	3.84	4.45	1.96	4.86	7.07	2.05	4.92	---	4.92	1.11	1.94	1.79	1.82
		2	3.16	3.07	1.51	1.60	3.22	2.82	4.76	3.97	4.33	1.88	4.82	7.00	2.01	5.00	---	4.57	1.03	1.83	1.74	1.77
Roof	51	1	2.18	2.26	1.05	1.44	3.35	2.22	4.29	4.18	3.55	1.56	4.15	6.29	1.04	4.67	---	4.50	---	1.22	1.07	1.38
Beams		2	2.52	2.57	---	1.70	3.55	2.46	4.55	4.46	3.76	1.79	4.42	6.70	1.30	5.06	---	4.90	---	1.50	---	1.68
	52	1	2.71	2.73	1.30	1.94	3.86	2.66	4.74	4.68	4.02	1.98	4.71	6.91	1.55	5.24	---	5.06	---	1.70	1.32	1.88
		2	2.80	2.92	1.38	1.98	3.93	2.82	4.95	4.89	4.15	2.14	4.78	7.10	1.55	5.30	---	5.37	---	1.76	1.38	1.94
	53	1	2.81	2.92	1.39	1.98	3.93	2.82	4.93	4.89	4.15	2.13	4.80	7.08	1.54	5.29	---	5.37	---	1.78	1.43	1.94
		2	2.69	2.73	1.31	1.93	3.87	2.66	4.77	4.68	4.02	1.97	4.67	6.96	1.55	5.24	---	5.06	---	1.66	1.30	1.88
	54	1	2.45	2.56	---	1.69	3.56	2.45	4.55	4.46	3.76	1.81	4.42	6.67	1.31	4.96	---	4.89	---	1.46	---	1.67
		2	2.21	2.25	1.07	1.43	3.36	2.21	4.29	4.19	3.54	1.51	4.14	6.36	1.02	4.72	---	4.52	---	1.23	1.09	1.37

Table 7-18. Curvature ductility envelopes (FR-6F-33) – 0.25×MCE

Floor	Member	End	TH-1	TH-2	TH-3	TH-4	TH-5	TH-6	TH-7	TH-8	TH-9	TH-10	TH-11	TH-12	TH-13	TH-14	TH-15	TH-16	TH-17	TH-18	TH-19	TH-20
Columns	**1**	1	---	---	---	---	---	---	---	---	---	---	---	---	---	---	---	---	---	---	---	---
	7	1	---	---	---	---	---	---	---	---	---	---	---	---	---	---	---	---	---	---	---	---
	13	1	---	---	---	---	---	---	---	---	---	---	---	1.04	---	---	---	---	---	---	---	---
	19	1	---	---	---	---	---	---	---	---	---	---	---	1.00	---	---	---	---	---	---	---	---
	25	1	---	---	---	---	---	---	---	---	---	---	---	1.11	---	---	---	---	---	---	---	---
2nd Floor	31	1	---	---	---	---	1.12	---	---	1.08	---	---	1.25	1.75	---	---	---	1.12	---	---	---	1.14
Beams		2	---	---	---	---	1.12	---	---	1.08	---	---	1.25	1.74	---	---	---	1.12	---	---	---	1.14
	32	1	1.10	1.14	---	1.10	1.36	1.19	---	1.32	---	1.22	1.51	2.02	---	1.15	---	1.38	---	---	---	1.39
		2	1.14	1.17	---	1.12	1.42	1.23	---	1.36	---	1.29	1.55	2.08	---	1.17	---	1.44	---	---	---	1.44
	33	1	1.14	1.17	---	1.12	1.43	1.23	---	1.35	---	1.29	1.55	2.06	---	1.17	---	1.44	---	---	---	1.44
		2	1.10	1.14	---	1.10	1.36	1.19	---	1.32	---	1.21	1.51	2.03	---	1.15	---	1.37	---	---	---	1.39
	34	1	---	---	---	---	1.11	---	---	1.08	---	---	1.23	1.75	---	---	---	1.13	---	---	---	1.14
		2	---	---	---	---	1.11	---	---	1.09	---	---	1.25	1.73	---	---	---	1.13	---	---	---	1.14
3rd Floor	35	1	1.15	1.14	1.26	1.09	1.60	1.39	---	1.44	---	1.53	2.18	2.68	---	1.71	---	1.64	---	---	---	1.48
Beams		2	1.15	1.14	1.26	1.09	1.59	1.39	---	1.44	---	1.53	2.17	2.68	---	1.71	---	1.64	---	---	---	1.47
	36	1	1.43	1.42	1.54	1.36	1.88	1.66	---	1.72	---	1.82	2.48	2.98	1.08	2.00	---	1.94	---	---	---	1.77
		2	1.49	1.46	1.59	1.41	1.92	1.74	---	1.75	---	1.86	2.52	3.08	1.12	2.07	---	1.95	---	---	---	1.80
	37	1	1.47	1.46	1.60	1.41	1.92	1.74	---	1.75	---	1.83	2.53	3.05	1.12	2.06	---	1.95	---	---	---	1.80
		2	1.44	1.42	1.55	1.36	1.88	1.66	---	1.73	---	1.83	2.49	2.99	1.09	2.00	---	1.94	---	---	---	1.77
	38	1	1.16	1.15	1.25	1.10	1.58	1.39	---	1.43	---	1.54	2.17	2.69	---	1.72	---	1.62	---	---	---	1.46
		2	1.17	1.15	1.25	1.10	1.59	1.42	---	1.43	---	1.54	2.17	2.70	---	1.72	---	1.63	---	---	---	1.47
4th Floor	39	1	1.41	---	1.55	1.80	1.23	1.22	---	1.90	---	1.38	2.28	2.69	---	2.23	---	1.68	---	---	---	2.00
Beams		2	1.41	---	1.54	1.84	1.22	1.20	---	1.89	---	1.38	2.27	2.65	---	2.29	---	1.68	---	---	---	2.04
	40	1	1.74	1.29	1.87	2.19	1.56	1.53	---	2.24	---	1.70	2.62	3.05	1.07	2.65	---	2.00	---	---	---	2.38
		2	1.75	1.35	1.93	2.21	1.57	1.56	---	2.25	---	1.74	2.64	3.10	1.11	2.67	---	2.02	---	---	---	2.41
	41	1	1.76	1.32	1.92	2.21	1.56	1.55	---	2.29	---	1.74	2.65	3.11	1.11	2.66	---	2.05	---	---	---	2.41
		2	1.74	1.30	1.88	2.18	1.56	1.53	---	2.23	---	1.71	2.62	3.03	1.07	2.65	---	2.00	---	---	---	2.38
	42	1	1.40	1.01	1.53	1.83	1.22	1.21	---	1.86	---	1.36	2.26	2.69	---	2.27	---	1.66	---	---	---	2.01
		2	1.40	1.01	1.53	1.83	1.21	1.23	---	1.89	---	1.36	2.27	2.69	---	2.27	---	1.66	---	---	---	2.00
5th Floor	43	1	1.11	1.09	1.18	2.00	1.61	---	---	1.85	1.19	1.69	1.42	1.71	---	2.51	---	1.42	---	---	---	2.15
Beams		2	1.11	1.12	1.18	2.07	1.61	---	---	1.85	1.19	1.69	1.40	1.75	---	2.51	---	1.45	---	---	---	2.15
	44	1	1.47	1.45	1.53	2.42	2.00	1.24	1.27	2.26	1.53	2.07	1.74	2.11	---	2.92	---	1.80	---	---	---	2.53
		2	1.51	1.43	1.57	2.46	2.03	1.27	1.33	2.24	1.57	2.11	1.83	2.13	---	2.96	---	1.84	---	---	---	2.57
	45	1	1.51	1.43	1.57	2.48	2.03	1.28	1.30	2.26	1.57	2.10	1.84	2.13	---	2.96	---	1.85	---	---	---	2.57
		2	1.47	1.45	1.54	2.39	1.99	1.25	1.27	2.23	1.53	2.07	1.75	2.10	---	2.92	---	1.80	---	---	---	2.53
	46	1	1.10	1.09	1.17	2.09	1.63	---	---	1.86	1.18	1.70	1.38	1.76	---	2.52	---	1.42	---	---	---	2.14
		2	1.09	1.09	1.16	2.03	1.63	---	---	1.87	1.18	1.71	1.40	1.73	---	2.52	---	1.42	---	---	---	2.14
6th Floor	47	1	---	---	---	1.55	1.41	---	1.10	1.56	1.02	1.59	---	1.07	---	1.95	---	---	---	---	---	1.49
Beams		2	---	---	---	1.59	1.41	---	1.11	1.66	1.07	1.60	---	1.13	---	1.95	---	---	---	---	---	1.53
	48	1	---	1.20	---	1.83	1.66	1.03	1.35	1.89	1.28	1.88	---	1.35	---	2.22	---	1.21	---	---	---	1.77
		2	---	1.28	---	1.91	1.76	1.08	1.44	1.91	1.35	1.90	---	1.39	---	2.30	---	1.28	---	---	---	1.80
	49	1	---	1.27	---	1.90	1.75	1.08	1.44	1.95	1.35	1.93	---	1.39	---	2.30	---	1.28	---	---	---	1.80
		2	---	1.19	---	1.83	1.66	1.04	1.35	1.82	1.28	1.82	---	1.36	---	2.22	---	1.22	---	---	---	1.77
	50	1	---	---	---	1.59	1.48	---	1.15	1.64	1.06	1.61	---	1.10	---	2.02	---	---	---	---	---	1.49
		2	---	---	---	1.58	1.41	---	1.11	1.63	1.00	1.60	---	1.05	---	1.94	---	---	---	---	---	1.48
Roof	51	1	---	---	---	---	---	---	---	---	---	---	---	---	---	---	---	---	---	---	---	---
Beams		2	---	---	---	---	---	---	---	---	---	---	---	---	---	---	---	---	---	---	---	---
	52	1	---	---	---	1.06	1.12	---	---	1.18	---	1.11	---	---	---	1.24	---	---	---	---	---	---
		2	---	---	---	1.18	1.21	---	---	1.30	---	1.20	---	---	---	1.38	---	---	---	---	---	1.07
	53	1	---	---	---	1.17	1.21	---	---	1.31	---	1.21	---	---	---	1.38	---	---	---	---	---	1.07
		2	---	---	---	1.06	1.11	---	---	1.15	---	1.08	---	---	---	1.22	---	---	---	---	---	---
	54	1	---	---	---	---	---	---	---	---	---	---	---	---	---	---	---	---	---	---	---	---
		2	---	---	---	---	---	---	---	---	---	---	---	---	---	---	---	---	---	---	---	---

Table 7-19. Curvature ductility envelopes (FR-6F-27) – 0.67×MCE

Floor	Member	End	TH-1	TH-2	TH-3	TH-4	TH-5	TH-6	TH-7	TH-8	TH-9	TH-10	TH-11	TH-12	TH-13	TH-14	TH-15	TH-16	TH-17	TH-18	TH-19	TH-20
Columns	**1**	1	2.69	1.02	---	1.23	5.14	2.53	1.05	---	1.18	---	2.34	5.87	---	3.94	---	2.99	3.42	---	---	1.52
	4	1	---	---	---	---	1.60	---	---	---	---	---	---	---	---	---	---	---	---	---	---	---
	7	1	2.91	1.07	---	1.26	4.76	2.41	1.30	---	1.40	---	2.51	5.37	1.23	3.62	---	3.03	3.60	---	---	1.74
	10	1	---	---	---	---	2.03	---	---	---	---	---	---	---	---	---	---	---	---	---	---	---
	11	1	---	---	---	---	1.18	---	---	---	---	---	---	---	---	---	---	---	---	---	---	---
	13	1	3.06	1.04	1.04	1.28	4.66	2.34	1.38	---	1.50	---	2.62	5.25	1.32	3.51	---	3.13	3.78	---	1.05	1.85
	15	1	---	---	---	1.16	---	---	---	---	---	---	1.15	1.02	---	---	---	---	---	---	---	---
	15	2	1.06	---	---	---	---	---	---	---	---	---	---	---	---	---	---	---	---	---	---	---
	16	1	---	1.23	---	1.56	2.68	---	1.27	---	1.33	---	---	1.24	---	---	---	---	---	---	---	---
	16	2	---	---	---	1.07	---	---	---	---	---	---	---	---	1.00	1.39	---	---	---	---	---	1.18
	17	1	---	1.02	---	1.02	1.63	---	1.34	1.30	---	---	---	1.02	---	---	---	---	---	---	---	---
	19	1	3.13	---	1.06	1.20	4.43	2.20	1.43	---	1.54	---	2.68	5.02	1.35	3.36	---	3.17	3.89	---	1.07	1.90
	22	1	---	---	---	---	1.91	---	---	---	---	---	---	---	---	---	---	---	---	---	---	---
	23	1	---	---	---	---	1.16	---	---	---	---	---	---	---	---	---	---	---	---	---	---	---
	25	1	3.33	---	1.05	1.00	4.29	1.99	1.44	---	1.53	---	2.64	4.99	1.39	3.17	---	3.14	4.31	---	---	1.93
	28	1	---	---	---	---	1.27	---	---	---	---	---	---	---	---	---	---	---	---	---	---	---
2nd Floor	31	1	4.76	1.68	2.02	1.90	6.50	3.79	2.88	1.88	2.77	1.67	4.75	7.27	2.64	4.96	1.11	4.88	5.78	1.59	1.77	3.32
Beams		2	4.70	1.68	2.07	1.91	6.51	3.85	2.85	1.92	2.79	1.75	4.66	7.28	2.61	4.93	1.12	4.87	5.72	1.60	1.81	3.26
	32	1	5.05	1.97	2.35	2.23	6.83	4.13	3.16	2.25	3.12	1.88	5.04	7.58	2.88	5.33	1.38	5.18	6.10	1.91	2.11	3.59
		2	4.91	1.89	2.28	2.15	6.75	4.07	3.05	2.12	2.90	2.00	4.94	7.53	2.84	5.21	1.34	5.09	5.94	1.79	1.99	3.51
	33	1	4.90	1.94	2.28	2.15	6.76	4.07	3.04	2.12	2.90	1.99	4.94	7.54	2.84	5.21	1.34	5.09	5.94	1.79	1.97	3.51
		2	5.01	1.95	2.35	2.25	6.85	4.17	3.12	2.26	3.09	1.87	5.03	7.59	2.85	5.36	1.38	5.15	6.06	1.91	2.11	3.56
	34	1	4.66	1.68	2.07	1.93	6.54	3.89	2.83	1.92	2.76	1.75	4.66	7.28	2.58	4.96	1.13	4.79	5.69	1.60	1.79	3.22
		2	4.68	1.68	2.02	1.95	6.53	3.88	2.75	1.89	2.70	1.67	4.78	7.23	2.55	5.04	1.09	4.81	5.64	1.59	1.77	3.25
3rd Floor	35	1	6.10	2.23	3.06	2.34	6.94	4.70	3.77	2.97	4.54	2.53	6.49	8.90	4.07	5.73	---	6.32	7.04	2.41	2.73	3.62
Beams		2	6.09	2.24	3.07	2.35	7.03	4.69	3.70	2.89	4.55	2.60	6.55	8.96	4.08	5.74	---	6.39	7.06	2.40	2.76	3.53
	36	1	6.44	2.52	3.38	2.64	7.43	5.07	4.16	3.29	4.76	2.87	6.84	9.26	4.40	6.08	1.27	6.73	7.42	2.73	3.01	3.89
		2	6.37	2.45	3.29	2.57	7.34	4.90	3.99	3.16	4.88	2.77	6.76	9.28	4.33	5.98	1.15	6.58	7.36	2.62	2.98	3.84
	37	1	6.37	2.45	3.31	2.58	7.34	4.90	3.99	3.16	4.88	2.77	6.72	9.29	4.33	5.99	1.17	6.58	7.35	2.62	2.98	3.79
		2	6.45	2.52	3.36	2.64	7.42	5.06	4.16	3.30	4.76	2.87	6.86	9.26	4.41	6.08	1.24	6.74	7.42	2.73	3.01	3.92
	38	1	6.12	2.24	3.07	2.35	7.05	4.68	3.69	2.89	4.57	2.60	6.54	8.95	4.08	5.74	---	6.41	7.07	2.40	2.75	3.53
		2	6.08	2.23	3.06	2.33	6.86	4.68	3.75	2.97	4.52	2.52	6.49	8.92	4.09	5.71	---	6.33	7.07	2.41	2.74	3.63
4th Floor	39	1	7.11	2.83	3.81	2.99	6.54	3.45	5.48	2.54	6.11	2.28	8.41	9.36	4.95	5.75	---	6.14	6.73	2.63	3.85	3.54
Beams		2	7.02	2.76	3.73	2.91	6.47	3.39	5.46	2.39	5.82	2.38	8.33	9.45	4.87	5.66	---	6.05	6.62	2.53	3.73	3.46
	40	1	7.59	3.28	4.18	3.56	6.95	3.87	6.10	2.90	6.57	2.72	8.84	10.00	5.36	6.20	1.14	6.60	7.18	3.03	4.27	3.97
		2	7.39	2.93	4.11	3.18	6.50	3.76	5.52	2.77	6.04	2.68	8.74	9.61	5.29	5.96	---	6.40	6.94	2.87	4.09	3.76
	41	1	7.35	2.93	4.11	3.18	6.56	3.76	5.53	2.78	6.10	2.68	8.74	9.61	5.24	5.96	---	6.39	6.93	2.87	4.04	3.76
		2	7.60	3.27	4.15	3.50	6.95	3.89	6.11	2.90	6.48	2.71	8.83	10.00	5.38	6.23	1.12	6.60	7.17	3.03	4.36	3.97
	42	1	7.01	2.72	3.71	2.90	6.48	3.39	5.45	2.44	5.82	2.37	8.33	9.46	4.86	5.66	---	6.04	6.61	2.53	3.77	3.46
		2	7.10	2.85	3.82	2.99	6.70	3.50	5.56	2.52	6.10	2.27	8.41	9.36	4.95	5.76	---	6.13	6.72	2.65	3.83	3.48
5th Floor	43	1	8.28	4.71	3.63	5.26	9.87	2.62	6.18	2.58	8.76	3.40	10.15	9.55	4.89	4.31	1.75	6.18	6.73	3.55	6.00	4.45
Beams		2	8.27	4.59	3.82	5.17	9.77	2.56	6.14	2.56	8.68	3.38	10.03	9.53	4.80	4.28	1.74	6.17	6.67	3.54	6.05	4.34
	44	1	8.94	5.24	4.44	5.75	10.44	3.11	6.61	3.13	9.32	3.90	10.56	10.26	5.36	4.85	2.24	6.74	7.25	4.12	6.63	4.96
		2	8.60	4.97	3.89	5.50	10.15	2.90	6.45	2.71	9.08	3.69	10.57	9.86	5.21	4.42	2.05	6.58	7.10	3.87	6.42	4.71
	45	1	8.60	4.96	3.83	5.53	10.18	2.90	6.45	2.71	9.07	3.69	10.52	9.86	5.20	4.44	2.04	6.53	7.06	3.87	6.42	4.70
		2	8.94	5.24	4.48	5.69	10.45	3.11	6.61	3.13	9.31	3.88	10.59	10.27	5.35	4.84	2.24	6.76	7.27	4.13	6.64	4.95
	46	1	8.26	4.59	3.83	5.17	9.79	2.59	6.12	2.56	8.69	3.38	10.02	9.53	4.80	4.29	1.69	6.17	6.67	3.55	6.05	4.35
		2	8.28	4.71	3.54	5.21	9.91	2.61	6.28	2.58	8.68	3.39	10.15	9.55	4.88	4.32	1.77	6.18	6.73	3.55	6.00	4.37
6th Floor	47	1	9.03	7.06	5.10	6.47	12.94	4.96	8.98	5.57	10.19	5.60	11.57	12.30	5.55	5.25	4.03	6.42	6.75	4.06	7.94	5.01
Beams		2	9.18	7.10	5.23	6.41	13.13	4.88	8.75	5.69	10.39	5.54	11.54	12.11	5.62	5.24	3.86	6.59	6.73	4.03	8.02	4.99
	48	1	9.63	7.51	5.60	6.71	13.61	5.33	9.34	6.11	10.66	6.02	12.05	12.97	6.04	5.66	4.27	7.02	7.16	4.41	8.45	5.43
		2	9.61	7.56	5.75	7.11	13.75	5.34	9.54	6.07	10.96	5.99	12.07	12.96	6.05	5.66	4.42	6.96	7.31	4.49	8.48	5.39
	49	1	9.60	7.56	5.75	7.11	13.75	5.29	9.55	6.02	10.95	5.98	11.94	12.97	6.06	5.65	4.42	6.98	7.18	4.52	8.48	5.39
		2	9.63	7.51	5.60	6.71	13.62	5.33	9.34	6.12	10.66	6.01	12.07	12.98	6.04	5.65	4.26	6.98	7.19	4.41	8.45	5.43
	50	1	9.20	7.10	5.31	6.45	13.13	4.89	8.74	5.68	10.40	5.56	11.54	12.12	5.63	5.23	3.86	6.58	6.73	4.05	7.99	4.98
		2	8.97	7.06	5.09	6.40	12.93	4.93	9.02	5.57	10.15	5.55	11.57	12.30	5.56	5.24	4.02	6.42	6.74	4.06	8.01	5.00
Roof	51	1	8.41	6.85	5.02	6.46	14.20	5.07	8.90	5.94	9.70	5.92	11.40	12.81	5.69	5.40	3.82	6.76	6.00	3.13	7.49	5.79
Beams		2	8.86	7.27	5.36	6.25	14.80	5.32	9.24	6.57	10.10	6.15	11.69	13.00	5.96	5.44	3.93	7.00	6.22	3.29	7.76	6.09
	52	1	9.11	7.53	5.81	6.69	15.20	5.60	9.45	6.72	10.63	6.39	12.23	13.44	6.28	5.98	4.30	7.10	6.53	3.60	8.07	6.37
		2	9.22	7.57	5.66	7.00	15.14	5.63	9.96	6.59	10.42	6.75	12.04	13.68	6.35	5.82	4.33	7.60	6.60	3.66	8.23	6.52
	53	1	9.22	7.56	5.67	6.99	15.15	5.62	9.94	6.59	10.45	6.74	12.03	13.68	6.35	5.89	4.32	7.59	6.60	3.75	8.23	6.52
		2	9.11	7.53	5.81	6.69	15.20	5.60	9.50	6.72	10.56	6.38	12.23	13.44	6.29	5.86	4.29	7.10	6.53	3.59	8.07	6.36
	54	1	8.83	7.26	5.37	6.28	14.81	5.31	9.23	6.56	10.10	6.14	11.68	13.01	5.97	5.43	3.93	6.98	6.22	3.40	7.76	6.08
		2	8.41	6.84	5.03	6.38	14.21	5.05	8.95	5.93	9.69	5.91	11.40	12.82	5.70	5.39	3.79	6.75	5.99	3.06	7.50	5.79

Table 7-20. Curvature ductility envelopes (FR-6F-33) – 0.67×MCE

Floor	Member	End	TH-1	TH-2	TH-3	TH-4	TH-5	TH-6	TH-7	TH-8	TH-9	TH-10	TH-11	TH-12	TH-13	TH-14	TH-15	TH-16	TH-17	TH-18	TH-19	TH-20
Columns	**1**	1	2.90	2.52	4.26	1.57	3.59	1.63	2.11	2.17	5.08	3.01	4.80	6.53	1.38	2.72	---	2.83	1.94	---	1.03	2.17
	2	1	---	---	---	---	---	---	---	---	---	---	1.09	---	---	---	---	---	---	---	---	---
	3	1	---	---	---	---	---	---	---	---	1.01	---	---	---	---	---	---	---	---	---	---	---
	4	1	---	1.04	---	---	---	---	---	---	---	---	---	1.08	---	---	---	---	---	---	---	---
	7	1	2.84	2.49	3.85	1.60	3.64	1.56	2.06	2.24	4.67	2.96	4.51	6.02	1.46	2.53	1.06	2.67	1.96	---	1.00	2.03
	9	1	---	---	---	---	---	---	---	---	1.00	1.01	---	---	---	---	---	---	---	---	---	---
	13	1	2.77	2.42	3.80	1.57	3.59	1.51	2.01	2.17	4.61	2.92	4.43	6.00	1.38	2.49	---	2.61	1.88	---	---	1.96
	19	1	2.81	2.46	3.87	1.63	3.64	1.58	2.06	2.24	4.66	2.99	4.45	6.09	1.42	2.56	1.04	2.68	1.92	---	1.03	2.04
	21	1	---	---	---	---	---	---	---	---	1.02	---	---	---	---	---	---	---	---	---	---	---
	22	1	---	---	---	---	---	---	---	---	---	---	---	1.02	---	---	---	---	---	---	---	---
	25	1	2.99	2.62	3.77	1.60	3.85	1.51	2.13	2.49	4.79	2.96	4.81	6.55	1.52	2.62	1.06	2.68	2.02	---	---	2.08
2nd Floor	31	1	3.31	2.79	3.76	2.33	3.93	1.96	2.32	2.72	4.66	3.13	5.27	6.50	1.83	3.14	1.62	2.70	2.70	---	1.63	2.18
Beams		2	3.28	2.77	3.70	2.30	3.86	1.97	2.31	2.56	4.66	3.13	5.25	6.50	1.80	3.14	1.61	2.66	2.66	---	1.64	2.18
	32	1	3.59	3.07	4.04	2.58	4.26	2.23	2.62	2.99	4.88	3.39	5.57	6.85	2.08	3.44	1.88	2.96	2.96	1.10	1.90	2.45
		2	3.63	3.11	4.10	2.58	4.16	2.29	2.65	2.95	5.08	3.46	5.61	6.90	2.15	3.49	1.93	3.05	3.01	1.11	1.94	2.57
	33	1	3.61	3.11	4.10	2.58	4.16	2.29	2.65	2.95	5.09	3.46	5.62	6.90	2.15	3.49	1.93	3.04	3.01	1.11	1.95	2.61
		2	3.60	3.07	4.05	2.59	4.25	2.22	2.63	3.00	4.87	3.36	5.56	6.85	2.09	3.43	1.88	2.96	2.97	1.10	1.90	2.44
	34	1	3.29	2.78	3.73	2.32	3.84	1.95	2.31	2.58	4.66	3.10	5.26	6.50	1.84	3.14	1.62	2.69	2.69	---	1.63	2.19
		2	3.29	2.78	3.75	2.30	3.96	1.98	2.34	2.71	4.61	3.15	5.26	6.53	1.78	3.17	1.61	2.68	2.66	---	1.64	2.20
3rd Floor	35	1	3.64	3.23	4.04	3.45	4.15	2.24	2.97	2.94	4.09	2.76	6.07	7.35	2.67	4.41	2.01	3.33	3.95	1.26	2.43	2.93
Beams		2	3.65	3.24	4.04	3.46	4.13	2.24	2.97	2.92	4.10	2.70	6.07	7.34	2.67	4.40	2.06	3.34	3.95	1.25	2.43	2.93
	36	1	3.97	3.56	4.38	3.77	4.49	2.55	3.28	3.26	4.44	3.01	6.44	7.70	2.99	4.73	2.35	3.66	4.28	1.54	2.70	3.27
		2	4.07	3.60	4.43	3.79	4.51	2.57	3.37	3.23	4.43	3.01	6.46	7.78	2.99	4.76	2.37	3.68	4.30	1.58	2.76	3.30
	37	1	4.07	3.60	4.43	3.78	4.52	2.57	3.37	3.23	4.42	3.03	6.46	7.78	3.00	4.76	2.36	3.69	4.30	1.57	2.76	3.30
		2	3.97	3.56	4.38	3.76	4.49	2.53	3.28	3.26	4.44	3.01	6.44	7.70	2.96	4.73	2.35	3.64	4.27	1.54	2.71	3.27
	38	1	3.66	3.25	4.06	3.47	4.13	2.25	2.98	2.92	4.09	2.70	6.08	7.33	2.68	4.38	2.09	3.34	3.95	1.27	2.43	2.95
		2	3.67	3.25	4.07	3.47	4.13	2.26	2.96	2.91	4.18	2.73	6.09	7.33	2.68	4.38	2.04	3.37	3.97	1.27	2.42	2.96
4th Floor	39	1	3.71	3.41	4.47	4.65	5.06	3.20	3.13	3.25	3.37	3.57	5.67	6.97	2.58	4.93	1.73	3.66	4.02	1.44	2.97	3.97
Beams		2	3.76	3.37	4.45	4.68	5.05	3.20	3.04	3.25	3.26	3.59	5.58	6.92	2.55	4.93	1.75	3.73	4.02	1.44	2.96	3.98
	40	1	4.15	3.73	4.83	5.08	5.44	3.59	3.46	3.65	3.74	4.02	6.14	7.35	2.92	5.32	2.11	4.08	4.40	1.77	3.36	4.38
		2	4.20	3.74	4.99	5.14	5.47	3.61	3.49	3.62	3.74	4.06	6.09	7.51	2.93	5.35	2.14	4.12	4.43	1.84	3.39	4.42
	41	1	4.20	3.73	4.99	5.13	5.47	3.61	3.49	3.62	3.74	4.06	6.02	7.51	2.93	5.38	2.16	4.12	4.43	1.84	3.39	4.42
		2	4.14	3.73	4.82	5.08	5.45	3.59	3.46	3.65	3.74	4.02	6.17	7.35	2.92	5.31	2.09	4.08	4.40	1.77	3.36	4.38
	42	1	3.80	3.37	4.44	4.69	5.03	3.21	3.04	3.26	3.33	3.62	5.63	6.91	2.58	4.91	1.76	3.73	4.03	1.44	2.97	3.99
		2	3.75	3.41	4.49	4.66	5.05	3.21	3.11	3.27	3.38	3.60	5.72	6.97	2.61	4.90	1.74	3.63	4.03	1.45	2.93	3.98
5th Floor	43	1	3.27	3.74	3.38	4.27	3.84	3.25	3.52	3.44	3.11	2.64	3.98	4.81	2.40	4.24	2.37	3.40	3.49	1.48	3.56	3.94
Beams		2	3.34	3.73	3.45	4.29	3.84	3.25	3.58	3.39	3.10	2.78	3.88	4.84	2.40	4.23	2.37	3.40	3.50	1.47	3.56	3.93
	44	1	3.73	4.14	3.84	4.71	4.25	3.65	3.99	3.89	3.55	3.11	4.37	5.23	2.79	4.65	2.79	3.78	3.93	1.86	3.97	4.38
		2	3.78	4.18	3.90	4.76	4.31	3.69	3.98	3.83	3.58	3.13	4.43	5.28	2.83	4.69	2.83	3.82	3.98	1.89	4.01	4.42
	45	1	3.78	4.18	3.90	4.76	4.31	3.64	3.98	3.83	3.57	3.13	4.42	5.27	2.78	4.69	2.83	3.83	3.98	1.88	4.01	4.42
		2	3.73	4.14	3.83	4.71	4.26	3.66	3.98	3.88	3.55	3.10	4.36	5.25	2.80	4.65	2.79	3.79	3.93	1.85	3.97	4.37
	46	1	3.35	3.72	3.43	4.30	3.83	3.24	3.57	3.37	3.11	2.80	3.89	4.81	2.41	4.22	2.38	3.39	3.51	1.51	3.54	4.00
		2	3.28	3.73	3.43	4.28	3.82	3.29	3.57	3.51	3.12	2.66	3.99	4.81	2.41	4.23	2.38	3.39	3.50	1.48	3.55	3.93
6th Floor	47	1	2.50	2.49	1.75	3.30	3.43	2.16	3.54	3.01	2.39	1.38	2.31	2.59	1.68	3.62	1.84	2.34	2.68	1.02	2.80	3.72
Beams		2	2.50	2.50	1.79	3.31	3.38	2.13	3.70	2.96	2.38	1.41	2.41	2.72	1.71	3.64	1.81	2.39	2.67	1.04	2.77	3.76
	48	1	2.77	2.73	2.04	3.57	3.60	2.37	3.83	3.19	2.68	1.65	2.62	2.97	1.93	3.78	2.11	2.62	2.94	1.32	3.07	3.94
		2	2.78	2.86	2.16	3.50	3.61	2.50	3.82	3.27	2.68	1.66	2.67	2.83	2.08	3.87	2.12	2.58	2.95	1.37	3.02	3.96
	49	1	2.78	2.86	2.12	3.50	3.61	2.46	3.81	3.25	2.68	1.66	2.67	2.83	2.08	3.87	2.11	2.54	2.95	1.37	3.03	3.95
		2	2.77	2.73	2.06	3.56	3.61	2.37	3.82	3.19	2.67	1.65	2.62	2.98	1.93	3.78	2.10	2.68	2.94	1.32	3.07	3.94
	50	1	2.49	2.49	1.81	3.32	3.41	2.16	3.64	3.01	2.49	1.41	2.44	2.67	1.74	3.62	1.93	2.37	2.69	1.08	2.77	3.75
		2	2.49	2.48	1.77	3.32	3.35	2.17	3.65	3.01	2.37	1.37	2.33	2.58	1.69	3.60	1.78	2.33	2.69	1.03	2.77	3.76
Roof	51	1	1.41	1.45	---	1.99	2.64	1.15	2.80	1.69	1.49	---	1.07	1.22	---	3.23	---	1.21	1.44	---	1.84	3.41
Beams		2	1.51	1.59	---	2.00	2.65	1.23	2.92	1.79	1.63	---	1.15	1.36	---	3.29	---	1.30	1.52	---	1.99	3.44
	52	1	1.77	1.85	---	2.29	2.90	1.52	3.18	2.07	1.89	---	1.42	1.55	---	3.48	1.12	1.54	1.84	---	2.20	3.70
		2	1.97	1.96	1.04	2.61	3.04	1.68	3.28	2.22	2.00	---	1.63	1.81	1.01	3.70	1.24	1.77	2.01	---	2.29	3.90
	53	1	1.98	1.96	1.02	2.56	3.12	1.69	3.27	2.25	1.99	---	1.58	1.81	1.00	3.70	1.24	1.77	2.02	---	2.42	3.90
		2	1.77	1.85	---	2.30	2.85	1.50	3.18	2.02	1.90	---	1.42	1.55	---	3.48	1.10	1.54	1.82	---	2.17	3.70
	54	1	1.49	1.56	---	2.05	2.58	1.28	2.90	1.77	1.63	---	1.14	1.34	---	3.30	---	1.27	1.57	---	1.88	3.46
		2	1.39	1.53	---	1.99	2.65	1.15	2.86	1.74	1.53	---	1.05	1.21	---	3.21	---	1.19	1.44	---	1.85	3.42

7.3.3.3 Story Shear Envelopes

Fig. 7-29 plots the story shear envelopes at the design-level earthquake. Good agreement exists between the mean and 'Protected' values. Higher mode demands on the upper floors are noticeable, possibly approaching column capacities.

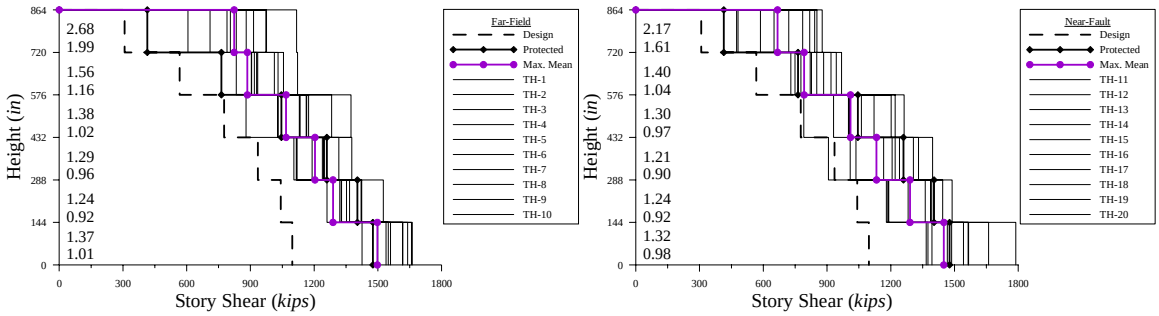

(b) FR-6F-27

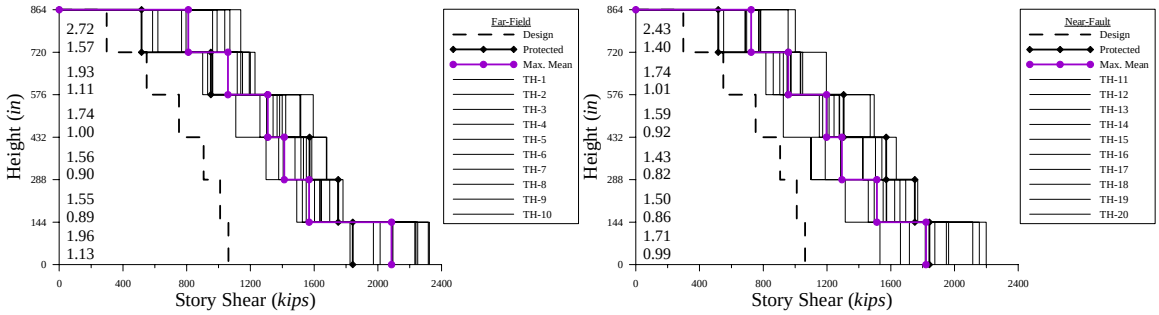

(c) FR-6F-33

Figure 7-29. Story shear envelopes

In comparison with Tables 7-19 and 7-20, it is evident that the proposed capacity design procedure adequately protects non-ductile members from the increase in design story shears due to flexural overstrength and contributions of higher modes. However, capacity design does not also equate to satisfactory performance. While a few columns develop plastic hinges, they do not destabilize the frame enough to develop a soft story.

7.3.3.4 Story Drift Envelopes

Fig. 7-30 illustrates the story drift envelopes at the design-level earthquake. Although cantilever action dominates the response of FR-6F-27, the mean frame response satisfies the drift limit below the effective height. In contrast, FR-6F-33 satisfies the drift limit on the low side due to high elastic stiffness requirements. Although this frame satisfies the drift limit, it has difficulty matching the performance objective.

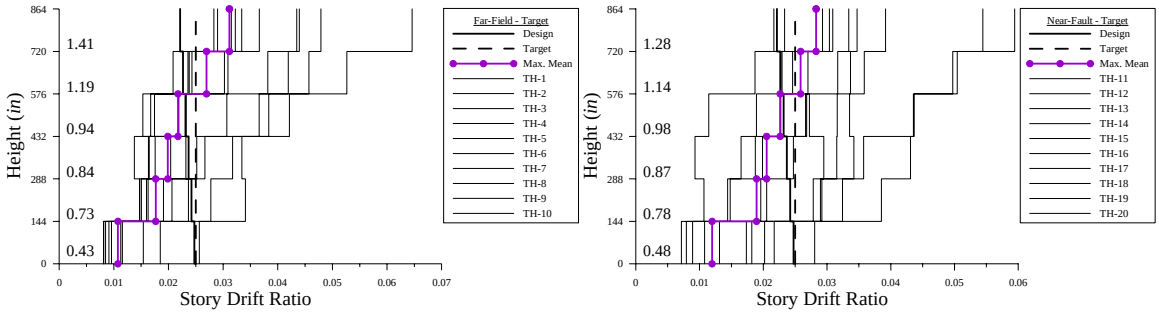

(b) FR-6F-27

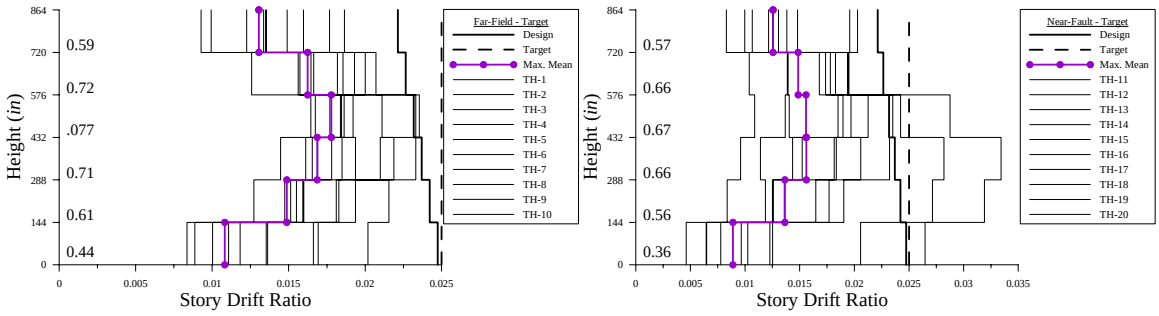

(c) FR-6F-33

Figure 7-30. Drift ratio envelopes (Target - 0.67×MCE)

Fig. 7-31 presents the story drift ratios at the yield-level earthquake. Similarly, frame response indicates that the proposed procedure provides an acceptable value for the yield drift angle.

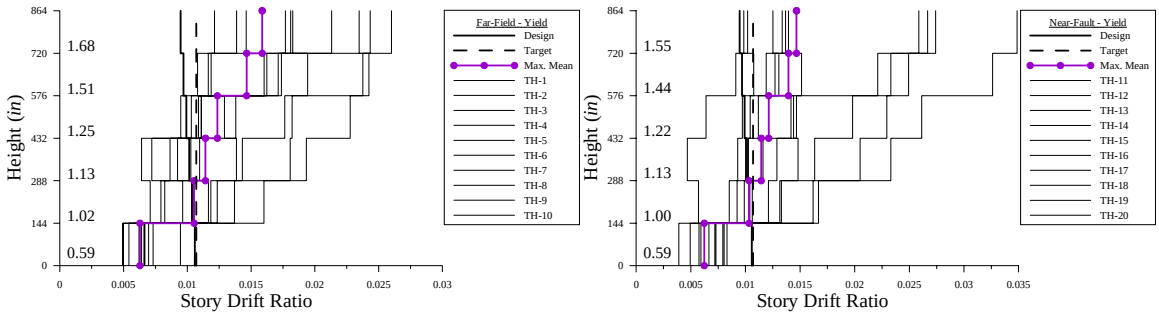

(b) FR-6F-27

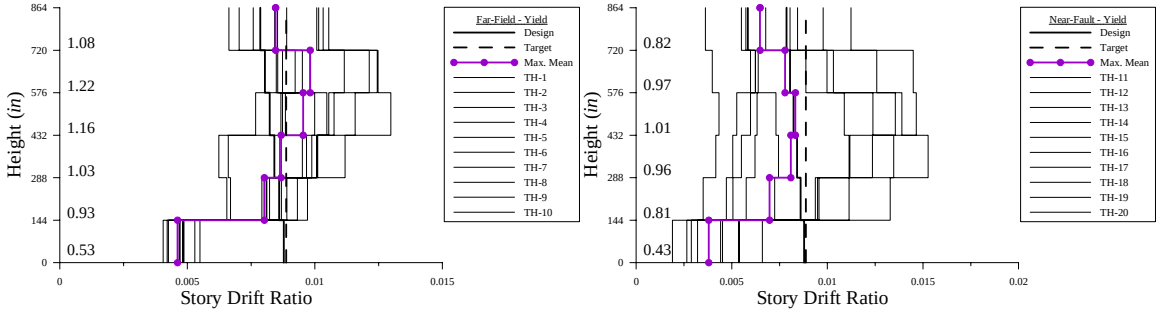

(c) FR-6F-33

Figure 7-31. Drift ratio envelopes (Target - ℜ ×MCE)

7.2.3.5 Effective Height

Fig. 7-32 plots the effective heights for the four levels of earthquake intensity at: (1) each maximum nodal displacement (six floors) and (2) each maximum story shear (six floors) – 120 points for each intensity.

Higher modes in these frames essentially contribute equally to displacement and story shear, a reduction to displacement contributions is evident in FR-6F-33. The standard deviations of these frames are approximately 40% (FR-6F-27) and 38% (FR-6F-33) of the design effective height for displacements and 51% and 52% for story shears respectively. Ultimately, this comparison indicates that these frames exhibit large higher mode contributions. While the analytical response generally agrees with that assumed in design, deviation between design displacement profile and actual benchmark shape is

evident. It is recommended that six-story frames with periods greater than 2 *seconds* be the starting point of a multi-mode DDBD philosophy. .

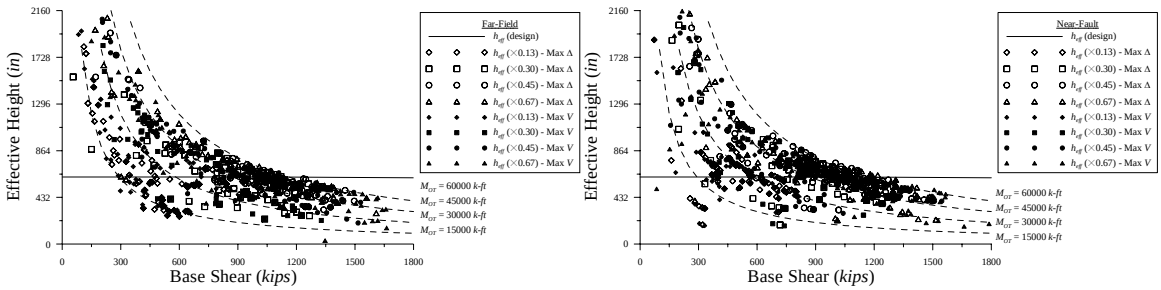

(a) FR-6F-27

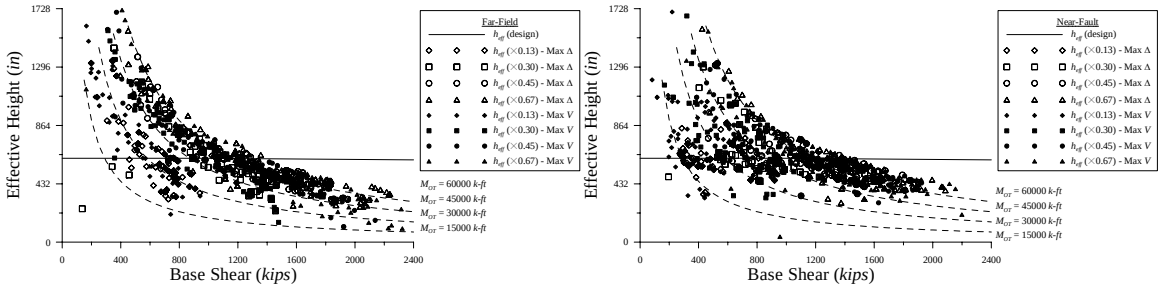

(b) FR-6F-33

Figure 7-32. Effective Height (0.13, ℜ , 0.45, 0.67 × MCE)

7.3.3.6 Serviceability

Figs. 7-33 and 7-34 present the displacement and drift angle envelopes at the service-level earthquake. Assuming the service-level earthquake intensity to be acceptable, FR-6F-27 does not perform satisfactorily in meeting the drift limit. Relaxing the drift limit, as suggested previously, would indicate satisfactory performance. FR-6F-33 indicates satisfactory performance in complying with the service-level drift limit.

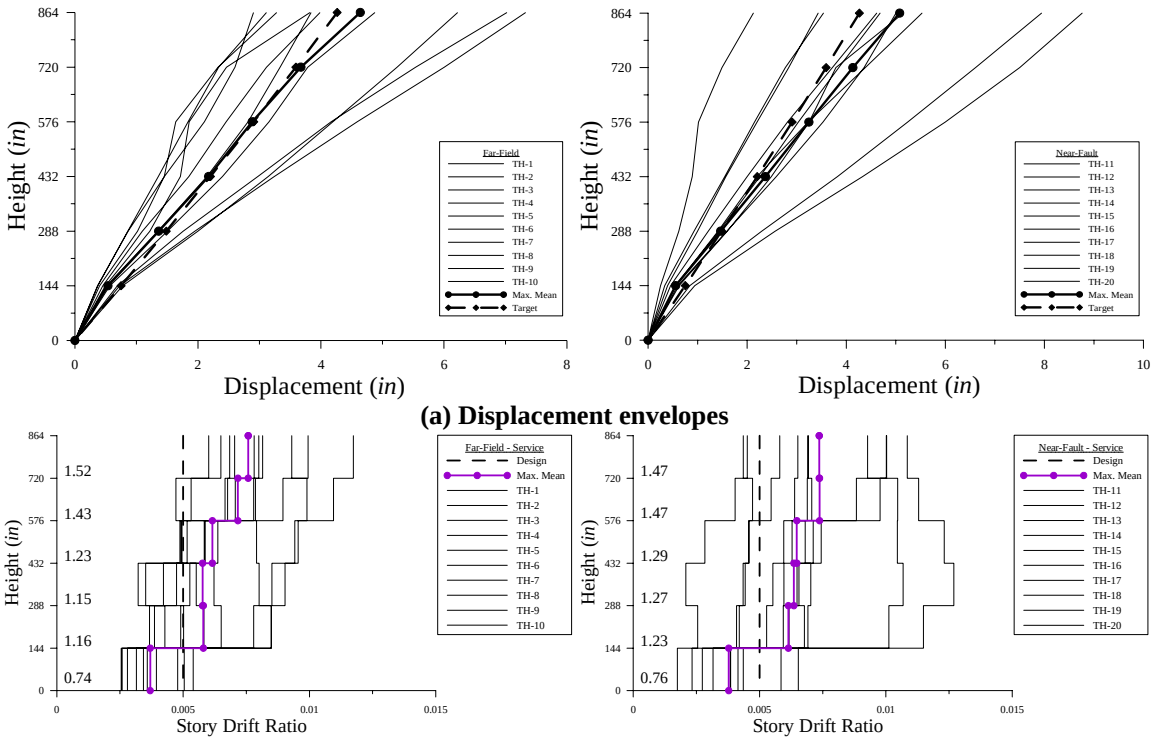

(a) Displacement envelopes

(b) Story drift ratio

Figure 7-33. Serviceability (FR-6F-27)

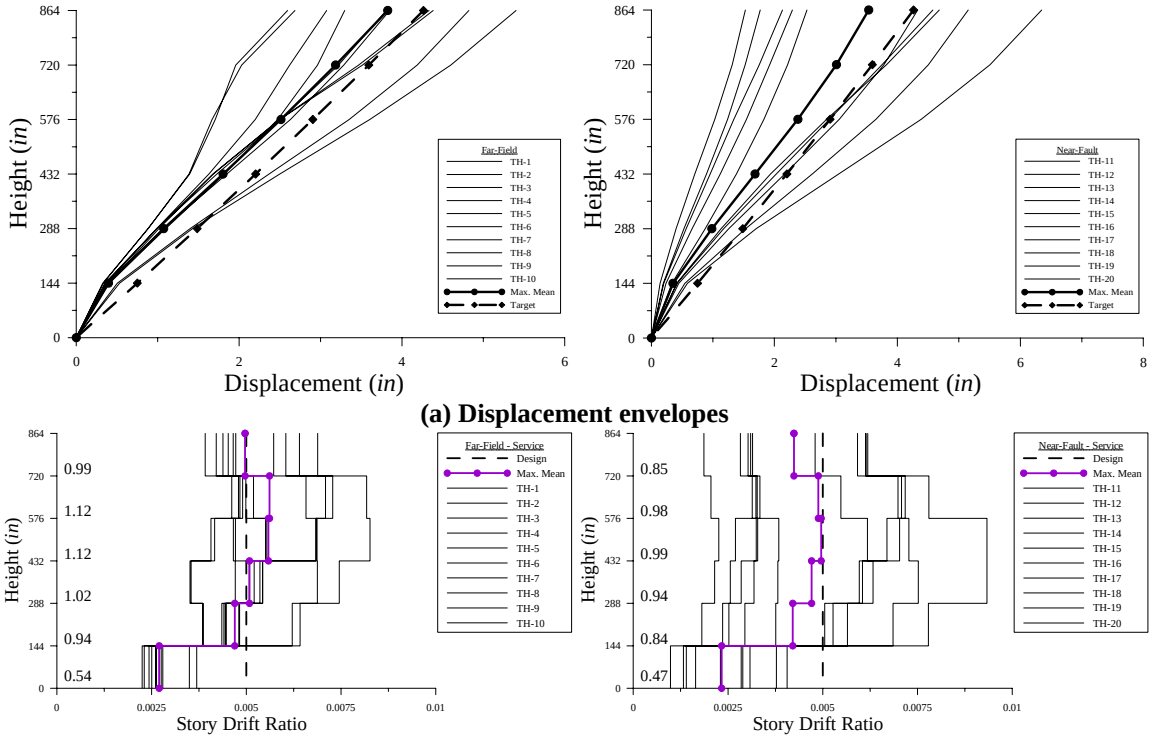

(a) Displacement envelopes

(b) Story drift ratio

Figure 7-34. Serviceability (FR-6F-33)

7.2.3.7 Effective SDOF Displacement Comparison

Fig. 7-35 plots the ratios of actual displacement at the design effective height to design displacement of the effective SDOF and displacement taken from the respective DRS at the target equivalent period and damping. The same conclusions provided for the three-story frame examples are applicable.

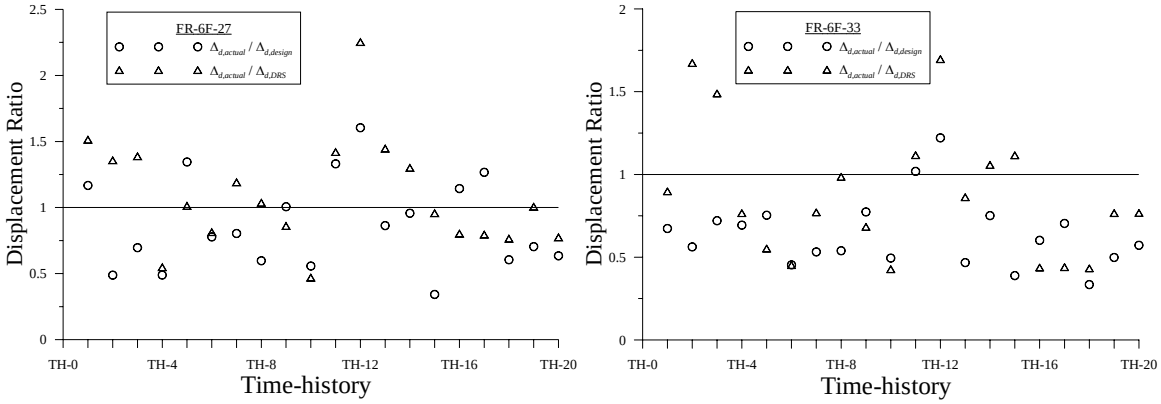

(a) FR-6F-27 **(b) FR-6F-33**

Figure 7-35. Displacement ratio

7.3.3.8 Force-Based Design Parameters

For comparison purposes, the strength-level fundamental period for FR-3F is

$$T_1 = C_u T_a = 1.4(0.028(72^{0.8})) = 1.2\ sec \begin{cases} \text{FR-6F-27 } T_1 = 2.13\ sec \rightarrow \overbrace{0.56}^{ratio} \\ \text{FR-6F-33 } T_1 = 1.97\ sec \rightarrow 0.61 \end{cases}$$

The corresponding strength-level design base shear at first significant yield is

$$V_{by'} = \frac{S_{D1}}{T_1\left(R/I\right)} W_t = \frac{0.66}{1.2(8)} W_t = 0.07 W_t = 619\ kips \begin{cases} \text{FR-6F-27 } V_{by} = 1097\ kips \rightarrow \overbrace{0.56}^{ratio} \\ \text{FR-6F-33 } V_{by} = 1062\ kips \rightarrow 0.58 \end{cases}$$

This yields a design lateral force distribution (k = 1.35) and magnitude of

$$\{\phi_f\} = \begin{Bmatrix} 0.33 \\ 0.25 \\ 0.19 \\ 0.13 \\ 0.07 \\ 0.03 \end{Bmatrix} = \begin{Bmatrix} 1.00 \\ 0.78 \\ 0.58 \\ 0.39 \\ 0.23 \\ 0.09 \end{Bmatrix} \overbrace{\begin{Bmatrix} 1.00 \\ 0.83 \\ 0.65 \\ 0.47 \\ 0.28 \\ 0.11 \end{Bmatrix}}^{\text{FR-6F-27}} \overbrace{\begin{Bmatrix} 1.00 \\ 0.85 \\ 0.67 \\ 0.46 \\ 0.26 \\ 0.09 \end{Bmatrix}}^{\text{FR-6F-33}} \text{ and } \{F_x\} = \begin{Bmatrix} 202 \\ 158 \\ 117 \\ 79 \\ 46 \\ 18 \end{Bmatrix} kips$$

As evident, the base shear and corresponding design forces are smaller than those used in the previous DDBD example, albeit independent of frame and member geometry. However, the force distribution agrees well with the fundamental mode shapes. It follows that the displacement profile due to the displacement-level lateral forces and expected inelastic displacements should be limited to

$$\{\delta_{ex}\} = \begin{Bmatrix} 3.00 \\ 2.35 \\ 1.74 \\ 1.18 \\ 0.68 \\ 0.27 \end{Bmatrix} in. \ (\theta_{ex} = 0.46\%) \text{ and } \{\delta_{in}\} = \begin{Bmatrix} 16.50 \\ 12.90 \\ 9.54 \\ 6.47 \\ 3.47 \\ 1.47 \end{Bmatrix} in. \ (\theta_{in} = 2.5\%)$$

7.4 Idealized Frames (FR-3F-24I and FR-6F-27I)

As illustrated previously, earthquake characteristics, higher mode contributions, flexural overstrength coupled with increased stiffness, and base hinge formations are the primary sources for variation between the analytical results and design parameters. Two idealized frames are evaluated in an effort to examine the extent of the latter two causes.

7.4.1 Frame Model and Design

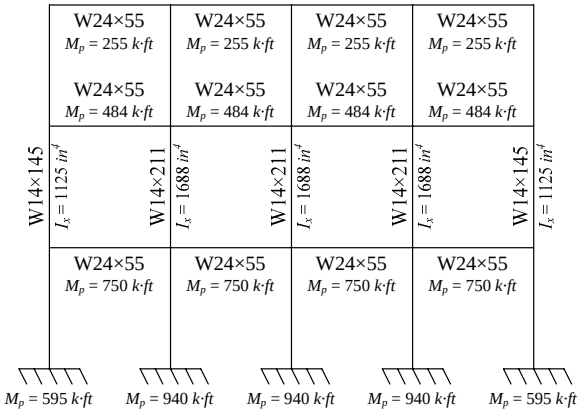

(i) Frame schematic

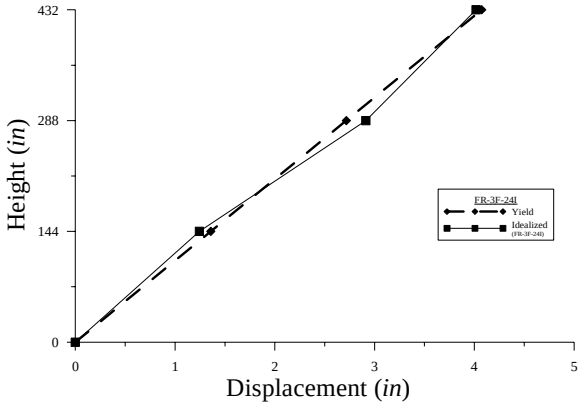

(ii) Displacement profile

(a) FR-3F-24I

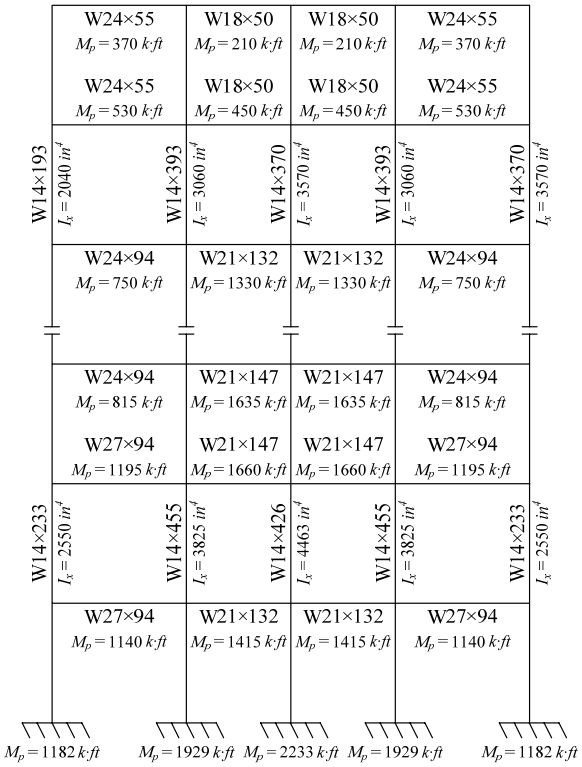

(i) Frame schematic

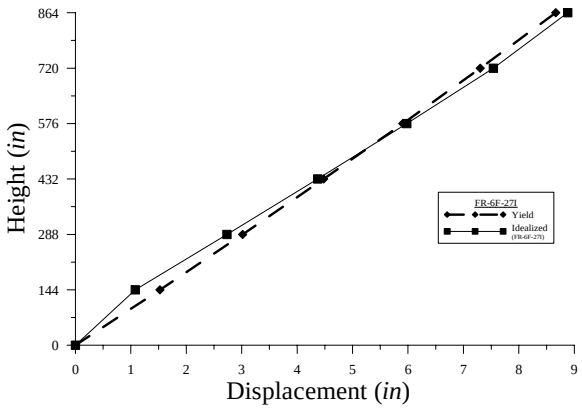

(ii) Displacement profile

(b) FR-6F-27I

Figure 7-36. Frame design

Fig. 7-36 presents the idealized frame designs and displacement profiles. In constructing the idealized frames, the moment of inertia of the columns, I_c, is varied

until convergence on the target fundamental period. The plastic moment capacities of the beams and base hinges are set equal to that developed under the design forces. Floor flexural overstrength values are thus all equal to 1.1.

Table 7-21. Actual dynamic properties (Idealized)

Property	FR-3F-24I		FR-6F-27I	
	Elastic	Ratio	Elastic	Ratio
M_{eff}	6612	0.99	18610	0.98
h_{eff} (*in*)	337	1.00	635	1.02
P_{eff} (*kips*)	2555	0.99	7017	0.95
Γ_1	1.253	0.97	1.365	0.99
T_{eff^2} (*sec*)	1.29	1.00	2.21	1.00
T_{eff^1} (*sec*)	1.26	1.00	2.13	1.00
K_{eff^2} (*kips/in*)	157.6	1.00	150.0	0.98
K_{eff^1} (*kips/in*)	165.7	1.00	161.6	0.98

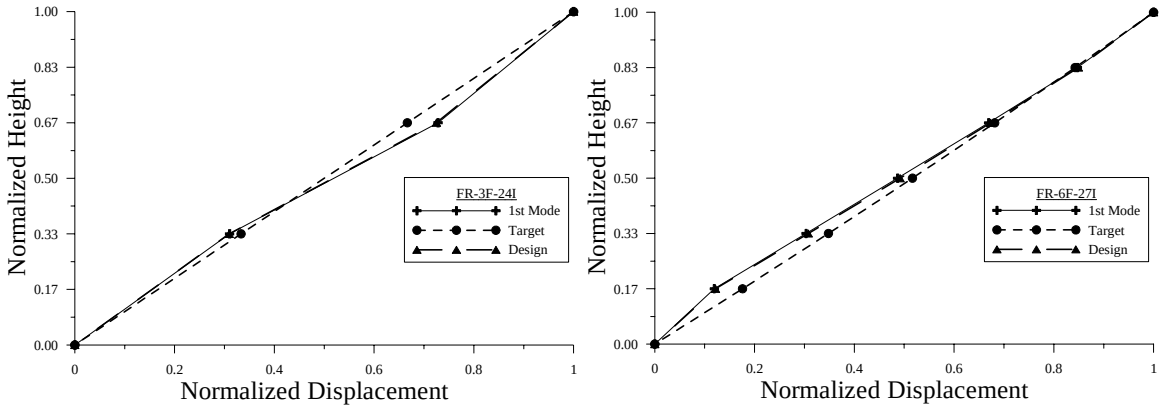

(a) FR-3F-24I **(b) FR-6F-27I**

Figure 7-37. Normalized 1st mode shape

Table 7-21 lists the actual dynamic properties of the designed frames. Fig. 7-37 illustrates the normalized 1st mode shapes. It is evident that the mode shapes are dependent on story stiffness distribution. The yield displacement profile for frames with *n* > 4could be revised to that indicated in Fig. 7-37.

7.4.2 Monotonic Static Pushover Analysis

Fig. 7-38 presents the pushover curves of each frame under the design force distribution. As evident, the assumed post-yield stiffness is not accurate compared to the actual pushover curve. The 1st order post-yield stiffness ratio, r_{Δ^1}, is 0.04.

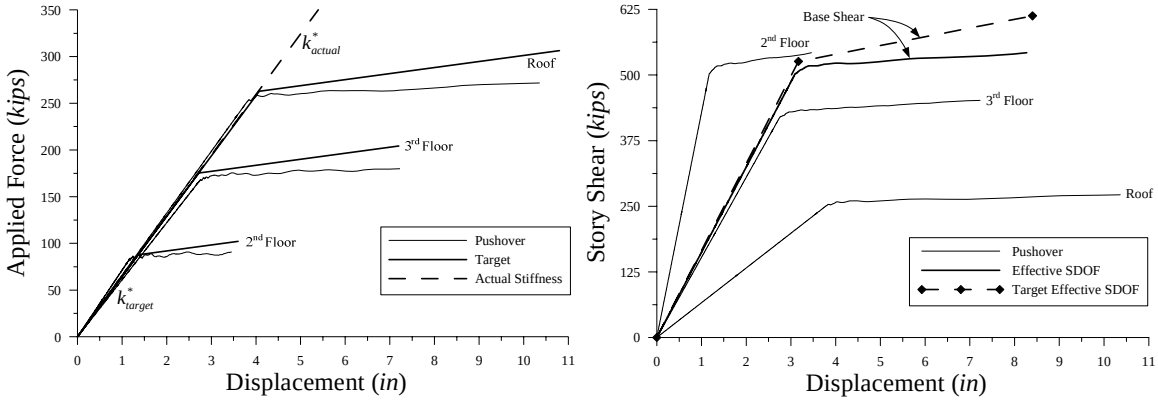

(i) Lateral force pushover **(ii) Story shear pushover**

(a) FR-3F-24I

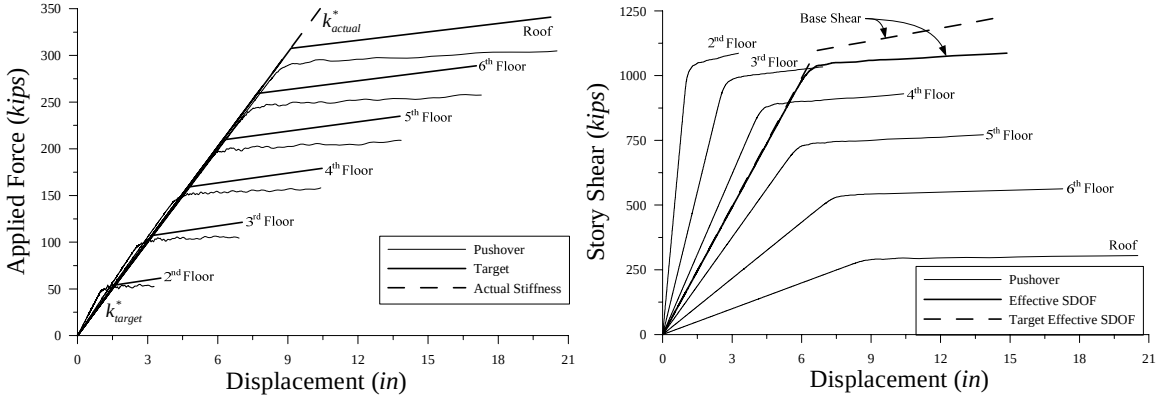

(i) Lateral force pushover **(ii) Story shear pushover**

(b) FR-6F-27I

Figure 7-38. 1st mode pushover curves

Applying the revised post-yield stiffness ratio in the proposed procedures and performing another pushover illustrates agreement (see Fig. 7-39). This suggests that post-yield stiffness is dependent upon column stiffness and base hinges formation.

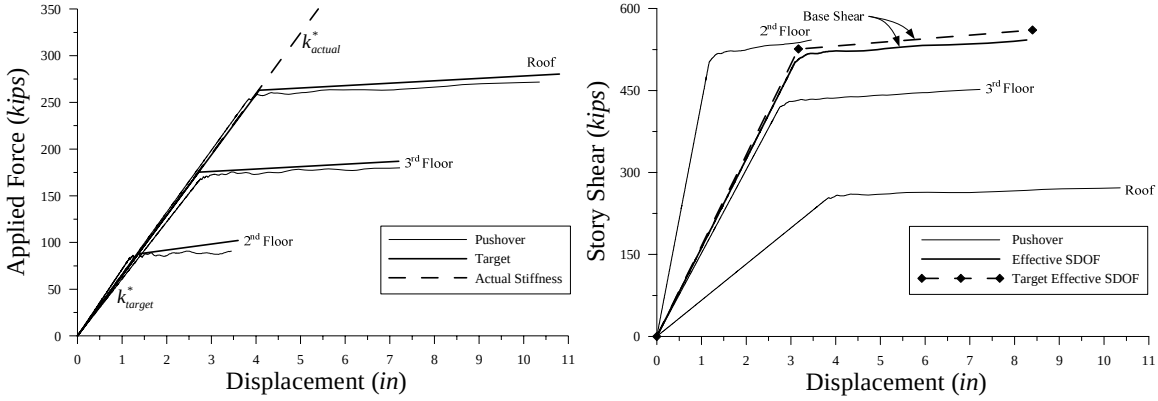

(i) Lateral force pushover **(ii) Story shear pushover**

(a) FR-3F-24I-A

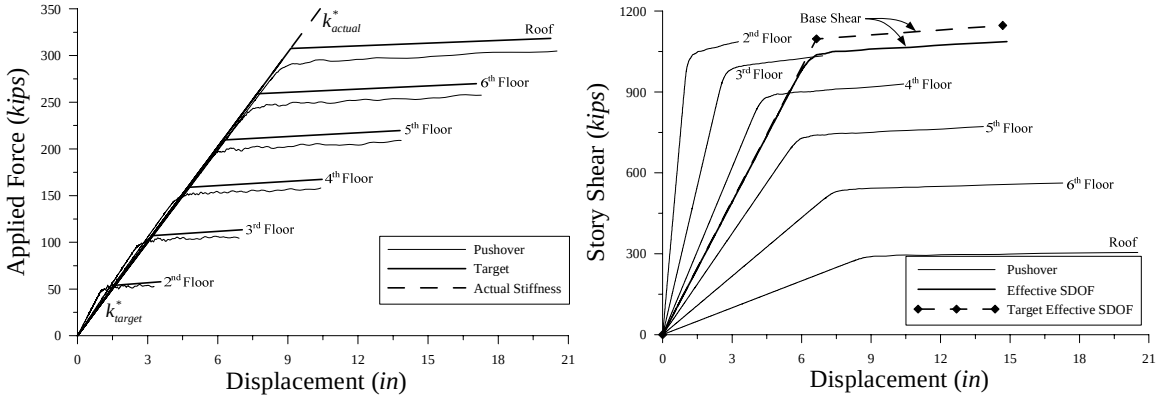

(i) Lateral force pushover **(ii) Story shear pushover**

(b) FR-6F-27I-A

Figure 7-39. Revised 1st mode pushover curves

Revising the post-yield stiffness, however, increases the degree of equivalent damping resulting in a lengthening of the equivalent period. As a result, the design forces would change accordingly. For this examination, the original elastic design values remain unchanged since the fundamental period is matched to the original target. Inelastic dynamic analysis results could therefore exceed the target values. Although analytical deviations are expected, the objective of this discussion is to examine the effects of matching the design objective at the yield point.

Table 7-22 presents the predicted static and dynamic response curve ordinates of the designed frames using the revised post-yield stiffness ratio. Fig. 7-40 illustrates the effective SDOF 'target' and expected 'static' and 'dynamic' pushover curves for each frame. The monotonic pushover curve for each frame subjected to the design force distribution is also shown. The original target curve is included for comparison purposes.

Table 7-22. Static and dynamic predicted pushover ordinates (Idealized)

Frame	Ω^o	Λ^o	Θ^o	Δ_y^o (*in*)	$F_{y^2}^o$ (*kips*)	$F_{y^1}^o$ (*kips*)	Δ_d^o (*in*)	$F_{d^2}^o$ (*kips*)	$F_{d^1}^o$ (*kips*)	ϕ_p^o	$F_{y^1}^d$ (*kips*)	$F_{d^1}^d$ (*kips*)
FR-3F-24I	1.00	0.98	0.99	3.12	492	516	8.27	485	548	1.17	601	639
FR-6F-27I	0.96	0.95	0.95	6.27	967	1041	13.92	988	1153	1.23	1275	1415

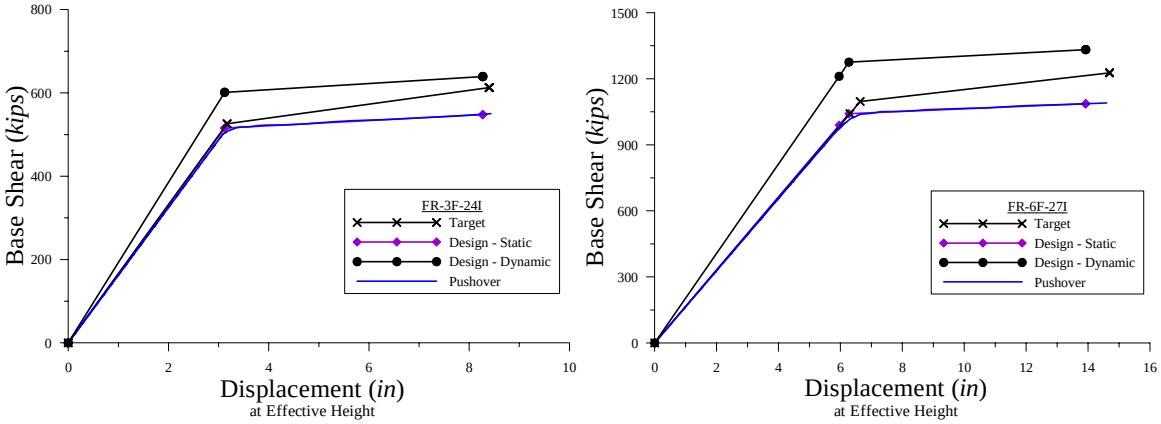

(a) FR-3F-24I **(b) FR-6F-27I**

Figure 7-40. Target and predicted pushover curves

7.4.3 Dynamic Analysis

7.4.3.1 Displacement Envelopes and Dynamic Response Curves

Figs. 7-41 and 7-42 present the displacement envelopes for the frames at the yield-level ($\Re \times$MCE) and design-level (0.67 × MCE) earthquake.

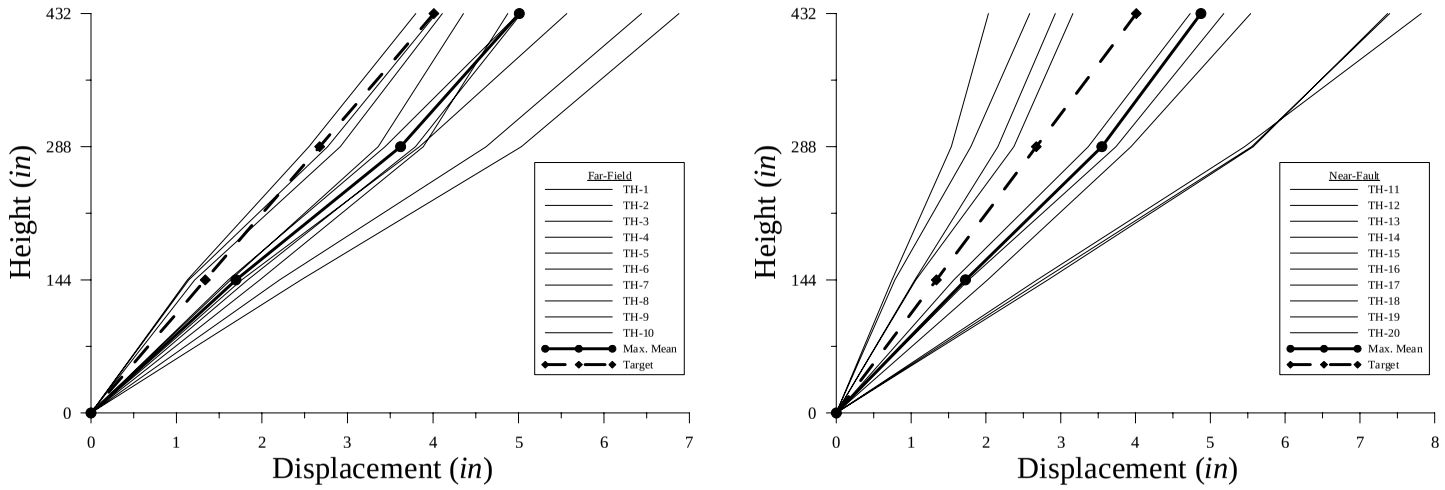

(a) Displacement profile (Yield – 0.25 × MCE)

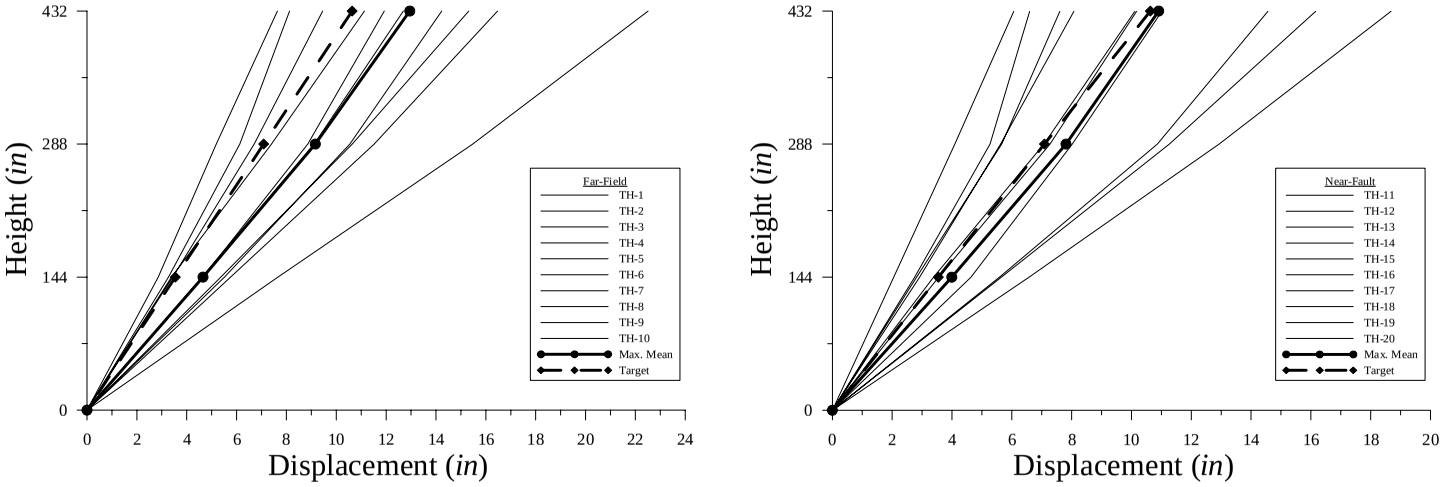

(b) Displacement profile (Target - 0.67 × MCE)

Figure 7-41. FR-3F-24I inelastic dynamic analysis results

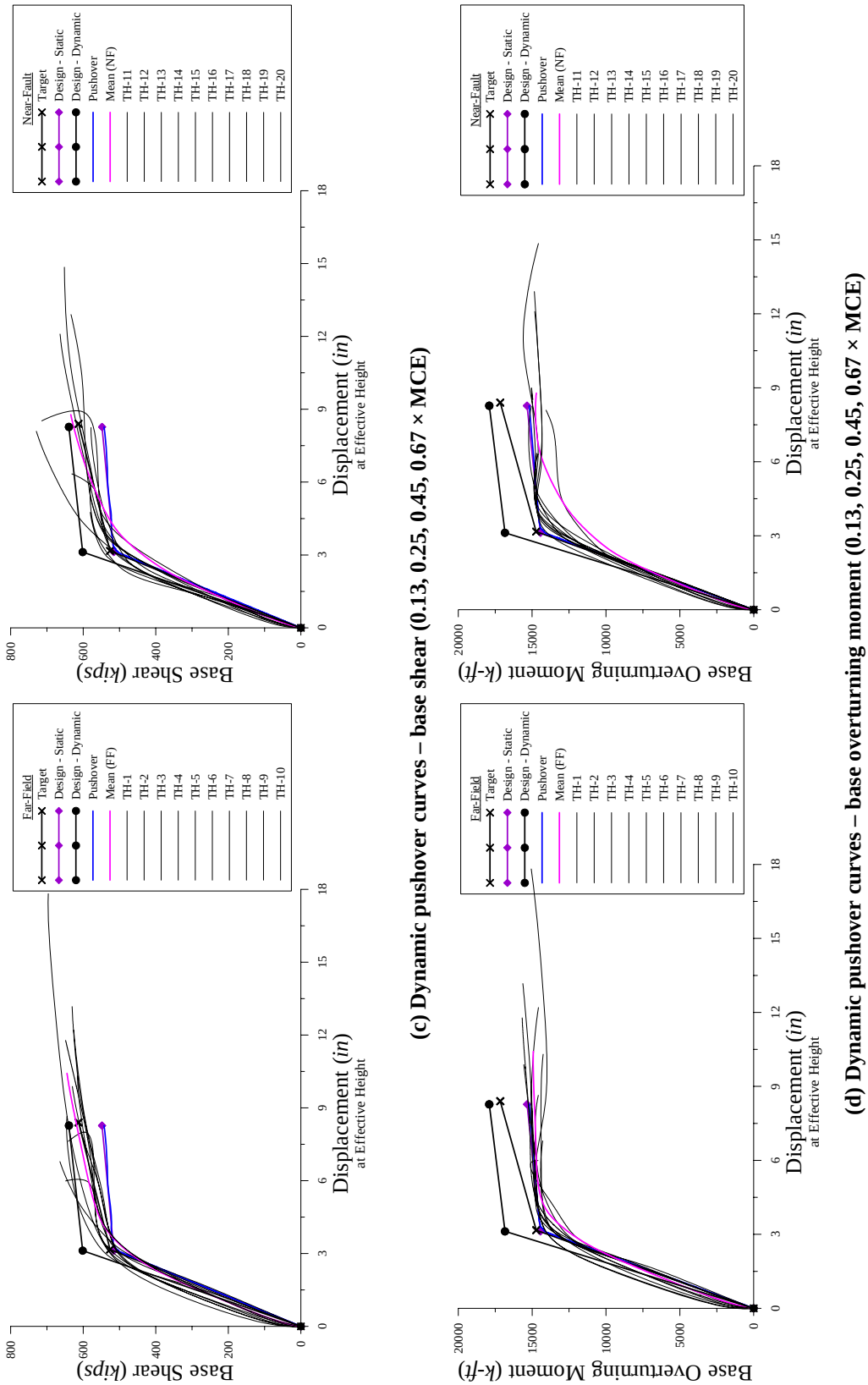

(c) Dynamic pushover curves – base shear (0.13, 0.25, 0.45, 0.67 × MCE)

(d) Dynamic pushover curves – base overturning moment (0.13, 0.25, 0.45, 0.67 × MCE)

Figure 7-41. FR-3F-24I inelastic dynamic analysis results (Cont'd)

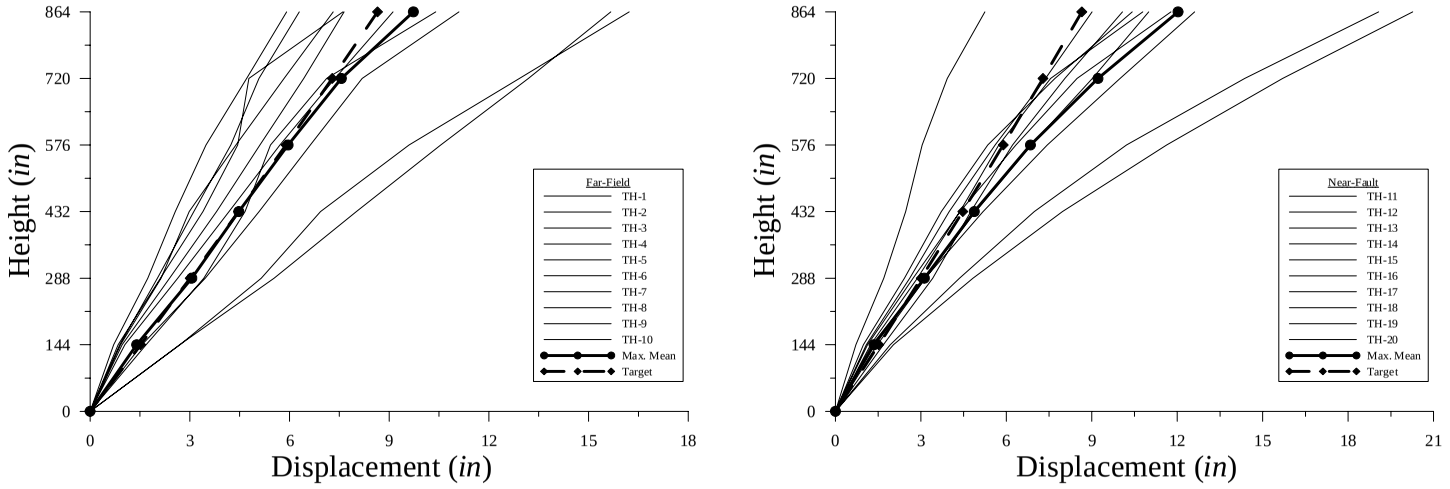

(a) Displacement profile (Yield – 0.30 × MCE)

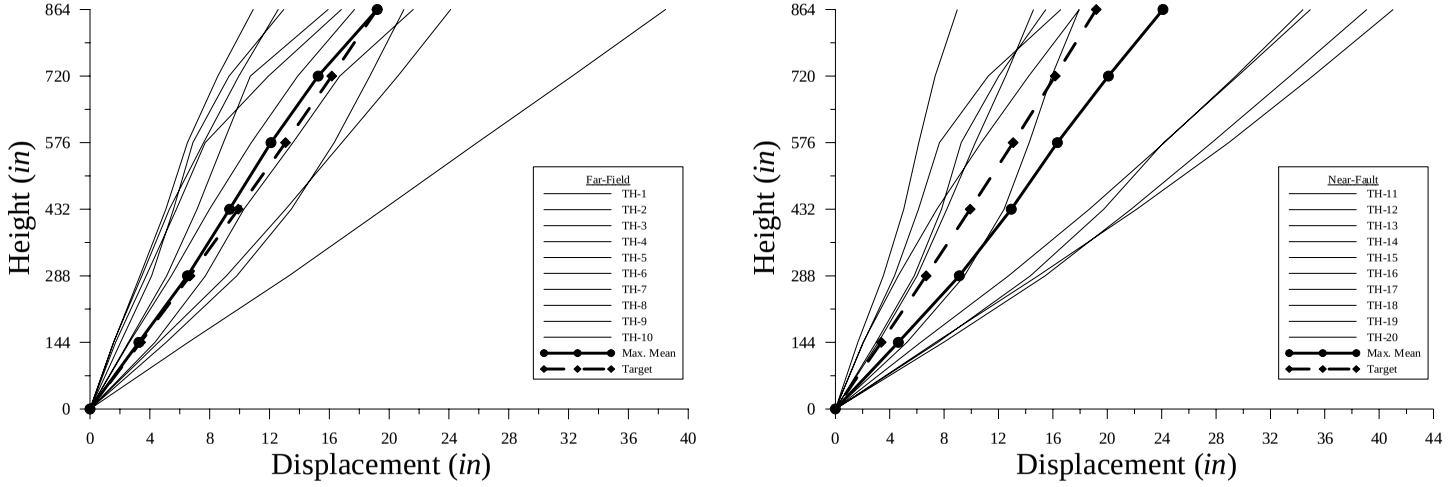

(b) Displacement profile (Target - 0.67 × MCE)

Figure 7-42. FR-6F-27I inelastic dynamic analysis results

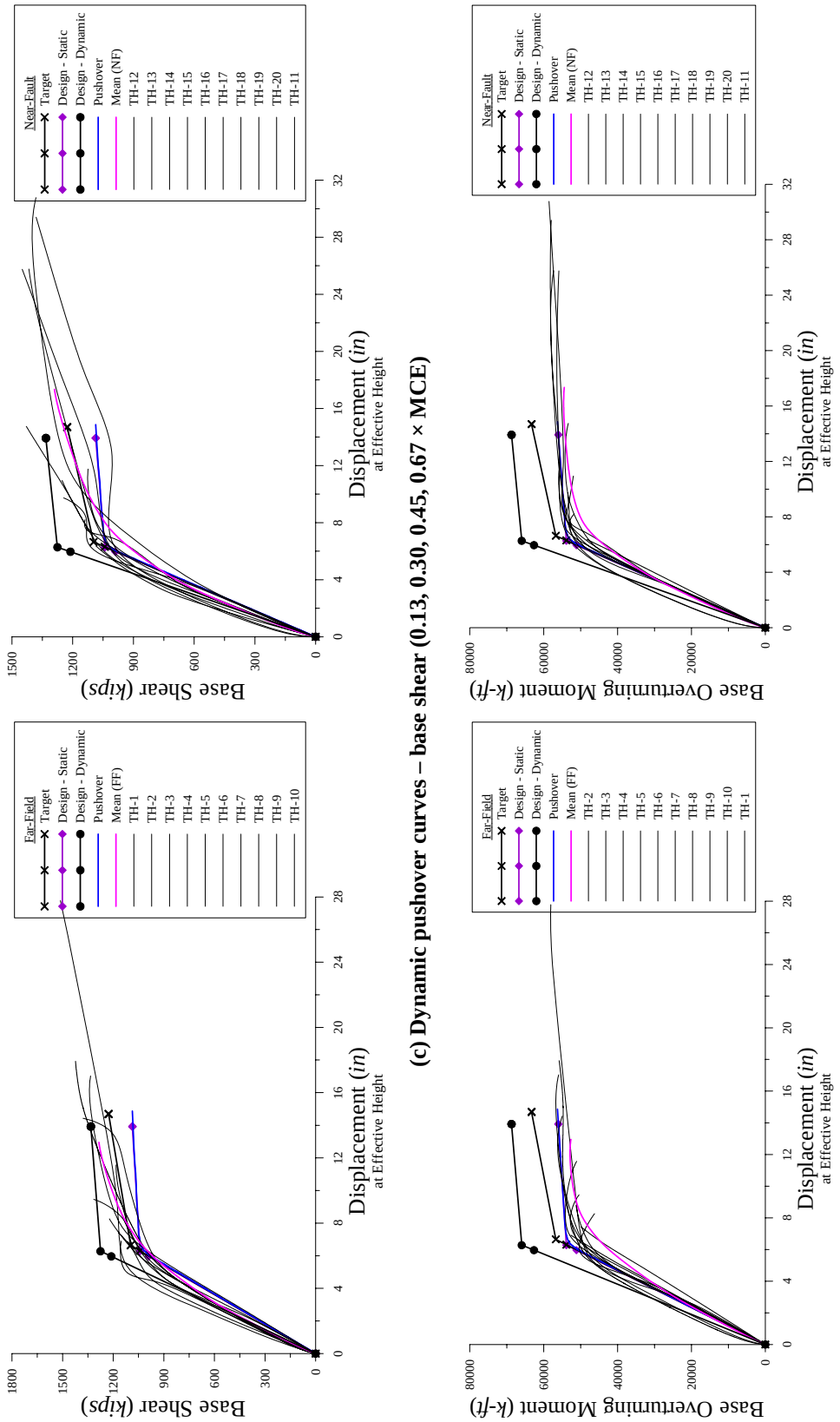

(c) Dynamic pushover curves – base shear (0.13, 0.30, 0.45, 0.67 × MCE)

(d) Dynamic pushover curves – base overturning moment (0.13, 0.25, 0.45, 0.67 × MCE)

Figure 7-42. FR-6F-27I inelastic dynamic analysis results (Cont'd)

FR-3F-24I

As seen in Fig. 7-41(a) and (b), the analytical results exceed the target values as previously discussed. In truth, the idealized frame would need to be redesigned since the elastic stiffness would change (via the revised beam yield rotations) thus altering the lateral force magnitude at yield. Still, a trend exists illustrating that cantilever action does not dominate frame response implying that base hinge formation is one way to counteract this phenomenon. The frequency content and magnitudes are such that higher modes from earthquake characteristics contribute little to frame behavior. Higher mode effects are mostly due to localized stiffness reductions.

FR-6F-27I

As seen in Fig. 7-42(a) and (b), excellent agreement exists between the mean envelopes and target profiles for the far-field earthquakes. Unlike FR-3F-24I, the increase in hysteretic damping does not lead to displacement results in excess of the target. This indicates that in longer period frames, peak displacements are somewhat insensitive to the degree of damping. The frequency content and magnitudes are such that higher modes contribute slightly to frame behavior for the far-field earthquakes. The results indicate that higher modes contribute more due to localized stiffness reduction in the inelastic range. Lastly, cantilever action does not dominate the response of this frame indicating that the target displacement profile is satisfactory for design and requires base hinges.

7.4.3.2 Story Shear Envelopes

Fig. 7-43 plots the story shear envelopes at the design-level earthquake. Similar story shear effects illustrated by the actual frames are evident. However, story shear amplification in this case is directly due to higher mode contributions and secondary behavioral response.

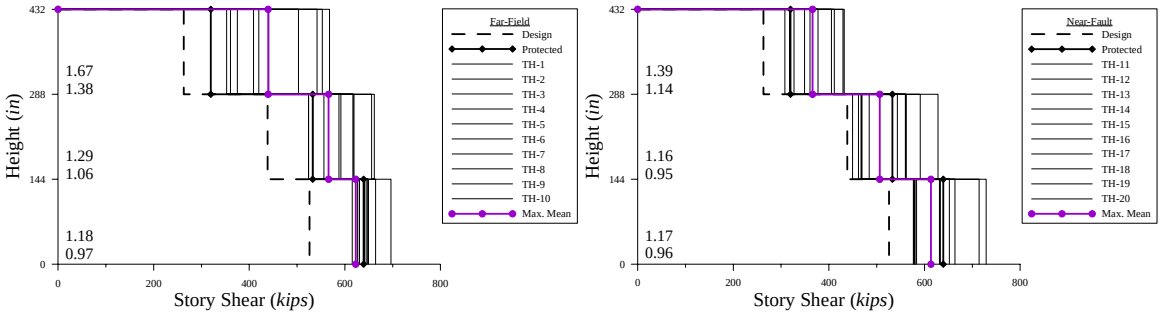

(b) FR-3F-24I

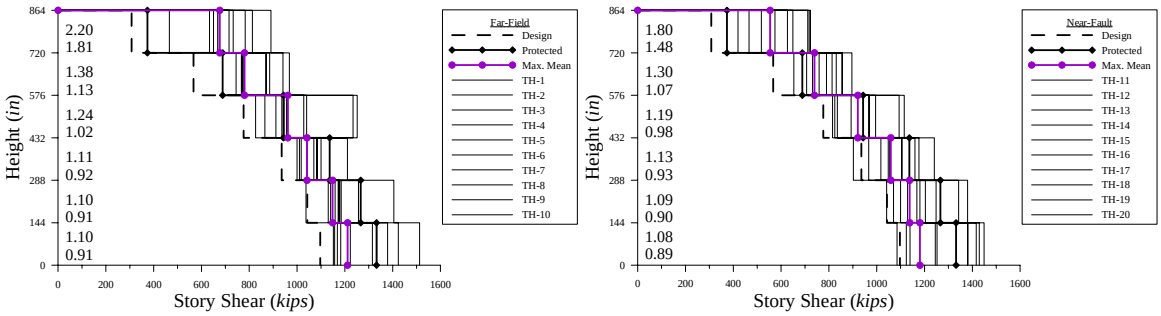

(c) FR-6F-27I

Figure 7-43. Story shear envelopes

7.4.3.3 Story Drift Envelopes

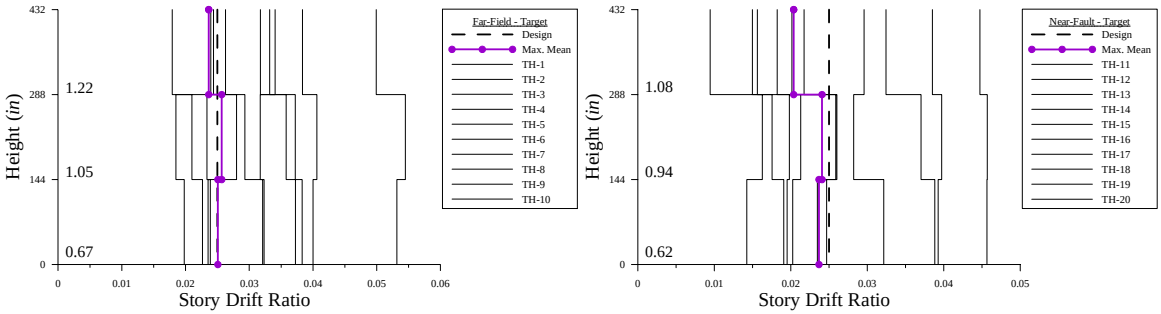

(b) FR-3F-24I

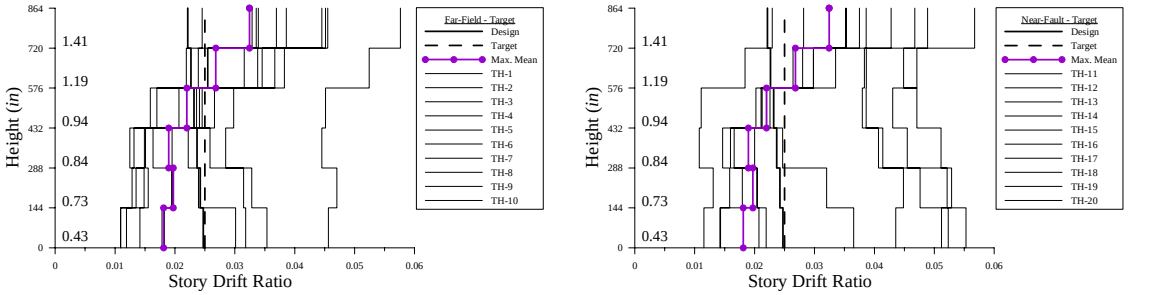

(c) FR-6F-27I

Figure 7-44. Drift ratio envelopes (Target - 0.67×MCE)

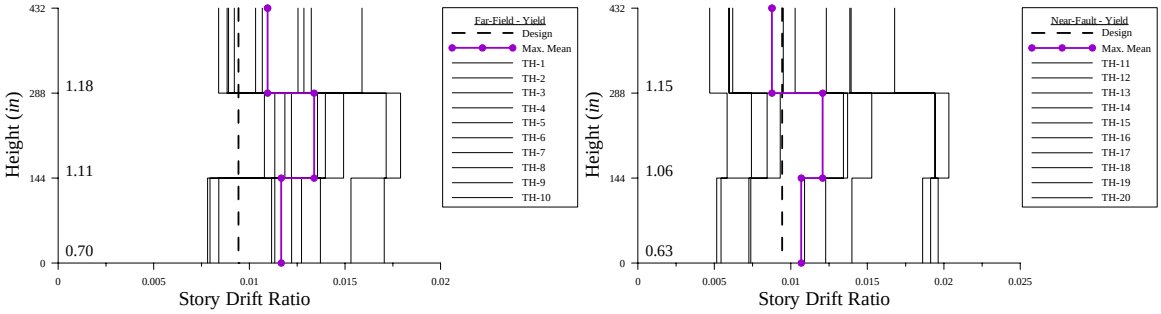

(b) FR-3F-24I

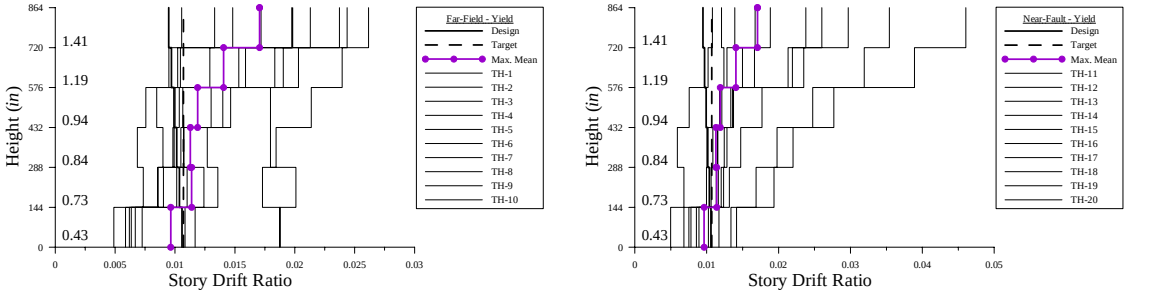

(c) FR-6F-27I

Figure 7-45. Drift ratio envelopes (Target - ℜ ×MCE)

Fig. 7-44 illustrates the story drift ratio envelopes. Both frames perform well in meeting the performance target.

Fig. 7-45 presents the story drift ratios at the yield-level earthquake. As indicated previously, the drifts exceed the target. FR-6F-27I indicates cantilever action at the yield-level further suggesting that the design displacement profile at yield could be revised accordingly. In this case, design forces would be amplified during capacity design to account for inelastic redistribution of the displacement profile.

7.4.3.4 Effective Height

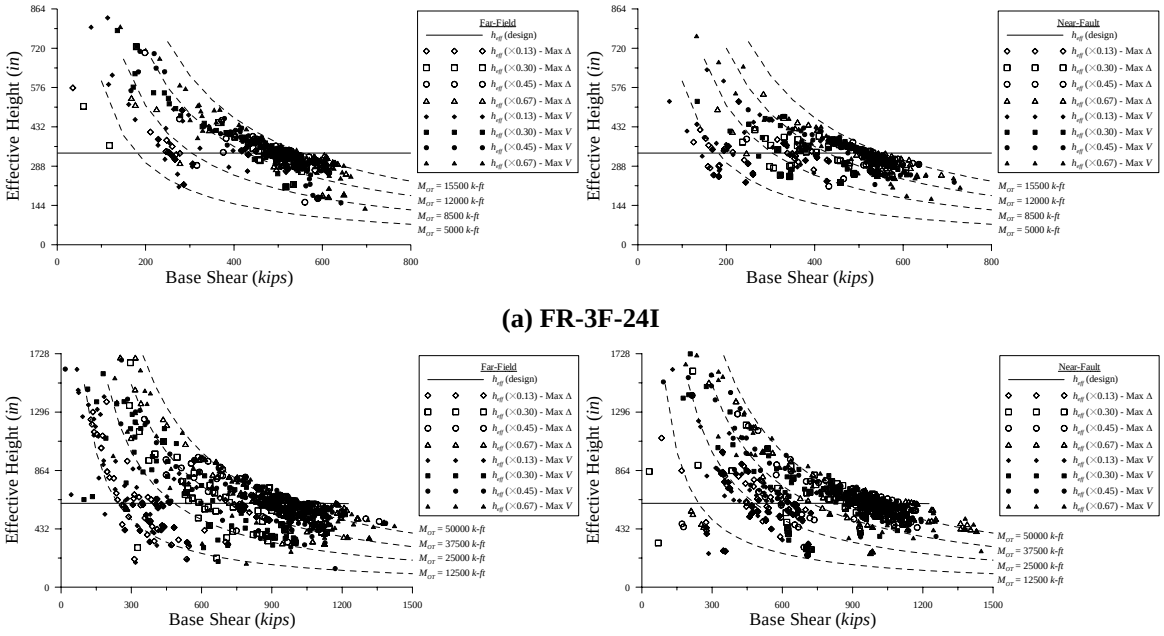

(a) FR-3F-24I

(b) FR-6F-27I

Figure 7-46. Effective Height (0.13, ℜ , 0.45, 0.67 × MCE)

Fig. 7-46 plots the effective heights for four levels of earthquake intensity at: (1) each maximum nodal displacement (three and six floors) and (2) each maximum story shear (three and six floors) – 60 and 120 points for each intensity respectively. FR-3F-24I

indicates good agreement with the design effective height whereas FR-6F-27I exhibits a wider dispersion due to higher mode contributions.

7.4.3.5 Serviceability

Figs. 7-47 and 7-48 present the displacement and drift angle envelopes at the service-level earthquake. Although the performance target is exceeded as was expected, the frames respond in a more linear fashion.

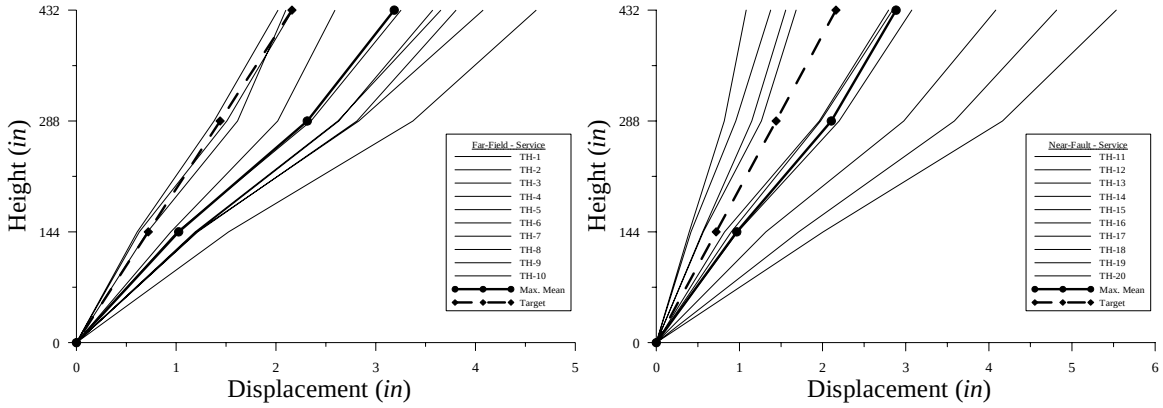

(a) Displacement envelopes

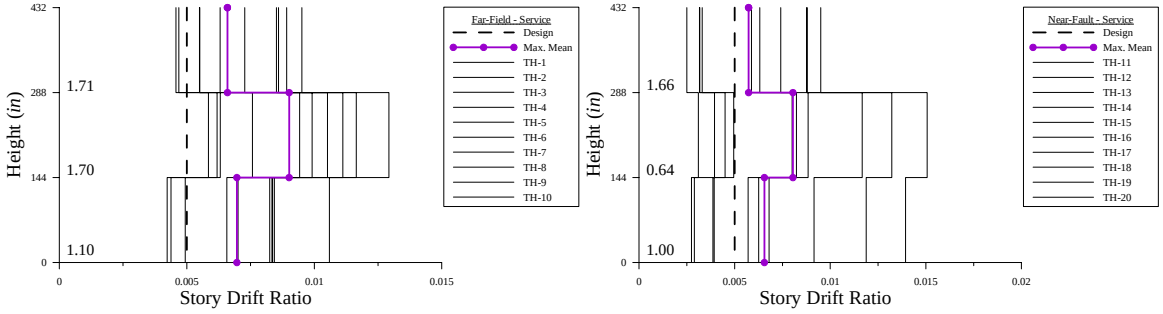

(b) Story drift ratio

Figure 7-47. Serviceability (FR-3F-24I)

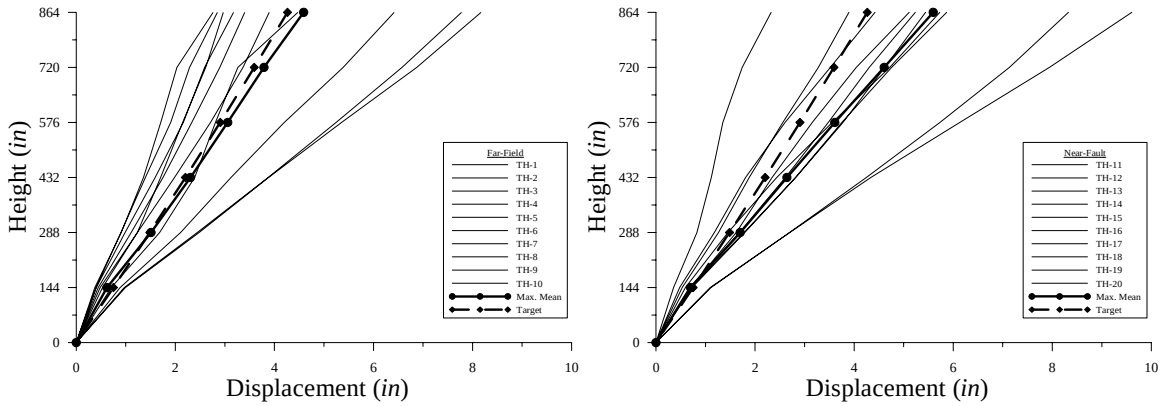

(a) Displacement envelopes

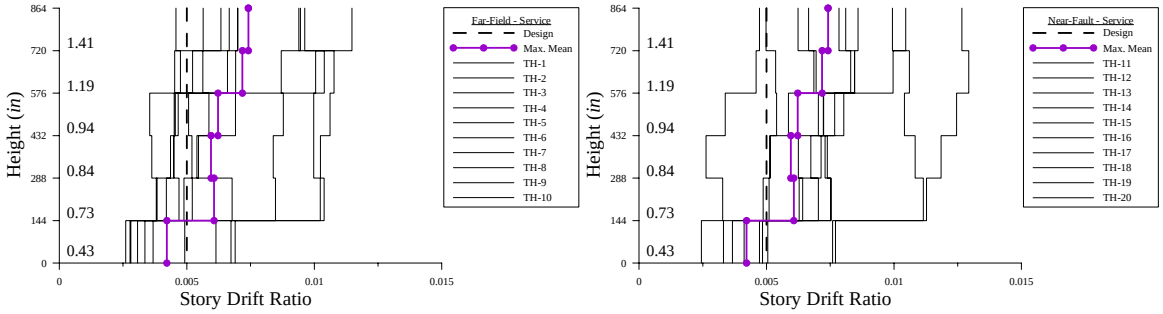

(b) Story drift ratio

Figure 7-48. Serviceability (FR-6F-27I)

7.5 Evaluation of Higher Modes (FR-3F-24H and FR-6F-27H)

As discussed in the previous sections, higher modes play a role in frame response. These higher modes originate from two factors: (1) excitation characteristics and (2) localized stiffness reduction due to formation of plastic hinges. It was noted that higher modes can contribute more to story shear than displacements. What is not clear is the magnitude of higher mode contributions to frame displacements. The target displacement profiles are based on the fundamental mode although the damping modification factor is statistically derived to include some contributions from higher modes. Therefore, it is important to examine the extents of higher modes.

7.5.1 Frame Model and Design

The two designed frames selected in Section 7.4, classified as FR-3F-24H and FR-6F-27H, are evaluated. For FR-3F-24H, earthquake records are filtered with a low-pass filter to remove excitation frequencies above the mean of: (1) first and second modes (f = 1.94 *Hz*) and (2) second and third modes (f = 4.41 *Hz*). For FR-6F-27H, earthquake records are filtered at: (1) first and second modes (f = 0.92 *Hz*), (2) second and third modes (f = 2.03 *Hz*), and (3) third and fourth modes (f = 3.60 *Hz*). This is done in an attempt to excite only the 1st, 1st and 2nd, and 1st through 3rd (FR-6F-27H only) modes.

7.5.2 Displacement Envelopes and Dynamic Response Curves

Figs. 7-49 and 7-50 present the displacement envelopes and dynamic pushover curves from the dynamic analysis for FR-3F-24H at the yield-level ($\Re \times$ MCE) and design-level (0.67 × MCE) earthquakes. Figs. 7-51 and 7-52 present the displacement envelopes and dynamic pushover curves for FR-6F-27H. The figures are categorized by the filtered records.

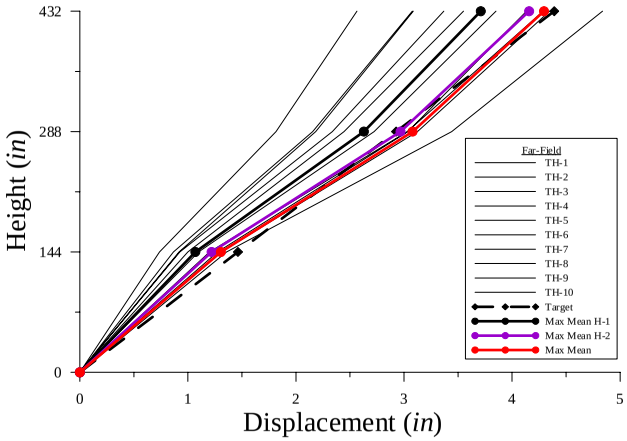

(i) 1st mode

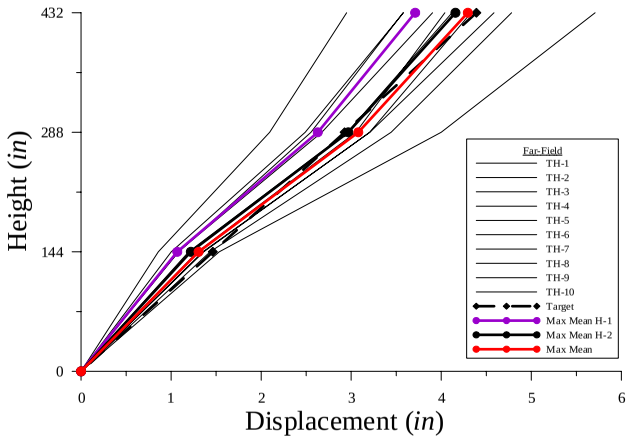

(ii) 1st and 2nd mode

(a) Displacement profile (Yield – 0.25 × MCE)

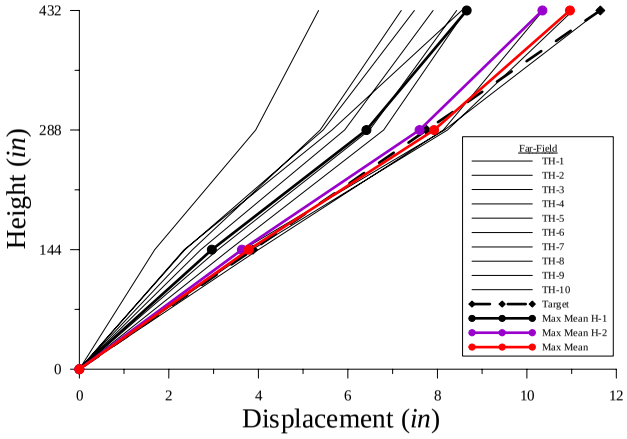

(i) 1st mode

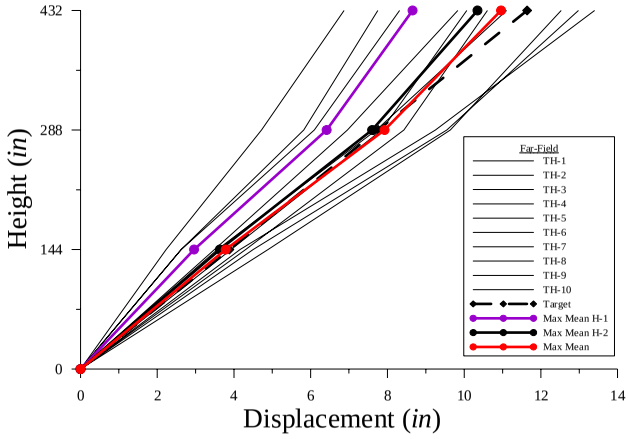

(ii) 1st and 2nd mode

(b) Displacement profile (Target - 0.67 × MCE)

Figure 7-49. FR-3F-24H inelastic dynamic analysis results (far-field)

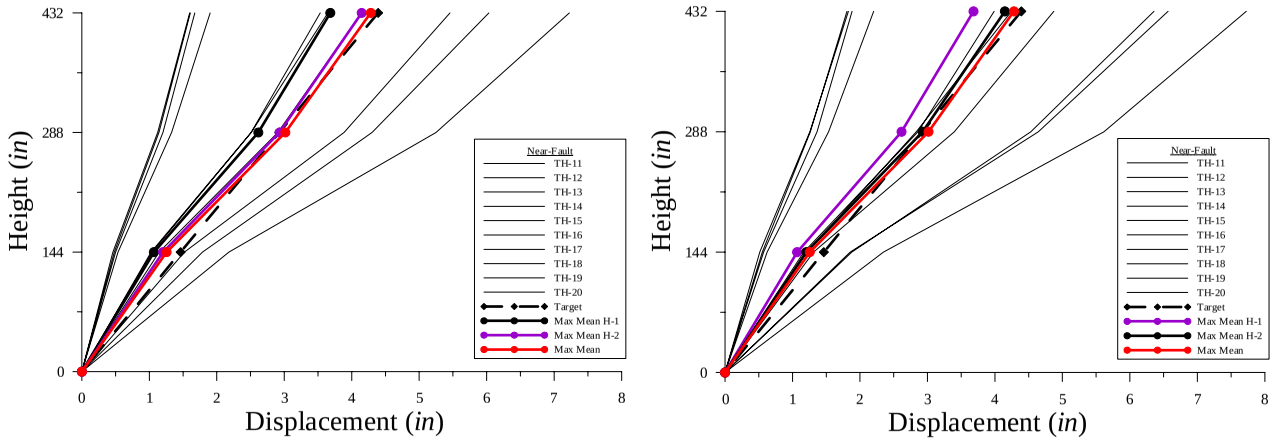

(i) 1st mode **(ii) 1st and 2nd mode**

(a) Displacement profile (Yield – 0.25 × MCE)

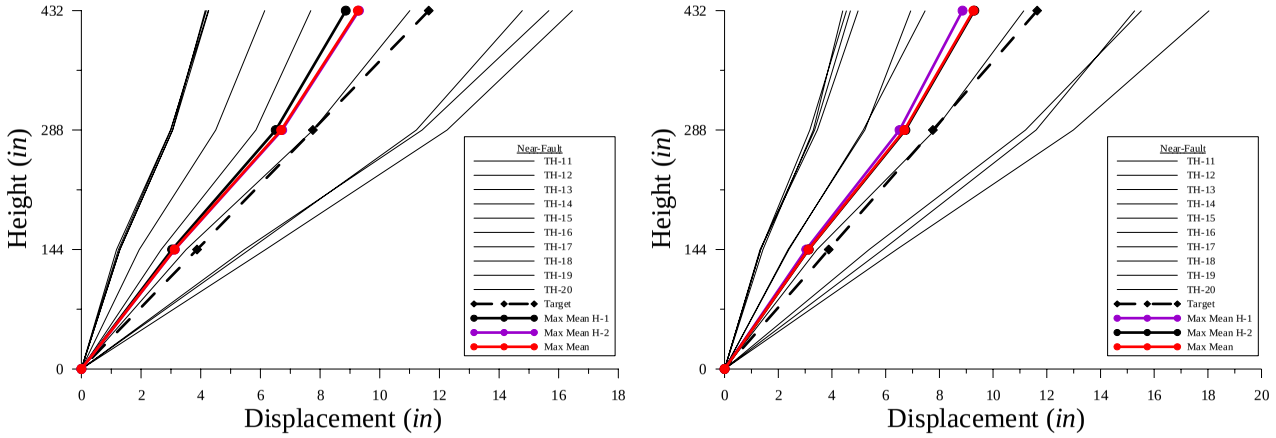

(i) 1st mode **(ii) 1st and 2nd mode**

(b) Displacement profile (Target - 0.67 × MCE)

Figure 7-50. FR-3F-24H inelastic dynamic analysis results (near-fault)

:

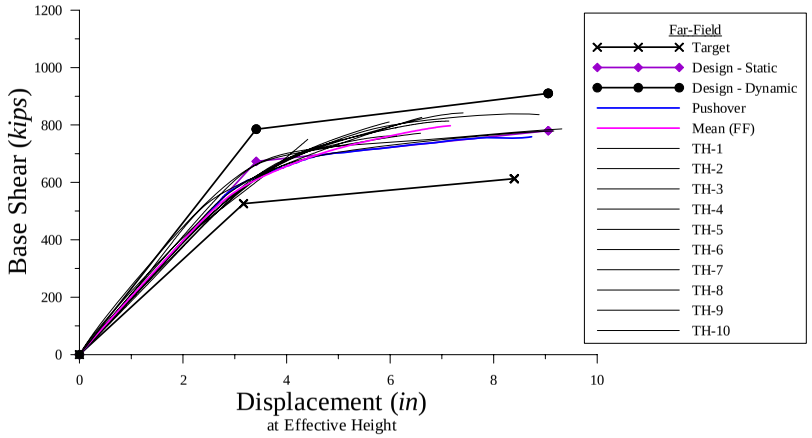

(i) 1st mode

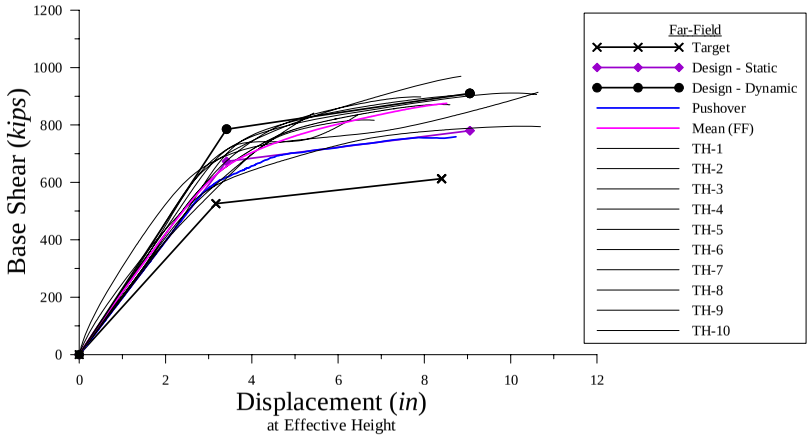

(ii) 1st and 2nd mode

Figure 7-49. FR-3F-24H inelastic dynamic analysis results (far-field) (Cont'd) - Dynamic pushover curves (0.13, 0.25, 0.45, 0.67 × MCE)

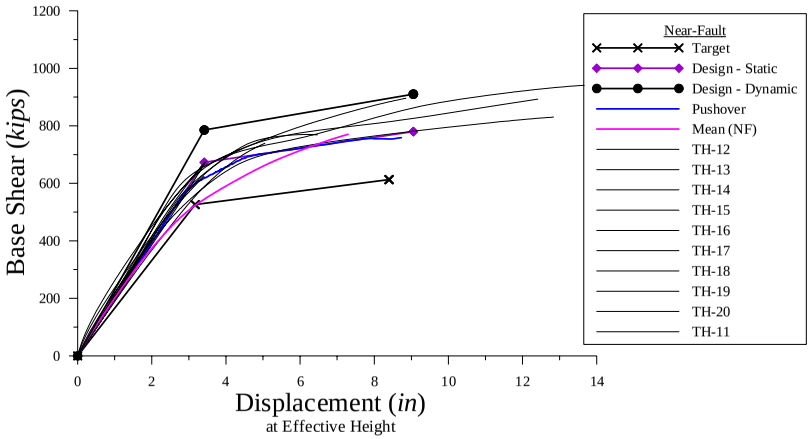

(i) 1st mode

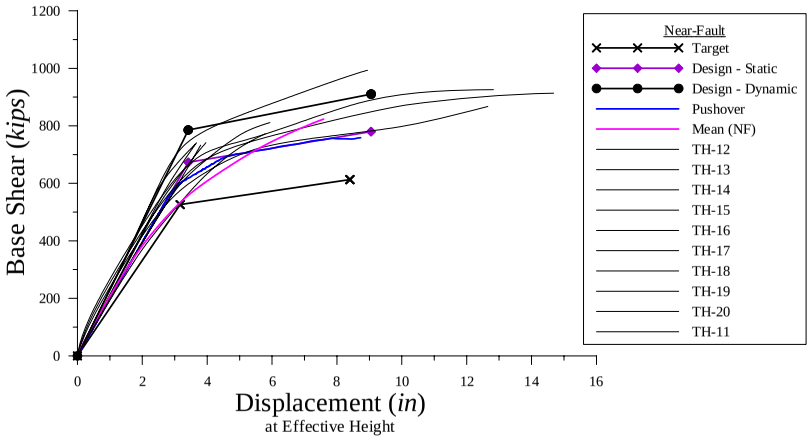

(ii) 1st and 2nd mode

Figure 7-50. FR-3F-24H inelastic dynamic analysis results (near-fault) (Cont'd) - Dynamic pushover curves (0.13, 0.25, 0.45, 0.67 × MCE)

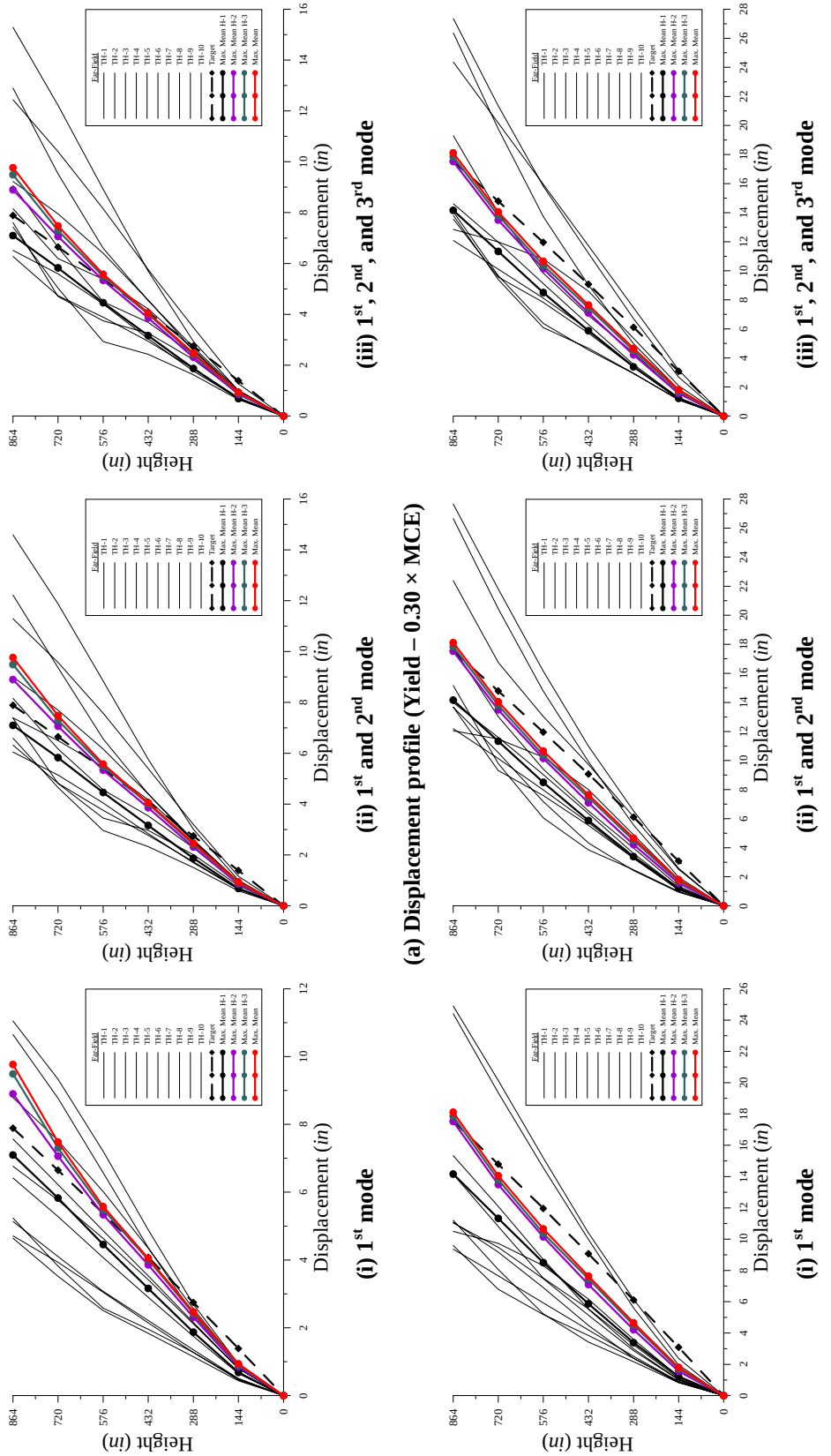

Figure 7-51. FR-6F-27H inelastic dynamic analysis results (far-field)

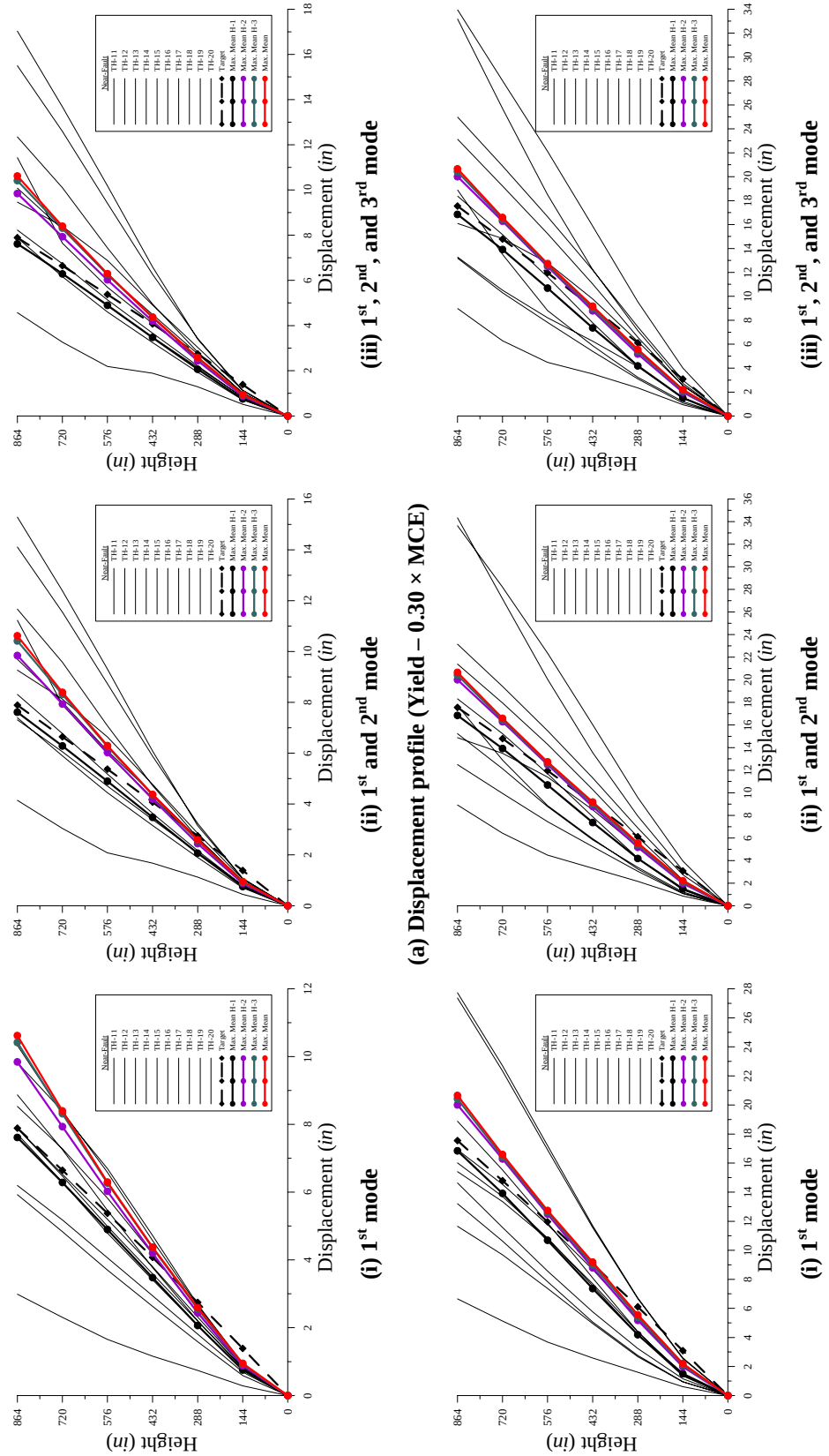

Figure 7-52. FR-6F-27H inelastic dynamic analysis results (near-fault)

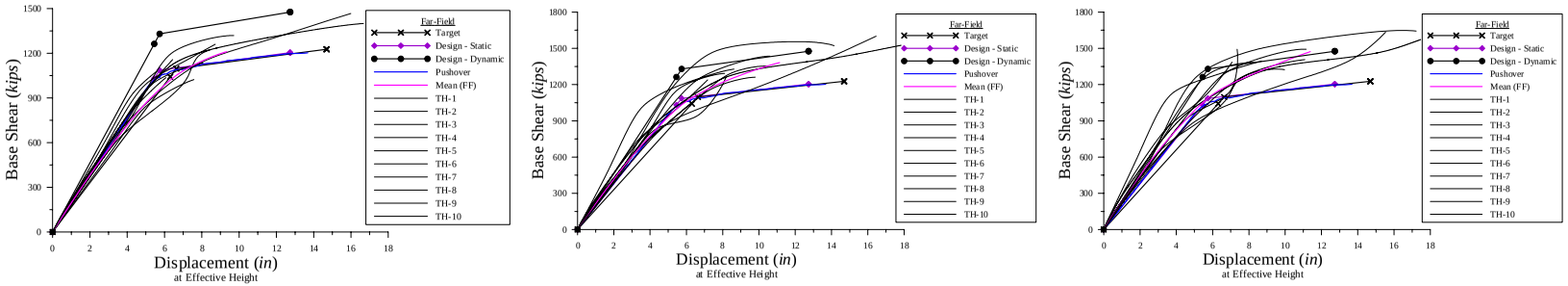

(i) 1st mode **(ii) 1st and 2nd mode** **(iii) 1st, 2nd, and 3rd mode**

Figure 7-51. FR-6F-27H inelastic dynamic analysis results (far-field) (Cont'd) - Dynamic pushover curves (0.13, 0.30, 0.45, 0.67 × MCE)

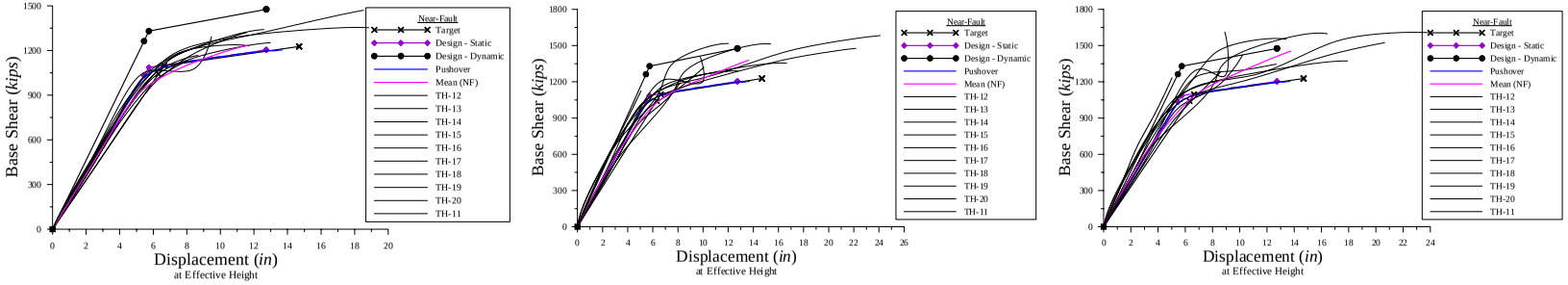

(i) 1st mode **(ii) 1st and 2nd mode** **(iii) 1st, 2nd, and 3rd mode**

Figure 7-52. FR-6F-27H inelastic dynamic analysis results (near-fault) (Cont'd) - Dynamic pushover curves (0.13, 0.30, 0.45, 0.67 × MCE)

FR-3F-24H

As seen in Fig. 7-49(a) and (b), FR-3F-24H indicates an average 15% and 21% reduction from the actual displacement profile at yield and design-level respectively when only the 1st mode is excited. The reduction is 4% and 5% respectively when the first two modes are excited. This effect is also seen in Fig. 7-49(c) where the dynamic pushover curve closely follows the static pushover curve in the elastic region then begins to shift towards the dynamic pushover curve upon adding the 2nd mode. The frame shows some higher mode contributions in the post-yield region due to localized stiffness reduction.

The response of FR-3F-24H when subjected to the near-fault records is similar to the far-field records. The average reduction in displacement is 14% and 3% respectively for 1st mode excitation and 3% and 0% when excited by the first two modes.

FR-6F-33H

As seen in Fig. 7-51(a), (b), and (c), FR-6F-27H indicates an average 24% reduction from the actual displacement profile at both yield and design-level when only the 1st mode is excited. When the first two modes are excited the reduction is 6% and 7% respectively and 2% and 3% respectively when the first three modes are excited. This effect is similarly evident in Fig. 7-51(c).

The response of FR-6F-27H when subjected to the near-fault records is similar to the far-field motions. The average reduction in displacement is 23% and 21%

respectively for 1st mode excitation, 6% and 5% respectively when excited by the first two modes, and 1% and 2% respectively when excited by the first three modes.

It can be concluded that while the target displacement profile adopted in the proposed DDBD procedure is based on the fundamental mode shape, it allows for some contributions from higher modes. This signifies that the frame is designed to resist some contributions from higher modes in the elastic region. The design engineer can negate some higher mode contributions by optimizing the beam-column depth ratios. As evident from the results, frames upwards of six stories begin to exhibit larger contributions from higher modes and the extent is dependent on the stiffness of the frame. Plotting the filtered DRS for TH-1 illustrates similar response to that indicated in the results (see Fig. 7-53). It can be concluded that the primary cause of displacement variation, disregarding ground motion characteristics, is due to the period shift associated with overstrength and capacity design, and that base hinges play a crucial role in the selection of the design displacement profile.

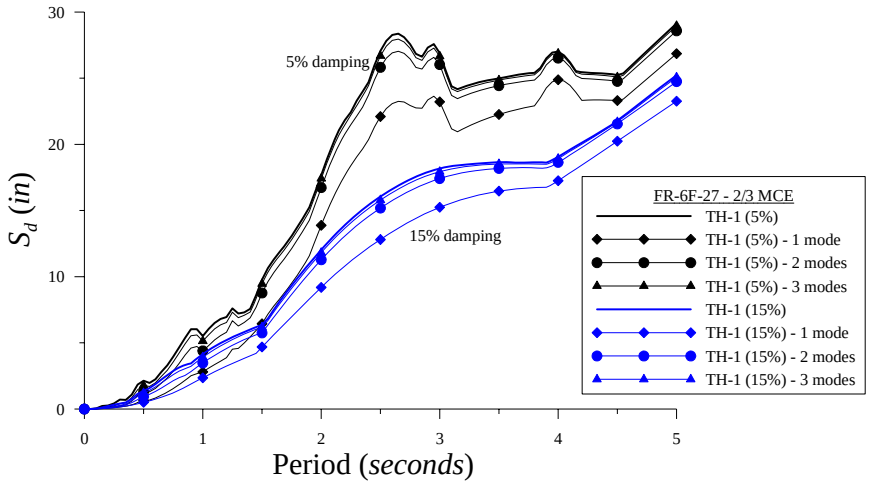

Figure 7-53. Filtered DRS (TH-1)

Lastly, only the first two modes of response are required in design of steel moment frames limited to six stories to adequately represent frame. Contributions from higher modes are very small since they are essentially damped out of the response due to inelastic response increasing the level damping. Moreover, higher mode contributions for these frames do not appear to affect the idealized yield displacement.

7.6 Evaluation of Higher Modes (FR-3F-24HI and FR-6F-27HI)

Similar to Section 7.5, the idealized frames presented in Section 7.4 are analyzed: FR-3F-24HI and FR-6F-27HI. For FR-3F-24HI, the earthquake records are filtered at: (1) f = 1.69 *Hz* and (2) f = 3.66 *Hz*. For FR-6F-24HI, earthquake records are filtered at: (1) f = 0.84 *Hz*, (2) f = 1.79 *Hz*, and (3) f = 3.05 *Hz*. These cutoff frequencies differ from Section 7.4 due to period variations between the designed and idealized frames.

Figs. 7-54 and 7-55 present the displacement envelopes and dynamic pushover curves from the dynamic analysis for FR-3F-24HI. Figs. 7-56 and 7-57 present the displacement envelopes and dynamic pushover curves for FR-6F-27HI. These figures are shown only for comparison purposes and no conclusions are drawn.

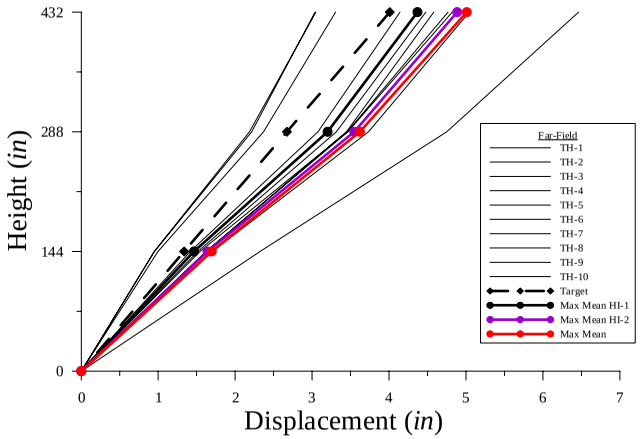

(i) 1st mode

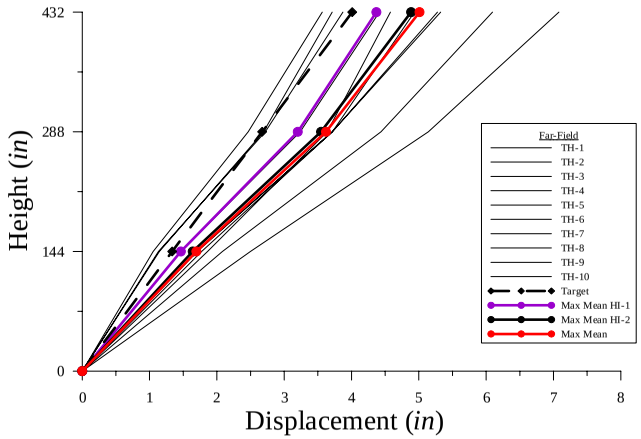

(ii) 1st and 2nd mode

(a) Displacement profile (Yield – 0.25 × MCE)

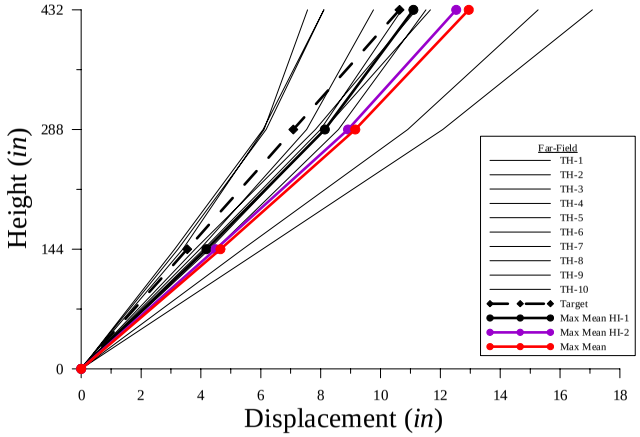

(i) 1st mode

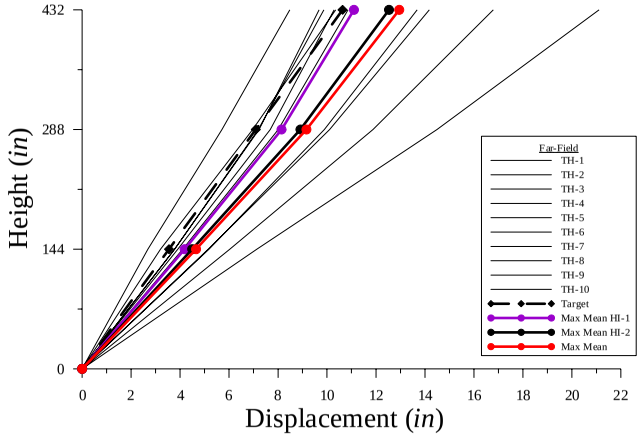

(ii) 1st and 2nd mode

(b) Displacement profile (Target - 0.67 × MCE)

Figure 7-54. FR-3F-24HI inelastic dynamic analysis results (far-field)

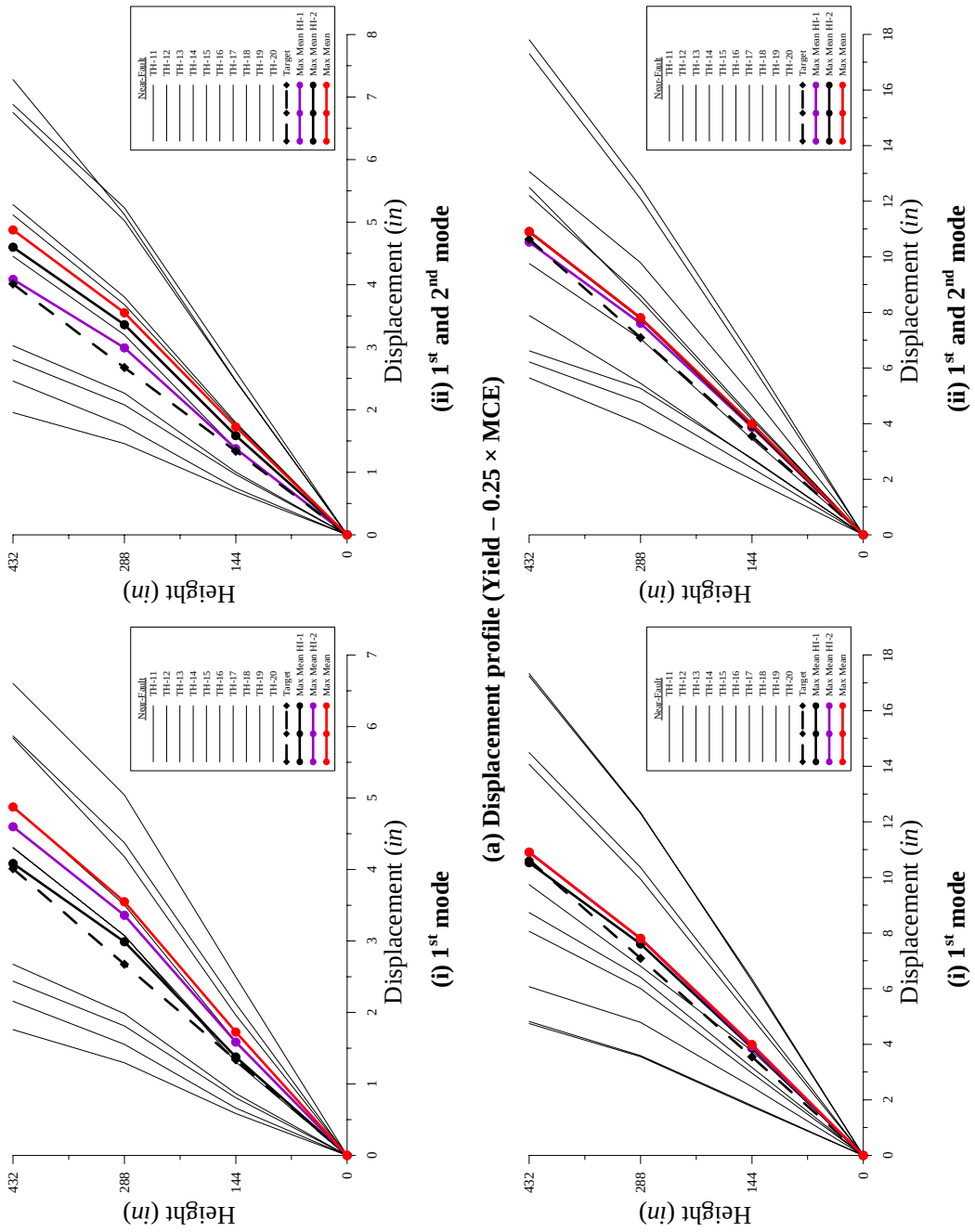

(i) 1st mode **(ii) 1st and 2nd mode**

(a) Displacement profile (Yield – 0.25 × MCE)

(i) 1st mode **(ii) 1st and 2nd mode**

(b) Displacement profile (Target - 0.67 × MCE)

Figure 7-55. FR-3F-24HI inelastic dynamic analysis results (near-fault)

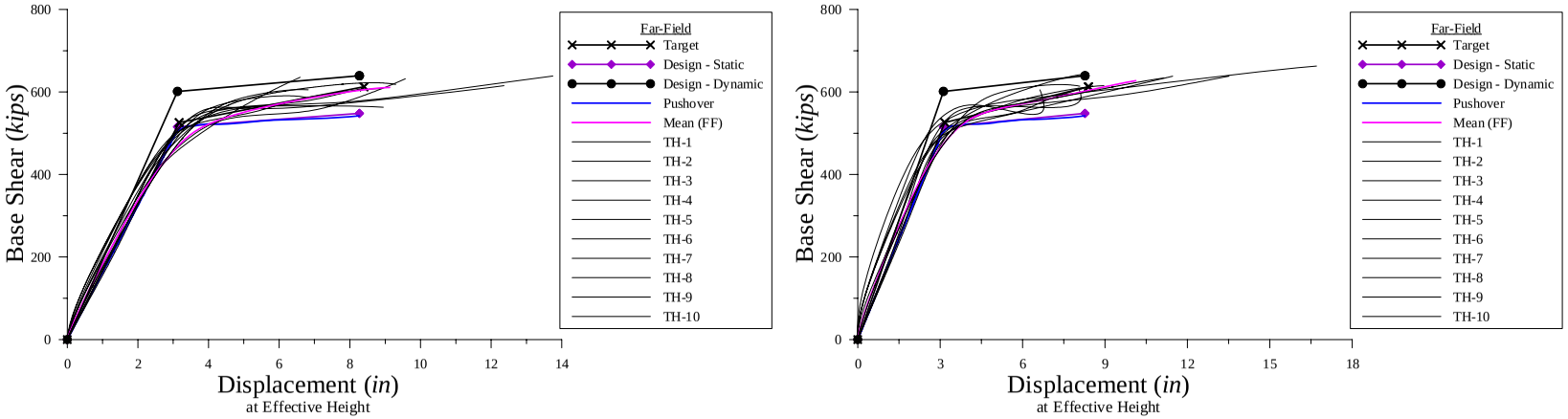

(i) 1st mode **(ii) 1st and 2nd mode**

Figure 7-54. FR-3F-24HI inelastic dynamic analysis results (far-field) (Cont'd) - Dynamic pushover curves (0.13, 0.25, 0.45, 0.67 × MCE)

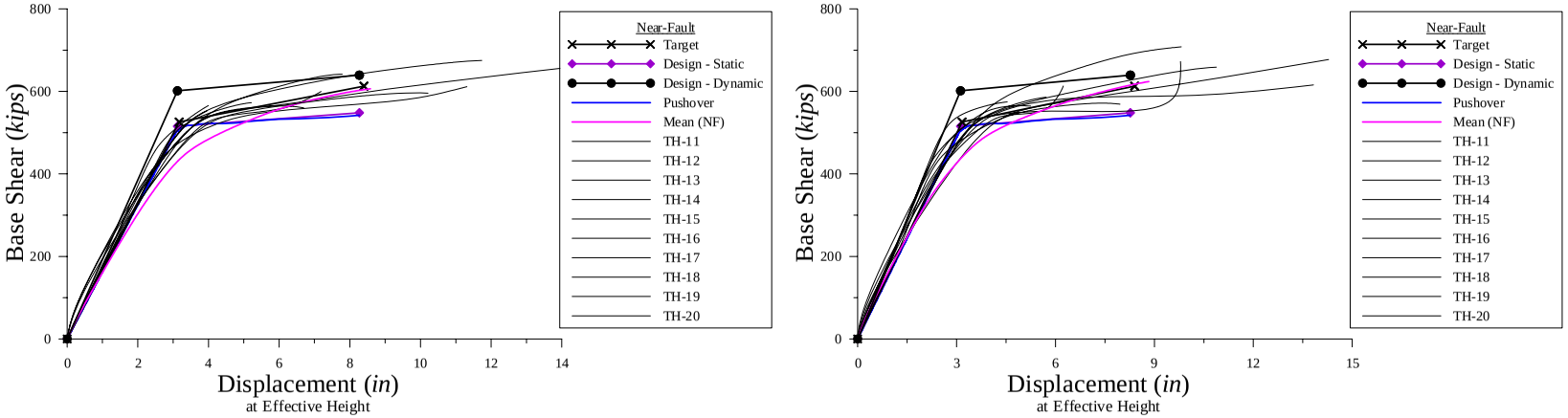

(i) 1st mode **(ii) 1st and 2nd mode**

Figure 7-55. FR-3F-24HI inelastic dynamic analysis results (near-fault) (Cont'd) - Dynamic pushover curves (0.13, 0.25, 0.45, 0.67 × MCE)

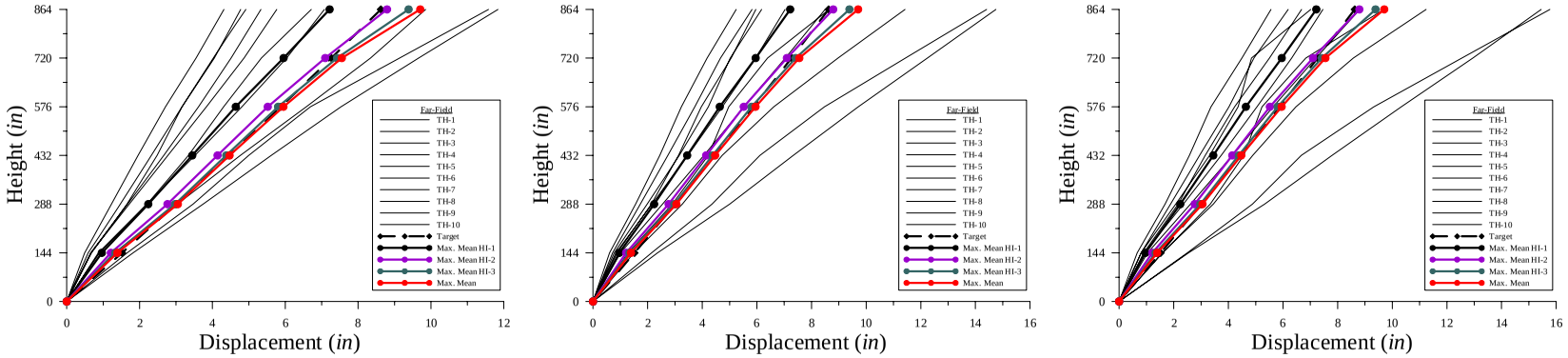

(i) 1st mode **(ii) 1st and 2nd mode** **(iii) 1st, 2nd, and 3rd mode**

(a) Displacement profile (Yield – 0.30 × MCE)

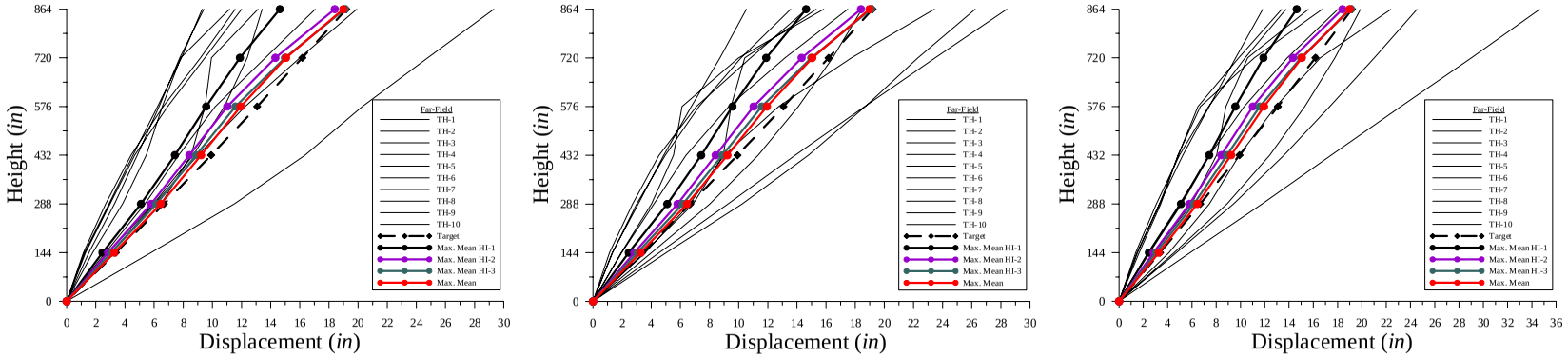

(i) 1st mode **(ii) 1st and 2nd mode** **(iii) 1st, 2nd, and 3rd mode**

(b) Displacement profile (Target - 0.67 × MCE)

Figure 7-56. FR-6F-27HI inelastic dynamic analysis results (far-field)

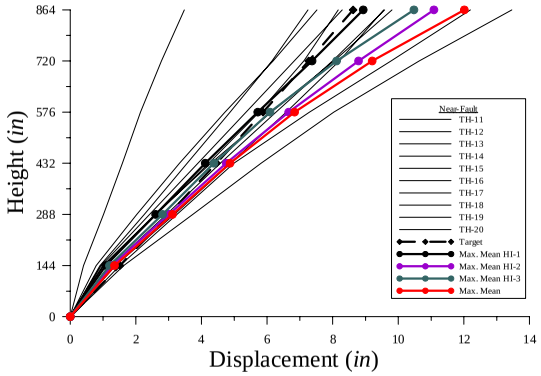

(i) 1st mode

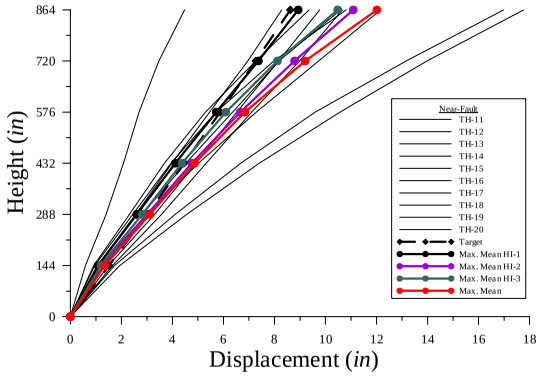

(ii) 1st and 2nd mode

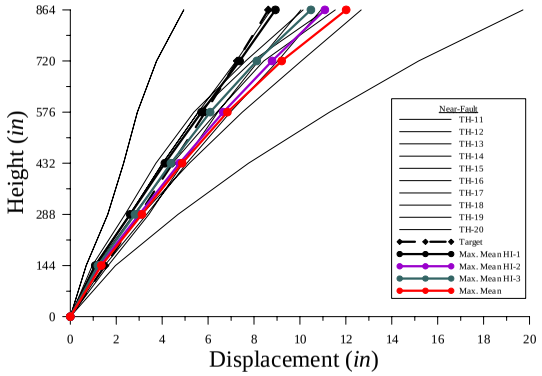

(iii) 1st, 2nd, and 3rd mode

(a) Displacement profile (Yield – 0.30 × MCE)

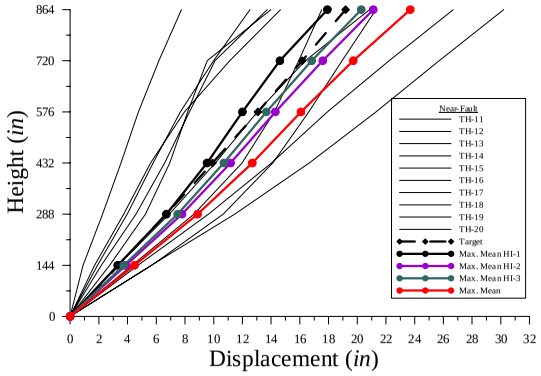

(i) 1st mode

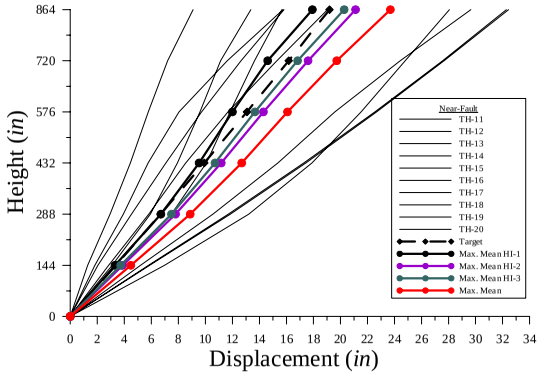

(ii) 1st and 2nd mode

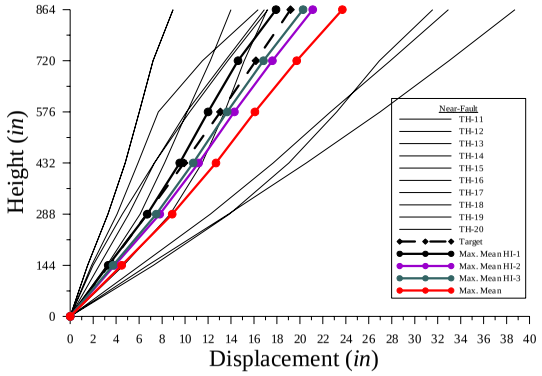

(iii) 1st, 2nd, and 3rd mode

(b) Displacement profile (Target - 0.67 × MCE)

Figure 7-57. FR-6F-27HI inelastic dynamic analysis results (near-fault)

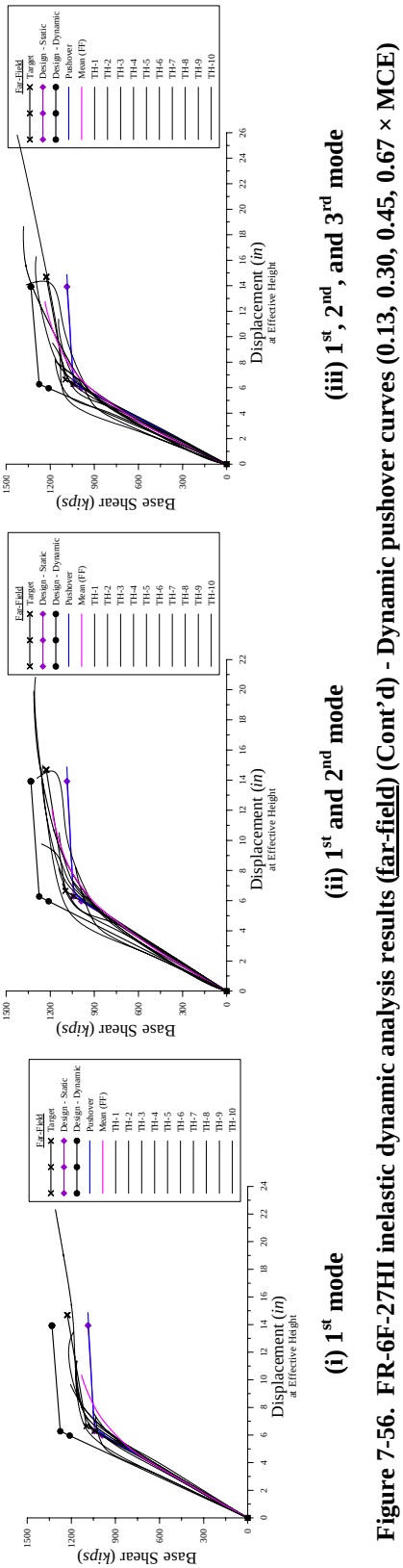

(i) 1st mode (ii) 1st and 2nd mode (iii) 1st, 2nd, and 3rd mode

Figure 7-56. FR-6F-27HI inelastic dynamic analysis results (far-field) (Cont'd) - Dynamic pushover curves (0.13, 0.30, 0.45, 0.67 × MCE)

(i) 1st mode (ii) 1st and 2nd mode (iii) 1st, 2nd, and 3rd mode

Figure 7-57. FR-6F-27HI inelastic dynamic analysis results (near-fault) (Cont'd) - Dynamic pushover curves (0.13, 0.30, 0.45, 0.67 × MCE)

Chapter 8 Conclusions and Future Research

8.1 Conclusions

This research has proposed a comprehensive Direct Displacement-Based Design procedure for low-rise seismic resistant steel moment frames. The analytical results demonstrate that the proposed procedure could be a viable seismic analysis and design procedure in order to satisfy a performance target set by PBSE. Further, the procedure conceptually bypasses the intrinsic limitations observed in conventional force-based design. Although no assessment is conducted within this document outside of key philosophical differences, future research efforts in the proposed methodology will perform such evaluation as well as experimental verification. The reader is referred to Harris (2004) for a comparison of two steel moment frames designed with the proposed procedure (earlier version of) and FBD. That study concluded that a steel moment frame designed in accordance with DDBD could be more efficient by means of ductility capacity and behavior while providing a reduction in frame weight. Additionally, the design engineer has a better sense of post-yield frame response and the various degrees and location of damage.

While the procedures outlined within this document give good comparisons at yield-level earthquakes, post-yield behavior is sporadic at best due to the effects of overstrength and earthquake characteristics leading to variations against the target. It is found that analytical results generally agree with the design parameters determined from an effective SDOF representation in the fundamental mode. This is in part a corollary of

the explicit consideration of the yield displacement profile resulting in an improved estimate of the design displacement ductility demands. The difficulty of predicting the post-yield response of longer period frames is noted. The results indicate that story drift ratios can reach upwards of 6% even when explicitly designing for 2.5%. Hence, the requirement to incorporate a capacity design procedure into analysis is recommended. As evident, capacity design, while an invaluable design tool, should not be applied without consideration of its effects on frame properties and response. While the inclusion of capacity design procedures aims to guarantee structural safety, it should not be assumed that it also produces a system that will perform satisfactorily in meeting a performance target.

Base hinges can also play a significant role in the response of a frame. However, there is no readily available procedure to optimize the frame such that base hinges develop concurrently with first-level hinges. To offset the penalty of capacity design on first story columns it appears plausible to incorporate Reduced Column Sections (RCS) in an effort to develop base hinges when desired. Unfortunately, to the authors' knowledge there is no information currently available to justify its use. Stability issues and the effect of RCS on the structural integrity of a frame would need to be examined. This is a topic of future research in seismic design of steel moment frames.

It is also found that the use of an equivalent modal damping based on a Modified Secant Stiffness method to represent the degree of damping in the inelastic system leads to a better approximation than examining a system-level force-displacement loop and applying a damping formulation explicitly derived for a SDOF system. The results

indicate that damping levels can be somewhat insensitive to design. Hence, a plausible concept would be to set equivalent damping fixed at 10% for frames less than three stories and 15% for frames three to six stories for design.

It can be seen from the analytical results that the force reduction factor, *R*, used in FBD cannot effectively represent all frames in a specific class when different beam and column depths are used. As a result, the response modification factors should be period dependent and a function of both overstrength and yield displacement. It is realistic to envision a future seismic design procedure that incorporates the best aspects of FBD and DDBD.

As elegant as the proposed procedure may appear, it is not without its limitations. Recommendations have been provided within the text concerning frame limitations. Conceptually, this procedure should be limited to regular frames up to six stories with fundamental periods less than 2 seconds (these limits also coincide with the limits of the ELFA). Taller moment frames (up to sixteen stories) and frames with longer periods indicate an increase in higher mode contributions thus limiting the proposed procedure and the use of a design spectrum based on SDOF response. It is additionally recommended that the proposed procedure be limited to frames with an equivalent period not exceeding 4 seconds. It is the aim of the author to evaluate a multi-mode DDBD procedure for frames outside these limits. Lastly, the question that still remains is what elastic stiffness should be provided as a minimum and what are the effects on yield displacements and design forces when considering all external stiffness contributions.

As illustrated within this document, the proposed method is relatively simple with the only complexities stemming from the determination of the degree of equivalent damping and displacement profiles. Additionally, current seismic design does not offer an analysis solution incorporating a comprehensive capacity design scenario nor the advantages of investigating post-yield frame response. Ultimately, the proposed method has a much greater potential for producing efficient structures since the proportionality between strength and stiffness is maintained in analysis and design. The true benefit of the proposed DDBD procedure could be the monetary savings gained by efficient member selection and level of repairs required after being subjected to certain earthquake intensities.

8.2 Future Research

A review of future research topics illustrates that this procedure is far from being adopted as a complete alternative design procedure. The following lists future research efforts in the proposed DDBD procedure.

- Refined hysteretic models
- Composite action and external stiffness contributions
- Capacity design adjustment factors for higher mode protection
- Multi-mode DDBD methodology for taller frames
- DDBD of steel braced frames (concentric and eccentric) and dual systems
- 3-Dimensional DDBD methodology
- Inelastic stability of steel members - Reduced Column Sections

- DDBD-FBD combination procedure
- Design displacement profiles for various framing systems
- Incorporation of *Advanced Analysis* ('Direct Analysis' per AISC) into DDBD

Lastly, the SCWB criteria, Eq. (6-15), should be further investigated. For example, Fig. 8-1 illustrates the beam-column joint in FR-3F-24 for Members 7 and 8 (columns) at t = 7.02 and 5.30 *sec* for TH-4. Although the SCWB criteria is met, Member 8 develops a plastic hinge at t = 5.30 *sec* as Member 7 exhibits single curvature bending. While this example uses $\phi_c = 0.9$ to compute $M_{p,c}$, it illustrates the potential of hinging.

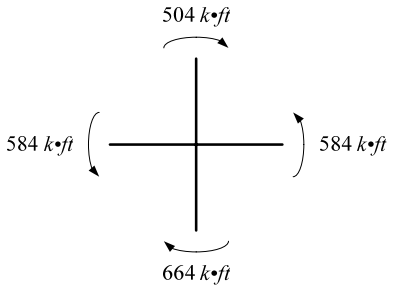

(a) Moments at joint

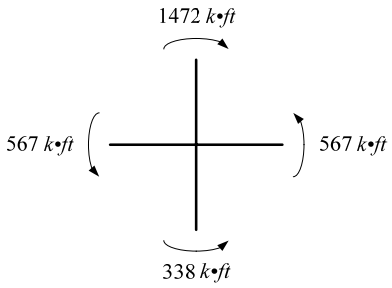

(b) Moments at joint

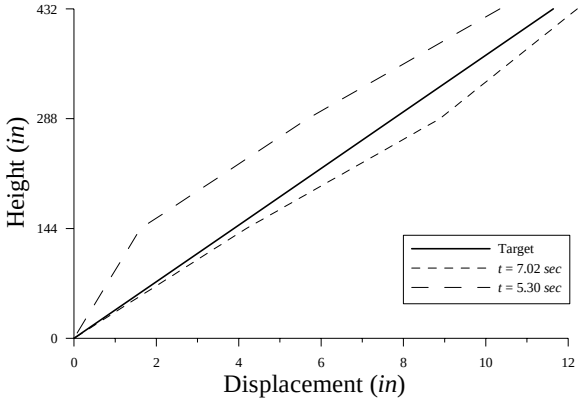

(c) Displacement profiles

$$M^{o}_{p,b} = 676\ k\bullet ft\ \ (50\ ksi)$$

$$M_{p,c} = 1463\ k\bullet ft\ \ (50\ ksi)$$

$$\frac{\sum M_{p,c}}{\sum M^{o}_{p,b}} = \frac{2926}{1352} = 2.2 \geq 1.0$$

(d) SCWB criteria

Figure 8-1. Beam-column joint

Appendix A Derivations

A.1 Chapter 2

Relationship between modal and effective Mass - Eq. (2-8)

From Eq. (2-4), $M_j = \sum_{i=1}^{n}\left(m_i \phi_{i,j}{}^2\right)$

From Eq. (2-5), $M_{eff,j} = \dfrac{\left(\sum_{i=1}^{n}\left(m_i \phi_{i,j}\right)\right)^2}{\sum_{i=1}^{n}\left(m_i \phi_{i,j}{}^2\right)}$

It follows that $\dfrac{M_{eff,j}}{M_j} = \left(\dfrac{\sum_{i=1}^{n}\left(m_i \phi_{i,j}\right)}{\sum_{i=1}^{n}\left(m_i \phi_{i,j}{}^2\right)}\right)^2 = \Gamma_j{}^2$

$\therefore M_{eff,j} = \Gamma_j{}^2 M_j$

Relationship between modal and effective Stiffness - Eq. (2-9)

From Eq. (2-7), $\dfrac{M_{eff,j}}{K_{eff,j}} = \dfrac{M_j}{K_j}$

Therefore, from Eq. (2-8), $\dfrac{\Gamma_j{}^2 M_j}{K_{eff,j}} = \dfrac{M_j}{K_j}$

$\therefore K_{eff,j} = \Gamma_j{}^2 K_j$

Displacement of Effective SDOF - Eq. (2-16)

From Eq. (2-12), $\Delta_{eff} = \dfrac{\sum_{i=1}^{n} F_i \delta_i}{F_{eff}}$

From Eq. (2-13) and (2-14), $\delta_i = c_i \Delta_{eff}$ and $a_i = c_i a_{eff}$

From Eq. (2-15), $F_{eff} = \sum_{i=1}^{n} F_i = \sum_{i=1}^{n} m_i a_i = a_{eff} \sum_{i=1}^{n} m_i c_i$

Therefore, $\Delta_{eff} = \dfrac{\sum_{i=1}^{n} F_i \delta_i}{a_{eff} \sum_{i=1}^{n} m_i c_i} = \dfrac{\sum_{i=1}^{n} m_i a_i \delta_i}{a_{eff} \sum_{i=1}^{n} m_i c_i} = \dfrac{\sum_{i=1}^{n} m_i c_i \delta_i}{\sum_{i=1}^{n} m_i c_i} = \dfrac{\sum_{i=1}^{n} m_i \delta_i^2}{\sum_{i=1}^{n} m_i \delta_i}$

Relationship between equivalent and elastic stiffness - Eq. (2-20)

$$K_{eff,eq} = \frac{F_m}{\Delta_d} = \frac{F_y + r_\Delta K_{eff}\left(\Delta_d - \Delta_y\right)}{\Delta_d}$$

$$K_{eff,eq} = \frac{F_y + r_\Delta F_y\left(\dfrac{\Delta_d - \Delta_y}{\Delta_y}\right)}{\Delta_d} = F_y\left(\frac{1 + r_\Delta\left(\mu_\Delta - 1\right)}{\Delta_d}\right)$$

$$K_{eff,eq} = F_y\left(\frac{1 + r_\Delta\left(\mu_\Delta - 1\right)}{\Delta_d}\right)\frac{\Delta_y}{\Delta_y} = K_{eff}\left(\frac{1 + r_\Delta\left(\mu_\Delta - 1\right)}{\mu_\Delta}\right)$$

$$\therefore K_{eff} = K_{eff,eq}\left(\frac{\mu_\Delta}{1 + r_\Delta\left(\mu_\Delta - 1\right)}\right)$$

A.2 Chapter 3

Idealized Yield Curvature - Eqs. (3-3) and (3-4)

From structural mechanics, the stress distribution for a member subjected to a bending moment, *M*, and an axial force, *P*, is

$$\sigma = \frac{Mc}{I} \pm \frac{P}{A_g}$$

For axial compression, the stress at the extreme compression fiber at yield is

$$\sigma_c = \frac{M}{S_x} + \frac{P}{A_g} = F_y$$

Similarly, at the extreme tension fiber, the flexural stress is

$$\sigma_t = \frac{M}{S_x} = F_y - \frac{P}{A_g}$$

Substituting Eq. (2.2.4.1-3) into Eq. (2.2.4.1-1), we have

$$\sigma_t = \frac{M}{S_x} - \frac{P}{A_g} = \left(F_y - \frac{P}{A_g} \right) - \frac{P}{A_g} = F_y - \frac{2P}{A_g}$$

Applying

$$P_y = A_g F_y$$

the resulting tensile stress can be expressed as

$$\sigma_t = F_y - \frac{2P}{A_g} = F_y - \frac{2PF_y}{P_y} = F_y \left(1 - \frac{2P}{P_y} \right)$$

Applying Hooke's Law and evaluating the strain distribution, we have from similar triangles

$$\frac{\varepsilon_y}{c} = \frac{\varepsilon_y \left(1 - \frac{2P}{P_y} \right)}{d_b - c}$$

Solving for *c*, the distance from the extreme compression fiber to the neutral axis, we have

$$c = \frac{d_b}{2\left(1 - \frac{P}{P_y} \right)}$$

By trigonometry, the section yield curvature for a member subjected to bending and an axial force can be expressed as

$$\phi_y = \frac{2\varepsilon_y}{d_b} \left(1 - \frac{P}{P_y} \right)$$

From Fig. 3-6, the idealized yield curvature is

For $0 \le P \le 0.15P_y$

$$\phi_y = \frac{\phi_b M_{pr}}{EI} = \frac{\phi_b M_p}{EI}$$

$$S_F = \frac{Z_x}{S_x} \text{ and } I = S_x \bar{y} = \frac{S_x d_b}{2} \text{ and } \varepsilon_y = \frac{F_y}{E}$$

$$\phi_b M_p = \phi_b \overbrace{Z_x \left(\phi_m^o \phi_{sr}^o F_y \right)}^{M_p}$$

$$\phi_y = \phi_b \phi_m^o \phi_{sr}^o \frac{2 S_F \varepsilon_y}{d_b}$$

For $0.15P_y \le P \le P_y$

$$\phi_b M_{pr} = \phi_b 1.18 M_p \left(1 - \frac{P}{P_y} \right) = 1.18 \phi_b \overbrace{Z_x \left(\phi_m^o \phi_{sr}^o F_y \right)}^{M_p} \left(1 - \frac{P}{P_y} \right)$$

$$\phi_y = \phi_b \phi_m^o \phi_{sr}^o \frac{2.36 S_F \varepsilon_y}{d_b} \left(1 - \frac{P}{P_y} \right)$$

Idealized Yield Rotation - Eqs. (3-7) and (3-8)

Stability functions will be employed to compute the idealized beam-column rotation at yield. Fig. App.A-1 shows a beam-column subjected to end moments, M_A and M_B, and a compressive axial force, P.

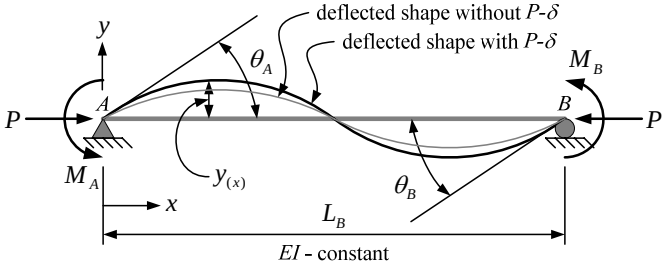

Figure App.A-1. Beam-Column subjected to end moments and axial force

From structural theory, the deflection formula (with *P*-δ) of the beam-column is

$$y_{(x)} = \frac{M_A}{EIk^2}\left(\frac{\cos kL}{\sin kL}\sin kx - \cos kx - \frac{x}{L} + 1\right) + \frac{M_B}{EIk^2}\left(\frac{1}{\sin kL}\sin kx - \frac{x}{L}\right)$$

where

$$k = \sqrt{\frac{P}{EI}}$$ (see Chapter 3 and below for simplification)

The slopes at the ends of the beam are determined from the 1st derivative of Eq. (X) using the boundary conditions $x = 0$ and $x = L$.

$$\theta_A = \frac{M_A L}{EI}\left(\frac{kL\cos kL - \sin kL}{(kL)^2 \sin kL}\right) + \frac{M_B L}{EI}\left(\frac{kL - \sin kL}{(kL)^2 \sin kL}\right)$$

$$\theta_B = \frac{M_A L}{EI}\left(\frac{kL - \sin kL}{(kL)^2 \sin kL}\right) + \frac{M_B L}{EI}\left(\frac{kL\cos kL - \sin kL}{(kL)^2 \sin kL}\right)$$

Solving for M_A and M_B in terms of θ_A and θ_B, we determine that

$$M_A = \frac{EI}{L}(s_{ii}\theta_A + s_{ij}\theta_B) \text{ and } M_B = \frac{EI}{L}(s_{ji}\theta_A + s_{jj}\theta_B)$$

where

$$s_{ii} = s_{jj} = \frac{kL\sin kL - (kL)^2\cos kL}{2 - 2\cos kL - kL\sin kL}$$

$$s_{ij} = s_{ji} = \frac{(kL)^2 - kL\sin kL}{2 - 2\cos kL - kL\sin kL}$$

From Fig. 3-5, when $P \le 0.15P_y$, using L'Hôpital's rule, these equations are simplified to the standard first-order slope-deflection equations.

$$M_A = \frac{EI}{L}(4\theta_A + 2\theta_B) \text{ and } M_B = \frac{EI}{L}(2\theta_A + 4\theta_B)$$

Solving for equal end plastic moments ($M_A = M_B = M_{pr}$)

For $0 \le P \le 0.15P_y$ (Compression)

$$\theta_{by,A} = \theta_{by,B} = \underbrace{\frac{\phi_b M_p}{EI}}_{\phi_y} \frac{L}{6}$$

For $0.15P_y \le P \le P_y$ (Compression)

$$\theta_{by,A} = \theta_{by,B} = \underbrace{\frac{\phi_b M_{pr}}{EI}}_{\phi_y} L\left(\frac{kL + kL\cos kL - 2\sin kL}{(kL)^2 \sin kL}\right)$$

Stability coefficient - Eq. (3-8a)

$$k = \sqrt{\frac{P}{EI}}$$

Setting $P = \chi P_y = \chi A_g F_y$ gives $k = \sqrt{\chi \frac{A_g F_y}{EI}}$

$$I = S_x \overline{y} = \frac{S_x d_b}{2} = \frac{Z_x d_b}{2S_F}$$

Therefore, $k = \sqrt{\chi \frac{2S_F A_g}{Z_x d_b} \frac{F_y}{E}} = \sqrt{\chi \frac{2S_F}{d_b} \frac{A_g}{Z_x} \varepsilon_y}$

From Fig. 3-10, $\frac{A_g}{Z_x} \approx \frac{2S_F}{d_b^{0.96}}$. It follows that $k = \sqrt{\chi \frac{4S_F^{\,2}}{d_b^{1.96}} \varepsilon_y}$

A.3 Chapter 4

Equivalent Hysteretic Damping - Eq. (4-31)

$$E_{D,h,sys} = A_{hyst} = 4F_y\Delta_y\left(\mu_\Delta - r_\Delta\left(\mu_\Delta - 1\right) - 1\right)$$

$$K_{eq} = K\left(\frac{1 + r_\Delta\left(\mu_\Delta - 1\right)}{\mu_\Delta}\right)$$

$$\therefore \zeta_{eq,h} = \frac{E_{D,h,sys}}{2\pi\eta_{eq}K_{eq}{\Delta_{in}}^2} = \frac{2}{\pi}\frac{\left(1-r_\Delta\right)\left(\mu_\Delta-1\right)}{\mu_\Delta\left(1+r_\Delta\left(\mu_\Delta-1\right)\right)}\frac{1}{\eta_{eq}}$$

Equivalent Hysteretic Damping - Eq. (4-37)

$$E_I = \pi F\Delta_{in}\sin\left(\tan^{-1}\left(\frac{2\zeta_{eq,h}\eta_{eq}}{1-{\eta_{eq}}^2}\right)\right) = \pi F\Delta_{in}\frac{2\eta_{eq}\zeta_{eq,h}}{\left(1-{\eta_{eq}}^2\right)\sqrt{1+\frac{\left(2\eta_{eq}\zeta_{eq,h}\right)^2}{\left(1-{\eta_{eq}}^2\right)^2}}}$$

$E_I = E_D$ and solving for $\zeta_{eq,h}$

$$\therefore \zeta_{eq,h} = \frac{E_D\sqrt{\left({\eta_{eq}}^2-1\right)^2}}{2\eta_{eq}\sqrt{\left(\pi F\Delta_{in}\right)^2-{E_D}^2}}$$

$$E_D = 4F_y\Delta_y\left(\mu_\Delta - r_\Delta\left(\mu_\Delta-1\right)-1\right)$$

$$\therefore \zeta_{eq,h} = \frac{{F_y}^2\sqrt{\left({\eta_{eq}}^2-1\right)^2}}{2\eta_{eq}\sqrt{\left(\frac{\pi}{4}\frac{F}{F_y}\frac{\mu_\Delta}{\mu_\Delta - r_\Delta\left(\mu_\Delta-1\right)-1}\right)^2-1}}$$

Energy Dissipated by System - Eqs. (4-52) and (4-53)

$$E_{D,h,sys} = \sum_{i=1}^{n}A_{hyst,i} = \sum_{i=1}^{n}4F_{y,i}\delta_{y,i}\left(\mu_{\delta,i} - r_{\delta,i}\left(\mu_{\delta,i}-1\right)-1\right)$$

$$A_{hyst,n} = 4F_{y,n}\delta_{y,n}\left(\mu_{\delta,n} - r_{\delta,n}\left(\mu_{\delta,n}-1\right)-1\right)$$

$$A_{hyst,i} = A_{hyst,n}\frac{4F_{y,i}\delta_{y,i}\left(\mu_{\delta,i} - r_{\delta,i}\left(\mu_{\delta,i}-1\right)-1\right)}{4F_{y,n}\delta_{y,n}\left(\mu_{\delta,n} - r_{\delta,n}\left(\mu_{\delta,n}-1\right)-1\right)} = A_{hyst,n}\frac{F_{y,i}\delta_{y,i}}{F_{y,n}\delta_{y,n}}\left(\frac{r_{\delta,i}-1}{r_{\delta,n}-1}\right)\left(\frac{\mu_{\delta,i}-1}{\mu_{\delta,n}-1}\right)$$

$$\frac{F_{y,i}\delta_{y,i}}{F_{y,n}\delta_{y,n}} = \frac{\phi_{f,i}F}{\phi_{f,n}F}\frac{\phi_i\delta_{y,n}}{\phi_n\delta_{y,n}} = \frac{\phi_{f,i}}{\phi_{f,n}}\frac{\phi_i}{\phi_n} = \frac{\phi_{f,i}}{1}\frac{\phi_i}{1} = \phi_{f,i}\phi_i$$

$$\therefore E_{D,h,sys} = A_{hyst,n}\sum_{i=1}^{n}\phi_{f,i}\phi_i\left(\frac{r_{\delta,i}-1}{r_{\delta,n}-1}\right)\left(\frac{\mu_{\delta,i}-1}{\mu_{\delta,n}-1}\right)$$

$$\therefore \tau_i = \frac{E_{D,h,i}}{E_{D,h,sys}} = \frac{A_{hyst,n}\phi_{f,i}\phi_i\left(\frac{r_{\delta,i}-1}{r_{\delta,n}-1}\right)\left(\frac{\mu_{\delta,i}-1}{\mu_{\delta,n}-1}\right)}{A_{hyst,n}\sum_{i=1}^{n}\phi_{f,i}\phi_i\left(\frac{r_{\delta,i}-1}{r_{\delta,n}-1}\right)\left(\frac{\mu_{\delta,i}-1}{\mu_{\delta,n}-1}\right)} = \frac{\phi_{f,i}\phi_i\left(\frac{r_{\delta,i}-1}{r_{\delta,n}-1}\right)\left(\frac{\mu_{\delta,i}-1}{\mu_{\delta,n}-1}\right)}{\sum_{i=1}^{n}\phi_{f,i}\phi_i\left(\frac{r_{\delta,i}-1}{r_{\delta,n}-1}\right)\left(\frac{\mu_{\delta,i}-1}{\mu_{\delta,n}-1}\right)}$$

Floor Stiffness – Eq. (4-56)

$$[K]\{\phi_j\} = \{k_j^*\} \text{ and } [K]\{\phi_j\} = \omega_j{}^2[M]\{\phi_j\}$$

Since no other modes of vibration are excited, $\{u_j(t)\} = \{\phi_j\}q_j(t) = \{\phi_{i,j}u_{i,j}(t)\}$

$$k_{i,j}^* = \omega_j{}^2 m_i$$

A.4 Chapter 5

First-order Design Displacement - Eq. (5-24)

$$\Delta_d = \frac{F_{d^2}}{K_{eff,eq^2}}$$

$$\Delta_{d^1} = \frac{F_{d^2}}{K_{eff,eq^1}} = \frac{K_{eff,eq^2}}{K_{eff,eq^1}}\Delta_d = \frac{K_{eff,eq^2}}{K_{eff,eq^2}+\frac{P_{eff,eq}}{h_{eff,eq}}}\Delta_d = \frac{\Delta_d}{\left(1+\theta_{eff,eq}\right)}$$

Elastic Second-order Stiffness - Eq. (5-25)

The 1st order elastic stiffness is

$$K_{eff1} = \frac{F_y}{\Delta_y} = \frac{\left(K_{eff,eq^2}+\frac{P_{eff,eq}}{h_{eff,eq}}\right)\Delta_d - r_{\Delta^1}K_{eff}{}^1\left(\Delta_d-\Delta_y\right)}{\Delta_y}$$

After simplification,

$$K_{eff^1} = \left(K_{eff,eq^2} + \frac{P_{eff,eq}}{h_{eff,eq}} \right) \frac{\mu_\Delta}{1 + r_{\Delta^1}\left(\mu_\Delta - 1\right)}$$

The 2nd order elastic stiffness is

$$K_{eff^2} = K_{eff^1} - \frac{P_{eff,eq}}{h_{eff,eq}}$$

Substituting and simplifying,

$$\therefore K_{eff^2} = \eta\Upsilon \left(K_{eff,eq^2} + \left(1 - r_{\Delta^1}\right)\left(1 - \frac{1}{\mu_\Delta}\right)\frac{P_{eff,eq}}{h_{eff,eq}} \right)\left(\frac{\mu_\Delta}{1 + r_{\Delta^1}\left(\mu_\Delta - 1\right)} \right)$$

Elastic First-order Stiffness - Eq. (5-28)

See Above (Eq. (5-25)

Second-order Post-yield Stiffness Ratio - Eq. (5-25)

$$r_{\Delta^2} = \frac{r_{\Delta^1} - \dfrac{P_{eff}}{K_{eff^1} h_{eff}}}{1 - \dfrac{P_{eff}}{K_{eff^1} h_{eff}}}$$

$$\therefore r_{\Delta^2} = \frac{r_{\Delta^1}\left(1 + \dfrac{h_{eff,eq}}{P_{eff,eq}} K_{eff,eq} \mu_\Delta \right) - 1}{\left(\mu_\Delta + r_{\Delta^1}\left(1 - \mu_\Delta\right) - 1 \right) + \dfrac{h_{eff,eq}}{P_{eff,eq}} K_{eff,eq} \mu_\Delta}$$

Equivalent Hysteretic Damping - Eq. (5-26)

$$\zeta^*_{eq,h,i} = \kappa \frac{E^*_{D,h,i} T_{eq,\delta^1}{}^2}{8\pi^3 m_{eq,i} \delta_{d,i}{}^2} = \kappa \frac{E^*_{D,h,i} T_{eq,\delta^2}{}^2}{8\pi^3 m_{eq,i} \delta_{d,i}{}^2 \left(1 + \theta_{eff,eq}\right)}$$

A.5 Chapter 6

Distance modification factor - Eq. (6-5)

Assuming a point of inflection at midspan, $\frac{M_{EQ,b}}{\frac{L_b}{2}} = \frac{\phi_{db}^o M_{EQ,b}}{\frac{L_b}{2} - \left(\frac{d_c + d_b}{2}\right)}$

$$\therefore \phi_{db}^o = \frac{\frac{L_b}{2} - \left(\frac{d_c + d_b}{2}\right)}{\frac{L_b}{2}} = 1 - \left(\frac{d_c + d_b}{2}\right)\frac{2}{L_b} = 1 - \left(\frac{d_c + d_b}{L_b}\right)$$

Distance modification factor - Eq. (6-6)

Assuming a point of inflection at midspan, from geometry $\frac{2M_{EQ,b}}{L_b - d_c} = \frac{2\phi_{db}^o M_{EQ,b}}{L_b - \left(d_c + d_b\right)}$

$$\therefore \phi_{db}^o = \frac{\frac{L_b}{2} - \left(\frac{d_c + d_b}{2}\right)}{\frac{L_b - d_c}{2}} = 1 - \left(\frac{d_c + d_b}{2}\right)\left(\frac{2}{L_b - d_c}\right) = 1 - \left(\frac{d_b}{L_b - d_c}\right)$$

Distance modification factor - Eq. (6-7b)

Assuming a point of inflection at midspan, from geometry $\frac{2M_{EQ,c}}{L_c} = \frac{2\phi_{dc}^o M_{EQ,c}}{L_c - d_b}$

$$\therefore \phi_{dc}^o = \frac{\frac{L_c}{2} - \frac{d_b}{2}}{\frac{L_c}{2}} = 1 - \frac{d_b}{2}\frac{2}{L_c} = 1 - \frac{d_c}{L_c}$$

Modified Yield Displacement - Eq. (6-19)

$$K_{eff} = \frac{F_y}{\Delta_{dy}} = \frac{F_y}{\mu_{\Delta,el}\Delta_y}$$

$$\Delta_y^o = \frac{F_y^o}{K_{eff}^o} = \frac{\Lambda^o}{\Omega^o}\frac{F_y}{K_{eff}} = \frac{\Lambda^o}{\Omega^o}\Delta_{dy} = \left(\mu_{\Delta,el}\frac{\Lambda^o}{\Omega^o}\right)\Delta_y$$

Appendix B Ground Motion Time-Histories and Response Spectra

Table App.B-1. MCE response spectrum parameters

Parameter	Value
Code	NEHRP (2003) (FEMA 450)
Location	Los Angeles (Zip Code: 90012)
Soil Type	C
S_S, S_1	2.33g, 0.77g
F_a, F_v	1.0, 1.3
S_{DS}, S_{D1}	1.49g, 0.66g
T_L	4 seconds
ζ_v	5%

Table App.B-2. Time-histories

Time History	Earthquake [1,2]	Station	Year	+ PGA (% g)	- PGA (% g)	Normalization Factor	Soil Type	Figure
TH-1	Cape Mendocino	Fortuna Blvd.	1992	0.50	-0.54	4.68	C	App.B-2
TH-2	Cape Mendocino	Rio Dell Overpass	1992	0.63	-0.99	2.56	C	App.B-3
TH-3	Landers	Desert Hot Springs	1992	0.45	-0.59	3.80	C	App.B-4
TH-4	Loma Prieta	Gilroy Array # 4	1989	0.90	-1.23	2.96	D	App.B-5
TH-5	Loma Prieta	Hollister Diff. Array	1989	0.82	-0.90	3.25	D	App.B-6
TH-6	Loma Prieta	Saratoga – W. Valley Coll.	1989	0.45	-0.61	1.83	C	App.B-7
TH-7	Northridge	Canoga Park – Topanga Can	1994	0.96	-0.83	2.70	D	App.B-8
TH-8	Northridge	LA-Hollywood Stor	1994	0.87	-0.86	3.78	D	App.B-9
TH-9	Northridge	N. Hollywood – Coldwater Can	1994	0.79	-1.01	3.73	C	App.B-10
TH-10	Superstition Hills	Plaster City	1997	0.74	-0.80	4.30	D	App.B-11
TH-11	Kobe	Takatori – 90°	1995	0.62	-0.58	1.00	---	App.B-12
TH-12	Kobe	Takatori – 0°	1995	0.61	-0.49	1.00	---	App.B-13
TH-13	Northridge	Rinaldi – 318°	1994	0.47	-0.44	1.00	---	App.B-14
TH-14	Northridge	Rinaldi – 228°	1994	0.62	-0.84	1.00	---	App.B-15
TH-15	Loma Prieta	UCSC Stn. 16 – 90°	1989	0.61	-0.43	1.00	---	App.B-16
TH-16	Loma Prieta	UCSC Stn. 16 – 0°	1989	0.56	-0.50	1.00	---	App.B-17
TH-17	El Centro	Array #6 – 230°	1979	0.32	-0.44	1.00	---	App.B-18
TH-18	El Centro	Array #6 – 140°	1979	0.31	-0.41	1.00	---	App.B-19
TH-19	Northridge	Sylmar – 90°	1994	0.60	-0.33	1.00	---	App.B-20
TH-20	Northridge	Sylmar – 360°	1994	0.84	-0.59	1.00	---	App.B-21

1. TH-1 to TH-10 are far-field records, TH-11 to TH-20 are near-fault records.
2. See Fig. App.B-2 to 21 for duration (All records are discretized into 0.005 second time-steps).
3. TH-1 to TH-10 are normalized by minimizing error between DRS and NEHRP DRS from 0.5 to 2.0 second periods.
4. Near-fault records are not normalized.

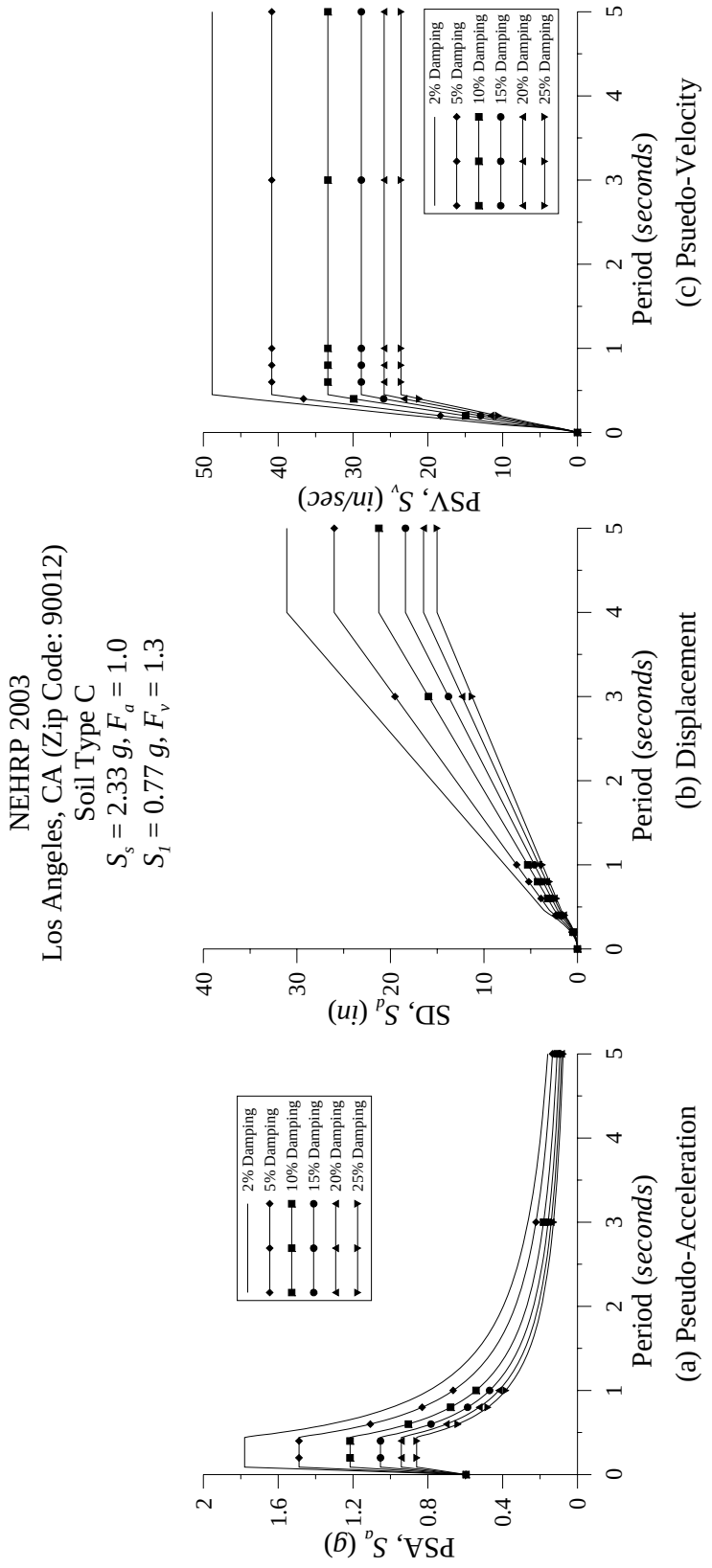

Figure App.B-1. MCE Response Spectra

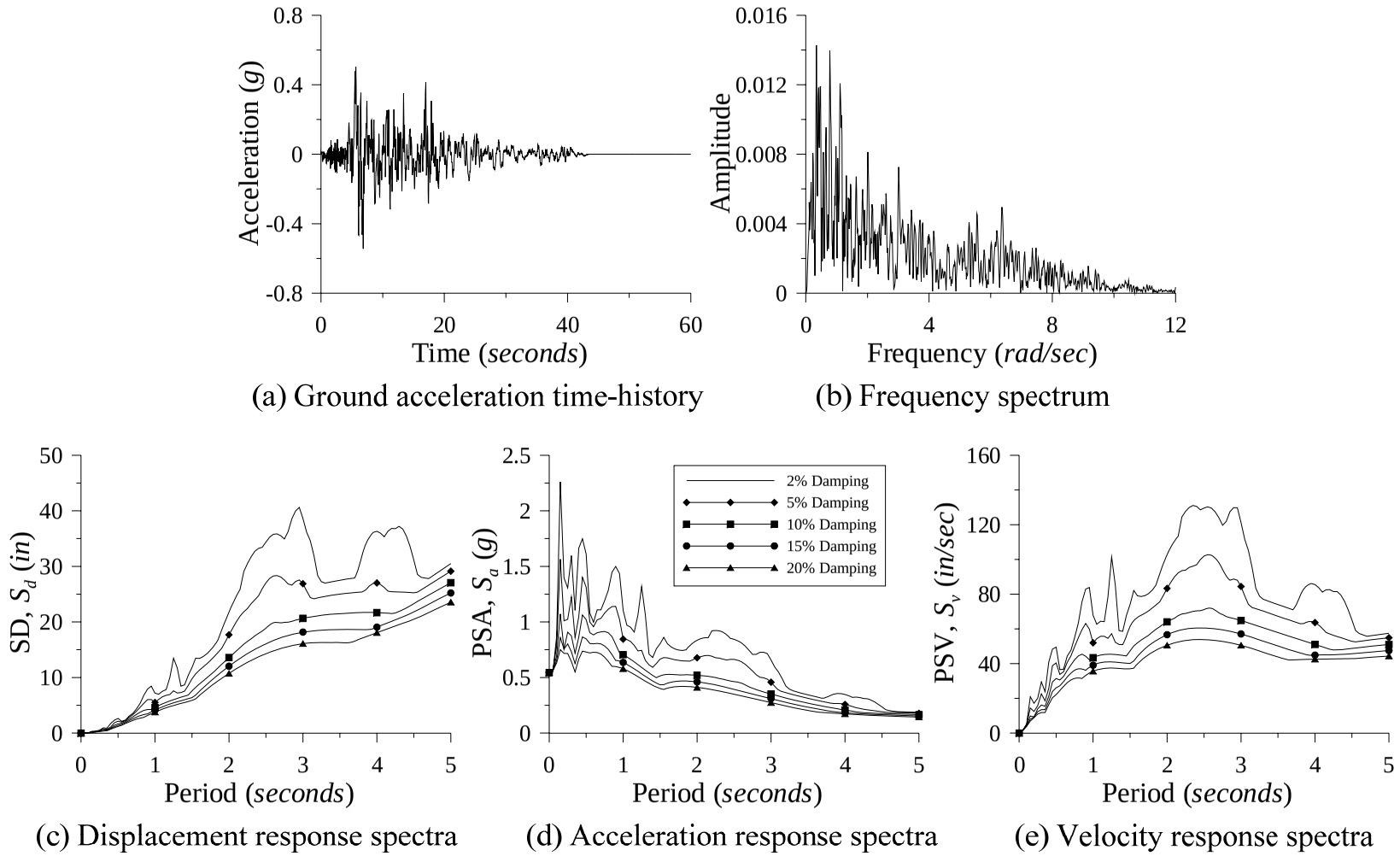

(a) Ground acceleration time-history (b) Frequency spectrum

(c) Displacement response spectra (d) Acceleration response spectra (e) Velocity response spectra

Figure App.B-2. TH-1

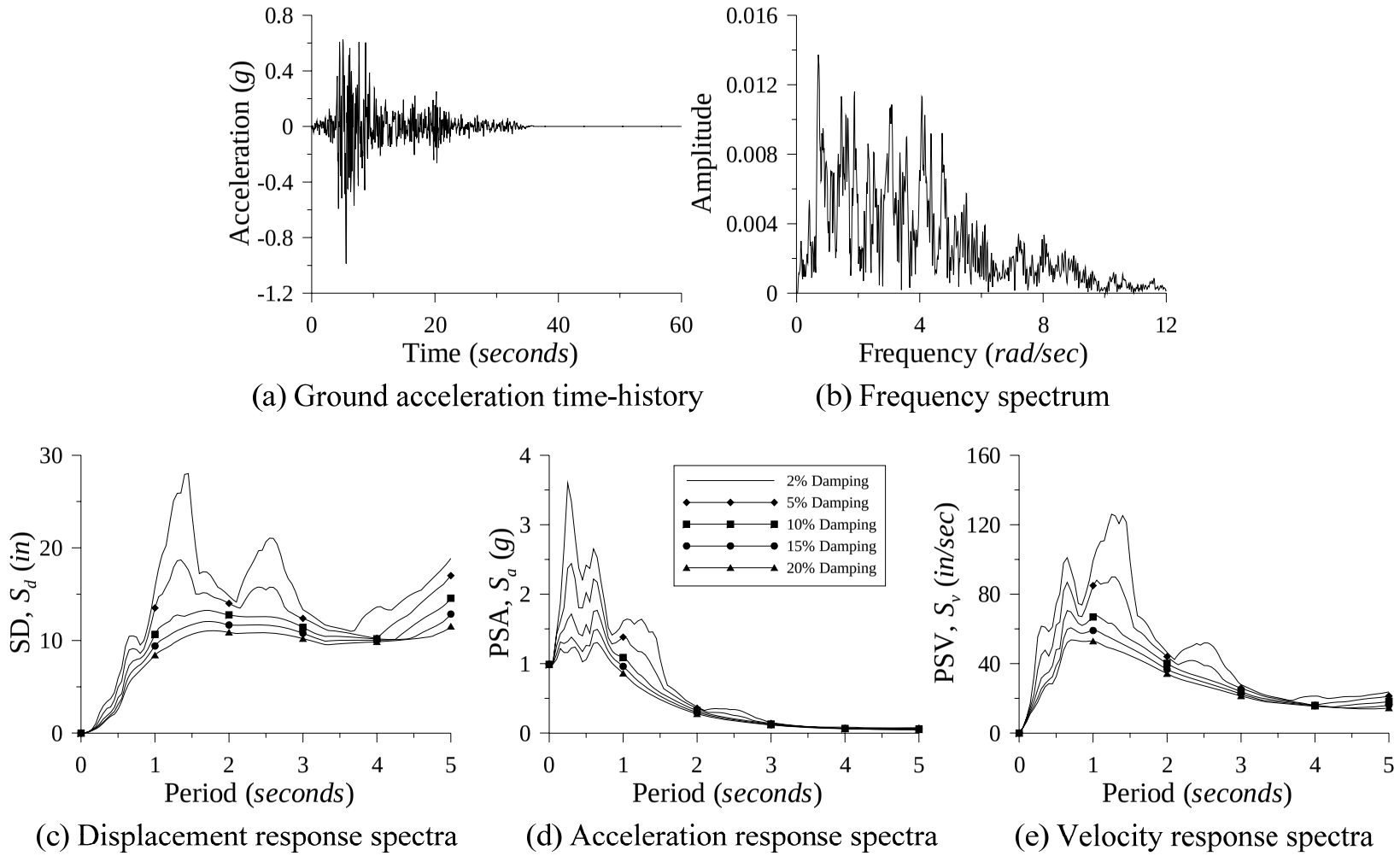

Figure App.B-3. TH-2

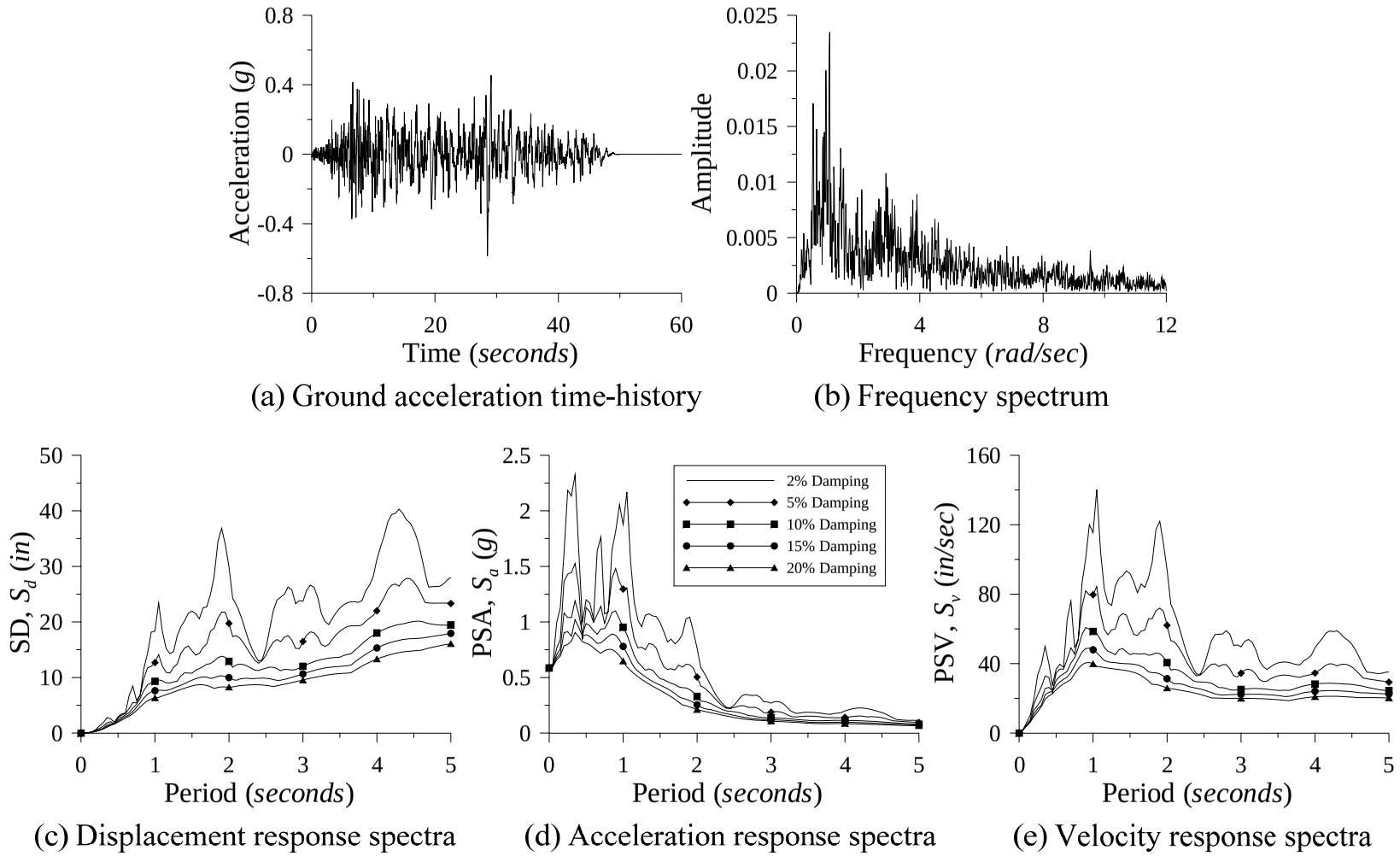

Figure App.B-4. TH-3

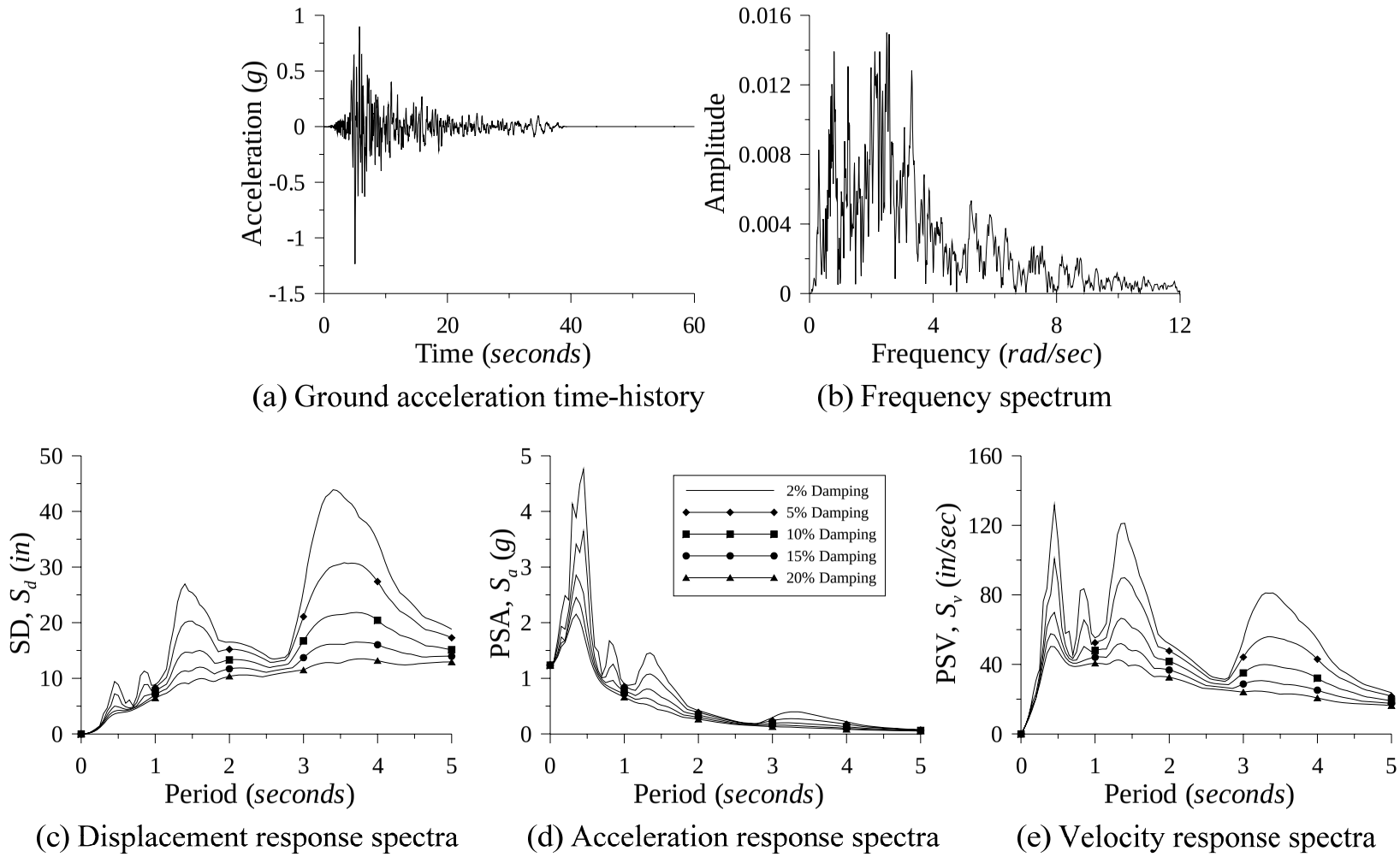

(a) Ground acceleration time-history (b) Frequency spectrum

(c) Displacement response spectra (d) Acceleration response spectra (e) Velocity response spectra

Figure App.B-5. TH-4

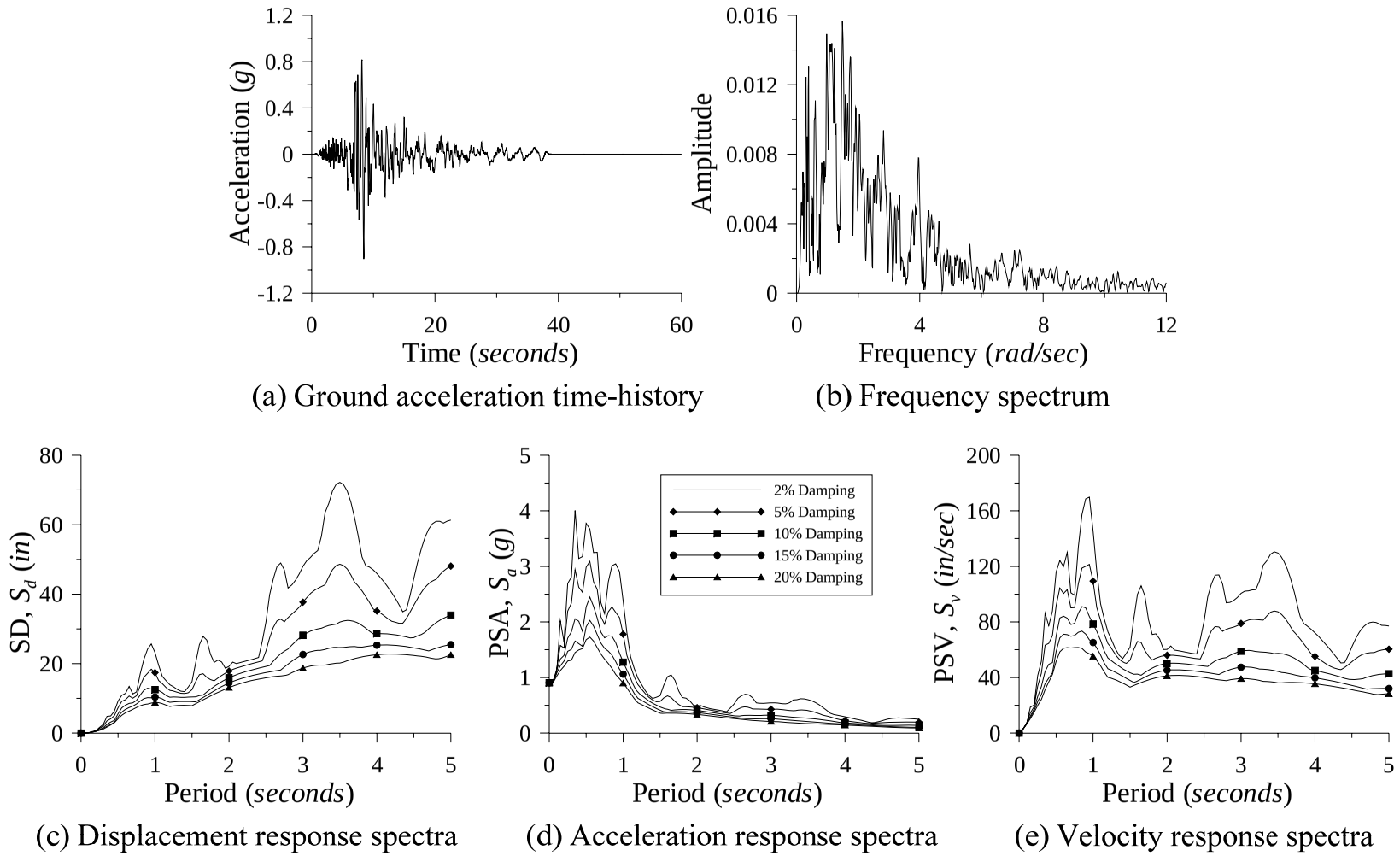

Figure App.B-6. TH-5

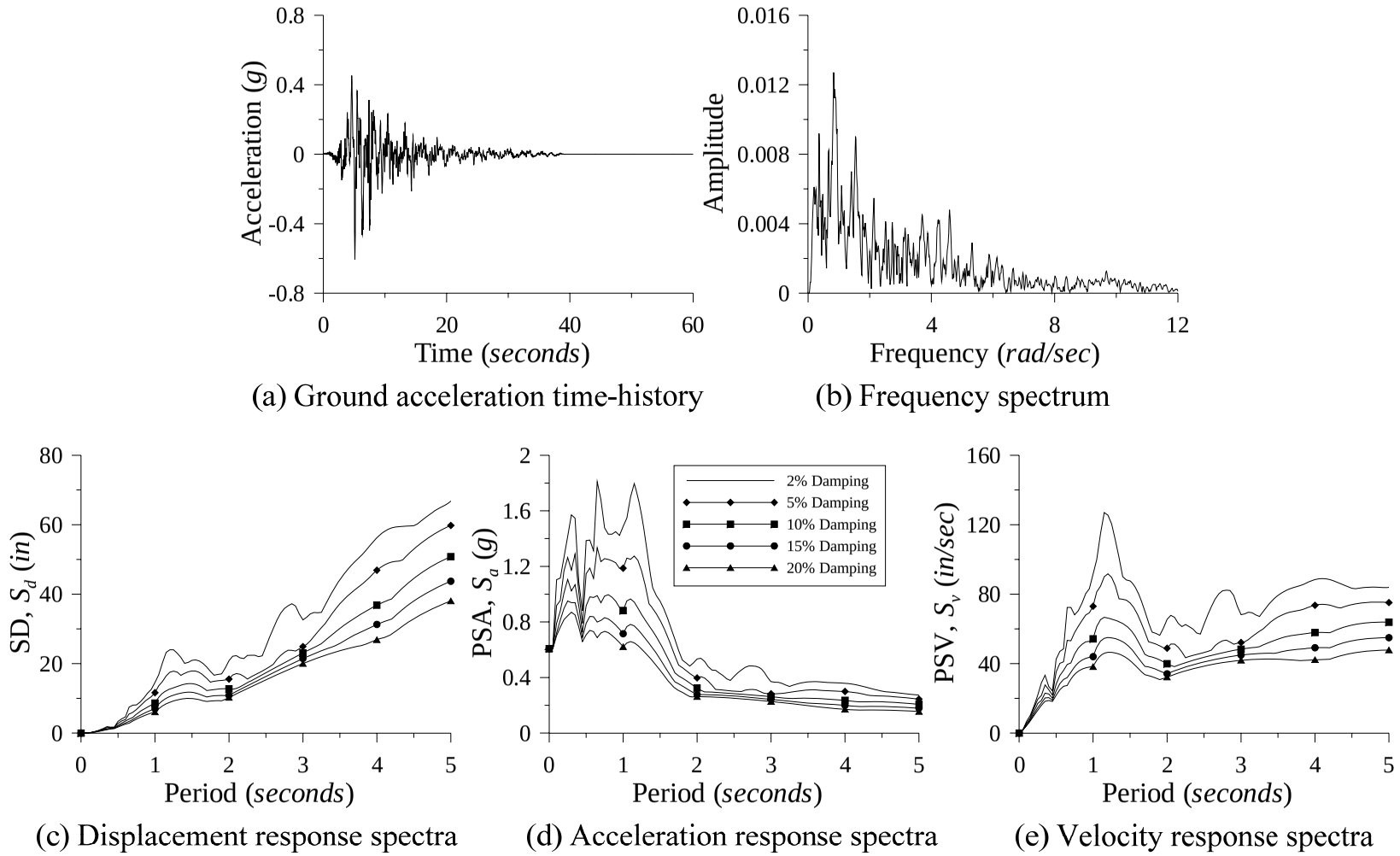

Figure App.B-7. TH-6

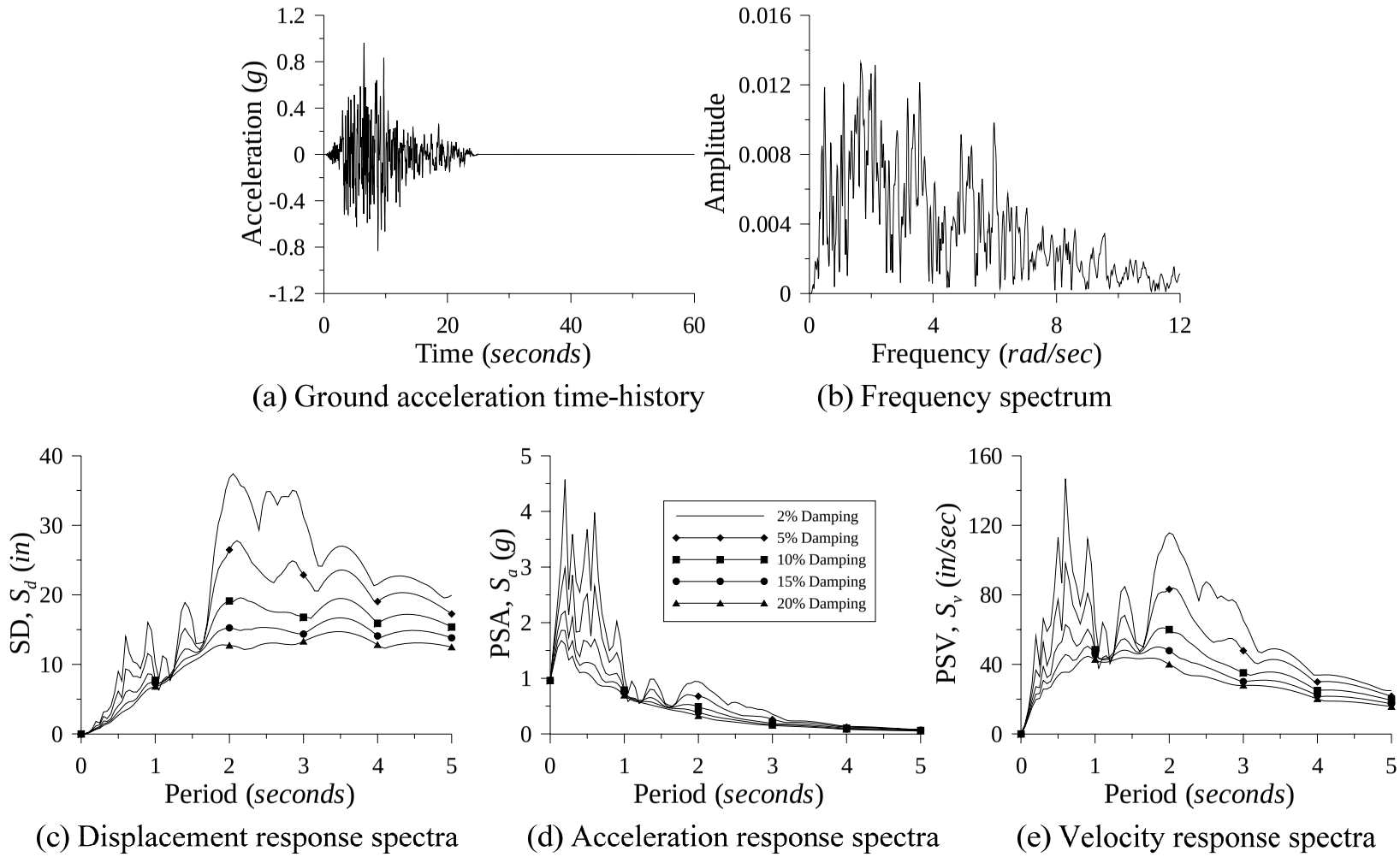

(a) Ground acceleration time-history (b) Frequency spectrum

(c) Displacement response spectra (d) Acceleration response spectra (e) Velocity response spectra

Figure App.B-8. TH-7

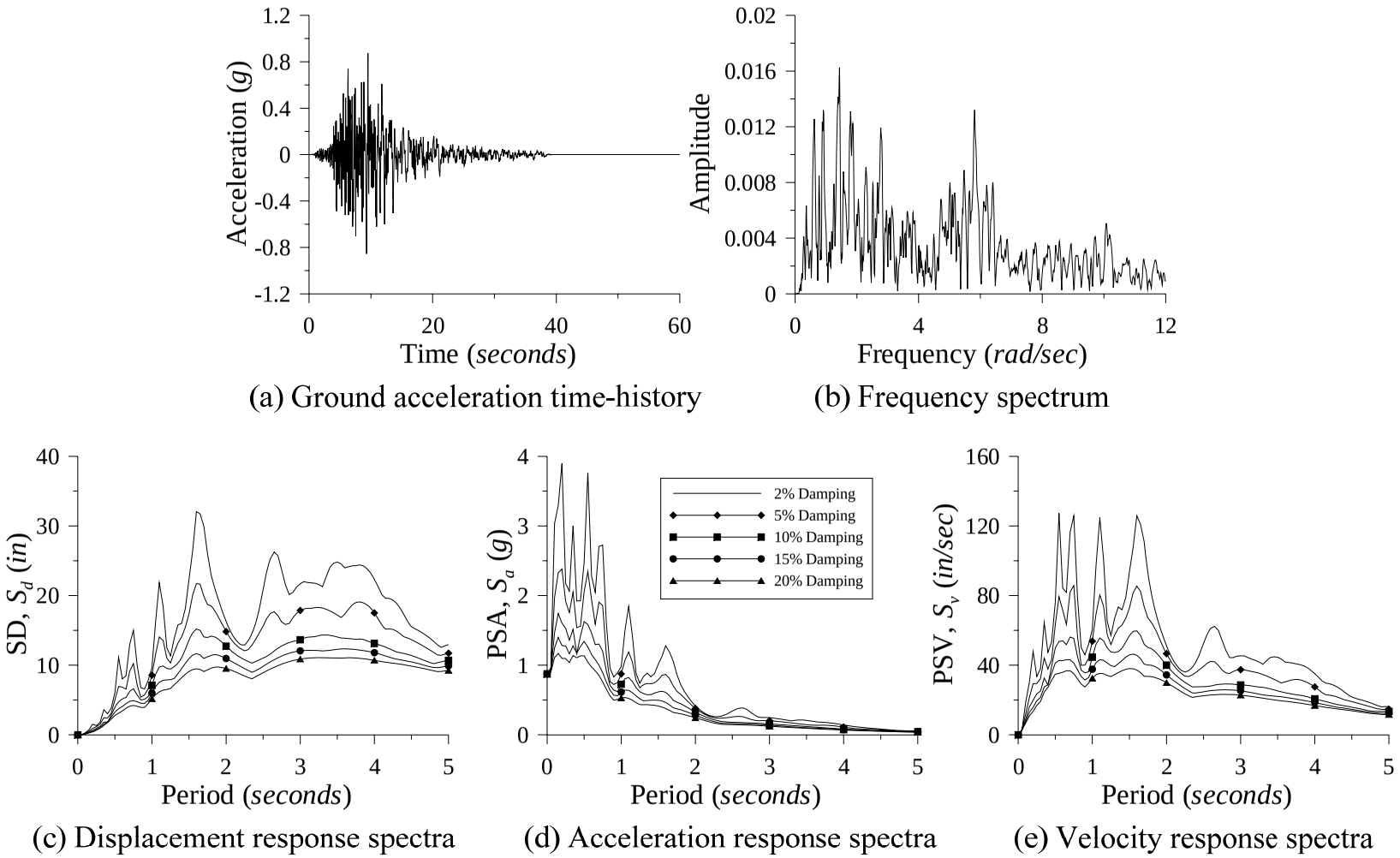

(a) Ground acceleration time-history (b) Frequency spectrum

(c) Displacement response spectra (d) Acceleration response spectra (e) Velocity response spectra

Figure App.B-9. TH-8

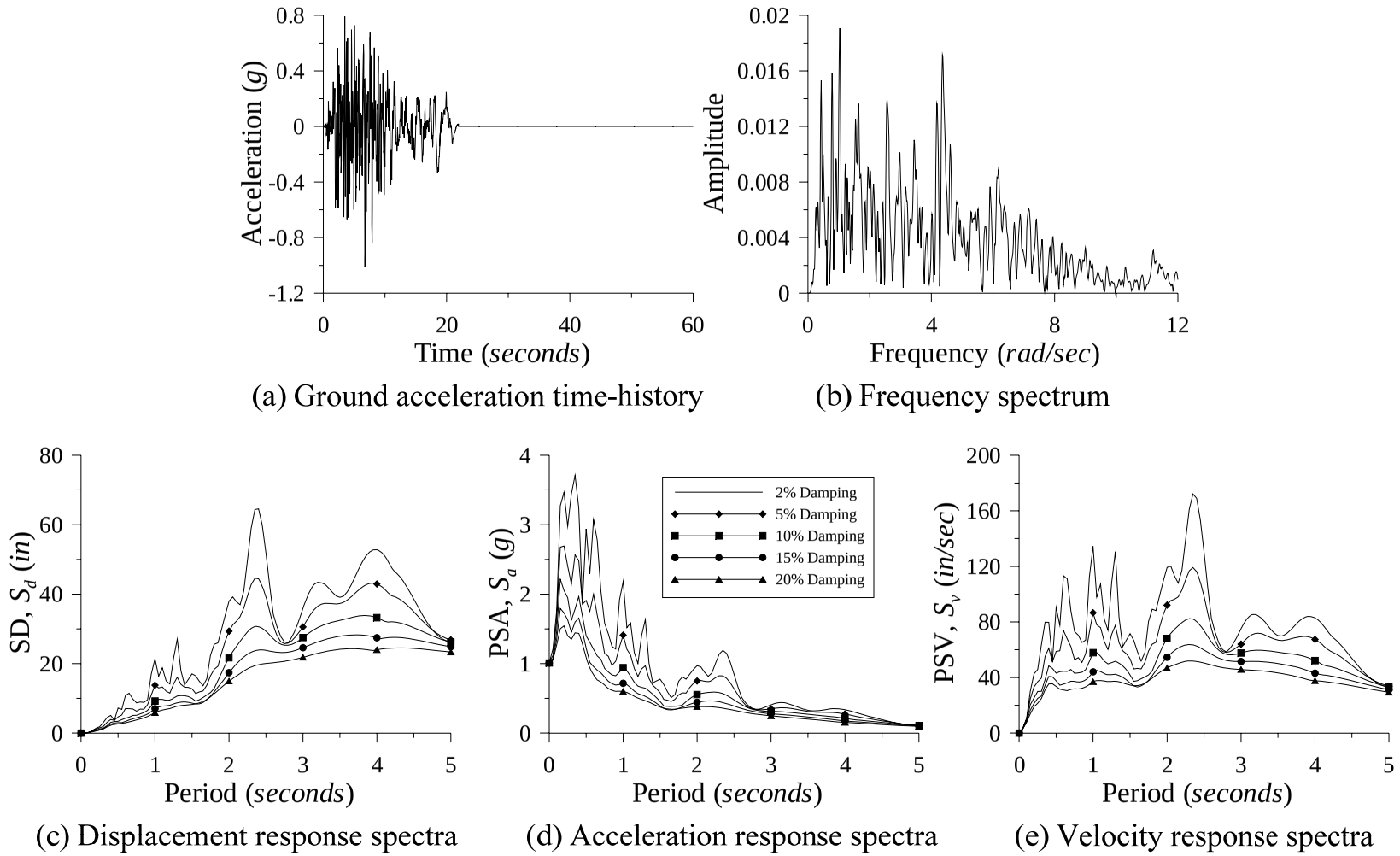

(a) Ground acceleration time-history (b) Frequency spectrum

(c) Displacement response spectra (d) Acceleration response spectra (e) Velocity response spectra

Figure App.B-10. TH-9

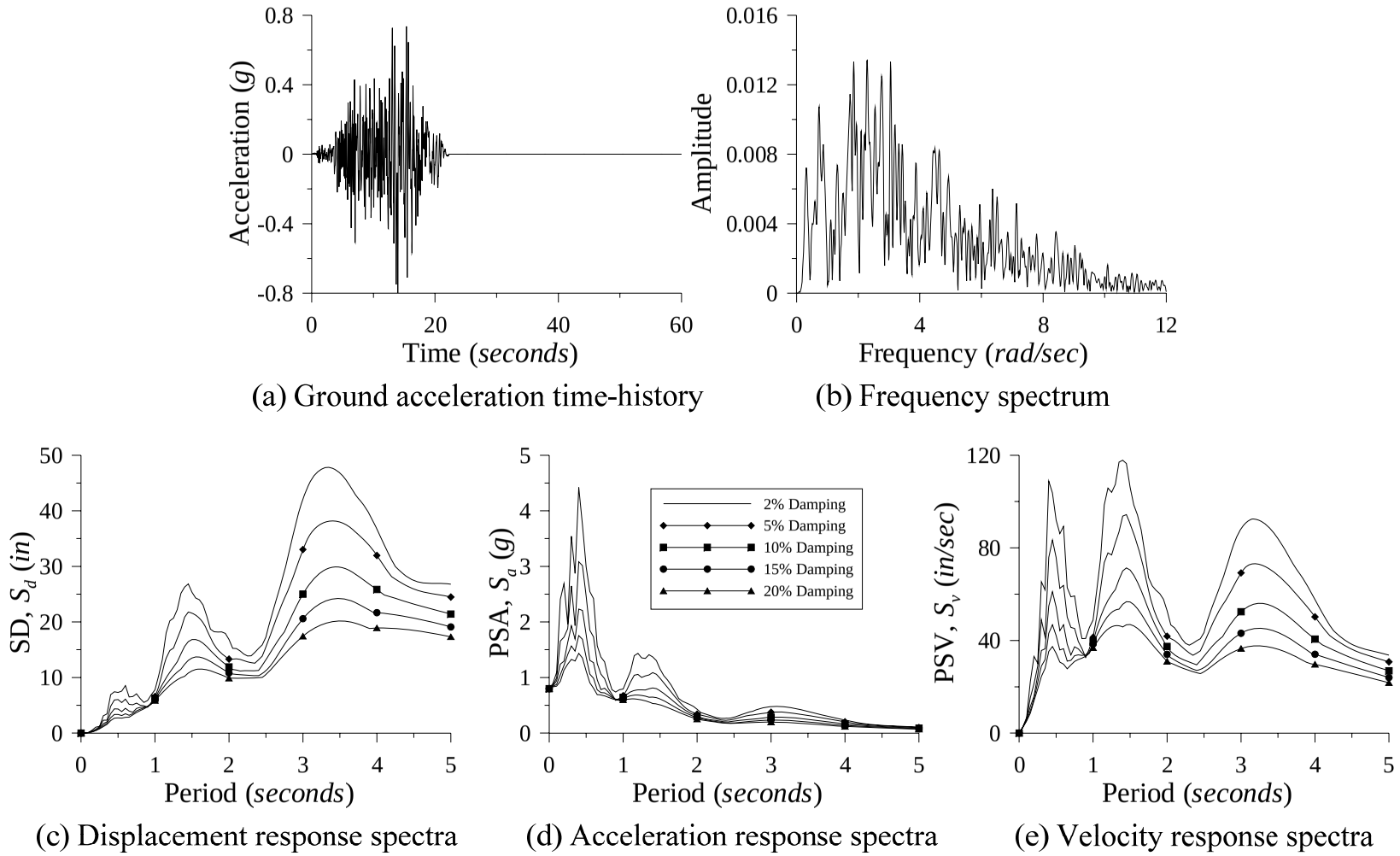

(a) Ground acceleration time-history (b) Frequency spectrum

(c) Displacement response spectra (d) Acceleration response spectra (e) Velocity response spectra

Figure App.B-11. TH-10

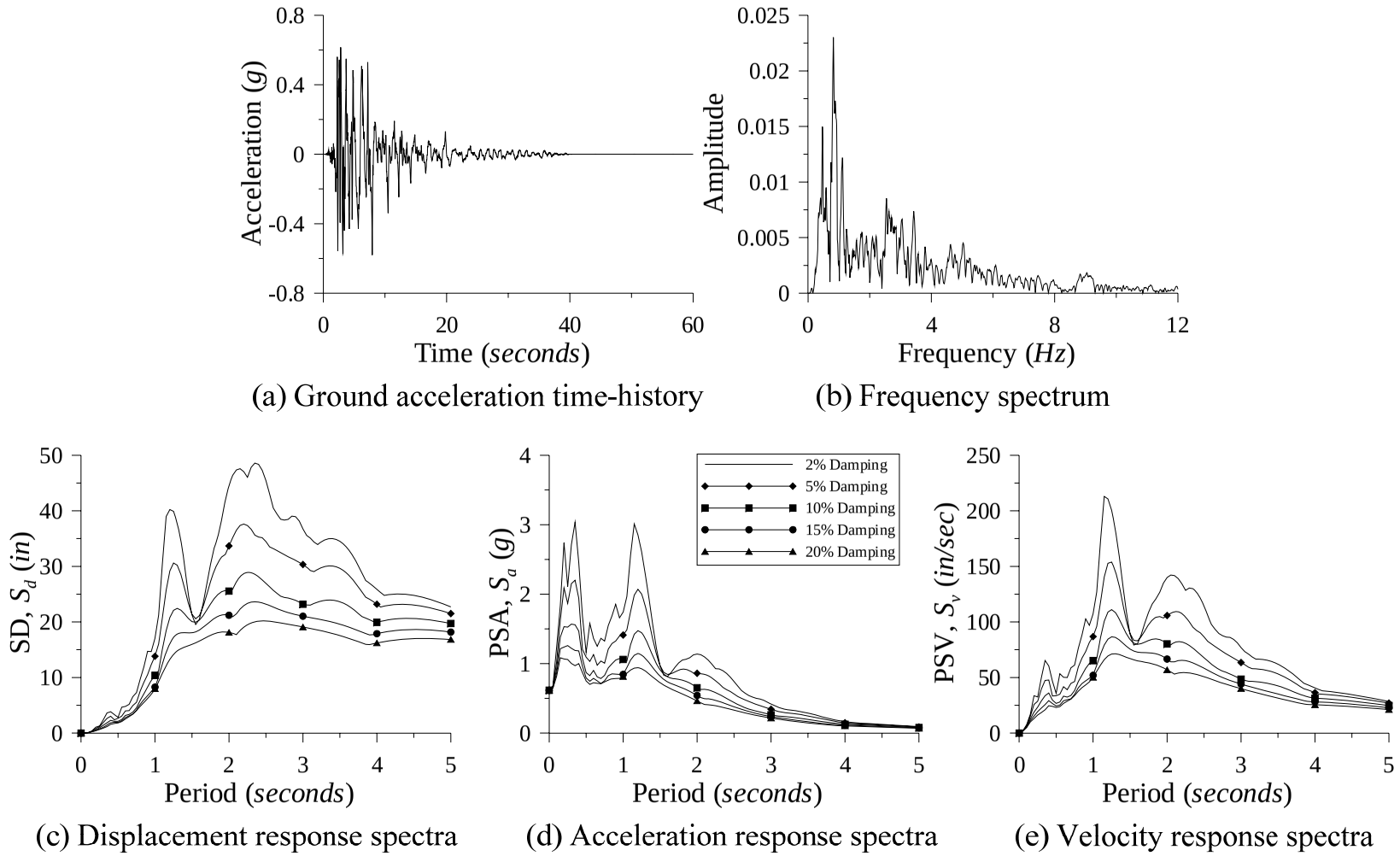

Figure App.B-12. TH-11

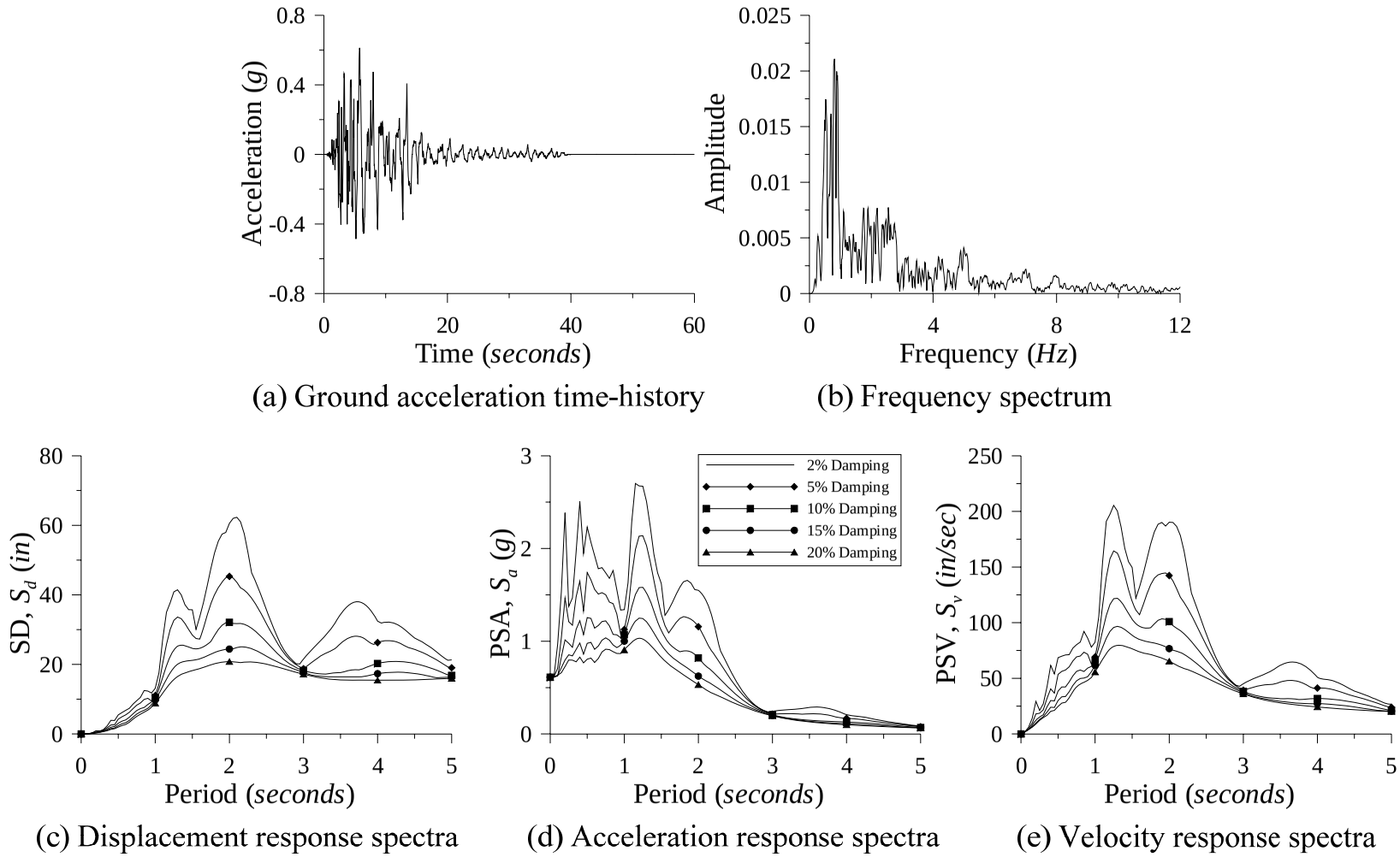

Figure App.B-13. TH-12

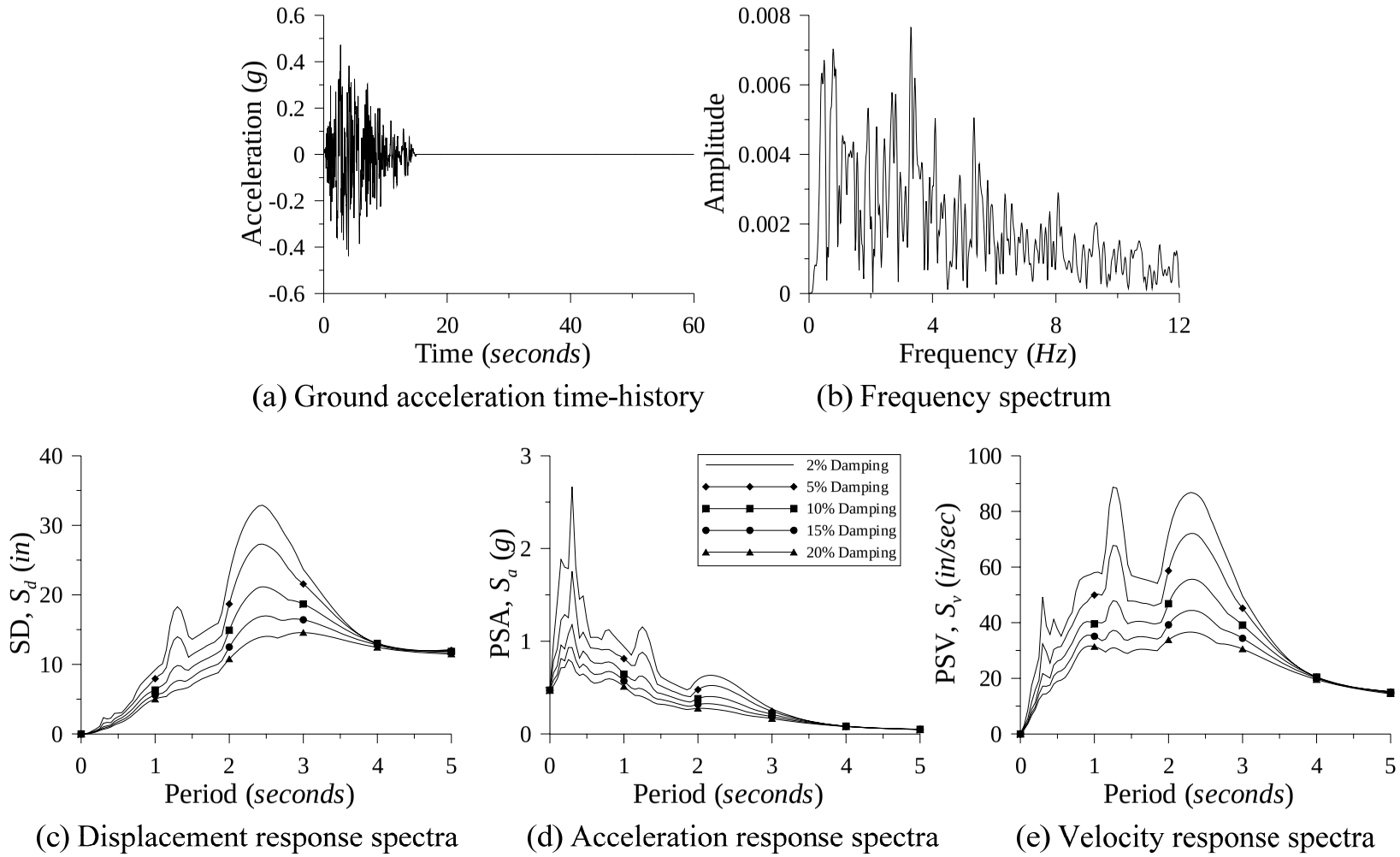

(a) Ground acceleration time-history (b) Frequency spectrum

(c) Displacement response spectra (d) Acceleration response spectra (e) Velocity response spectra

Figure App.B-14. TH-13

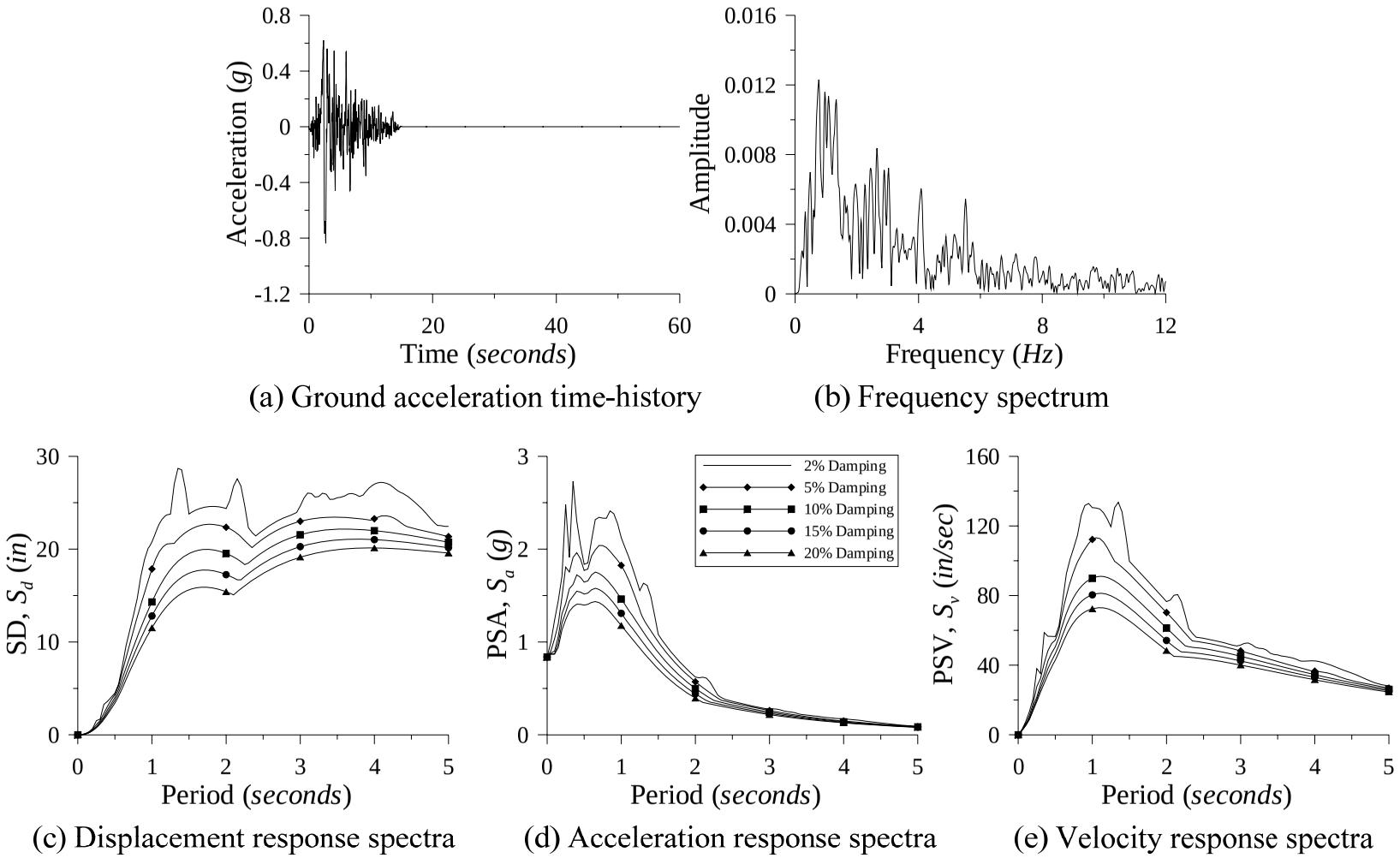

Figure App.B-15. TH-14

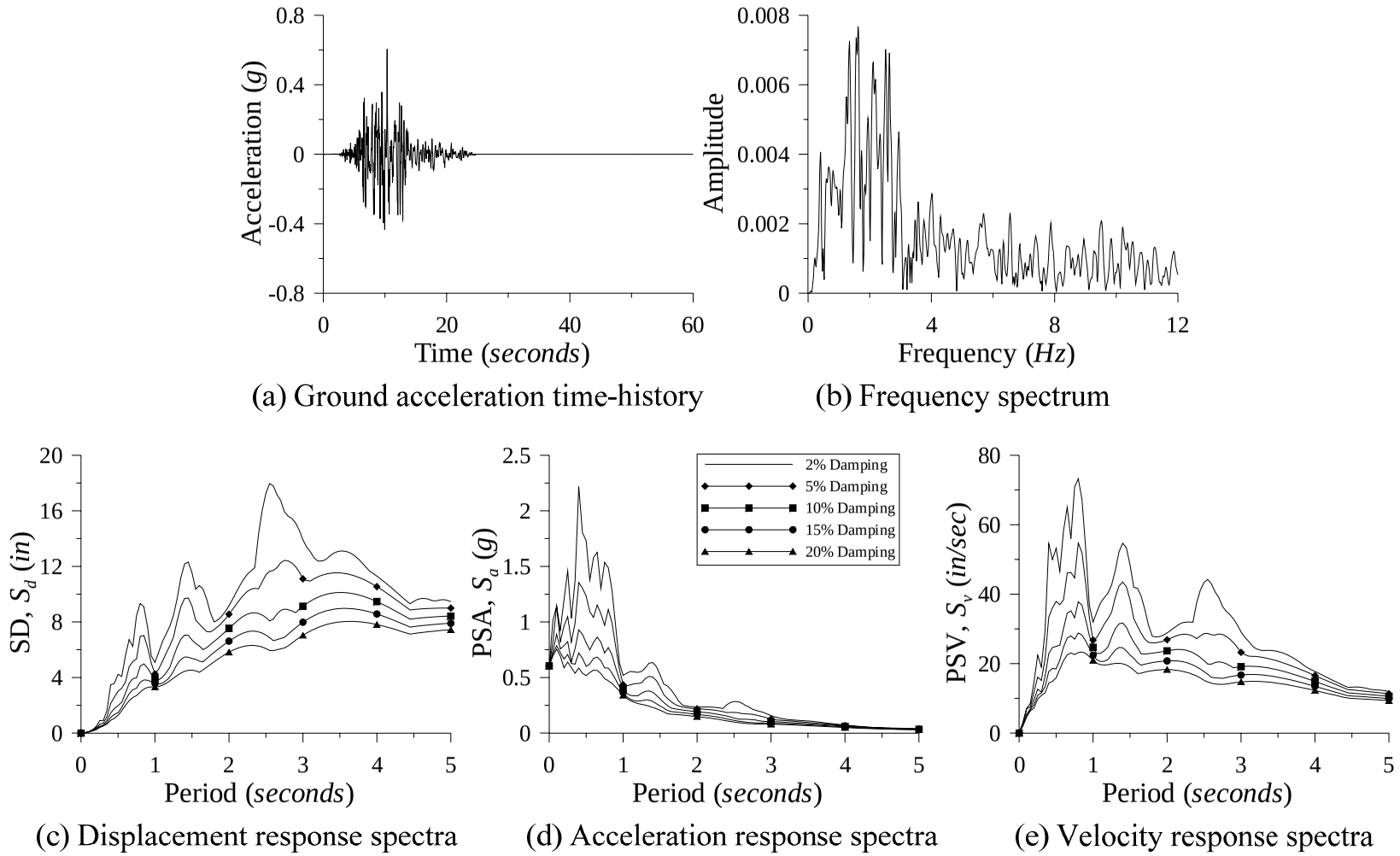

(a) Ground acceleration time-history (b) Frequency spectrum

(c) Displacement response spectra (d) Acceleration response spectra (e) Velocity response spectra

Figure App.B-16. TH-15

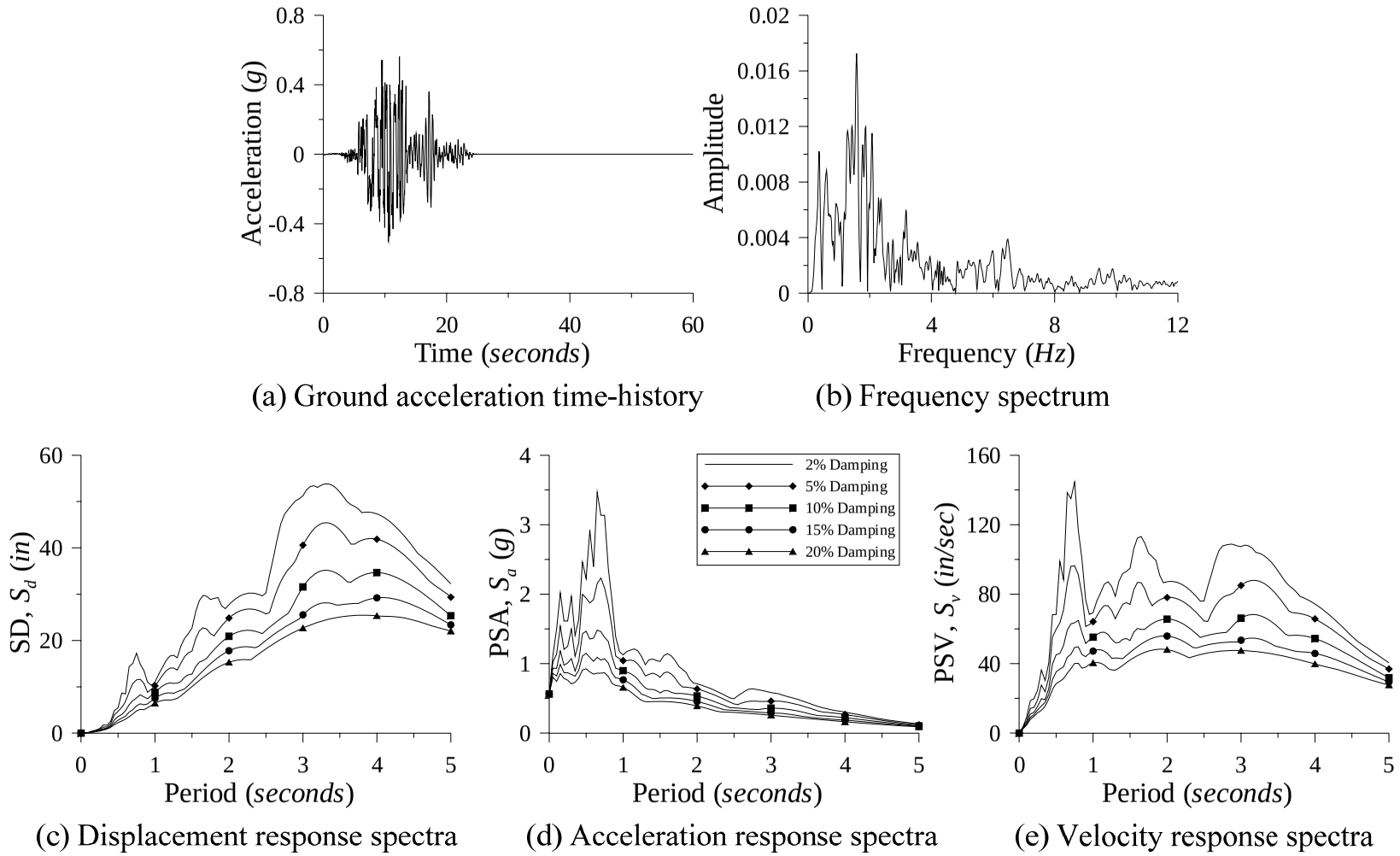

Figure App.B-17. TH-16

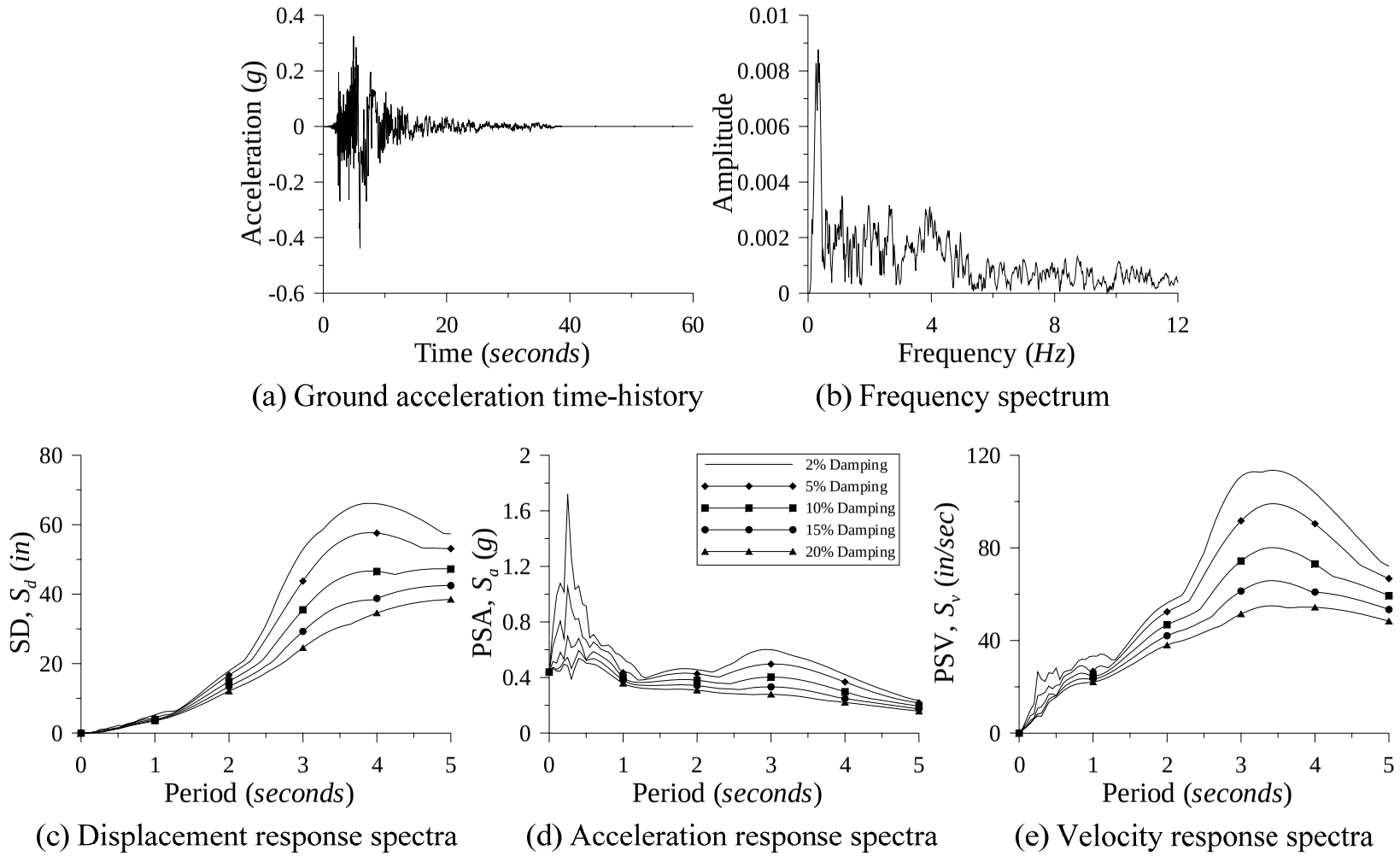

(a) Ground acceleration time-history (b) Frequency spectrum

(c) Displacement response spectra (d) Acceleration response spectra (e) Velocity response spectra

Figure App.B-18. TH-17

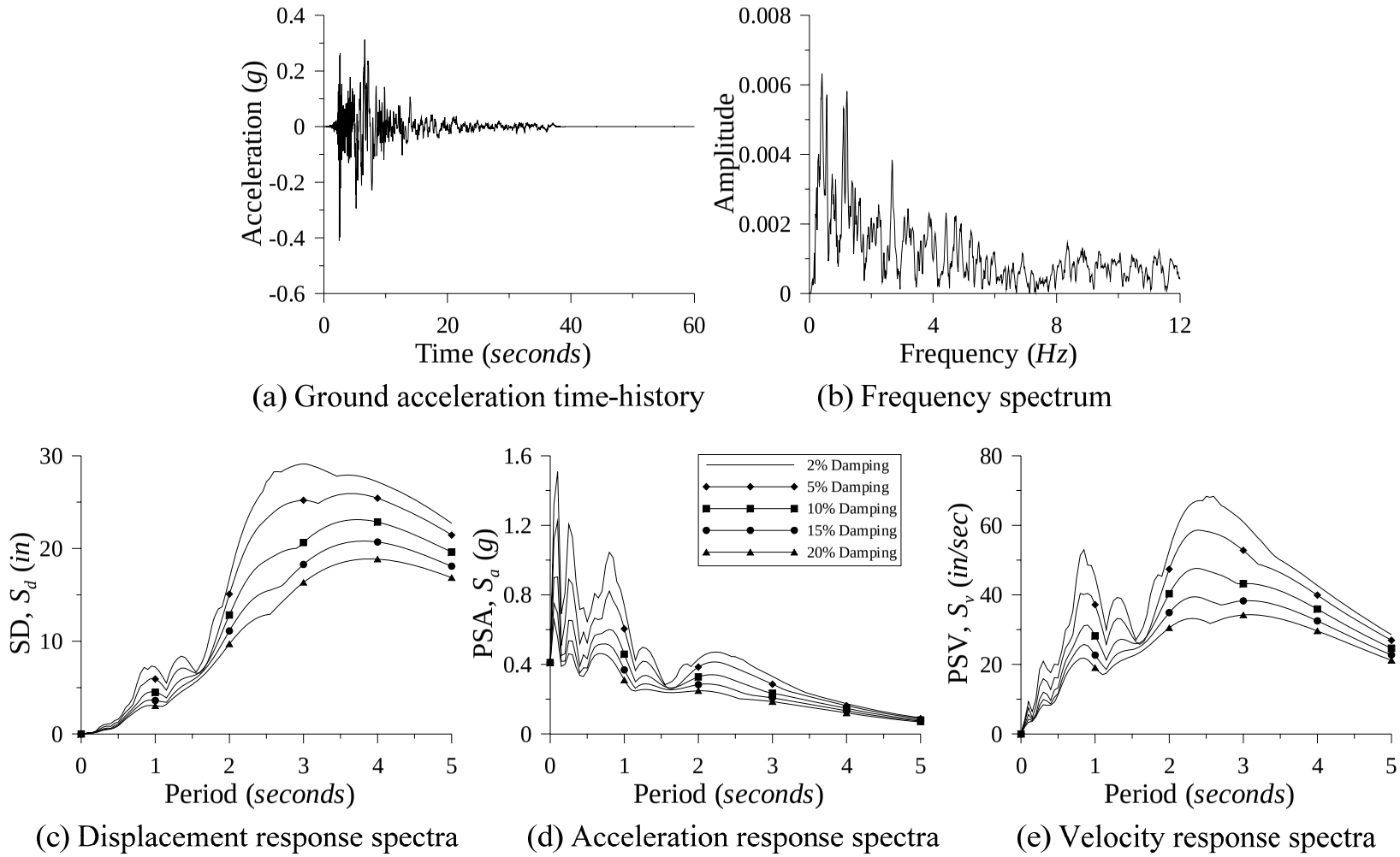

Figure App.B-19. TH-18

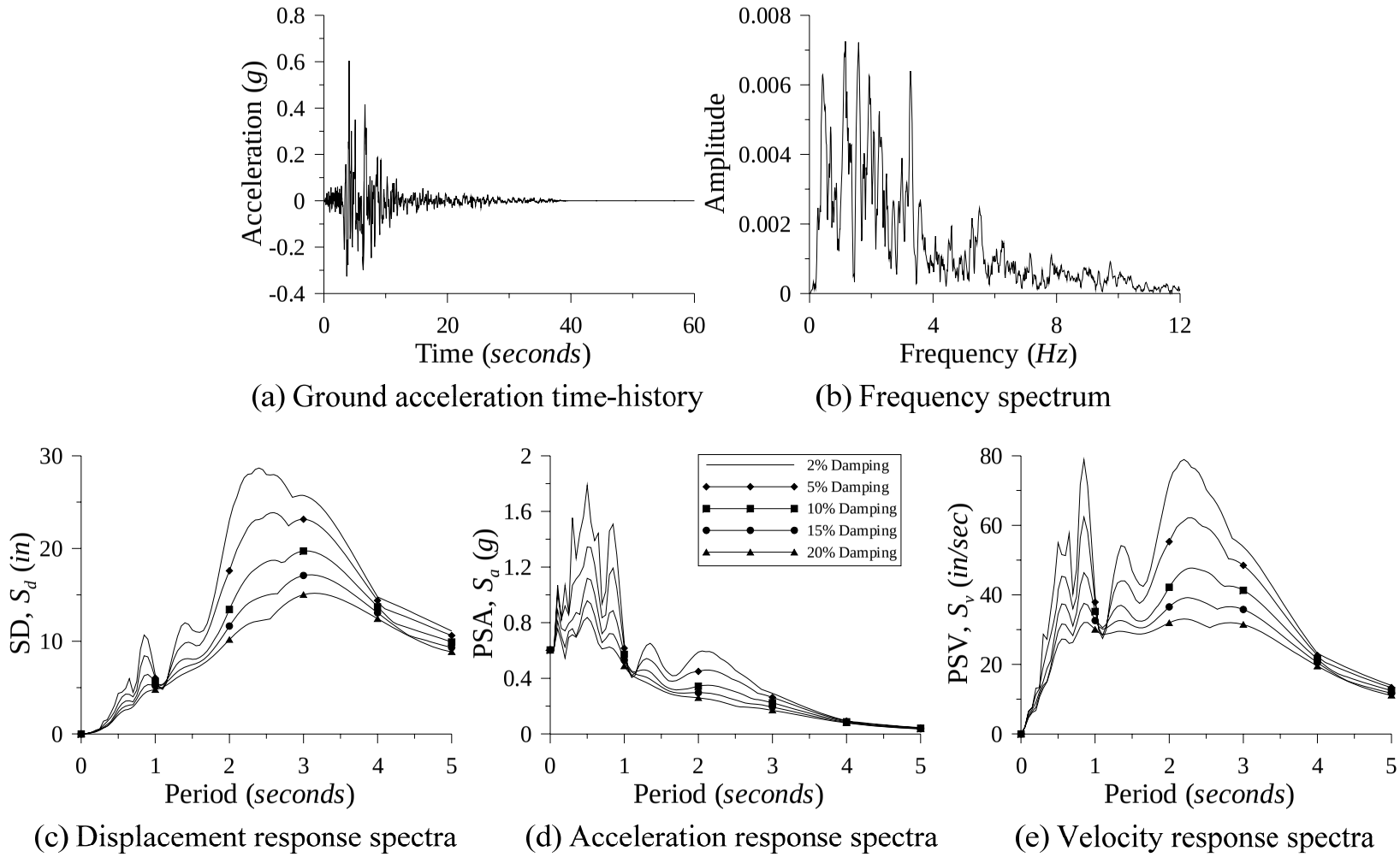

Figure App.B-20. TH-19

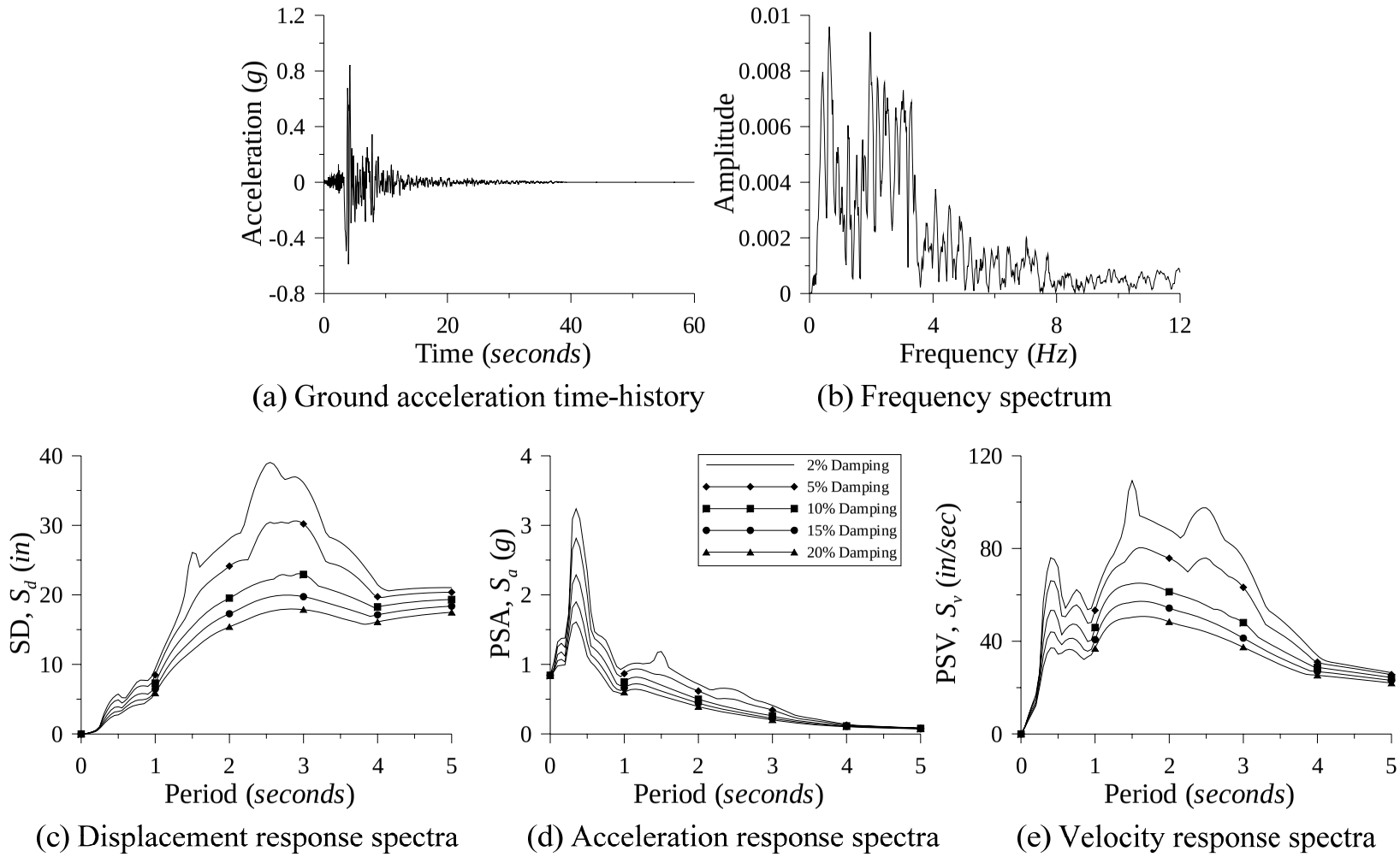

(a) Ground acceleration time-history (b) Frequency spectrum

(c) Displacement response spectra (d) Acceleration response spectra (e) Velocity response spectra

Figure App.B-21. TH-20

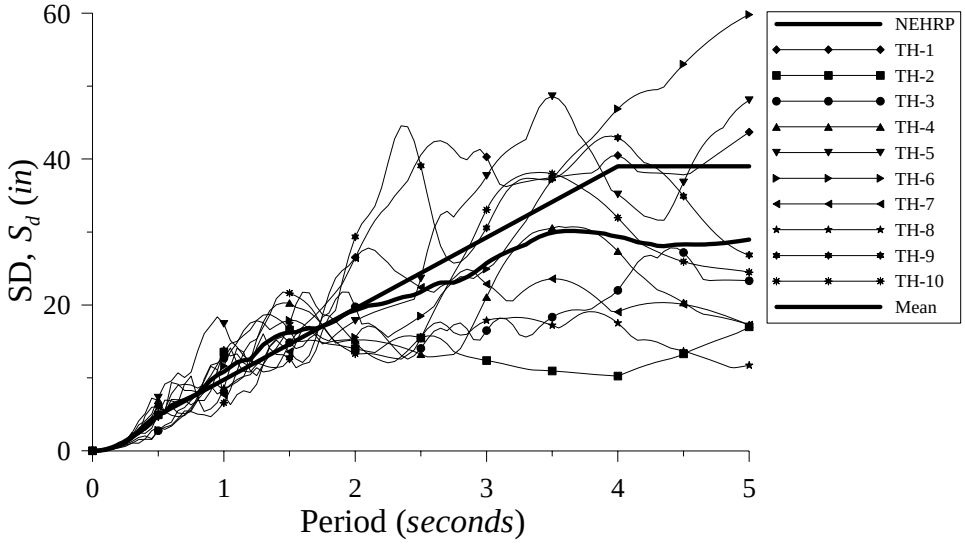

Figure App.B-22. DRS Comparison (MCE – 5% damping – Far-Field)

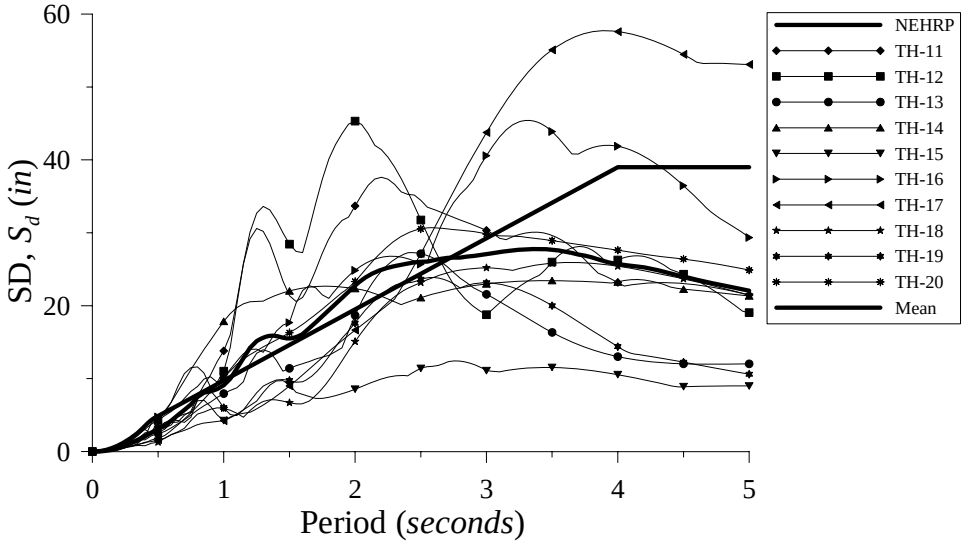

Figure App.B-23. DRS Comparison (MCE – 5% damping – Near-Fault)

Appendix C Supplementary Data

C.1 Chapter 4

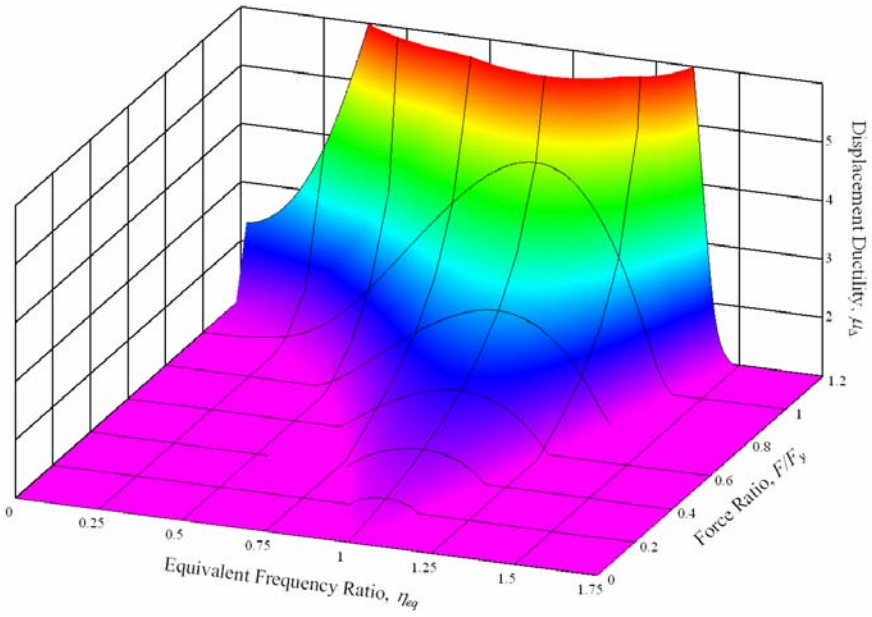

Figure App.C-1. Displacement Ductility (r_Δ = 0)

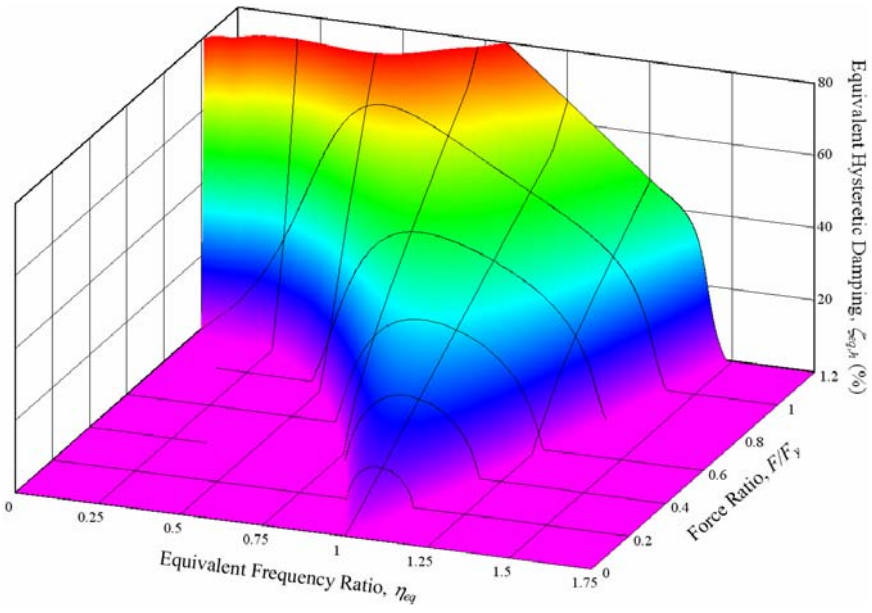

Figure App.C-2. Equivalent hysteretic damping (r_Δ = 0)

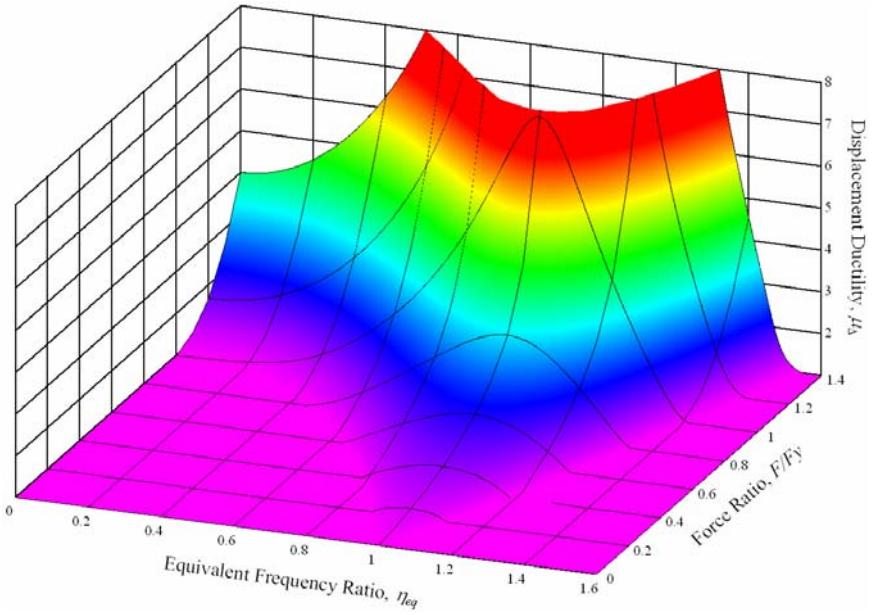

Figure App.C-3. Displacement Ductility (r_Δ = 0.1)

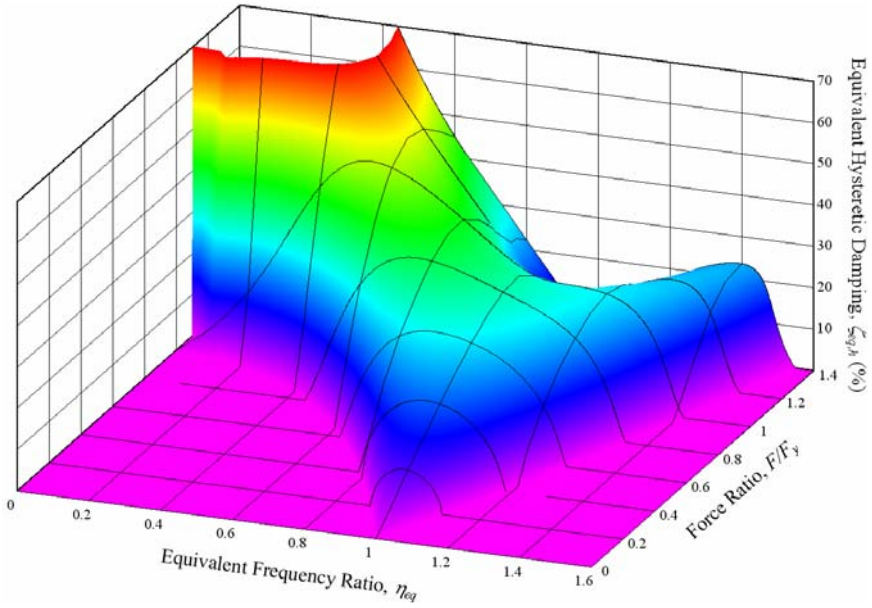

Figure App.C-4. Equivalent hysteretic damping (r_Δ = 0.1)

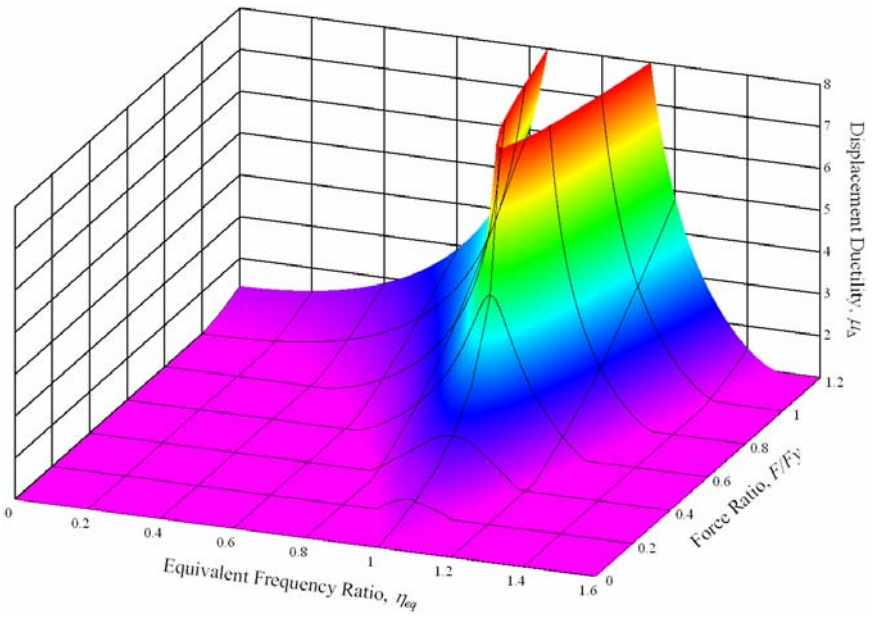

Figure App.C-5. Displacement Ductility (r_Δ = 0.4)

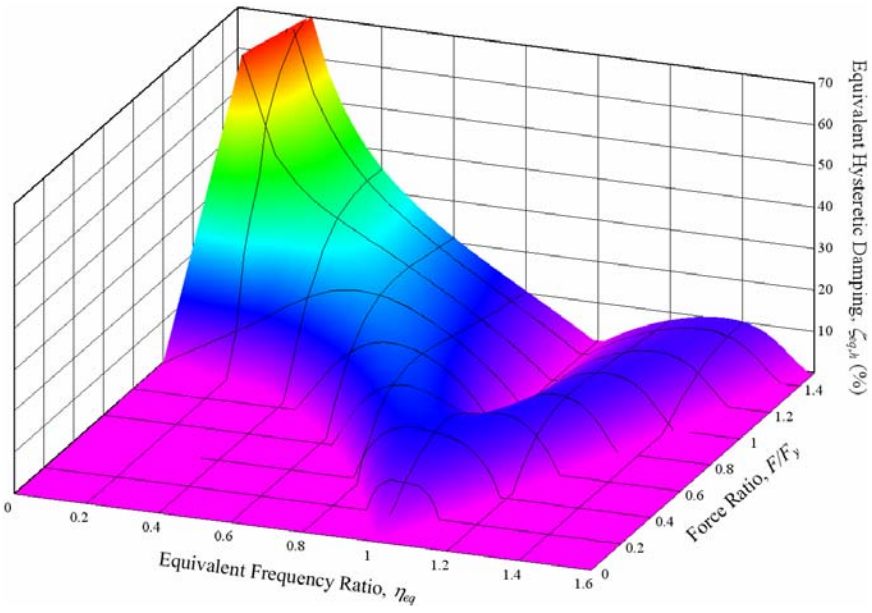

Figure App.C-6. Equivalent hysteretic damping (r_Δ = 0.4)

References

Adam, C., Ibarra, L.F., and Krawinkler, H. (2004). "Evaluation of P-Delta Effects in Non-deteriorating MDOF Structures from Equivalent SDOF Systems." *Proc., 13th World Conf. on Earthquake Eng.*, Vancouver, B.C., Canada, August 1-6 2004, Paper No. 3407.

Adams, P.F. (1979). "Overall Stability Considerations in the Design of Steel Structures." *Engineering Structures*, Vol. 25, 236-244.

Akkar, S. and Miranda, E. (2003). "Critical Review of Equivalent Linear Methods in ATC-40." *Proc., 1st National Conf. on Earthquake Engineering*, Brebbia, C.A. and Corz, A. (Eds.), Bled, Slovenia, June 24-27 1997, WIT Press, Southampton, 101-110.

Albanesi, T., Nuti, C., and Vanzi, I. (2000). "A Simplified Procedure to Assess the Seismic Response of Nonlinear Structures." *Earthquake Spectra*, EERI, Vol. 16(4), 715-734.

American Institute of Steel Construction (AISC) (2001). *Manual of Steel Construction - Load and Resistance Factor Design Specification for Structural Steel Buildings*. Chicago, IL.

American Institute of Steel Construction (AISC) (2005). *Steel Construction Manual*. Chicago, IL.

American Institute of Steel Construction (AISC) (2002). *Seismic Provisions for Structural Steel Buildings*. Chicago, IL

American Institute of Steel Construction (AISC) (2005). *Seismic Provisions for Structural Steel Buildings*. Chicago, IL.

American Society of Civil Engineers (ASCE) (2005). *ASCE 7-05: Minimum Design Loads for Buildings and Other Structures*. Herndon, VA.

American Society of Civil Engineers (ASCE) (2000). *FEMA 356: Prestandard and Commentary for the Seismic Rehabilitation of Buildings*. Washington, D.C.: Federal Emergency Management Agency (FEMA).

Andrews, A.L. (1977). "Slenderness Effects in Earthquake Resisting Frames." *Bulletin of the New Zealand Society for Earthquake Engineering*, Vol. 10(3), 154-158.

Applied Technology Council (ATC) (1978). *Tentative Provisions for the Development of Seismic Regulations of Buildings*. ATC 3-06 Report, Redwood City, CA.

Applied Technology Council (ATC) (1996a). *Structural Response Modification Factors*. ATC 19 Report, Redwood City, CA.

Applied Technology Council (ATC). (1996b). *Seismic Evaluation and Retrofit of Concrete Buildings, Volumes 1 and 2*. ATC-40 Report, Redwood City, CA.

Applied Technology Council (ATC). (1997a). *FEMA 273: NEHRP Guidelines for the Seismic Rehabilitation of Buildings*. ATC-33 Project, Washington, D.C.: Building Seismic Safety Council (BSSC) and Federal Emergency Management Agency (FEMA).

Applied Technology Council (ATC). (1997b). *FEMA 274: NEHRP Commentary on the Guidelines for the Seismic Rehabilitation of Buildings.* ATC-33 Project, Washington, D.C.: Building Seismic Safety Council (BSSC) and Federal Emergency Management Agency (FEMA).

Applied Technology Council (ATC). (2005) *FEMA 440: Improvement of Inelastic Seismic Analysis Procedures*. ATC 55 Project, Washington, D.C.: Federal Emergency Management Agency (FEMA).

Applied Technology Council (ATC). *FEMA 445: Program Plan for Development of Next-Generation Performance-Based Seismic Design Guidelines.* ATC 58-1 Project, Washington, D.C.: Federal Emergency Management Agency (FEMA). (in preparation)

Applied Technology Council (ATC) *FEMA 446: Characterization of Seismic Performance for Buildings*. ATC 58-2 Project, Washington, D.C.: Federal Emergency Management Agency (FEMA). (in preparation)

Araki, Y. and Hjelmstad, K.D. (2000). "Criteria for Assessing Dynamic Collapse of Elastoplastic Structural Systems." *Earthquake Eng. and Structural. Dynamics*, Vol. 29, 1177-1198.

Aschheim, M.A. (2002). "Seismic Design Based on the Yield Displacement." *Earthquake Spectra*, EERI, Vol. 18(4), 581-600.

Aschheim, M.A. and Black, E.F. (2000) "Yield Point Spectra for Seismic Design and Rehabilitation" *Earthquake Spectra*, EERI, Vol. 16(2), 317-336.

Aschheim, M. and Montes, E.H. (2003). "The Representation of P-Δ Effects Using Yield Point Spectra." *Engineering Structures*, Vol. 25, 1387-1396.

Asimakopoulus, A.V., Karabalis, D.L., and Beskos, D.E. (2003). "Treatment of P-Δ Effect in a Direct Displacement-Base Design Procedure of Steel Moment Resisting Frames." *Proc: Behavior of Steel Structures in Seismic Areas – STESSA 2003*, F.M. Mazzolani, Ed., Naples, Italy, 2003, pp. 9-15.

Beedle, L.S. *Plastic Design of Steel Frames*. New York: John Wiley & Sons, 1958.

Berg, G.V. (1983). *Seismic Design Codes and Procedures*. Earthquake Engineering Research Institute (EERI), Oakland, CA.

Berg, G.V. *Elements of Structural Dynamics*. Englewood Cliffs, NJ: Prentice Hall, 1989.

Bernal, D. (1987). "Amplification Factors for Inelastic Dynamic P-Δ Effects in Earthquake Analysis." *Earthquake Eng. and Structural. Dynamics*, Vol. 15, 635-651.

Bernal, D. (1992). "Instability of Buildings Subjected to Earthquakes." *J. Struct. Eng.*, ASCE, Vol. 118(8), 2239-2260.

Bernal, D. (1994). "Viscous Damping in Inelastic Structural Response." J. Struct. Eng., ASCE, Vol. 120(4), 1240-1254.

Bernal, D. (1998). "Instability of Buildings During Seismic Response." *Engineering Structures*, Vol. 20(4-6), 496-502.

Bertero, V.V. (1986). "Evaluation of Response Reduction Factors Recommended by ATC and SEAOC." *Proc.: 3rd U.S. Natl. Conf. on Earthquake Eng.*, Charleston, SC, 1663-1673.

Blandon, C.A. and Priestley, M.J.N. (2005). "Equivalent Viscous Damping Equations for Direct Displacement-Based Design." J. Earthquake Engineering, Vol. 9, SP 2, 257-278.

Bommer, J.J. and Elnashai, A.S. (1999). "Displacement Spectra for Seismic Design." *Earthquake Eng. and Struct. Dyn*. Vol. 3(1), 1-32.

Bommer, J.J., Elnashai, A.S., and Weir, A.G (2000). "Compatible Acceleration and Displacement Spectra for Seismic Design Codes." *Proc., 12th World Conference on Earthquake Engineering*, Auckland, New Zealand, Jan. 30 – Feb. 4, 2000.

Bommer, J.J. and Mendis, R. (2005). "Scaling of Spectral Displacement Ordinates with Damping Ratios." *Earthquake Eng. and Struct. Dyn*. Vol. 34(2), 145-165.

Bonacci, J.F. (1994). "Design Forces for Drift and Damage Control: A Second Look at the Substitute-Structure Approach." *Earthquake Spectra*, EERI, Vol. 10 (2), 319-331.

Bozorgnia, Y. and Bertero, V.V. (Eds.). *Earthquake Engineering: from engineering seismology to performance-based engineering*. Boca Raton, FL: CRC Press, 2004.

Borzi, B. and Elnashai, A.S. (2000). "Assessment of Inelastic Response of Buildings Using Force- and Displacement-Based Approaches." *The Struct. Design of Tall Buildings*, Vol. 9(4), 251-277.

Borzi, B., Calvi, G.M., Elnashai, A.S., and Bommer, J.J. (2001). "Inelastic Spectra for Displacement-Based Seismic Design." *Soil Dynamics and Earthquake Eng.*, Vol. 21, 47-61.

Browning, J.P. (2001) "Proportioning of Earthquake-Resistant RC Building Structures" *J. Struct. Div.*, ASCE, Vol. 127(2), 145-151.

Bruneau, M., Uang, C.M., and Whittaker, A. *Ductile Design of Steel Structures*, New York, NY: McGraw Hill, 1998.

Building Officials Code Administrators International (BOCAI) (1999). *National Building Code*. Country Club Hills, IL.

Building Seismic Safety Committee (BSSC) (2003a). *FEMA 450-1: NEHRP Recommended Provisions for Seismic Regulations for New Buildings and Other Structures, Part I: Provisions*. Washington, D.C.: Federal Emergency Management Agency (FEMA).

Building Seismic Safety Committee (BSSC) (2003b). *FEMA 450-2: NEHRP Recommended Provisions for Seismic Regulations for New Buildings and Other Structures, Part II: Commentary*. Washington, D.C.: Federal Emergency Management Agency (FEMA).

California Department of Transportation (Caltrans). (2001). *Seismic Design Criteria 1.2*. Sacramento, CA, December 2001, pp. 121.

Calvi, G.M. (1999). "A Displacement-Based Approach for Vulnerability Evaluation of Classes of Buildings." *J. Earthquake Eng.*, Vol. 3(3), 411–438.

Calvi, G.M. and Kingsley, G.R. (1995). "Displacement-Based Seismic Design of Multi-Degree-of-Freedom Bridge Structures." *Earthquake Eng. and Structural. Dynamics.*, Vol. 24, 1247-1266.

Calvi, G.M. and Pavese, A. (1995). "Displacement-Based Design of Building Structures." *European Seismic Design Practice: Research and Application, Proceedings of the Fifth SECED Conference*, Elnashai, A.S. (Ed.), Chester, United Kingdom, October 26-27 1995, A.A. Balkema, Rotterdam, 127-132.

Carr, A.J. (2004). "RUAUMOKO – Program for Inelastic Dynamic Analysis." Dept. of Civil Engineering, University of Canterbury, New Zealand.

Caughey, T.K. (1960a). "Sinusoidal Excitation of a System with Bilinear Hysteresis." *J. Appl. Mech.*, ASME, Vol. 27, 640-643.

Caughey, T.K. (1960b). “Forced Oscillations of a Semi-Infinite Rod Exhibiting Weak Bilinear Hysteresis.” *J. Appl. Mech.*, ASME, Vol. 27, 644-648.

Caughey, T.K. (1960c). “Random Excitation of a System with Bilinear Hysteresis.” *J. Appl. Mech.*, ASME, Vol. 27, 648-652.

Celebi, M. (1996). “Radiation Damping Observed from Seismic Responses of Buildings.” *Proc., 12th World Conference on Earthquake Engineering*, Auckland, New Zealand, Jan. 30 – Feb. 4, 2000.

Chandler, A.M. and Mendis, P.A. (2000). “Performance of Reinforced Concrete Frames using Force and Displacement-based Seismic Assessment Methods.” *Engineering Structures*, Vol. 22, 352-363.

Chen, W.F. and Kim, S.E. *LRFD Steel Design using Advanced Analysis*. Boca Raton, FL: CRC Press, 1997.

Chen, W.F. and Toma, S. *Advanced Analysis of Steel Frames*. Boca Raton, FL: CRC Press, 1994.

Chen, W.F. and Lui, E.M. *Stability Design of Steel Frames*. Boca Raton, FL: CRC Press, 1992.

Chen, W.F. and Sohal, I. *Plastic Design and Second-order Analysis of Steel Frames*. New York: Springer-Verlag, 1995.

Chen, W.F. *Practical Analysis for Semi-Rigid Frame Design*, Princeton, NJ: World Scientific, 2000.

Chopra, A.K. *Dynamics of Structures – Theory and Applications to Earthquake Engineering*, Englewood Cliffs, NJ: Prentice Hall, 2001.

Chopra, A. (1981). *Earthquake Dynamics of Structures, A Primer, 1st Ed.*. Earthquake Engineering Research Institute (EERI), Oakland, CA.

Chopra, A. (2005). *Earthquake Dynamics of Structures, A Primer, 2nd Ed.*. Earthquake Engineering Research Institute (EERI), Oakland, CA.

Chopra, A.K. and Goel, R.K. (1999) "Capacity-Demand-Diagram Methods Based on Inelastic Design Spectrum" *Earthquake Spectra*, EERI, Vol. 15(4), 637-656.

Chopra, A.K. and Goel, R.K. (2001). “Direct Displacement-Based design: Use of Inelastic vs. Elastic Design Spectra.” *Earthquake Spectra*, EERI, Vol. 17(1), 47-64.

Christopoulos, C., Pampanin, S., and Priestley, M.J.N. (2003). "Performance-based Seismic Response of Frame Structures Including Residual Deformations. Part I: Single-Degree-of-Freedom Systems." *J. Earthquake Eng.*, Vol. 7 (1), 97-118.

Clough, R.W. and Penzien, J. *Dynamics of Structures*. New York: McGraw-Hill, 1993.

Davidson, B.J., Chung, B.T., and Fenwick, R.C. (1991). "The Inclusion of P-Delta Effects in the Design of Structures." *Proc., Pacific Conf. on Earthquake Eng.*, New Zealand, November 20-23 1991, 37-48.

Davidson, B.J., Judi, H. and Fenwick, R.C. (2002). "Force-Based Seismic Design: A Displacement-Based Focused Approach." *Proc. of the 12th European Conference on Earthquake Engineering*, London, UK, September 9-13, 2002, SAFERR.

Decanini, L., M. Mollaioli, F. and Mura, A. (2001). "Equivalent SDOF Systems for the Estimation of Seismic Response of Multistory Frame Structures." *Proc., Earthquake Resistant Engineering Structures III*, Brebbia, C.A. and Corz, A. (Eds.), Bled, Slovenia, June 24-27 1997, WIT Press, Southampton, 101-110.

Doherty, K., Griffith, M.C., Lam, N. and Wilson, J. (2002). "Displacement-Based Seismic Design for Out-of-Plane Bending of Unreinforced Masonry Walls." *Earthquake Eng. and Structural Dynamics*, Vol. 31, 833-850.

Dwairi, H. and Kowalsky, M.J. (2004). "Investigation of Jacobsen's Equivalent Viscous Damping Approach as Applied to Displacement-Based Seismic Design." *Proc., 13th World Conference on Earthquake Engineering*, Vancouver, B.C., Canada, Aug. 1-6 2004, NZNCEE??, No. 228.

Dwairi, H., Kowalsky, M.J. and Nau, J.M. (2005). "Equivalent Damping in Support of Direct Displacement-Based Design." *Earthquake Eng. and Structural Dynamics*, submitted for review.

Earthquake Engineering Research Institute (EERI) (2000). *FEMA 349: Action Plan for Performance Based Seismic Design*. Washington, D.C.: Federal Emergency Management Agency (FEMA).

European Committee for Standardization (ECS). (1998). *EC8: Design Provisions for Earthquake Resistant of Structures*. Brussels, Belgium.

Faccioli, E., Paolucci, R., and Rey, J. (2004). "Displacement Spectra for Long Periods." *Earthquake Spectra*, EERI, Vol. 20(2), 347-376.

Fajfar, P., Yi, J., and Fischinger, M. (1988). "Comparison of Modal Analysis and Equivalent Lateral Force Procedure for Seismic Analysis of Buildings." *European Earthquake Engineering*. Vol. 2(2), 3-14

Fajfar, P. (2000) "A Nonlinear Analysis Method for Performance-Based Seismic Design." *Earthquake Spectra*, EERI, Vol. 16(3), 573-592.

Fardis M. N. and Panagiotakos, T. B. (1996). "Hysteretic Damping of Reinforced Concrete Elements," Elsevier Science Ltd, 1996, *Eleventh World Conference on Earthquake Engineering*, Paper No. 464.

Fardis, M.N., Panagiotakos, T.B., and Telemachos, B. (1997). "Displacement-Based Design of RC Buildings: Proposed Approach and Application." *Proc., Seismic Design Methodologies for the Next Generation of Codes*, Fajfar, P. and Krawinkler, H. (Eds.), Bled, Slovenia, June 24-27 1997, A.A. Balkema, Rotterdam, 195-206.

Fenwick, R.C. and Davidson, B.J. (1994). "The Influence of Different Hysteretic Forms on Seismic P-Delta Effects." *Proc., 2nd International Workshop on Seismic Design and Retrofitting of R.C. Bridges*, Queenstown, New Zealand, 1994, 57-82.

Filiatrault, A. (2003). "Advanced Seismic Design of Structures." Class manuscript, University of California, San Diego, La Jolla, CA.

Freeman, S.A. (1978). "Prediction of Response of Concrete Buildings to Severe Earthquake Motion." *ACI Special Publication SP-55*, ACI, 589-605.

Goel, R.K. and Chopra, A. (1997). "Period Formulas for Moment-Resisting Frame Buildings." *J. Struct. Eng.*, Vol. 123(11), 1454-1461.

Gulkan, P. and Sozen, M.A. (1974). "Inelastic Responses of Reinforced Concrete Structures to Earthquake Motion." *ACI Journal*, ACI, Vol. 17(12), 604-610.

Gupta, A. and Krawinkler, H. (2000a). "Estimation of Seismic Drift Demands for Frame Structures." *Earthquake Eng. and Structural. Dynamics*, Vol. 29, 1287-1305.

Gupta, A. and Krawinkler, H. (2000b). "Dynamic P-Delta Effects for Flexible Inelastic Steel Structures." *J. Struct. Eng.*, ASCE, Vol. 126(1), 145-154.

Gutierrez, J. and Alpizar, M. (2004). "An Effective Method for Displacement-Based Earthquake Design of Buildings." *Proc., 13th World Conference on Earthquake Engineering*, Vancouver, B.C., Canada, Aug. 1-6, 204.

Hadjian, A.H. (1982). "A Re-evaluation of Equivalent Linear Models for Simple Yielding Systems." *Earthquake Eng. and Structural Dynamics*, Vol. 10, 759-767.

Harris, J.L. (2002). *Seismic Analysis and Design of Type FR Steel Frames using Displacement-Based Design and Advanced Analysis*. MS Thesis, North Carolina State University, Raleigh, NC, 2002.

Harris, J.L. (2004). "Comparison of Steel Moment Frames Designed in Accordance with Force-Based and Direct Displacement-Based Design." *Proceedings: SEAOC Convention*, Aug. 2004, Monterey, CA.

Hayashi, M., Fu, J., Ichisawa, Y., Teshigawara, M., Fukuyama, H.and Kato, H. (2000). "Study for Seismic Criteria by Equivalent Linearization." *Proc., 12th World Conference on Earthquake Engineering*, Auckland, New Zealand, Jan. 30 – Feb. 4, 2000.

Heidebrecht, A.C.and Naumoski, N.D. (1997). "Development and Application of a Displacement-Based Design Approach for Moment Resisting Frame Structures." *Proc., Seismic Design Methodologies for the Next Generation of Codes*, Fajfar, P. and Krawinkler, H. (Eds.), Bled, Slovenia, June 24-27 1997, A.A. Balkema, Rotterdam, 217-228.

Hudson, D.E. (1965). "Equivalent Viscous Friction for Hysteretic Systems with Earthquake-like Excitations." *Proc., 3rd World Conference on Earthquake Engineering*, Auckland and Wellington, New Zealand, January 22 – February 1 1965, NZNCEE, Vol. II, 185-206.

International Code Conference (ICC). (2003). *International Building Code*. Falls Church, VA.

International Conference and Building Officials (ICBO) (1997). *Uniform Building Code*. Whittier, CA.

Iwan, W.D. and Gates, N.C. (1979). "The Effective Period and Damping of a Class of Hysteretic Structures." *Earthquake Eng. and Structural Dynamics*, Vol. 7, 199-211.

Iwan, W.D. (1980). "Estimating Inelastic Response Spectra from Elastic Spectra." *Earthquake Eng. and Structural Dynamics*, Vol. 8, 375-388.

Iwan, W.D. (2002). "The Use of Equivalent Linearization in Performance Based Engineering." *J. Struct. Eng.*, ASCE, Vol. 127(5), 506-516.

Jacobsen, L.S. (1930). "Steady Forced Vibration as Influenced by Damping." *Trans. of the ASME*, ASME, Vol. ?, 169-181.

Jacobsen, L.S. (1960). "Damping in Composite Structures." *Proc., 2nd World Conference on Earthquake Engineering*, Tokyo and Kyoto, Japan, July 11-18 1960, Science Council of Japan, 1029-1044.

Jennings, P.C. (1968). "Equivalent Viscous Damping for Yielding Structures." *J. Eng. Mech. Div.*, ASCE, Vol. 94, 2(EM1), 103-116.

Judi, H.J., Davidson, B.J. and Fenwick, R.C. (2002). "Damping for the Nonlinear Static Procedure in ATC-40." *Engineering Structures*, Vol. 25, 1803-1813.

Kappos, A.J. and Manafpour, A. (2001). "Seismic Design of R/C Buildings with the Aid of Advanced Analytical Techniques." *Engineering Structures*, Vol. 23(4), 319-332.

Kim, J. and Seo, Y. (2004). "Seismic Design of Low-Rise Steel Frames with Buckling-Restrained Braces." *Engineering Structures*, Vol. 26, 543-551.

Kim, S.E. and Chen, W.F. (1996). "Practical Advanced Analysis for Braced Steel Frame Design." *J. Struct. Eng*., ASCE 122(11).

Kim, S.E. and Chen, W.F. (1996). "Practical Advanced Analysis for Unbraced Steel Frame Design." *J. Struct. Eng*., ASCE 122(11).

Kircher, C.A. (1999). "United States Building Code Approach to Variations in Regional Seismicity." *Bulletin of the New Zealand Society for Earthquake Engineering*, 33(1), 48-55.

Kowalsky, M.J. (2001). "RC Structural Walls Designed according to UBC and Displacement-Based Methods." *J. Struct. Eng.*, ASCE, Vol. 127(5), 506-516.

Kowalsky, M.J. (2002). "A Displacement-Based Approach for the Seismic Design of Continuous Bridges." *Earthquake Eng. and Structural Dynamics*, Vol. 31 (3), 719-747.

Kowalsky, M.J., Priestley, M.J.N. and MacRae, G.A. (1994). "Displacement-Based Design: A Methodology for Seismic Design Applied to Single Degree of Freedom Reinforced Concrete Structures." Structural Systems Research Report, University of California, San Diego.

Kowalsky, M.J., Priestley, M.J.N. and MacRae, G.A. (1995) "Displacement-Based Design of RC Bridge Columns in Seismic Regions" *Earthquake Engineering and Structural Dynamics*, Vol. 24(12), 1623-1643.

Kowalsky, M.J. and Ayers, J.P. (2002). "Investigation of Equivalent Viscous Damping for Direct Displacement-Based Design." *Proc.: The Third U.S.-Japan Workshop on Performance-Based Earthquake Engineering Methodology for Reinforced Concrete Building Structures*, 16-18 August 2001, Seattle, Washington , pp. 173-185. 2002

Karavasilis, T.L., Bazeos, N. and Beskos, D.E. (2006). "Maximum Displacement Profiles for the Performance-Based Seismic Design of Plane Steel Moment Resisting Frames." Engineering Structures, Vol. 28, 9 -22.

Kryloff, N. and Bogoliuboff, N. *Introduction to Non-linear Mechanics*. Princeton, NJ: University Press, 1943.

Kwan, W-P. and Billington, S.L. (2003). "Influence of Hysteretic Behavior on Equivalent Period and Damping of Structural Systems." *J. Struct. Eng.*, ASCE, Vol. 129(5), 576-585.

Lee., S.-H., Min, K.-W., Hwang, J-S. and Kim, J. (2004). "Evaluation of Equivalent Damping Ratio of a Structure with Added Dampers." *Engineering Structures*, Vol. 26, 335-346.

Lee, S.-S. and Goel. S.C. (2001). "Performance-Based Design of Steel Moment Frames Using Target Drift and Yield Mechanism." Research Report No. UMCEE 01-17, Department of Civil & Environmental Engineering, University of Michigan, Ann Arbor, MI, December 2001.

Lee, S.-S., Goel, S.C. and Chao, S.-H. (2004). "Performance-Based Design of Steel Moment Frames Using Target Drift and Yield Mechanism." *Proc., 13th World Conference on Earthquake Engineering*, Vancouver, B.C., Canada, Aug. 1-6, 2004.

Levy, R., Rutenberg, A., and Qadi, K. (2006). "Equivalent Linearization Applied to Earthquake Excitations and the R-μ-T_0 Relationships." *Engineering Structures*, submitted for review.

Liew, J.Y.R., White, D.W., and Chen, W.F. (1993) Second-Order Refined Plastic Hinge Analysis of Frame Design: Part I, *J. Struct. Eng*., ASCE 119(11).

Liew, J.Y.R., White, D.W., and Chen, W.F. (1993) Second-Order Refined Plastic Hinge Analysis of Frame Design: Part II, *J. Struct. Eng.*, ASCE 119(11).

Lin, Y.Y., Chang, K.C., Tsai, M.H., and Wang, T.F. (2002). "Displacement-Based Seismic Design for Buildings." *J. Chinese Inst. Engineers*, Vol. 25(1), 89-98.

Lin, Y.Y., Tsai, H.M., Hwang, J.S. and Chang, K.C. (2003). "Direct Displacement-Based Design for Building with Passive Energy Dissipation Systems." *Engineering Structures*, Vol. 25, 25-37.

Loeding, S., Kowalsky, M.J., and Priestley, M.J.N. (1998a). "Displacement-Based Design Methodology Applied to R.C. Building Frames." Structural Systems Research Report, SSRP -98/06, University of California, San Diego.

Loeding, S., Kowalsky, M.J., and Priestley, M.J.N. (1998b). "Displacement-Based Design of Reinforced Concrete Building Frames." Structural Systems Research Report, SSRP -98/08, University of California, San Diego.

Mahin, S. and Boroschek, R. (1991). "Influence of Geometric Non-linearities on the Seismic Response and Design of Bridge Structures." *Report to California Department of Transportation*, Division of Structures.

Mazzolani, F.M. and Piluso, V. *Theory and Design of Seismic Resistant Steel Frames*. London: E&FN Spon, 1996.

Mazzolani, F.M., Montuori, R., and Piluso, V., (2000). "Performance-Based Design of Seismic Resistant MR Frames." *Behavior of Steel Structures in Seismic Area – STESSA 2000*, F.M. Mazzolani, Ed., Montreal, Canada, 2000, p. 611-618.

MacRae, G.A. (1994). "P-Δ Effects on Single-Degree-of-Freedom Structures in Earthquakes." *Earthquake Spectra*, EERI, Vol. 10(3), 539-568.

MacRae, Priestley, M.J.N., and Tao, J. (1993). "P-Δ Design in Seismic Regions." *Structural Systems Research Project*, Report No. 93/05, Dept. of Applied Mechanics and Engineering Sciences, University of California, San Diego, 115 pp.

Medhekar, M.S. and Kennedy, D.J.L. (2000a). "Displacement-Based Seismic Design of Buildings - Theory." *Engineering Structures*, Vol. 22, 201-209.

Medhekar, M.S. and Kennedy, D.J.L. (2000b). "Displacement-Based Seismic Design of Buildings - Application." *Engineering Structures*, Vol. 22, 210-221.

Merritt, R.G. (1978). "Equivalent Viscous Damping of Elastoplastic Systems Under Sinusoidal Loading." Construction Engineering Research Laboratory.

Mesa, A. and Priestley, M.J.N., "Dynamic Amplification of Seismic Moment and Shear Forces in Cantilever Walls", Master's Thesis, Rose School, Pavia, Italy, 2002, 95 pp.

Miranda, E. and Ruiz-Garcia, J. (2002). "Evaluation of Approximate Methods to Estimate Maximum Inelastic Displacement Demands." *Earthquake Eng. and Structural Dynamics*, Vol. 31, 539-560.

Miranda, E. and Lin, Y.-Y. (2004). "Non-iterative Equivalent Linear Method for Displacement-Based Design." *Proc., 13th World Conference on Earthquake Engineering*, Vancouver, B.C., Canada, Aug. 1-6, 2004.

Moehle, J.P. (1992). "Displacement-Based Design of RC Structures Subjected to Earthquakes." *Earthquake Spectra*, EERI, Vol. 8 (3), 403-428.

Montgomery, C.J. (1981). "Influence of P-Delta Effects on Seismic Design." *Canadian J. of Civil Eng.*, Vol. 8, 31-42.

Moss, P.J. and Carr, A.J. (1980). "The effects of Large Displacements on the Earthquake Response of Tall Concrete Frame Structures." *Bulletin of the New Zealand Society for Earthquake Engineering*, Vol. 13(4), 317-328.

National Fire Protection Agency (NFPA) (2003). *Building Construction and Safety Code*. Quincy, MA.

Newmark, N.M. and Hall, W.J. (1982). *Earthquake Spectra and Design*. Earthquake Engineering Research Institute (EERI), Oakland, CA.

Otani, S. (1981) "Hysteresis Models of Reinforced Concrete for Earthquake Response Analysis." *J. Faculty of Eng.*, University of Tokyo XXXVI(2), 407–441.

Pampanin, S., Christopoulos, C., and Priestley, M.J.N. (2003). "Performance-based Seismic Response of Frame Structures Including Residual Deformations. Part II: Multi-Degree-of-Freedom Systems." *J. Earthquake Eng.*, Vol. 7 (1), 119-147.

Panagiotakos T.B. and Fardis M.N. (1999) "Deformation-Controlled Earthquake-Resistant Design of RC Buildings" *J. of Earthquake Eng.*, Vol. 3(4), 498-518.

Paret, T.F, Sasaki, K.K., Eilbeck, D.H., and Freeman, S.A. (1996). "Approximate inelastic procedures to identify failure mechanisms from higher mode effects." *11th World Conference on Earthquake Engineering*, Acapulco, Mexico.

Park, H. and Taesung, E. (2005). "Direct Inelastic Earthquake Design Using Secant Stiffness." *J. Struct. Eng.*, ASCE, Vol. 131(9), 1355-1362.

Paulay, T. (1978). "A Consideration of P-Delta Effects in Ductile Reinforced Concrete Frames." *Bulletin of the New Zealand Society for Earthquake Engineering*, Vol. 11(3), 151-160.

Paulay, T. and Priestley, M.J.N. *Seismic Design of Reinforced Concrete and Masonry Buildings*, New York: John Wiley & Sons, 1992.

Pettinga, J.D. and Priestley, M.J.N. (2005). "Dynamic Behavior of Reinforced Concrete Frames Designed with Direct Displacement-Based Design." *J. Earthquake Eng*., Vol. 9, SP2, 309-330.

Priestley, M.J.N. (1993). "Myths and Fallacies in Earthquake Engineering – Conflicts between Design and Reality." *Bulletin of the New Zealand Society for Earthquake Engineering*, 26(3), 329-341.

Priestley, M.J.N. (1998a). "Brief Comments on Elastic Flexibility of Reinforced Concrete Frames and Significance to Seismic Design." *Bulletin of the New Zealand Society for Earthquake Engineering*, 31(4), 246-259.

Priestley, M.J.N. (1998b). "Direct Displacement-Based Seismic Design of Buildings." *Proc., Asia-Pacific Workshop on Seismic Design and Retrofit of Structures*, Taipei, China, August 10-12 1998, NCREE, 549-569.

Priestley, M.J.N. (2003). "Myths and Fallacies in Earthquake Engineering, Revisited." *The 9th Mallet Milne Lecture, 2003*, IUSS Press (Rose School), Pavia, Italy, 121 pp.

Priestley, M.J.N. and Calvi, G.M. (1997). "Concepts and Procedures for Direct Displacement-Based Design and Assessment." *Proc., Seismic Design Methodologies for the Next Generation of Codes*, Fajfar, P. and Krawinkler, H. (Eds.), Bled, Slovenia, June 24-27 1997, A.A. Balkema, Rotterdam, 171-182.

Priestley, M.J.N. and Calvi, G.M. (2003). "Direct Displacement-Based Seismic Design of Concrete Bridges." *Proc.: ACI 2003 International Conference: Seismic Bridge Design and Retrofit for Earthquake Resistance*, December 8-9, 2003, La Jolla, CA.

Priestley, M.J.N., Kowalsky, M.J., Ranzo, G. and Benzoni, G. (1996). "Preliminary Development of Direct Displacement-Based Design for Multi-Degree of Freedom Systems", *Proc.: 65th Annual SEAOC Convention*, Maui, Hawaii, U.S.A., 47-66.

Priestley, M.J.N. and Kowalsky, M.J. (2000). "Direct Displacement-Based Seismic Design of Concrete Buildings." *Bulletin of the New Zealand Society for Earthquake Engineering*, 33(4), 421-444.

Priestley, M.J.N. and Grant, D.N. (2004). "Viscous Damping in Seismic Design and Analysis." *J. Earthquake Eng.*, Vol. 9, SP 2, 229-255.

Qi, X. and Moehle, J.P. (1991). "Displacement Design Approach for Reinforced Concrete Structures Subjected to Earthquakes." Struct. Res. Series No. 413, Civ. Eng. Studies, University of Illinois, Urbana, Illinois.

Reddy, C.K. and Pratap, R. (2000). "Equivalent Viscous Damping for a Bilinear Hysteretic Oscillator." *J. Eng. Mechanics*, ASCE, Vol. 126 (11), 1189-1196.

Reinhorn, A.M. (1997). "Inelastic Analysis Techniques in Seismic Evaluations." *Proc., Seismic Design Methodologies for the Next Generation of Codes*, Fajfar, P. and Krawinkler, H. (Eds.), Bled, Slovenia, June 24-27 1997, A.A. Balkema, Rotterdam, 277-287.

Riddell, R., Garcia, J.E. and Garces, E. (2002). "Inelastic Deformation Response of SDOF Systems Subjected to Earthquakes." *Earthquake Eng. and Structural Dynamics*, Vol. 31, 515-538.

Rosenblueth, E. (1965). "Slenderness Effects in Buildings." *TJ. Of Struct. Div.*, ASCE, Vol. 91 (ST1), 229-254.

Rosenblueth, E. and Herrera, I. (1964). "On a Kind of Hysteretic Damping." *J. Eng. Mech. Div.*, ASCE, Vol. 90, 8(EM4), 37-48.

SAC Joint Venture. *FEMA 350: Steel Moment Frame Buildings: Design Criteria for New Buildings*. Washington, D.C.: Federal Emergency Management Agency (FEMA), 2000.

--Salmon, C.G. and Johnson, J.E. *Steel Structures – Design and Behavior*. New York: Harper Collins, 1996.

Shibata, A. (1975). "Equivalent Linear Models to Determine Maximum Inelastic Response of Nonlinear Structures for Earthquake Motion." *Earthquake Eng. and Structural. Dynamics.*, Vol. 24, 1247-1266.

Shibata, A. and Sozen, M.A. (1976a). "Substitute-Structure Method for Seismic Design in R/C." *J. Struct. Div.*, ASCE, Vol. 102, 1(ST1), 1-18.

Shibata, A. and Sozen, M.A. (1976b). "Use of Linear Models in Design to Reflect the Effect of Nonlinear Response." Proc.: Review Meeting, U.S.-Japan Cooperative Research Program in Earthquake Engineering with Emphasis on the Safety of School Buildings, 274-290.

Shibata, A. and Sozen, M.A. (1977). "Substitute-Structure Method to Determine Design Forces in Earthquake-Resistant Reinforced Concrete Frames." *Proc., 6th World Conference on Earthquake Engineering*, Auckland and Wellington, New Zealand, January 22 – February 1 1965, ISET, Vol. II, 1905-1910.

Shimazaki, K. (2000). "Evaluation of Structural Coefficient by Displacement Response Estimation Using the Equivalent Linear Method." *Proc., 12th World Conference on Earthquake Engineering*, Auckland, New Zealand, Jan. 30 – Feb. 4, 2000.

Smith, R.S.H. and Tso, W.K. (2002). "Inconsistency of Force-Based Design Procedure." *J. Seismology and Earthquake Eng.*. Vol. 4(1), 47-54.

Southern Building Code Congress International (SBCCI) (1999) *Standard Building Code*. Birmingham, AL.

Structural Engineering Association of California (SEAOC). *Recommended Lateral Force Requirements and Commentary*. Sacramento, CA, 1999.

Structural Engineering Association of California (SEAOC). *Vision 2000: Performance-Based Seismic Engineering of Buildings*, Sacramento, CA, 1995.

Structural Stability Research Council (SSRC) (1993). "Plastic-Hinge Based Methods for Advanced Analysis and Design of Steel Frames." White, D.W. and Chen, W.F., Eds., SSRC, Lehigh University, Bethlehem, PA, 299 pp.

Sullivan, T.J., Calvi, G.M., Priestley, M.J.N. and Kowalsky, M.J. (2003). "The Limitations and Performances of Different Displacement-Based Design Methods." *J. Earthquake Eng.*, Vol. 7 (SP1), 201-241.

Sullivan, T.J., Calvi, G.M., and Priestley, M.J.N. (2004). "Initial Stiffness Versus Secant Stiffness in Displacement-Based Design." *Proc., 13th World Conference on Earthquake Engineering*, Vancouver, B.C., Canada, Aug. 1-6, 2004. No. 2888.

Takeda, T, Sozen, M.A. and Nielsen, N.N. (1970). "Reinforced Concrete Response to Simulated Earthquakes." *J. Struct. Div.*, ASCE, Vol. 96, 12(ST12), 2557-2573.

Teshigawara, M., Isoda, H. and Izumi, N. (2000). "Deviation of Plastic Deformations and Equivalent Damping Ratio on Single-Degree-of-Freedom System." *Engineering Structures*, Vol. 25, 75-87.

Thomsen, J.H. and Wallace, J.W. (2004). "Displacement-Based Design of Slender Reinforced Concrete Structural Walls – Experimental Investigation." *J. Struct. Eng.*, ASCE, Vol. 103(4), 618-630.

Tjondro, J.A., Moss, P.J., and Carr, A.J. (1992). "Seismic *P*-δ Effects in Medium Height Moment Resisting Steel Frames." *Engineering Structures*, Vol. 14(2), 75-90.

Tolis, S.V. and Faccioli, E. (1999). "Displacement Design Spectra." *J. of Earthquake Eng.*, Vol. 3(1), 107-125.

Tremblay, R., Duval, C., and Léger, P. (1998). "Effects of Viscous Damping Models, Hysteretic Models, and Ground Motion Characteristics on Seismic P-Delta Strength Amplification Factors." *Stability and Ductility of Steel Structures*, Usami Tsutomu, Itoh Yoshito, Eds., Amsterdam, Elsevier, 1998, 103-18.

Tsai, K.C., Lai, J.W., Chen, C.H., Hsiao, B.C, Weng, Y.T., and Lin, M.L. (2003). "Pseudo Dynamic Tests of a Full Scale CFT/BRB Composite Frame." Proc.: 2004 Structures Congress, May 22-26, 2004, Nashville, TN.

Tzan, S-R. and Pantelides, C.P. (1998). "Active Structures Considering Energy Dissipation Through Damping and Plastic Yielding." *Computers and Structures*, Vol. 66 (4), 411-433.

Uang, C.-M. (1991a) "Establishing R (or R_w) and C_d Factors for Building Seismic Provisions." *J. Struct. Eng.*, ASCE, Vol. 117(7), 19-28.

Uang, C.-M. (1991b). "Comparison of Seismic Force Reduction Factors Used in U.S.A. and Japan." *Earthquake Eng. and Struct. Dyn.*, Vol. 20, 389-397.

Uang, C.-M. (1993) “An Evaluation of Two-Level Seismic Design Procedure.” *Earthquake Spectra*, EERI, Vol. 9(1), 121-135.

Uang, C.-M. and Bertero, V.V. (1991). “UBC Seismic Serviceability Regulations: Critical Review.” *J. Struct. Eng.*, ASCE, Vol. 117(7), 2055-2068.

Uang, C.-M. and Maarouf, A. (1993). “Safety and Economical Considerations of UBC Seismic Force Reduction Factors.” *Proc.: 1993 Natl. Earthquake Conf.*, Memphis, TN.

Uang, C.-M. and Maarouf, A. (1994). “Deflection Amplification Factor for Seismic Design Provisions”, *J. Struct. Eng.*, ASCE, Vol. 120(8), 2423-2436.

Xue, Q. (2001). “A Direct Displacement-Based Seismic Design Procedure of Inelastic Structures.” *Engineering Structures*, Vol. 23, 1453-1460.

Xue, Q. (2001). “Assessing the Accuracy of the Damping Models Used in Displacement-based Seismic Demand Evaluation and Design of Inelastic Structures.” *Earthquake Eng. and Eng. Seismology*, Vol. 3 (2), 37-45.

Xue, Q. and Chen, C-C. (2003). “Performance-Based Seismic Design of Structures: A Direct Displacement-Based Approach.” *Engineering Structures*, Vol. 25, 1803-1813.

Xue, Q. and Wu, C.-W. (2006). “Preliminary Detailing for Displacement-Based Seismic Design of Buildings.” *Engineering Structures*, submitted for review.

Yavas, A. and Saylan, S. (2004). “Effect of Equivalent Linearization in Direct Displacement Based Seismic Design of Bridge Columns.” *Proc., 13th World Conference on Earthquake Engineering*, Vancouver, B.C., Canada, Aug. 1-6, 2004.

Yura, J.A., Galambos, T.V., and Ravindra, M.K. (1978). “The Bending Resistance of Steel Beams.” *J. Struct. Div.*, ASCE, Vol. 104(ST9), 1355-1370.